

# **OPERATION HARDTACK**

411003

## **PROJECT 2.3 - Characteristics of the Radioactive Cloud from Underwater Bursts**

**E. C. Evans III, Project Officer  
T. H. Shirasawa  
U.S. Naval Radiological Defense Laboratory  
San Francisco, California**

**15 January 1962**

### **NOTICE:**

**This is an extracted version of (WT-1621), OPERATION HARDTACK, Project 2.3.**

**Approved for public release;  
distribution is unlimited.**

**Extracted version prepared for  
Director  
DEFENSE NUCLEAR AGENCY  
Washington, DC 20305-1000**

**1 September 1985**

**BEST COPY AVAILABLE**

Destroy this report when it is no longer needed. Do not return to sender.

PLEASE NOTIFY THE DEFENSE NUCLEAR AGENCY  
ATTN: TITL, WASHINGTON, DC 20305 1000, IF YOUR  
ADDRESS IS INCORRECT, IF YOU WISH IT DELETED  
FROM THE DISTRIBUTION LIST, OR IF THE ADDRESSEE  
IS NO LONGER EMPLOYED BY YOUR ORGANIZATION.



UNCLASSIFIED

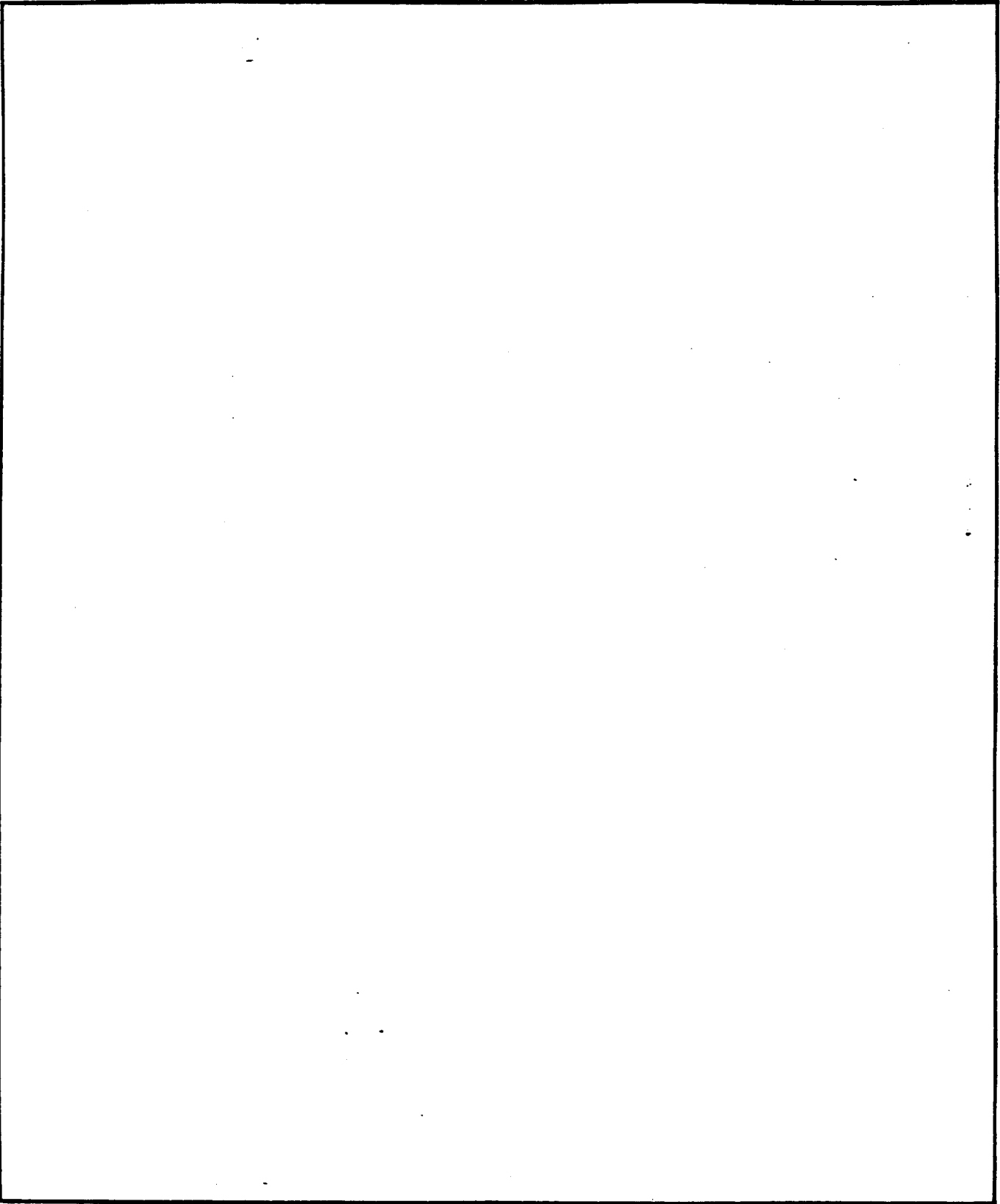
SECURITY CLASSIFICATION OF THIS PAGE

REPORT DOCUMENTATION PAGE				
1a. REPORT SECURITY CLASSIFICATION <b>UNCLASSIFIED</b>		1b. RESTRICTIVE MARKINGS		
2a. SECURITY CLASSIFICATION AUTHORITY		3. DISTRIBUTION / AVAILABILITY OF REPORT Approved for public release; distribution is unlimited.		
2b. DECLASSIFICATION / DOWNGRADING SCHEDULE				
4. PERFORMING ORGANIZATION REPORT NUMBER(S)		5. MONITORING ORGANIZATION REPORT NUMBER(S) <b>WT-1621 (EX)</b>		
6a. NAME OF PERFORMING ORGANIZATION <b>Naval Radiological Defense Laboratory</b>	6b. OFFICE SYMBOL (If applicable)	7a. NAME OF MONITORING ORGANIZATION <b>Defense Atomic Support Agency</b>		
6c. ADDRESS (City, State, and ZIP Code) <b>San Francisco, California</b>		7b. ADDRESS (City, State, and ZIP Code) <b>Washington, DC</b>		
8a. NAME OF FUNDING / SPONSORING ORGANIZATION	8b. OFFICE SYMBOL (If applicable)	9. PROCUREMENT INSTRUMENT IDENTIFICATION NUMBER		
8c. ADDRESS (City, State, and ZIP Code)		10. SOURCE OF FUNDING NUMBERS		
		PROGRAM ELEMENT NO.	PROJECT NO.	TASK NO.
				WORK UNIT ACCESSION NO.
11. TITLE (Include Security Classification) <b>OPERATION HARDTACK, PROJECT 2.3 - Characteristics of the Radioactive Cloud from Underwater Bursts, Extracted Version</b>				
12. PERSONAL AUTHOR(S) <b>E. C. Evans III and T. H. Shirasawa</b>				
13a. TYPE OF REPORT	13b. TIME COVERED FROM TO	14. DATE OF REPORT (Year, Month, Day) <b>620115</b>	15. PAGE COUNT <b>434</b>	
16. SUPPLEMENTARY NOTATION <b>This report has had sensitive military information removed in order to provide an unclassified version for unlimited distribution. The work was performed by the Defense Nuclear Agency in support of the DoD Nuclear Test Personnel Review Program.</b>				
17. COSATI CODES		18. SUBJECT TERMS (Continue on reverse if necessary and identify by block number)		
FIELD	GROUP	HARDTACK		
18	3	Umbrella Shot		
18	8	Fallout		
		Radioactive Clouds		
19. ABSTRACT (Continue on reverse if necessary and identify by block number)				
<p>The purpose of this project was to (1) measure the complex gamma field at a number of positions within 10,000 yards of each of the two underwater nuclear detonations (Wahoo and Umbrella); (2) collect limited samples of airborne debris resulting from these detonations; and (3) expose a number of test panels to this same debris.</p> <p>The total gamma field was measured by means of about 20 gamma-intensity-time recorders installed on floating platforms located within a radius of 10,000 yards from surface zero. Samples of radioactive materials deposited from the cloud were obtained by incremental collectors associated with the basic gamma-intensity-time recorders. During both shots, nearly all of the total gamma dose occurred within 20 minutes after zero time and was due to the passage of airborne radioactive material.</p>				
20. DISTRIBUTION / AVAILABILITY OF ABSTRACT <input checked="" type="checkbox"/> UNCLASSIFIED/UNLIMITED <input type="checkbox"/> SAME AS RPT <input type="checkbox"/> OTIC USERS		21. ABSTRACT SECURITY CLASSIFICATION <b>UNCLASSIFIED</b>		
22a. NAME OF RESPONSIBLE INDIVIDUAL <b>Mark D. Flohr</b>		22b. TELEPHONE (Include Area Code) <b>(202) 325-7559</b>	22c. OFFICE SYMBOL <b>DNA/ISCM</b>	

DD FORM 1473, 84 MAR

83 APR edition may be used until exhausted.  
All other editions are obsolete.SECURITY CLASSIFICATION OF THIS PAGE  
**UNCLASSIFIED**

SECURITY CLASSIFICATION OF THIS PAGE



SECURITY CLASSIFICATION OF THIS PAGE

## FOREWORD

Classified material has been removed in order to make the information available on an unclassified, open publication basis, to any interested parties. The effort to declassify this report has been accomplished specifically to support the Department of Defense Nuclear Test Personnel Review (NTPR) Program. The objective is to facilitate studies of the low levels of radiation received by some individuals during the atmospheric nuclear test program by making as much information as possible available to all interested parties.

The material which has been deleted is either currently classified as Restricted Data or Formerly Restricted Data under the provisions of the Atomic Energy Act of 1954 (as amended), or is National Security Information, or has been determined to be critical military information which could reveal system or equipment vulnerabilities and is, therefore, not appropriate for open publication.

The Defense Nuclear Agency (DNA) believes that though all classified material has been deleted, the report accurately portrays the contents of the original. DNA also believes that the deleted material is of little or no significance to studies into the amounts, or types, of radiation received by any individuals during the atmospheric nuclear test program.

**OPERATION HARDTACK—PROJECT 2.3**

**CHARACTERISTICS OF THE RADIOACTIVE CLOUD  
FROM UNDERWATER BURSTS**

**E. C. Evans III, Project Officer  
T. H. Shirasawa**

**U. S. Naval Radiological Defense Laboratory  
San Francisco 24, California**

## ABSTRACT

The general objectives were: (1) to measure the complex gamma field at a number of positions within 10,000 yards of each of the two underwater nuclear detonations (Wahoo and Umbrella), (2) to collect limited samples of airborne debris resulting from these detonations, and (3) to expose a number of test panels to this same debris.

The total gamma field was measured by means of about 20 gamma-intensity-time recorders installed on floating platforms located within a radius of 10,000 yards from surface zero. Samples of radioactive material deposited from the cloud were obtained by incremental collectors associated with the basic gamma-intensity-time recorders. Surface water activity was measured, and certain physicochemical parameters of the radioactive cloud were measured to calculate the free-field dose rates from the records obtained. Similar instruments supplemented by National Bureau of Standards film packs were used to determine gamma fields and total doses at various positions aboard three destroyers and a Liberty ship located within the area covered by the floating platforms. A comparison between shipboard fields and the local free-field is thus possible.

During both Wahoo and Umbrella, nearly all of the total gamma dose occurred within 25 minutes after zero time and was due to the passage of airborne radioactive material. The gamma-dose-rate records show pronounced and characteristic differences in the transiting gamma fields resulting from each of the two detonations. Gamma doses in excess of 100 r occurred within the first 15 minutes at downwind distances less than 16,000 feet from Wahoo and 14,000 feet from Umbrella. In both instances the residual field due to deposited radioactive material was relatively insignificant, although radioactive foam may represent a radiological hazard.

## PREFACE

The preparation of any report is necessarily the direct work of only a few people; yet the very existence of this final product is the summation of the material contributions of a large number of persons who remain anonymous.

The authors thank the many members of the Army Signal Engineering Laboratory (ASEL) who were responsible for the development and construction of the gamma-intensity-time recorders loaned to the project for Operation Hardtack. Special thanks are due Mr. Basil Markow and Mr. Richard G. Rast of ASEL who joined the project as consultants in the field and as specialists in ASEL instrumentation.

Special thanks are also due Mr. Samuel C. Rainey of the Bureau of Ships (Code 372) who assisted with much of the theoretical work and with final data reduction in the field.

Lastly, special thanks are due to Mr. Lansing E. Egeberg and Mr. Glynn A. Pence of the Naval Radiological Defense Laboratory, both for their ceaseless and invaluable efforts as deputy project officers for operations in the field and for their continued work on many and varied problems of data reduction during the preparation of the final report.

In a project of the size and complexity of the one reported on, the number of contributions is so large as to require brevity, yet the gratitude of the authors for both material assistance and moral support is nonetheless genuine. The following list is by no means complete but represents a summary of principal contributors:

For deep-anchoring theory and coracle design; James L. Faughn and Lyle D. Johnson.

For radiation field theory; Rodney Buntzen, Arthur B. Denison, and Edwin S. Shapiro.

For design of specialized electronic instrumentation; Benjamin Chow, Philip A. Covey, Richard R. Soule, and Harry A. Zagorites.

For design of specialized mechanical instruments; Robert A. Nelson and John I. Pond.

For design and implementation of special site chemistry; Roger Caputi, William R. Schell, and Edward R. Tompkins.

For devising specialized readout techniques and reduction of taped data; Walter J. Gurney.

For data reduction and preparation of the final report; Esther N. Guffy, Ichiro Hayashi, Morris Pasternak, Jean V. Sanderson, and Ann Swanson.

For general assistance in many and varied problems; Roger Caputi, Louis B. Gomez, Gordon L. Jacks, Walter W. Perkins, Jack A. LaSpada, Dale H. Williams, and many others.

## CONTENTS

ABSTRACT-----	5
PREFACE -----	6
CHAPTER 1 INTRODUCTION -----	23
1.1 Objectives -----	23
1.2 Background-----	24
1.3 Theory-----	25
1.3.1 Components of the Radiation Field -----	31
1.3.2 Properties of Moving Fields -----	37
1.3.3 Supplementary Measurements -----	39
CHAPTER 2 PROCEDURE -----	48
2.1 General Operations and Shot Participation -----	48
2.1.1 Shot Wahoo-----	52
2.1.2 Shot Umbrella-----	53
2.2 Instruments -----	55
2.2.1 Gamma-Intensity-Time Recorder (GITR)-----	55
2.2.2 Underwater GITR -----	55
2.2.3 High-Range GITR -----	57
2.2.4 Incremental Fallout Collector -----	57
2.2.5 Film Packs -----	57
2.2.6 Supplementary Fallout Collectors-----	60
2.2.7 Instrument Control -----	63
2.2.8 GITR Tape Readout -----	65
2.3 Special Operations -----	65
2.3.1 Calculation of the Deep Moor-----	67
2.3.2 Properties and Placement of Coracles -----	72
CHAPTER 3 RESULTS AND DISCUSSION -----	76
3.1 General Description of the Data -----	76
3.1.1 Data Reduction -----	79
3.1.2 Data Obtained from Other Agencies -----	83
3.2 Early Gamma Radiation -----	83
3.3 Gamma Radiation Fields Resulting from Airborne Radioactive Material -----	89
3.3.1 Deposited Radioactive Material -----	105
3.3.2 Free-Field Dose Rates-----	113
3.3.3 Free-Field Isodose Contours-----	139
3.3.4 Transport Phenomena -----	228
3.3.5 Estimated Waterborne Radioactivity-----	244
3.4 Gamma Radiation Fields Aboard Target Ships-----	276
3.4.1 Gamma Dose Rate versus Time -----	276
3.4.2 Variation of Shipboard Dose with Position -----	284
3.4.3 Conversion Factors -----	311

3.5 Characteristics of Airborne Radioactive Material	318
3.5.1 Fractionation	320
3.5.2 Physical and Chemical Properties	326
CHAPTER 4 CONCLUSIONS AND RECOMMENDATIONS	343
4.1 Conclusions	343
4.2 Recommendations	345
APPENDIX A THEORY AND PREDICTION	347
A.1 Factors for Theoretical Calculations	347
A.2 Theoretical Deposition from a Radioactive Cloud	347
A.3 Model for an Inclined Wall of Approaching Base Surge	348
A.4 Wind Correction Factors	348
A.5 Predicted Radiation Contours	359
APPENDIX B INSTRUMENTS AND DECAY	359
B.1 Instruments	360
B.2 Decay Curves	366
APPENDIX C CALIBRATION AND RESPONSE	366
C.1 Standard GTR Calibration and Response	366
C.2 ASEL-GTR Calibration and Response	367
C.3 End-Window Gamma Counter Response	367
C.4 Film Calibration	367
C.5 Empirical Correlation Between Std-GTR and IC	368
C.6 Underwater Response of Std-GTR	379
APPENDIX D ORIGINAL DATA	379
D.1 Linear Free-Field and Shipboard Records	379
D.2 Meter Survey Data for Coracles	379
D.3 IC Counting Data	380
D.4 IC Decay Data	414
APPENDIX E SUMMARY OF OTHER UNDERWATER DETONATIONS	414
E.1 General Conditions	414
E.2 Shot Baker	414
E.3 Shot Wigwam	417
APPENDIX F GLOSSARY	424
REFERENCES	
TABLES	26
1.1 Depths and Bottom Slopes at Proposed Stations	35
1.2 Falling Velocities for Liquid Droplets	42
1.3 Estimated Relative Dose and Distance of Drift for FFP's	49
2.1 Instrumentation and Actual Position of Stations	68
2.2 Assumed Subsurface Currents Southwest of Eniwetok Atoll	
2.3 Estimated Drag Forces on Coracle Station and on Deep Mooring Components	68

2.4	Estimated Excursion and Depression of 1,200-Fathom Moor	68
2.5	Estimated Excursion and Depression of 400-Fathom Moor	68
2.6	Coracle Recovery Data, Shot Wahoo	73
2.7	Time of Arrival of Device-Generated Water Waves at Stations	73
3.1	Shot Data and Surface Weather at Shot Time	78
3.2	Correction Factors for Directional Response	78
3.3	Summary of Time Adjustments	84
3.4	Initial Dose Rate Peaks	87
3.5	Estimated Cumulative Doses for Initial Radiation	90
3.6	Deposit Dose Determined from GITR Background, Meter Survey Reading, and IC Collections	106
3.7	Relative Activity of Later Incremental Collections	112
3.8	Times and Dose Rates for Significant Peaks in the Gamma Records	123
3.9	Cumulative Doses Calculated from Std-GITR Records	125
3.10	Cumulative Doses Calculated from Normalized Rate Curves	126
3.11	Master Table for Base Surge Transit, Shots Wahoo and Umbrella	135
3.12	Coracle Film Pack, Shipboard Film Pack, and Floating Film Pack Data	202
3.13	Dose Rate and Distance from Hypothetical Surge Center, H, for Various Times After Zero Time	205
3.14	Time of Arrival (TOA) at Coracles and Ships	229
3.15	Visual Approach Velocities	233
3.16	Velocity of Approach Calculated from Rate of Rise of Std-GITR	235
3.17	Radial Velocity of Expansion Computed from Rate of Rise of Std-GITR	235
3.18	Time of Cessation (TOC) at Coracles	238
3.19	Photographic Cloud Boundary as a Function of Time Along Various Radial Lines	239
3.20	Radial Distances to Hypothetical Surge Center at Time of Passage of Base Surge Boundaries	241
3.21	Summary for Second FFP Drop	245
3.22	Dose Rate Peaks and TOA for UW-GITR Records	246
3.23	Comparison of Standard and Underwater Gamma Records	248
3.24	Summary of White Water Movement	250
3.25	Calculated Water and Foam Movement	253
3.26	Positions and Attitudes of Target Ships	277
3.27	Summary of Cumulative Doses Obtained from Shipboard GITR's and Film Packs	279
3.28	Times and Dose Rates for Significant Peaks in the Shipboard Gamma Records	280
3.29	Cumulative Doses Calculated from Normalized Rate Curves, Ships	281
3.30	Shipboard Film Pack Doses and Associated Survey Readings	309
3.31	Average Shipboard Survey Readings Not Associated with Film Packs	310
3.32	Average Shipboard Doses and Dose Ratios	316
3.33	Conversion Factors for Superstructure Shielding	317
3.34	Characteristic Decay Curves for IC Collections	321
3.35	Miscellaneous Sample Data	327
3.36	Summary for Funnel Samples	327
3.37	Activity of Air Filtration Instrument (AFI) Samples	332
3.38	Summary of Liquid Fraction Measurements	337
3.39	Summary of Solid Fraction Measurements	338
3.40	Spectrochemical Analysis of Selected Samples	340
3.41	Mo <sup>99</sup> Analysis of IC Trays	342
A.1	Summary of U <sup>235</sup> Fission Product Gamma Ray Properties	349
A.2	Characteristics of Absorbing Materials	349

A.3	Pertinent Attenuation Coefficients	350
A.4	Geometric Parameters of Coracle	350
A.5	Buildup Factors for Water	350
A.6	Gamma Intensities of Finite Clouds Expressed as a Percentage of -an Infinite Cloud, 1-Mev Gamma Energy	351
A.7	Directional Response of Low-Range Std-GITR Detector	351
A.8	Value of $I_A$ Expressed as a Percentage of $I_G$	352
A.9	Wind Corrections	353
C.1	Relative Energy Response for End-Window Gamma Counter 2 for a Point Source on Shelf 5	368
D.1	Meter Survey of Coracle Decks	381
D.2	U 4.5 IC Tray Counts, Shot Wahoo	381
D.3	CL 3.9 IC Tray Counts, Shot Wahoo	381
D.4	CL 4.6 IC Tray Counts, Shot Wahoo	382
D.5	DL 7.1 IC Tray Counts, Shot Wahoo	382
D.6	D 8.0 IC Tray Counts, Shot Wahoo	382
D.7	DR 4.5 IC Tray Counts, Shot Wahoo	382
D.8	DR 14.4 IC Tray Counts, Shot Wahoo	383
D.9	DR 24.0 IC Tray Counts, Shot Wahoo	383
D.10	DRR 6.8 IC Tray Counts, Shot Wahoo	383
D.11	DRR 12.8 IC Tray Counts, Shot Wahoo	384
D.12	CR 6.4 IC Tray Counts, Shot Wahoo	384
D.13	U 2.7 IC Tray Counts, Shot Umbrella	384
D.14	U 3.9 IC Tray Counts, Shot Umbrella	385
D.15	CL 4.0 IC Tray Counts, Shot Umbrella	385
D.16	CL 6.0 IC Tray Counts, Shot Umbrella	385
D.17	DL 6.2 IC Tray Counts, Shot Umbrella	386
D.18	DL 16.0 IC Tray Counts, Shot Umbrella	386
D.19	DL 18.6 IC Tray Counts, Shot Umbrella	386
D.20	D 10.4 IC Tray Counts, Shot Umbrella	386
D.21	D 18.2 IC Tray Counts, Shot Umbrella	387
D.22	D 22.0 IC Tray Counts, Shot Umbrella	387
D.23	DR 12.2 IC Tray Counts, Shot Umbrella	387
D.24	CR 4.9 IC Tray Counts, Shot Umbrella	387
D.25	CR 6.6 IC Tray Counts, Shot Umbrella	388
D.26	DD-592 (Port) IC Tray Counts, Shot Umbrella	388
D.27	DD-592 (Stbd) IC Tray Counts, Shot Umbrella	388
D.28	CL 3.9 Decay of IC Tray (2 Minutes), Shot Wahoo	388
D.29	CL 3.9 Decay of IC Tray (3 Minutes), Shot Wahoo	388
D.30	CL 4.6 Decay of IC Tray (3 Minutes), Shot Wahoo	389
D.31	DL 7.1 Decay of IC Tray (4 Minutes), Shot Wahoo	389
D.32	DL 7.1 Decay of IC Tray (9 Minutes), Shot Wahoo	389
D.33	D 8.0 Decay of IC Tray (19 Cont), Shot Wahoo	389
D.34	D 23.1 Decay of IC Tray (54), Shot Wahoo	389
D.35	DR 4.5 Decay of IC Tray (9 minutes), Shot Wahoo	389
D.36	DR 4.5 Decay of IC Tray (19 Cont), Shot Wahoo	390
D.37	DR 24.0 Decay of IC Tray (52 Minutes), Shot Wahoo	390
D.38	DRR 6.8 Decay of IC Tray (2 Minutes), Shot Wahoo	390
D.39	DRR 6.8 Decay of IC Tray (3 Minutes), Shot Wahoo	390
D.40	DRR 12.8 Decay of IC Tray (44 Minutes), Shot Wahoo	390
D.41	CR 4.1 Decay of IC Tray (19), Shot Wahoo	390
D.42	CR 5.2 Decay of IC Tray (2 Cont), Shot Wahoo	391
D.43	CR 6.4 Decay of IC Tray (2 Minutes), Shot Wahoo	391

D.44	CR 6.4 Decay of IC Tray (3 Minutes), Shot Wahoo	391
D.45	U 2.7 Decay of IC Tray (2 Minutes), Shot Umbrella	391
D.46	U 2.7 Decay of IC Tray (3 Minutes), Shot Umbrella	391
D.47	CL 4.0 Decay of IC Tray (2 Minutes), Shot Umbrella	391
D.48	CL 4.0 Decay of IC Tray (4 Minutes), Shot Umbrella	392
D.49	CL 6.0 Decay of IC Tray (19 Cont), Shot Umbrella	392
D.50	DL 6.2 Decay of IC Tray (2 Minutes), Shot Umbrella	392
D.51	DL 16.0 Decay of IC Tray (6 Minutes), Shot Umbrella	392
D.52	DL 16.0 Decay of IC Tray (8 Cont), Shot Umbrella	392
D.53	D 10.4 Decay of IC Tray (20 Cont), Shot Umbrella	392
D.54	D 18.2 Decay of IC Tray (7 Minutes), Shot Umbrella	392
D.55	D 22.0 Decay of IC Tray (9 Minutes), Shot Umbrella	393
D.56	DR 12.2 Decay of IC Tray (5 Minutes), Shot Umbrella	393
D.57	CR 2.7 Decay of IC Tray (37 Minutes), Shot Umbrella	393
D.58	CR 2.7 Decay of IC Tray (40), Shot Umbrella	393
D.59	DD-592 (Port) Decay of IC Tray (4 Minutes), Shot Umbrella	393
D.60	DD-592 (Stbd) Decay of IC Tray (4 Minutes), Shot Umbrella	393
D.61	IC Decay Slopes Determined on the Basis of Two Points	394
E.1	Shot Data and Surface Weather at Shot Time, Shots Baker and Wigwam	416
E.2	Column and Base Surge Data, Shot Baker	416
E.3	Spray Dome and Base Surge Data, Shot Wigwam	416

**FIGURES**

1.1	Originally intended array of coracles and floating film packs (FFP)	27
1.2	Coracle	28
1.3	Simplified elevation, cross section, and plan view of coracle	28
1.4	NRDL gamma-intensity-time recorder	29
1.5	Free-field response expressed as a percentage of gross response ( $t_0 = 3$ minutes)	36
1.6	Free-field response expressed as a percentage of gross response ( $t_0 = 10$ minutes)	36
1.7	Radiation intensity from a circular upwelling of radioactive water (computed for a standard GITR at its center)	38
1.8	Relative intensity from an enveloping base surge (90° cloud model, 1 Mev gamma)	38
1.9	Relative intensity from an enveloping base surge (90° cloud model, 1.25 Mev gamma)	40
1.10	Relative intensity from an enveloping base surge (60° cloud model, 1.25 Mev gamma)	40
1.11	Relative intensity for moving circular patches of radioactive water (circular disk model, 1½ feet thick, 1.25 Mev gamma)	40
1.12	Target ship instrument layout aboard DD-474 and DD-593	44
1.13	Target ship instrument layout aboard DD-592	45
1.14	Target ship instrument layout aboard EC-2	46
1.15	NRDL instrument platform aboard DD-474 and DD-592	47
1.16	NRDL instrument platform aboard DD-592	47
2.1	Master plot of stations, Shot Wahoo	50
2.2	Master plot of stations, Shot Umbrella	51
2.3	GITR mounting for ships	56
2.4	ASEL gamma-intensity-time recorder	58
2.5	Incremental collector	59
2.6	Various types of floating film packs	61
2.7	Open-close collector	62

2.8 Air flow instrument	62
2.9 Relative positions of components in AFI sampling head	64
2.10 GITOUT equipment	64
2.11 Elements of GITOUT system	66
2.12 Maximum horizontal drag forces for various anchors on sloping bottoms	70
2.13 Measured coracle drag forces	70
2.14 Comparison of float excursion and net reaction of anchor on the bottom as a function of subsurface float size ( $\frac{5}{32}$ -inch cable, 1,200-fathom moor)	71
2.15 Deep-anchoring system	71
2.16 Coracle drift rates	74
3.1 Relative response of ASEL-GITR detector for an enveloping base surge. (Source: 120 kev X-ray)	80
3.2 Relative response of secondary-GITR detector for an enveloping base surge. (Source: Co <sup>60</sup> )	80
3.3 Relative response of standard-GITR detector for an enveloping base surge. (Source: Co <sup>60</sup> )	80
3.4 Initial dose rate versus distance, Shots Wahoo and Umbrella	88
3.5 Gross gamma record, 0 to 2.5 minutes, coracle at 4,500 feet, 66° T from surface zero (std-GITR), Shot Wahoo	91
3.6 Gross gamma record, 0 to 2.5 minutes, coracle at 3,900 feet, 159° T from surface zero (std-GITR), Shot Wahoo	91
3.7 Gross gamma records, 0 to 2.5 minutes, coracle at 4,600 feet, 151.5° T from surface zero (ASEL- and std-GITR's), Shot Wahoo	92
3.8 Gross gamma record, 0 to 2.5 minutes, coracle at 4,500 feet, 263° T from surface zero (std-GITR), Shot Wahoo	92
3.9 Gross gamma records, 0 to 2.5 minutes, coracle at 4,100 feet, 336° T from surface zero (ASEL- and std-GITR's), Shot Wahoo	93
3.10 Gross gamma record, 0 to 2.5 minutes, coracle at 5,200 feet, 334.5° T from surface zero (std-GITR), Shot Wahoo	93
3.11 Gross gamma record, 0 to 2.5 minutes, EC-2 at 2,300 feet, 28.5° T from surface zero (GITR installed inside pilot house), Shot Wahoo	94
3.12 Gross gamma records, 0 to 2.5 minutes, EC-2 at 2,300 feet, 28.5° T from surface zero (GITR installed on centerline, Frame 48, forward, and Frame 137.5, aft), Shot Wahoo	94
3.13 Gross gamma records, 0 to 2.5 minutes, coracle at 1,760 feet, 51.8° T from surface zero (ASEL- and std-GITR), Shot Umbrella	95
3.14 Gross gamma records, 0 to 2.5 minutes, coracle at 2,700 feet, 67° T from surface zero (ASEL-, std-, and sec-GITR's), Shot Umbrella	95
3.15 Gross gamma records, 0 to 2.5 minutes, coracle at 3,890 feet, 68° T from surface zero (ASEL- and std-GITR's), Shot Umbrella	96
3.16 Gross gamma records, 0 to 2.5 minutes, coracle at 3,060 feet, 163.7° T from surface zero (ASEL- and std-GITR's), Shot Umbrella	96
3.17 Gross gamma record, 0 to 2.5 minutes, coracle at 3,990 feet, 158.5° T from surface zero (ASEL-GITR), Shot Umbrella	97
3.18 Gross gamma record, 0 to 2.5 minutes, coracle at 6,010 feet, 158.9° T from surface zero (std-GITR), Shot Umbrella	97
3.19 Gross gamma record, 0 to 2.5 minutes, coracle at 6,220 feet, 230.4° T from surface zero (std-GITR), Shot Umbrella	98

3.20	Gross gamma records, 0 to 2.5 minutes, coracle at 2,670 feet, 248° T from surface zero (ASEL-, std-, and sec-GITR's), Shot Umbrella -----	98
3.21	Gross gamma records, 0 to 2.5 minutes, coracle at 4,770 feet, 247.9° T from surface zero (ASEL-, std-, and sec-GITR's), Shot Umbrella -----	99
3.22	Gross gamma record, 0 to 2.5 minutes, coracle at 4,530 feet, 263.5° T from surface zero (ASEL-GITR), Shot Umbrella -----	99
3.23	Gross gamma records, 0 to 2.5 minutes, coracle at 3,940 feet, 279.1° T from surface zero (ASEL- and std-GITR's), Shot Umbrella ----	100
3.24	Gross gamma record, 0 to 2.5 minutes, coracle at 6,740 feet, 278.1° T from surface zero (std-GITR), Shot Umbrella -----	100
3.25	Gross gamma records, 0 to 2.5 minutes, coracle at 4,910 feet, 334° T from surface zero (ASEL- and std-GITR's), Shot Umbrella -----	101
3.26	Gross gamma record, 0 to 2.5 minutes, EC-2 at 1,650 feet, 158° T from surface zero (GITR installed inside pilot house), Shot Umbrella -----	101
3.27	Gross gamma records, 0 to 2.5 minutes, EC-2 at 1,650 feet, 158° T from surface zero (GITR installed on centerline, Frame 48, forward, and Frame 137.5, aft, main deck), Shot Umbrella -----	102
3.28	Gross gamma record, 0 to 2.5 minutes, DD-474 at 1,900 feet, 245.7° T from surface zero (GITR installed on centerline at Frame 21, bow), Shot Umbrella -----	102
3.29	Gross gamma records, 0 to 2.5 minutes, DD-474 at 1,900 feet, 245.7° T from surface zero (GITR installed on main deck, Frame 136, port, and Frame 136, starboard), Shot Umbrella -----	103
3.30	Gross gamma records, 0 to 2.5 minutes, DD-592 at 3,000 feet, 248.5° T from surface zero (GITR installed on centerline, Frame 21, bow, and top of 5-inch gun director, platform), Shot Umbrella -----	103
3.31	Gross gamma records, 0 to 2.5 minutes, DD-592 at 3,000 feet, 248.5° T from surface zero (GITR installed on main deck, Frame 136, port, and Frame 136, starboard), Shot Umbrella -----	104
3.32	Deposit dose rate versus distance (calculated from GITR background), Shot Wahoo-----	108
3.33	Deposit dose rate versus distance (calculated from GITR background), Shot Umbrella-----	108
3.34	Deposit dose rate versus distance (calculated from total IC collection), Shots Wahoo and Umbrella -----	108
3.35	Plume trajectories determined from documentary photography, Shot Wahoo -----	110
3.36	Family of decay curves for IC collections, Shots Wahoo and Umbrella-----	110
3.37	Deposit dose rate histogram for IC at 4,500 feet, 66° T from surface zero, Shot Wahoo -----	114
3.38	Deposit dose rate histogram for IC at 3,900 feet, 159° T from surface zero, Shot Wahoo-----	114
3.39	Deposit dose rate histogram for IC at 4,600 feet, 151.5° T from surface zero, Shot Wahoo -----	114
3.40	Deposit dose rate histogram for IC at 7,100 feet, 231.5° T from surface zero, Shot Wahoo -----	114
3.41	Deposit dose rate histogram for IC at 8,000 feet, 256.5° T from surface zero, Shot Wahoo -----	114

3.42	Deposit dose rate histogram for IC at 4,500 feet, 263° T from surface zero, Shot Wahoo-----	114
3.43	Deposit dose rate histogram for IC at 14,400 feet, 265° T from surface zero, Shot Wahoo-----	115
3.44	Deposit dose rate histogram for IC at 24,000 feet, 263° T from surface zero, Shot Wahoo-----	115
3.45	Deposit dose rate histogram for IC at 6,800 feet, 281° T from surface zero, Shot Wahoo-----	115
3.46	Deposit dose rate histogram for IC at 12,800 feet, 276° T from surface zero, Shot Wahoo-----	115
3.47	Deposit dose rate histogram for IC at 6,400 feet, 332° T from surface zero, Shot Wahoo-----	115
3.48	Deposit dose rate histogram for IC at 2,700 feet, 67° T from surface zero, Shot Umbrella-----	115
3.49	Deposit dose rate histogram for IC at 3,890 feet, 68° T from surface zero, Shot Umbrella-----	116
3.50	Deposit dose rate histogram for IC at 3,990 feet, 158.5° T from surface zero, Shot Umbrella-----	116
3.51	Deposit dose rate histogram for IC at 6,010 feet, 158.9° T from surface zero, Shot Umbrella-----	116
3.52	Deposit dose rate histogram for IC at 6,220 feet, 230.4° T from surface zero, Shot Umbrella-----	116
3.53	Deposit dose rate histogram for IC at 15,980 feet, 237.1° T from surface zero, Shot Umbrella-----	117
3.54	Deposit dose rate histogram for IC at 18,650 feet, 233.5° T from surface zero, Shot Umbrella-----	117
3.55	Deposit dose rate histogram for IC at 10,380 feet, 247.5° T from surface zero, Shot Umbrella-----	117
3.56	Deposit dose rate histogram for IC at 18,220 feet, 250.2° T from surface zero, Shot Umbrella-----	117
3.57	Deposit dose rate histogram for IC at 22,000 feet, 248° T from surface zero, Shot Umbrella-----	117
3.58	Deposit dose rate histogram for IC at 12,230 feet, 262.5° T from surface zero, Shot Umbrella-----	117
3.59	Deposit dose rate histogram for IC at 4,910 feet, 334° T from surface zero, Shot Umbrella-----	118
3.60	Deposit dose rate histogram for IC at 6,610 feet, 337.3° T from surface zero, Shot Umbrella-----	118
3.61	Deposit dose rate histogram for IC aboard DD-592 at 3,000 feet, 248.5° T from surface zero, platform starboard, Shot Umbrella-----	118
3.62	Deposit dose rate histogram for IC aboard DD-592 at 3,000 feet, 248.5° T from surface zero, platform port, Shot Umbrella-----	118
3.63	Illustration of special base surge transit terms-----	121
3.64	Normalized peak dose rates as a function of time, Shot Wahoo-----	128
3.65	Normalized peak dose rates as a function of time, Shot Umbrella-----	128
3.66	Transit dose rate record and data summary for U 4.5, Shot Wahoo-----	140
3.67	Transit dose rate record and data summary for CL 3.9, Shot Wahoo-----	142
3.68	Transit dose rate record and data summary for CL 4.6, Shot Wahoo-----	144
3.69	Transit dose rate record and data summary for DL 7.1, Shot Wahoo-----	146
3.70	Transit dose rate record and data summary for D 8.0, Shot Wahoo-----	148
3.71	Transit dose rate record and data summary for DR 4.5, Shot Wahoo-----	150
3.72	Transit dose rate record and data summary for DR 9.0, Shot Wahoo-----	152
3.73	Transit dose rate record and data summary for DR 14.4, Shot Wahoo-----	154

3.74	Transit dose rate record and data summary for DR 24.0, Shot Wahoo	156
3.75	Transit dose rate record and data summary for DRR 6.8, Shot Wahoo	158
3.76	Transit dose rate record and data summary for DRR 12.8, Shot Wahoo	160
3.77	Transit dose rate record and data summary for CR 4.1, Shot Wahoo	162
3.78	Transit dose rate record and data summary for CR 5.2, Shot Wahoo	164
3.79	Transit dose rate record and data summary for CR 6.4, Shot Wahoo	166
3.80	Transit dose rate record and data summary for U 1.8, Shot Umbrella	168
3.81	Transit dose rate record and data summary for U 2.7, Shot Umbrella	170
3.82	Transit dose rate record and data summary for U 3.9, Shot Umbrella	172
3.83	Transit dose rate record and data summary for CL 3.1, Shot Umbrella	174
3.84	Transit dose rate record and data summary for CL 6.0, Shot Umbrella	176
3.85	Transit dose rate record and data summary for DLL 6.6, Shot Umbrella	178
3.86	Transit dose rate record and data summary for DL 6.2, Shot Umbrella	180
3.87	Transit dose rate record and data summary for DL 16.0, Shot Umbrella	182
3.88	Transit dose rate record and data summary for D 2.7, Shot Umbrella	184
3.89	Transit dose rate record and data summary for D 4.8, Shot Umbrella	186
3.90	Transit dose rate record and data summary for D 18.2, Shot Umbrella	188
3.91	Transit dose rate record and data summary for D 22.0, Shot Umbrella	190
3.92	Transit dose rate record and data summary for DR 12.2, Shot Umbrella	192
3.93	Transit dose rate record and data summary for DR 18.6, Shot Umbrella	194
3.94	Transit dose rate record and data summary for DRR 3.9, Shot Umbrella	196
3.95	Transit dose rate record and data summary for DRR 6.7, Shot Umbrella	198
3.96	Transit dose rate record and data summary for CR 4.9, Shot Umbrella	200
3.97	Comparison of cumulative doses determined by std-GITR and by film pack	203
3.98	One-minute isodose contours and base surge boundaries, Shot Wahoo	206
3.99	Two-minute isodose contours and base surge boundaries, Shot Wahoo	207
3.100	Three-minute isodose contours and base surge boundaries, Shot Wahoo	208
3.101	Three-and-a-half-minute base surge boundaries, Shot Wahoo	209
3.102	Five-minute isodose contours, Shot Wahoo	210
3.103	Final isodose contours (GITR cumulative dose to 6 hours), Shot Wahoo	211
3.104	One-minute isodose contours and base surge boundaries, Shot Umbrella	212
3.105	Two-minute isodose contours and base surge boundaries, Shot Umbrella	213
3.106	Three-minute isodose contours and base surge boundaries, Shot Umbrella	214
3.107	Five-minute isodose contours and base surge boundaries, Shot Umbrella	215
3.108	Six-minute base surge boundaries, Shot Umbrella	216
3.109	Final isodose contours (GITR cumulative dose to 6 hours), Shot Umbrella	217
3.110	One-minute cumulative dose versus distance, Shot Wahoo	218
3.111	Two-minute cumulative dose versus distance, Shot Wahoo	218
3.112	Three-minute cumulative dose versus distance, Shot Wahoo	219
3.113	Five-minute cumulative dose versus distance, Shot Wahoo	219
3.114	Six-hour cumulative dose versus distance, Shot Wahoo	220
3.115	One-minute cumulative dose versus distance, Shot Umbrella	221
3.116	Two-minute cumulative dose versus distance, Shot Umbrella	221
3.117	Three-minute cumulative dose versus distance, Shot Umbrella	222
3.118	Five-minute cumulative dose versus distance, Shot Umbrella	222
3.119	Six-hour cumulative dose versus distance, Shot Umbrella	223
3.120	One-minute dose rates versus distance from hypothetical surge center, Shot Wahoo	224
3.121	Two-minute dose rates versus distance from hypothetical surge center, Shot Wahoo	224
3.122	Three-minute dose rates versus distance from hypothetical surge center, Shot Wahoo	225

3.123	Five-minute dose rates versus distance from hypothetical surge center, Shot Wahoo-----	225
3.124	One-minute dose rates versus distance from hypothetical surge center, Shot Umbrella-----	226
3.125	Two-minute dose rates versus distance from hypothetical surge center, Shot Umbrella-----	226
3.126	Three-minute dose rates versus distance from hypothetical surge center, Shot Umbrella-----	227
3.127	Five-minute dose rates versus distance from hypothetical surge center, Shot Umbrella-----	227
3.128	Time of arrival versus distance, Shot Wahoo. (TOA defined as 38 percent of peak.) Official Task Force surface wind: 15 knots from 090° T -----	230
3.129	Time of arrival versus distance, Shot Umbrella. (TOA defined as 38 percent of peak.) Official Task Force surface wind: 20 knots from 050° T -----	230
3.130	Time of arrival versus distance, Shot Wahoo. (TOA defined as 100 percent of peak.) Official Task Force surface wind: 15 knots from 090° T -----	231
3.131	Time of arrival versus distance, Shot Umbrella. (TOA defined as 100 percent of peak.) Official Task Force surface wind: 20 knots from 050° T -----	231
3.132	Radial velocity of base surge, Shot Wahoo-----	236
3.133	Radial velocity of base surge, Shot Umbrella-----	236
3.134	Comparison of time of peak with earliest time of arrival, Shot Wahoo -----	240
3.135	Comparison of time of peak with earliest time of arrival, Shot Umbrella ---	240
3.136	Hypothetical base surge radius versus time, Shot Wahoo-----	242
3.137	Hypothetical base surge radius versus time, Shot Umbrella-----	242
3.138	Ratio of underwater dose rate as a function of depth -----	248
3.139	Time of arrival of radioactive water, Shot Wahoo-----	251
3.140	Time of arrival of radioactive water, Shot Umbrella-----	251
3.141	Accelerated decay of radioactive water, Shot Wahoo-----	254
3.142	Accelerated decay of radioactive water, Shot Umbrella-----	254
3.143	UW-GITR record, 0 to 15 minutes, coracle at 3,900 feet, 159° T from surface zero, Shot Wahoo-----	255
3.144	UW-GITR record, 0 to 15 minutes, coracle at 4,600 feet, 151.5° T from surface zero, Shot Wahoo -----	255
3.145	UW-GITR record, 0 to 15 minutes, coracle at 8,000 feet, 256.5° T from surface zero, Shot Wahoo -----	256
3.146	UW-GITR record, 0 to 15 minutes, coracle at 4,500 feet, 263° T from surface zero, Shot Wahoo-----	256
3.147	UW-GITR record, 0 to 30 minutes, coracle at 24,000 feet, 263° T from surface zero, Shot Wahoo-----	257
3.148	UW-GITR record, 0 to 30 minutes, coracle at 4,100 feet, 336° T from surface zero, Shot Wahoo-----	257
3.149	UW-GITR record, 0 to 15 minutes, coracle at 5,200 feet, 334.5° T from surface zero, Shot Wahoo -----	258
3.150	UW-GITR record, 0 to 15 minutes, coracle at 1,760 feet, 51.8° T from surface zero, Shot Umbrella -----	258
3.151	UW-GITR record, 0 to 15 minutes, coracle at 4,530 feet, 263.5° T from surface zero, Shot Umbrella -----	259
3.152	UW-GITR record, 0 to 30 minutes, coracle at 3,940 feet, 279.1° T from surface zero, Shot Umbrella -----	259

	U-GITR record, 0 to 15 minutes, coracle at 6,740 feet, 278.1° T from surface zero, Shot Umbrella -----	260
3.154	Std-GITR record, 0 to 6 hours, coracle at 4,500 feet, 66° T from surface zero, Shot Wahoo -----	261
3.155	Std- and UW-GITR records, 0 to 8 hours, coracle at 3,900 feet, 159° T from surface zero, Shot Wahoo-----	261
3.156	Std-GITR record, 0 to 6 hours, coracle at 4,600 feet, 151.5° T from surface zero, Shot Wahoo -----	262
3.157	Std-GITR record, 0 to 6 hours, coracle at 7,100 feet, 231.5° T from surface zero, Shot Wahoo -----	262
3.158	Std- and UW-GITR records, 0 to 8 hours, coracle at 8,000 feet, 256.5° T from surface zero, Shot Wahoo -----	263
3.159	Std- and UW-GITR records, 0 to 8 hours, coracle at 4,500 feet, 263° T from surface zero, Shot Wahoo-----	263
3.160	Std-GITR record, 0 to 6 hours, coracle at 8,950 feet, 263° T from surface zero, Shot Wahoo-----	264
3.161	Std-GITR record, 0 to 6 hours, coracle at 24,000 feet, 263° T from surface zero, Shot Wahoo-----	264
3.162	Std- and sec-GITR records, 0 to 6 hours, coracle at 6,800 feet, 281° T from surface zero, Shot Wahoo-----	265
3.163	Std- and sec-GITR records, 0 to 6 hours, coracle at 12,800 feet, 276° T from surface zero, Shot Wahoo-----	265
3.164	Std- and UW-GITR records, 0 to 6 hours, coracle at 4,100 feet, 336° T from surface zero, Shot Wahoo-----	266
3.165	Std- and UW-GITR records, 0 to 6 hours, coracle at 5,200 feet, 334.5° T from surface zero, Shot Wahoo -----	266
3.166	Std-GITR record, 0 to 6 hours, coracle at 6,400 feet, 332° T from surface zero, Shot Wahoo-----	267
3.167	Std-GITR record, 0 to 6 hours, coracle at 1,760 feet, 51.8° T from surface zero, Shot Umbrella -----	267
3.168	Std- and UW-GITR records, 0 to 6 hours, coracle at 2,700 feet, 67° T from surface zero, Shot Umbrella -----	268
3.169	Std-GITR record, 0 to 6 hours, coracle at 3,060 feet, 163.7° T from surface zero, Shot Umbrella -----	268
3.170	Std-GITR record, 0 to 6 hours, coracle at 6,010 feet, 158.9° T from surface zero, Shot Umbrella -----	269
3.171	Std-GITR record, 0 to 6 hours, SIO Skiff at 6,580 feet, 207.5° T from surface zero, Shot Umbrella -----	269
3.172	Std-GITR record, 0 to 6 hours, coracle at 6,220 feet, 230.4° T from surface zero, Shot Umbrella -----	270
3.173	Std-GITR record, 0 to 6 hours, coracle at 15,980 feet, 237.1° T from surface zero, Shot Umbrella -----	270
3.174	Std- and sec-GITR records, 0 to 6 hours, coracle at 2,670 feet, 248° T from surface zero, Shot Umbrella-----	271
3.175	Std- and sec-GITR records, 0 to 6 hours, coracle at 4,770 feet, 247.9° T from surface zero, Shot Umbrella -----	271
3.176	Std-GITR record, 0 to 6 hours, coracle at 18,220 feet, 250.2° T from surface zero, Shot Umbrella -----	272
3.177	Std-GITR record, 0 to 6 hours, coracle at 22,000 feet, 248° T from surface zero, Shot Umbrella-----	272
3.178	UW-GITR record, 0 to 6 hours, coracle at 4,530 feet, 263.5° T from surface zero, Shot Umbrella -----	273

3.179	Std-GITR record, 0 to 6 hours, coracle at 12,230 feet, 262.5° T from surface zero, Shot Umbrella -----	273
3.180	Std-GITR record, 0 to 6 hours, coracle at 18,600 feet, 261° T from surface zero, Shot Umbrella-----	274
3.181	Std- and UW-GITR records, 0 to 6 hours, coracle at 3,940 feet, 279.1° T from surface zero, Shot Umbrella -----	274
3.182	Std-GITR record, 0 to 6 hours, coracle at 6,740 feet, 278.1° T from surface zero, Shot Umbrella -----	275
3.183	GITR record, 0 to 15 minutes, for EC-2 at 2,300 feet, 28.5° T from surface zero, Shot Wahoo -----	285
3.184	Transit dose rate record and data summary for EC-2, Shot Wahoo -----	286
3.185	Transit dose rate record and data summary for DD-593, Shot Wahoo-----	288
3.186	GITR record, 0 to 30 minutes, for DD-593 at 8,900 feet, 250° T from surface zero, Shot Wahoo-----	290
3.187	GITR record, 0 to 15 minutes, for EC-2 at 1,650 feet, 158° T from surface zero, Shot Umbrella-----	291
3.188	Transit dose rate record and data summary for EC-2, Shot Umbrella -----	292
3.189	Transit dose rate record and data summary for DD-474, Shot Umbrella -----	294
3.190	GITR record, 0 to 30 minutes, for DD-474 at 1,900 feet, 245.7° T from surface zero, Shot Umbrella -----	296
3.191	GITR record, 0 to 30 minutes, for DD-592 at 3,000 feet, 248.5° T from surface zero, Shot Umbrella -----	297
3.192	Transit dose rate record and data summary for DD-592, Shot Umbrella -----	298
3.193	Transit dose rate record and data summary for DD-593, Shot Umbrella -----	300
3.194	GITR record, 0 to 15 minutes, for DD-593 at 7,900 feet, 249.2° T from surface zero, Shot Umbrella -----	302
3.195	GITR record, 0 to 6 hours, for EC-2 at 2,300 feet, 28.5° T from surface zero, Shot Wahoo -----	302
3.196	GITR record, 0 to 6 hours, for EC-2 at 2,300 feet, 28.5° T from surface zero, Shot Wahoo -----	303
3.197	GITR record, 0 to 6 hours, for DD-593 at 8,900 feet, 250° T from surface zero, Shot Wahoo-----	303
3.198	GITR record, 0 to 6 hours, for DD-593 at 8,900 feet, 250° T from surface zero, Shot Wahoo-----	304
3.199	GITR record, 0 to 6 hours, for EC-2 at 1,650 feet, 158° T from surface zero, Shot Umbrella-----	304
3.200	GITR record, 0 to 6 hours, for EC-2 at 1,650 feet, 158° T from surface zero, Shot Umbrella-----	305
3.201	GITR record, 0 to 6 hours, for DD-474 at 1,900 feet, 245.7° T from surface zero, Shot Umbrella -----	305
3.202	GITR record, 0 to 6 hours, for DD-474 at 1,900 feet, 245.7° T from surface zero, Shot Umbrella -----	306
3.203	GITR record, 0 to 6 hours, for DD-592 at 3,000 feet, 248.5° T from surface zero, Shot Umbrella -----	306
3.204	GITR record, 0 to 6 hours, for DD-592 at 3,000 feet, 248.5° T from surface zero, Shot Umbrella -----	307
3.205	GITR record, 0 to 6 hours, for DD-593 at 7,900 feet, 249.2° T from surface zero, Shot Umbrella -----	307
3.206	GITR record, 0 to 6 hours, for DD-593 at 7,900 feet, 249.2° T from surface zero, Shot Umbrella -----	308
3.207	Plot of film pack dose readings on main deck of destroyers versus position along ship, Shot Wahoo -----	312

3.208	Plot of film pack dose readings on superstructures of destroyers versus position along ship, Shot Wahoo	312
3.209	Plot of film pack dose readings on main deck of destroyers versus position along ship, Shot Umbrella	313
3.210	Plot of film pack dose readings on superstructure of destroyers versus position along ship, Shot Umbrella	313
3.211	Plot of film pack dose readings on main deck of EC-2 versus position along ship, Shots Wahoo and Umbrella	314
3.212	Plot of film pack dose readings on superstructure of EC-2 versus position along ship, Shots Wahoo and Umbrella	314
3.213	Estimated solid angle of cloud subtended by film packs plotted against frame number, destroyers	315
3.214	Estimated solid angle of cloud subtended by film packs plotted against frame number, EC-2	315
3.215	Dose rate difference shown by the bow GTR aboard the DD-593	319
3.216	Family of decay curves for early IC collections	322
3.217	Family of decay curves for late IC collections	322
3.218	Comparison of characteristic decay curves with standard decay curve	323
3.219	Family of decay curves for various continuous collections	323
3.220	Possible subfamily of early decay curves, Shot Wahoo	324
3.221	Possible subfamily of early decay curves, Shot Umbrella	324
3.222	Decay of funnel and cloud samples determined by End-Window Gamma Counter 2, Shot Wahoo	328
3.223	Decay of funnel, cloud, ocean-water, and crater samples determined by End-Window Gamma Counter 2, Shot Umbrella	329
3.224	Decay of funnel and cloud samples determined by 4π gamma ionization chamber, Shot Wahoo	330
3.225	Decay of liquid and solid fractions of AFI Sample 10-3, Shot Umbrella	333
3.226	Decay of liquid and solid fractions of AFI Sample 10-8, Shot Umbrella	334
3.227	Decay of liquid and solid fractions of AFI Sample 2-11, Shot Umbrella	335
A.1	Coracle dimensions	354
A.2	Relative gamma intensity for finite hemispheres of uniformly distributed activity (1 Mev gamma energy)	355
A.3	Diagram of 60° cloud model	356
A.4	Proposed array including FFP positions and predicted radiation fields, Shot Wahoo	357
A.5	Proposed array including FFP positions and predicted radiation fields, Shot Umbrella	358
B.1	Block diagram of GTR 103 with remote detector	361
B.2	Simplified schematic diagram of GTR 103 recycling electrometer	361
B.3	GTR 103 low-range detector output pulse period as a function of gamma intensity for Co <sup>60</sup> and Cs <sup>137</sup>	362
B.4	GTR 103 high-range detector output pulse period as a function of gamma intensity for Co <sup>60</sup> and Cs <sup>137</sup>	362
B.5	Comparison of standard decay curve with crystal, IC, and GIDU decay curves	363
B.6	Early decay determined by GIDU aboard DD-592	364
B.7	Scintillation counter decay of fission products following thermal neutron fission of U <sup>235</sup>	365
C.1	Energy response characteristics of the GTR 103 detector for parallel beam radiations	369
C.2	Directional response characteristics of the std-GTR detector for parallel beam radiation (Co <sup>60</sup> )	369

C.3	Directional response characteristics of UW-GITR detector for parallel beam radiation (Co <sup>60</sup> )	370
C.4	Directional response of ASEL-GITR low range detector in a plane perpendicular to the detector axis	370
C.5	Directional response of ASEL-GITR low-range detector in the plane of the detector axis	371
C.6	Directional response of ASEL-GITR high-range detector in a plane perpendicular to the detector axis	371
C.7	Directional response of ASEL-GITR high-range detector in the plane of the detector axis	372
C.8	Energy response characteristics of the ASEL-GITR for parallel beam radiations	372
C.9	Typical calibration curve for ASEL-GITR high-range detector	373
C.10	Relative energy response for End-Window Gamma Counter 2 (for a point source on Shelf 5)	374
C.11	Co <sup>60</sup> calibration curves for 502 emulsion	375
C.12	Co <sup>60</sup> calibration curves for 834 emulsion	375
C.13	Co <sup>60</sup> calibration curves for 1290 emulsion	376
C.14	Co <sup>60</sup> calibration curves for 548-0 emulsion	376
C.15	Energy response for emulsions used in film packs (dose inaccuracy)	377
C.16	Energy response for emulsions used in film packs (density inaccuracy)	377
C.17	Relationship between std-GITR response and deposited activity determined by IC	378
C.18	Variation of GITR reading as a function of height above a contaminated coracle deck	378
D.1	Approximate linear gamma dose rate record for coracle at 3,900 feet, 159° T from surface zero, Shot Wahoo	395
D.2	Approximate linear gamma dose rate record for coracle at 4,600 feet, 151.5° T from surface zero, Shot Wahoo	395
D.3	Approximate linear gamma dose rate record for coracle at 7,100 feet, 231.5° T from surface zero, Shot Wahoo	396
D.4	Approximate linear gamma dose rate record for coracle at 8,000 feet, 256.5° T from surface zero, Shot Wahoo	396
D.5	Approximate linear gamma dose rate record for coracle at 4,500 feet, 263° T from surface zero, Shot Wahoo	397
D.6	Approximate linear gamma dose rate record for coracle at 8,950 feet, 263° T from surface zero, Shot Wahoo	397
D.7	Approximate linear gamma dose rate record for coracle at 14,400 feet, 265° T from surface zero, Shot Wahoo	398
D.8	Approximate linear gamma dose rate record for coracle at 24,000 feet, 263° T from surface zero, Shot Wahoo	398
D.9	Approximate linear gamma dose rate record for coracle at 6,800 feet, 281° T from surface zero, Shot Wahoo	399
D.10	Approximate linear gamma dose rate record for coracle at 12,800 feet, 276° T from surface zero, Shot Wahoo	400
D.11	Approximate linear gamma dose rate record for coracle at 4,100 feet, 336° T from surface zero, Shot Wahoo	400
D.12	Approximate linear gamma dose rate record for coracle at 5,200 feet, 334.5° T from surface zero, Shot Wahoo	401
D.13	Approximate linear gamma dose rate record for coracle at 2,700 feet, 67° T from surface zero, Shot Umbrella	402
D.14	Approximate linear gamma dose rate record for coracle at 3,060 feet, 163.7° T from surface zero, Shot Umbrella	403

32

- D.15 Approximate linear gamma dose rate record for coracle at 6,010 feet,  
158.9° T from surface zero, Shot Umbrella -----
- D.16 Approximate linear gamma dose rate record for coracle at 6,580 feet,  
207.5° T from surface zero, Shot Umbrella -----
- D.17 Approximate linear gamma dose rate record for coracle at 6,220 feet,  
230.4° T from surface zero, Shot Umbrella -----
- D.18 Approximate linear gamma dose rate record for coracle at 15,980 feet,  
237.1° T from surface zero, Shot Umbrella -----
- D.19 Approximate linear gamma dose rate record for coracle at 2,670 feet,  
248° T from surface zero, Shot Umbrella-----
- D.20 Approximate linear gamma dose rate record for coracle at 4,770 feet,  
247.9° T from surface zero, Shot Un.brella -----
- D.21 Approximate linear gamma dose rate record for coracle at 18,220 feet,  
250.2° T from surface zero, Shot Umbrella -----
- D.22 Approximate linear gamma dose rate record for coracle at 22,000 feet,  
248° T from surface zero, Shot Umbrella-----
- D.23 Approximate linear gamma dose rate record for coracle at 12,230 feet,  
262.5° T from surface zero, Shot Umbrella -----
- D.24 Approximate linear gamma dose rate record for coracle at 18,600 feet,  
261° T from surface zero, Shot Umbrella-----
- D.25 Approximate linear gamma dose rate record for coracle at 3,940 feet,  
279.1° T from surface zero, Shot Umbrella -----
- D.26 Approximate linear gamma dose rate record for coracle at 6,740 feet,  
278.1° T from surface zero, Shot Umbrella -----
- D.27 Approximate linear gamma dose rate record for coracle at 4,910 feet,  
334° T from surface zero, Shot Umbrella-----
- D.28 Approximate linear gamma dose rate record for ship at 2,300 feet,  
28.5° T from surface zero, Shot Wahoo -----
- D.29 Approximate linear gamma dose rate record for ship at 8,900 feet,  
250° T from surface zero, Shot Wahoo-----
- D.30 Approximate linear gamma dose rate record for ship at 1,650 feet,  
158° T from surface zero, Shot Umbrella-----
- D.31 Approximate linear gamma dose rate record for ship at 1,900 feet,  
245.7° T from surface zero, Shot Umbrella -----
- D.32 Approximate linear gamma dose rate record for ship at 3,000 feet,  
248.5° T from surface zero, Shot Umbrella -----
- D.33 Approximate linear gamma dose rate record for ship at 7,900 feet,  
249.2° T from surface zero, Shot Umbrella -----
- D.34 Variation of meter survey of coracles with distance  
(converted to std-GITR response at 1 minute)-----
- D.35 Tray set background for IC collections -----



Specifically, the total gamma dose rate as a function of time was to be determined at 21 floating stations in a manner that would permit resolution into an initial dose occurring during the first minute after detonation, a free-field (Appendix F) dose rate resulting from the composite cloud only, and a residual dose rate due to radioactive material deposited from the cloud in transit. Since heavy deposits of radioactive material on the gamma detector itself—or upwelling of highly contaminated water around the floating platform carrying the detector—could have masked the free-field dose, additional instrumentation was installed at specific locations indicated by a theoretical analysis of the situation. The basic time-based gamma measurements were to be augmented by cloud-movement data obtained from photographs and by total dose data obtained from film packs mounted in fixed and free-floating stations.

The gamma fields due to airborne radioactive material only were to be correlated with the gamma fields measured aboard three destroyers (DD's) and one Liberty ship (EC-2) in the proposed target array. The data could then be used in conjunction with current theories of aerial transport in the determination of optimum conditions for antisubmarine warfare (ASW) delivery by a destroyer. Such an operations analysis was, however, specifically not an objective of the project.

Samples of airborne debris were to be collected aboard the three destroyers to provide additional information on the nature of both base surge and fallout. This information was needed for interpretation of contamination ingress studies and for development of better fallout simulants for underwater detonations. Also, test panels were to be exposed for use in later comparative decontamination studies of actual and simulated contaminants. Measurements obtained from the fallout collections and test panels are reported here only to the extent that they influence the basic gamma field determinations made by the project.

## 1.2 BACKGROUND

Shot Baker of Operation Crossroads and the single shot of Operation Wigwam represent the only underwater detonations of nuclear devices prior to Operation Hardtack.

Although the gamma dose and dose rates had been predicted for shallow underwater detonations by means of current scaling theories (References 11 and 12), high-explosive (HE) data (Reference 13), and photographic evidence (Reference 14), these predictions had to rely heavily on data from underground detonations (References 15, 16, and 17) and could therefore be in error by as much as two orders of magnitude. Although the paucity of underwater information justified this use of underground data, correspondence between the two types of detonations was not established, and speculations on the mechanism of formation and dispersion of radioactive material suggested substantial differences.

Specifically, the formation of fallout particles in underwater bursts by solution of fission products in liquid spheres condensed from the vaporized device casing (Reference 18) was thought to be analogous to airbursts rather than underground bursts. The greater ambient pressure might cause condensation to commence at earlier times; thus, an underwater burst could produce particle sizes slightly larger than those for an airburst (Reference 19), their

exact median size being a function of depth. However, due to the lower concentrations of vaporized material, the final particle size in either case was expected to be significantly smaller than those typical of the underground case. The gamma field resulting from the dispersion of such particles by meteorological processes was expected to differ significantly in the area of interest, because the mass subsidence of large amounts of water was expected to confine the total event to a much smaller area than that normally expected from an underground burst. The initial dose for an underwater shot could also be significantly altered both by shielding effects of the water itself and by the absence of nitrogen, thus preventing the high-energy gamma emission (average 6.5 Mev, Reference 20) due to the  $(n,\gamma)$  reaction on  $N^{14}$ . Gamma fields associated with the radiating cloud could be further altered by differences in gamma spectrum due to the presence or absence of specific induced radionuclides.

The similarity between underground and underwater bursts, therefore, appeared tenuous at best; and while it was recognized that HE models might effectively simulate the dynamics of clouds resulting from underwater nuclear detonations, insufficient data then existed for the calculation of the associated gamma fields. Although the peak dose rates during transit for Crossroads and Wigwam compare favorably (see Appendix E), the authors concluded that precise documentation of the total gamma environment resulting from the underwater detonation of a nuclear device was definitely required.

### 1.3 THEORY

The project proposed measurement of the gamma fields at 21 locations, selected after consideration of the best available information (References 21 through 25), to obtain data from three substantially different areas of the total event, viz, base surge without fallout, combination of base surge and fallout, and fallout only. For convenience, these locations were given nominal position designators stated in terms of the probable wind direction (References 26 and 27) as indicated in Table 1.1 and Figure 1.1. These nominal positions, which indicate the originally intended location of a station, are used throughout this chapter. The original nominal positions are changed at the beginning of Chapter 2 (Table 2.1) to reflect changes in intended position necessitated by operational conditions in the field. This second set of nominal position designators is used throughout the remainder of the report.

At each location, a number of detecting and collecting instruments were placed on specially designed floating platforms, termed "coracles" to distinguish them from skiffs previously used as deep-anchored stations (Figures 1.2 and 1.3). The coracles were circular, to facilitate interpretation of instrument responses, and were held to the smallest practical diameter to minimize corrections to the free-field dose rate due to deposited activity (actual dimensions are given in Figure A.1). They were also designed (1) to minimize wash over the deck, (2) to withstand overpressures of 2,000 psi, and (3) to reduce a shock of 200 g delivered to the coracle hull to 5 g delivered to instruments mounted in an internal instrument well. A fully instrumented coracle weighed approximately 1,700 pounds and drew 14 inches of water.

The use of shielded detectors to eliminate contributions from deposited activity was considered as a means of obtaining free-field measurements, but the interpretation of the record from single shielded detectors appeared difficult. Previous measurements of the directional characteristics of nonhomogeneous gamma fields (References 28 and 29) had indicated that the greatest directional contribution could be expected in that direction which transected the greatest thickness of the radioactive cloud. The principal component of the complex gamma field at most times and at most stations was therefore expected to be nearly horizontal. Although directional shielding has been attempted (References 30 and 31), the interpretation of records from shielded detectors mounted on the rolling platform afforded by a coracle would involve considerably more instrumentation than that allowed by funds then available to the project. Therefore, unshielded gamma detectors were employed.

When using unshielded detectors (Figure 1.4), the project had to consider the possibility that deposits of radioactive material on the coracle decks and the detector casing itself might be

TABLE 1.1 DEPTHS AND BOTTOM SLOPES AT PROPOSED STATIONS

For diagram of proposed array, see Figure 1.1.

WAHOO				UMBRELLA			
Position *	Approximate Depth		Bottom Slope	Position *	Approximate Depth		Bottom Slope
	fathoms	ft	deg		fathoms	ft	deg
U 3.2	400	2,400	22	U 2.0	20	120	0
U 4.0	360	2,200	23	U 3.0	20	120	0
U 4.8	310	1,900	23	U 4.0	20	120	0
CL 4.0	620	3,700	6	CL 3.0	16	100	0
CL 4.8	640	3,800	6	CL 4.0	16	100	0
DL 7.2	710	4,300	10	DL 6.5	18	110	0
DL 12.0	810	4,900	3	DL 13.0	130	780	31
DL 19.2	860	5,200	3	DL 19.0	520	3,100	12
D 4.8	650	3,900	10	D 4.5	18	110	0
D 8.0	730	4,400	10	D 7.5	18	110	0
D 14.4	850	5,100	3	D 14.5	140	840	27
D 24.0	900	5,400	2	D 22.0	510	3,100	12
DR 4.8	620	3,700	10	DR 4.5	18	110	0
DR 5.0	700	4,200	10	DR 7.5	18	110	0
DRR 14.4	820	4,900	3	DR 12.0	18	110	0
DR 24.0	920	5,500	2	DR 22.0	330	2,000	19
DRR 7.2	650	3,900	10	DRR 6.5	18	110	0
DRR 12.0	740	4,400	10	DRR 11.0	18	110	0
CR 4.0	400	2,400	19	CR 3.0	16	100	0
CR 4.8	380	2,300	20	CR 4.0	16	100	0
CR 6.0	340	2,000	20	CR 5.5	16	100	0

\* Positions are given relative to surface zero. Directions are stated with reference to a predicted surface wind from 068° T, viz: U = upwind; CL and CR = crosswind to the left and right respectively looking in the direction the wind is blowing; D = downwind; DL and DR = 15° to the left or right of downwind; DRR = 30° to the right of downwind. Distances to surface zero are expressed in thousands of feet.

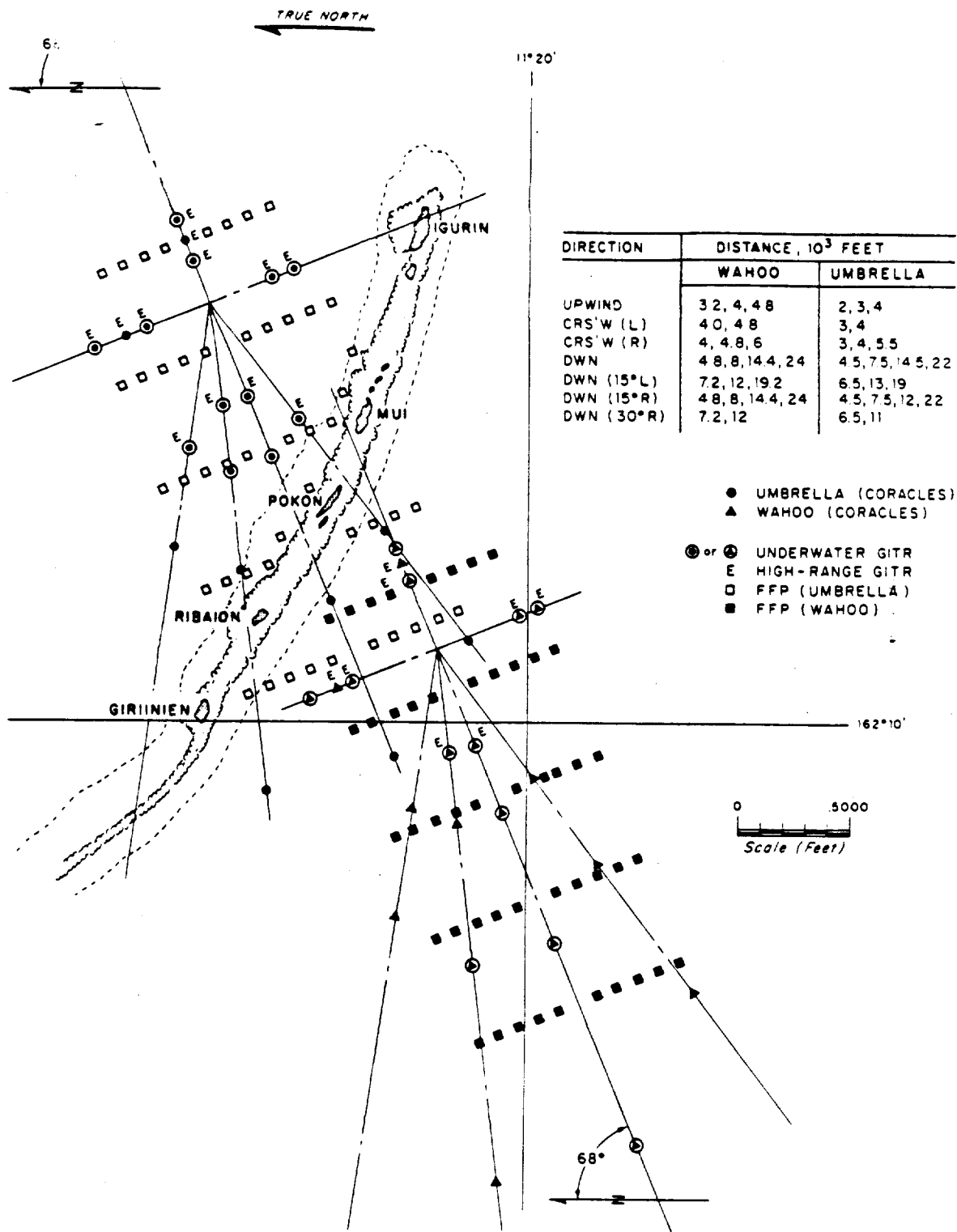
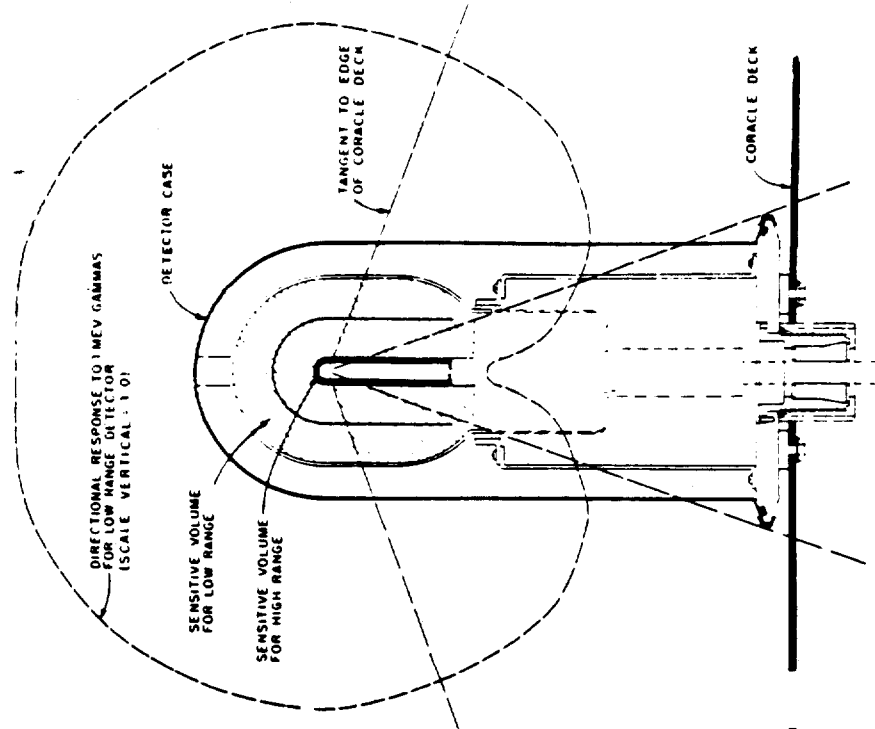
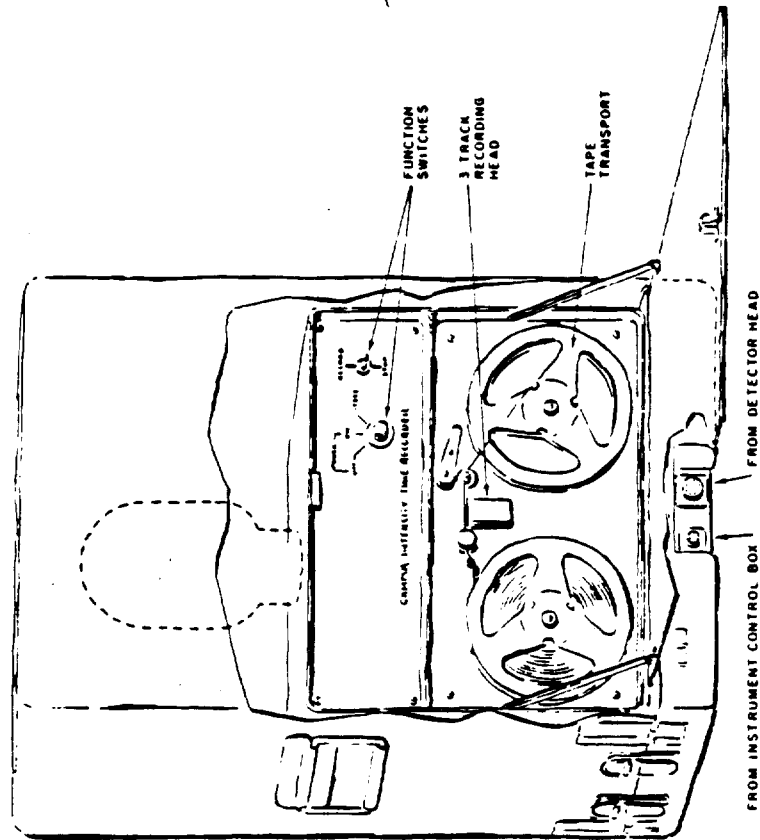


Figure 1.1 Originally intended array of coracles and floating film packs (FFP).





STANDARD DETECTOR MOUNTING FOR CORACLE



RECORDER UNIT WITHOUT DETECTOR

Figure 1.4 NRDL gamma-intensity-time recorder.

large enough to alter the free-field measurements significantly. Such heavy deposition contributing up to 50 percent of the recorded dose rate had, for instance, been experienced on Operations Castle and Redwing (References 32 and 33). During Operation Hardtack, the proximity of some proposed stations to surface zero placed the gamma-intensity-time recorders (GITR)—developed by the Naval Radiological Defense Laboratory (NRDL)—in areas where large amounts of erupted water with presumably high scavenging efficiency could be expected. The radioactive material remaining on coracle and detector surfaces might therefore be sufficient to represent a significant contribution to the gross gamma record; thus, some approximate means of correcting for such deposition appeared necessary.

Consequently, the GITR's were used in conjunction with an incremental collector (IC) capable of collecting radioactive material deposited at the detector for short increments of time during transit of the radiating cloud. These collections were to be counted after coracle recovery, corrected for decay, and applied to the gross gamma record, using conversion factors for detector response to known concentrations of deposited activity (Section C.5).

Other possible sources of radiation such as deposited radioactive material suspended in the water surrounding the coracle or the upwelling of water directly contaminated by the detonation were also examined and considered to be of secondary importance in comparison to deposits on coracle surfaces (Section 1.3.1). Although later experience in the field demonstrated that such corrections were unnecessary, the relative insignificance of deposited activity is in itself of particular importance.

An alternative method of deducing the free-field gamma intensity  $I_A$  was also available. This method was first employed on Operation Redwing data (Reference 34) and is based on the assumption that the rate of deposition is a function of the concentration of fallout in the air immediately over the point of deposition. Thus,

$$I_A = K_1 S(t) t^{-1.2}$$

where  $S(t)$  is the concentration of fallout per unit volume of air,  $K_1$  is a constant of proportionality for instrument response to a radiating cloud, and  $t$  represents time. The rate of deposition  $dD/dt$  is therefore defined by

$$\frac{dD}{dt} = K_2 S(t)$$

where  $K_2$  is a constant of proportionality describing deposition from the cloud.

The response  $I_D$  due to the deposited material is necessarily some function of the amount of deposited material  $D(t)$ . Thus,

$$I_D = K_3 D(t) t^{-1.2}$$

where  $K_3$  is a constant of proportionality for instrument response to a deposited field. The gross radiation intensity  $I_G$  is therefore

$$I_G = K_1 S(t) t^{-1.2} + K_3 D(t) t^{-1.2}$$

This equation is solved for  $S(t)$  in terms of  $I_G$ , yielding the expression:

$$S(t) = e^{-K_4 t} \int_{t_0}^t F(t) e^{K_4 t} dt$$

where  $K_4 = \frac{K_3 K_2}{K_1}$

and

$$F(t) = \frac{1}{K_1} \left( 1.2 t^{0.2} I_G + t^{1.2} \frac{dI_G}{dt} \right)$$

This equation offered a possible check on the empirical free-field determination by electronic analog, provided that  $dI_G/dt$  could be properly described by an arbitrary function generator. Otherwise a simplified version of the expression for  $S(t)$  could be solved by graphic iteration as demonstrated in Reference 34. The analog solution requires the determination of the various constants of proportionality  $K_1$ ,  $K_2$ , and  $K_3$  and a precise knowledge of decay at early times. Although values for  $K_1$  and  $K_3$  can be easily determined and it might be possible to estimate  $K_2$  by a statistical analysis of the incremental collections, complete information concerning early decay is required before an actual analog solution can be attempted. In fact both methods of correcting for deposited activity are necessarily dependent upon an accurate knowledge of early decay. Unfortunately, the project was unable to include a detailed study of early decay among its objectives because of lack of both funds and personnel.

**1.3.1 Components of the Radiation Field.** Proper interpretation of the gross gamma record depends upon the evaluation of the various sources of radiation outlined in the previous section. Considering first only sources resulting from deposition during passage of airborne radioactive material over the coracle, it is obvious that such sources do not exist until the station has been engulfed by the radiating cloud. These deposited sources increase in relative importance as long as the station remains within the cloud, finally becoming the principal source of radiation after transit. Possible gamma radiation resulting from the upwelling of radioactive water directly contaminated by the nuclear detonation is considered as a separate case later in this section. The gross gamma record is therefore separated into radiation received from the cloud itself, from deposits on the coracle decks, and from deposited material suspended in the surrounding water.

The relative magnitudes of these contributing components are estimated using the general expression (Reference 35)

$$dI = I_0 B(E_0, \Sigma \mu x) e^{-\Sigma \mu x} \frac{dA}{4\pi (\Sigma x)^2}$$

where  $dI$  is incident radiation intensity from a source of intensity  $I_0$  and area  $dA$  at a distance  $x$ ,  $B(E_0, \Sigma \mu x)$  is the buildup factor which is a function of radiant energy  $E_0$  and the sum of the mean free paths  $\Sigma \mu x$ , and  $e^{-\Sigma \mu x}$  is the attenuation factor also dependent on the number of mean free paths involved. The gross gamma intensity  $I_G$  is expressed as the summation of the radiation intensities from the cloud  $I_A$  from material deposited on the deck and the incident case  $I_D$  and from fallout suspended in the surrounding water  $I_W$ .

The cloud intensity  $I_A$  is determined by integrating over a hemisphere with the detector at its center and adding the contribution from a radiating slab whose thickness is equivalent to the detector distance above the water surface (see Section A.1 for dimensions). Allowing the detector and the hemisphere to extend to infinity, the integrated expression simplifies to

$$I_A = (1+K) \frac{J_A(t)}{2\mu_A} \left\{ 2 - e^{-\mu_A z} + \frac{\mu_A z}{1+K} [-Ei(-\mu_A z)] \right\}$$

where  $K$  is a constant approximating the buildup factor in an expression of the form  $(1+K)J_A(t)$  is the source intensity for a unit volume of cloud,  $\mu_A$  is the linear attenuation coefficient for air, and  $z$  is the thickness of the slab.  $U^{235}$  fission data (Reference 36) indicates that the average gamma photon energy over the period of interest probably lies between 1.2 and 0.5 Mev, thus, a weighted average for linear attenuation coefficients and buildup factors can be determined from standard references (References 37 and 38). Using the values tabulated in Section A.1, the expression for the cloud intensity was evaluated at

$$= 1.76 \times 10^4 J_A(t)$$

Radiation from the deposited material  $I_D$  is determined by subdividing it into two components, viz, that due to deposits on the coracle decks  $I_{dd}$ , and that due to deposits on the detector case  $I_{dc}$ ; thus,

$$I_D = I_{dd} + I_{dc}$$

Neglecting decay for the moment, the radiation intensity due to both deposited sources increases at a rate primarily determined by the terminal falling velocity  $V_p$  of the fallout material. Under the worst conditions, the radiation intensity due to material deposited on the detector case (which is a domed cylinder, see Figure 1.4) may be approximated by assuming a uniform deposition on a spherical shell surrounding the sensitive volume; thus,

$$I_{dc} = J_D(t) = J_A(t) V_p (t - t_0)$$

where  $J_D(t)$  is the radiation intensity deposited per unit area and  $(t - t_0)$  is the time elapsed since the arrival of fallout. This approximation probably overestimates  $I_{dc}$  by a factor ranging between 1 and 2, since only the upper hemisphere is equivalent to the actual detector case, and the shorter radial distance and normal photon incidence over the lower hemisphere probably overcompensates for the increased surface area of the cylinder. The radiation intensity due to the deck deposit was calculated from an expression developed in Reference 39 for a point above a smooth, uniformly contaminated plane:

$$I_{dd} = \frac{J_D(t)}{2} \left\{ [-E_1(-\mu_A x_0)] + K e^{-\mu_A x_0} \right\}$$

where  $x_0$  is the slant range between the sensitive volume and the edge of a nonradiating disk whose center is a distance  $h$  below the sensitive volume. With a deck radius of 3.7 feet, this expression was evaluated at

$$I_{dd} = 0.55 J_D(t) = 0.55 J_A(t) V_p (t - t_0)$$

As might be expected from its proximity to the sensitive volume, the deposition on the instrument case itself causes a greater instrument response than deposition on the coracle deck. Therefore, it appears more important to reduce deposition on the detector case than to shield the detector from the deck deposits. The total radiation due to deposited activity is:

$$I_D = 1.55 J_D(t) = 1.55 J_A(t) V_p (t - t_0)$$

The radiation  $I_W$  resulting from fallout material deposited in the surrounding water is estimated on the basis of Redwing data (Reference 40). For water surface bursts, the general behavior of that portion of fallout remaining near the ocean surface may be approximated by certain simple parameters. Assuming that these parameters also apply to subsurface detonations and assuming further that all fallout material remains in the surface layer, the maximum concentration of suspended fallout  $J_W(t)$  is approximated as follows:

$$J_W(t) = \frac{J_A(t) V_p (t - t_0)}{M}$$

where  $M$  is the depth of surface mixing. Redwing data (Reference 33) indicates that fallout reached a depth of 7 to 20 meters shortly after deposition in surface waters and, after cessation of fallout, settled to the thermocline at a rate of 2.6 m. hr. A value of 7 meters is there-

fore selected for the depth of surface mixing. The radiation intensity at a point above an infinite slab of uniformly distributed activity is calculated from the following simplified expression, which assumes that the buildup factors for the two media are the same:

$$I_W = \frac{J_W(t) h}{2 \mu_W x_0} \left\{ [1+K] e^{-\mu_A x_0} - \mu_A x_0 [-Ei(-\mu_A x_0)] \right\}$$

In order to estimate attenuation due to the coracle itself, the value for  $I_W$  is separated into two components, viz, that due to water beyond the intersection of a tangent to the coracle edge and the water surface, and that transmitted through portions of the coracle itself. The effective Z numbers calculated for various coracle materials by the method in Reference 41 are used to compute an average linear attenuation coefficient (Section A.1). The expression for  $I_W$  using these coefficients is:

$$I_W = 0.019 J_A(t) V_p (t - t_0)$$

It was therefore apparent that, with the exception of upwelling radioactive water, the principal factors affecting the gross intensity  $I_G$  are the radiation from deposited material  $I_D$  and radiation from the cloud  $I_A$ . The GTR, however, does not have a  $4\pi$  response (Figure 1.4). The corrected expression for  $I_G$  determined by averaging instrument response over the solid angle subtended by the deck is:

$$I_G = 1.02 I_A + 0.98 I_D + 0.98 I_W$$

The general expression for  $I_G$  in which the relative contribution for all deposited sources is represented by the sum of  $I_D$  and  $I_W$  is:

$$I_G = 1.8 \times 10^4 J_A(t) + 1.54 J_A(t) V_p (t - t_0)$$

To estimate the relative contribution from the radiating cloud, some expression must be assumed for  $J_A(t)$ . The mathematical complications of moving fields are avoided by assuming an infinite stationary cloud, and motion is simulated by allowing the concentration of radioactive material to change as a function of time. This approximation, of course, overestimates the relative importance of the deposit dose rate during the simulated approach and underestimates it during the latter phases of the simulated departure. Since the matter of primary interest is the approximate maximum contribution due to deposited activity prior to and during the peak dose rate, both these inaccuracies in the model can be tolerated. An analysis of previous gamma dose rate histories (Reference 42) has indicated that the time to reach peak activity is approximately twice the time of arrival; thus, by assuming further that cessation occurs at eight times the time of arrival, cloud movement is simulated by varying the concentration factor  $J_A(t)$  as follows:

$$J_A(t) = kt^{-1.2} [n'_A(t) + n''_A(t)]$$

where

$$n'_A(t) = \frac{t - t_0}{2 t_0} \quad \text{for } t_0 \leq t \leq 3 t_0$$

and

$$n''_A(t) = \left[ 1 - \frac{t - 3 t_0}{5 t_0} \right] \quad \text{for } 3 t_0 \leq t \leq 8 t_0$$

In these expressions,  $k$  is a factor converting the number of disintegrations per radiating particle into Mev/sec,  $n_A$  is the number of particles per unit volume of cloud, and  $t_0$  is the time of simulated arrival. A factor for radioactive decay is also included in the expression for  $J_A(t)$  by assuming the  $t^{-1.2}$  approximation applies. These expressions also contain the tacit assumptions that the average gamma energy per photon remains reasonably constant over the period under consideration, and that the vertical dimension of the cloud is large enough to neglect depletion of cloud activity through deposition, i.e., greater than five mean free paths, or 2,300 feet for a 1-Mev gamma. Although the radiation due to the airborne material can be estimated from the instantaneous value of  $J_A(t)$ , the contribution from deposited material must be integrated from the simulated time of arrival. Thus,

$$I_D + I_W = 1.54 k t^{-1.2} V_p \int_{t_0}^t n_A(t) dt$$

Although the concentration factor was determined by assuming certain arrival times, the use of such words in conjunction with a stationary model is misleading; therefore the term "cloud slope"  $C_s$  is coined. This term refers to the rate of increase in the concentration factor  $J_A(t)$ , a characteristic which completely describes the particular situation; thus,

$$C_s = \frac{1}{2t_0}$$

Using terminal velocities of 0.3, 3.0, and 30 cm/sec, which bracket those most probable for base surge (Table 1.2), the expected free-field intensity  $I_A$  is calculated for a number of cloud slopes and expressed as a percentage of  $I_G$ . Values for cloud slopes typical of early and late arrival times are presented in Figures 1.5 and 1.6, and the remainder of the calculations are tabulated in Section A.2. Both these curves and the tabulated data clearly demonstrate the pronounced decrease in the relative response to free-field intensity as the terminal velocity and, hence, the particle size increase. This situation becomes progressively worse for cloud slopes characteristic of late arrival times corresponding to those experienced during Operations Castle and Redwing. Since arrival of base surge at most of the proposed Hardtack stations was predicted (Reference 22) prior to 3 minutes, it seemed probable that the cloud slopes greater than 0.1 would be experienced at all project stations.

Since the estimated relative intensity  $I_W$  due to fallout suspended in the surface layer of the ocean is small, the most obvious means of improving detector response to the cloud radiation is to reduce the contribution due to deposited material. Any fallout associated with the proposed underwater detonations was expected to be in the form of liquid droplets; therefore, the most effective approach was to increase runoff from the detector case. In the event of high terminal falling velocities (or large fallout droplets), most of the material deposited on the detector case was expected to roll off to the deck, where its relative contribution would be reduced by a factor of 3. Further improvements in detector response could have been accomplished by shielding; however, about 500 pounds of lead would have been required to reduce the deck contribution to 1 percent, a weight that was obviously impractical for coracle application. The deck contribution could have been reduced to 50 percent by the addition of a 10-pound lead shield; however, the same reduction could also have been accomplished without the risk of deposition on the shield itself by raising the detector 1.7 feet above its present position. The simple deck mounting shown in Figure 1.2 was finally selected as the best compromise between experimental and operational requirements.

In the light of Wahoo and Umbrella results, the deposited activity actually observed is characteristic of that predicted for high cloud slopes and small individual droplet sizes; specifically, the relative response follows the curve for  $V_p = 0.3$  cm/sec as shown in Figure 1.5. A similar response could also have resulted from heavy deposition that immediately ran off the coracle surfaces, and it appears that, depending upon station location, the observed low residual activity

TABLE 1.2 FALLING VELOCITIES FOR LIQUID DROPLETS

Description *	Diameter of Drops **	Velocity of Fall (dist. H <sub>2</sub> O)	Velocity of Fall (salt H <sub>2</sub> O)	mg of H <sub>2</sub> O per m <sup>3</sup> of air *
	μ	cm/sec	cm/sec	
Fog	10	0.3	0.3	6.0
	20	1.2	1.2	-
	80	19	19	-
Mist	100	27	27	55.5
Drizzle	200	72	73	92.6
	300	117	119	-
	400	162	164	-
Light rain	450	-	-	139
	500	206	209	-
	600	247	250	-
	800	327	331	-
Moderate rain	1,000	403	408	278
	1,200	464	470	-
	1,400	517	524	-
Heavy rain	1,500	-	-	833

\* Reference 43.

\*\* Reference 44.

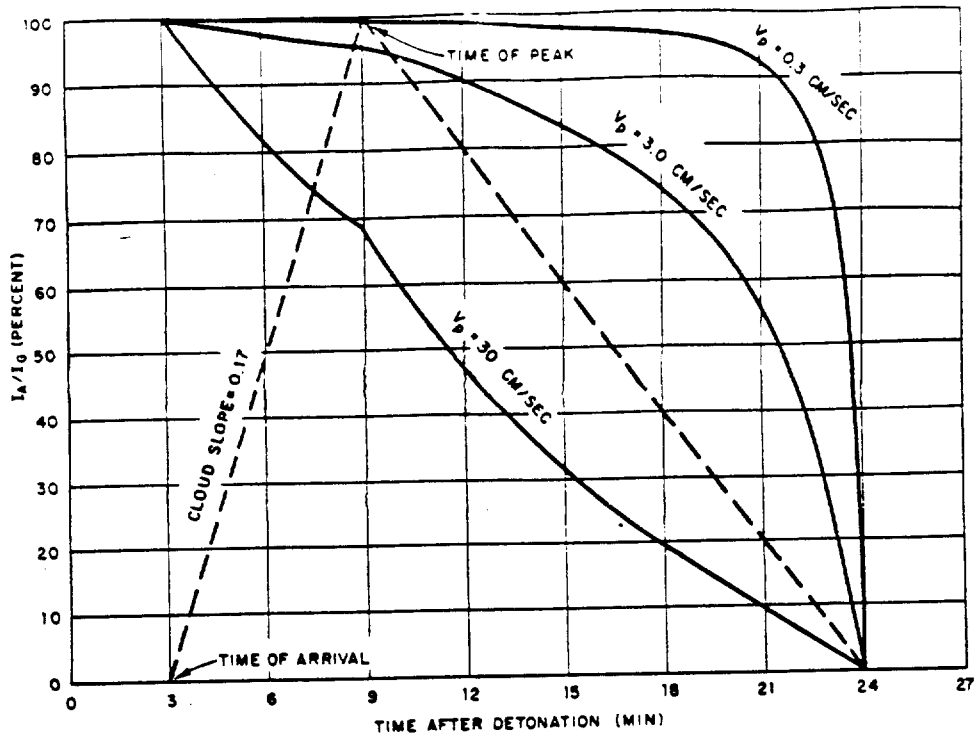


Figure 1.5 Free-field response expressed as a percentage of gross response ( $t_0 = 3$  minutes).

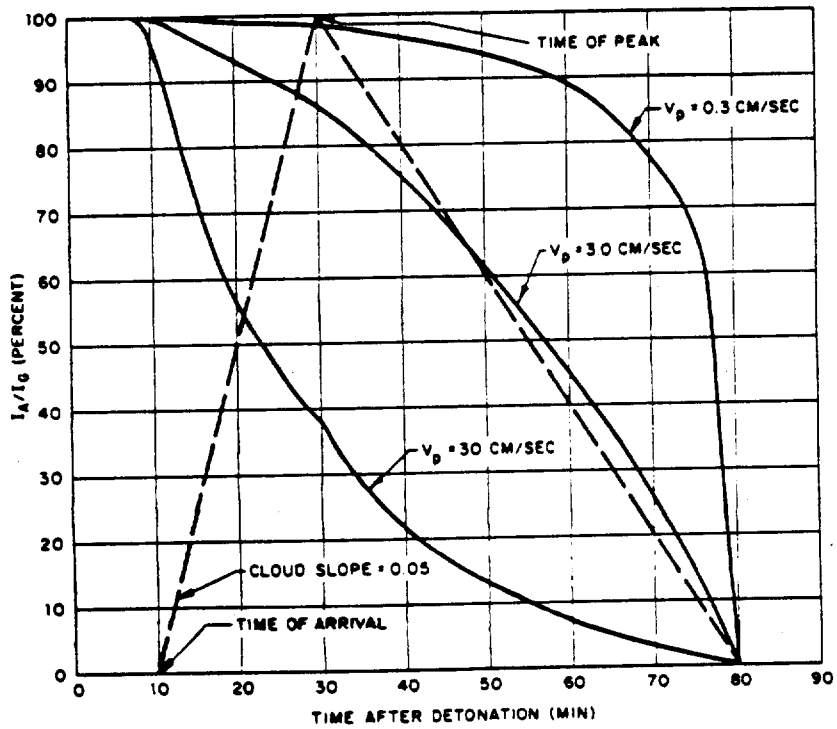


Figure 1.6 Free-field response expressed as a percentage of gross response ( $t_0 = 10$  minutes).

may result from either or both suggested causes. Thus, the gross gamma-intensity record in all cases be considered the free-field record without further correction. Presentation of a detailed theoretical treatment may therefore appear somewhat academic; however, the approach as given is considered useful both for interpreting the range of effects observed during Operation Hardtack and for predicting the relative magnitude of various contributing components in future underwater detonations where larger amounts of deposited radioactive material may logically be expected.

The radiation intensity due to the upwelling of contaminated water is treated in exactly the same manner as that already presented for  $I_W$ . In this case no mixing factor  $M$  is required. The intensity  $I_{UW}$  at the GTR detector, due to an infinitely large body of such contaminated water, is computed to be:

$$I_{UW} = 13.5 J_W(t)$$

If an equivalent source concentration is assumed for both the airborne and the waterborne material, i.e., that  $J_A(t) = J_W(t)$ , the intensity due to an infinite cloud is roughly a thousand times that due to an infinite water source. Although significant contributions from such sources were not considered likely, the intensities due to circular upwellings of various radii were calculated as a percentage of the intensity from an infinite water source and are presented in Figure 1.7. An inspection of this figure indicates that an upwelling 50 feet in radius would be nearly equivalent to an infinite water source. The mathematical model employed implies an absolutely smooth interface; therefore, the actual intensities could be reduced 20 percent or more by surface roughness (Reference 45). The approximate intensities resulting from the movement of such circular bodies of radioactive water past a coracle are presented in the following section.

1.3.2 Properties of Moving Fields. Although consideration of stationary radiation fields can indicate the relative magnitudes of possible contributing sources, such models are of no use in deducing cloud dynamics or transport mechanisms. The general solution for the passage of a radiating cloud would be a powerful tool for the analysis of dose rate histories, but such a general treatment rapidly runs into mathematical difficulties beyond the scope of this project. A few simple cases are investigated, however, and are used later in this report for interpretation of the GTR records.

The approach of an infinite rectangular radioactive cloud may be treated as a special case of the intensity above an infinite radiating slab developed in Reference 39. The approximate expression for the radiation intensity  $I_{ap}$  at a point on a nonradioactive plane and at distance  $x$  from the forward boundary of such a rectangular cloud of radioactivity is:

$$I_{ap} = \frac{J_A(t)}{4 \mu_A} \left\{ (1+K) e^{-\mu_A x} - \mu_A x [-Ei(-\mu_A x)] \right\}$$

where  $J_A(t)$  remains the source intensity per unit volume of cloud,  $\mu_A$  is the linear attenuation coefficient for air,  $K$  is a constant approximating the buildup factor in an expression of the form  $(1+K \mu_A x)$ , and  $\mu_A x$  is the mean-free-path length in air for gamma rays of a stated energy. Since radiation from sources approaching from a distance are to be considered, the errors inherent in the buildup approximation must be carefully inspected. Ignoring contributions from scattered photons with ultimate energies less than 0.068 Mev, the linear buildup approximation used is good to within  $\pm 16$  percent for a gamma source energy of 1 Mev up to distances of 10 mean free paths. When the distance to the approaching cloud becomes zero, the intensity is given by the expression:

$$(I_{ap})_{x \rightarrow 0} = I_0 = \frac{J_A(t)}{4 \mu_A} (1+K)$$

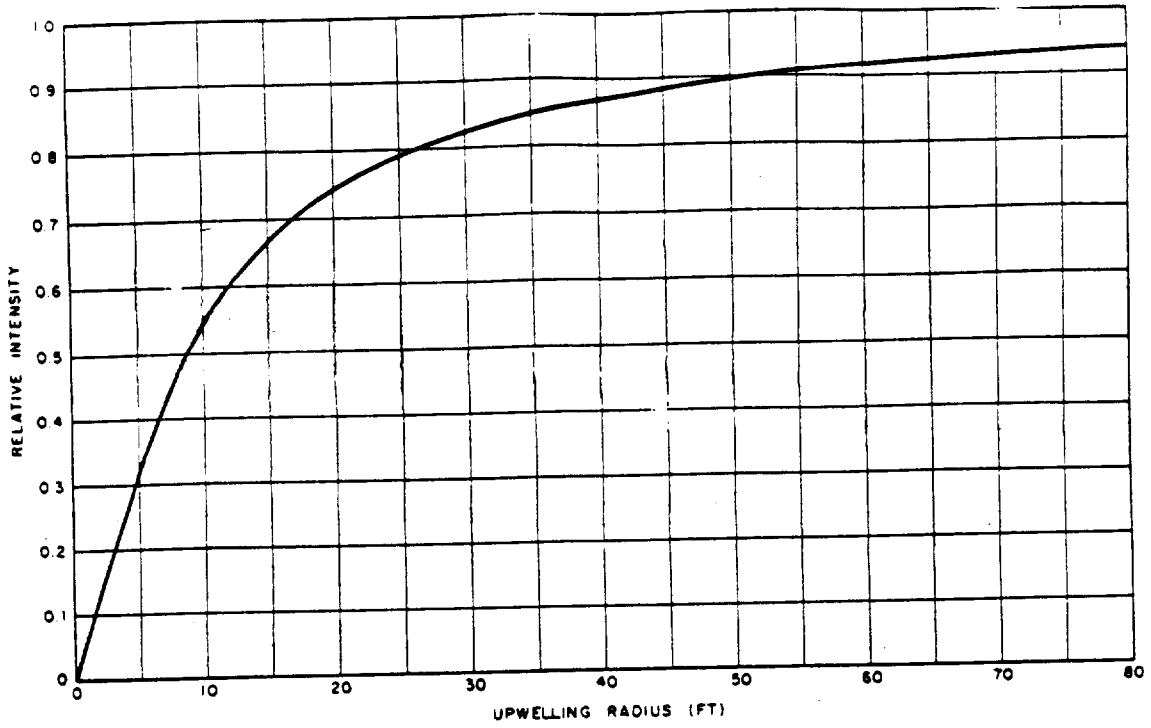


Figure 1.7 Radiation intensity from a circular upwelling of radioactive water (computed for a standard GTR at its center).

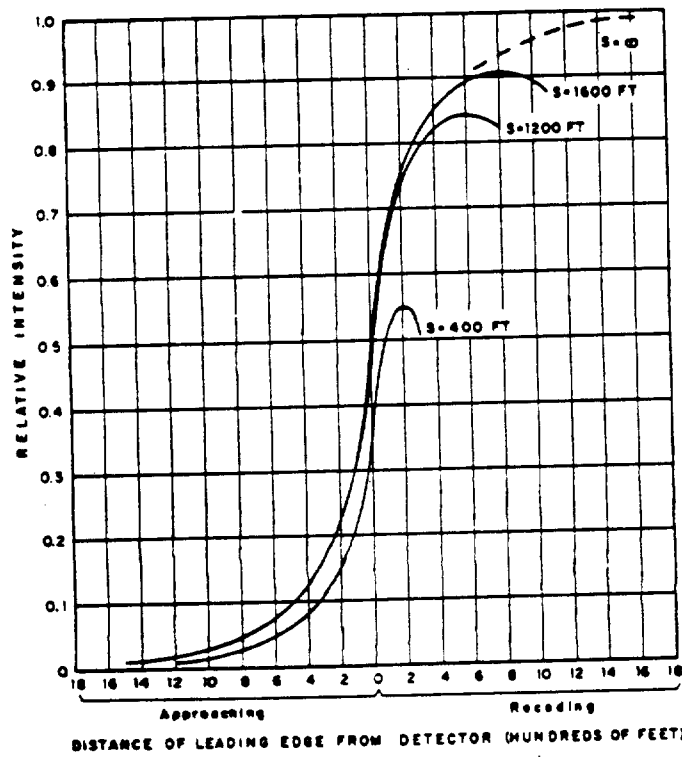


Figure 1.8 Relative intensity from an enveloping base surge (90° cloud model, 1 Mev gamma).

where  $I_0$  is the radiation intensity at the point in question when the approaching radioactive cloud reaches this point. If the cloud continues past the point a distance  $y$ , the intensity becomes:

$$I_{dp} = \frac{J_A(t)}{4\mu_A} (1+K) + \frac{J_A(t)}{4\mu_A} \left\{ y \mu_A [-Ei(-\mu_A y)] + (1+K) (1 - e^{-\mu_A y}) \right\}$$

and

$$(I_{dp})_{y \rightarrow \infty} = I_T = \frac{J_A(t)}{2\mu_A} (1+K)$$

where  $I_T$  is the radiation intensity at the center of an infinite hemisphere of radioactive cloud.

To simulate actual conditions, however, clouds of finite thickness must be considered. The difference between values obtained for two infinite rectangular clouds at different distances from the detection point approximates the desired intensity for clouds of finite thickness. Base surge is thus approximated by a vertical wall of radioactive material infinite in length and height but of finite thickness. Values of  $K$  corresponding to energies of 1.0 and 1.25 Mev were selected, and the intensity as a function of distance to the leading edge was calculated for various thicknesses  $s$  and expressed as a fraction of  $I_T$ . These results are presented in Figures 1.8 and 1.9. By assuming a surface wind speed, relative intensities as a function of time may be obtained from these plots. However, most photographs of base surge from underwater detonations reveal that, although the vertical wall approximation may be reasonable for the upwind case, the surge front at downwind and crosswind positions usually approaches at an obtuse angle. According to Reference 46, this angle is approximately  $120^\circ$ , a value which is usually substantiated by photographic measurements. The general expression for a wall approaching at a  $120^\circ$  angle could not be integrated. However, approximate solutions for a number of thicknesses were obtained by geometric means fully described in Section A.3. The computed intensities relative to  $I_T$  are presented in Figure 1.10 as a function of distance to the leading edge. Both the vertical and the  $120^\circ$  approach curves proved useful in the determination of base surge velocities and in the definition of time of arrival (Section 3.3.4).

Analysis of the gamma dose rate histories at late times (5 minutes or greater) revealed peak activities that can best be explained by assuming the presence of radioactive water or foam in the vicinity of the coracles. The shape of these later peaks could not be reproduced by areas of upwelling, which were large in comparison to the mean free path of 1-Mev gammas, a configuration which has been calculated in Reference 47. Consequently, a special case of the model currently being investigated (Reference 48) was extended to dimensions that would approximate the passage of a relatively small patch of radioactive water or foam. The approximation used yielded the intensities due to passage of a thin disk of uniformly distributed activity beneath a point whose distance above the plane of the disk was equivalent to that of the GTR detector above the ocean surface. The computed intensities normalized to the intensity at the center of the circular radioactive area are plotted against the distance from this center for a number of radii (Figure 1.11). These curves were employed to determine whether the dose rate peaks observed could indeed have been caused by such bodies of radioactive water or foam.

**1.3.3 Supplementary Measurements.** The basic instrumentation of the project consisted therefore of GTR's and IC's mounted in pairs on coracles arrayed about surface zero. This array was supplemented at specific locations by other instruments designed for more specialized measurements. Several underwater gamma detectors were used to detect activity due to upwelling contaminated water. Their locations were selected on the basis of the predicted movement of radioactive water (Section A.5). The data obtained was intended primarily for the correction of gross gamma records in cases where both the radiating cloud and heavily contaminated water arrived simultaneously. However, these water corrections were never applied, since on both Wahoo and Umbrella the base surge rapidly outdistanced the contaminated water

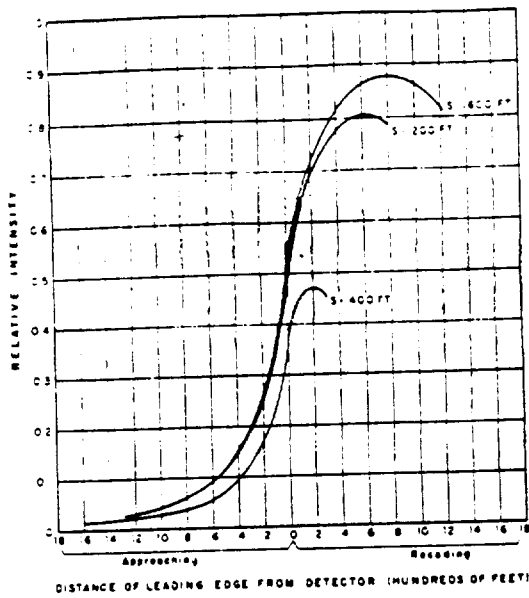


Figure 1.9 Relative intensity from an enveloping base surge (90° cloud model, 1.25 Mev gamma).

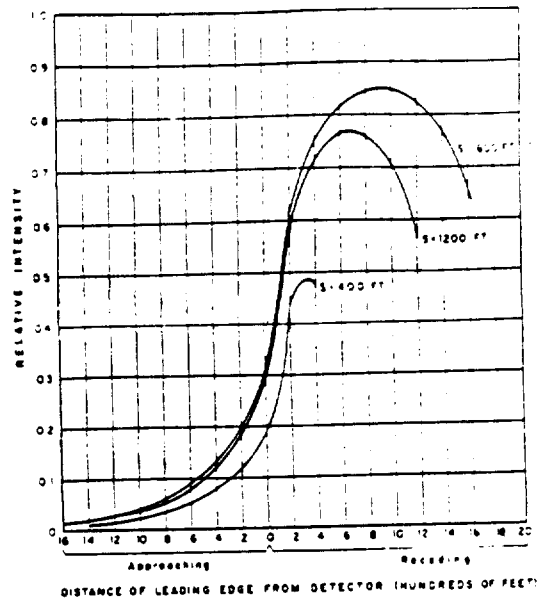


Figure 1.10 Relative intensity from an enveloping base surge (60° cloud model, 1.25 Mev gamma).

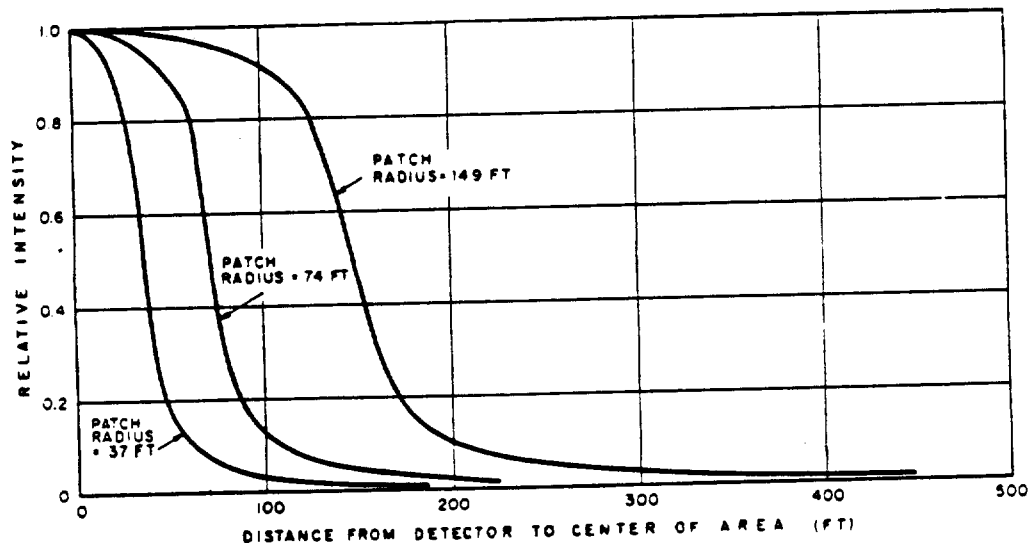


Figure 1.11 Relative intensity for moving circular patches of radioactive water (circular disk model, 1 1/2 feet thick, 1.25 Mev gamma).

and produced a sufficiently characteristic dose rate record so that the presence of waterborne radiation can be detected by inspection. At some locations, radiation due to contaminated water became important at later times (5 minutes or greater) when, in the absence of free-field radiation, the water intensities can be determined directly from the GTR record.

Although the underwater detectors were not needed as originally intended, these instruments provide attenuated traces of the free-field record which are used as a check on the standard instrument. A distinction between the attenuated free-field record and the water record as seen by an underwater detector was possible through a comparison of curve shapes, since the two phenomena produce a characteristic record.

Calculations based on predicted venting times (Reference 24) and previous measurements of dose rates occurring at early times (References 20 and 49 through 52) indicated that rates as high as  $10^6$  to  $10^8$  r/hr were possible at close ranges, particularly on Umbrella. Although the duration of these early peak rates would be very short, these peak dose rates could result in doses of tactical significance. Since these rates were beyond the range of the NRDL gamma detectors (maximum rate  $10^3$  r/hr), and since high time resolution would be advantageous in any analysis of early dose rates, the project borrowed a number of high-range gamma detectors developed by the Army Signal Engineering Laboratory (ASEL) with a maximum rate of  $10^6$  r/hr and a possible time resolution of 0.1 msec. These units, called Gustave I's (References 49 and 50), were installed on coracles closer than 6,500 feet from surface zero and provided a record of gamma radiation intensity for the first 85 seconds after zero time.

The project also requested detailed photographic coverage of cloud movement on both Wahoo and Umbrella so that the visual phenomena could be correlated with the time-based gamma intensity records obtained at all locations. By means of these visual records, meteorological parameters and current theories of fallout transport mechanisms, the project intended to correlate the gamma records at the coracle locations to gamma-intensity-time contours about surface zero. The production of such contours obviously requires a far greater station density than that permitted by available funds; therefore, the project had to rely heavily on photographic tracking of the base surge. Since the operational limitations on both photographic and meteorological coverage would affect the reliability of these contour plots, the project attempted to augment the station density through the use of approximately 70 floating film packs (FFP), which were either anchored or so placed as to drift into preselected locations throughout the coracle array. Data recorded by these FFP's were interpreted by means of similar film packs installed aboard the coracle station. Redwing experience (Reference 33) had shown that a good correlation existed between National Bureau of Standards (NBS) film pack measurements and the integrated total gamma dose obtained from an associated time-based gamma detector; therefore, the use of these FFP's made possible a finer grid of correlation points for the analysis of visual cloud phenomena and the construction of gamma contours.

The FFP's placed for Wahoo were necessarily free-floating, which greatly increased both operational and analytical difficulties. An analysis of current data taken by the Scripps Institution of Oceanography (SIO) during its November-December 1956 survey of the proposed shore area (Reference 53) and additional information provided by the Office of Naval Research (ONR) indicated that an average surface drift of 1 ft/sec could be assumed over the entire array. In the use of suitable drogues, the project hoped to reduce drift rate to about 0.5 ft/sec, which drift speed was used for computing the distance traveled during film pack exposure. The relative cloud dose  $D_A$ , expressed as a percentage of the total dose  $D_A + D_W$  accrued from both the cloud and deposited radioactive material suspended in the surface-water layer  $D_W$ , was computed by integrating the expressions derived earlier for cloud intensity  $I_A$  and water intensity  $I_W$ . Selected values, together with the estimated distances traveled during exposure were then used to evaluate the feasibility of attempting this FFP operation (Table 1.3). As indicated earlier in this chapter and borne out by actual experience in the field, cloud slopes (Appendix F) greater than 0.1 (corresponding to a time of arrival 5 minutes or less) were expected within the range of project stations for both Wahoo and Umbrella; therefore, drift distances were expected to exceed 1,000 feet.

TABLE 1.3 ESTIMATED RELATIVE DOSE AND DISTANCE OF DRIFT FOR FFP'S

Time of Arrival of Cloud	Assumed Duration of Fallout	FFP Movement During Exposure	Est. Percent of FFP's Moving Stated Distance or Less	D <sub>A</sub> as Percent of D <sub>A</sub> + D <sub>W</sub>		
				V <sub>p</sub> = 0.3 cm/sec	V <sub>p</sub> = 3.0 cm/sec	V <sub>p</sub> = 30 cm/sec
min	min	ft	pct	pct	pct	pct
1	8	240	—	100	99.3	93.0
2	16	480	37	99.9	98.5	87.0
3	24	720	—	99.8	97.8	81.5
4	32	960	—	—	—	—
5	40	1,200	58	99.6	96.4	72.6
6	48	1,440	—	—	—	—
8	64	1,920	79	—	—	—
10	80	3,000	—	99.2	93.0	57.1
20	160	6,000	—	87.5	86.9	39.8

Because Shot Umbrella was located inside Eniwetok lagoon, most FFP's could be anchored prior to the shot, which substantially increased their value. In both shots, however, some provision for assessing dose accumulated from radioactive water after passage of the cloud had to be made. This requirement was met by dropping a second group of FFP's as soon after cessation of fallout as radiological safety permitted; thus, the continuing water dosage was measured directly. All FFP positions were to be determined from locally measured drift rates and from two photomosaic maps flown as near zero time as was practicable, one before and one after the shot.

The only anomalous exposures of FFP's considered possible were those due to the upwelling (Appendix F) of contaminated water; however, Wigwam data (Reference 54) indicated that only about 8 percent of the FFP record would be so vitiated. Therefore, while the FFP's were not considered entirely essential, they were considered a valuable means of increasing the density of total dose measurements. They had the additional advantage of late placement, which would permit adjustment of the final array to surface winds existing at shot time.

Three additional GTR's and a number of film packs were installed aboard each of the three DD's and the EC-2 in the target array (Figures 1.12 through 1.14). These shipboard detectors were used as correlation points for a detailed radiological survey of these vessels. Predictions of the total gamma dose at specific locations aboard a DD maneuvering close to similar underwater atomic bursts could then be made by combining the gamma dose over a sequence of positions on various isodose contours and by applying the empirical conversion factor for a particular location aboard the vessel. Such predictions of gamma dose aboard a maneuvering DD were not undertaken by the project but presumably will be done in the analyses of subsequent operations.

In addition to shipboard gamma detectors, a number of aerosol collections and test-panel exposures were made aboard each of the target destroyers. Two smaller platforms were installed aboard the DD-474 and DD-593 on top of the after stacks, as shown in Figure 1.12; these platforms were equipped with four open-close collectors (OCC) and a control box (Figure 1.15). One larger platform installed aboard DD-592 was equipped with four OCC's, four always-open collectors (AOC), two IC's corresponding to those installed aboard the coracles, an air-filtration instrument (AFI), a wind-speed-and-direction indicator (WSDI), and an additional GTR (Figures 1.13 and 1.16).

Samples collected by the AFI, the OCC's and the AOC's provided information on the fraction of device deposited per unit area and on particle-size distribution required for interpretation of the gamma field. The OCC's were also used to expose test panels, which were later analyzed to develop better simulants of fallout originating from an underwater burst. Collections made by the AFI and the two IC's were analyzed for physical and chemical parameters of the base surge. A few additional collections were made simply by placing bottles equipped with funnels at certain locations in the array. These so-called funnel samples (FS) were used only for chemical analysis. Measurements obtained from these limited aerosol collections are reported here only to the extent that they influence the basic gamma-field determinations made by the project.

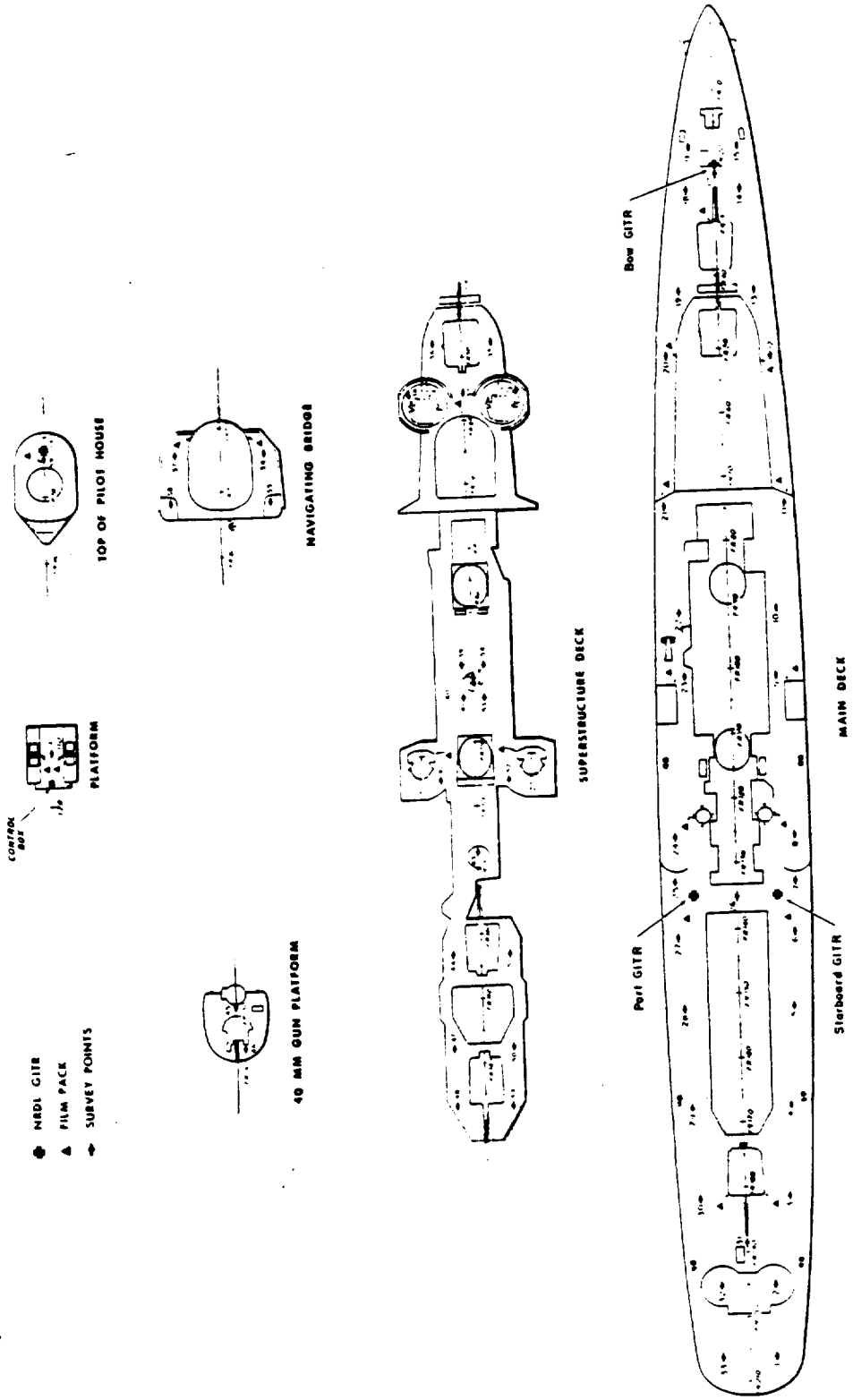


Figure 1.12 Target ship instrument layout aboard DD-474 and DD-593 (survey points also shown).

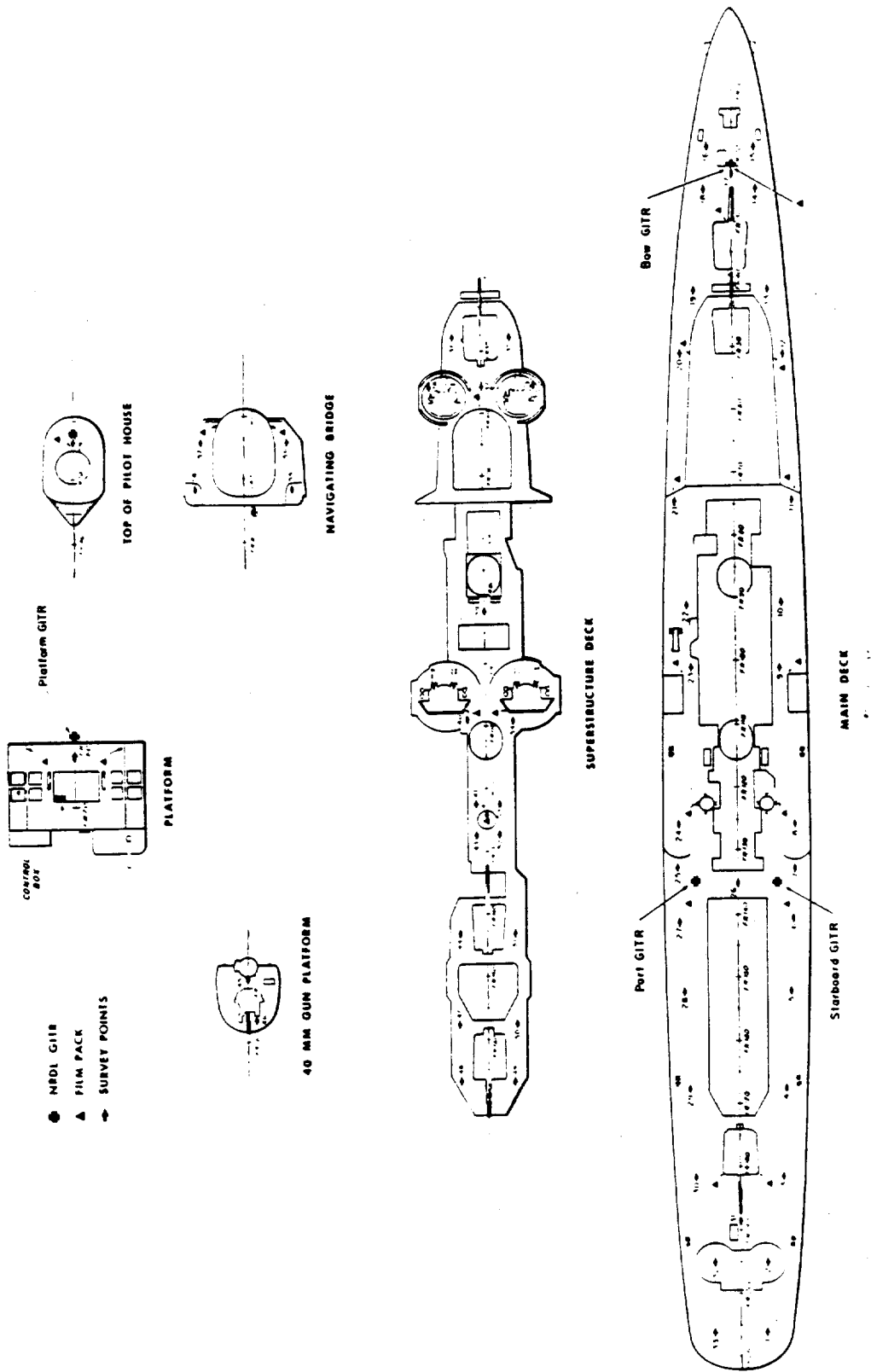


Figure 1.13 Target ship instrument layout aboard DD-592 (survey points also shown).

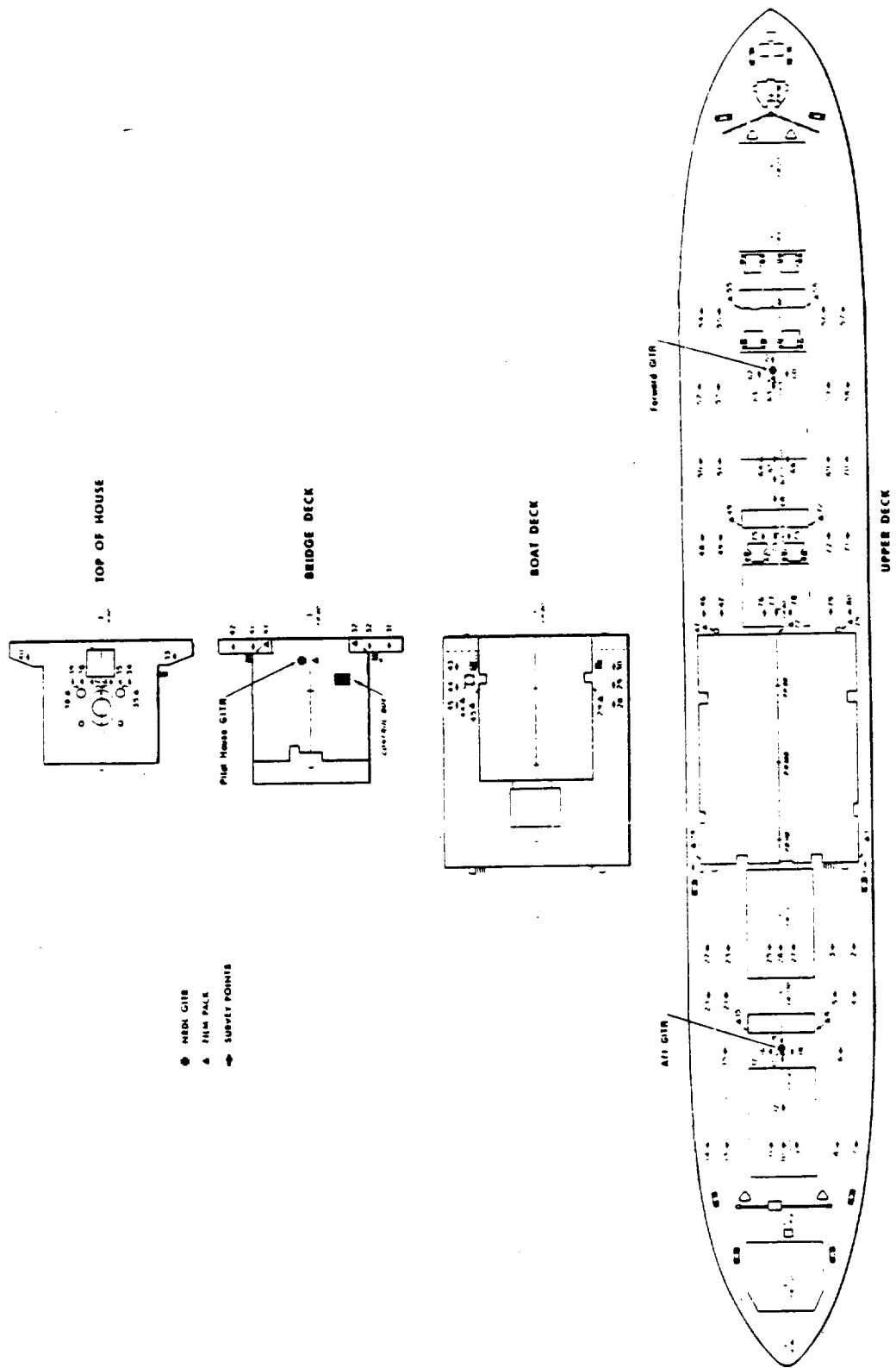


Figure 1.14 Target ship instrument layout aboard EC-2 (survey points also shown).

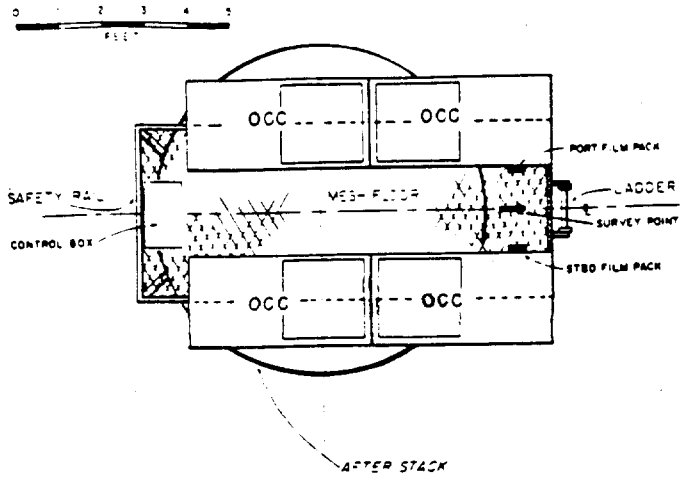


Figure 1.15 NRDL instrument platform aboard DD-474 and DD-592.

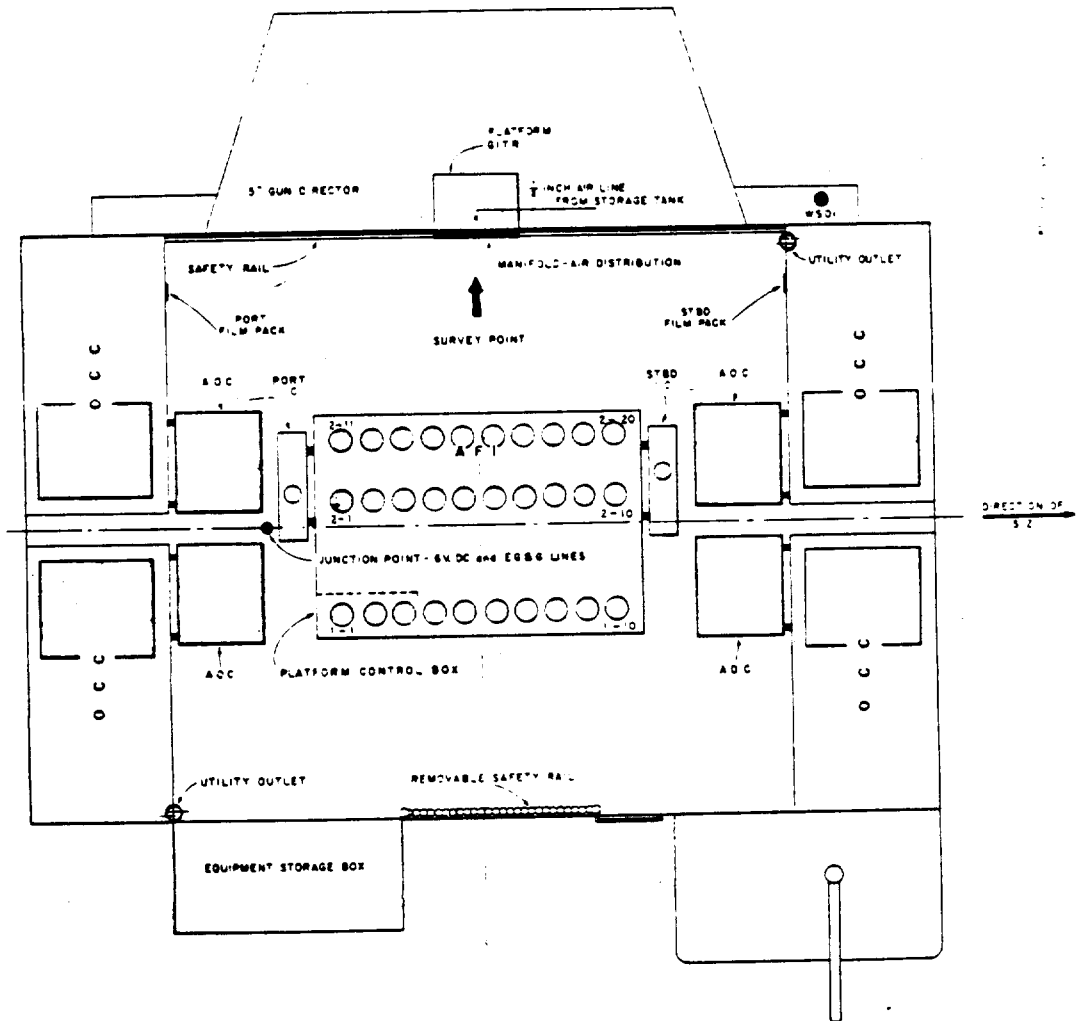


Figure 1.16 NRDL instrument platform aboard DD-592 (collecting areas shaded).

## Chapter 2

### PROCEDURE

#### 2.1 GENERAL OPERATIONS AND SHOT PARTICIPATION

The project participated in two scheduled underwater detonations in the Hardtack series at the Eniwetok Proving Ground (EPG): Shots Wahoo and Umbrella.

Operational limitations on accuracy of placement and conflicts with other elements of the total shot array necessitated modification of the idealized station array presented in Chapter 1. As originally planned, 21 coracles were placed for Wahoo; but, on the basis of Wahoo experience, the Umbrella array was modified to include 26 coracles and one skiff armed and placed by SIO. The coracle stations placed by the project, together with the instruments installed in each, are tabulated against their nominal positions in Table 2.1 and plotted in Figures 2.1 and 2.2. The estimated positions of all elements moving after the detonations are also plotted in these figures; however, throughout the remainder of this report, all coracles and all collections or records obtained aboard them will be referred to by means of the nominal position designators used in Table 2.1 regardless of later position. The coracle stations were supplemented by additional instrumentation installed aboard all major target vessels and by approximately 70 FFP's distributed throughout the fixed array.

Since climatological averages (References 26 and 27) indicated that surface winds tended to shift to the right during the May-June season, the station array for both Wahoo and Umbrella was skewed to the right of the downwind leg that had been selected by Joint Task Force 7. Deep-anchoring was required for all 21 coracle Wahoo locations, whereas only 5 Umbrella locations required such mooring. The remaining Umbrella stations were anchored by standard naval techniques in depths not exceeding 30 fathoms. Experience during Operation Redwing (References 55 and 56) had shown that properly installed deep-anchors could be relied upon for the mooring of skiffs. This fact was most definitely borne out by the Hardtack experience, since only 1 deep moor in 30 failed because of inherent defects, viz, a leaking fiberglass subsurface buoy. No coracles were lost during the entire operation, although two broke free due to chafing of the surface pennants.

All deep moors were placed by the USS Munsee (ATF-107), which had been specially equipped with a Markey hydrographic winch and AN/UQN-1B sonar sounding equipment modified to have a continuous fathometer scale from 0 to 1,200 fathoms. No difficulty was experienced in over-the-side handling of coracles in seas up to Class 5 (winds 17 to 21 knots, waves pronounced and long with white foam crests). An entire deep moor could be placed in about an hour starting from the time of the ATF's approach. A maximum of six deep moors could conveniently be placed in a normal working day; however, the actual placement of deep moors was controlled by the Task Group 7.3 mooring schedule for placement of the major target elements. The assistance of one LCM was required for the placement of coracle moors in shoal waters inside the lagoon. A maximum of eight such shallow moors could be placed in a normal working day. After surface currents were measured in the area, placement of the deep moors for Wahoo commenced on 16 April 1958. Placement of deep moors and lagoon anchorages for Umbrella was started on 27 May. Both areas were completely cleared of all remaining mooring components by 12 June. During this 60-day period, the USS Munsee was used by the project on nearly continuous assignment.

Concurrently with mooring operations, all project instruments were bench-checked and installed in coracles at the beach work area (BWA) on Parry Island. For Shot Wahoo, placement

TABLE 2.1 INSTRUMENTATION AND ACTUAL POSITION OF STATIONS

For target ship information, see Tables 3.26 and 3.27. The following abbreviations are used: std, standard gamma-intensity time recorder (GTR); UW, underwater GTR; ASEL, Army Signal Engineering Laboratory GTR; IC, incremental collector; (NR), station not rearmed after accidental firing; (CO), coracle overturned; (D), coracle drifting after the event; (reef), coracle placed on atoll reef; (deep) coracle placed outside lagoon for Umbrella.

Nominal Position	Coracle Number	Bearing		Distance		Instruments at Station	Nominal Position	Coracle Number	Bearing		Distance		Instruments at Station
		From Surface	Zero	From Surface	Zero				From Surface	Zero	From Surface	Zero	
		deg (true)		ft				deg (true)		ft			
Shot Whahoo:													
U 3.2	6	066	3,250	std, UW, ASEL, IC, (NR, D)	U 1.8	36	051.8	1,760	std, UW, ASEL, IC, (CO)				
U 4.0	-	-	-	Not placed**	U 2.7	11	067	2,700	std, UW, ASEL, IC				
U 4.5	1	066	4,500	std, IC(D)	U 3.9	2	068	3,900	std, ASEL, IC				
CL 3.9	26	159	3,900	std, UW, IC(D)	CL 3.1	21	163.7	3,060	std, UW, ASEL, IC, (CO)				
CL 4.6	17	151 1/2	4,600	std, UW, ASEL, IC	CL 4.0	13	158.5	3,990	std, ASEL, IC				
DL 7.1	3	231 1/2	7,100	std, UW, IC	CL 6.0	14	158.9	6,010	std, ASEL, IC				
DL 12.0	23	237	12,000	std, IC, (NR, D)	DL 5.6	SIO Skiff	207.5	6,580	std				
DL 18.3*	43	241	18,300	std, IC, (NR, D)	DL 6.2	32	230.4	6,220	std, IC				
D 4.8	-	-	-	Not placed**	DL 16.0	7	237.1	15,980	std, IC (deep)				
U 8.0	4	256 1/2	8,000	std, UW, IC(D)	DL 18.6	1	233.5	18,650	std, IC (deep)				
D 14.4	-	-	-	Not placed**	D 2.7	31	248	2,670	std, UW, ASEL, IC, (CO)				
D 23.1	11	249	23,100	std, IC, (NR)	D 4.8	4	247.9	4,770	std, UW, ASEL, IC, (CO)				
DR 4.5	21	263	4,500	std, UW, ASEL, IC, (D)	D 6.5	22	248	6,500	std, UW, IC				
DR 9.0	36	263	8,950	std, IC, (D)	D 10.4	37	247.5	10,380	std, IC				
DR 14.4	13	265	14,400	std, UW, IC	D 15.5	41	249.1	15,470	std, IC, (reef)				
DR 24.0	14	263	24,000	std, UW, IC	D 18.2	16	250.2	18,220	std, IC, (deep)				
DRR 6.8	41	281	6,800	std, UW, IC, (D)	D 22.0	23	248	22,000	std, IC, (deep)				
DRR 12.8	34	276	12,800	std, UW, IC	DR 4.6	26	263.5	4,530	std, UW, ASEL, IC, (CO)				
CR 4.1	27	336	4,100	std, UW, ASEL, IC, (CO, D)	DR 7.5	3	265.5	7,530	std, UW, IC				
CR 5.2	31	334 1/2	5,200	std, UW, IC	DR 12.2	6	262.5	12,230	std, UW, IC				
CR 6.4	22	332	6,400	std, IC, (D)	DR 18.6	17	261	18,600	std, IC, (reef)				
					DR 23.2	43	264.5	23,210	std, IC, (deep)				
					DRR 3.9	33	279.1	3,940	std, UW, ASEL, IC, (CO)				
					DRR 6.7	44	278.1	6,740	std, UW, IC				
					CR 2.7	12	310.9	2,670	std, UW, ASEL, IC (CO)				
					CR 4.9	24	334	4,910	std, ASEL, IC				
					CR 6.6	34	337.3	6,610	std, ASEL, IC				

\* The DD-474 collided with station during placement of the destroyer in the array and dragged the coracle to the estimated position given.  
 \*\* Deep moors were installed at these locations, but, because of the limited time available during the emergency rearming, coracles could not be placed at those locations.

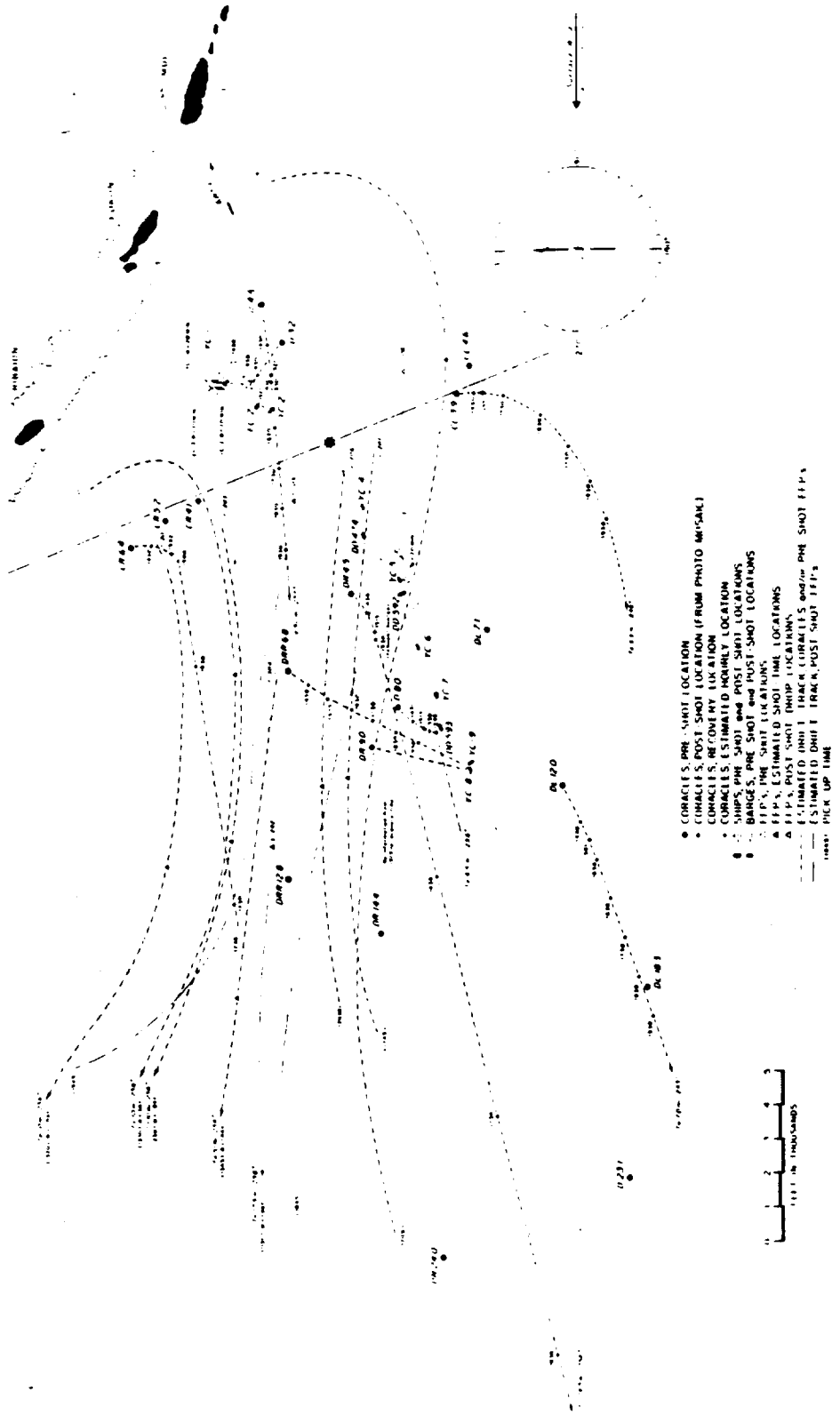


Figure 2.1 Master plot of stations, Shot Wahoo.

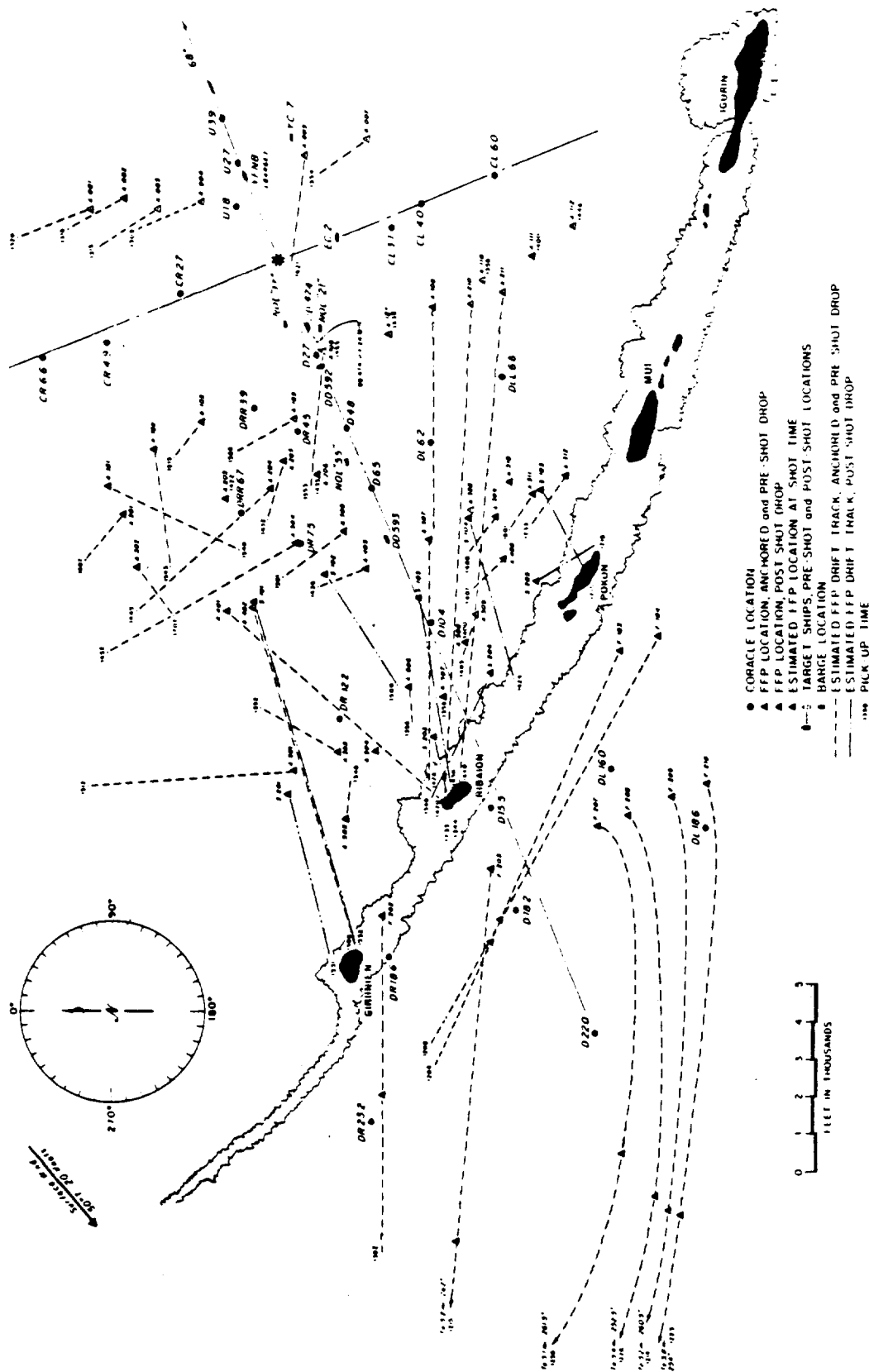


Figure 2.2 Master plot of stations, Shot Umbrella.

of fully instrumented and armed coracles began on D-4 days. For Umbrella, placement of partially armed coracles began on D-5 days, with final arming being accomplished after the last test signal in the afternoon of D-1 day.

Although line-of-sight radio signals had been thought necessary, all stations received radio signals with antennas placed 6 feet above the ocean surface. Installation and maintenance of the additional instruments aboard the major target ships were accomplished by a special crew using available shuttle services. Thus, no special logistic support was required for this phase of the project.

One FFP practice run, including the camera aircraft assigned responsibility for photomosaic coverage, was performed to gain operational experience in FFP placement, location, and recovery. On the basis of this experience, the operational procedure for Wahoo was planned. This plan was modified for Umbrella to include helicopter pickup of all FFP's, coupled with radar location of all positions before and after the shot.

**2.1.1 Shot Wahoo.** The placement of deep moors for Shot Wahoo, beginning on 16 April, proceeded slowly because of unavoidable delays caused by high winds and difficulties Task Group 7.3 was having with the mooring of the major target ships. By 29 April, 5 moors had been placed; by 8 May, 12 moors; and by 14 May, all moors except D 4.8 and D 8.0, which had to be withheld until DD-592 was placed in the target array. Final arming of coracles could not commence until 11 May (D-5) because Edgerton, Germeshausen and Grier (EG&G) was having difficulties with radio-signal transmission. Final arming of coracles therefore was accomplished according to the following schedule:

11 May DL 12.0, DL 18.3, D 23.1, DR 24.0, CR 6.4;  
12 May CL 3.9, CL 4.6, DL 7.1, DRR 6.8, CR 4.1;  
13 May U 4.5, D 14.4, DR 4.5 (operational difficulties precluded further arming);  
14 May U 3.2, DR 9.0, DR 14.4, DRR 12.8, CR 5.2;  
15 May U 4.0, D 4.8, D 8.0 (last two positions required both placement of moors and arming).

Shortly after 1600 on 15 May (D-1), an accidental radio signal triggered all coracles, thus canceling participation in the shot unless re-arming could be effected. The project therefore attempted an emergency re-arming operation the night of D-1. A priority list for the re-arming of coracles was established, and the USS Munsee, which was working the array at the time of the accidental signal, was instructed to pull and re-arm coracles without interruption. All available project personnel, plus volunteers from Project 2.1, SIO, and the USS Hooper Island (ARG-17) were ferried from Parry Island to the USS Munsee, where they formed three re-arming crews, which operated continuously until the ship was ordered to leave the array at H-2 hours. During this period of approximately 18 hours, 14 coracles were re-armed; however, the unavoidable fatigue and confusion that attended this work, combined with the necessity for rapidity, greatly increased the probability of instrument failure due to arming errors. The coracles finally re-armed were U 4.5, CL 3.9, CL 4.6, DL 7.1, D 8.0, DR 4.5, DR 9.0, DR 14.4, DR 24.0, DRR 6.8, DRR 12.8, CR 4.1, CR 5.2, and CR 6.4.

At H-5 hours, a crew of five men returned to Parry Island to carry out previously planned shot day activities. Forty-eight FFP's were dropped into the target array from two helicopters between H-2 and H-1 hours. No operational difficulties were experienced and all FFP drops were executed as planned (Section A.5). The first photomosaic was flown between H-1 hour and H-15 minutes at an altitude of 1,500 feet, a large number of FFP's being visible from the aircraft. The FFP's drifted 30 minutes longer than anticipated due to a delay in the shot and were moved an unexpected distance radially by water waves resulting from the detonation.

At H+1 hour, a second drop of 17 FFP's was made from an SA-16 aircraft concurrently with the postshot photomosaic. Also at H+1 hour an FS was recovered from the YC-2 barge by helicopter and returned to Parry Island for C<sup>14</sup> analysis and beta-gamma decay measurements. This helicopter and a second then returned to the target area to spot FFP's for the

pickup vessels. The project had personnel aboard the USS Munsee, the USS Mactobi (ATF-105), and the Task Group 7.4 crash boat (AVR), all of which were assigned to FFP pickup. Although many FFP's were seen by both aerial and surface units, only 10 out of a total of 65 were recovered, an effective recovery of about 15 percent. The principal difficulty lay in a failure of communication between Rad-Safe control and the task force elements attempting to retrieve FFP's. Consequently, ships that were to have recovered FFP's would not enter the presumed radex area where most of the FFP's happened to be concentrated. FFP recovery was terminated at H+4 hours, since Task Group 7.4 required all spotting helicopters to return to Eniwetok Island by 1800.

Rad-Safe control permitted D-day entry on DD-593 only; therefore, early recovery was effected only on this ship. This recovery was performed at H+4 $\frac{1}{2}$  hours, and these samples, together with aliquots of all sample solutions used in early chemistry were placed aboard the H+8 hour flyaway (Appendix F). Three coracles were also recovered on D-day by the USS Munsee. One coracle was overturned, and 10 deep moors were parted by the detonation. (Section 2.3.2). All moors broke near the bottom; therefore, the coracle drift rates were substantially reduced, which greatly simplified recovery on the following day.

On D+1 day a number of Task Group 7.3 ships recovered all remaining coracles and returned them to the BWA on Parry Island for further processing. The USS Bolster (ARS-38) recovered two coracles; the USS Grasp (ARS-24), seven; the USS Mactobi, two; and the USS Munsee, six. Although these additional vessels were able to perform effective coracle recovery, damage (particularly to the coracle hulls) was understandably increased through the lack of previous handling experience.

On D+1, it was found that radio signals starting project instrumentation aboard DD-474 and DD-592 were not received because of a failure of ship's power; therefore, minimal data was obtained from these ships. Since the target ships were being towed into the lagoon, all project operations aboard were suspended until they were reestablished at their lagoon moors.

On D+2, the project performed a complete recovery and survey of all target ships. Complete stripping of coracles was started at the BWA, all samples being processed through the Sample Recovery Center (SRC) established near the Parry Island airstrip to maintain proper contamination control and to insure proper logging of all pertinent data.

During the interval between shots, all coracles and instruments were overhauled, recalibrated, and repaired. Because of the low degree of radioactive contamination, no special decontamination was necessary. All GTR detectors were recalibrated on a radiation range established on Parry Island. All IC trays were counted in an end-window gamma counter as soon as they could be recovered, decay was followed on a few trays, and the remaining trays were returned to NRDL for further analysis. The GTR tapes from the coracles and the ships were read out on an electronic readout device (GITOUT), a procedure of several weeks' duration. Site chemistry was limited to beta and gamma decay measurements, and to Cl<sup>38</sup> analysis of early fallout samples and cloud samples obtained for the project by Los Alamos Scientific Laboratory (LASL). All further analytical work was performed at NRDL. Project instrumentation aboard the major target ships suffered only minor damage and was overhauled in situ with the exception of the GTR detectors, which were removed for recalibration on Parry Island.

2.1.2 Shot Umbrella. The placement of deep moors for Shot Umbrella commenced on 27 May. By 31 May, the 5 deep moors and 12 of the lagoon moors had been placed. The remaining moors, including two stations on the atoll reef, were placed during the final installation of coracles at the moors. During this period, seven lagoon moors had to be replaced because the counterweight on the Dan buoy chafed through the mooring cable. When this trouble was corrected by removal of the counterweight, no further difficulty was experienced with the lagoon moors. Starting on 3 June, coracles in a pre-armed condition were placed at the moors at a rate of five or six a day; these stations were later armed by pulling a lanyard attached to a dead-safe switch that had been installed in the instrument control box after Wahoo.

Considerable difficulty was experienced by the project in placing anchored FFP's in the array. Although the anchoring system had been successfully tested in the Umbrella area several times prior to final placement, only 16 out of 36 anchored FFP's placed the afternoon of 6 June were still in position the following morning. The high percentage of failure was probably due to short choppy seas that had blown up the day before in the Umbrella area. The project redesigned and remade 36 new anchored FFP's, improvising somewhat from depleted stocks. On the morning of D-1 day, the new anchored FFP's were placed in the array and remained in position until the shot. After the final test signal at 1340 on D-1, the project armed all coracles, using the USS Munsee outside the lagoon and the AVR inside. All stations except two were armed and ready by 1800 on D-1. Two of the coracles had pretripped during placement and were therefore removed from their moors, re-armed during the night, and replaced at their stations the morning of D-day.

D-day activities were considerably modified from those of Wahoo. Instead of photomosaic mapping, all preshot positions were obtained by M-33 radar on Eniwetok Island, which ranged on a spotting helicopter as it hovered over a given station. Postshot positions were obtained similarly with Mark 25 fire-control radar aboard the USS Boxer (LPH-4) ranging on the Marine helicopters performing FFP recovery. Also, because of the possibility that a large number of coracles would break their moors and drift onto the reef, the project had two recovery teams standing by during the shot; each team consisted of one LCU with a crane aboard, one LCM, and one DUKW with A-frame carried aboard the LCU. All project recovery was coordinated by Task Group 7.3 from the CIC aboard the USS Boxer.

At H-2 hours, 14 FFP's were dropped by the Task Group 7.4 helicopter outside the lagoon along previously planned drop lines (Section A.5). At H-1 hour, project control of the recovery operation moved aboard the Boxer. The two lagoon recovery teams, the AVR, and the USS Munsee with another LCM remained near the Boxer during the shot. At H+30 minutes, two Marine helicopters departed the Boxer to recover the free-floating FFP's outside the lagoon; meanwhile, a second drop of self-anchoring FFP's was made inside the lagoon from an SA-16. Also, two FS's were recovered from the target array by the Task Group 7.4 helicopter and returned to Parry Island for  $Cl^{38}$  analysis and beta-gamma decay measurements.

Recovery of the free-floating FFP's outside the lagoon proceeded rapidly and was completed at H+1½ hours. The two Marine helicopters then moved inside the lagoon and continued FFP recovery. Between H+1 and H+1½ hours, project crews performed early recovery of samples from the DD-474, DD-592, and DD-593, all samples being processed through the SRC. All ship samples, together with aliquots of all sample solutions used in early chemistry, were placed aboard the H+6 hour flyaway. Also at about H+1½ hours, the two special recovery teams and the AVR moved into the array to check for drifting coracles and assist in FFP recovery. No coracles had broken loose from their moors; however, seven had been overturned by the detonation.

At H+3½ hours, recovery of the coracles began with the USS Munsee operating outside the lagoon, one LCU and LCM team in the north section of the array, and the second LCU and LCM team in the south section. The AVR and the two Marine helicopters continued FFP search and recovery, completing this operation at about H+5 hours. By H+7 hours all coracles except the two reef stations had been recovered, and 63 FFP's had been retrieved. (Task Group 7.3's efficient and effective recovery unquestionably increased the value of the data obtained on Shot Umbrella and is greatly appreciated by the project.) Coracles were returned to the BWA, where pulling and counting of IC trays started immediately and continued throughout the night.

On D+1 day, the USS Munsee, assisted by an LCM, recovered the two coracles on the atoll reef and completely cleared the entire Umbrella array of remaining mooring components. Also on that morning, the project performed a complete recovery and survey of all target ships. Complete stripping of all coracles was started at the BWA, and again all samples were processed through the SRC to assure both proper logging of data and contamination control. By 1430 of that day the IC count on all 24 sets of trays had been completed, and the trays were ready for air shipment to NRDL for further analysis.

On D+3 days, the USS Munsee rechecked the old Wahoo array for possible mooring components, and that evening the project indicated that it had no further need for its services. Rollup proceeded rapidly. By D+5 days, essentially all project equipment, except that used for data reduction, was packed and ready for shipment.

## 2.2 INSTRUMENTS

**2.2.1 Gamma-Intensity-Time Recorder (GITR).** The primary instrument used by the project was a portable, self-contained GITR (or std-GITR), which represents a further development of a gamma-detecting instrument used during Operation Redwing (Reference 33). The instrument (Reference 57) is 16 by 13 by 21 inches high, weighs approximately 55 pounds with power supply, and consists of the following units: (1) a radiation detector and amplifier with time base, (2) a recording system, (3) a battery pack, and (4) miscellaneous instrument control switches and associated circuitry (Section B.1). The detector unit can be mounted either inside the recorder case or as a separate unit connected with the recorder by a cable not exceeding 25 feet in length (Figures 1.4 and 2.3). The sensitive element is a low-range ionization chamber containing a concentric, high-range chamber. The common base of these chambers contains the associated recycling electrometer circuits.

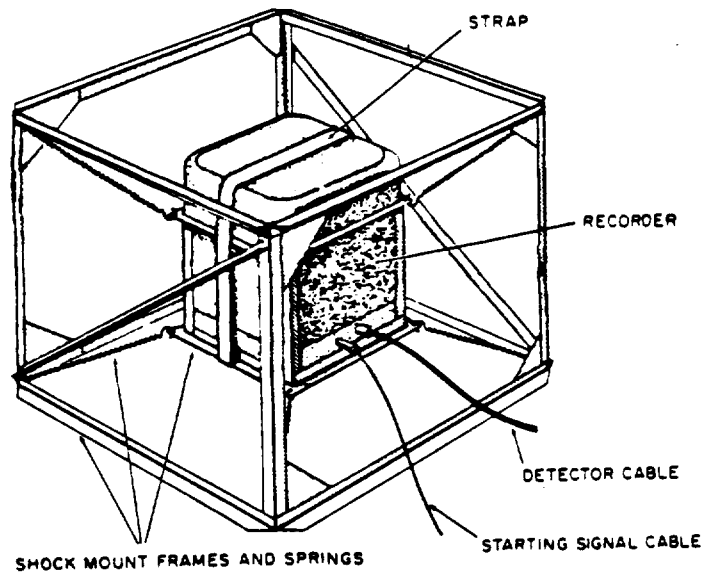
Both chambers have nearly a  $4\pi$  response and are independent of incident gamma energy to within  $\pm 20$  percent from 100 kev to 1.3 Mev (Section C.1). The discharge of either chamber fires its associated electrometer, giving a square-wave pulse that is amplified and recorded on magnetic tape. The transducer automatically recycles to the original charged condition in approximately 0.5 msec. Each recorded pulse represents an increment of gamma dose which, by means of time pulses indicating tape speed, can be converted to dose rate. The dose increments from the two chambers and the time base are recorded as three channels of information on a  $\frac{1}{4}$ -inch magnetic tape.

One of two types of tape transports can be coupled with the basic transducer unit, thus giving two instruments: one with a tape speed of 0.25 in/sec, giving 12 hours of operation with a range of 10 mr/hr to  $10^5$  r/hr; the other with a tape speed of 0.05 in/sec, giving 60 hours of operation with a range of 10 mr/hr to  $2 \times 10^4$  r/hr. All GITR's were actuated by a signal from a trigger-control box and shut themselves off automatically when the end of the tape was reached.

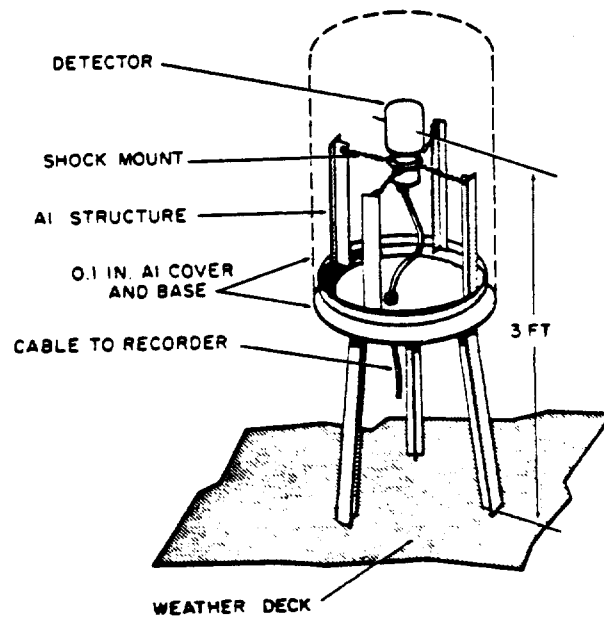
On a coracle installation, the detector was housed inside a watertight, 14-gage aluminum case mounted directly on the deck (Figure 1.4). All coracle recorders were the 12-hour type and were mounted below the deck in the instrument well. This mounting arrangement was selected after experimental checks of directional response with the detector mounted inside the recorder proved to be unsatisfactory. The detector response to known deck activity, as indicated by IC collections, was experimentally determined using exact coracle geometry (Section C.5).

For Wahoo, all shipboard GITR's were of the 60-hour type to insure a GITR record that would overlap the planned ship surveys. All shipboard GITR's were mounted with the detector and recorder installed separately. For Umbrella, two of the GITR's aboard the EC-2 were exchanged for 12-hour types in order to obtain the higher peak dose rate capability of these instruments. No special determination of detector response to particular shipboard geometry was attempted, although all locations were specifically selected to reduce anomalous contributions from ships' structures.

**2.2.2 Underwater GITR.** The underwater GITR (UW- or sec-GITR) is a simple modification of the standard GITR. The basic instrument consists of the 12-hour GITR described above with its detector housed in a deck mounting case identical to that used for the std-GITR (Figure 1.4). The detector, however, was placed on a 25-foot cable and was mounted at the edge of the coracle in a dropping mechanism actuated by a small cylinder of carbon dioxide upon receipt of a signal from the trigger-control box (Figures 1.2 and 1.3). The detectors were so weighted and the length of cable so chosen that after release they would be suspended approximately 6 feet



RECORDER



DETECTOR

Figure 2.3 GITR mounting for ships.

below the water surface in the attitude depicted in Figure 1.2. The drop was made after passage of the water shock waves by means of a preset time delay.

**High-Range GITER.** ASEL Gustave I recorders (ASEL-GITER) were borrowed by the project for use as high-range detectors. The units originally designed and built by ASEL were repackaged by NRDL (Figure 2.4). Because the basic device is described in existing literature (References 49 and 50), only a brief description is included here. The instrument is capable of recording dose rates as high as  $10^8$  r/hr with a time resolution of 0.1 msec. The gamma intensity record is made on 450 feet of 1-inch magnetic tape, which travels at 60 in./sec, providing a 90-second record. The basic circuit was modified by the elimination of the cathode follower originally used between the detector and the amplifier unit. The repackaged instrument is 19 by 16 $\frac{1}{2}$  by 16 inches high and weighs approximately 110 pounds with power supply.

The ASEL detectors were calibrated on a special range set up on Parry Island with a 200-curie Co<sup>60</sup> source. ASEL-GITER's were installed only on coracles less than 6,500 feet from surface zero, the recording element being placed in the instrument well with the detecting elements installed on the deck (Figure 1.2). The ASEL-GITER received a warmup signal at minus 5 minutes, and a minus-5-second signal to start the rapid tape transport. Both signals were received from the trigger-control box.

**2.2.4 Incremental Fallout Collector.** The incremental collector (IC) has been used on many field operations and has been frequently described (References 33 and 58 through 60). The current instrument was redesigned to reduce the unit cost and to bring the collecting surface as near the top of the instrument as possible (Figure 2.5 and Insert A of same figure). The instrument is 6 by 29 by 32 inches high and weighs 95 pounds with a complete set of trays. In essence, the IC obtains a series of 58 fallout collections over uniform time intervals regulated by the trigger-control box. Fifty-eight specially prepared trays are placed upon a spring-compensated elevator platform so that the stack of trays is directly below a sampling port approximately 3 inches in diameter, the top tray being exposed. The trays are then individually indexed onto a receiving platform by an electrically actuated pneumatic system. The exposure interval planned for Hardtack was 1 minute, and the instrument was timed and actuated by the trigger-control box. IC's were installed flush with the coracle deck (Figure 1.3) or flush with the general level of the platform instruments on DD-592 (Figure 1.16).

To reduce shadow bias (Appendix F and Reference 61), the collecting surface was brought to within  $\frac{1}{8}$  inch of the top of the instrument. Lucite trays 4 inches square and containing a circular well,  $3\frac{3}{4}$  inches in diameter and  $\frac{1}{4}$  inch deep, were used (Figure 2.5, Insert B). The well contains several thicknesses of filter paper capped with a perforated 20-mil polyethylene disk. The polyethylene disk is inserted by rotating it through a key slot in a  $\frac{1}{16}$ -inch lip projecting inward from the top of the well; thus, the disk with the filter papers beneath it is held firmly within the tray well. The perforated disk was coated with a thin layer of a grease specially developed for use at the EPG (Reference 33). This grease is made by adding polyethylene to Lubriseal (about 3 percent by weight) to raise its melting point to 130° F. The grease was intended to trap solid particulate matter, while the filter paper beneath the perforations retained the liquid fraction. The trays were designed so that the IC could be loaded or unloaded in a single operation, which alleviated recovery problems in high-radiation fields.

**2.2.5 Film Packs.** A large number of film packs were used by the project on the coracles, aboard the target ships, and as FFP's, which were either free-floating or anchored. Regardless of the manner in which these film packs were placed in the array, the basic element consisted of two packets of film placed inside an NBS holder (Reference 62). This holder was sealed inside a plastic cigarette case, which in turn was placed into two independently sealed plastic bags; this procedure both reduced humidity and oxygen damage to the films and afforded a rapid means of decontaminating film packs upon recovery. The whole package was then wrapped in aluminum foil to reduce absorbed heat, since the film used deteriorated under elevated temperatures.

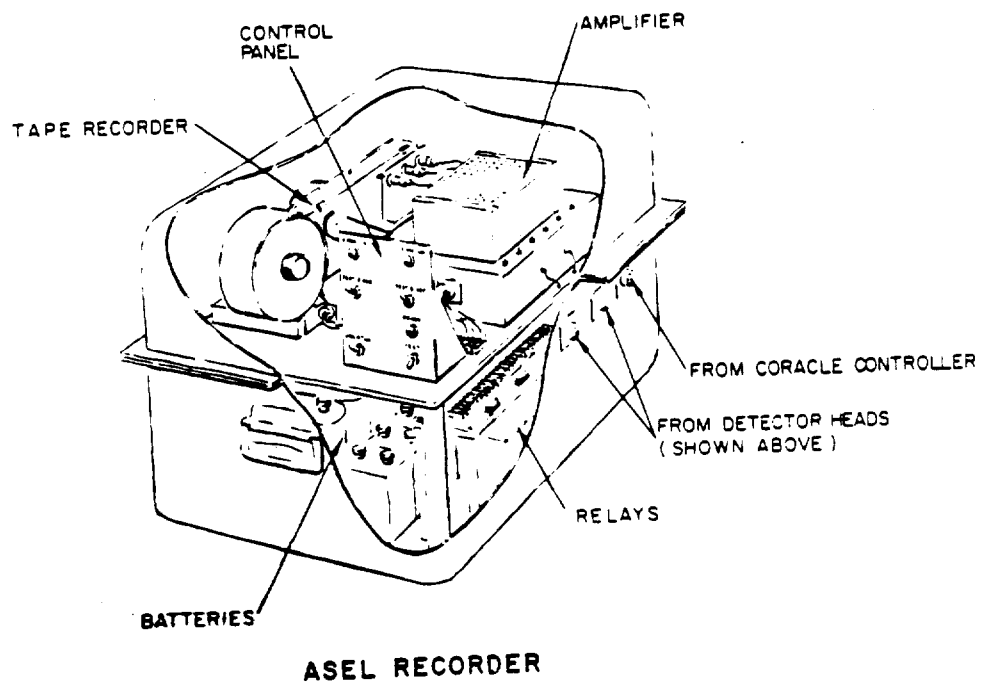
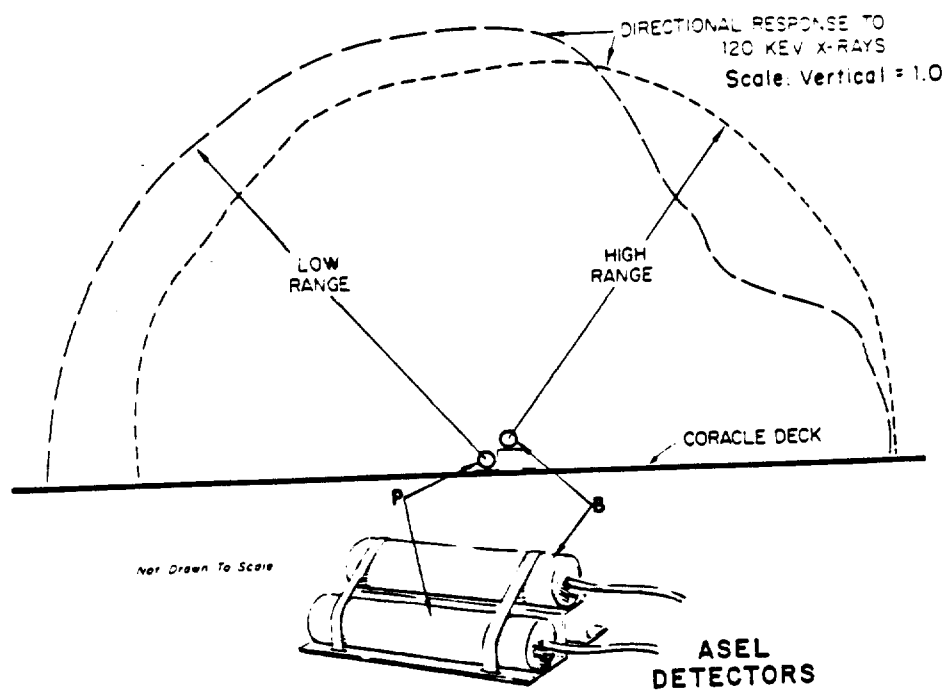


Figure 2.4 ASEL gamma-intensity-time recorder.

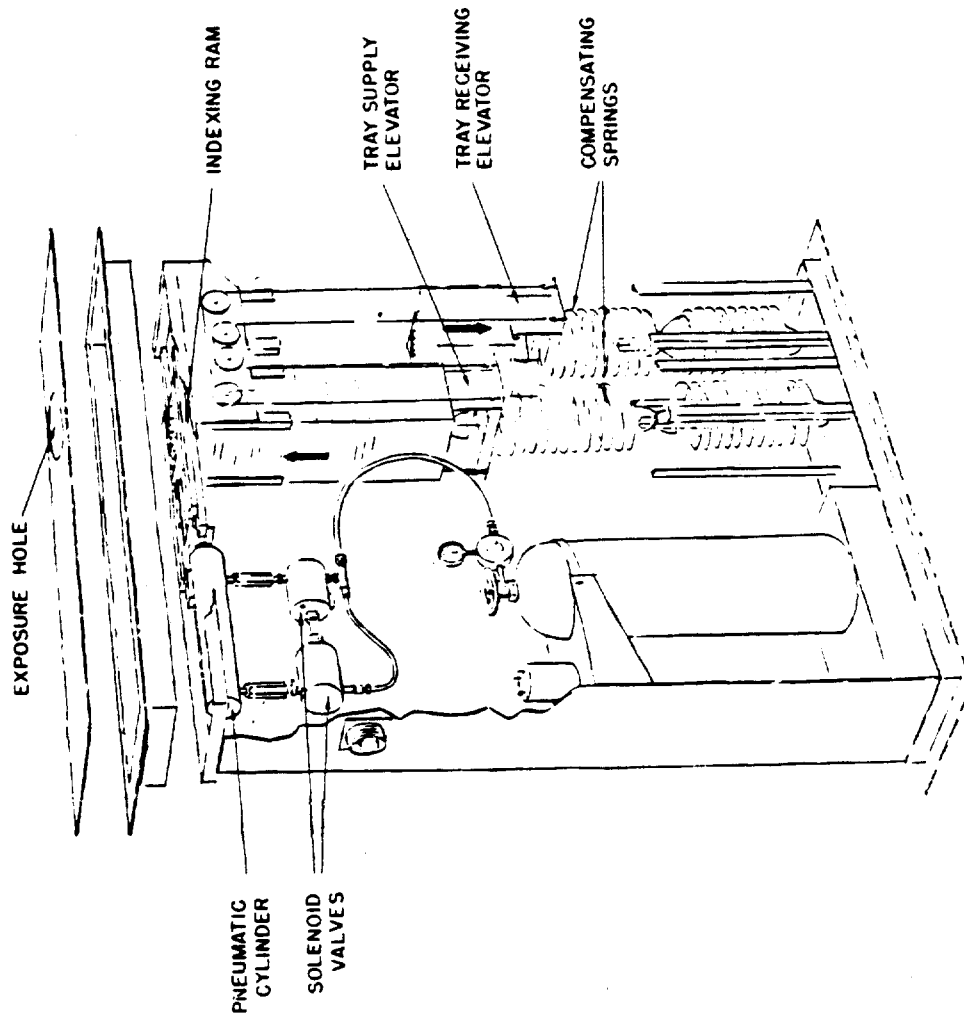
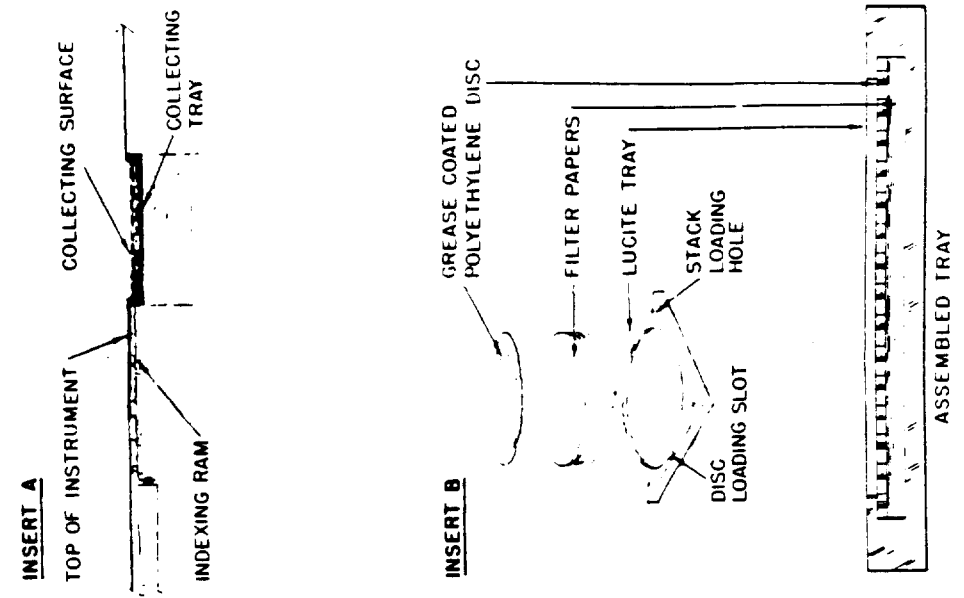


Figure 2.5 Incremental collector.

The NBS holder consists of a bakelite container with an 8.25-mm wall thickness covered with a 1.07-mm layer of tin and a 0.3-mm layer of lead. The thickness of the bakelite was experimentally determined to produce electron equilibrium (Reference 49). The lead and tin layers act as filters, which suppress lower energy components sufficiently to obtain a linear response similar to the GTR (linear above approximately 100 kev).

In the energy range from 115 kev to 2 Mev, this film pack is considered accurate to  $\pm 20$  percent (References 63 and 64) for the film emulsions tested. Two of the five emulsions (Dupont 834 and 1290) had not been extensively tested, but were expected to fall within the same range of accuracy. Two film packets were placed inside the NBS holder, one packet containing Dupont emulsions 502, 834, and 1290, which provided a combined range of 0.2 to 2,000 r, and a second containing Eastman emulsions SO-112 and 548-0 dc, which provided a combined range of 10 to 100,000 r. Latent image fading was counteracted by making film calibration runs at shot time for each shot.

Approximately 20 of the film packs described were placed in holders 3 feet above the deck aboard each of the target ships (Figures 1.12 through 1.14).

One film pack was taped to each coracle tripod at a height of 3 feet; another was mounted in an 8-inch-diameter Styrafoam float identical to that used on the FFP's and streamed 10 feet behind each coracle (Figure 1.2).

The remainder of the film packs were placed in the array as either anchored or free-floating FFP's (Figure 2.6). The FFP's were of three different types, all of which represented minor modifications of the same basic design. In all types, an 8-inch-diameter Styrafoam float 2 inches thick and faced with two sheets of 10-gage aluminum held the pack. This small float was designed so that the film pack was supported horizontally just at the water surface and was connected by means of a 10-foot wire to a second 3-foot-square Styrafoam float, called the FFP identifier, whose sole purpose was to aid aerial spotting and identification.

This basic unit was variously modified as follows: (1) a free-floating type, in which a standard 2.5-foot canvas drogue was attached to the identifier by 50 feet of line; (2) a self-anchoring type, in which a 2.5-pound Danforth anchor was attached to the identifier by means of a ball of light twine mounted in a cardboard ice-cream carton to prevent fouling as the line payed out; and (3) a second anchored type, requiring installation by a surface craft in which the same 2.5-pound Danforth was used with  $\frac{5}{32}$ -inch cable. Both the free-floating and the self-anchoring types were rigged so that they could be dropped from aircraft. All components were gathered into a compact package, which was firmly held together by a string harness containing a soluble link. Within 30 seconds after striking the water, this soluble link dissolved, thus releasing the harness and allowing either the anchor to drop or the drogue to set itself. The FFP's were specifically designed to keep unit cost to a minimum (approximately \$30.00 each).

**2.2.6 Supplementary Fallout Collectors.** A number of supplementary collectors were used at a few locations in the target array. These collectors included an OCC, an AOC, an AFI, and an FS.

The OCC and the AOC are briefly described together, since the latter is simply a mounted collection tray of the former. Both devices have been fully described in previous reports (Reference 33). In essence, the OCC is a large splashproof box, 27 by 53 inches by 5 inches high, weighing approximately 100 pounds and possessing a sliding lid (Figures 1.15, 1.16, and 2.7). The instrument is designed to withstand peak air pressures of 3.5 psi and will open with a 200-pound weight placed on the sliding lid. The sliding lid is moved on a roller track by a pneumatic cylinder using air at 60 psi and actuated by solenoid valves upon receipt of a signal. When sampling, the collecting tray is raised  $\frac{1}{2}$  inch above the top of the collector to reduce shadow bias. The device was actuated by a signal from the platform control box and remained in the open position until receipt of a closing signal.

The aluminum collecting tray is approximately 18 by 21 inches by 2 inches deep, weighs 6 pounds empty, and is used both in the OCC and as an AOC. The tray was lined with a preformed polyethylene liner and contained an insert consisting of four sections of aluminum hexcell coated

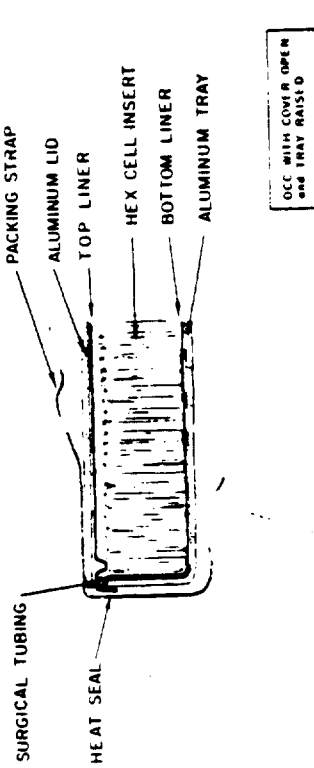
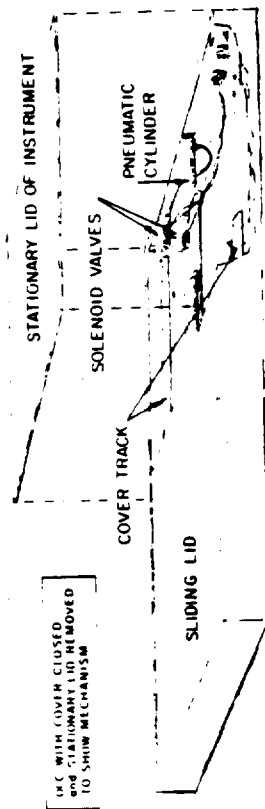


Figure 2.7 Open-close collector.

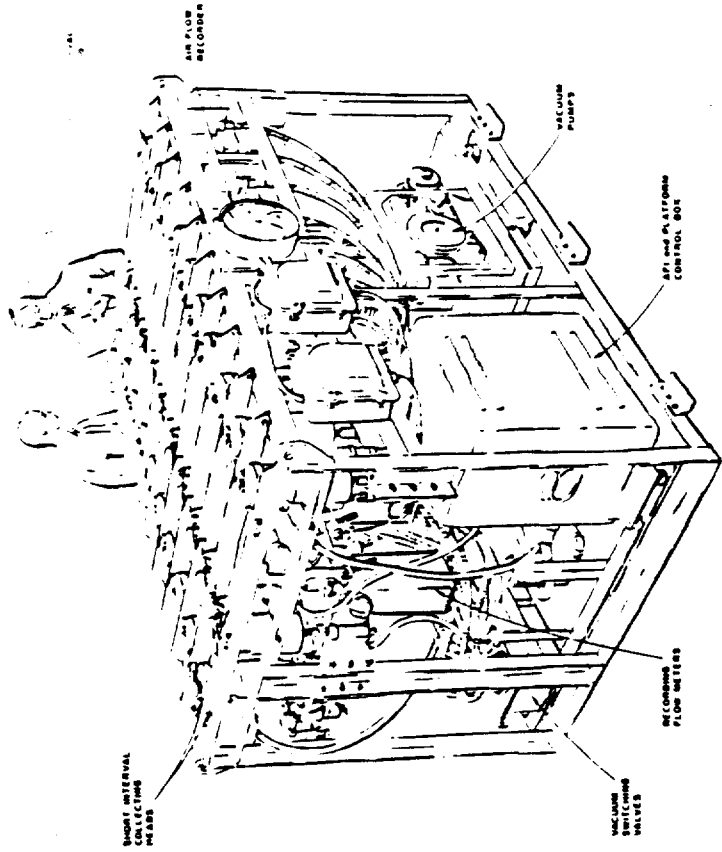


Figure 2.8 Air filtration instrument.

with Number 100 black Epo-lux. The hexcell inserts were used to prevent collected material from being subsequently swept out by winds and were black to aid in the location of individual fallout particles, the majority of which were expected to be light in color. The hexcell was coated, and the aluminum tray was lined to obtain chemically inert surfaces from which the fallout material could be easily removed. Upon recovery, the trays were closed with a preformed polyethylene lid over which was placed an aluminum cover; the whole assembly was then temporarily sealed by means of a gasket of surgical tubing, which was compressed by external pressure maintained by two cloth cinches (Figure 2.7). The polyethylene liner and lid were later permanently heat-sealed together. With an aluminum cover banded to the tray, the sealed assembly could maintain internal pressures of 7 psi indefinitely.

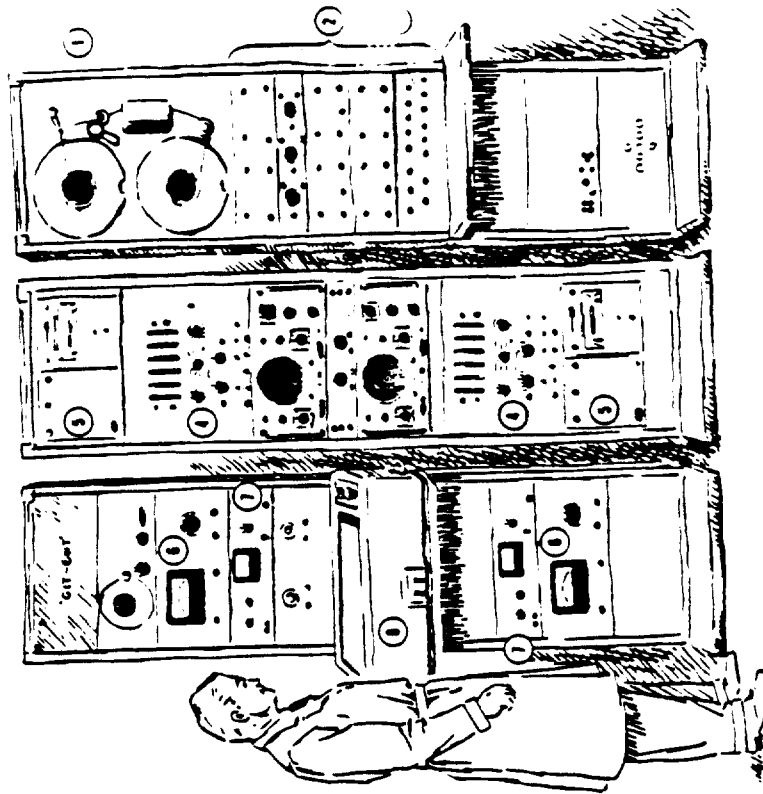
The AFI was installed on the instrument platform aboard the DD-592 (Figures 1.16 and 2.8). The present model represents the redesign of an instrument used during Operation Redwing (Reference 33). The original design was modified to obtain a more complete series of fallout and base surge samples. The instrument used a series of chemical filters so designed that any large amounts of water arriving with fallout would be immediately removed from the solid material and stored in a separate water reservoir (Figure 2.9). Dimethylterephthalate (DMT), recrystallized into its acicular form, was used as the filter material (Reference 65). Such a filter had been determined to have a high efficiency for 0.3-micron-diameter particles and permitted later recovery of solids by sublimation. The filter head is  $3\frac{3}{4}$  inches in diameter (inside diameter, 3.55 inches), uses a  $\frac{3}{8}$ -inch filter bed of DMT crystals, and is known to withstand very heavy rains (50 in/hr) without plugging or loss of efficiency. The filter also is so designed that both the solid and the liquid fractions, together with all surfaces contacted, can be shipped as a single sealed package (Figure 2.9).

Mechanically, the AFI can be considered as an assemblage of the following units: the filter heads and the filter-head-raising mechanisms, the pneumatic system, the vacuum pumps, the vacuum switching valves, the recording flow meters, and the control box. The instrument has a series of 30 filter heads, each covered when not actually sampling, and each raised above the level of the other heads when drawing a sample. All heads sample vertically at a constant rate of 10 ft<sup>3</sup>/min. One series of 10 heads sampled in numerical sequence for intervals of 10 minutes each, the entire sequence being started at zero time by the control box. A second series of 20 heads sampled in numerical sequence for intervals of 2 minutes each, the entire sequence being triggered by a preset increase in background.

Flow through the filters is maintained by a pair of constant-flow vacuum pumps, which have a line-vacuum-sensing control valve to compensate for increases in pressure drop across the filter due to filter loading. By means of the vacuum-switching valves, this controlled vacuum is applied only to the chamber containing the water reservoir of the filter actually sampling, thus minimizing vacuum evaporation of the water fraction. A pair of recording Flow-rators are incorporated into the vacuum lines of both the short and the long interval filters. The AFI control box governed and recorded the filtering sequences and the other instruments on the DD-592 platform. The activities of all platform instruments including the AFI flow rates were automatically recorded by the AFI control box, so that all samples collected could be correlated in time. The AFI control box was in turn activated by EG&G radio signals received at minus 5 minutes, minus 1 minute and minus 5 seconds.

The FS's were installed at various locations aboard barges or on islands and were specifically designed for very early recovery. They simply consisted of a large polyethylene funnel (2.6-ft<sup>2</sup> collecting area), which was fitted into a 2-gallon polyethylene bottle. The bottles were mounted on top of a 10-foot pipe stand in a special bracket that permitted helicopter recovery. Helicopter pickup was effected by snagging a 2-foot diameter sphere made of two hoops welded at right angles. The bottles were set in the previously installed stands just prior to shot time so that the collection of extraneous material before the shot would be reduced to a minimum.

**2.2.7 Instrument Control.** All project instrumentation was activated upon receipt of an EG&G radio signal at the instrument control box (ICB). This control box, designed for installation aboard the coracles, started both the standard and the underwater GTR's, provided



- ① FOUR-SPEED, THREE-CHANNEL TAPE TRANSPORT
- ② AMPLIFIERS
- ③ PULSE SHAPERS AND DISCRIMINATORS
- ④ ELECTRONIC COUNTERS
- ⑤ PRINTER-ANALOG CONVERSION UNIT
- ⑥ DC AMPLIFIER
- ⑦ LOG CONVERTER
- ⑧ X-Y RECORDER

Figure 2.10 GITOUT equipment.

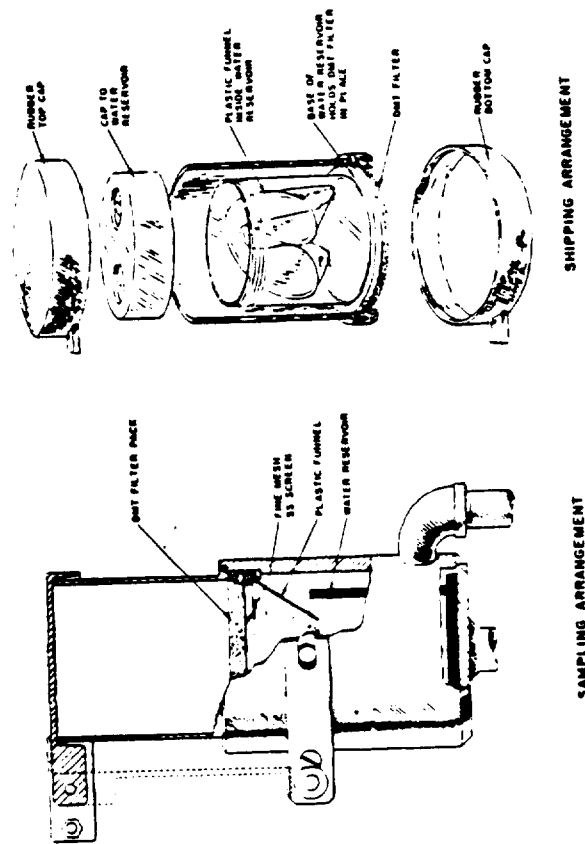


Figure 2.9 Relative positions of components in AFI sampling head.

power and control pulses for the IC, timed and actuated the dropping mechanism for the underwater detector, and recorded receipt of test signals on a series of mechanical registers that could be read from a small boat alongside the coracle.

The ICB's contain their own power supply, are packaged in vaporproof Plexiglass cases 10½ by 14½ by 12 inches high, and weigh about 15 pounds. The ICB's receive the minus-5-minute, minus-1-minute, and minus-5-second signals and are designed for a closed-contact signal of not less than ½-second duration. The units have a reset button, which disarms all latched components and returns all timing devices to their zero position. A cross-reference time mark is obtained by blanking the timing pulses on both the standard and the underwater GTR tapes upon receipt of a minus-1-minute signal and by reinstating these timing pulses upon receipt of a minus-5-second signal. By this means, the IC and all GTR records could be correlated in time. This time-blanking circuit had a backup feature that restored the timing pulses automatically after 60 seconds in the event of failure of the minus-5-second signal.

Although the ICB register system worked as designed, it could be used only if there were regularly scheduled timing signal runs. The fact that EG&G sent many hand signals on demand between the scheduled timing runs rendered the register system entirely useless. After the accidental radio signal before Shot Wahoo, the project cannibalized the control box register and installed a dead-safe switch arrangement with its own batteries and arming light in the old register housing. This switch completely deactivated the entire coracle system, regardless of any signals received by the EG&G radio trigger. The coracle was armed by pulling a lanyard connected to this switch. This modification gave the project partial protection against accidental firing of the coracle stations; however, if a signal was on the EG&G radio or if any of the EG&G relays had been closed by jarring, the coracle would fire when the dead-safe switch was thrown. Three such accidental firings did occur on the final arming run for Umbrella.

**2.2.8 GTR Tape Readout.** The GTR tape readout (GITOUT) was an electronic readout device developed at NRDL for converting radiation pulses (Appendix F) on the recorded tapes into dose rate information (Figure 2.10). The GITOUT employed digital techniques with a digital-to-analog conversion near the end of the system to give an x-y presentation of time versus data on graph paper. The system (Figure 2.11) was composed of commercially available components so that no electronic development was required. The instrument is more fully described in Reference 66.

Tapes are placed in the tape transport and are played at a speed depending upon the field resolving-time desired. The information from the timing channel and from one of the radiation channels is read off the tape and shaped into square-wave pulses. The timing pulses are sent to a time counter, where they are accumulated and converted by an associated printer to an analog voltage which, in turn, drives the x axis of the plotter. Radiation pulses are sampled by the other counter at a rate determined by the timing pulses. This counter either accumulates the pulses or resets itself after each time increment, depending upon whether total dose or dose rate is required. The data counter controls a second printer, which also converts the radiation pulse count into an analog voltage to drive the y axis of the plotter. Log converters can be inserted between the printers and the x-y plotter to give a log-log or semilog presentation of the data versus time. A digital record of the information can also be obtained directly from the printers.

### 2.3 SPECIAL OPERATIONS

Although only a support activity, the maintenance of fixed coracle stations in deep water represented a major operational problem. Since the installation of deep moors on the steep slopes of coral atolls may be again required, a brief description of the specially adapted moor employed by the project is given here. Deep-anchoring techniques, developed at SIO (Reference 67), had been used on a small scale during Operations Ivy and Wigwam but were first used extensively during Operation Redwing where 13 deep-anchored positions were maintained in depth.

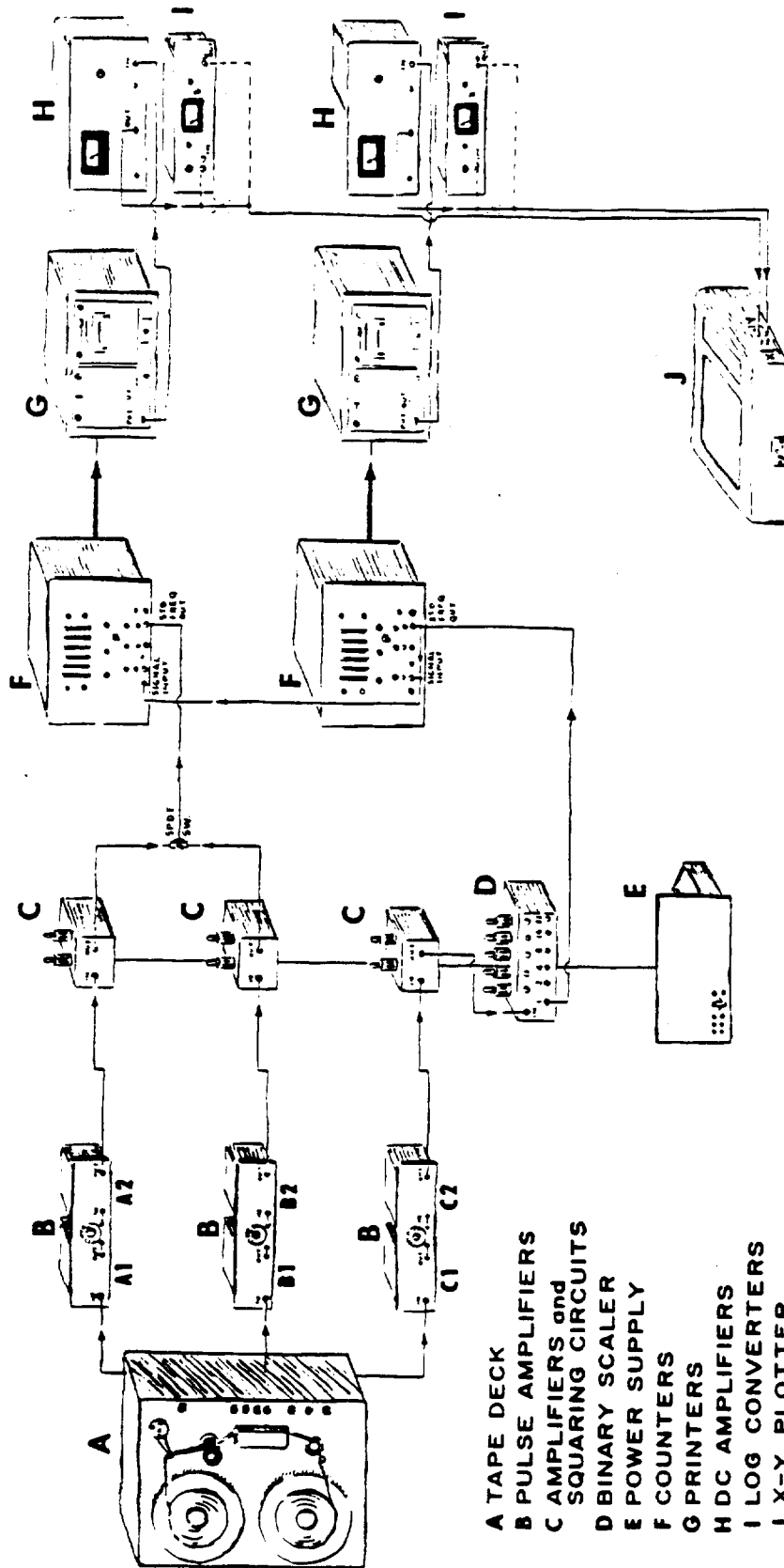


Figure 2.11 Elements of CITOOUT system.

up to 100 fathoms for about 2 months (Reference 33). The operational and theoretical aspects of deep mooring have been set forth by SIO in its report on Operation Redwing activities (Reference 34). However, the anchoring problem as it existed for Redwing was complicated in this operation by the stringent limitations on accuracy of placement, by the fact that mooring had to be effected on steep bottom slopes (Table 1.1), and by the increased horizontal drag forces due to the larger sail area of the coracles.

Although errors in placement as large as  $\pm 1/2$  nautical mile could be tolerated on past operations, a consideration of predicted radiation fields (Reference 22) and cloud diameters (Reference 17) for Operation Hardtack indicated that on each event approximately 70 percent of the total coracle array had to be more accurately located. Despite operational limitations on the accuracy of placement, the project attempted to keep the placement error within  $\pm 300$  feet, an error representing nearly half the predicted distance between upwind and crosswind isodose contours (Appendix F) differing by one order of magnitude. Other factors requiring high accuracy of placement were the estimated arrival time of the base surge, which influenced the dropping time of the underwater detectors, and the predicted magnitude of underwater snock (References 23 and 68 through 70).

Consequently, the nominal positions shown in Table 1.1 were intended to represent the actual position of the coracle relative to surface zero, and not the point of contact of the moor with the bottom. Therefore, the excursion of the subsurface floats was calculated, using experimentally determined currents for the area in question, and the probable position of the coracle relative to the subsurface float was estimated from known coracle parameters. The most desirable point of bottom contact was thus estimated and used in the installation of the deep moors.

**2.3.1 Calculation of the Deep Moor.** Briefly, the basic principle of deep anchoring is the reduction of the horizontal excursion of the moored element by the application of vertical tension to the mooring cable. Cable tension is obtained by means of a submerged float placed so that the orbital motion is less than 1 percent of the surface waves.

The buoyancy of this float is adjusted so that maximum cable tension is obtained without reducing the net reaction of the anchor with the bottom below the total horizontal drag forces for the complete system. Buoyant mooring lines are used above the subsurface float to damp periodic motion due to surface waves and to reduce abrasion at the junction with the surface element. The entire system is determined by a series of graphical approximations, and the exact excursion of the submerged float is determined by iterative vector addition from the bottom to the surface.

All proposed deep moors for Hardtack were therefore calculated using known coracle characteristics and the following regional information:

1. **Bottom:** On the ocean side of Eniwetok Atoll, the steeper portions of the atoll slope are hard, barren, coralline ridges whereas the flat plateau extending southwest is thinly covered to a depth of about  $2\frac{1}{2}$  feet with coral sand and debris interrupted by occasional large coral blocks fallen from the atoll slope (Reference 71). Neither surface affords sufficient loose bottom material for a Danforth anchor to develop maximum holding power. The coralline ridges run at right angles to the normal direction of wind and current in the region; however; thus, considerable holding power due to fouling was expected. The lagoon bottom was assumed to be the usual thick covering of foraminiferal debris dotted with occasional coral heads.

2. **Currents:** Normal surface currents in the area were assumed to be 1 knot in the Wahoo target area and 0.4 knot in the Umbrella target area (Reference 53). The idealized subsurface currents used are given in Table 2.2. Tidal currents were not considered in the calculations, since all proposed mooring sites were sufficiently distant from the shoreline.

3. **Wind and Waves:** Surface winds of 15 to 25 knots are considered normal to both target areas at the time of the proposed shot schedule. Ocean waves in the lee of Eniwetok Atoll were expected to range between 3 and 8 feet in height with periods from 2 to 9 seconds (Reference 53). Long swells reaching the atoll from southern winter storms were not considered important. Wave conditions within the lagoon were expected to be worse because of a short chop with heights

TABLE 2.2 ASSUMED SUBSURFACE CURRENTS SOUTHWEST OF ENIWEKOK ATOLL

Derived from the SIO survey of 1956.

Depth ft	Current ft/sec
0 to 150	1.69
150 to 300	1.39
300 to 450	1.15
450 to 600	0.92
600 to 750	0.73
750 to 900	0.65
900 to 1,050	0.57
1,050 to 1,200	0.45
1,200 to 1,350	0.42
1,350 to 1,500	0.35
1,500 to 1,650	0.27
Below 1,650	0.20

TABLE 2.3 ESTIMATED DRAG FORCES ON CORACLE STATION AND ON DEEP MOORING COMPONENTS

	Coracle Station				Deep Mooring Components (1,200 fathoms)					
	Water Drag (1-knot current)	Wind Drag			Cable (Snuckles and clamps incl.) Diameter Drag		Submerged Float Diameter Drag		Nylon Line (1/2-inch diameter) Drag	Surface Float (5- by 9-inch plastic) Drag
		lb	15-knot wind	20-knot wind	35-knot wind	in	lb	ft	lb	lb
Minimum	0.23	1.3	2.0	3.2	1/8	12.9	2.6	2.0	14.7*	2.5 each*
Maximum	30	26	45	76	3/32	15.6	2.9	2.3	14.7*	2.5 each*
					3/16	18.2	3.0	2.7	14.7*	2.5 each*

\* Estimated total drag for buoyant line with five floats and disconnect linkages = 29.2 pounds.

TABLE 2.4 ESTIMATED EXCURSION AND DEPRESSION OF 1,200-FATHOM MOOR

Cable Diameter	Submerged Float Diameter	Gross Buoyancy of Float	Net Buoyancy of Float	Cable Tension at Anchor	Excursion		Depression	
					Minimum	Maximum	Minimum	Maximum
					ft	ft	ft	ft
1/8	2.6	587	487	284	600	2,500	28	475
1/8	2.8	733	633	430	450	1,800	14	200
1/8	3.0	900	800	598	350	1,400	9	125
5/32	2.6	587	487	148	975	3,125	78	750
5/32	2.8	733	633	306	625	2,225	45	350
5/32	3.0	900	800	474	450	1,625	21	225
3/16	2.6	587	487	59	1,950	4,800	425	1,775
3/16	2.8	733	633	205	900	2,800	125	650
3/16	3.0	900	800	373	600	1,900	90	325

TABLE 2.5 ESTIMATED EXCURSION AND DEPRESSION OF 400-FATHOM MOOR

Cable Diameter	Submerged Float Diameter	Gross Buoyancy of Float	Net Buoyancy of Float	Cable Tension at Anchor	Excursion		Depression	
					Minimum	Maximum	Minimum	Maximum
					ft	ft	ft	ft
1/8	2.6	587	487	396	250	750	14	87
1/8	2.8	733	633	344	150	525	5	66
1/8	3.0	900	800	712	125	400	3	34
5/32	2.6	587	487	365	200	775	10	129
5/32	2.8	733	633	511	175	550	5	74
5/32	3.0	900	800	679	150	450	3	42
3/16	2.6	587	487	330	250	800	12	136
3/16	2.8	733	633	476	175	600	10	73
3/16	3.0	900	800	644	125	425	6	33

to 6 feet. The most severe waves expected were those generated by the underwater detonations themselves. The forces on the moor from these waves were calculated, using the wave heights and velocities estimated in Reference 21.

The required depth for the subsurface float was determined by calculating the orbital motion of normal surface waves at depth using the formulas (Reference 72):

$$H_d = H_o e^{-(2\pi d/L)}$$

and

$$L = \frac{g}{2\pi} T^2$$

where  $H_d$  is the diameter of the orbit at depth  $d$ ;  $H_o$  is the height of the surface wave from trough to crest;  $L$  is the length of the wave from crest to crest;  $g$  is the acceleration of gravity; and  $T$  is the period of the wave. Thus, for periods of 2 and 9 seconds, the depth at which the orbital motion is 1 percent of surface is approximately 60 and 300 feet, respectively. A depth of 150 feet for the subsurface float was selected as the best compromise between expected extremes. Although the hydrostatic pressure at this depth is relatively insignificant, calculated overpressure due to the detonation required that close-in subsurface floats be capable of withstanding pressures of about 2,000 psi. The maximum capability of the floats finally used in these locations was calculated to be 1,450 psi, using a modified Timoshenko formula. This strength proved sufficient.

To maintain a deep moor on either a sloping or a flat bottom, the weight of the anchor used by SIO (Reference 55) was doubled. The maximum horizontal force  $F_H$  that can be sustained by the deep moor may be expressed as a function of the anchor weight in air  $W$ , as follows:

$$F_H = (bW - T) \cos \theta (f \cos \theta - \sin \theta)$$

where  $b$  is the buoyancy factor characteristic of the anchor material;  $T$  is the vertical component of tension in the mooring cable;  $\theta$  is the angle of the bottom; and  $f$  is the coefficient of friction. Assuming an angle of friction of  $45^\circ$ , this maximum force was calculated for iron and concrete weights on a number of bottom slopes (Figure 2.12). At the cable tensions and anchor weights used (tension approximately 500 pounds, anchor weight approximately 1,500 pounds in air), the difference in density between iron and concrete permits a smaller weight of iron to be used for a given bottom reaction. Furthermore, the compact shapes obtainable with iron weights permit greater lowering speeds.

Both minimum and maximum values for wind and water drag forces were calculated for the coracle. The maximum case for water was calculated, using the profile drag coefficient for a flat disk whose diameter was equivalent to the coracle diameter at the waterline, and the profile drag coefficient for a flat plate was used in calculating the maximum case for air. These maximum and minimum drag forces on the coracle, presented in Table 2.3, bracket those actually observed for the winds or currents encountered (Figure 2.13). Similarly, the expected drag forces on various possible mooring components were calculated for the assumed surface and subsurface currents and are also summarized in Table 2.3. The maximum and minimum excursions were then determined for a number of possible moors and are tabulated, together with the approximate subsurface float depressions, in Tables 2.4 and 2.5. A safety factor greater than that employed by SIO (Reference 55) was incorporated in the specified mooring cable, since calculations showed that this increase was possible without materially altering drag forces or cable costs.

Selection of the final moor represented a compromise between various opposing factors as demonstrated for a 1,200-fathom moor in Figure 2.14. The final system is schematically represented in Figure 2.15. In brief, the specifications for the major components are from the bottom up: a bottom detecting device (SIO drawing E-834), a No. 16 grapnel, a 1,500-pound

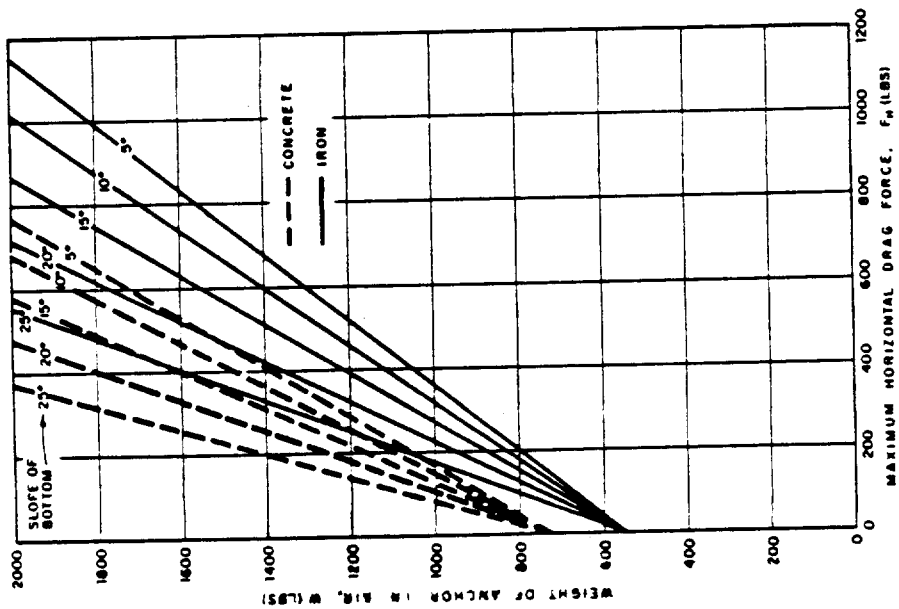


Figure 2.12 Maximum horizontal drag forces for various anchors on sloping bottoms. (Coefficient of friction assumed to be unity; tension calculated for case of 3-foot subsurface float supporting 1,200 fathoms of  $\frac{5}{32}$ -inch wire;  $b = 0.87$  for iron;  $b = 0.66$  for concrete.)

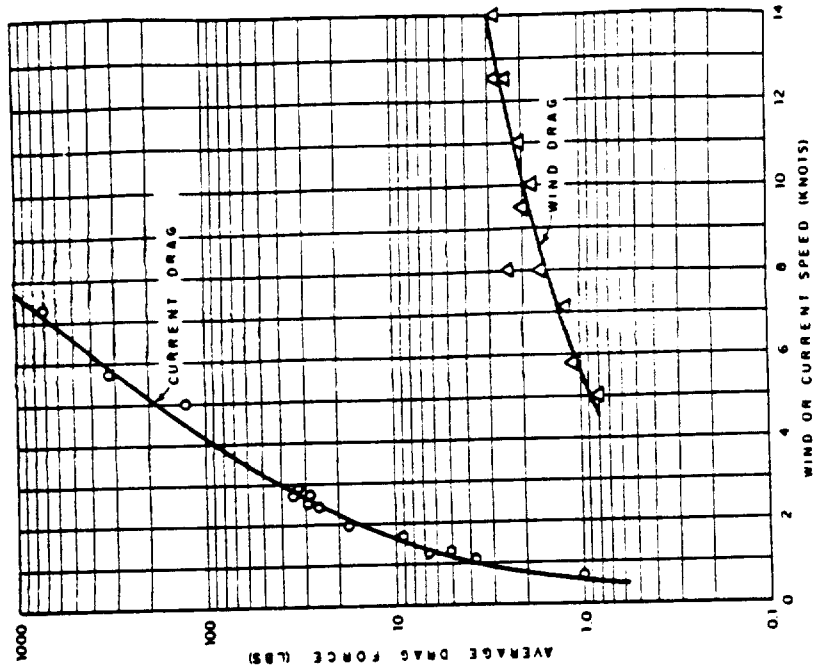


Figure 2.13 Measured coracle drag forces.

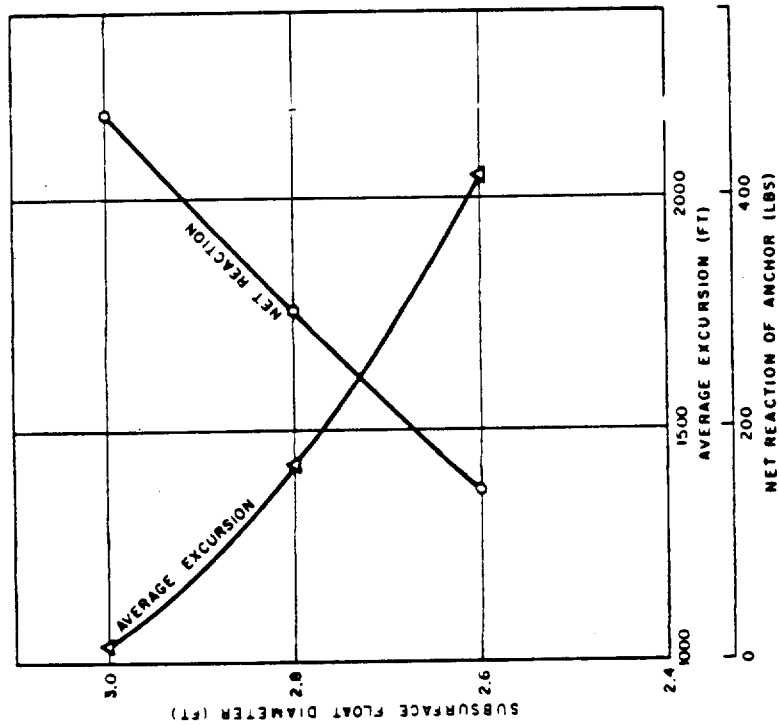


Figure 2.14 Comparison of float excursion and net reaction of anchor on the bottom as a function of subsurface float size (5/32-inch cable, 1,200-fathom moor).

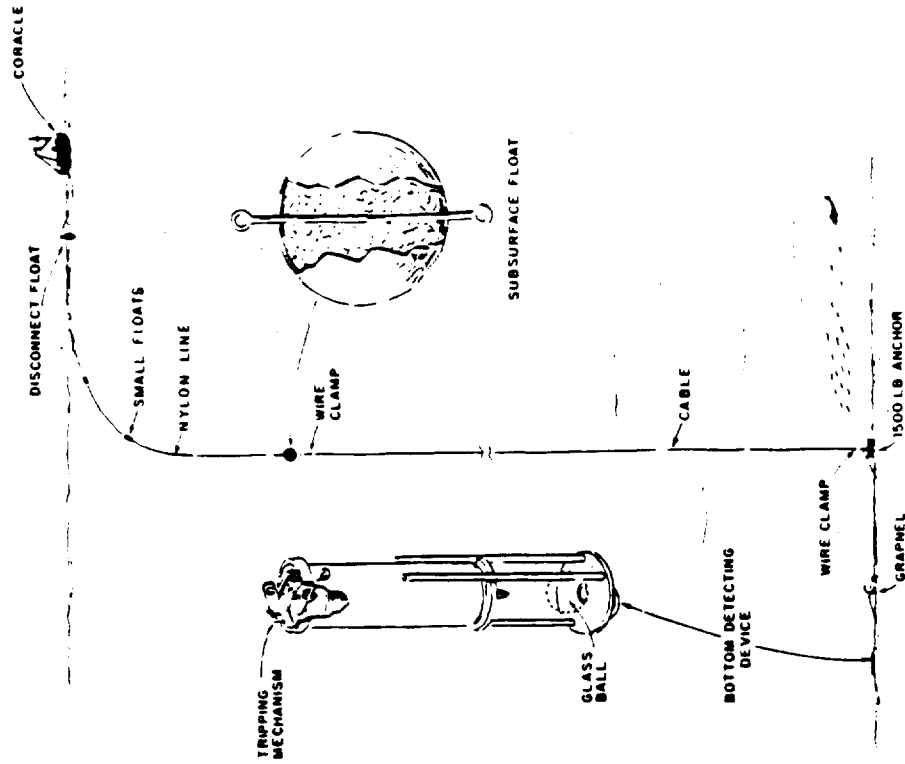


Figure 2.15 Deep-anchoring system.

anchor made of two railroad wheels, a  $1\frac{1}{2}$ -ton swivel, a wire clamp (SIO drawing A-832, X dimension = 0.144 inch with a tolerance of + 0.000 to - 0.002 inch), a length of  $\frac{5}{32}$ -inch-diameter cable determined by the depth of the moor (guaranteed ultimate tensile strength 3,300 pounds), a second wire clamp, 15 feet of  $\frac{3}{16}$ -inch-diameter wire rope, a second  $1\frac{1}{2}$ -ton swivel, a subsurface float of net buoyancy determined by the depth of moor, 300 feet of  $\frac{1}{2}$ -inch nylon line with 5- by 9-inch plastic floats as required. No attempt was made to insulate the various components of the moor electrically. The deep moor is described in greater detail in Reference 73.

Since little advantage could be gained through applying deep-anchoring techniques to the shallow anchorages required for placement of coracles within Eniwetok lagoon, all such coracles were moored to Navy Dan buoys by 150-foot pennants. This type of mooring is a standard Navy procedure requiring no special theoretical considerations. The major components of the moor from the bottom up were: a 25-pound Danforth anchor, 30 feet of  $\frac{3}{8}$ -inch chain, a 15-pound concrete clump, 5 feet of  $\frac{3}{8}$ -inch chain, a length of  $\frac{3}{8}$ -inch-diameter wire rope dependent upon depth, and a standard Navy Dan buoy.

**2.3.2 Properties and Placement of Coracles.** Operational experience with the coracles is reported in detail in Reference 73 and is, therefore, reviewed only briefly here. About an hour was required for installation of a complete deep moor, starting from the time of the ship's approach run on a desired location. Coracles could be handled over the side, using the ATF ship's boom if proper precautions were taken to protect the coracle from swinging against the side. The accuracy of coracle placement was principally limited by the accuracy of the ship's navigating equipment at short range. For Wahoo, the placement accuracy for stations within 10,000 feet of surface zero was approximately  $\pm 300$  feet. Stations beyond 10,000 feet could be placed within an ellipse with a 600-foot minor axis and a 1,000-foot major axis parallel to the downwind leg of the array. The observed coracle excursions were within the calculated limits. No variation with tide was discernible. The direction and extent of the observed excursions, however, appeared entirely random; therefore, recalculation of the point of contact with the bottom to effect more accurate station positioning was not possible. For Umbrella, an accuracy of  $\pm 200$  feet was obtained for all positions.

The coracle locations reported in Table 2.1 and plotted in various figures throughout this report were determined from an analysis of photomosaic maps made at approximately H-1 hour and H+1 hour for Wahoo and by means of a series of pre- and postshot radar fixes for Umbrella. Although 11 coracles for Shot Wahoo were found drifting, their positions during the time of principal interest did not change more than about 300 feet. The drift rates for coracles dragging their moors may be estimated from Wahoo recovery data presented in Table 2.6 and the observed drift rates presented in Figure 2.16. Estimated positions for drifting coracles are plotted for the first 6 hours after zero time in Figures 2.1 and 2.2.

During Shot Wahoo, roughly 70 percent of the deep moors failed. Of the 20 moors in position at the time of detonation (2 were without coracles), only 7 at the more distant locations survived. The relatively slow drift rates observed indicated that most of these coracles were dragging the greater portion of their mooring cable; therefore, it was presumed that failure occurred near the bottom. At no time was there any evidence of dragging anchors. Because of limitations on time, only one broken moor (DL 12.0) was completely recovered. Inspection of the cable revealed a pure tension break at a depth of 5,000 feet with no sign of kinking, corrosion, or abrasion. Failure of the moor at DL 18.3 was undoubtedly caused by damage incurred prior to the shot, during a collision with one of the target vessels as it was being towed into its final position. The reasons for failure of the remaining moors cannot be precisely determined because of the lack of detailed information. Strain on the cable due to waves or submarine avalanches caused by the detonation do not appear sufficient to have caused failure. At locations closer than 3,500 feet, the violent upwelling of water after the detonation may have created radial currents along the surface of sufficient magnitude to cause failure. The drag due to the coracle alone in a current of 10 knots would be 3,500 pounds. However, on

TABLE 2.6 CORACLE RECOVERY DATA, SHOT WAHOO

Nominal Position	Position at Recovery		Recovery Time	Estimated Time of Failure		Remarks
	Bearing From Surface Zero	Distance From Surface Zero		Wire	Pennant	
	deg (true)			date time	date time	
U 3.2	Alongside EC-2		17 1501	16 1330	-	Arrived at EC-2 approximately D - 1½ hours
U 4.5	257	9 n. mi.	17 1225	16 1330	17 0300	
CL 3.9	246	5½ n. mi.	17 1440	16 1330	-	
CL 4.6	151½	4,600 ft	17 1604	-	-	
DL 7.1	232	7,100 ft	17 1617	-	-	
DL 12.0	240	7 n. mi.	17 1403	16 1330	-	
DL 15.3	253	15 n. mi.	17 1105	-	16 2130	Failure due to collision with TG 7.3 vessel on D-1 day
D 9.0	256	4½ n. mi.	17 1635	16 1330	-	Hung up near bow of DD-593 for approximately 10½ hours
D 23.1	249	23,100 ft	17 1418	-	-	
DR 4.5	256	24½ n. mi.	17 1135	16 1330	16 1530	
DR 9.0	Alongside YC-9		17 1400	16 1330	-	Arrived at YC-9 no earlier than D - 4 hours
DR 14.4	265	14,400 ft	17 1420	-	-	
DR 24.0	263	24,000 ft	17 1530	-	-	
DRR 6.8	Alongside YC-9		17 1400	16 1330	-	Arrived at YC-9 no earlier than D - 8 hours
DRR 12.8	276	12,800 ft	17 1405	-	-	
CR 4.1	286½	7,600 ft	17 1425	16 2140	-	
CR 5.2	332	5,100 ft	17 1501	-	-	
CR 6.4	291	13,600 ft	16 1836	16 1330	16 1730	

TABLE 2.7 TIME OF ARRIVAL OF DEVICE-GENERATED WATER WAVES AT STATIONS

Calculated from Reference 74. Underlined times indicate the highest wave when given. (D) = a drifting coracle. (CO 1.1 min) = an overturned coracle with estimated time of overturn. When no GTR record was obtained this estimate cannot be made.

Nominal Position	Time of Arrival (secs)				Remarks
	First Wave	Second Wave	Third Wave	Fourth Wave	
Wahoo:					
U 3.2	48	70	91	109	(D)
U 4.5	55	80	103	121	(D)
CL 3.9	52	75	97	114	(D)
CL 4.6	55	81	104	122	
DL 7.1	69	102	129	150	
D 8.0	74	109	137	160	(D)
DR 4.5	55	90	103	121	(D)
DR 9.0	79	118	147	171	(D)
DRR 6.8	67	100	125	147	(D)
CR 4.1	53	77	99	116	(D, CO 1.1 min)
CR 5.2	59	87	111	130	
CR 6.4	65	96	122	142	(D)
Umbrella:					
U 1.8	<u>29</u>	55	80		(CO 1.5 min)
U 2.7	<u>41</u>	68	91		
U 3.9	58	93	107		
CL 3.1	<u>44</u>	70	95		(CO 1.5 min)
CL 4.0	56	83	107		
CL 6.0	86	108	131		
DL 6.2	93	113	137		
D 2.7	<u>41</u>	76	92		(CO 2.4 min)
D 4.8	65	89	112		(CO 1.5 min)
D 6.5	93	113	137		
DR 4.5	65	89	112		(CO 1.0 min)
DR 7.5	93	113	137		
DRR 3.9	58	83	107		(CO 2.5 min)
DRR 6.7	93	113	137		
CR 2.7	<u>44</u>	70	95		(CO 2, no GTR)
CR 4.9	58	83	107		
CR 6.6	96	108	131		

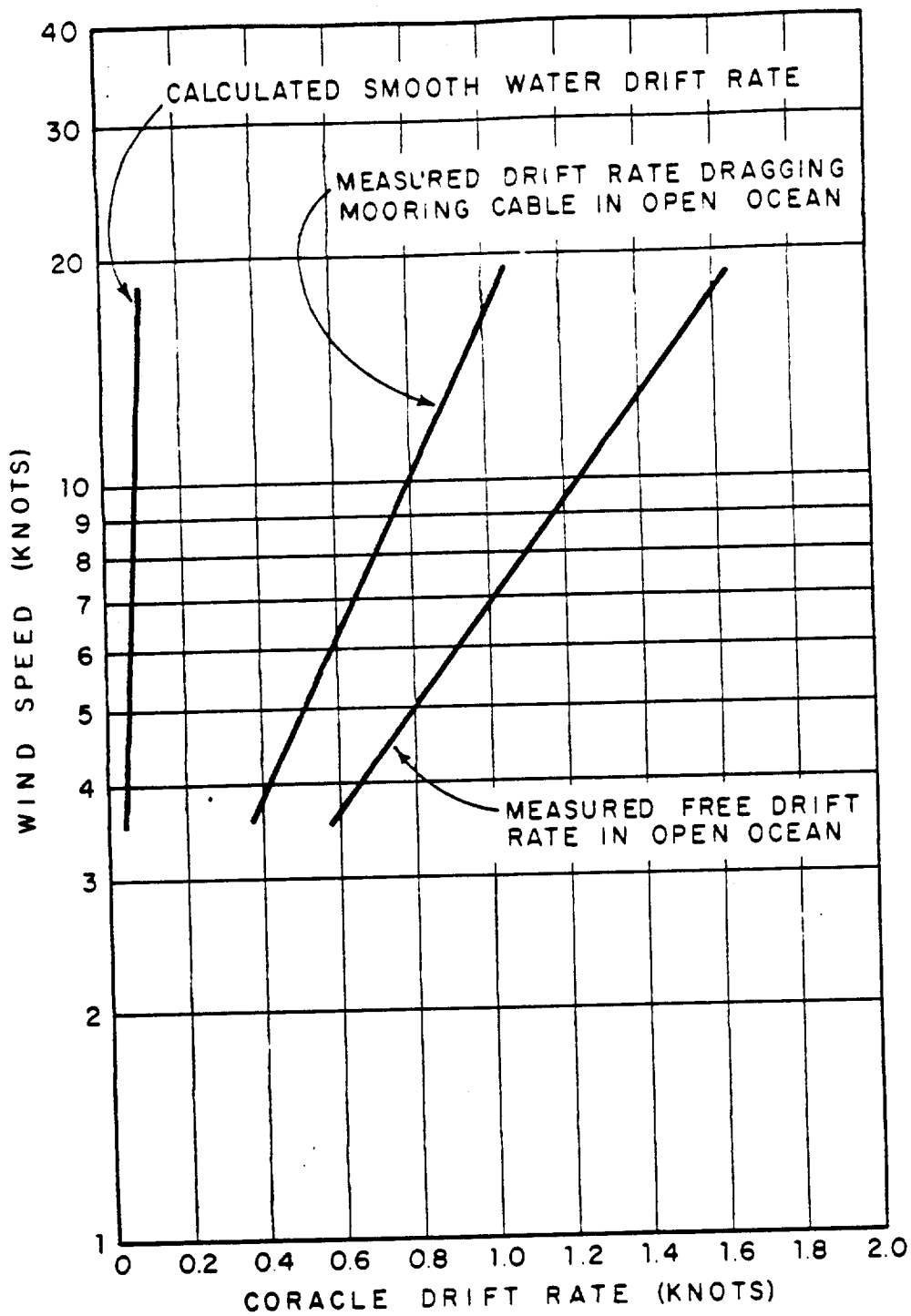


Figure 2.16 Coracle drift rates.

the basis of available photographic information, these surface currents cannot even be extended to the closest coracles. Although the reason remains unknown, failures under similar conditions in the future can probably be prevented by using heavier mooring cable; cable diameters as large as  $\frac{1}{4}$  inch can be used without greatly increasing horizontal drag forces.

During Shot Umbrella, none of the moors failed; however, seven of the close-in coracles overturned shortly after zero time. The precise reason for capsizing also remains a subject for speculation. Device-generated water waves do not appear sufficient as a single agent. The force on a coracle in a horizontal attitude, due to the 100-knot water-laden winds observed near surface zero, was estimated to be about 160 pounds. Increasing the water burden from an assumed 3 to 100 gm/ft<sup>3</sup> of air and increasing the sail area to that of a coracle rolled 30° to the horizontal raises this force to about 680 pounds. A force of this magnitude, if properly applied, is capable of overturning a coracle. Without experimental measurements of metacentric shift at high angles of inclination, a precise approach to this problem is not possible. It seems unlikely, however, that the proper conditions for coracle overturn due to base surge forces alone could have been reached. Perhaps, such base surge forces operating in conjunction with the turbulent water conditions existing inside the foam ring could have been sufficient for capsizing.

If, in spite of the previous discussion, device-generated water waves are assumed to be the reason for capsizing, their arrival times at the closer project stations have been calculated using data presented by SIO in Reference 74 and are given in Table 2.7 for comparison with the estimated time of overturn. Sometimes the time of overturn may be estimated from the GTR record (Section 3.3.2). In about half the cases a sharp decline in the peak dose rate is roughly coincident with the calculated arrival of the device-generated waves, but the later GTR record does not appear to be that of an overturned coracle. Sharp decreases in dose rate could also be the result of a rapidly transiting radioactive cloud. Inspection of the preliminary photographic information appears to support this latter hypothesis. The estimated times of coracle overturn have been arrived at through a careful comparison of all gamma records along a given line of radial expansion and all currently available photographic information. In any event the estimated times of overturn appear to be so late as to preclude action of base surge drag forces.

## Chapter 3

### RESULTS AND DISCUSSION

#### 3.1 GENERAL DESCRIPTION OF THE DATA

In any consideration of the results presented in this and following chapters, a number of points should be borne in mind. Because of the nature of weapon-effect tests, investigations in the field must be conducted for single shots fired at a time that may not be convenient to the individual project. This condition is not conducive to precise work, particularly in situations requiring the maintenance of numerous stations over large areas of deep water, a situation peculiar to this project. These difficulties were further augmented by the fact that little concrete information on the complex gamma fields associated with underwater nuclear detonations existed during the planning and operative stages of the project. Nevertheless, the data obtained and reported here, when taken as a whole, exhibits a degree of internal consistency that is surprising considering the conditions under which it was collected. This consistency suggests greater reliability than that indicated by the stated limits of accuracy that were established on the basis of maximum possible experimental error.

Since, however, so little is currently known about gamma fields associated with underwater nuclear detonations, some data that might otherwise have been omitted has been purposely included. To interpret such data, the treatment has in some instances been carried beyond that warranted by statistical reliability. Special corrections have been applied, and certain portions have been emphasized on the basis of an intimate knowledge of conditions existing in the field. This extended treatment is based on the assumption that an estimate by persons completely familiar with the project is better than no information whatever. In all such cases, the uncertainties and assumptions are fully stated in the body of the report. The unmodified data is presented in Appendix D.

It should be reiterated that in most instances the data contained in this report is considered sufficient and presents a consistent and logical picture of both shots. All material contained in this report was obtained at fixed locations within the specific radiological environments generated by the two underwater nuclear detonations documented; therefore, its extension to other devices and particularly to moving objects must be performed with special caution.

During Shot Wahoo, the project recovered an estimated 60 percent of the maximum possible coracle data. This general index of success was arrived at by weighting each instrument according to the relative importance of the data it obtained. Using the same arbitrary system of evaluation, the project also recovered about 60 percent of the maximum possible data from the target ships. These low figures are primarily due to the accidental firing of all coracles on D-1 day, to the limited number of FFP's recovered, and to a power failure on the DD-474 and DD-592 prior to the shot—all of which were beyond project control. Nine out of the 12 critical stations re-armed the night of D-1 showed a high percentage of proper instrument operation; thus, a fairly complete gamma-field history can be reconstructed with the help of photographic data. Although essentially no significant data was recovered from FFP's on this shot, the project at least demonstrated that it was operationally feasible to obtain supplementary data in this manner. All correlation between free-field radiation and that occurring aboard ships must be based on the EC-2 and DD-593 records supported by film pack information from the DD-474 and DD-592.

An estimated 80 percent of the maximum possible data from the coracle and FFP array was recovered during Shot Umbrella. Although some project instrumentation aboard the DD-474

was severely damaged due to shock or base surge action, an estimated 90 percent of the maximum data was recovered from the target ships. Most of the records obtained from overboard coracles are considered valid, since the most important phase of base surge transit was often completed prior to overturn and since an apparently accurate although attenuated record of airborne radiation fields was obtained after overturn. There was, unfortunately, a high percentage of instrument failure during Umbrella due to a combination of cable failure and exhausted batteries. Both these difficulties can be partially attributed to the accidental firing during Wahoo, since the project supply of batteries was depleted and instrument cables necessarily received rough handling under the less-than-ideal re-arming conditions extant on the fantail of the USS Munsee. Because of these failures, little data exists on the downwind leg in the neighborhood of the DD-593; however, the highly successful FFP operation permits the construction of isodose contours in this area. With the help of photographic data, these contours can be used to interpret the DD-593 records.

In summary, the data obtained by the project comprises:

1. Records of the total gamma dose rate as a function of time from unshielded detectors installed aboard 14 coracles and 2 target ships for Wahoo, and aboard 17 coracles and 4 target ships for Umbrella. These were recorded on magnetic tape for a period of 12 hours or longer after detonation and have an estimated accuracy of  $\pm 30$  percent after correction for detector response.
2. A series of incremental collections of deposited activity taken at uniform time intervals after zero time at 11 coracle locations for Wahoo and at 13 coracle locations and 1 ship for Umbrella. These collections were counted for gamma activity after recovery of the coracles; however, since the degree of fractionation is largely unknown, the estimated activity at the time of deposition could be in error by an order of magnitude.
3. Records of the early gamma dose rate as a function of time with high time resolution from coracles at 2 locations for Wahoo and at 10 locations for Umbrella. These were recorded with a time resolution of 0.1 msec on magnetic tape for a period of approximately 80 seconds after detonation and are probably accurate to within  $\pm 30$  percent when corrected for detector response.
4. Records of the underwater gamma dose rate as a function of time from detectors placed below the ocean surface at 7 locations for Wahoo and at 4 locations for Umbrella. These were recorded on magnetic tape for a period of 12 hours after detonation with an estimated accuracy of  $\pm 30$  percent after correction for detector response.
5. Total gamma dose accumulated during the radiological event measured by film packs at all coracle locations and at approximately 20 locations aboard each target ship for both shots. Film pack data was also obtained at 10 additional locations within the Wahoo array and at 62 additional locations within the Umbrella array. The accuracy of the film dose is at least  $\pm 20$  percent.

Additional samples collected primarily for other projects included total and time-based fallout collections and exposed test panels aboard the DD-592 for Umbrella only. Gross collections of fallout deposited on a  $2\frac{1}{2}$ -ft<sup>2</sup> area were obtained from time of fallout arrival to 1 hour after detonation by OCC collectors, and from time of arrival to time of cessation by AOC collectors. Standard test panels were exposed over the same time period specified for OCC collections. A series of fallout collections made at a constant sampling rate of 10 ft<sup>3</sup>/min were obtained for a sequence of 10- and 2-minute sampling intervals.

Aboard the DD-593, additional OCC collections and exposed standard test panels were obtained for Wahoo and Umbrella.

For greater convenience, information on shot yields and positions, together with meteorological conditions prevailing at the time of detonation have been obtained from the best available sources (References 75 through 81) and are summarized in Table 3.1. Similar data for Shots Baker and Wigwam and a summary of attendant radiation phenomena are presented in Appendix E.

**3.1.1 Data Reduction.** A discussion of data reduction is presented here to indicate the limitations and accuracy of the results. More detailed treatment, if required, will be found in particular sections dealing with each aspect of the phenomenon. The main body of the Project 2.3 results are dependent upon GTR measurements and subsequent readout by the GITOUT device. Because of the nature of the two shots studied, all other measurements were found to be of secondary importance. Therefore, matters of principal interest are GTR response corrections, errors and limitations due to the GITOUT, and possible errors due to time resolution plotting, and plot-reading procedures.

As described in detail in Section C.1 of this report, the directional response of the GTR detectors was determined using a number of X-ray energies, a  $\text{Cs}^{137}$  source, and a  $\text{Co}^{60}$  source (Figures 1.4, C.2, and C.3). All detectors were calibrated before and after each shot, using a 30°-beam, 120-curie  $\text{Cs}^{137}$  source, which was directed toward the top of the detector dome (the direction of the calibrating source is designated as zero degrees in all response plots). All components were precisely positioned; thus, the calibration procedure accurately reproduced detector response to a known source carefully aligned with the vertical axis of the detecting chamber. The high-range chamber showed an appreciable increase in response when positioned at right angles to the calibration beam; thus, it was necessary to apply a correction factor in the case of a detector completely surrounded by a radiating source.

An integrated detector response was determined by weighting each measured response for a given 5° segment by the total solid angle subtended by that segment. The reciprocal of this integrated response thus represented a correction factor that normalized the total response to unity. Since the maximum roll of a coracle is 45° and since the principal radiating source was found to be airborne material, the total response for the vertically mounted standard GTR was numerically integrated over a figure of revolution representing the measured directional response from 0° to 135°. Thus, the factors employed in this report correct for radiation incident over  $3.41\pi$  rather than  $4\pi$  steradians (a response normalized to  $4\pi$  steradians would be 10 and 4 percent greater than those reported for the high- and low-range chambers, respectively).

Since the detectors for both the ASEL and UW-GTR's were mounted with their axes of symmetry in the horizontal plane, at least half the effects due to roll would cancel out; thus, correction factors for these detectors were approximated by those for a  $4\pi$  response. A weighted average of the detector response was determined both for the effects of roll and for attenuation due to the coracle itself in these two latter cases. Both calculations resulted in only small deviations from the  $4\pi$  response. Because the UW detector case was wrapped in the instrument control cable, a 2-percent attenuation factor was applied when it was used as a secondary coracle. A simple  $4\pi$  response was employed for the UW-GTR when used underwater.

Correction factors were calculated for each energy for which directional response measurements had been made and were then combined by weighting each factor in accordance with the gamma energy groupings for instantaneous thermal neutron fission of  $\text{U}^{235}$  (Reference 83). Final correction factors, which were nearly equal to those determined for the  $\text{Co}^{60}$  directional response, are presented in Table 3.2. These correction factors have been applied to all GTR data presented in this report; the original gamma dose rates may be obtained from tabulated or plotted data by applying the reciprocal of the appropriate factor.

These correction factors are strictly applicable only to the case of a uniform radiating source completely surrounding the detector, a condition that is most closely approximated during peak dose rates. The actual response of the GTR will vary as the radiating cloud approaches and departs; however, for the conditions encountered during these events, this variation is always less than the stated limits of accuracy. Since neither the distribution of radioactive material within the base surge, nor the velocity of approach is accurately known, no attempt has been made to correct for changes in total response due to moving sources.

Although no directional response corrections for source movement were made, the differences between ASEL and std-GTR dose rate records at early times can be partially explained by this means (Section 3.2). The differences in detector response during the approach of a finite source are shown in Figures 3.1 through 3.3. These responses were determined as p

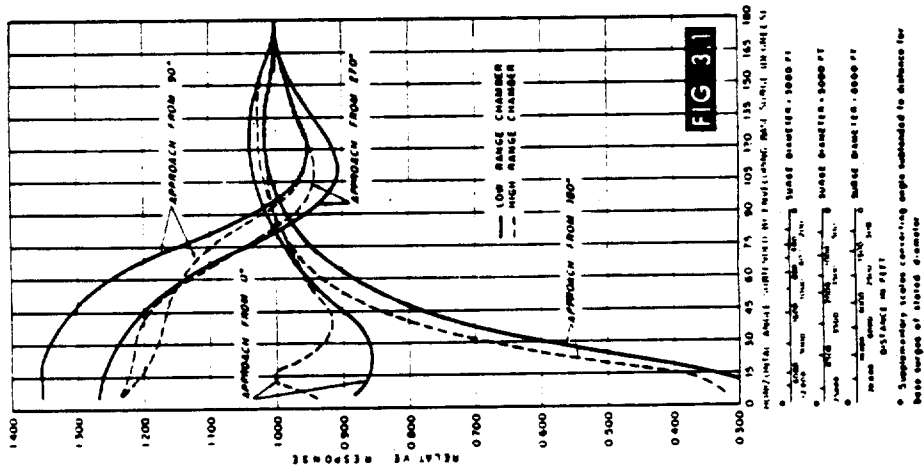


Figure 3.1 Relative response of ASEL-GTR detector for an enveloping base surge. (Source: 120 kev X-ray.)

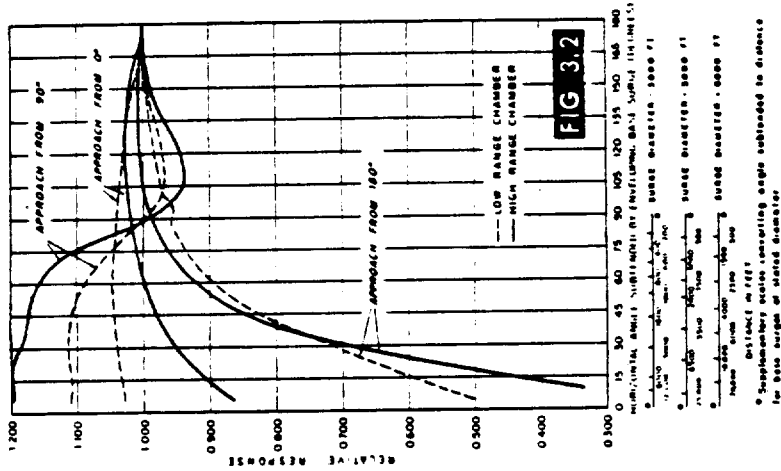


Figure 3.2 Relative response of secondary-GTR detector for an enveloping base surge. (Source: Co<sup>60</sup>.)

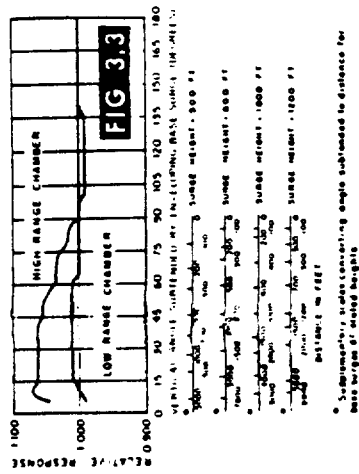


Figure 3.3 Relative response of standard-GTR detector for an enveloping base surge. (Source: Co<sup>60</sup>.)

viously described by using the data in Section C.2 and assuming that the total incident radiation was contained within the same angle at each detector. The integrated response for various assumed angles was then normalized to a response of unity for a completely surrounded detector. Since the ASEL and sec-GITR response is equivalent to a figure of revolution whose axis is parallel to the ocean surface, only variation in the horizontal angle subtended by the source causes a difference in response. Conversely, since the std-GITR response is analogous to a figure of revolution perpendicular to the ocean surface, only variation in the vertical angle subtended causes a change in response. For greater convenience, the assumed angles have been converted to the distance at which base surges of various assumed dimensions would subtend a similar angle at the detector. These calculations are presented as alternate scales beneath the scale of assumed angles.

The importance of the gamma-intensity time records requires a more detailed description of the limits of accuracy imposed by the detecting system and readout procedure. The stated limits of accuracy are  $\pm 30$  percent except at peak dose rate where the accuracy becomes indeterminate. Because the std-GITR is a recycling dosimeter, it tends to average out rapid changes in dose rate. This defect is an essential characteristic of the detecting device and cannot be rectified; thus, all peak dose rates reported are probably lower than the actual peak rates by an indeterminate amount. The ionization chambers can respond accurately to dose rates as high as 500,000 r/hr; however, their associated electrometer circuits begin to introduce appreciable recycling errors at rates above 87,500 r/hr for the 12-hour GITR. In most instances the GITR record can be used to rates of about 100,000 r/hr with errors ranging between 2 and 7 percent. At higher rates the spacing of individual radiation pulses on the magnetic tape becomes too close for resolution, and the record is said to be saturated.

The information on these tapes is in the form of two channels of radiation pulses (Appendix F) and one channel of timing pulses. Each radiation pulse on the high-range channel represents a dose increment of 0.243 r; for the low-range channel the value is one-thousandth of the high-range increment. The time channel consists of a square-wave pulse created by a mechanical timing motor every 3.75 seconds. Dose rate was obtained from GITR tapes utilizing the GITOUT in one of two possible ways: (1) the fixed-interval-counting method, and (2) the time-between-pulses method. Since the GITR tape transport operates at a nonstandard speed and since the GITOUT was constructed of standard commercial elements, the slowest transport speed for readout is 3.75 in/sec or 15 times the speed at which the 12-hour GITR records. Therefore, when considering GITOUT procedures, a careful distinction must always be made between playback time and real time.

The fixed-interval-counting method was used most frequently. The length of the counting interval is determined by the timing channel, the shortest interval being 3.75 seconds of real time. During each counting interval, all radiation pulses are summed by a digital counter. At the end of each interval, the cumulated total is printed out, and the summation operation is simultaneously switched to a second digital counter so that the tapes can be monitored continuously. Average dose rate in r/hr over a counting interval of 3.75 seconds is obtained by multiplying the sum of the radiation pulses accumulated by 233 for the high-range channel and by one-thousandth of this value for the low-range channel. The GITOUT can reproduce dose rate to an accuracy of  $\pm 1$  radiation pulse per counting interval; thus, the accuracy of the fixed-interval counting method for dose rates represented by less than 10 radiation pulses per interval is no better than  $\pm 10$  percent.

The time-between-pulse method of readout is highly accurate at any dose rate but has disadvantages in that it is more time consuming than the fixed-interval counting method and frequently requires electronic tape stretching. Dose rate is determined directly by measuring the time required to accumulate the preset dose increments, i.e., 0.243 r or 0.243 mr. Total running time, however, must now be determined by summing all time intervals instead of simply multiplying the number of intervals by a constant as in the fixed-interval method. Furthermore a minimum of 200 msec is required to complete any given print-out cycle. As the dose rate increases, the spacing between radiation pulses on the tape decreases. At the min

imum tape transport speed of the GITOUT, the time interval between successive radiation pulses can become shorter than 200 msec, at which point radiation pulses will be lost during the print-out operation. Thus, the maximum dose rates that can be read out by the time-between-pulse method without electronic stretching are 280 r/hr and 280 mr/hr for the high- and low-range channels, respectively. Higher dose rates can be read out only after tapes are rerecorded at speeds higher than those used for the original recording so that the physical spacing between radiation pulses on the tape is expanded. This process is called electronic stretching. The time-between-pulse method was used for all ASEL tapes and on all NRDL tapes in the 100- to 2,000-r/hr dose rate range where difficulties resulted from the crossover between the low- and high-range channels. All peak dose rates were measured by a modified time-between-pulse method in which a sweep-calibrated oscilloscope trace of the radiation pulses was photographed in the neighborhood of peak and the minimum distance between successive pulses converted to peak rate (Reference 66).

The direct plotting capability of the GITOUT was used only to obtain qualitative dose rate information for the preliminary report (ITR-1621). All GITR dose rates reproduced in this report were obtained by converting digital print-out information into dose rate, which was then plotted against the total number of counting intervals converted from playback to real time. For the ASEL records, digital time-between-pulse information was converted to dose rate using a calibration curve for each detector (Section C.2). The resulting dose rates were similarly plotted against real time. This readout and plotting procedure is estimated to be within the stated limits of accuracy.

For the higher dose rates, the time resolution of radiation pulses is approximately  $\pm 10$  msec on the NRDL tapes, whereas the resolution on the ASEL tapes is  $\pm 0.1$  msec. Although high resolution is possible between any two events on a given tape, the time of the entire gamma record relative to zero time for the detonation cannot be as precisely determined. The project received EG&G radio signals at minus 5 minutes, minus 1 minute, and minus 5 seconds, the two latter signals being used to determine time relative to zero time. According to EG&G (References 84 and 85), the accuracy of these keyed signals is  $\pm 0.05$  second relative to zero time; however, a delay as great as 0.25 second can be experienced between the time of the keyed signal and closure of the signal relay in the EG&G radio receiver. All delays in the coracle control box are at least an order of magnitude less than those enumerated. Zero time for the ASEL tapes was determined on the assumption that this instrument received its starting signal at minus 5 seconds; the accuracy of this assumption is within  $+0.05$  to  $-0.30$  second. Zero time for all NRDL tapes was determined by means of a timing blank which started at minus 1 minute and ceased at minus 5 seconds (Section 2.2.7). Although this procedure synchronized all instruments within a coracle, it did not permit the determination of zero time with an accuracy greater than  $\pm 1.25$  seconds.

All gamma dose rates were plotted on semilogarithmic paper, and straight lines were drawn between the points. These plots were later used to calculate the cumulative dose by a process of numerical integration. Both the use of semilogarithmic presentation and the construction of straight lines on such a plot contain inherent errors that depend on the actual shape of the dose rate curve. In determining cumulative doses, a linear dose rate function was assumed over each increment of time. If the dose rate is actually a logarithmic function of time, then the logarithmic presentation is correct, but the linear averaging technique employed is high by a factor dependent upon the distance between data points. If, on the other hand, the dose rate is actually a linear function of time, then construction of straight lines on a semilogarithmic plot is incorrect and the linear averaging is low by a factor dependent upon the distance between data points. However, a high density of plotted points reduces the errors inherent in either assumption.

For the linear averaging technique employed, the area under the curve can be as much as 30 percent low for a time interval so selected that the dose rate falls exactly midway between two plotted points a decade apart. If the separation of the plotted points is reduced by a factor of 10, the calculated area under the curve would be 2.4 percent low, with continued increases

TABLE 3.3 SUMMARY OF TIME ADJUSTMENTS

Shct	Nominal Position	Instrument	Time Change	Basis for Change
Wahoo	CL 4.6	ASEL-GITR	Matched with std-GITR	No timing channel.
Wahoo	CR 4.1	ASEL-GITR	Retarded 5 seconds	Matched with std-GITR record to show first pulse at known time of surfacing of explosion bubble.
Umbrella	U 1.8	std-GITR	Advanced 3 seconds	Matched with ASEL-record.
Umbrella	U 2.7	ASEL-GITR	Advanced 5 seconds	Changed so that the time of arrival agreed with other upwind stations and with velocity of approach determined from rate of rise (Section 3.3.4).
Umbrella	D 2.7	ASEL-GITR	Matched with std-GITR	No timing channel.
Umbrella	CR 4.9	std-GITR	Advanced 2 seconds	Matched with ASEL-record.

tion was observed, a period of greatly reduced radiation intensity is clearly indicated. To emphasize this reduced rate, the following criteria were used. When the peak dose rate exceeded the next plotted point by a factor of 10 and the interval between the two points was greater than 10 seconds, a minimum dose rate  $R_m$  was defined for the interval by:

$$R_m = \frac{R_t^2}{R_{pk}}$$

where  $R_t$  is the dose rate indicated by the plotted point terminating the interval and  $R_{pk}$  is the peak dose rate starting the interval. A point on this minimum dose rate line was then selected so that the area under the figure formed by connecting the peak dose rate, the selected point, and the terminating dose rate was the same as that obtained when the terminating dose rate was assumed constant over the whole interval. Simple geometric considerations demonstrate that such a point is uniquely determined. This treatment is admittedly arbitrary, but it at least approximates the true shape of the dose rate function more closely than the straight line connection, which is obviously in error. Although such treatment is also warranted for the other initial peaks reported, it has not been applied since both the peak rates and the time intervals involved were small enough so that the additional refinement appeared unnecessary.

The early gamma records presented in Figures 3.5 through 3.31 are in excellent general agreement. No correction has been made for deposit dose, since this correction may be safely ignored (Section 3.3.1). The records show a number of initial peaks followed by a period of essentially no radiation and then by a rapid increase to peak dose rate. The first part of this increase is always steeper than the latter part. This latter, more gradual rise is undoubtedly due to the approach of the base surge and its subsequent envelopment of the detector. By superimposing these early gamma records, it is generally apparent that a similar series of events occurs during both shots, the Umbrella sequence being about 10 to 20 seconds earlier.

The records obtained from different instruments at the same station show some interesting differences that are attributed to variations in detector response. The difference between the ASEL- and std-GITR records at Stations CL 4.6 and CR 4.1 on Wahoo and at Station DRR 3.9 on Umbrella are of particular interest (Figures 3.7, 3.9, and 3.23). These records show that, although both instruments record nearly the same peak dose rate, the rise in dose rate recorded by the ASEL-GITR always lags behind that of the std-GITR, this effect being greatest for CL 4.6 and least for DRR 3.9. In the confusion of the emergency re-arming for Wahoo, the ASEL detectors were erroneously oriented so that surface zero subtended an area of low directional response (Figures C.5 and C.7; direction of surface zero in these figures is 180° and 0° for detectors at CL 4.6 and CR 4.1, respectively). These orientations are confirmed by photographs taken during instrument recovery after Wahoo. In the case of DRR 3.9 for Umbrella, the coracle was so positioned by the wind that an area of low response was directed toward the hot line (Appendix F and Figures C.5 and C.7; direction of hot line in these figures is 0°). Therefore, it is possible that the differences between the ASEL- and std-GITR records are the result of differences in directional response made evident by the approach of base surge.

An application of the calculated detector responses (Figures 3.1 through 3.3) for the total angle subtended by an approaching base surge brings the two instruments into closer agreement, but complete agreement cannot be achieved until surge dimensions of 300 feet are assumed. This type of hypothetical approach suffers from the fact, inherent in the mathematical model, that the dimensions of the assumed radiating cloud varies as a function of distance to the detector unless it is assumed to lag a certain distance behind the visible base surge boundary. This lag distance is approximately 1,000 feet in all three cases, a distance which is in accord with other observations discussed more fully in Section 3.3.2. Photographic records indicate much larger maximum dimensions for the visible base surge; however, there are many indications (Sections 3.3.2, 3.3.4, and 3.4.1) that radioactive material is not uniformly distributed throughout the visible surge. No particular emphasis is placed on these speculations except to note that highly radioactive clouds of small dimensions are not impossible, and that these and other

considerations often strongly suggest their existence. Usually the ASEL- and std-GITR's are in close agreement since, when properly oriented toward surface zero, there are only small differences in response as a radioactive cloud approaches.

A second difference shown by both the sec- and ASEL-GITR's with respect to the std-GITR is best illustrated by the records obtained from Umbrella Stations D 4.8 and DRR 3.9 (Figures 3.21 and 3.23). The ASEL- and sec-GITR's track each other after the peak dose rate but rise above the std-GITR trace. Similar differences are also seen for some records at 0 to 15 minutes and 0 to 6 hours presented in Sections 3.3.2 and 3.3.5. Although changes in detector response as the radiating cloud recedes might be a contributing factor, these differences are most probably due to the combined effect of radioactive material on coracle surfaces and in the water immediately surrounding the coracle. The center of the sensitive volume for the std-GITR stands 14.7 inches above the coracle deck whereas those for the sec-GITR and the ASEL-GITR are about 3 inches above the deck; thus, the relative effect of deck deposits is greater for the lower detectors. An empirically determined curve (Figure C.18) indicates that the response of the lower detectors should be about three times that of the std-GITR. The ratio between the recorded dose rates for these instruments at Stations D 4.8 and DRR 3.9 does approach this value as the downwind segment of the base surge recedes. Radioactivity in the water can cause an even greater difference between the std- and sec-GITR records and is undoubtedly the principal cause at later times; however, at these early times the visible boundary of white water (Appendix F) has not yet reached these stations. Unfortunately, the combined effects of overturn, washoff at close-in positions, and the relatively light deposition over the more distant array afford insufficient opportunity to check this hypothesis.

The remaining differences in the composite records cannot yet be satisfactorily explained. The flat plateau shown by the ASEL-GITR at Station CL 3.1 on Umbrella (Figure 3.16) may have been produced by a radiating cloud that passed off to the right of the station through a region of low directional response; however, the suggestion raises nearly as many difficulties as it solves. The 15-second dip occurring between 32 and 47 seconds in the sec-GITR record at Station D 2.7 on Umbrella (Figure 3.20) may be due to capsizing, although this possibility seems unlikely, since the std-GITR record appears reasonable until 2.4 minutes.

The early gamma records obtained aboard the target ships are not necessarily comparable with those obtained from the coracles, because little is known of the directional response of GITR's installed in such complex surroundings. The shipboard records are in general agreement with those obtained from the coracles although most of the Umbrella records are incomplete because of saturation. The maximum dose rates for some saturated records have been estimated from the records of GITR's installed inside the ships by Project 2.1 (Reference 86) and are presented on the appropriate plots.

The initial radiation recorded at stations closer than 6,000 feet during both Wahoo and Umbrella was a sharp peak in dose rate occurring at about the time the explosion bubble first reached the ocean surface. Usually it was recorded as a single radiation pulse by both the ASEL- and std-GITR's. Unfortunately, the first radiation pulse on an ASEL record cannot be considered valid, since any leakage occurring between the warmup signal at minus 5 minutes and the first pulse must be included as an indeterminate part of the initial dose increment. Consequently, the initial dose rate peak has been omitted from the ASEL records except when substantiated by more than one radiation pulse. All initial dose rates obtained from the ASEL records have been included in Table 3.4 and in Figure 3.4 to show the extent of scatter. Because the std-GITR ion chambers are recharged by the minus-5-second signal, their records are considered reliable. Although a plot of these initial dose rates versus distance exhibits considerable scatter, the std-GITR peaks and some of the ASEL peaks are reasonably approximated by a straight line whose slope is similar to that for the attenuation of gamma radiation with distance from a distributed source of mixed fission products at early time (Figure 3.4). Note that the initial dose rate peaks measured by the ASEL-GITR at Stations CL 4.6 and CR 4.1 during Wahoo (Figures 3.7 and 3.9), both of which are substantiated by more than one radiation pulse, show an attenuation with distance that is too great unless a point source of radiation

is assumed. All initial dose rate data is summarized in Table 3.4. The variation in the time of initial peak is probably due to errors in determining true zero time on individual GTR records. As the initial peak dose rates for Umbrella are plotted without decay correction. To correct the initial dose rate peaks for Wahoo in the average time of the initial peaks (0.3 seconds) has been corrected to the average time of the Umbrella peaks (1.6 seconds) using a decay curve recently determined (Section B.2 and Reference 87).

Unfortunately, the station density is too low to permit any conclusions; however, the following observations can be made: (1) a period of low radiation intensity definitely follows an initial dose rate peak that appears to be associated with the surfacing of the explosion bubble, and (2) there is the suggestion that this initial radiation was registered at greater distances during Umbrella. The single Wahoo station between radial distances of 4,600 to 6,000 feet did not register an initial dose rate peak, whereas three out of three stations in this same range of distances registered such a peak during Umbrella.

The existence of a period of low radiation intensity after the initial dose rate peak poses some difficult questions. The decline in dose rate immediately after the initial peak is too abrupt to be caused solely by decay and therefore implies some sort of shielding between the source and the detector. Rough calculations indicate that the amount of water comprising the plumes and column cannot afford sufficient shielding to produce the observed effects. Therefore some physical action that accomplishes the temporary submergence of the principal radiating source below the ocean surface appears to be required. Further speculation is left to those more familiar with the hydrodynamics of these events. Because of the extremely short duration of the initial radiation, little can be inferred concerning the true initial dose or the shape of the initial dose rate peak. The data obtained from the coracles strongly suggests that the true peak is much sharper than that reconstructed by Project 2.1 (Reference 86); their data is, however, the best available until more precise measurements can be made.

The second portion of the early gamma record is the dose due to shine (Appendix F) from the column and approaching base surge. Photographic evidence (Reference 88) indicates that for Wahoo the primary plumes reached maximum height at 15.5 seconds (maximum height of secondary plumes at 30.5 seconds), and the base surge was clearly distinguishable by about 25 seconds; for Umbrella the column reached its average maximum height at 15 seconds, and the base surge was clearly distinguishable at about 13 seconds. On both shots a steep rise in dose rate occurs before the time of base surge emergence established by photographs. This first steep rise may also be associated with the initial surfacing of the explosion bubble. For Wahoo it is more pronounced and is usually followed by a short plateau, which is terminated at about the time of base surge emergence by a more gradual increase in dose rate. For Umbrella it is evident only as a change in slope, which again corresponds roughly to base surge emergence. Using the times of arrival (TOA) defined in Section 3.3.4, the cumulative dose from zero time to TOA has been calculated as an estimate of the shine dose. For greater convenience, the cumulative dose due to initial radiation, shine and the total dose to 1 minute are presented in Table 3.5. Because of its short duration, the initial radiation dose must also be regarded as an estimate. This initial dose is considered too uncertain to justify the construction of isodose contours. Contours of cumulative dose at 1 minute may be found in Section 3.3.3.

### 3.3 GAMMA RADIATION FIELDS RESULTING FROM AIRBORNE RADIOACTIVE MATERIAL

As stated in the introduction of this report, radiation from the airborne radioactive material may be divided into radiation from (1) the base surge, (2) the column and transiting cloud, and (3) material deposited from either of these two sources. The deposited material may be further subdivided into that deposited on retentive surfaces and that deposited in the ocean where mixing can occur. Radiation fields resulting from the airborne radioactive material specifically exclude those due to waterborne radioactive material, shine from the column, and secondary fallout, which is improbable in the case of an underwater burst. The two latter sources did not

make significant contributions to the gross gamma fields observed; however, radiation due to radioactive water remains a possible undetected addition to the free-field dose at the close-in stations. Consequently, the discussion of the gamma dose rate resulting from deposited radioactive material remaining suspended in the surface water layer is extended to include radiation from the passage or upwelling of water directly contaminated by the nuclear device even though such discussion is not properly included in this section.

**3.3.1 Deposited Radioactive Material.** The fact that any detector records the summation of radiation received from airborne, waterborne, and deposited material requires that at least two of these three potential sources be individually evaluated. Consequently, considerable effort was devoted to the prediction and assessment of possible deposited and waterborne radiation. In the light of the results from Wahoo and Umbrella, these efforts may appear to have been unnecessary; however, the very fact that the large deposits expected did not occur is in itself of particular significance. This fact has therefore been substantiated by all available evidence in addition to that obtained from the IC collections themselves. These measurements were not originally intended to provide such information, and thus, precision is understandably lacking. Evidence proving the deposit dose to be tactically unimportant is provided by: (1) the IC collections, (2) the standard GTR records after passage of the base surge, and (3) radiac meter surveys of the coracles upon recovery.

The relative contribution of the deposited material to the gross gamma field may be estimated from the data presented in Table 3.6 in which all values are converted to std-GTR response. The GTR and meter survey readings have been brought to a common time of 1 minute, using the ionization chamber decay curve in Reference 89 extended to early time by normalization with the decay curve in Reference 36 (Section B.2). For brevity, this combined decay curve is hereafter referred to as the standard decay curve. The IC collections were also corrected to the common time of 1 minute by a method described later.

A plot of the deposit dose rate estimated from meter survey data versus distance from surface zero (Figure D.34) shows no significant variation with distance, a fact which suggests that the meter survey readings are not representative of the deposition phenomena. The meter survey data indicates rather that the general background on Wahoo was approximately 10 times higher than on Umbrella. This increase in background, which was detected in other data (see Figure D.35), is attributed to the fact that Eniwetok Atoll was subjected to secondary fallout just prior to Wahoo from Shot Koa fired at Bikini. If Koa is accepted as the origin, the application of the standard decay curve on the assumption that the material was deposited from Wahoo is obviously false, and consequently the high meter survey estimates for Wahoo cannot be accepted. Even if meter survey estimates are accepted, they are less than 3 percent of the recorded peak dose rate at stations that were transited by the base surge.

The std-GTR records after passage of the base surge provide a better estimation of the deposit dose (Appendix F). A background dose rate after passage of the base surge was selected from each gamma record at a time not later than 3 hours after zero time and in a region where there was no immediate evidence of sources other than material deposited on the coracle decks. This background dose rate was then corrected by means of the standard decay curve (Appendix F) to the rate of 1 minute after zero time. A plot of these deposit dose rates (Figures 3.32 and 3.33) shows some scatter, which must be expected when all positions are represented without wind corrections, but which may also result from bodies of waterborne radioactive material in the neighborhood of the coracle. Nevertheless, the plotted points show some dependence on distance from surface zero and thus are more acceptable as an indication of deposition phenomena. If only points from downwind stations are considered, a straight line may be drawn through the points from the Wahoo close-in stations. Unfortunately, due to the large number of overturned coracles, there are almost no close-in points for Umbrella; however, a straight line parallel to that drawn through the Wahoo data fits the few Umbrella points reasonably well. If these straight line plots are accepted, the deposit dose rate may be approximated by the expression:

$$D_x = D_0 e^{-\alpha d}$$

where  $D_x$  is the deposit dose rate at some distance  $d$ ,  $D_0$  is an intercept constant representing a virtual deposit dose rate at zero distance, and  $\alpha$  is a constant representing the decrease in deposit dose rate with distance. For the data presented in Figures 3.32 and 3.33 these constants are:  $\alpha = 3.6 \times 10^{-4} \text{ ft}^{-1}$ ,  $D_0 = 5,400 \text{ r/hr}$  at 1 minute for Wahoo, and  $D_0 = 260 \text{ r/hr}$  at 1 minute for Umbrella. These plots cannot be considered in themselves sufficient evidence for an exponential decrease of deposited material with distance, but they do indicate that there is essentially no significant deposition beyond 15,000 feet for Wahoo and at 11,000 feet for Umbrella. The value of  $D_0$  for Wahoo is 21 times that for Umbrella, which could be caused by the combined effect of a heavier Wahoo deposition and the higher general background for all Wahoo samples. Total depositions over the shot arrays estimated from IC collections do not, however, indicate a significantly greater deposition after Wahoo. Finally, the few data points along upwind and crosswind radii show an abrupt decrease in deposit dose with distance as might well be expected.

The sum of IC collections attributed to base surge plotted against distance from surface zero (Figure 3.34) shows even wider scatter yet a similar decrease with distance. A straight line with nearly the same slope as that obtained from the GTR background data may be drawn through the Wahoo points; the slope and intercept values are:  $\alpha = 3.0 \times 10^{-4} \text{ ft}^{-1}$  and  $D_0 = 1,100 \text{ r/hr}$  at 1 minute. The fact that this line appears to fit the Umbrella data points is undoubtedly coincidental. If the close-in Umbrella stations are ignored, the Umbrella IC collections show little tendency to vary with distance from surface zero and are again about a factor of 10 lower than the Wahoo collections.

In the case of Station U 2.7 on Umbrella, the very large IC collection suggests that this station was involved in primary throwout (Appendix F). The additional fact that the early collections made at this station exhibit a decay curve that is characteristic of depositions accompanied by large amounts of water would seem to bear out this assumption. Photographic evidence for Umbrella is poor, but analysis of Wahoo plume trajectories (Figure 3.35) would indicate that the maximum throwout radius for that shot is about 1,800 feet. The possibility of a greater throwout radius existing for Umbrella appears unlikely; therefore, this explanation for the large collection at U 2.7 is not acceptable.

Collections made aboard the DD-592 platform also indicate such a heavy deposit accompanied by large amounts of water (Section 3.5.2). Reference 90 postulates that heavy rains of short duration fall from the base surge soon after its formation, the exact time being dependent upon the average size of the original base surge droplets. Although the time of both observed depositions is much earlier than that calculated in Reference 90, it is still possible that these two stations were exposed to such rainfall if original droplets of 20 to 50 microns are assumed. On the basis of these two records, heavy rains possibly accompanied by large amounts of radioactive material may be postulated to distances of  $3,000 \pm 500$  feet. Such heavy deposition of water would probably cross-contaminate (Appendix F) the uppermost IC trays, which may account for the fact that these IC collections appear to have continued after passage of the base surge (Figures 3.48, 3.61, and 3.62). If such deposition actually did occur, the meter survey and the GTR background data indicate that the majority of this material washed off the coracle decks, probably within a short space of time.

The IC trays were counted in an end-window gamma counter, consisting of a  $1\frac{1}{2}$ -inch-diameter NaI thallium-activated crystal,  $\frac{1}{2}$  inch thick, mounted in a lead shield (Technical Associates Lead Shield, Model LS-6) with appropriate photomultiplier and scaling circuits (Nuclear Instrument and Chemical Corporation, Model 162 scaler backed up with a Model 182 scaler). The crystal was shielded with  $\frac{1}{4}$  inch of aluminum to eliminate all contributions from beta activity. All trays were counted on Shelf 5 (distance: 84 mm from shelf support to bottom of crystal); the efficiency for gamma 0.7-Mev photons is approximately 0.35 percent for this position. The efficiency of the crystal system for a given sample can best be determined empirically.

cally, since counting efficiency is greatly influenced by the soft gamma spectra of the sample. Because the IC data presented in the body of this report has been greatly modified to permit interpretation of the GTR records, all observed tray counts, together with an approximate spectral response of the crystal counter are presented in Sections C.3 and D.2.

To compare the IC collections with the GTR records, both observations had to be brought to a common time, a correction that afforded particular difficulty, since at first inspection each separate collection appeared to exhibit an individual decay. However, after detailed comparison of the various individual decays (described in Section 3.5.1), it was found that nearly all observed decays for both Wahoo and Umbrella IC collections could be approximated by a family of five curves (Figure 3.36). If the apparent dependence upon time of collection is accepted, criteria based on known conditions of sampling can be established for the selection of a specific decay curve for a given IC collection. Thus, these empirically determined decay curves offer a means of correcting the observed tray counts to time of deposition, which is an improvement over the application of a single calculated decay curve for all samples.

The fact that the observed decay curves when normalized at 22 days again approach each other to within a factor of 3 at 0.2 day, permits the assumption that the relative magnitude of the tray counts at 0.2 and 22 days must also be the same within a factor of 3 regardless of the decay curve actually followed by the individual collections. Usually, the tray counts were made at 2 and at 6 days, times when the differences due to fractionation could be as high as a factor of 8.5. Since the decay curves at later times are better known, all IC tray counts were brought to a common time of 22 days using the following criteria for the selection of decay curves:

- Curve SI : deposition at 1 minute accompanied by large amounts of water.
- Curve SII : deposition at 1 or 2 minutes without large amounts of water.
- Curve SIII : deposition at 3 or 4 minutes.
- Curve SIV : deposition at 5 minutes or more as long as the GTR record indicates the presence of base surge at the station.
- Curve W : all other deposition.

The tray counts were then converted to a std-GTR response for a deposit of corresponding magnitude distributed uniformly over the coracle deck, using an empirically determined conversion factor  $\beta = 0.71 \times 10^{-7}$  (r/hr)/cpm (Section C.5). This factor was determined using a  $\text{La}^{140}$  slurry and exactly the same GTR exposure geometry and tray counting equipment. The value of such a conversion factor will, of course, vary as the energy spectrum of the deposited material changes. However, since the base surge samples were known to be enriched in  $\text{Ba}^{140}$ - $\text{La}^{140}$  and since these products represent better than 25 percent of the total activity in normal fission products at 20 days, the application of this conversion factor at 22 days is at least most consistent with the known energy of the material used for its determination. The hypothetical GTR response at 22 days was then converted to the GTR response at 1 minute, using the standard decay curve. The standard decay curve, when normalized with the five empirical decays at 22 days, also passed through the region of closest approach at 0.2 day and in fact agreed within a factor of 2 with an ionization chamber decay curve obtained by Project 2.1 to a time of 6 minutes.

This somewhat elaborate technique of correcting the IC collections to a common time was evaluated by examining all trays, which were counted once in the EPG at about 2 days and again at NRDL about 4 to 8 days after zero time. If the decay curve used for each of these individual samples was correct, both counts should yield the same results at any stipulated common time. Therefore, in all cases where trays had been doubly counted, the two counts were converted to the simulated GTR response at 1 minute both by the process just described and by the simple application of the standard decay curve together with the conversion factor  $\beta$ . In all except two cases, the values determined by means of the standard decay curve alone showed considerably more variation. Specifically, values calculated by means of the empirically determined decay curves showed an average variation of 19 percent of the mean, whereas those determined by means of the standard decay curve showed an average variation of more

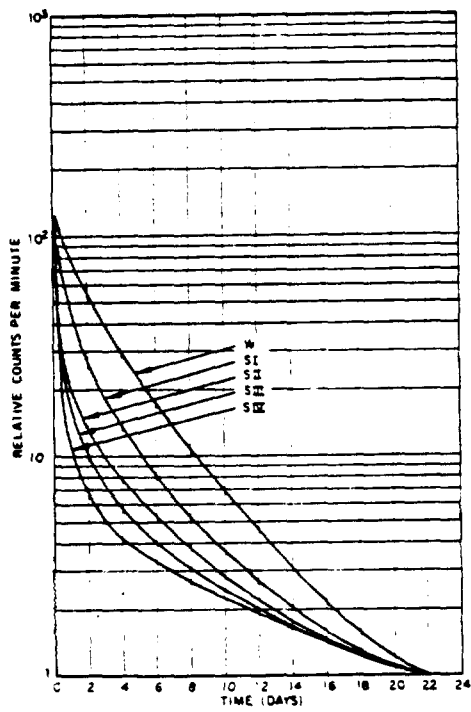


Figure 3.36 Family of decay curves for IC collections, combined (normalized to 22 days), Shots Wahoo and Umbrella.

than twice this amount. The values are finally presented as histograms on which the standard GTR record corrected to 1 minute using the standard decay curve (called the normalized rate curve) has been superimposed for ease of comparison (Figures 3.37 through 3.62). The plotted values may be converted to counts/min at 22 days by dividing by 0.015; the values may also be converted to GTR response to an infinite plane contaminated to the same degree by multiplying by 6.

When comparing the GTR record with the IC collections, it should be remembered that the sequence in which the trays were exposed, and therefore the time of exposure, was determined from the order of the trays upon recovery. Mechanical limitations of the IC itself cannot permit a time resolution better than  $\pm \frac{1}{2}$  minute for early collections, increasing to  $\pm 4$  minutes at the end of the tray sequence. Furthermore, difficulties experienced in the emergency re-arming for Wahoo resulted in a number of arming errors such as incomplete restacking or the loading of trays in improper numerical sequence. In all cases of such difficulty, exposure time was adjusted to that which seemed most probable on the basis of field notes, and this fact is indicated on all plots of the data.

The comparison of the IC and the GTR records at a given station is usually quite reasonable. The maximum possible contribution due to deposited radioactivity is usually less than 1 percent of the gross gamma record; thus, within the accuracy claimed for the GTR records, no correction for the contribution due to deposited radioactive material need be applied. The close-in stations, particularly on Shot Umbrella, show no pronounced deposition at the time of the dose rate peak. The known instrument bias under the high initial velocities of the base surge would preclude the collection of a representative sample in cases of light deposition. On both shots, the period of deposition from the base surge is usually short at the upwind and crosswind positions. The longest periods of deposition occur at the downwind positions; none, however, exceed 10 minutes during Wahoo or 7 minutes during Umbrella. The Wahoo histograms frequently show two peaks of deposited activity whereas those from Umbrella usually display a single peak. The rate of deposition is difficult to ascertain for depositions as short as those observed because of the large time increments of the IC collections.

The histograms were terminated at 15 minutes although most of the coracles showed IC collections at later times when no remnant of the base surge can be reasonably postulated. In the few cases where decays were observed, these late collections exhibited the characteristic water decay and were probably due to spray from radioactive water in the vicinity of the coracle. A series of prolonged IC collections in the target area prior to Wahoo indicates that approximately 300 cc/day of ocean spray entered the IC port. The value given has been corrected for rainfall reported in the area during the period of exposure; however, salt analysis of the liquid collected indicates that this correction may have been low. A similar value would be expected for the Umbrella target area.

The IC collections after 15 minutes were treated in exactly the same manner described for the other collections using the water decay curve. Collections significantly above background are presented without further discussion in Table 3.7. The IC collections are designated by the location of the collection, followed by a time indicating the time at which each 1-minute collection ceased. The abbreviation "cont" following the time designator indicates that the IC stuck at the tray in question; therefore, the tray was exposed continuously from 1 minute prior to the indicated time until the coracle was recovered. A more complete description of the symbols used in IC tabulations is given in Appendix D.2.

Although station density for the IC collection was very low, IC data was also used to estimate the total deposition over the target array. These estimates were made by mapping the total activity deposited from the base surge as determined by the IC collections and performing approximate isodeposition contours through these points. Total deposited activity in counts/min was determined over equal areas for both shots by numerical integration. Because no reliable deposition information existed at distances closer than 3,500 feet for Umbrella, an area of this radius was omitted from both summations. These calculated total depositions were then converted to fissions using the standard decay curve and the factor  $3.73 \times 10^5$  fissions/counts per

minute at 12 hours, which had been determined by Reference 36 for fission products, and the end-window counter used to determine IC tray activities.

This data suggests that the total Wahoo deposition was slightly greater than Umbrella; however, considering the assumptions required for these calculations, the differences between Wahoo and Umbrella shown by the deposit dose versus distance curves (Figures 3.32 through 3.34) are more probably due to the generally higher background of the Wahoo collections.

**3.3.2 Free-Field Dose Rates.** The free field is arbitrarily defined for the purposes of this report as the gamma radiation field near the water surface resulting from a cloud of airborne radioactive material unmodified by any projections above that surface. The GTR records best describing the free-field dose rates are those obtained from the coracles and presented in this section (Figures 3.66 through 3.96). Since these records are necessarily the summation of a complex sequence of interrelated phenomena, their interpretation requires considerable discussion.

The corrections and modifications of both the gamma records and base surge photography with which they are compared are first described. On the basis of radiological and photographic evidence, a simple base surge model is next proposed together with some specialized terminology required for greater brevity and clarity. The general features of the two underwater detonations can then be summarized and are later substantiated by more detailed discussion. The general discussion is intended to provide an approximate description of the gross base surge phenomena suitable for estimates of tactical hazards. The detailed discussions are presented to suggest hypotheses, which may be later used as guides for a combined analysis of all final Hardtack results. The limitations and justifications for any extended treatment of the data have been stated in the introduction to this chapter (Section 3.1).

Each gamma dose rate record is presented with a summary of all pertinent information considered necessary for the complete interpretation of that record. A brief synoptic description of the two underwater detonations is attempted by collecting some of this individual information into a master table (Table 3.11). All general or detailed descriptions of the records and all speculations on surge transport mechanisms are based on this material. Although the postulated base surge models and distinctions in surge structure cannot be conclusively demonstrated, they at least fit all radiological observations. Other models or structures can, of course, be postulated, and the project places no particular emphasis on those elaborated here.

Some of the material presented in this section must be abstracted from other sections of this report, since an intelligent interpretation of the free-field dose rate requires a nearly complete synthesis of all radiological observations. This material is properly abbreviated in this section; however, complete presentation of all such data is found elsewhere, viz, cloud and foam models are presented in Sections 1.3.1 and 1.3.2, instrument response in Section 3.1.1, isodose contours in Section 3.3.3, approach velocities and general base surge dynamics in Section 3.3.4, waterborne sources and their movement or sinking in Section 3.3.5, and shipboard records in Section 3.4.1. Reduction of surge photography was performed by the project from preliminary prints of aerial photographs supplied by Project 1.3, Naval Ordnance Laboratory (NOL), prior to publication of Reference 91, to which the reader is referred for final reduced data. Some of these NOL radii have been incorporated into this report with the kind permission of Project 1.3 (Figures 3.21 and 4.20 of Reference 91 for Wahoo and Umbrella radii, respectively). Finally, the linear presentations of dose rate which appeared in the preliminary report (ITR-1621) are presented in Section D.1. To conserve space, only parenthetical reference to sources of additional information is made throughout the remainder of this section.

All dose rate records obtained aboard coracles are given from zero time to H-15 minutes, a time interval that includes the major radiation phenomena associated with underwater nuclear

detonations. In some cases where radiation fields of tactical significance were still being recorded at 15 minutes, the record is extended. All dose rates presented have been corrected for response as described in Section 3.1.1. No corrections have been made for deposited activity (Section 3.3.1) or for waterborne radioactive sources, viz, (1) radioactive material remaining suspended after being deposited from the base surge, (2) water directly contaminated by the device, and (3) radioactive foam generated during eruption and collapse of the column. Since the presence and relative importance of these sources cannot be precisely determined, the unmodified gamma records are presented with a brief discussion of possible errors.

The extreme complexity of the gamma records, especially those for Wahoo, fosters the suspicion that at least the minor variations are generated by the detecting instrument itself. This suspicion is not sustained by a comparison of standard and secondary GITS records. When the LW-GITS detector failed to drop, a second record, called sec-GITS record, was produced by a completely independent instrument at the same location. Where such dual records were obtained, the two nearly duplicate each other (Figures 3.75, 3.76, 3.81, 3.88, and 3.89). The slight variations between these two records are usually explained by the differences in position and response of the two detectors (Section 3.1.1 and Figure 1.2) or by the fact that the coracle overturned. The following interpretation of the gamma dose rate records is based, therefore, on the assumption that both the variations in the recorded dose rate and all differences between two instruments at the same location do in fact represent actual changes in the radiation field.

Before further examination of the gamma dose rate records is attempted, the fact that many of the coracles were drifting after Wahoo and that many were overturned after Umbrella must be considered. Both occurrences could severely modify or even vitiate the gamma records affected; however, a careful evaluation demonstrates that very few records are greatly changed. All coracles that broke free after Wahoo were dragging long lengths of mooring cable, which greatly diminished their rate of drift (Section 2.3.2). In each case the rate of drift has been estimated and coracle movement during surge transit has been calculated (Table 3.11). In no instance does this distance exceed 200 feet, which is less than the theoretical limits placed on coracle positioning accuracy. Care must, however, be exercised when interpreting the later records, since some coracles drifted with the white water (Appendix F) while others became entangled with various elements of the target array. This information on later behavior is summarized in Table 2.6 and Figure 2.1.

Coracle overturn after Umbrella represents a more serious difficulty; however, if the std-GITS was not damaged during overturn, an attenuated record is obtained through the coracle bottom, which is sufficient for an analysis of surge transit if allowance is made for possible masking by white water. This attenuation factor has been evaluated at 0.18, using the known std-GITS response through its own electronics further attenuated by the coracle components (Section A.1). The sec-GITS in the capsized position is prevented from obtaining an accurate record of the radiological event through the bottom of the coracle by a layer of water that varies in thickness from 0 to about 5 inches depending on wave action. The time of coracle overturn is difficult to estimate, since a rapid decrease in dose rate may indicate either a rapidly transiting surge or an overturn. The estimated times of overturn (Table 3.11) are determined by comparing the GITS records of all adjacent stations. Where there is good agreement with neighboring stations, both coracles are assumed to be upright; where the two records do not track, an overturn is assumed. Additional evidence of overturn is also obtained by comparing the std-GITS and sec-GITS records when available. Thus only the latter part of the records from Umbrella coracles U 1.8 and D 2.7 (Figures 3.80 and 3.88) are considered invalid because of std-GITS damage resulting from overturn.

The interpretation of any dose rate record is obviously dependent upon some knowledge of visible base surge position relative to the instrument providing the record. These visible boundaries (photo-boundaries) were determined at 1-minute intervals after zero time from prints of oblique aerial photographs, which were geometrically corrected for the known distance and altitude of the aircraft (Section 3.3.3). The boundaries obtained cannot be more

accurate than  $\pm 1,000$  feet and may be in error by as much as  $\pm 1,000$  feet. When making prints from the original negative, an overexposure can result in the disappearance of some detail in the surge outline. By superimposing the time sequence of surge outlines for a given shot, a few such photographic disappearances become apparent. Since the base surge should not retract from a region where it is once photographically detected, the largest photographically determined boundary is always continued into later time; these maintained boundaries are indicated as dashed lines in the transit plots (Appendix F) to be described later. Times cannot be more accurate than  $\pm 2$  seconds, a limitation determined by the accuracy with which the gamma records can be related to the photographic data. Therefore, the analysis presented, while useful for the purposes of this report, must be substantiated by repetition with final reduced photographic information (Reference 91). These limitations also apply to other sections of this report (especially Section 3.3.4) where the position of the visible boundary is used.

On the basis of both radiological and photographic evidence, the base surge may be generally described as a low torus-shaped cloud that expands radially as it is transported downwind. Although roughly circular in outline, definite lobes or irregularities can be observed in the aerial photographs and are suggested by the final isodose patterns (Figures 3.103 and 3.105). Such irregularities are probably caused by nonsymmetrical interaction of the explosion bubble with the surface or by local retardation due to turbulence resulting from surface obstructions such as the target ships or the atoll reef. On both shots, the base surge did not exceed an altitude of about 2,000 feet; thus, after cessation of energetic radial expansion, surge movement is controlled by local surface winds. Difficulties caused by incomplete knowledge of local wind speed and direction are met by assuming that the photographically determined center X (Appendix F) represents the true surge center up to the last reliable photographically determined position (3.5 minutes for Wahoo and 6.0 minutes for Umbrella), after which the surge center is assumed to move in accordance with the official Task Force surface winds (15 knots from  $090^\circ$  T for Wahoo and 20 knots from  $050^\circ$  T for Umbrella).

As will be substantiated in detail later, the downwind gamma dose rate records for Wahoo suggest the generation of at least two base surges after Wahoo, forming a series of roughly concentric expanding toroids. Such a complex surge structure could result from a sequence of interactions between the explosion bubble and the water surface, a postulate that is supported by photographic evidence showing secondary plumes rising above an already well developed base surge at about 26 seconds (Reference 88). A similar phenomena (with perhaps tertiary plumes) was photographically recorded after Shot Wigwam, the only other deep-water nuclear detonation for which such data is available (Reference 14). Additional plume development may be presumed to have created a second base surge in a manner similar to primary surge genesis. The multiple surges so formed might mix or remain as partially or wholly separate cloud masses. Aerial photographs of the Wahoo surge at times greater than 2 minutes show two concentric rings of cloud separated by an annulus of relatively clear air. The center of the inner surge ring contains a number of irregular clouds. Prior to 2 minutes, white water masks any internal details of the base surge. Thus, both the dose rate records and later aerial photography favor the hypothesis that at least a primary and a secondary base surge did exist and that these surges were at least partially separate. For Umbrella, however, a single base surge torus seems adequate for an analysis of the gamma dose rate records. Aerial photographs show a single base surge toroid with a nearly cloud-free center. Very diffuse remnants of the Umbrella column moving centrally but above the surface base surge are apparent in some photographs.

A schematic representation of the more complex Wahoo surge is presented in Figure 3.63 together with a number of additional terms and symbols needed for a description of photographically distinguishable surge features or the manner of base surge passage over a given station. For greater simplicity of presentation, the surge is illustrated as stationary while the coracles are indicated as moving through it. The nine different types of transit illustrated together with their letter designators are self-explanatory. Use of these letter designators permits a maximum condensation of descriptive material and pertinent data. The designators

are used to serve as mnemonic devices once the reader is familiar with them. All symbols are summarized in a key placed at the beginning of the individual record sequence and again in Appendix F in addition to being defined as they appear in the text.

The initial presumed base surge is called the primary base surge, and the assumed second surge is called the secondary base surge. The terms "inner" and "outer" are used to describe surge boundaries, since the adjectives "leading" and "trailing" fail when describing upwind events. In the ensuing discussion two visible surge boundaries are used: an irregular photographically determined boundary (photo-boundary) and a smooth boundary defined by a circle best approximating the photo-boundary. Thus four visible boundaries of the primary surge are employed: the outer and inner photo-boundary ( $P_o$  and  $P_i$  respectively) and the outer and inner smooth boundary ( $B_o$  and  $B_i$  respectively). The secondary base surge is photographically indistinct; therefore, the smooth boundary of the secondary surge  $B_s$  is used unless otherwise noted. The final Project 1.3 (Reference 91) radii mentioned above are employed to construct another smooth boundary (labeled "NOL") using the center of the circle defining the primary smooth boundary (the photographic surge center X). The base surge torus is also divided into upwind, crosswind, and downwind segments always with respect to the official Task Force surface wind (15 knots from  $090^\circ$  T for Wahoo and 20 knots from  $050^\circ$  T for Umbrella).

Presumed areas of decreased radioactivity either between the primary and secondary base surge or at the center of the surge are called the intersurge decrement and central decrement, respectively. As suggested previously, these areas are apparently coincident with photographically clear areas within the base surge. In any discussion, a careful distinction must be maintained between photographically and radiologically established parameters; thus, wherever ambiguity is possible, the modifiers photo- or rad- will be prefixed to the parameter in question. Although the treatment of the two shots is similar, it cannot be identical because of the pronounced phenomenological differences. In all cases where more than one similar gamma record was obtained at a single location, only that record most closely approximating the free field is analyzed, i.e., the coracle record from the std-GITR or the shipboard record from the GITR facing surface zero or the hot line (Appendix F).

In general, base surge transit is responsible for all dose received at locations more than 1,500 feet from surface zero, as far as tactical considerations are concerned. Surge transit time varies with position relative to surface zero. For Wahoo, transit times range from approximately 3 minutes at upwind and crosswind locations to approximately 20 minutes at distant downwind positions; for Umbrella, these approximate times are 3 minutes and 10 minutes, respectively. Thus, the area in the immediate vicinity of surface zero should be safe for entry by combatant ships approximately 25 minutes after detonation. The generalization is correct as stated for larger combatant ships, but a consideration of waterborne material (discussed later) requires an exception for small boats operating in the vicinity of surface zero. The gamma dose rate record characteristic of Wahoo starts with a relatively blunt first major dose rate peak followed by a shallow valley, which in turn is followed by a series of blunt dose rate peaks slowly decreasing in magnitude over a period of about 10 to 15 minutes. A characteristic Umbrella record begins with a high, sharp peak in dose rate followed by a prolonged period of low dose rate, which finally increases to a flat-topped rise of approximately 4 minutes' duration. These characteristic records, supported by additional photographic evidence, indicate fundamental differences in the complex structure of the base surge produced by the two detonations. Such differences are not surprising but require considerable interpretation.

All peak dose rates and times of peaks are summarized for both shots in Table 3.8 (also see discussion in second preceding paragraph). The valley occurring immediately after the first major peak in dose rate has also been included in this table, since it is often indicative of an important feature of the base surge. The fact that all weather-deck GITR's

aboard ships 3,000 feet or closer to Umbrella saturated during the first major dose rate peak should be noted. Maximum dose rates 0.35 minute have been estimated by Project 2.1 from the records of instruments shielded below decks (Reference 86).

The cumulative dose at various times after zero time has been calculated by numerical integration and is presented in Table 3.9. Despite the higher peak dose rates observed during Umbrella, the average total dose for downwind stations closer than 12,000 feet is approximately two to three times higher for Wahoo than for Umbrella because of the longer surge transit times. The fact that many of the close-in stations on Umbrella overturned has little effect on the relative magnitude of the cumulative dose, since all these coracles received most of their total dose prior to the estimated time of overturn. A rough check of all GTR records demonstrates the observed dose rates to be consistent with a base surge containing

fission product activity available. As indicated later, the assumption that the radioactive base surge from an underwater detonation disappears solely by a process of decay appears justified for estimates of tactical hazards during the first 15 minutes after detonation.

To limit weather deck exposures a combatant ship must remain downwind of Wahoo and downwind of Umbrella. Closer upwind and crosswind approaches without exceeding these total weather deck exposures are of course possible, but, due to the unpredictability of close-in phenomena, these closer approaches must be determined by careful operations analysis. Another important tactical consideration in problems involving ship maneuvers immediately upwind of a receding surge is the possible existence of relatively invisible radioactive remnants streaming behind the visible surge. All radiological observations, however, indicate that base surge is the controlling tactical problem and that waterborne radioactivity is definitely of secondary importance. The passage of radioactive foam is, however, presumed to cause the spikes (Appendix F) in dose rate of 3,000 to 6,200 r/hr between 5 and 15 minutes observed at some crosswind coracles and would represent a serious hazard to small boats.

Any more detailed comparison of the gamma dose rate records with various features of the base surge requires the application of some correction for radioactive decay and the adoption of some formal means of estimating the combined effects of surge irregularities, radial expansion, and local surface winds. Because of the limited data available, no proper solution to any of these problems exists. The observed gamma dose rates are corrected to 1 minute after zero time by applying the standard decay correction (Figure B.5) to dose rates read off the std-GTR record (unless otherwise noted) at intervals of a tenth of a minute. The resulting curve called the normalized dose rate has been superimposed as a dashed line on each gamma record and is also used in Section 3.3.1. The approximate effect of surge movement and irregularity at a given coracle is estimated from base surge photography as previously described. Two representations of the approximate base surge position—the boundary plot and the transit plot (Appendix F) to be described later—are presented with each gamma record together with a number of tables summarizing important information and assumptions relevant to that particular record.

The application of a single decay curve (Figure B.5) to obtain the normalized rate curve is considered justified, since the principal clouds of airborne radioactive material appear to have been small enough to be seen as a whole by the std-GTR. The resulting normalized rate curve is useful for studying surge dynamics where radioactive decay is simply an additional and irrelevant complication. It cannot, however, be considered as accurate as the observed gamma dose rate because of possible deviations from the standard decay curve and because of unavoidable mathematical approximations used in its determination. Although the normalized rate curve is sometimes continued after passage of the base surge, its use for other radiating sources is not justified. The cumulative dose under the normalized rate curves has also been calculated for various times after zero time by numerical integration and is presented in Table 3.10. Because of complications due to waterborne sources, the calculation of the cumulative normalized dose is stopped as soon as the gamma record indicates completion of surge transit. Although the cumulative normalized dose contains a number of inherent inaccuracies, it may be

used to compare the total amount of radioactive material seen at different stations. The normalized dose should be comparable with the observed dose cumulated over the same time interval; however, the relative contribution from waterborne sources is unavoidably exaggerated in the former.

The normalized rate curve can be regarded as an approximation of the dose rate that would have resulted had the entire radiological event taken place so rapidly that no significant dilution occurred. In its calculation, no correction for dilution has been applied, since a plot of the normalized dose rate peaks versus time of peak shows no appreciable dilution due to diffusion or deposition from 3 minutes to 15 minutes (Figures 3.64 and 3.65). The possibility that the standard decay curve just compensates for dilution exists but is considered remote. The absence of dilution effects suggests that the radioactive fraction of the base surge remaining after 3 minutes is a very fine aerosol existing as a number of discrete clouds that maintain their identity. This physical model of the base surge is supported by the IC collections at distances greater than  $3,000 \pm 500$  feet (Section 3.3.1), by the lobes in the downwind isodose contours (Section 3.3.3), and by differences in instrument response during base surge approach (Sections 3.2 and 3.3.4). An analysis of the gamma dose rate records for Umbrella station outside the lagoon suggests modification of this simple model to include moderate expansion of the base surge torus due to increased turbulence caused by passage over the reef. This effect may also be reflected in Figure 3.65 by points D 18.2 and D 22.0 but is not supported by the point for DR 18.6 (reef station). These observations are the basis of the suggestion made in the general discussion that the decline of base surge radioactivity for the 15 minutes after detonation is primarily due to decay, the effects of deposition and continued eddy diffusion being of minor to negligible importance.

The total effect of the complex base surge movement is approximated by the photographic determination of surge boundaries as previously described from about  $\frac{1}{2}$  minute to the last time at which reliable boundaries can be so determined. Although diffuse remnants of the surge are detectable to approximately 25 minutes after both shots, the final photographic boundaries selected are the 3.5-minute boundary for Wahoo and the 6-minute boundary for Umbrella (Figures 3.101 and 3.108). The 3.5-minute boundary for Wahoo is expanded pantographically to an average smooth radius of 5 minutes and is then assumed to maintain this boundary throughout the remainder of recorded transit time. The 6-minute boundary for Umbrella is assumed to represent maximum surge expansion for all stations outside the lagoon, an assumption that is in apparent disagreement with the Project 1.3 report that the Umbrella surge still exhibited a 3-knot crosswind growth at 20 minutes (Reference 1). Although this 6-minute boundary results in reasonable agreement between photo-arrival times and rad-arrival times (photo-TOA and rad-TOA) determined from the gamma records for stations inside the lagoon (Table 3.11), it does not yield proper arrival times for the remaining stations, using various assumed wind speeds and directions within the limits set forth in Section 3.1.

At shot time for Umbrella, the tide is at approximately midstage (2.9 feet and falling); the partially exposed reef in addition to the sun-warmed islands of Giriinien, Ribaion, and Pokon could have introduced both turbulent and thermal energy into the base surge. Such introduction could result in increased eddy diffusion, in partial evaporation of surge droplets, in increased vertical surge development, or in raising the entire surge off the water surface. If increased diffusion did occur, the resultant dilution was not sufficient to produce a pronounced decrease in the normalized peak dose rate (Figure 3.65). The gamma dose rate records indicate a decreased wind speed after reef transit although the visual approach velocities determined for stations outside the lagoon (14 to 15 knots) and particularly for the reef station (10 knots) suggest such a decrease (Table 3.11). Although the precise mechanism of the post-reef surge modifications due to the reef remains uncertain, the effect is presumed analogous to that of the reef and the additional expansion arbitrarily set at 1,000 feet. The final radius  $B_0$  of the smooth boundary



(Appendix F) for Umbrella thus becomes 7,800 feet (the similarity of the final surge diameter for the two shots is entirely coincidental). Although the postulated two-stage radial expansion resulting from the influence of the atoll reef cannot be conclusively demonstrated, such behavior is in better agreement with the reported observations of Project 1.3 (Reference 1). The final radii adopted for analysis of the gamma records are essentially the same as those arrived at in Section 3.3.4 from analyses using the hypothetical surge center H (Appendix F and Figures 3.136 and 3.137).

The centers of all photo-boundaries just described for the Wahoo and the Umbrella surges are considered to be coincident with that of the primary smooth boundary  $B_0$ . This center is called the photographic surge center X (Appendix F), is assumed to be independent of the reported surface wind speeds up to the time of the last photographically determined surge boundary (3.5 minutes for Wahoo and 6 minutes for Umbrella). After this time it is presumed to move in accordance with the official Task Force surface winds (15 knots from  $090^\circ$  T for Wahoo and 20 knots from  $050^\circ$  T for Umbrella). Since two methods of determining the surge center are employed in this report, special care should be taken to note the difference between the photographic surge center X just described and the hypothetical surge center H, which is simply the point defined by moving surface zero downwind in accordance with official surface winds starting at zero time. The photographic surge center X is used exclusively throughout this section; similar calculations using the hypothetical surge center H and arriving at essentially the same conclusions are presented in Section 3.3.4. Although the difference between these two centers is never large, the photographic surge center X for Wahoo undergoes a somewhat abrupt change in direction of travel between 3 and 4 minutes, which probably results in fictitious variations in the boundary plots (Appendix F) between these times.

The two representations of visible surge position accompanying each gamma record have been graphically determined for each coracle location, using the photo-boundaries and wind movement just described. Although these procedures are admittedly rough, actual base surge movement is sufficiently approximated to reveal some of the subtler aspects of the gamma dose rate records. For brevity these two plots are hereinafter referred to as the "transit plot" and the "boundary plot" (Appendix F). The transit plot consists of a plan view of the most probable photo- and smooth boundaries at the times of their individual initial and final transit at a given station. These transit plots are presented to indicate appropriate intercomparison between the given record and other records at similar stages of transit or base surge development. The boundary plot is determined by measuring the shortest distance from the given station to the appropriate photo-boundary at 1-minute intervals. The smooth curve drawn through these points is considered only an estimate of the actual surge position, which includes variations due to local irregularities in boundary, changes in surface wind speed and direction, and changes in the rate of base surge expansion. The sign of the plotted values indicates whether the particular boundary is radially closer to the surge center than the station (negative value) or radially beyond the station (positive value). These boundary plots are used to correlate various photographically detectable features of the surge with specific portions of the gamma dose rate record.

The base surge approach velocity is a vectorial combination of the radial surge expansion and the local surface wind. At least two (not necessarily identical) approach velocities must be considered, viz, that of the visible surge and that of the airborne radioactive material. The visual approach velocity may be calculated for either the primary photo-boundary  $P_0$  (Appendix F) or for the outer smooth boundary  $B_0$ . Since the distance of either boundary as a function of time is given in the boundary plots, the slope of the appropriate curve at some time (or distance) prior to surge arrival yields the desired velocities. In most instances these slopes are changing rapidly, thus the approach velocities are quite sensitive to the point at which the slope is determined. The point giving the most favorable comparison with radiological approach velocities is one representing a distance of 500 feet from the station at the time of the first major peak in dose rate. All visible approach velocities tabulated in Table 3.11 are determined for this point (estimated values are enclosed in parentheses). Agreement

between the approach velocities determined for the primary photo-boundary and the outer smooth boundary indicates a relatively even surge outline in the neighborhood of the station; conversely, large discrepancies suggest lobes or irregularities. The approach velocity for the airborne radioactive material is determined from the gamma dose rate record by the rate of rise to the first major peak, a process fully described in Section 3.3.4. The value obtained depends on the surge model used (Section 1.3.2). Only the range of possible rate-of-rise velocities is tabulated in Table 3.11. The rough general agreement between the several velocity determinations suggests that the visible surge and the radioactive aerosol are moved by the same mechanical forces but does not necessarily imply that they are the same body of airborne material. For both shots, a somewhat better comparison results for rate-of-rise velocities determined with surge models of greater thickness. Since all these derived velocities are affected by a large number of arbitrary assumptions necessary for their determination, this distinction may indeed be fictitious.

A more consistent difference between the Wahoo and Umbrella records becomes apparent when the shortest distance to the outer primary photo-boundary  $P_0$  at the time of the major dose rate peak is considered. These distances obtained from the boundary plots are given in Table 3.11. In accordance with the sign conventions previously described, a negative value indicates that the outer primary boundary has not yet reached the station; a zero value indicates that its arrival is coincident with the time of the first major peak; and a positive value indicates that it has already passed the station. The major dose rate peak may be assumed to correspond to a position of optimum detector geometry relative to the airborne radioactive material or to a region of maximum radioactive concentration within the visible base surge (such regions of increased radioactivity were previously suggested in Section 3.2 by variations in instrument response). Regardless of its actual cause, this point is referred to as the source center.

Although no particular significance is placed on the numerical values because of the stated limitations on the accuracy of all photo-boundaries, the fact that the values for Wahoo are preponderantly positive suggest that the source center lags approximately 1,000 feet behind the outer visible boundary somewhere near the inner edge of the primary base surge. This suggestion is also supported by the observation in Section 3.2 that a source center approximately 1,000 feet behind the photo-boundary is required in correcting the differences between ASEL-GITR and std-GITR responses at Wahoo Stations CL 4.6 and CR 4.1 (Figures 3.7 and 3.9). For Umbrella the preponderantly negative values suggest a source center closely associated with the outer primary photo-boundary or possibly somewhat in advance of that boundary. At the distant stations, such differences might be ascribed to errors in assumed surface winds, but at the closer stations, which constitute approximately 80 percent of all records, the position of the surge boundary is a matter of photographic record. Use of the NOL radii places the source center even farther behind the visible surge boundary for Wahoo, whereas for Umbrella their use moves the source center to an apparently more reasonable 500 feet behind the outer primary photo-boundary. The distinction that the source center for Wahoo lags far behind that for Umbrella, however, remains essentially unchanged.

As already indicated, existence of an invisible radioactive material in advance of the primary photo-boundary might be the result of an overexposure in the photographic printing process. Indeed, the anomalous behavior shown by Station DRR 12.8 during Wahoo is probably due to such photographic disappearance. If the section of the primary surge boundary that finally intersects this station is assumed to expand from its 2-minute position in a manner exactly similar to the remainder of the surge, the source center lies behind the primary photo-boundary at a position similar to that observed at other Wahoo stations. Nevertheless, an exactly similar disappearance could result from evaporation at the outer surge boundaries. Under the appropriate ambient conditions, the base surge droplets could evaporate leaving a more or less invisible radioactive aerosol. Thus, these differences in source center position relative to visible boundaries suggest that, although the airborne radioactive material is often closely associated with the visible material, such association cannot be tacitly assumed.

In the preceding general discussion the Wahoo base surge is described as a double toroid having a number of diffuse clouds at its center whereas the Umbrella base surge is described

the upwind direction but were then transported downwind after their initial energy had been dissipated against existing surface winds. Alternatively, originally coherent masses of radioactive aerosol could have been broken up by turbulence and small variations in wind structure.

The simpler Umbrella dose rate records show no evidence of an intersurge decrement but indicate a comparatively large central decrement, a structure again corroborated by aerial photography. The fact that this central decrement is recorded at coracles experiencing only an inner edge transit (U 1.8, CL 3.1, DLL 6.6, DRR 3.9; Figures 3.80, 3.83, 3.85, and 3.94 respectively) indicates that the central decrement is at least as large as 3,000 feet in radius. Thus, both the photographic evidence and the simpler dose rate records suggest that a relatively large nonradioactive center was followed by the rapid passage of a compact, highly radioactive aerosol over the stations and then by the longer transit of a more diffuse cloud, which again probably represents base surge originally moving in an upwind direction. Similar conclusions on the general structure of both base surges are arrived at using the hypothetical surge center H (Section 3.3.4; Figures 3.120 through 3.127).

Further analysis of the Umbrella central decrement is complicated by the presence of white water, by expansion of the base surge torus, and by the fact that no two stations record exactly the same transit. After radial expansion ceases, inward diffusion of the surge boundary might be expected to eradicate any central decrement; however, there is only indirect evidence for any such process. Of the four coracles providing central transit records, two overturned during transit; therefore, any comparison must be made between coracle and shipboard records. Because of the possible persistence of radioactive aerosols in the neighborhood of obstructions causing turbulence (Section 3.4.3), this particular comparison is not desirable. The minimum normalized dose rates during central transit for Coracles DL 6.2 and DL 16.0 are 29 r/hr at 3.70 minutes and 37 r/hr at 7.80 minutes, respectively, whereas those for the three destroyers in order of increasing distance from surface zero are 400 r/hr at 2.19 minutes, 160 r/hr at 2.30 minutes, and 55 r/hr at 3.91 minutes, respectively. All usable records suggest that expansion of the central decrement ceased after about 3 minutes. Since the outer base surge boundary is photographically observed to continue radial expansion until at least 6 minutes, this earlier stabilization of the inner boundary may be the only evidence for inward diffusion. Coracle D 4.8, although overturned, was not quite in white water at the time of central transit; thus, its minimum normalized dose rate corrected for attenuation (110 r/hr) may be tentatively included in the above comparison.

The continued persistence of gamma activity after final transit of the surge photo-boundary is a phenomenon frequently observed for both shots. Generally, gamma records showing the longest persistence are those from coracles that experience central transits or are located where turbulence from target ships upwind is possible. A number of explanations for the observed persistence are possible; the simplest, however, is that turbulence resulting from passage of the base surge over the ocean surface and around large obstacles separates diffuse radioactive remnants, which stream out behind the surge. Indirect evidence of surface drag forces necessary to the formation of such remnants is implicit in the photographic observation that, in later time, the base surge torus tends toward an ellipse with its major axis in the direction of the surface wind (Reference 91). For brevity, these postulated remnants are referred to as "tails." Simple hydrodynamic considerations indicate that the length of such tails should increase with increasing distance downwind of surface zero and should decrease as the transit path approaches the crosswind edge of the base surge torus. Although interference by target ships must be considered in nearly all cases, the persistence in dose rate expected of the suggested tails roughly fits such predictions.

In cases where target ships are involved (Table 3.11), prolonged gamma dose rates may be caused by both ship retardation and by streaming of surge remnants detained in turbulent eddies generated by the superstructure (Section 3.4.2). Surge retardation by the target ships, apparent in base surge photography (Reference 91), is not detectable in surge arrival times derived from the gamma dose rate records. The prolonged dose rate records after surge transit may, however, be radiological evidence for such retardation. If the postulated tails following the base

surge proper and temporarily streaming from the target ships are accepted, the fact that Umbrella tails are consistently somewhat shorter than Wahoo tails may indicate another difference between the two base surges. Shorter tails, for instance, might be expected from a higher, thinner base surge torus presenting a smaller basal area to surface drag.

Alternative explanations for the persistence of the dose rate record after surge transit include: (1) changes in wind speed and direction after downwind surge arrival, (2) continued surge expansion or increased eddy diffusion resulting in a thicker base surge torus, (3) presence of a second radioactive aerosol moving above the surface base surge at a different speed or direction, or (4) the prolonged generation of a radioactive mist by some process of white water out-gassing or wind dispersal of foam. Full evaluation of all these possibilities was not attempted, although each was investigated briefly before the tail hypothesis was selected as the most probable on the basis of the observed gamma records. Other surface wind speeds (or directions) within the reported limits of variation (Table 3.1) not only fail to eliminate all observed tails but also frequently create apparent tails at crosswind locations. Furthermore, because these assumed changes are only applicable after the last photographically established base surge position, they must often occur after the downwind surge transit but before arrival of the upwind surge (Appendix F). The time of the presumed change would thus differ for the various coracle positions. Continuous radial expansion or greater eddy diffusion of the base surge partially eliminates the observed tails at some locations (particularly for Umbrella) but requires either longer tails or, in some cases, negative tails at other locations.

More recent calculations using surge toroids having somewhat greater radii than those assumed in this report fit some downwind gamma records very well; therefore, this postulate is the most probable alternate to the tail theory described above. The postulated influence of the atoll reef should also be remembered when considering any later base surge expansion. A radioactive cloud moving at higher altitude also appears unlikely. For Wahoo, no such upper cloud was photographically detected nor is any significant wind shear reported up to an altitude of 5,000 feet (base surge height is 2,000 feet). The Umbrella case is more favorable, since a diffuse remnant of the central column was photographically detected; however, this remnant moved centrally with the base surge torus. Again, no significant wind shear is reported up to an altitude of 5,000 feet (base surge height is 2,000 feet), although some shear is apparent in surge photography (Reference 91). Finally, although a mist emanating from white water was observed for a period of 13 to 14 minutes after Umbrella (Reference 91) and may also have existed undetected after Wahoo, such tertiary processes should not contain as much radioactivity as a secondary process derived from base surge directly. Furthermore, the dose rate record of such a radioactive mist would be expected to terminate gradually rather than abruptly as is observed for base surge. None of these alternative explanations can, however, be definitely eliminated or accepted without analysis that is beyond the scope of the project.

During the discussion above, a number of structural differences between the base surges generated by the two underwater nuclear detonations have been indicated. The Wahoo base surge appears to be a double toroid with the primary and secondary surges separated by an essentially surge-free annulus (intersurge decrement). The center of the second torus contains a number of diffuse clouds, which could represent additional degenerate base surges. The source center (Appendix F) appears to be situated well behind the visible surge front, somewhere near the inner boundary of the primary base surge. The Umbrella base surge is much simpler in comparison, being a single torus with a large surge-free central decrement, although faintly visible remnants of a central column are observed to move with but above the base surge. The source center appears to be situated at or in advance of the visible surge front.

Some indirect evidence suggests that the Wahoo surge may have a greater horizontal thickness than the Umbrella surge; this observation, however, could simply be a result of the former's compound structure. Preliminary studies indicate that the Wahoo explosion bubble went through its first maximum expansion and surfaced just prior to its first minimum at an internal pressure somewhat greater than atmospheric. Conversely, the Umbrella explosion

bubble broke surface well before its first maximum expansion, at a time when its internal pressure was less than atmospheric; therefore, an implosion is possible. These differences appear to be caused by the two base surge structures, which suggest a different sequence of events in base surge genesis. The two processes might be distinguished by the terms "exogenic" (eruptive) and "endogenic" (irruptive) base surge generation. Such speculations are actually beyond the scope of this report, and this summary is presented to suggest that a more rigorous analysis of surge structure might provide additional information on bubble action at the surface and subsequent surge generation.

In some cases, the gamma dose rate record continues even after any reasonable final transit by the surge tails postulated above. Typical examples of such records are those from Coracles CL 3.9, CR 4.1, and CR 5.2 for Wahoo and Coracles CL 3.1 and DRR 3.9 for Umbrella (Figures 3.67, 3.77, 3.78, 3.83, and 3.94). Between 5 and 15 minutes after zero time, these records show an irregular series of sharp dose rate peaks ranging between 3,000 and 6,200 r/hr. These peaks are undoubtedly due to bodies of waterborne radioactive material. The important sources are water directly contaminated by the detonation (white water) and small patches of radioactive foam, the existence of which is discussed in Section 3.3.5. Of the two sources the foam would have the more pronounced effect, since it would be largely unshielded. Small patches of foam approximately 100 feet in diameter, moved by the wind past a coracle, could produce the sharp dose rate peaks observed (Sections 1.3.1 and 1.3.2).

Although the shape of the observed dose rate peaks favors the foam hypothesis, the evidence is at best circumstantial principally because the white water contribution to the observed dose rate cannot be positively eliminated; only Stations DR 4.5 for Wahoo and DRR 3.9 for Umbrella (Figures 3.71 and 3.94) provide definite evidence of waterborne activity that cannot be white water. Interpretation of the waterborne record is further complicated by drifting coracles after Wahoo and overturned coracles after Umbrella. Calculations indicating the most probable movement of waterborne radioactive material are included in Table 3.11. The white water boundaries used in this analysis are reproduced in the transit plots (defined in Appendix F).

For Wahoo, expected arrival and cessation times for foam were calculated for various assumed sets and drifts, using the measured distance to the closest and furthest white water boundaries at a known time and allowing for the movement of drifting coracles. Sets ranging from 250° T (average direction of coracle drift) to 302° T (Reference 92) and drifts of 1, 2, and 6 knots were used. Movement toward 270° T at 6 knots is both in reasonable agreement with the observed gamma dose rate records and is compatible with the official surface wind direction and reported ocean currents (References 53 and 93, and project observations). Similarly, white water arrival and cessation times calculated on the basis of a set and drift of 270° T and 1 knot are also in reasonable agreement with the observed gamma records, although sets of 250° and 302° T give equally good or slightly better comparisons.

For Umbrella, foam is again assumed to move with the official surface wind, but a speed of 2 knots compares more favorably with the observed dose rate records. The slower rate of foam movement may possibly be due to smoother water conditions inside the lagoon. Since the effect of the atoll reef on waterborne movement cannot yet be properly evaluated, no comparisons are made for coracles outside the lagoon. The assumption that white water moves with the surface wind at 1 knot yields arrival times comparable with the gamma records but results in times of cessation that are much too early. An assumed radial expansion at 0.5 knot gives better general agreement with the gamma records and observed expansion rates. Since the limited current data available for lagoons (Reference 94) indicates surface currents about 1.6 percent of wind speed, the assumed radial expansion appears at least reasonable. For Umbrella, it is also assumed that the white water is composed largely of radioactive bottom material, which sinks with a speed comparable to that observed in the laboratory for Umbrella crater material, viz, 0.96 m/hr. On the basis of water shielding alone, such a sinking rate would result in a decrease in dose rate of 1 decade in the first 21 minutes of settling. Such decreases are observed at the close-in stations after Umbrella (Section 3.3.5).

KEY FOR TABLE 3.11 AND FIGURES 3.66 THROUGH 3.96

1. Gamma dose rate record: Gamma dose rate versus time corrected for instrument response; type of detector indicated. Normalized rate curve for instrument shown from 1 minute until end of record.
2. Plan view plot: Plan view of various surge boundaries at beginning and end of transit. Boundaries shown for times indicated. Letter designators for boundaries same as those given in tabulated section of this key.
3. Tabular data: Same key is applicable for Table 3.11.

General: Letter designators and other general symbols used in table:

- |                                      |  |                                   |
|--------------------------------------|--|-----------------------------------|
| - = no data available                | ( ) = value is estimated                       | [ ] = see notes for boundary plot |
| CA = point of closest surge approach | mag = observation expected but not observed    |                                   |
| calc = calculated data               | mak = observation masked by a concurrent event |                                   |
| CR = point where $B_0$ recedes       | n.a. = not applicable, occurrence is unlikely  |                                   |
| DD = drifting                        | NC = not central decrement                     |                                   |
| ED = inner edge influences           | neg = negative value                           |                                   |
| EX = expanded surge boundary         | RF = reef station                              |                                   |
| OL = station outside lagoon          | sat = instrument saturated                     |                                   |
| OV = coracle overturned              | WW = interference due to white water           |                                   |
| obs = observed data                  | XTP = extrapolated data                        |                                   |
| poss = possibly                      |  |                                   |

Records: records given are complete unless parenthetically indicated or modified as stated.

Modifying conditions: basis of estimated time of overturn given in parentheses: (no 2nd rise) = the instrument failed to record the passage of the upwind surge accurately, (sec-GITR track) = the secondary GITR tracked the std-GITR until the time of the estimate. GITR OK = std-GITR was not damaged by overturn. GITR damaged = std-GITR damaged by overturn.

Types of transit are illustrated in Figure 3.63; the letter designators used are:

- |                                       |  |
|---------------------------------------|--|
| C = central transit                   | SN = skirting transit, an upwind event                           |
| D = distant transit                   | TN = total envelopment, an upwind event                          |
| E = edge transit                      | TTC = transit thru the center, center passes at 1,000 ft or less |
| IE = inner edge transit               |  |
| OE = outer edge transit               |  |
| PN = partial transit, an upwind event |  |

Types of records: more fully described in Section 3.3.2; the letter designators used are:

- |   |   |
|---|---|
| M = record typical for station almost missed by surge                     | $W_1$ & $W_2$ = characteristic Wahoo records    |
| $N_1$ & $N_2$ = records typical for stations experiencing an edge transit | $U_1$ & $U_2$ = characteristic Umbrella records |

Surge boundaries: These and other surge parameters are illustrated in Figure 3.63; the letter designators used are:

- |   |   |
|---|---|
| $B_1$ = inner primary smooth boundary   | NOL = NOL smooth boundary                       |
| $B_0$ = outer primary smooth boundary   | $P_1$ = inner photo-boundary of primary surge   |
| $B_s$ = outer secondary smooth boundary | $P_0$ = outer photo-boundary of primary surge   |
| H = hypothetical surge center           | $S_0$ = outer photo-boundary of secondary surge |
|   | X = photographic surge center                   |

Total surge: normalized dose cumulated over time indicated.

Surge boundaries: photo-TOA and photo-TOC given for outer primary photo-boundary only; distance and time of closest approach of X given if < 5,000 feet; rad-TOA = average of 38 and 100 percent of TOP; rad-TOC = time normalized rate curve drops below  $10^3$  r/hr; source center = distance of  $P_0$  at TOP (time of peak); length of tail calculated using official surface wind speed.

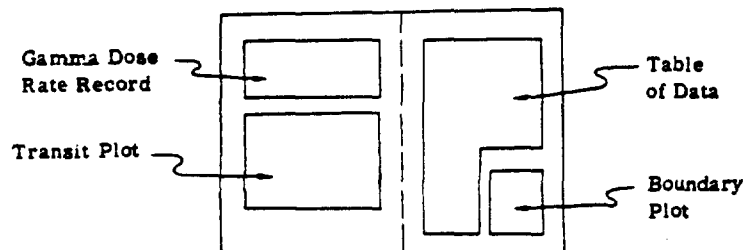
Approach velocities: Photo-velocities calculated for boundary indicated at specified distances greater than that at TOP. Rad-velocities calculated for rise from 5 to 100 percent of peak for models indicated (see Section A.3).

Waterborne sources: Calculated water and foam movements for drifts and sets or radial expansions indicated.

Bomb-generated waves: Calculated as described in Section 2.3.2.

4. Boundary plot: Distance of various surge boundaries shown as a function of time; normalized rate curve with logarithmic scale superimposed; calculated water and foam movements shown at bottom; values in brackets are read from dashed boundaries, which compensate for photographic disappearance of the surge (see text).

#### CHART IDENTIFYING SECTIONS OF ILLUSTRATIONS



Only a few of the gamma records require additional individual interpretation. The Wahoo record from Coracle CR 4.1 (Figures 3.77 and 3.164) may be useful for determining the decay rate of water directly contaminated by the detonation. This coracle overturned at an estimated time of 1.1 minutes and remained at its moored position until approximately 8 hours after zero time. White water reached the coracle at approximately 6 minutes and remained in the vicinity for about an hour. When recovered, the instrument well of this coracle contained about an inch of radioactive water (approximately 180 liters, reading 160 mr/hr at 75.6 hours), which presumably represents a sample of white water taken sometime within the first hour after the detonation. The 0- to 6-hour record for CR 4.1 (Figure 3.164) is a smoothly decreasing decay curve from about 30 minutes to the end of the record. Since the std-GITR dome is sealed directly to the instrument well cover, this record is then a decay curve for white water obtained through approximately  $\frac{1}{4}$  inch of aluminum.

The gamma record from Coracle CL 6.0 for Umbrella (Figure 3.84) represents a distant transit, but the observed dose rate is complex, showing a second rise in dose rate higher than the first, an occurrence which at first appears contradictory. A number of similar occurrences are revealed when the normalized rate curves for other distant or edge transits are inspected, viz, CL 4.6 for Wahoo and CR 4.9 for Umbrella (Figures 3.68 and 3.96, respectively). Such records are probably caused by a temporary decrease in surface wind speed at a time when the base surge is still actively expanding.

All free-field gamma dose rate records, together with their respective boundary plots, transit plots, and additional tabular data, are presented on the pages that follow. Coding must be used in order to condense a maximum amount of information into a minimum space. The coded designators have been selected so that, with some familiarity, their meanings should be immediately apparent. Many of the terms or coded designators have already been explained in the text of this section; however, all designators and special conditions of tabulation are fully described in the keys preceding the free-field records themselves or at the front of Appendix F.

**3.3.3 Free-Field Isodose Contours.** The principal sources of contour data are: (1) cumulative doses at various times after zero time from the std-GITR for the early time contours, augmented in the final contours by (2) film pack information. The GITR cumulative doses are presented in Table 3.9 and all film pack information is summarized in Table 3.12. Oblique photography of the base surge taken by aircraft circling the event at an altitude of 10,000 feet and a slant range of approximately 23,000 feet was used to check contour shapes against base surge positions at early time, (the estimated accuracy of these surge boundaries is presented in Section 3.3.2).

The total cumulative dose recorded by a std-GITR and the total dose registered by a NBS film pack installed at the same location show good correspondence (Figure 3.97). Similar correlation has been previously reported for similar combinations of film packs and recording ion chambers (References 33 and 132). Both the directional and energy response of the NBS film packs are considered compatible with the std-GITR (Section C.4). Thus, the film pack dose may be converted to an equivalent total GITR dose by the factor of 1.25, the slope of the straight line through the data plotted in Figure 3.97. Tripod film packs (Section 2.2.5) are considered directly comparable with the std-GITR when the coracle did not overturn, whereas FFP's are converted to an equivalent std-GITR dose by comparing them with the float packs attached to nearby coracles. The variation between the three types of film packs is usually small, being caused primarily by differences in the total solid angle of the radiating cloud subtended and by the effects of radioactive water. The few large discrepancies between a tripod and an FFP dose may be explained by overturn and subsequent passage of radioactive foam (Section 3.3.5).

The contours presented in this section are constructed by means of the logarithmic method described in References 95 and 96. All cumulative dose information is first converted to an equivalent std-GITR dose for a given station. These data points are mapped and then connected by straight lines along which the difference in dose between the two positions is marked off ac-

ording to a logarithmic scale. The contours are then constructed through the resultant field of logarithmic scales. The first isodose contours to be constructed are the final contours, since all information for a given shot can be used. After this map is completed, the contours for earlier times are constructed from the final map with the aid of photographic information on base surge shape and position.

All isodose contours presented suffer from the fact that the point density is too low to permit reliable construction. Maximum reliance is placed in the final isodose contours (Figures 3.103 and 3.109) in which 21 data points have been used for the Wahoo construction and 79 for Umbrella. Since no film pack information and only a portion of the total GTR array may be used in the construction of the early time contours, these contours are no better than estimates based on the limited data available and complete familiarity with conditions in the field at the time of the shot. On the basis of reliability, only the final contours should be presented, and even this presentation in the case of Wahoo may be questioned; however, since it is realized that a series of isodose contours at various times shortly after zero time are needed and will probably be constructed by persons making an operational analysis of ships maneuvering in the vicinity of an underwater detonation, the estimated isodose contours at these earlier times are also reproduced (Figures 3.98 through 3.102 and 3.104 through 3.107). These contours are, therefore, presented under the assumption that estimates made by persons completely familiar with all currently available information and with the situation in the field at the time the measurements were made are preferable to no information whatsoever. All contours, especially those for early times, must, however, be used with caution.

The protrusions shown in some early time contours and in the final contour for Wahoo may be questioned; however, those for Umbrella appear to be supported by sufficient data to be accepted. Such protrusions might have been caused by discrete bodies of radioactive aerosol moving only along specific radii. Alternatively, discrete masses of radioactive aerosol might have been propelled ahead of the rapidly advancing plumes and thus might have arrived at times substantially ahead of the main body of activity along a given radius. There is some evidence for this latter hypothesis in plots of base surge radius versus time (Section 3.3.4). Although the data is insufficient to substantiate either hypothesis, the requirement in both cases for a relatively small, discrete body of radioactive aerosol should be noted, since this notion is contrary to the usual concept of massive toroidal expansion.

Plots of GTR cumulative dose at various times versus distance from surface zero may be more useful than contours for the operational analysis of situations involving moving ships, since the direction of the surface wind and the approximate location of surface zero are the two factors having the highest probability of being known. The basic cumulative dose information has been discussed in Section 3.3.2 (Table 3.9), and the plots for 1, 2, 3, and 5 minutes and 6 hours after zero time are presented in Figures 3.110 through 3.119. The points are somewhat scattered, particularly for cumulative periods less than 5 minutes, a fact that is probably a result of the variable nature of the contaminating event at close distances. The plots for Umbrella also exhibit a hump or plateau extending to approximately  $7,500 \pm 1,500$  feet, a distance that corresponds to the point at which the radial expansion of the base surge essentially ceases and the principal transport mechanism becomes the surface wind (Section 3.3.4). It is possible that this change in transport mechanism is reflected in the cumulative dose.

Further information useful in a study of cloud dynamics is obtained by plotting the dose rate versus distance from the moving cloud center, a presentation that should correct for the effects of surface wind. Although considerable latitude exists in the choice of surface wind, the plot is reasonably insensitive to changes of the same order of magnitude as those listed in Section A.4. Consequently, the surface winds reported by the Task Force (15 knots from  $090^\circ$  T for Wahoo and 20 knots from  $050^\circ$  T for Umbrella) were used to compute the location of a hypothetical surge center H at various times. The distance of all stations from this moving hypothetical center were determined graphically and are summarized together with dose rate information in Table 3.13. Only the data for the first 5 minutes has been plotted in Figures 3.120 through

3.127, since at later times the fact that the center of the radioactive cloud and the center of the radioactive water are separated by a considerable distance makes interpretation difficult. The most probable position of the radioactive cloud is indicated in these plots as a shaded area; the points not included in this area are considered to be dose rates arising primarily from radioactive water. These plots are too scattered for any precise cloud shape to be established; however, they do indicate that the radioactive cloud for Wahoo is apparently continuous through its center whereas the center of the Umbrella cloud was relatively free of radioactive aerosol. These general distributions of airborne radioactive material have already been suggested in Section 3.3.2, and the presentation in this section is simply a means of summarizing the dose rate information from all stations in a single plot.

3.3.4 Transport Phenomena. Analysis of transport phenomena has been performed only to the extent necessary to interpret the gamma dose rate records. The material presented in this section is again based upon an analysis of the GTR records and surge boundary positions derived from photography as described in Section 3.3.2. The limitations of this preliminary treatment have been explicitly stated in Section 3.3.2. In general, however, there is reasonable agreement between data derived from photographic positions of the surge (Section 3.3.2) and that determined by use of the hypothetical surge center H (Section 3.3.3, and this section). Although the individual numerical values can only be accepted within wide limits of error, the internal consistency of data from several different analytical treatments is considered indicative of the validity of the general interpretation.

Time of arrival (TOA) (see Appendix F) of radioactive material at a given station is the first obvious parameter for inspection; however, TOA may be defined as (1) time to the first pronounced increase in dose rate, (2) time to first peak in dose rate, or (3) time to some specified point on the increasing slope of the first major dose rate peak. The last definition of TOA is undoubtedly best, yet the selection of the specific point depends on the base surge model assumed. By use of the computed dose rate curves for the approach of various hypothetical cloud models (Figures 1.9 and 1.10, and Section A.3), an average TOA may be defined as 38 percent of peak dose rate for any of the 60° cloud models, as 54 percent of peak for the 90° models over 1,200 feet in thickness, or as 74 percent of peak for 90° cloud models in the neighborhood of 400 feet thick. Accordingly, TOA has been read from the standard GTR records for 38, 54, 74, and 100 percent of the first major peak in dose rate. These values are tabulated in Table 3.14. The average of the 38- and 100-percent values is frequently used for the radiologically determined TOA (rad-TOA). This value is given in Table 3.11; as also indicated by this table, the photographically determined TOA (photo-TOA) occurs after the rad-TOA for Wahoo, whereas the reverse is true for Umbrella.

A comparison between various photographically and radiologically determined approach velocities (discussed later in this section) indicates some preference for the thicker cloud models and a more definite preference for all 60° cloud models. Since only rough general agreement is shown, no positive selection of cloud models can be made; however, if the 60° cloud models are accepted, the 38-percent TOA should be correct for most downwind arrivals. A plot of TOA thus defined is presented for each shot in Figures 3.128 and 3.129. Since this definition does not satisfy all observed phenomena, a similar plot of TOA defined as 100-percent peak dose rate is also presented for each shot in Figures 3.130 and 3.131. A comparison of these plots reveals that they are relatively insensitive to the definition of TOA.

After the break, the slope of the best straight line for Wahoo is 15 to 16 knots, which is the same as the reported surface wind speed at shot time. For Umbrella, arrival times at the more distant stations show considerable scatter, which may be due to the effect of the atoll reef (Section 3.3.2). Visual

approach velocities for these stations are, however, fairly consistent with the reported surface wind. It seems reasonable to assume, therefore, that the primary transport mechanism at downwind distances greater than  $7,500 \pm 1,500$  feet is the surface wind. The upwind and crosswind arrivals cannot be analyzed in this simple manner, since the radial expansion in these cases is being bucked to varying extents by the surface wind. Since the TOA at most upwind and crosswind stations is less than 1 minute, the base surge center can be considered nearly stationary, in which case radial expansion seems to carry the base surge to distances of 3,000 to 4,000 feet and 4,000 to 5,000 feet in the upwind and crosswind directions, respectively.

Although there are insufficient data points to be conclusive, these TOA plots suggest that the base surge may have moved at different speeds in specific downwind directions. For Umbrella, the slopes of the best straight lines through all stations at distances greater than 6,000 feet on legs DL, D and DR indicate apparent speeds of 35, 23, and 17 knots, respectively. Since surface winds have been assumed to be the primary transport mechanism at these greater distances, the suggestion of different radial speeds is apparently contradictory. This contradiction may be resolved by postulating a nonuniform distribution of radioactivity within the visual base surge when radial expansion effectively ceases. Since the time intervals required for these masses to reach the stations concerned are short, this nonuniform distribution could be reflected as apparent differences in speed along specific radii. As previously suggested, this explanation is at least consistent with the downwind protrusions on the isodose contours presented in Section 3.3.3. Alternatively, variable effects due to the atoll reef discussed later could result in apparent differences in speed of approach.

The rapid radial expansion of the base surge predominating at closer distances is probably due to collapse of the central column. This transport energy is dissipated at approximately 7,500 feet downwind of surface zero and at smaller distances in the upwind and crosswind directions. Although average downwind radial velocities for this expansion have been approximated by determining the slope of a straight line through these closer points, the treatment oversimplifies the situation, since the decrease in radial velocity with distance from surface zero is probably not linear and since wind effects are tacitly ignored.

More reasonable estimates of base surge approach velocities can be determined both for the visible surge from the boundary plots (Section 3.3.2) and for the airborne radioactive material from an analysis of the rate of rise to the first gamma dose rate peak. The visual approach velocity may be calculated for either the primary photo-boundary  $P_0$  or the outer smooth boundary  $B_0$ . Since the distance of both boundaries as a function of time is given in the boundary plots, the slope of the appropriate curve at some time (or distance) prior to surge arrival yields the desired velocities. In most instances, these slopes are changing rapidly; thus, the approach velocities are quite sensitive to the point at which the slope is determined. The most informative comparison is that between the photographically and the radiologically determined approach velocities; therefore the points are defined with respect to the time of peak dose rate (TOP). Visual approach velocities are determined for times when  $P_0$  or  $B_0$  are 100, 200, 300, and 500 feet more distant than at TOP. These velocities are presented in Table 3.15 (estimated values enclosed in parentheses). Agreement between the approach velocities determined for the primary photo-boundary and the outer smooth boundary indicates a relatively even surge outline in the neighborhood of the station; conversely, large discrepancies suggest lobes or irregularities.

The approach velocity for the airborne radioactive material is determined by the rate of rise (r of r) to the first major gamma dose rate peak (hence the r-of-r velocity). To determine velocity in this manner, some shape has to be assumed for the approaching body of airborne radioactive material. The radiation intensity for several cloud models has been calculated as a function of distance between the cloud source and the detector (Section 1.3.2). Assuming that these models approximate actual surge shapes, the distance required for an increase in dose rate from 5 to 100 percent of peak value may be obtained from these computed intensities. This distance divided by the time required for a similar increase in recorded gamma dose rate yields a velocity of approach dependent upon the cloud model assumed. These approach velocities calculated for a number of cloud models using a gamma energy of 1.25 Mev are presented in Table

TABLE 3.15 VISUAL APPROACH VELOCITIES

$F_0/B_0$  determined at indicated distances greater than measured boundary distance at TCP.

	minus 100 ft (k)	minus 200 ft (k)	minus 300 ft (k)	minus 500 ft (k)
<b>MAHOO:</b>				
U 4.5	-5, -12	-2, -9	0, -7	?, ?
CL 3.9	37, 19	39, 22	48, 24	46, 40
CL 4.6	13, 5	16, 7	15, 12	25, 21
DL 7.1	11, 20	15, 20	16, 20	20, 20
D 3.0	11, 28	12, 25	14, 24	15, 24
DR 4.5	17, 20	14, 20	13, 20	13, 20
DR 9.0	32, 13	32, 13	32, 17	32, 27
DR 14.4	14, 16	15, 16	16, 14	16, 14
DR 24.0	16, 14	16, 14	16, 14	15, 14
DRR 6.8	14, 14	14, 17	15, 19	26, 24
DRR 12.8	19, 19	19, 19	19, 19	22, 19
CR 4.1	25, 17	29, 26	46, 38	60, 69
CR 5.2	6, 7	8, 14	21, 23	33, 45
CR 6.4	----- (26)/(3) at 1.5 min -----			
EC-2 fwd	32/36	32/36	32/36	32/36
DD-593 stbd	17/26	17/26	17/26	17/26
<b>UMBRELLA:</b>				
U 1.8	----- (40-60) -----			
U 2.7	----- (35-45) -----			
U 3.9	----- (20-25) -----			
CL 3.1	----- (35-45) -----			
CL 6.0	6/7	17/9	23/11	37/15
DLL 6.6	17/12	18/12	18/13	20/15
DL 6.2	20/19	21/20	22/21	26/26
DL 16.0	20/21	20/21	20/21	20/21
D 2.7	----- (40-70) -----			
D 4.8	38/32	44/38	45/46	52/53
D 18.2	15/15	15/15	15/16	15/15
D 22.0	13/14	13/14	14/14	14/15
DR 12.2	3/7	4/10	5/11	9/12
DR 18.6	4/3	5/4	5/5	7/7
DRR 3.9	27/50	27/52	30/55	54/70
DRR 6.7	6/5	7/6	8/8	12/11
CR 4.9	12/16	16/22	19/32	35/46
EC-2 fwd	----- (40-60) -----			
DD-474 stbd	----- (40-50) -----			
DD-592 stbd	----- (40-50) -----			
DD-593 port	12/14	10/13	9/13	9/11

3.16. The obvious difference between the assumed cloud models, which describe the approach of a linear cloud front, and true base surge, which probably approaches as a segment of a circle of finite radius, is negligible for the large surge dimensions observed.

As stated above, only a rough general agreement exists between the visual and radiological approach velocities (Tables 3.15 and 3.16). The most favorable comparison is obtained for the visual approach velocity determined at minus 500 feet. Lack of better agreement is probably due to variations in the generation and behavior of different segments of total base surge and to uncertain knowledge of local surface winds. Further difficulties are caused by double spikes (Appendix F) in the first major peak and by obvious changes in the slope of the dose rate curve, which are associated with base surge emergence at early times (Section 3.2). R-of-r velocities determined for rises from 1, 5, and 10 percent to 80 and 100 percent of peak in an attempt to circumvent these difficulties do not yield any significant improvement. The 5- to 100-percent determinations are simply presented as representative. Thus, although the comparison between visual and radiological approach velocities gives somewhat better agreement for the thicker 60° cloud models, distinctions made on this basis may be entirely fictitious. The rough general agreement between the visual and radiological approach velocities does suggest that the visible surge and the radioactive aerosol are moved by the same mechanical forces but does not necessarily imply that they are the same body of airborne material.

The velocities tabulated in Table 3.16 represent a best estimate of the speed with which the major radiating source approached the detector. They are, therefore, the vector sum of the velocity due to radial expansion and the surface wind velocity. An approximate value for the radial velocity may be deduced from the approach velocity by assuming that movement of the photographic surge center X (Appendix F) actually represents local variations in surface winds. The instantaneous radial component of the local wind at the rad-TOA for each station can then be estimated and is presented in Table 3.17. This radial component is small for rad-TOA's less than 1 minute, because the surge requires about that amount of time to accelerate to surface wind speed. The appropriate approach velocities corrected for the wind component represent radial velocities due to expansion and are also presented in Table 3.17. The negative velocities obtained at DR 9.0 for Wahoo may reflect possible ship retardation (Section 3.3.2) whereas those obtained at the more distant stations for Umbrella probably indicate that local wind variations based on movements of the photographic surge center X do not necessarily correspond to those existing at the surge periphery.

For both shots, records from the Eniwetok weather station show enough variation in both surface wind speed and direction to cause errors in the computed radial components as large as  $\pm 5$  knots. These approximate radial velocities are plotted for Wahoo and Umbrella in Figures 3.132 and 3.133. Because expansion of the base surge into an opposing wind would tend to increase the angle of the front, radial velocities derived from the 90° cloud model are used for the upwind stations. Velocities derived from the 60° model are used in all other directions. Cloud thicknesses of 1,600 feet and 1,200 feet are used for Wahoo and Umbrella, respectively. The scatter in the radial velocity data is partially due to uncertainties in the basic assumptions underlying the calculations but may also be due to actual differences in the initial velocity of expansion along specific radii. Furthermore, local vertical surge development caused by the atoll reef could be reflected as an apparent increase in radiologically determined approach velocity. The high approach velocity reported for Umbrella Station DR 18.6 may represent such a case. Local vertical development over the reef could increase the radiating area without greatly changing horizontal motion. Such action would result in an apparent increase in approach velocity.

These approximate radial velocities may be compared with the fluid models of References 97 through 100. In all investigations, fluid columns of a uniform density greater than that of the ambient fluid were released from rest and their collapse studied photographically. A similar collapse has been suggested as the primary mechanism for the formation of base surge. Unfortunately, Reference 97 is for a solid column, and insufficient information is available in the published work to make an exact conversion to Wahoo and Umbrella conditions. The data

TABLE 3.16 VELOCITY OF APPROACH CALCULATED FROM RATE OF RISE OF STD-GTTR

Nominal Position	Velocity of Approach (5% to 100% of peak) 90° Model*			Velocity of Approach (5% to 100% of peak) 50° Model*		
	thickness = 1600 ft	thickness = 1200 ft	thickness = 400 ft	thickness = 1600 ft	thickness = 1200 ft	thickness = 400 ft
	(k)	(k)	(k)	(k)	(k)	(k)
<b>WABDO:</b>						
U 4.5	14	13	11	16	14	11
CL 3.9	17	14	11	16	14	11
CL 4.6	20	18	16	22	20	16
DL 7.1	25	21	20	27	24	18
D 8.0	34	31	26	37	32	27
DR 4.5	22	20	16	24	22	17
DR 9.0	14	13	11	15	14	11
DR 14.0	-	-	-	-	-	-
DR 24.0	7	6	6	8	7	5
DRN 6.6*	37	34	29	40	35	27
DRN 12.8**	19	17	15	20	18	14
CR 4.1	67	61	52	72	64	49
CR 5.2	41	38	32	45	39	30
CR 6.4	-	-	-	-	-	-
RC-2 ftvd	43	39	34	47	41	32
RD-593 stbd	28	26	22	31	27	21
<b>UMBRELLA:</b>						
U 1.8	66	61	53	74	64	47
U 2.7	51	46	40	56	49	36
U 3.9	16	16	14	19	16	13
CL 3.1	62	56	49	66	60	43
CL 6.0	21	20	17	24	21	14
DL 6.6	30	27	24	33	29	21
DL 6.2	62	56	49	66	60	43
DL 16.0	20	18	17	22	19	13
D 2.7	100	93	80	111	99	72
D 4.8	48	44	38	54	47	34
D 18.2	12	12	10	14	12	9
D 22.0	12	10	9	13	11	8
DR 12.2	7	8	6	8	7	5
DR 18.6	13	12	10	14	12	9
DRN 3.9	48	44	38	54	48	34
DRN 6.7	19	18	16	21	18	13
CR 4.9	25	23	20	26	24	18
RD-593 port	35	32	27	38	33	26

\*See Section 1.3.2 and Appendix A-3.  
\*\*Note: record obtained from sec-GTTR.

TABLE 3.17 RADIAL VELOCITY OF EXPANSION COMPUTED FROM RATE OF RISE OF STD-GTTR (Movement of photographic surge center used to estimate surface wind)

Nominal Position	Bearing and Distance of Photographic Surge Center, X		Rad-TCA (avg 38% ± 100%)	Wind Component Along Station Radius	Radial Velocity (upwind stations 90°; other stations 50°)**		
	Bearing from Station	Distance from Station			thickness = 1600 ft	thickness = 1200 ft	thickness = 400 ft
	deg (true)	ft			min	knots	knots
<b>WABDO:</b>							
U 4.5	070	6000	1.25	+13.7	28	27	25
CL 3.9	146-1/2	4390	0.85	+6.5	46	42	34
CL 4.6	134-1/2	5390	1.40	+4.3	26	24	19
DL 7.1	223-1/2	5660	1.46	-12.6	14	11	5
D 8.0	256	5360	2.08	-15.8	21	16	9
DR 4.5	265-1/2	2790	1.46	-12.4	12	10	5
DR 9.0	269-1/2	5100	2.99	-15.4	0	-1	-4
DRN 6.6*	266-1/2	5350	1.28	+9.9	30	25	17
DRN 12.8**	291-1/2	7980	4.20	-13.4	7	5	1
CR 4.1	351	3600	0.92	+1.8	74	66	51
CR 5.2	350	4700	1.25	+2	49	41	34
RC-2 ftvd	247-1/2	5500	0.63	+6.6	54	48	39
RD-593 stb	041-1/2	2700	2.61	-14.9	16	12	6
<b>UMBRELLA:</b>							
U 2.7	068-1/2	2850	0.60	+9.1	60	56	50
U 3.9	069-1/2	4325	0.86	+9.1	26	25	23
CL 3.1	160-1/2	3090	0.62	+4.7	71	64	48
CL 6.0	147-1/2	6140	1.10	+0.7	24	21	14
DL 6.6	197	5200	1.66	+6.8	27	22	14
DL 6.2	226-1/2	5150	1.18	-11.2	55	48	32
DL 16.0	240	8600	4.22	-19.0	3	0	-6
D 2.7	248	2590	0.2	+9.1	103	90	62
D 4.8	247-1/2	4240	0.83	+8.9	45	38	25
D 18.2	276	8490	6.51	-13.1	1	-2	-4
D 22.0	275-1/2	9410	7.92	-14.0	-1	-3	-6
DR 12.2	282	6100	4.83	-12.7	4	-6	-8
DR 18.6	322-1/2	9410	8.86	+4.1	10	8	5
DRN 3.9	262	3650	0.79	-10.5	43	36	24
DRN 6.7	251	5330	1.81	-7.5	14	11	6
CR 4.9	140	4620	0.80	+9	23	19	13
RD-593 port	250-1/2	6200	1.56	-11.4	27	22	15

\*Record obtained from secondary GTTR  
\*\*See Section 1.3.2 for description of cloud models used.

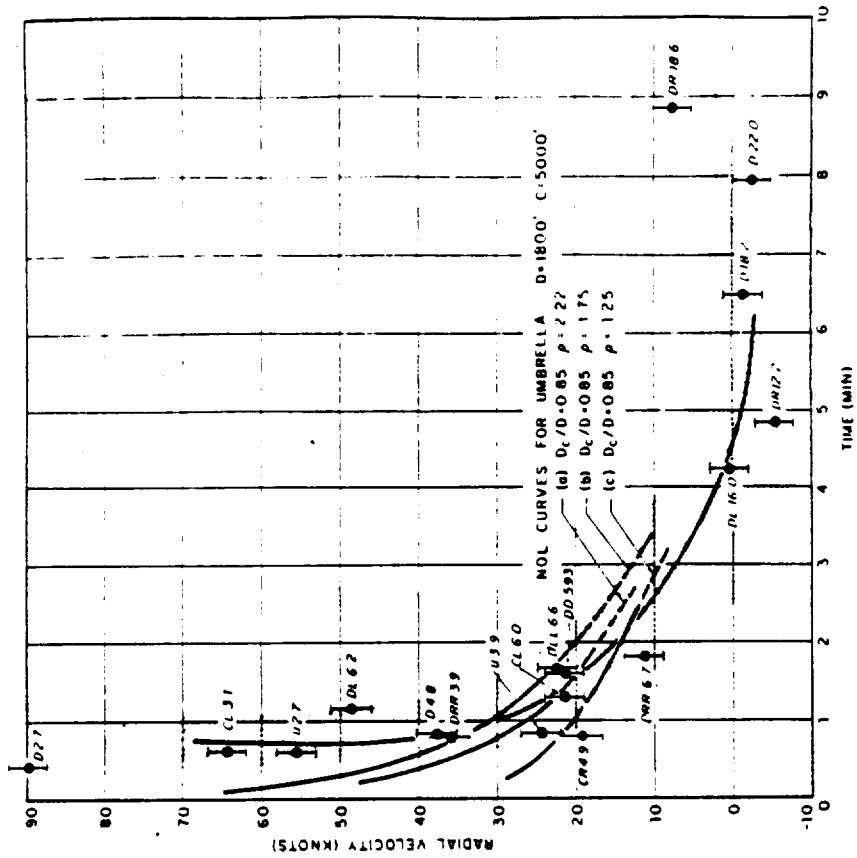


Figure 3.133 Radial velocity of base surge, Shot Umbrella. (Determined from rate-of-rise: 90° cloud model for the upwind stations, all others 60° cloud model; thickness = 1,200 feet.) Assumed surface wind: 16 knots from 053° T.  $\rho$  = the density of the collapsing fluid column relative to that of the ambient fluid.

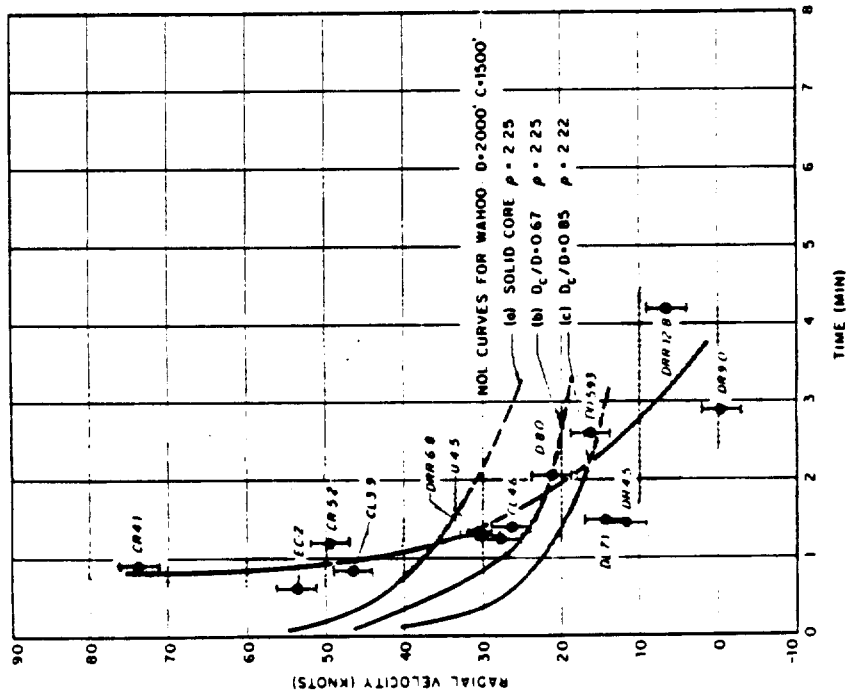


Figure 3.132 Radial velocity of base surge, Shot Wahoo. (Determined from rate-of-rise: 90° cloud model for the upwind stations, all others 60° cloud model; thickness = 1,600 feet.) Assumed surface wind: 14 knots from 070° T.  $\rho$  = the density of the collapsing fluid column relative to that of the ambient fluid.

given by Reference 98, however, has been converted to the Wahoo and Umbrella cases, using a column diameter  $D$  of 2,000 feet and a column height  $C$  of 1,500 feet for Wahoo; similar parameters for Umbrella are 1,800 feet and 5,000 feet, respectively. The cases for a solid column and for two hollow columns (one with an inner core  $D_c$ , 67 percent of the outer diameter, and a second with an inner core  $D_c$ , 85 percent of the outer diameter) are computed for both shots. None of the resultant radial velocity curves compare with those obtained for Wahoo; three such curves representing the three types of columns have been superimposed on the observed curve in Figure 3.132. All velocities are plotted relative to zero time instead of relative to the time of base surge formation as suggested by Reference 98. The case for a hollow core, 85 percent of the outer diameter, most closely approximates the radial velocities observed for Umbrella, and three such curves representing the collapse of columns of three different densities have been superimposed on the observed curve in Figure 3.133. The comparison with these fluid models is, however, poor at best. The collapse of the fluid models starts with the column at rest, a static condition that only approximates the actual situation. The collapsing column, particularly on Wahoo, must have had some initial radial velocity before collapse as indicated by the throwout plumes. A more extensive study of these phenomena is required before any definite conclusions can be drawn.

The time of cessation (TOC) (see Appendix F) is subject to a number of definitions even greater than TOA. TOC may be defined either as the time at which the normalized rate curve becomes essentially horizontal after registering the passage of the main series of dose rate peaks or as that point at which the normalized rate curve drops permanently below  $10^3$  r/hr. Both TOC's have been determined for each station, and these values are presented in Table 3.18. A plot of cessation times defined either way versus distance is badly scattered particularly for the close-in stations where TOC is influenced both by surge development and by contributions from waterborne radioactive sources. At greater distances, the slope of the data points roughly approximates the reported surface winds. Since the latter definition of the TOC sometimes indicated by the abbreviation "norm  $10^3$  ↓", is more readily corrected for the effects of waterborne sources, this TOC is used for the study of the surge tails, the postulated diffuse remnants which trail behind the base surge (Section 3.3.2). The length of these tails is computed on the basis of the time difference between the photo-TOC and the rad-TOC, using the official Task Force surface wind speed.

The distance of the primary surge photo-boundary  $P_0$  along each of the station legs has been determined at various times after zero time (Table 3.19). A plot of these distances versus time may be approximated by a straight line for most downwind legs. The slopes of these straight lines are also given in Table 3.19. At approximately 4 minutes after Umbrella, a break occurs in the downwind plots, which probably represents the passage of the downwind surge over the atoll reef (Section 3.3.2). The slopes for Umbrella are, therefore, given both before and after this time. In general, the slopes of all lines are close to the reported surface wind speeds; however, once again there is some evidence of a difference in base surge velocity along specific radii. There is also some indication that the point of maximum dose rate (source center) recedes farther behind the surge front at later times. Since the later visible boundaries are rather diffuse, the postulated recession can only be illustrated by comparing the time at which the dose rate reached 0.1 percent of peak values with time of the peak value (Figures 3.134 and 3.135). The tendency for the time of peak to fall farther behind the time of the first rise in dose rate is, however, so slight that it cannot be conclusively demonstrated with the available data. If this phenomenon is real, it may possibly be explained by the fact that the base surge increases in height with time and thus increases its effective radiating area.

The base surge radius has been determined by calculating the position of the hypothetical surge center for the time of peak dose rate recorded at a given station and measuring the distance from the station to this center. These measurements have been made, both for the first peak representing the downwind surge transit and for the completion of the upwind surge transit (photo-TOC). These radii are presented in Table 3.20. The measured radii for the first peak are also plotted in Figures 3.136 and 3.137. For Wahoo, the surge radii at time of peak appear

TABLE 3.18 TIME OF CESSATION (TOC) AT CORACLES

Nominal Position	Bearing From	Distance From	TOC	TOC
	Surface Zero	Surface Zero	Norm. Horiz.	norm 10 <sup>3</sup> †
	deg (true)	ft	min	min
WAHOO:				
U 4.5	066	4,500	6	3.03
CL 3.9	159	3,900	5	(5.2)**
CL 4.6	151-1/2	4,600	7	4.45
DL 7.1	231-1/2	7,100	14	11.34
D 8.0	256-1/2	8,000	17	15.80
DR 4.5	263	4,500	15	?
DR 9.0	263	8,950	17	15.42
DR 14.4	265	14,400	16	(>20)**
DR 24.0	263	24,000	27	25.26
DRR 6.8	281	6,800	16	13.52
DRR 6.8*	281	6,800	16	13.37
DRR 12.8	276	12,800	18	14.51
DRR 12.8*	276	12,800	18	14.45
CR 4.1	336	4,100	5	(3.8)**
CR 5.2	334-1/2	5,200	6	5.13
CR 6.4	332	6,400	9	(4.8)**
UMBRELLA:				
U 1.8	051.8	1,760	10	?
U 2.7	067	2,700	8	(3.2)**
U 2.7*	067	2,700	8	(3.2)**
U 3.9	068	3,890	7	1.41
CL 3.1	163.7	3,060	6	(5.4)**
CL 6.0	158.9	6,010	8	4.00
DLL 6.6	207.5	6,580	12	9.05
DL 6.2	230.4	6,220	14	9.45
DL 16.0	237.1	15,980	20	14.23
D 2.7	248	2,670	8	?
D 2.7*	248	2,670	8	?
D 4.8	247.9	4,770	12	(7.7)**
D 4.8*	247.9	4,770	12	(7.7)**
D 18.2	250.2	18,220	16	12.95
D 22.0	248	22,000	20	14.72
DR 12.2	262.5	12,230	12	8.54
DR 18.6	261	18,600	16	12.98
DRR 3.9	279.1	3,940	10	(6.8)**
DRR 6.7	278.1	6,740	10	6.45
CR 4.9	334	4,910	7	2.47

\*Record obtained from secondary GIER.

\*\*Values in parentheses are estimated or extrapolated.



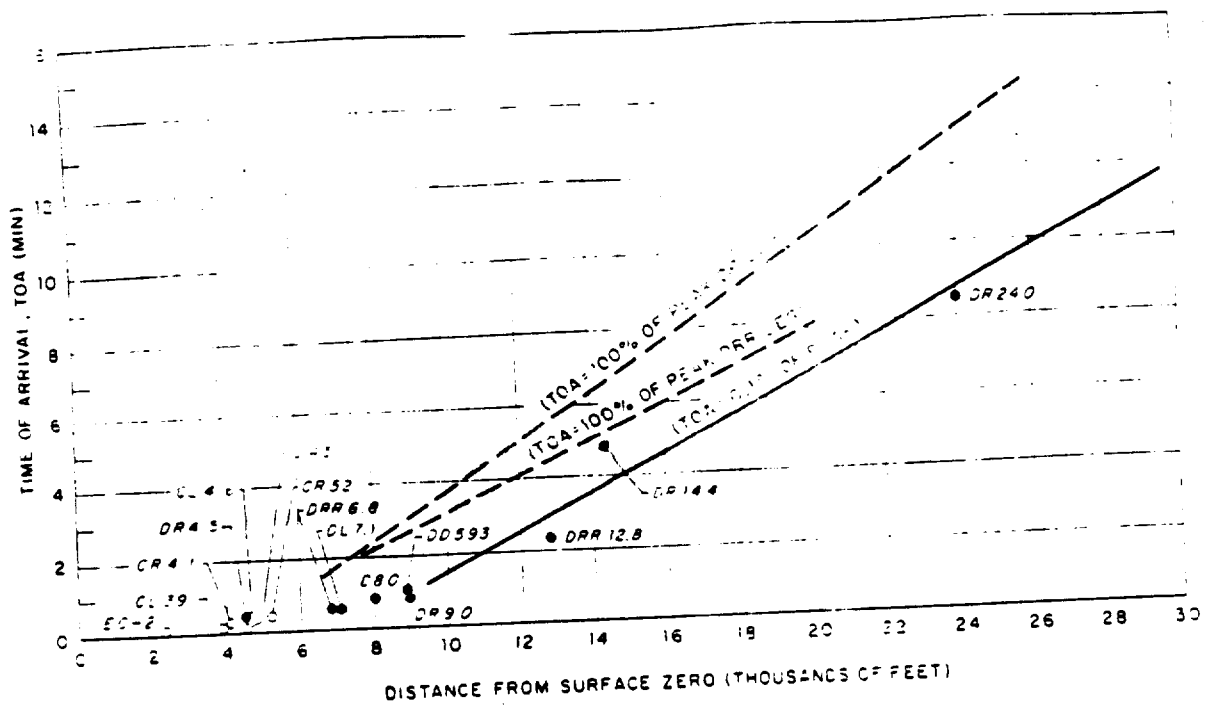


Figure 3.134 Comparison of time of peak with earliest time of arrival, Shot Wahoo. Note: For greater convenience, dashed lines represent TOA information transferred from Figure 3.131.

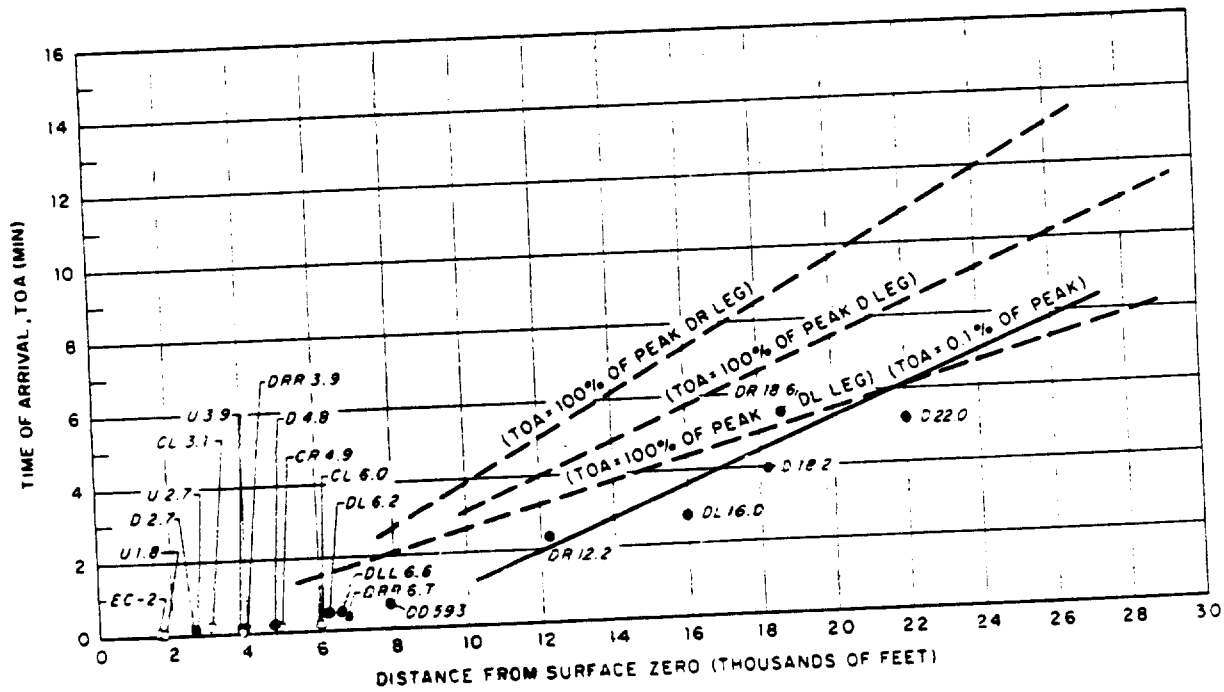


Figure 3.135 Comparison of time of peak with earliest time of arrival, Shot Umbrella.

TABLE 3.20 RADIAL DISTANCES TO HYPOTHETICAL SURGE CENTER AT TIME OF PASSAGE OF BASE SURGE BOUNDARIES\*\*

Nominal Position	Actual Position		Base Surge Radius				Remarks	
	Bearings from Surface Zero	Distance from Surface Zero	Determined at Downwind Transit		Determined at Upwind Transit			
			Time of Peak	Dist to Center	Time	Dist to Center, H		
deg (True)	ft	min	ft	min	ft			
<b>WAHOO:</b>								
U 4.5	066	4,500	1.7	6,200	3.5	9,610	closest approach	
CL 3.9	155	3,900	0.98	4,630	4.25	9,450		
CL 4.6	151-1/2	4,600	1.67	6,240	4.10	9,350		
DL 7.1	231-1/2	7,100	1.66	5,400	9.50	9,920		
D 8.0	256-1/2	8,000	2.17	4,850	10.90	8,980		
DR 4.5	263	4,500	1.63	2,100	8.35	8,250		
DR 9.0	263	8,950	3.23	4,220	11.60	8,830		
DR 14.4	265	14,400	5.6	4,500	15.10	8,720		
DR 24.0	263	24,000	12.85	5,200	21.25	9,020		
DRR 6.3*	281	6,800	1.37	4,780	9.85	8,400		
DRR 12.8	276	12,300	4.47	6,130	13.75	8,320		
CR 4.1	336	4,100	0.97	3,770	5.10	7,150		
CR 5.2	334-1/2	5,200	1.26	4,720	3.9	5,980		
CR 6.4	332	6,400	No high range channel.					
<b>UMBRELLA:</b>								
U 1.8	051.8	1,760	0.47	2,700	2.3	6,420	overturn	
U 2.7	067	2,700	0.68	4,050	1.90	6,490		
U 3.9	068	3,890	1.25	6,350	1.4	6,660	closest approach	
CL 3.1	163.7	3,060	0.67	2,500	2.35	5,360	overturn	
CL 6.0	158.9	6,010	1.50	5,800	4.0	8,410	closest approach	
DLI 6.6	207.5	6,580	1.77	3,540	6.85	8,220		
DL 6.2	230.4	6,220	1.23	3,730	7.20	8,400		
DL 15.0	237.1	15,980	4.5	7,070	12.50	5,710		
D 2.7	248	2,570	0.45	1,500	4.9	7,450	overturn	
D 4.5	247.9	4,770	0.90	3,100	6.2	8,150	overturn	
D 15.2	250.2	18,220	6.82	7,100	11.70	9,130		
D 22.0	245	22,000	8.2	8,100	13.30	9,080		
DF 12.2	262.5	12,230	5.13	6,550	5.50	6,600		
DR 13.6	261	18,600	9.15	9,550	10.0	10,510	closest approach	
DRR 3.9	275.1	3,940	0.88	3,100	4.5	7,210	overturn	
DRR 6.7	278.1	6,740	2.02	5,050	4.90	7,400		
CR 4.9	334	4,910	0.98	5,750	2.0	7,110	closest approach	

\* Record obtained from secondary GIBS.

\*\* First major ice rate peak assumed to correspond to the passage of the downwind edge of the base surge. The peak corresponding to passage of the upwind surge selected on the basis of cloud photography. The position of the hypothetical surge center, H, was determined assuming a surface wind 15k from 090° for Wahoo and 20k from 050° for Umbrella.

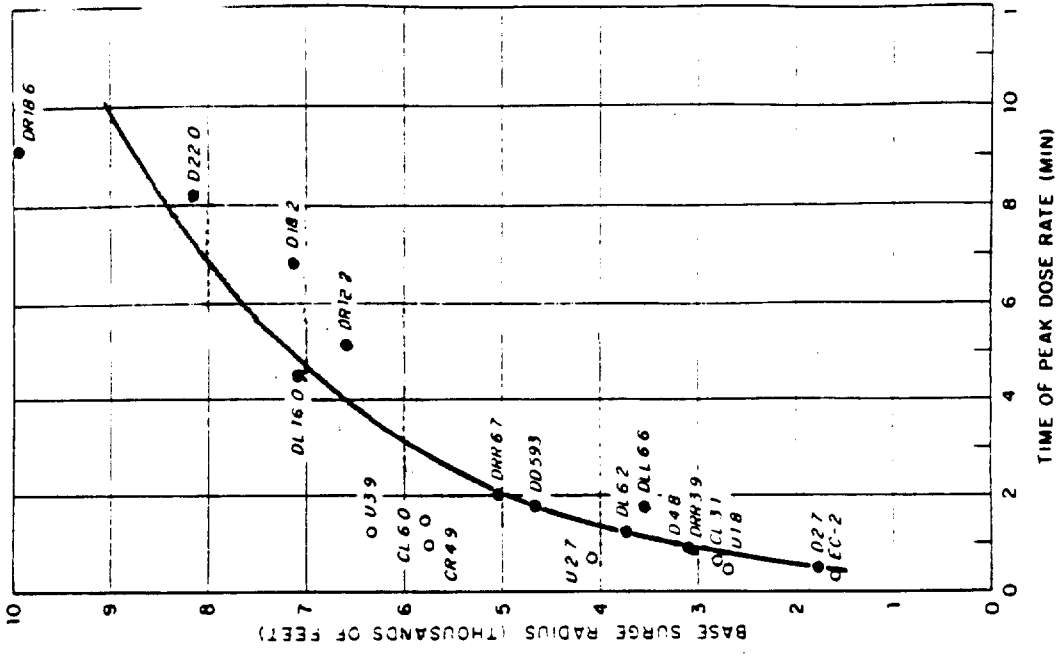


Figure 3.136 Hypothetical base surge radius versus time, Shot Wahoo. (Determined from time of first major peak dose rate.)

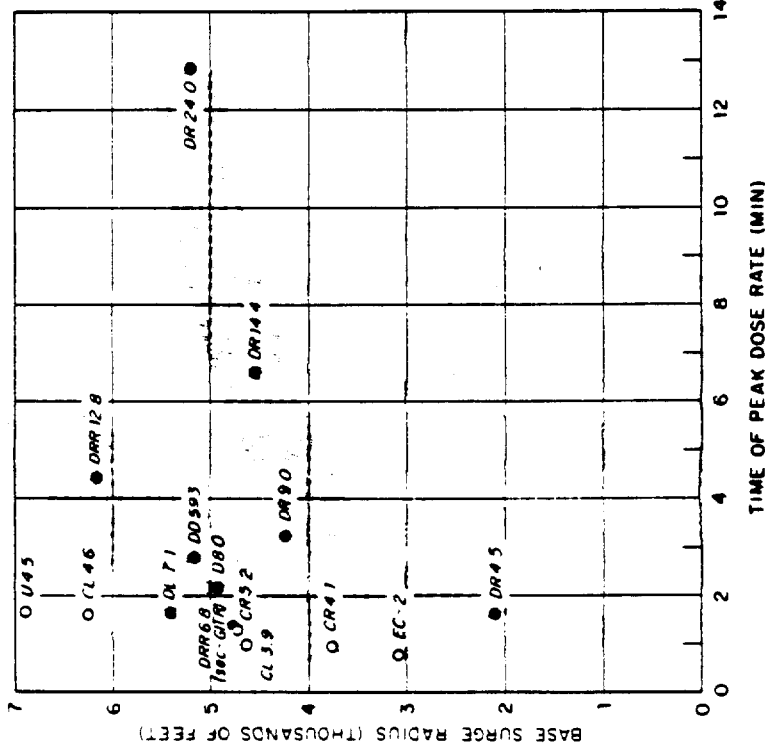


Figure 3.137 Hypothetical base surge radius versus time, Shot Umbrella. (Determined from time of first major peak dose rate.)

to fall on two separate curves, the possible existence of which may again indicate differences in radial transport velocities or may be due to the discrepancy between the official Task Force surface wind (15 knots from 090° T) and that indicated by surge photography (14 knots from 070° T). For Umbrella, the hypothetical surge radii tend to fall on a definite curve, although again two separate branches at later times could be drawn because of the postulated effects of the atoll reef and because of slight differences between the reported and photographically observed surface winds (Task Force weather report: 050° T, 20 knots; surge photography: 053° T, 16 knots). The radii determined at photo-TOC are fairly constant. Furthermore, they are similar both to the radii determined at TOP for the later transits and to those determined from base surge photography (Section 3.3.2).

Although only a few points of comparison exist, there are certain general similarities between Wahoo and Wigwam and between Umbrella and Shot Baker (Operation Crossroads) despite the large differences in yield in both instances. The Wigwam base surge, like Wahoo, first appears at about 13 seconds and expands at similar velocities; the visible surge velocities for Wigwam have been calculated from photographs (Reference 14) and are presented for comparison in Appendix E. Each shot generated secondary and perhaps tertiary plumes, which possibly resulted in secondary or tertiary base surges. Fallout or deposited material from the base surge seems to have been light at the greater distances. GITR's installed aboard the YAG-39, which was steaming at approximately 10 knots about 28,000 feet downwind of Wigwam, recorded peak dose rate of 550 r/hr at 16 minutes and a second peak of 640 r/hr at 19.7 minutes (Reference 9). The GITR at Station DR 24.0 on Wahoo recorded a peak dose rate of 589 r/hr at 12.7 minutes followed by a gradual decrease in dose rate, which continued to approximately 25 minutes. Although the shape of the dose rate peaks differ, possibly because one detector was moving while the other was stationary, both the peak dose rates and the time of arrival are comparable (surface wind for Wigwam was 18 knots from 031° T). Furthermore, film packs on the weather decks of the YAG-39 registered cumulative doses ranging from 26 to 35 r, values which compare favorably with the tripod film pack dose of 33 r registered at DR 24.0. Thus, despite the fact that the yields of the two detonations differ by a factor of 3, essentially the same doses and dose rates were observed at similar locations.

Umbrella and Baker were quite dissimilar events; however, in the few instances where comparison can be made, nearly the same dose rates during base surge transit were observed on both shots. The column for both shots was probably hollow. During Baker, the fireball was briefly visible at the top of the column. Later a cumuliform cloud similar to those from surface shots was formed, and the column was seen to be open to the atmosphere. During Umbrella, no cumuliform cloud was formed, and the column was probably never open to the atmosphere. The Baker column could have collapsed in a manner approximated by the fluid models just discussed; however, as the Umbrella column collapsed, two high energy jets of water, one vertically upward and the second downward, have been postulated at the collapsing apex.

During Baker, a heavy rain was observed to fall from the cumuliform cloud at about 3 minutes (References 35, 90, and 99) whereas for Umbrella a similar heavy rainfall from the base surge may have occurred continuously during the first minute after zero time. If the hypothesis (Reference 90) concerning the formation of this rain is accepted (Section 3.3.1), the early occurrence of rain would indicate that the individual droplets comprising the Umbrella base surge at formation were much larger than those postulated for Baker. The initial base surge velocities of the two shots are comparable; however, at later times the velocity for Umbrella falls considerably below that for Baker (Appendix E).

Comparison of dose rate information for the two shots is difficult, since so little rate information is available for Baker. Instruments similar to the std-GITR installed aboard LCT-874 and LCT-332 appear to have recorded an initial dose when the explosion bubble first reached the water surface. The instruments saturated; therefore, the peak dose rate cannot be determined (Reference 5). The record of the LCT-874 (7,500 feet, bearing 045° T from surface zero) is probably most similar to that obtained at DRR 6.7 on Umbrella; the peak dose rates were 4,000 r/hr at 1.7 minutes for the LCT-874 record and 6,000 r/hr at 2.0 minutes for DRR 6.7.

A comparison of the LCT-332 (5,700 feet, bearing 089° T from surface zero) record with that from the CR 4.0 shows that the first peak dose rates were at 0.9 minute and at 1.0 minute, respectively. The peak dose rates for the two shots appear, on the basis of this limited data, to be about the same order of magnitude; however, the total dose registered by film packs on the weather decks of the target ships for Baker are one or two orders of magnitude larger than total doses registered at similar locations for Umbrella (References 7 and 101). A detailed description of the film packs employed for Baker has not been located; however, it is probable that they were packets of Eastman Kodabromide G-3 and Eastman 548-0 double and single coat film shielded with a lead cross approximately 1 mm thick. Although the increased sensitivity of this type of film pack to beta and soft gamma radiation and the effects of heat prior to recovery may have increased the recorded total dose, neither effect could cause the large differences observed. It appears, therefore, that a very much heavier deposition of radioactive material occurred during Baker. The large deposit dose from Baker is thought to be due to fallout from the cumuloform cloud, which contained large amounts of radioactive coral from the lagoon bottom. Bottom material, however, does not appear to have been important during Umbrella even though this shot was fired on the bottom. A satisfactory explanation of this difference between Baker and Umbrella has not yet been advanced; however, it should be noted that the column was observed to vent to the atmosphere on the former shot, while no such observation exists for the latter.

3.3.5 Estimated Waterborne Radioactivity. The contribution to the free-field gamma dose rate from radioactive material falling into the ocean is negligibly small in comparison to the other radiation sources. Since only small amounts of radioactive material appear to have fallen from the base surge at distances greater than 3,500 feet (assumed maximum distance of heavy rain, see Section 3.3.1), the relative insignificance of radiation due to material suspended in the water is not surprising. This statement, however, is definitely not true of the other sources of waterborne activity discussed later in this section. The relative unimportance of radioactive material deposited from the base surge and remaining suspended in the surface waters is indicated in two ways. First, in all instances where the gamma record is not complicated by other waterborne sources, the underwater gamma records drop abruptly after registering passage of the airborne material, without showing any appreciable residual radiation. Second, FFP's dropped into the downwind array after the event do not register any dose significantly above the background. These FFP's were dropped 120 minutes after Wahoo and 60 minutes after Umbrella; therefore, the film pack data certainly indicates that no significant contribution for suspended material exists after these times. This data cannot be considered conclusive, since if all suspended material is assumed to sink at a rate of 0.96 m/hr (discussed later in this section), the postshot FFP drops are too late to register any significant dose from suspended material. The data dose imply either that the dose from suspended material remaining near the surface is insignificant or that, because of the sinking rate of this material, all important radiation ceases shortly after passage of the base surge (for the stated sinking rate, this time would be approximately 30 minutes). The doses obtained from these postshot FFP drops are summarized in Table 3.21.

Records from the underwater GTR (UW-GTR), described in Section 2.2.2, are subject to the same limitations set forth in Section 3.1. Unfortunately, a great deal of difficulty was experienced with the underwater detector cables and with the probe-dropping mechanism; therefore, only seven underwater records were obtained for Shot Wahoo and four for Shot Umbrella (Figures 3.143 through 3.153). The majority of the underwater records show a high dose rate peak at a time roughly corresponding to the peak registered by the std-GTR upon passage of the airborne radioactive material (compare Tables 3.8 and 3.22). The fact that the underwater detectors frequently produce records similar to those of the std-GTR leads to the suspicion that these detectors were much closer to the surface than the planned 6 feet.

Accordingly, in all cases where both a standard and an underwater record exists, the two records are compared. Since peak dose rates do not provide a reliable basis for comparison,

the 3-minute cumulative doses are used (Table 3.23). The possibility of radiation due to white water cannot be excluded from the closer stations; therefore, the calculated depth of the underwater detector in these instances must be regarded as a minimum possible depth. These depths are calculated by modifying the expression for the radiation intensity at a point above an infinite slab of uniformly distributed activity. In this case the radiation intensity at a depth beneath the water surface  $I_{uw}$ , due to a radiating cloud above the surface, is expressed by:

$$I_{uw} = \frac{J_A d}{2 \mu_A} \left\{ \left[ \frac{1+K}{d} \right] e^{-\mu_W d} - \mu_W [-Ei(-\mu_W d)] \right\}$$

- Where:  $J_A$  = source intensity per unit volume of the cloud  
 $\mu_A$  = linear attenuation coefficient for air  
 $\mu_W$  = linear attenuation coefficient for water  
 $K$  = a constant approximating the buildup factor in an expression of the form  $(1+K \mu_W d)$   
 $\mu_W d$  = the path length in water expressed in units of mean free path for gamma rays of a stated energy  
 $d$  = depth of the detector below the water surface.

The radiation intensity at the interface  $I_s$  is given by the expression:

$$I_s = \frac{J_A (1+K)}{2 \mu_A}$$

Thus, the ratio between  $I_{uw}$  and  $I_s$  is:

$$\frac{I_{uw}}{I_s} = e^{-\mu_W d} - \frac{\mu_W d}{1+K} [-Ei(-\mu_W d)]$$

Values of this ratio have been calculated for a 1-Mev gamma energy and are plotted as a function of depth in Figure 3.138. These values were used in conjunction with the 3-minute cumulative dose figures to estimate the depth of the underwater detectors given in Table 3.23. They indicate that the underwater detector bobbed up to or near the surface, probably because of the action of device-generated water waves, although there is some suggestion that a combination of current and normal wave action may occasionally have brought the detector near the surface at later times. After analysis of the data, this hypothesis was experimentally verified. This behavior had not been previously noted, since the detectors were dropped into the water only after zero time, and coracle recoveries after Wahoo were performed principally by nonproject personnel. Because of the particular nature of both events, this attitude of the underwater detectors does not vitiate their records; in fact, this occurrence permits checks on the std-GITR records, which would not have been possible had the underwater detectors dropped to their planned depth.

Radiation due to waterborne material other than that deposited from the base surge is discussed here, since these phenomena are definitely a part of the total gamma records. The gamma records show evidence of two such sources, viz, (1) radiation due to water directly contaminated by the device (white water) and (2) radiation due to patches of radioactive foam.

During the early recovery of the target ships about 2 hours after Umbrella, a patch of radioactive foam, which pinned a survey meter set for a maximum rate of 50 r/hr, was observed by Project 2.1 personnel. Although this report represents the only direct observation of radioactive foam, it seems probably that such a waterborne source would be generated both by the collapse of the column and by the violent upwelling of water immediately after the detonation. The presence of spikes in the std-GITR records, after the passage of airborne material

TABLE 3.23 COMPARISON OF STANDARD AND UNDERWATER GAMMA RECORDS

Nominal Position	Actual Position		Standard GTR Cumulative Dose at 3 Minutes	Underwater GTR Cumulative Dose at 3 Minutes	Ratio UW/Std	Calculated Depth of UW GTR
	Bearing From Surface Zero	Distance From Surface Zero				
	deg (true)	ft	r	r		inches
Wahoo:						
CL 3.9	159	3,900	234	16.6	0.0769	12
CL 4.6	151 $\frac{1}{2}$	4,600	150	0	0	72
D 8.0	256 $\frac{1}{2}$	8,000	69.6	0.000251	0.0000365	68
DR 4.5	263	4,500	527	0.133	0.00252	45
DR 2.0	263	24,000	0	0	-	-
CR 4.1	336	4,100	142	3.99	0.0261	18
CR 5.2	334 $\frac{1}{2}$	5,200	316	21.3	0.0674	13
Umbrella:						
U 1.8	051.6	1,760	735	604	0.876	1
DR 4.5	263.5	4,530	No data	14.4	-	-
DRR 3.9	279.1	3,940	165	17.3	0.105	11
DRR 6.7	278.1	6,740	108	0.0048	0.000444	55

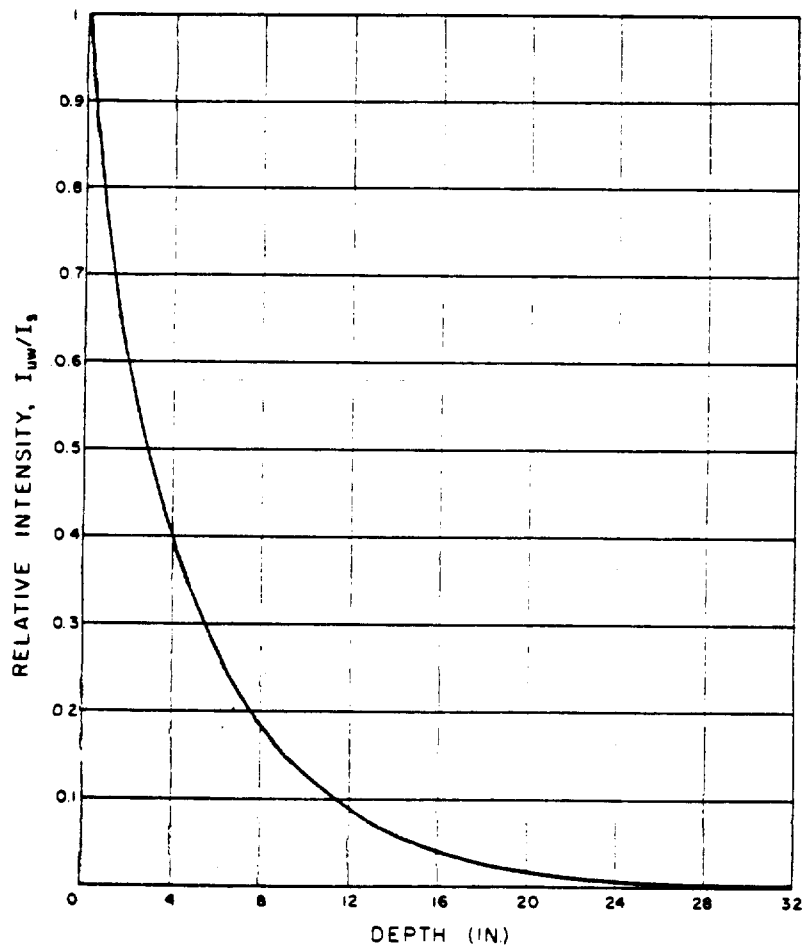


Figure 3.138 Ratio of underwater dose rate as a function of depth (calculated for 1-Mev gammas).

157

but at times requiring speeds two to five times the known ocean surface currents in the area. gives further indirect evidence for such sources (Section 3.3.2). A comparison of the std-GITR and the UW-GITR records from Stations DR 4.5, CR 4.1, and CR 5.2 for Wahoo and DRR 3.9 for Umbrella reveals several instances at later times where the std-GITR shows a spike in dose rate, which is either not recorded or recorded at a much lower intensity by the UW-GITR; such differences could be the result of radioactive foam.

Finally, a careful inspection of photographs taken at an altitude of 24,000 feet over Wahoo surface zero shows a white border, which is probably foam, persisting along the downwind edge of the white water area as late as 24 minutes after zero time. After about 13 minutes, the white water area becomes indistinct, being distinguished only by the foam border along the downwind edge and by a discontinuity in the surface roughness of the ocean observable along the other edges.

Photographic evidence indicates that the spread of the white water itself is probably not a toroidal circulation as suggested in Reference 102 but rather an overlaying of the surface water by the violent upwelling of contaminated waters near the surface zero. This water, which is white in appearance probably due to included bubbles (and bottom material in the case of Umbrella), spreads out radially along the surface to a distance of about 3,500 feet at velocities not less than 10 knots. Evidence for overlaying is found by inspection of the white water boundaries presented with the isodose contours in Section 3.3.3, which reveal an indentation on their outer perimeter associated with each of the closer target ships. These indentations are located radially beyond the ships and are particularly pronounced for Wahoo. It seems more probable that they would have been caused by surface interference with the suggested radial overlaying phenomenon rather than by the interruption of a toroidal circulation extending to greater depths.

Additional evidence of radioactive surface water is provided by the 0- to 6-hour records of both the standard and the underwater GITR's (Figures 3.154 through 3.182). When considering these figures, it should be remembered that many of the coracles on Wahoo were drifting; their estimated positions at later times are indicated in Figure 2.1. Recovery, when it occurred during the record, is also indicated. The observed times of arrival and cessation for white water are presented in Table 3.24.

Times of cessation are particularly difficult to read from the gamma record and in many instances are little better than guesses. For Wahoo, the TOA have been plotted as a function of distance (Figure 3.139). Although the points show some scatter, a straight line with a slope of approximately 1 knot may be faired through them. The fact that these later events occur at times and in directions that are compatible with known ocean surface currents in the region further supports the assumption that they are indeed due to the movement of water directly contaminated by the nuclear device. The reported dose rates may be converted to fission product concentrations as indicated in Section C.6.

Assuming a speed of 1 knot, the path lengths through the white water have been computed for the Wahoo stations and are also included in Table 3.24. These path lengths are usually shorter than the last observed white water diameter (about 10,000 feet at 24 minutes), probably because corrections for drift can only be approximate. They suggest, however, that this body of radioactive water does not greatly increase its boundaries after about 24 minutes.

The 0- to 6-hour records for Umbrella do not show much evidence of radioactive water at later times. Since all deep-moored stations were recovered before any white water could have crossed the reef and reached their positions, these stations are omitted from the analysis of white water movement. Consequently, not all the 0- to 6-hour records for Umbrella have been reproduced. The more distant stations within the lagoon indicate white water arrival at a time compatible with an assumed radial expansion of 0.5 knot from the photographically established 23-minute white water boundary (Section 3.3.2). An assumed movement in the direction of the surface wind at a speed of 1 knot also fits the water data nearly as well. Movement of lagoon waters by the wind at comparable speeds has been reported for Bikini (Reference 94). A plot of the Umbrella TOA for water is scattered; however, a line with a slope of approximately 2 knots may be faired through the points (Figure 3.140). This line is presumed to represent the

movement of radioactive foam (Section 3.3.2).

Complete analysis of the waterborne record requires consideration of both the 0- to 15-minute and the 0- to 6-hour records. Most of this analysis is presented as part of the free-field dose rate discussion (Section 3.3.2), since certain spikes in dose rate presumed due to radioactive foam might be mistaken for radiation from the base surge. The arrival and departure of both foam and white water, computed for a number of speeds and directions, are presented in Table 3.25. Drifting coracles are assumed to move with the wind at speeds determined for a dragging mooring cable unless there is good photographic evidence of free drift (Figure 2.16). Foam is assumed to move in directions and at speeds determined by the combined effects of ocean currents, sea conditions, and the surface wind. For Wahoo, directions ranging from 250° T (average direction of coracle drift) to 302° T (Reference 92) and speeds of 1, 2, and 6 knots are calculated. For Umbrella, the same range of speeds is used, but the direction of movement is limited to that of the surface wind. As shown in Table 3.11, the best agreement between the gamma records and these assumed foam movements is obtained for a set and drift of 270° T at 6 knots after Wahoo and 230° T at 2 knots after Umbrella. Although all evidence for foam is at best circumstantial, the assumed foam movement after Wahoo is compatible with the official surface wind direction and the reported ocean currents (References 53 and 93, and project observations). The slower rate of foam movement after Umbrella is presumed to be a consequence of smoother water conditions inside the lagoon, which would reduce stripping action by the wind.

For Wahoo, white water arrival and cessation times calculated on the basis of a set and drift of 270° T and 1 knot are also in reasonable agreement with observed dose rate values, although sets of 250° T and 302° T give equally good or slightly better comparisons. For Umbrella, the assumed radial expansion at 0.5 knot gives best general agreement with both the gamma records and the observed early white water expansion. This radial expansion cannot of course be used for calculation of cessation times. Since the limited current data available for lagoons (Reference 94) indicates little surface current, the assumed radial expansion is at least reasonable, although such continued expansion is not indicated by other late-time observations currently available to the project. At 5 or 6 hours after Umbrella, the white water patch was still in the neighborhood of surface zero but was transected at least at the surface by a channel of clear water roughly parallel to the surface wind direction (observation by project personnel aboard the USS Munsee).

For Umbrella, white water is assumed to contain a suspension of pulverized coral from the lagoon bottom. A significant fraction of the residual radioactivity is probably associated with this suspension. The closer stations located within or near the white water boundary show a steady decline in dose rate due to a combination of decay and sinking of the radioactive material below the surface. Laboratory tests of Umbrella crater material indicate that its sinking rate in sea water is about 0.96 m/hr, a rate about a third that observed during Operation Redwing (Section 1.3.1 and Reference 33). This difference is probably due to the finely pulverized condition of the bottom material. Using the total linear attenuation coefficient for 1-Mev gammas in water, this would indicate a decrease in dose rate of 1 decade per 21 minutes due to sinking alone. Such slopes are observed in the normalized rate curves (Section 3.3.2).

An indication of the combined sinking and dilution rate for water sources is obtained by comparing the observed and the standard decay rates as shown in Figures 3.141 and 3.142 (the standard decay curve is described in Section B.2). In these figures the average dose rates for the later Wahoo records and the decay rates for a number of close-in Umbrella stations are plotted as a function of time. The decrease in average dose rate shown by the later Wahoo records is probably due to sinking or mixing with deeper water, since the white water area at the surface remains unchanged.

For Umbrella, the decrease in dose rate after 30 minutes agrees closely with the standard decay curve, which could mean that a fine radioactive suspension persists after the sinking of the coarser material. Such agreement also implies no dilution by expansion or by surface currents. A survey meter 15 feet above the center of the white water at H+4 hours read 200

TABLE 3.25 CALCULATED WATER AND FOAM MOVEMENT  
(Time of arrival over time of cessation, both in minutes)

Station	Set 250°T		Set 270°T		Set 302°T	
	16 min bound. drift = 1 k	2 min bound. = 2 k	16 min bound. = 1 k	2 min bound. = 2 k	16 min bound. = 1 k	2 min bound. = 2 k
U 4.5	<16/18	<16/17	(5-16)/never*	<16/17	<16/18	<16/17
CL 3.9	<16/30	<16/23	(3-5)/18	<16/17	<16/17	<16/17
CL 4.6	misses station	misses station	does not reach station	misses station	does not reach station	misses station
DL 7.1	37/112	26/64	52/78	34/47	misses station	misses station
D 8.0	37/148	25/78	36/128	26/71	misses station	misses station
DR 4.5	<16/117	<16/61	9.3/150*	<16/58	misses station	misses station
DR 9.0	41/142	28/79	42/138	29/77	misses station	misses station
DR 14.4	105/191	61/104	96/193	56/104	misses station	misses station
DR 24.0	270/356	120/136	208/279	112/148	misses station	misses station
DRR 6.8	25/121	21/64	20/129	18/68	misses station	misses station
DRR 12.8	111/136	63/76	73/180	49/98	misses station	misses station
CR 4.1	<16/36	<16/36	(3-5)/59	<16/37	misses station	misses station
CR 5.2	<16/48	<16/24	(5-16)/61	<16/23	misses station	misses station
CR 6.4	16/29	16/22	16/36	16/24	misses station	misses station

Station	Set 230°T		Radial Expansion	
	23 min bound. drift = 1 k	3 min bound. = 2 k	23 min bound. rate = 0.3 k	3 min bound. = 0.3 k
U 1.8	<23/40	<23/32	<23	<23
U 2.7	<23/36	<23/29	<23	<23
U 3.9	does not reach station	does not reach station	26	25
CL 3.1	<23/53	<23/38	<23	<23
CL 6.0	misses station	misses station	92	65
DL 6.6	43/102	33/62	82	59
DL 6.2	36/120	29/71	66	49
DL 16.0	131/210	77/115	66	49
D 2.7	<23/84	<23/53	<23	<23
D 4.8	38/95	30/59	51	40
D 18.2	misses station	misses station	250	159
D 22.0	misses station	misses station	250	159
DR 12.2	misses station	misses station	250	159
DR 18.6	misses station	misses station	250	159
DRR 3.9	<23/67	<23/45	90	63
DRR 6.7	misses station	misses station	62	46
CR 4.9	misses station	misses station	62	46

Station with white water until indicated TOC.  
( ) Parenthetic entries were determined using intermediate water boundaries between the earliest and latest boundary times tabulated here.



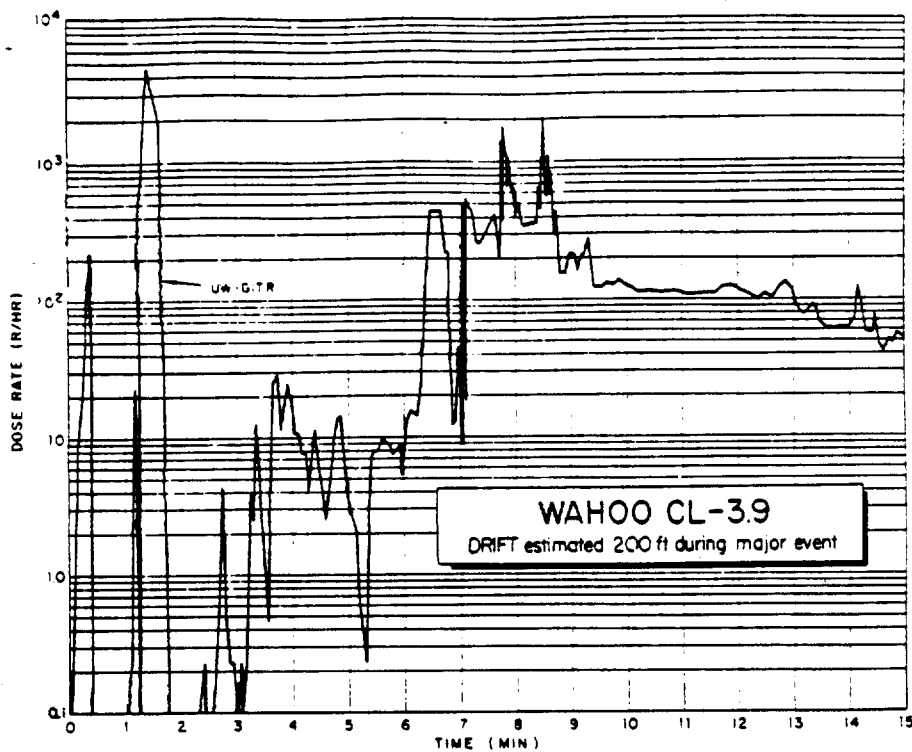


Figure 3.143 UW-GITR record, 0 to 15 minutes, coracle at 3,900 feet, 159° T from surface zero, Shot Wahoo.

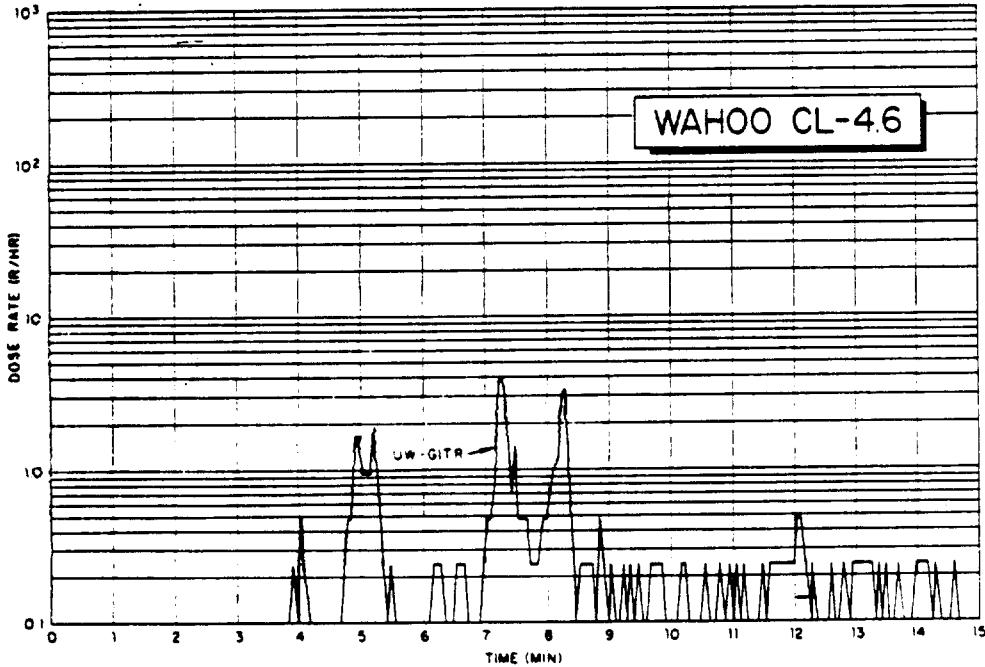


Figure 3.144 UW-GITR record, 0 to 15 minutes, coracle at 4,600 feet, 151.5° T from surface zero, Shot Wahoo.

167

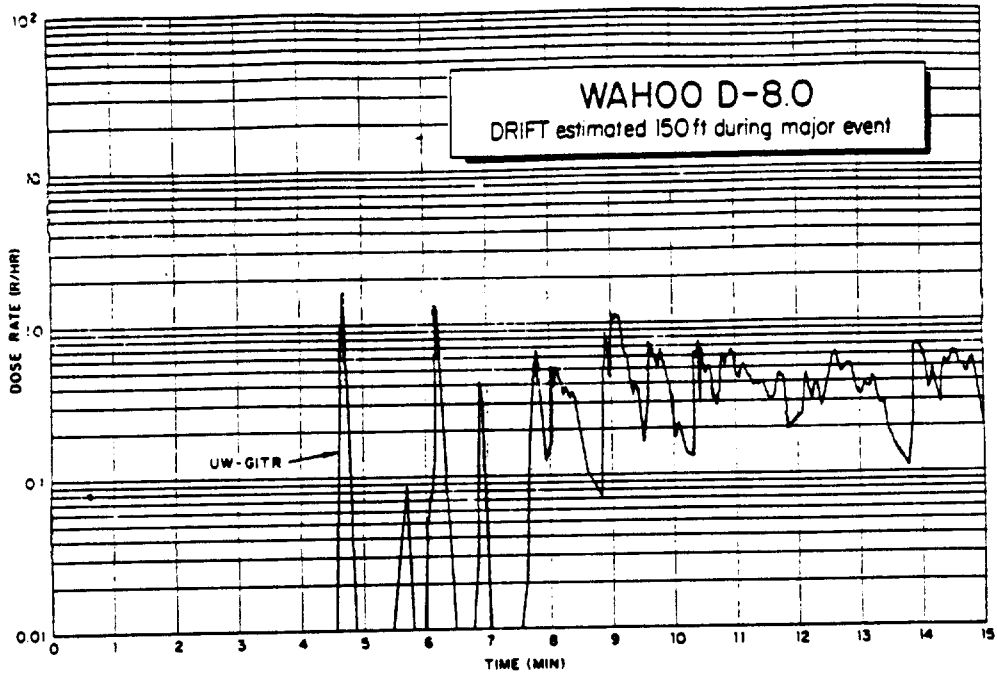


Figure 3.145 UW-GITR record, 0 to 15 minutes, coracle at 8,000 feet, 256.5° T from surface zero, Shot Wahoo.

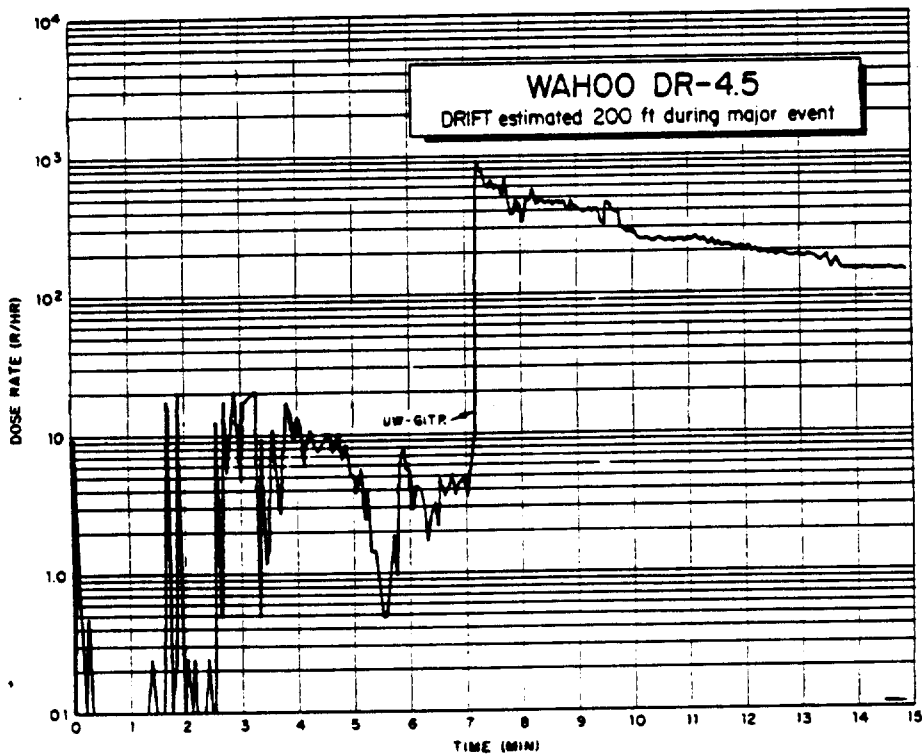


Figure 3.146 UW-GITR record, 0 to 15 minutes, coracle at 4,500 feet, 263° T from surface zero, Shot Wahoo.

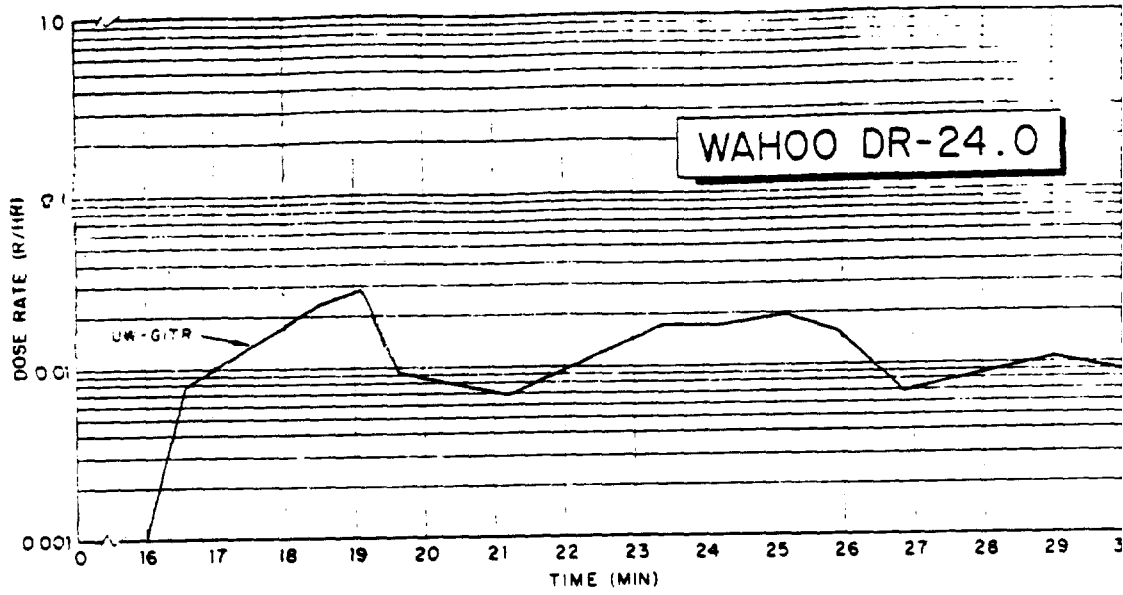


Figure 3.147 UW-GITR record, 0 to 30 minutes, coracle at 24,000 feet, 263° T from surface zero, Shot Wahoo.

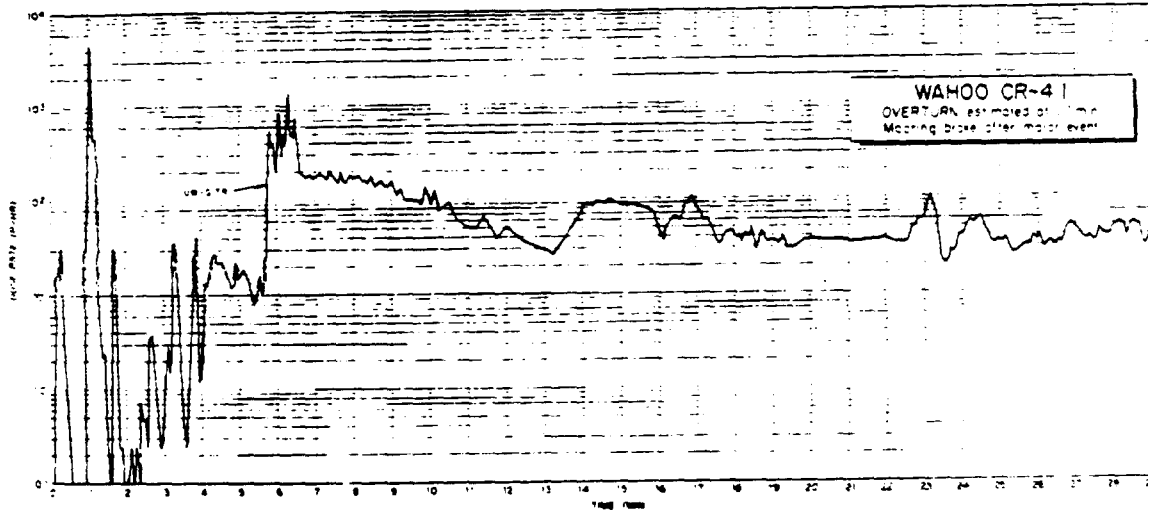


Figure 3.148 UW-GITR record, 0 to 30 minutes, coracle at 4,100 feet, 336° T from surface zero, Shot Wahoo.

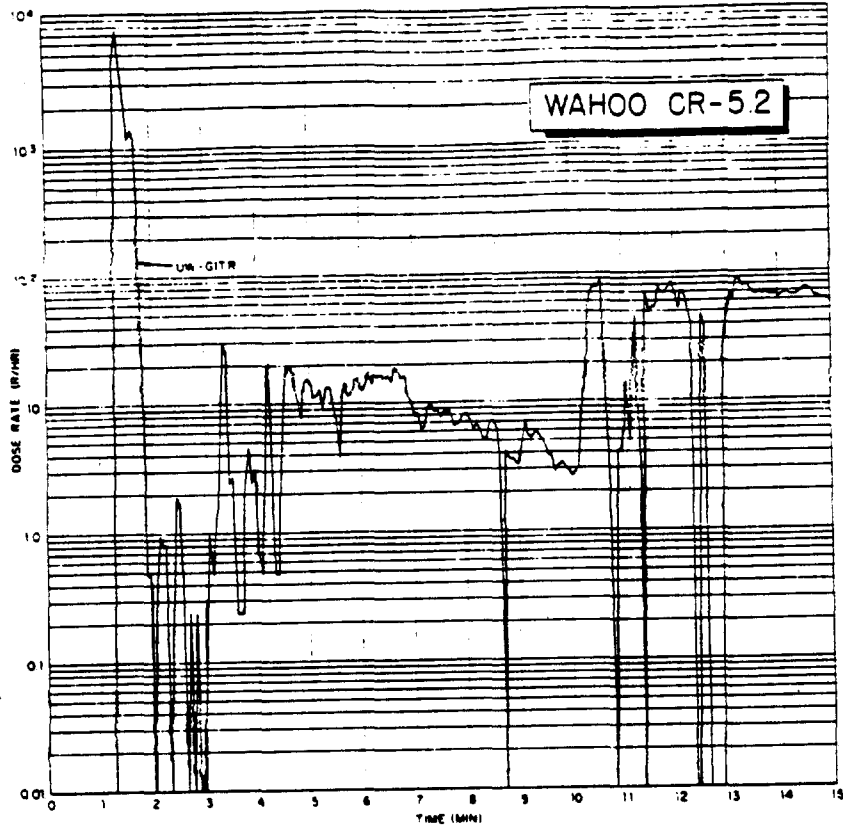


Figure 3.149 UW-GITR record, 0 to 15 minutes, coracle at 5,200 feet, 334.5° T from surface zero, Shot Wahoo.

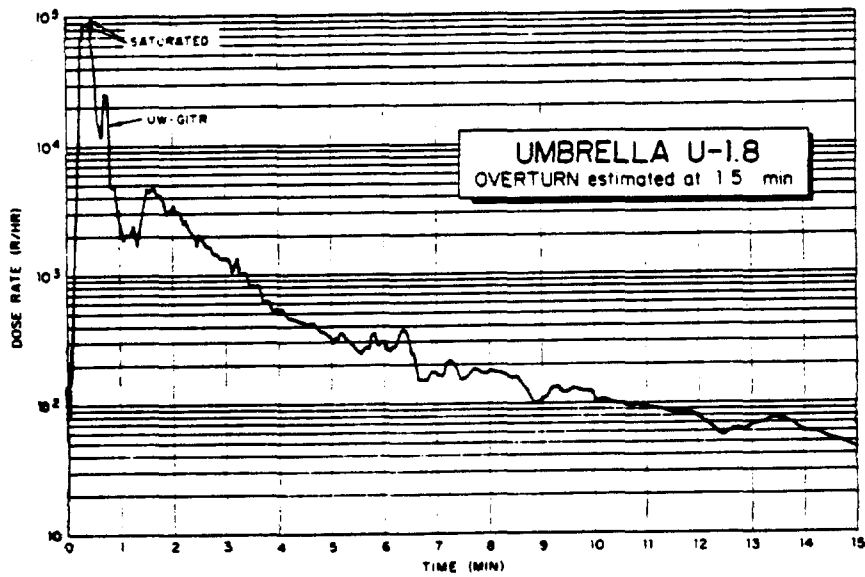


Figure 3.150 UW-GITR record, 0 to 15 minutes, coracle at 1,760 feet, 51.8° T from surface zero, Shot Umbrella.

122

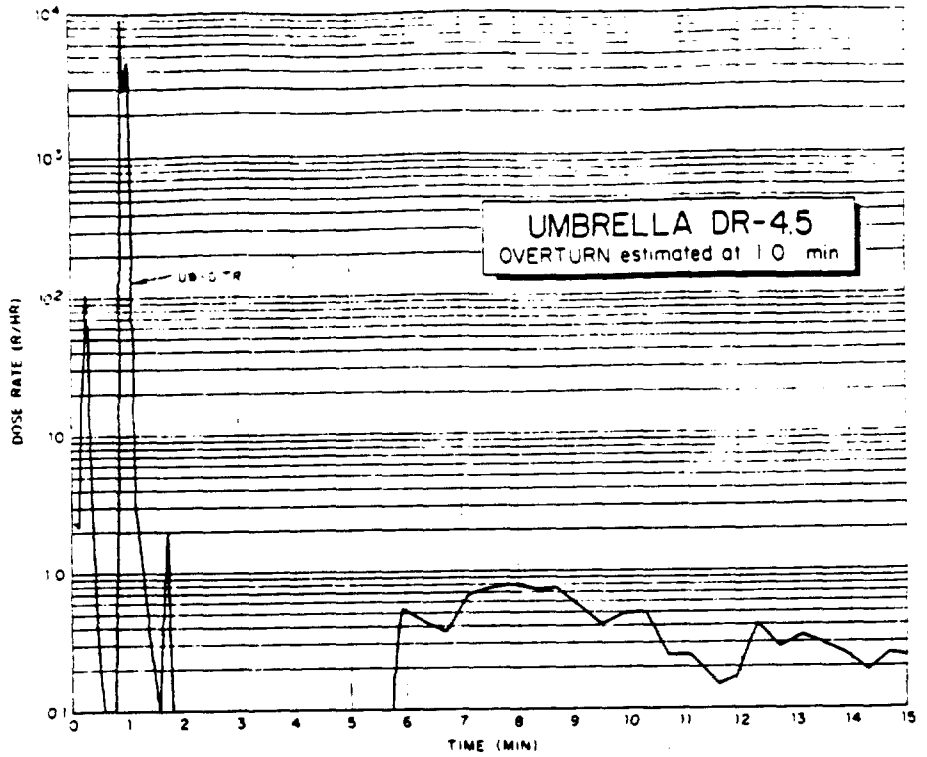


Figure 3.151 UW-GITR record, 0 to 15 minutes, coracle at 4,530 feet, 263.5° T from surface zero, Shot Umbrella.

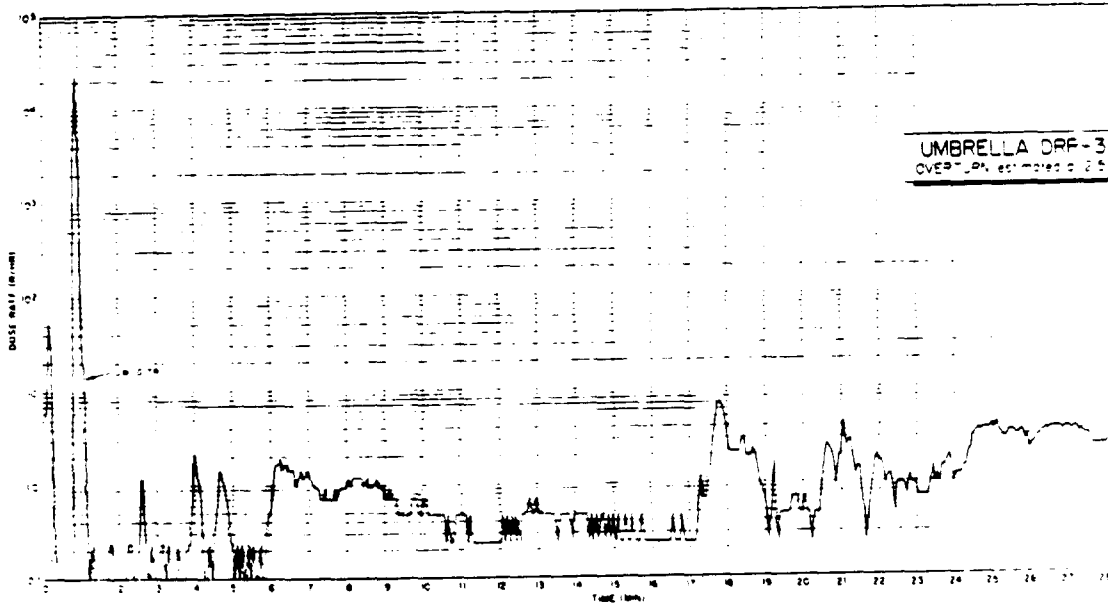


Figure 3.152 UW-GITR record, 0 to 30 minutes, coracle at 3,940 feet, 279.1° T from surface zero, Shot Umbrella.

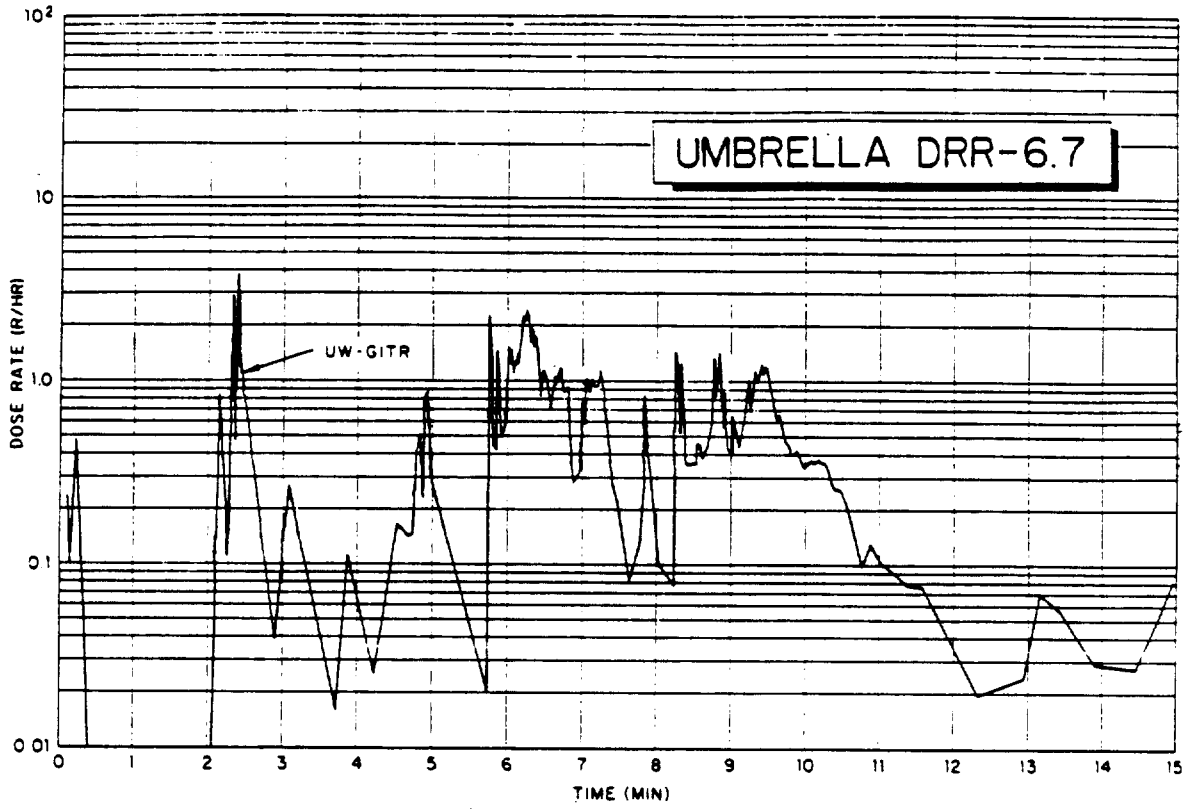


Figure 3.153 UW-GITR record, 0 to 15 minutes, coracle at 6,740 feet, 278.1° T from surface zero, Shot Umbrella.

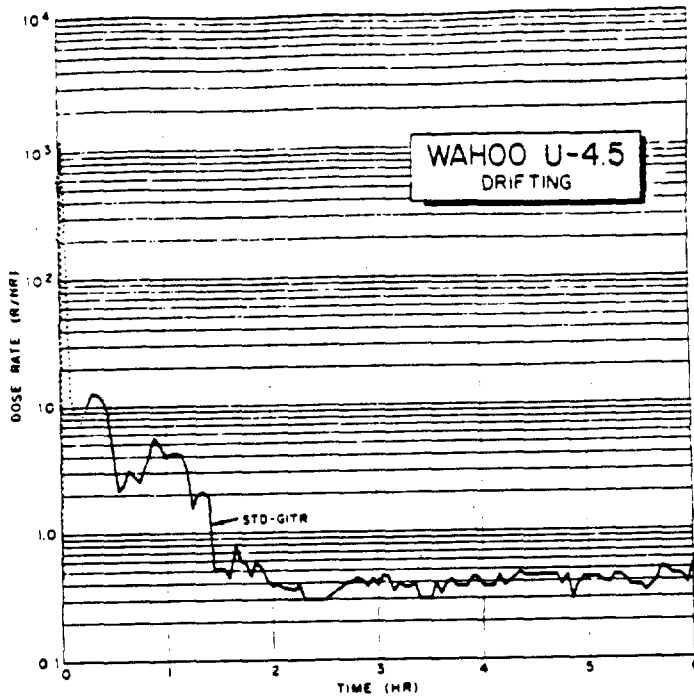


Figure 3.154 Std-GITR record, 0 to 6 hours, coracle at 4,500 feet, 66° T from surface zero, Shot Wahoo.

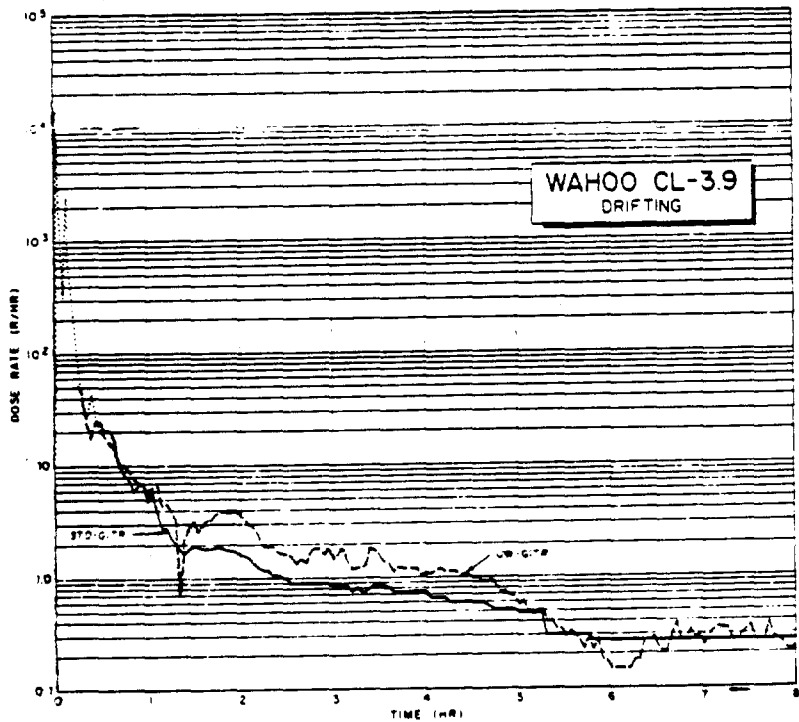


Figure 3.155 Std- and UW-GITR records, 0 to 8 hours, coracle at 3,900 feet, 159° T from surface zero, Shot Wahoo.

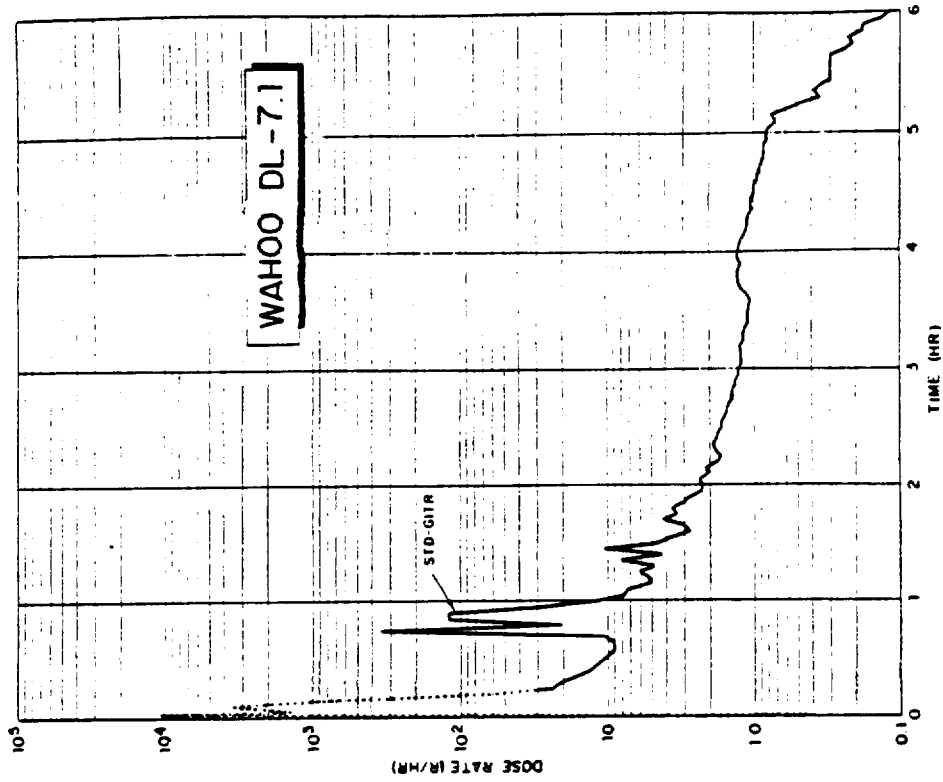


Figure 3.157 Sid-GITR record, 0 to 6 hours, coracle at 7,100 feet, 231.5° T from surface zero, Shot Wahoo.

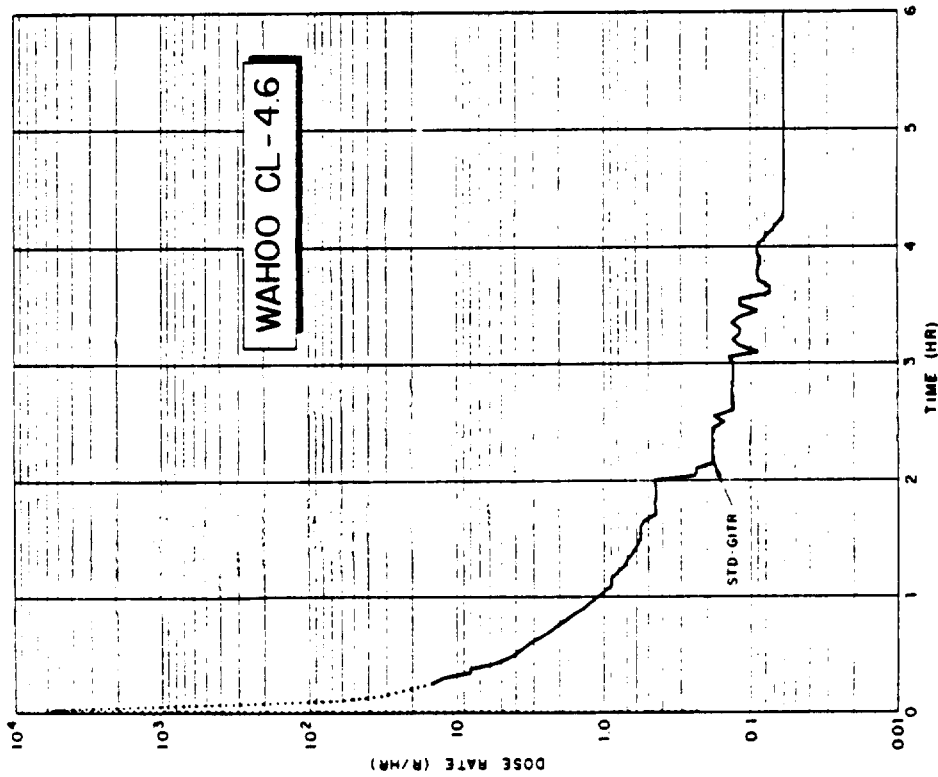


Figure 3.156 Sid-GITR record, 0 to 6 hours, coracle at 4,600 feet, 151.5° T from surface zero, Shot Wahoo.

130

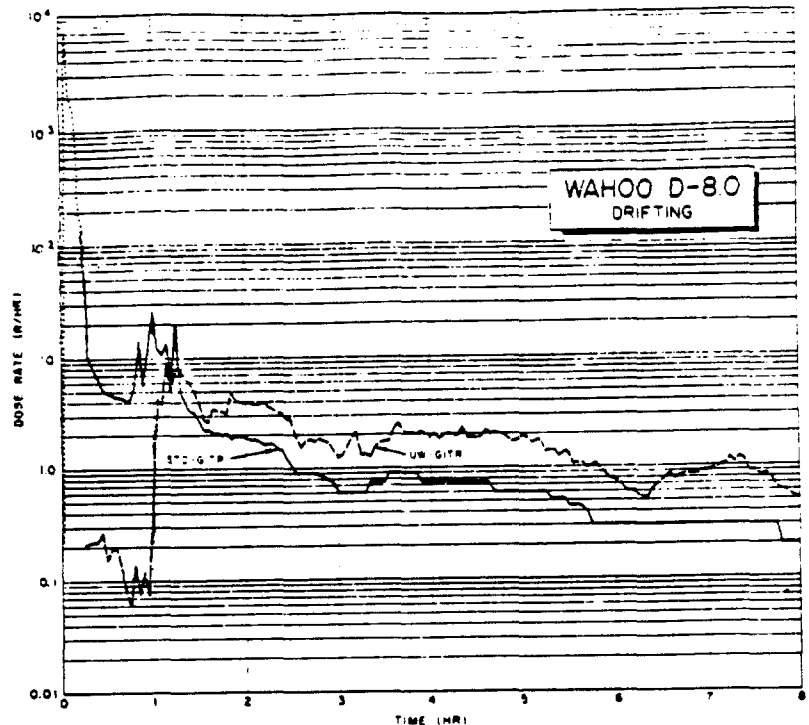


Figure 3.158 Std- and UW-GTR records, 0 to 8 hours, coracle at 8,000 feet, 256.5° T from surface zero, Shot Wahoo.

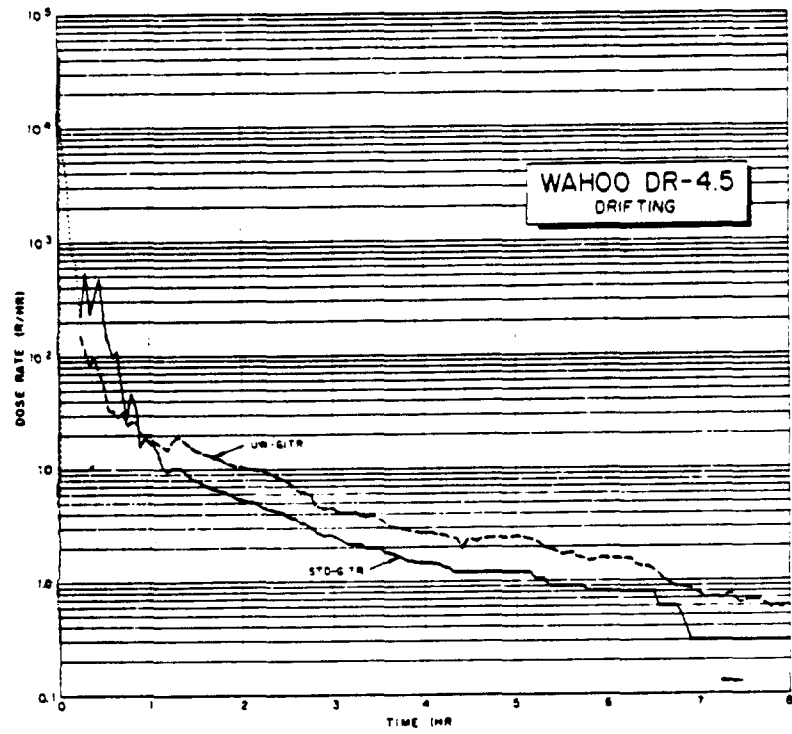


Figure 3.159 Std- and UW-GTR records, 0 to 8 hours, coracle at 4,500 feet, 263° T from surface zero, Shot Wahoo.

152

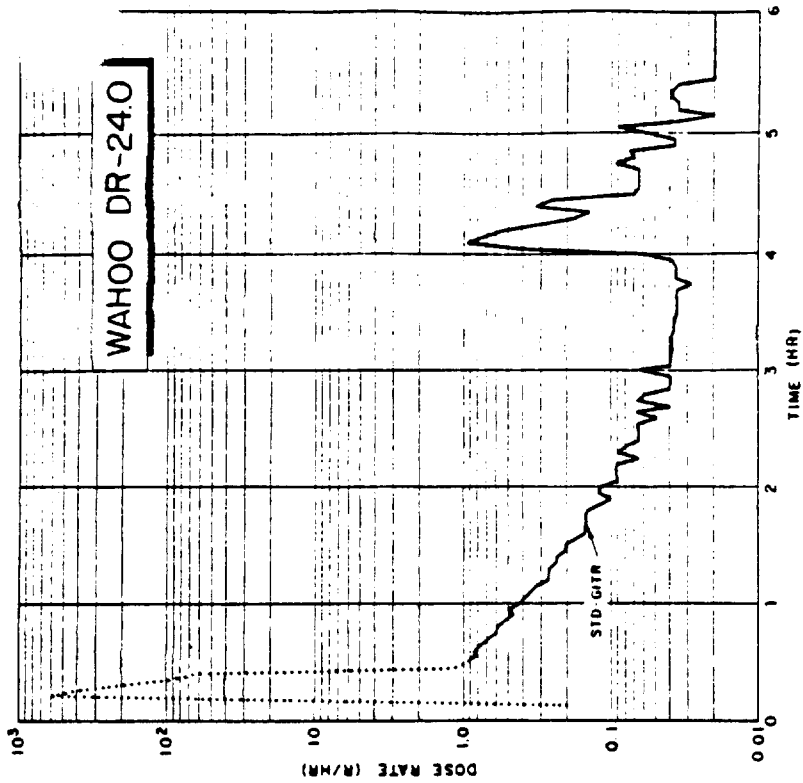


Figure 3.161 Sid-GITR record, 0 to 6 hours, coracle at 24,000 feet, 263° T from surface zero, Shot Wahoo.

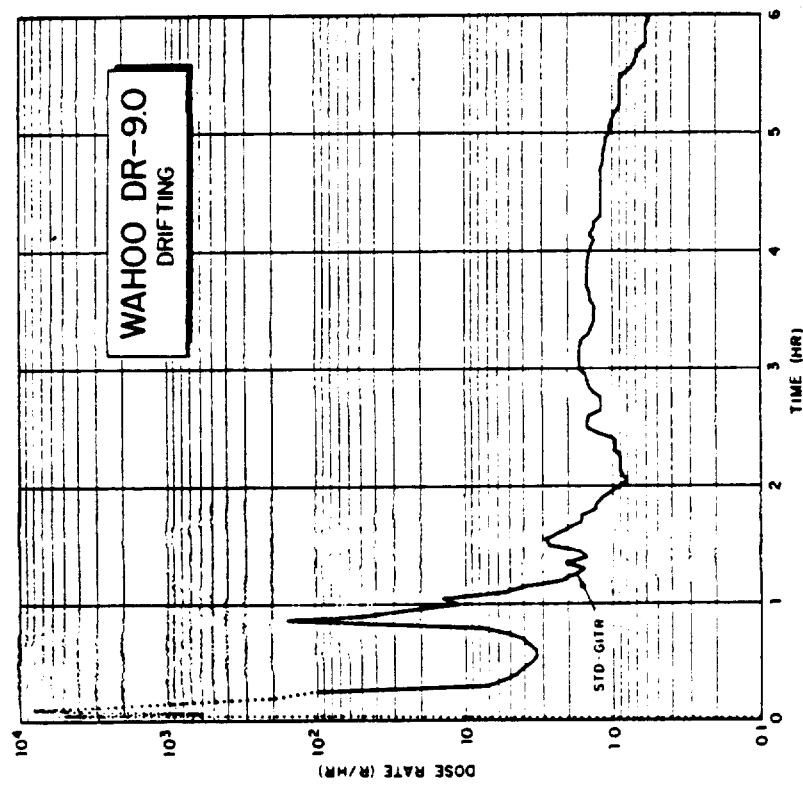


Figure 3.160 Sid-GITR record, 0 to 6 hours, coracle at 9,950 feet, 263° T from surface zero, Shot Wahoo.

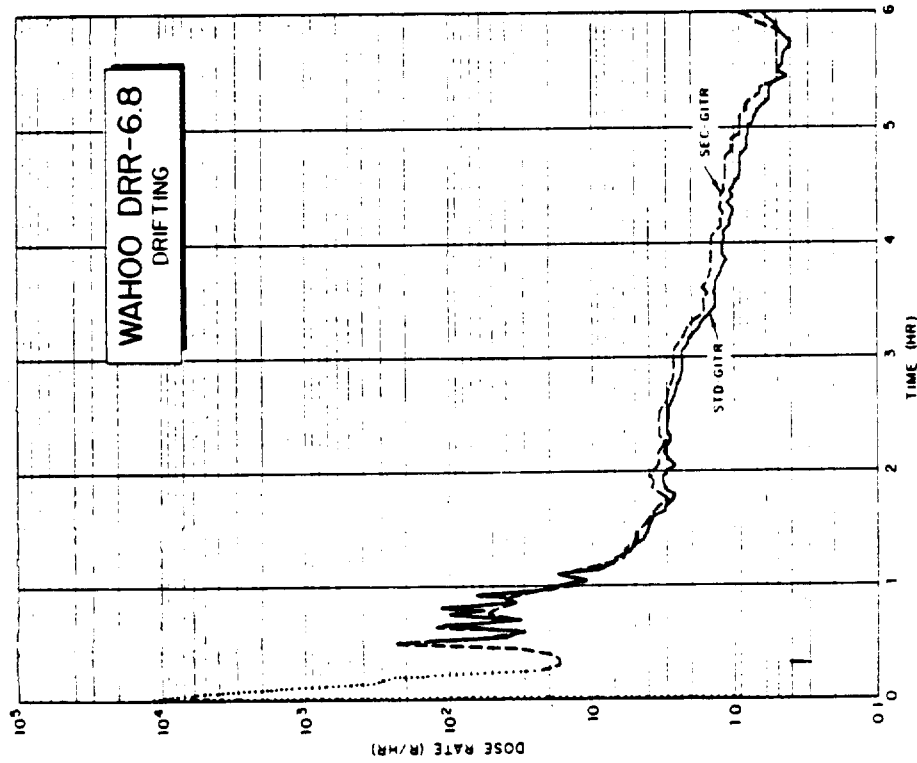


Figure 3.162 Std- and sec-GTR records, 0 to 6 hours, coracle at 6,800 feet, 281° T from surface zero, Shot Wahoo.

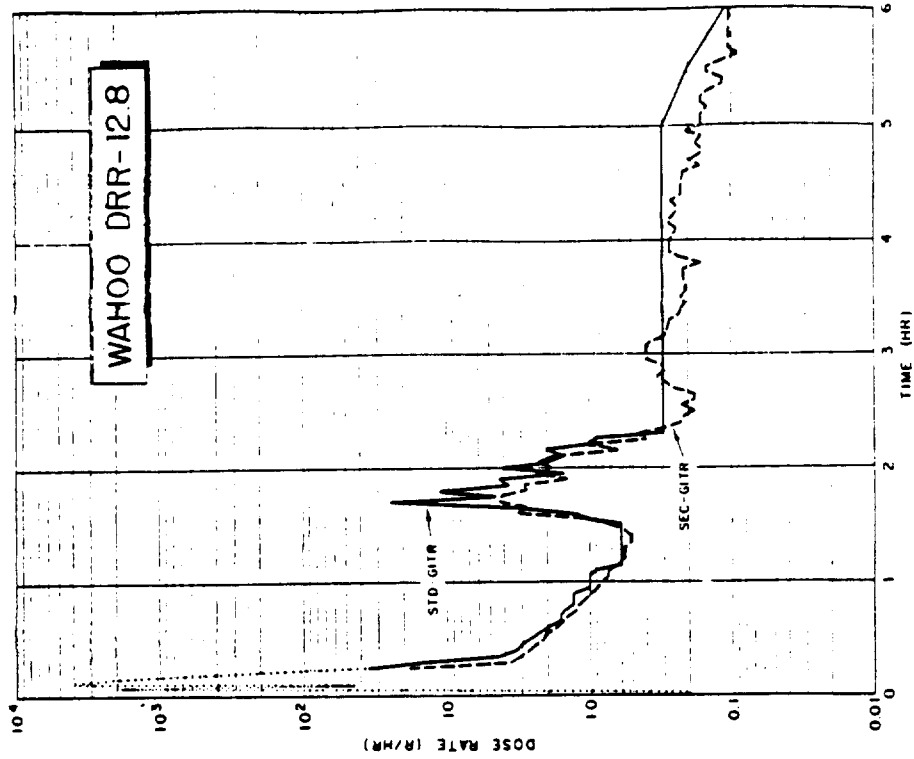


Figure 3.163 Std- and sec-GTR records, 0 to 6 hours, coracle at 12,800 feet, 276° T from surface zero, Shot Wahoo.

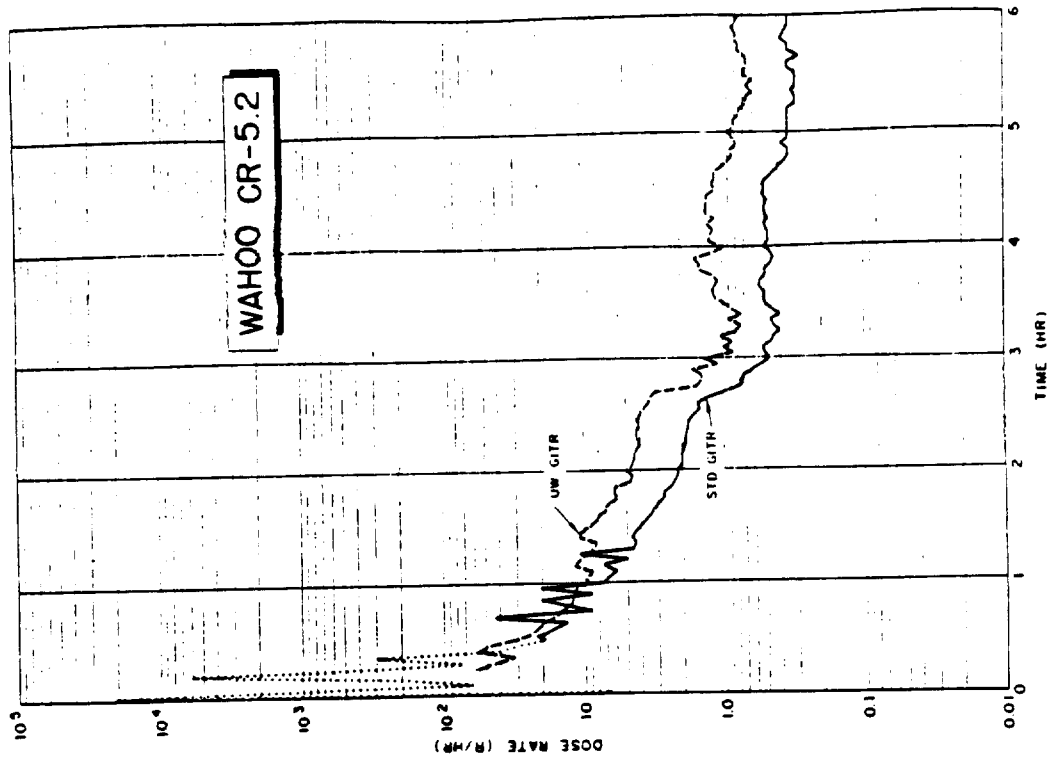


Figure 3.165 Std- and UW-GTR records, 0 to 6 hours, coracle at 5,200 feet, 334.5° T from surface zero, Shot Wahoo.

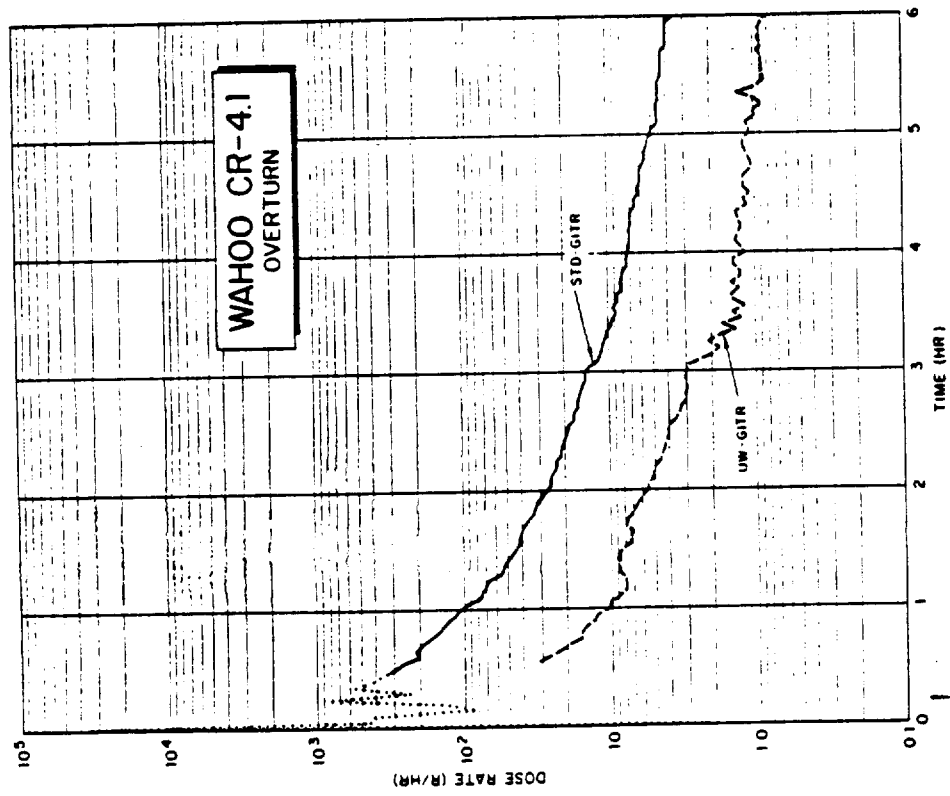


Figure 3.164 Std- and UW-GTR records, 0 to 6 hours, coracle at 4,100 feet, 336° T from surface zero, Shot Wahoo.

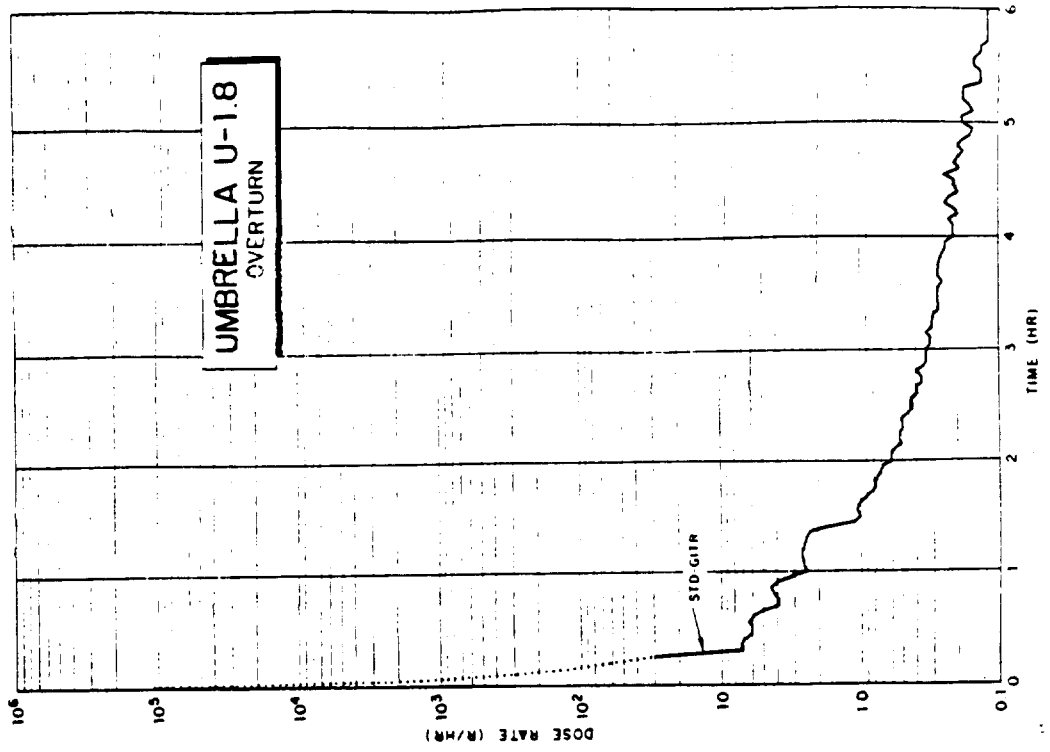


Figure 3.167 Std-GTR record, 0 to 6 hours, coracle at 1,760 feet, 51.8° T from surface zero, Shot Umbrella.

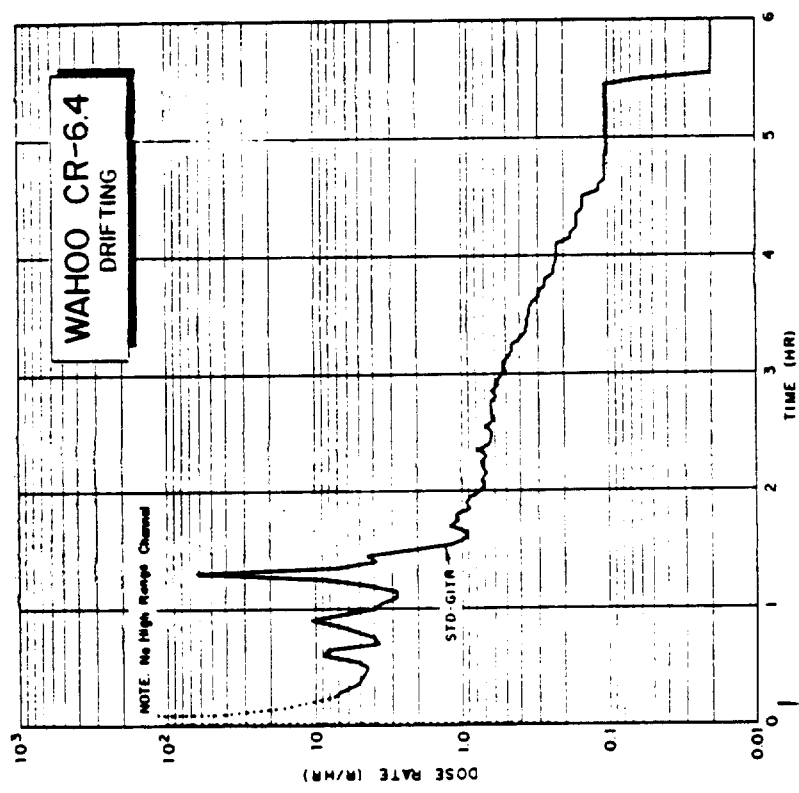


Figure 3.166 Std-GTR record, 0 to 6 hours, coracle at 6,400 feet, 332° T from surface zero, Shot Wahoo.

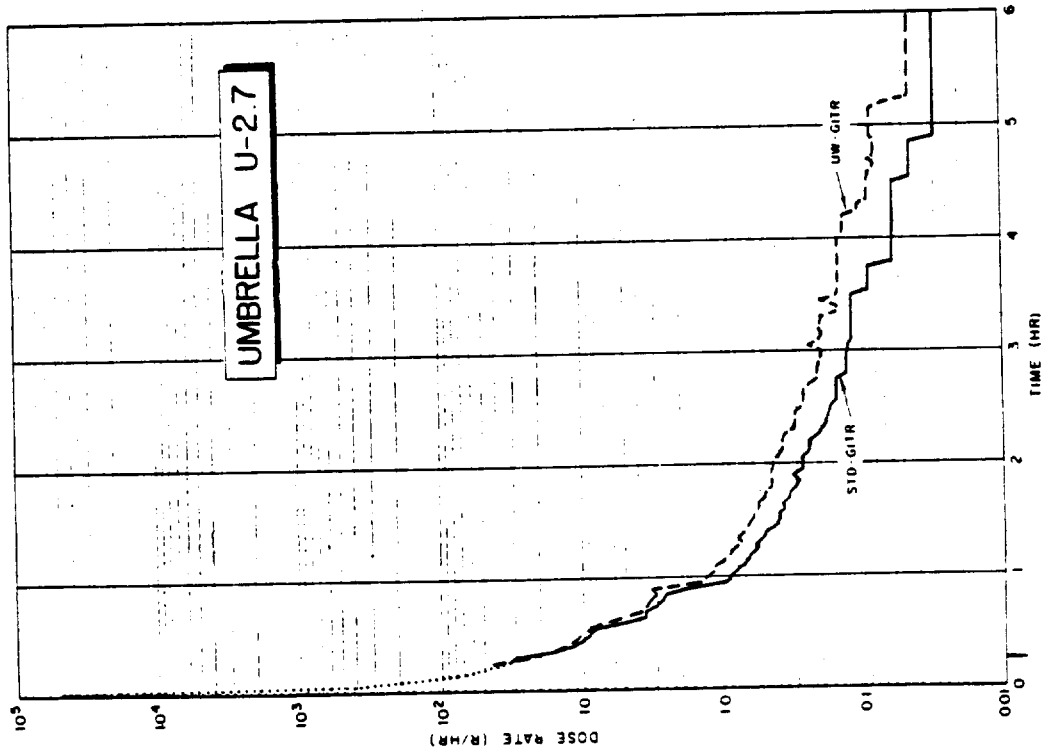


Figure 3.168 Sid- and UW-GTR records, 0 to 6 hours, coracle at 2,700 feet, 67° T from surface zero, Shot Umbrella.

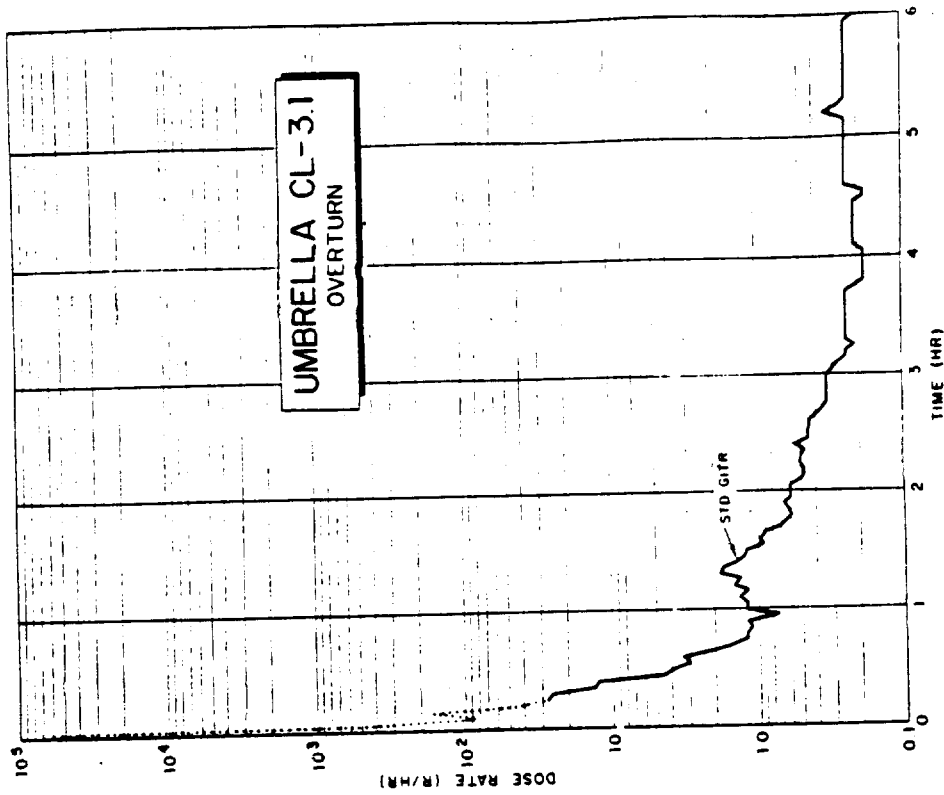


Figure 3.169 Sid-GTR record, 0 to 6 hours, coracle at 3,060 feet, 163.7° T from surface zero, Shot Umbrella.

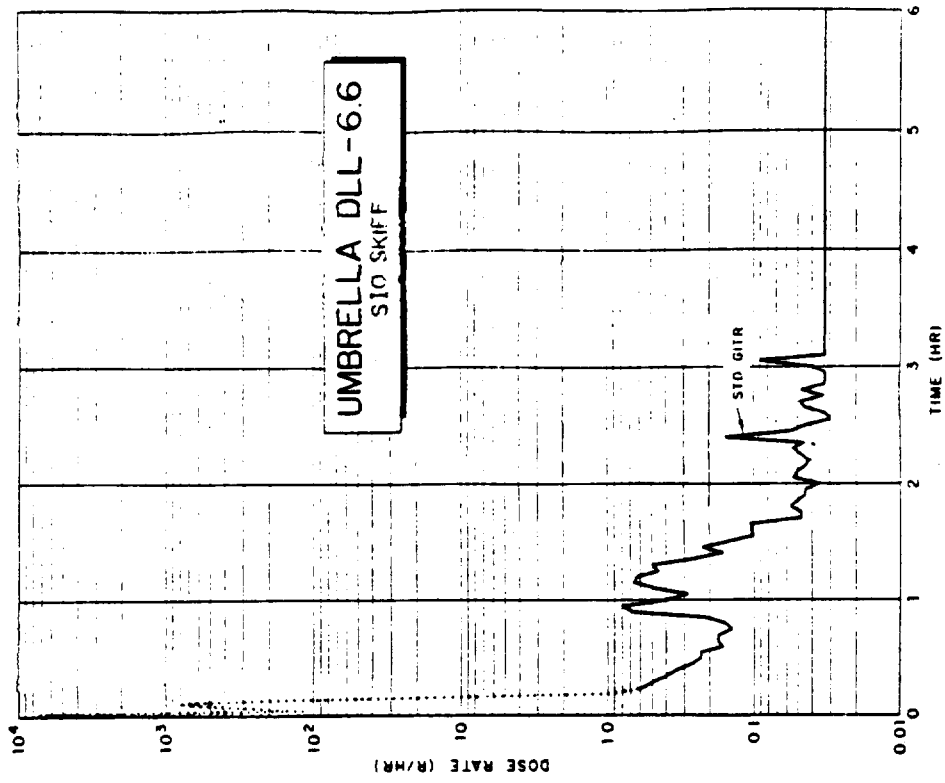


Figure 3.171 Sid-GITR record, 0 to 6 hours, SIO Skiff at 6,580 feet, 207.5° T from surface zero, Shot Umbrella.

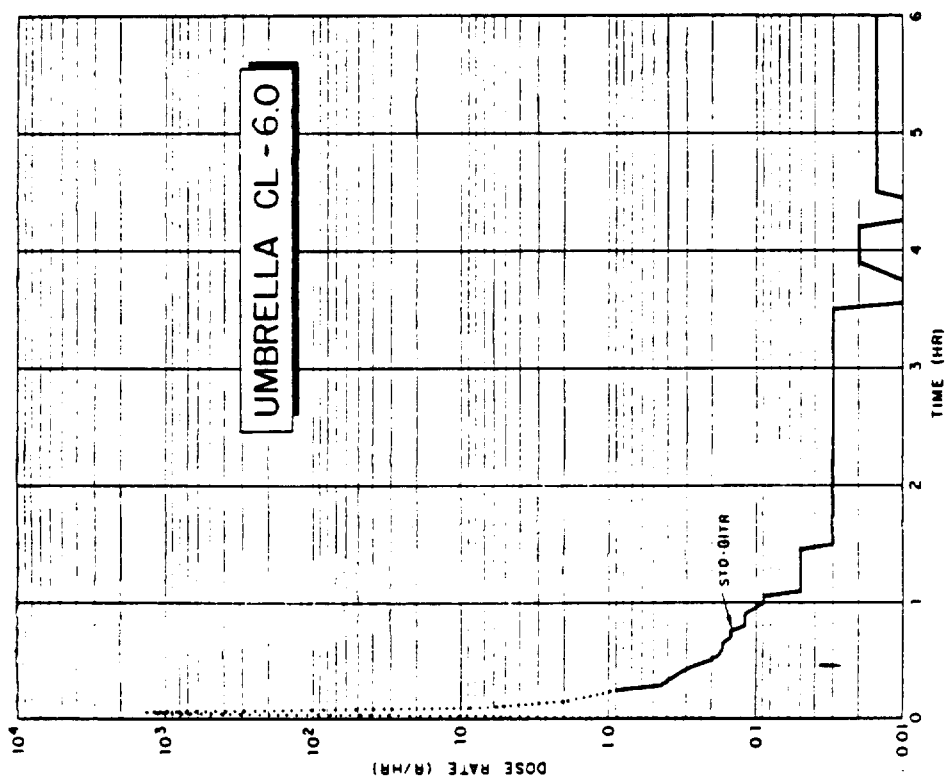


Figure 3.170 Sid-GITR record, 0 to 6 hours, coracle at 6,010 feet, 158.9° T from surface zero, Shot Umbrella.

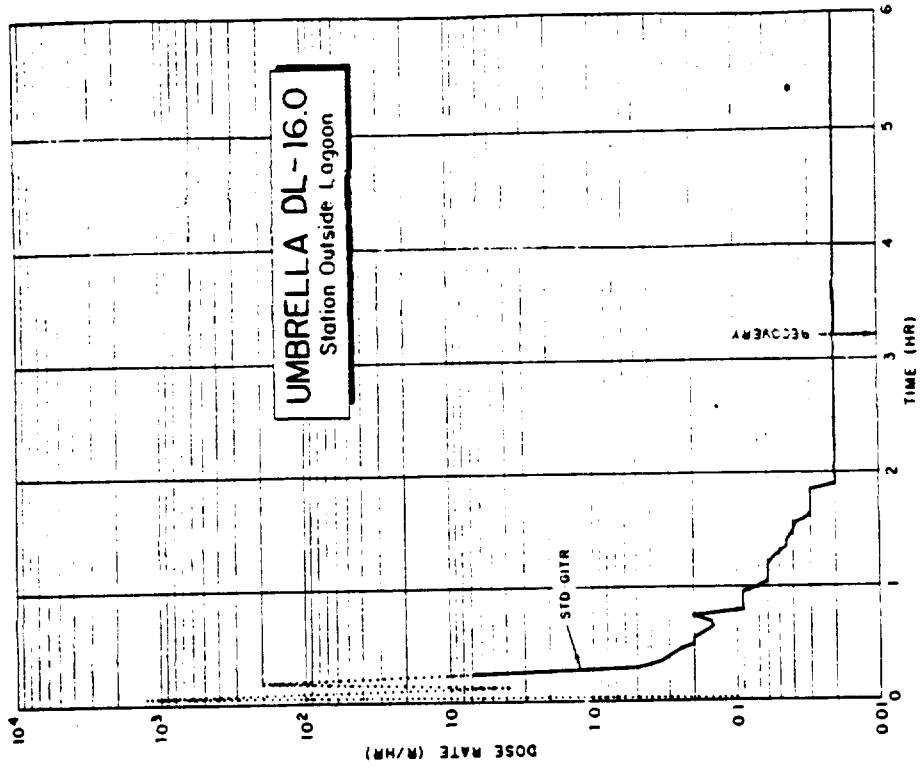


Figure 3.173 Sid-GITR record, 0 to 6 hours, coracle at 15,980 feet, 237.1° T from surface zero, Shot Umbrella.

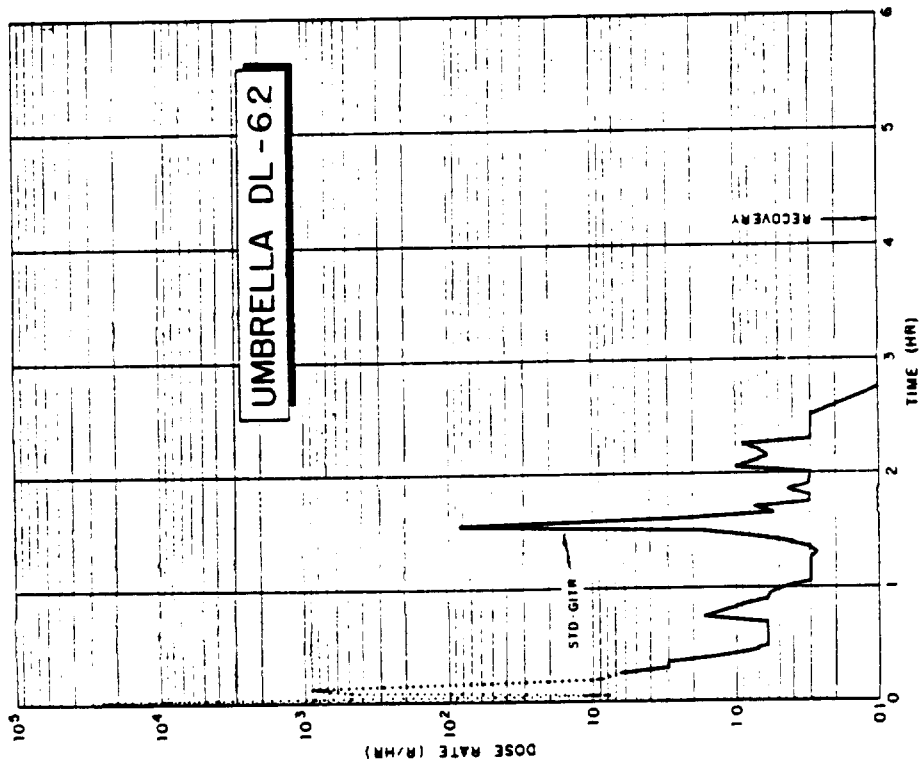


Figure 3.172 Sid-GITR record, 0 to 6 hours, coracle at 6,220 feet, 230.4° T from surface zero, Shot Umbrella.

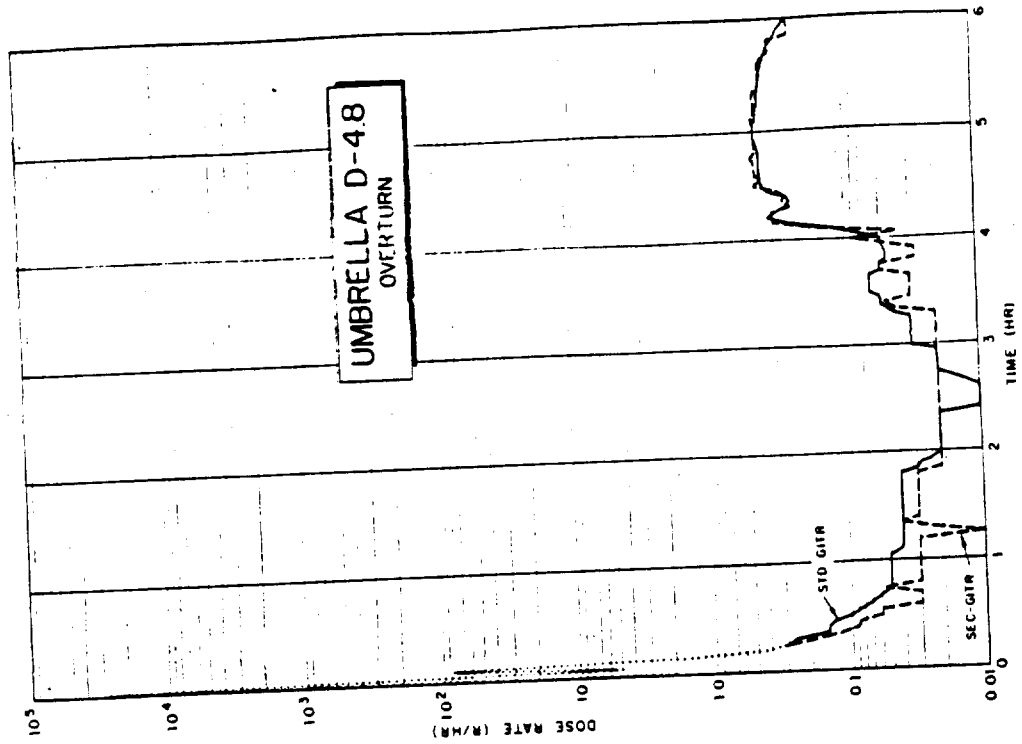


Figure 3.175 Std and sec-G1TR records, 0 to 6 hours, coracle at 4,770 feet, 247.9° T from surface zero, Shot Umbrella.

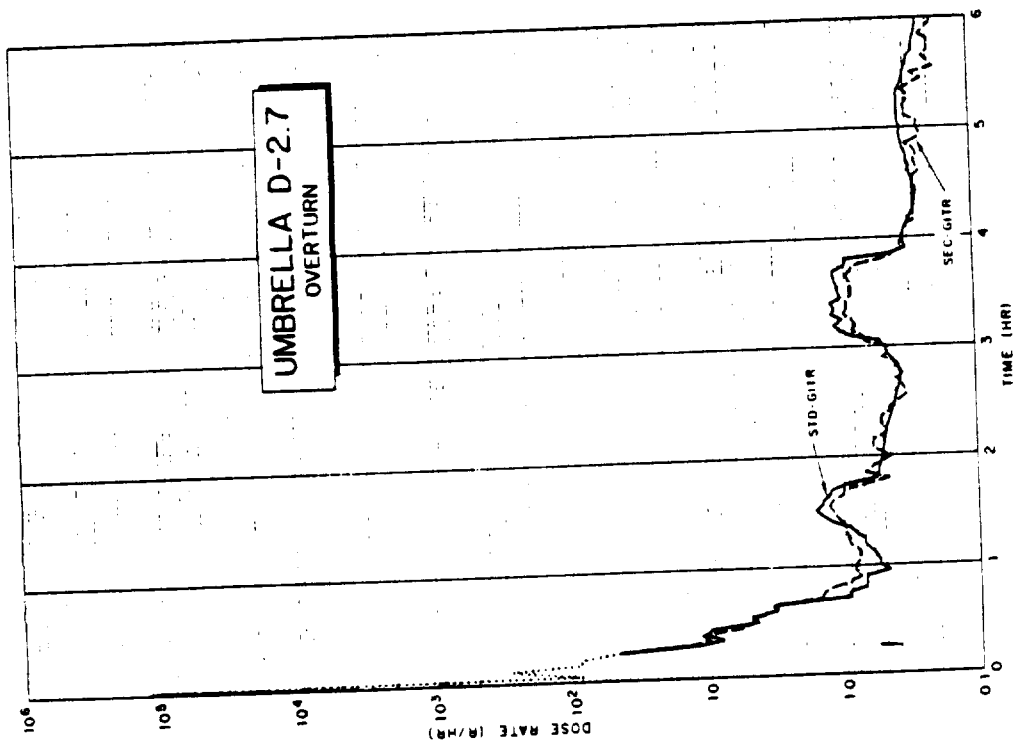


Figure 3.174 Std- and sec-G1TR records, 0 to 6 hours, coracle at 2,670 feet, 248° T from surface zero, Shot Umbrella.

145

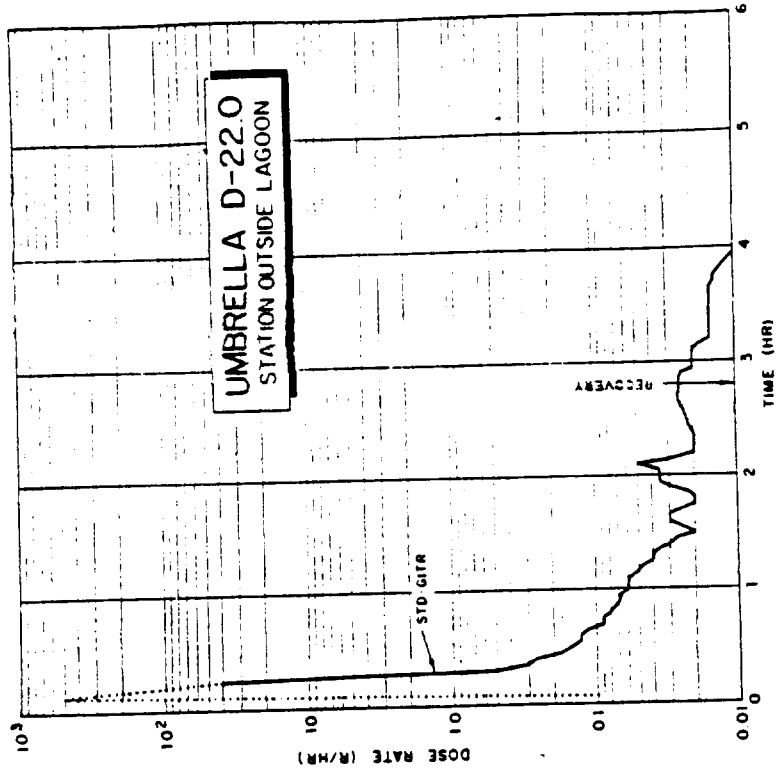


Figure 3.177 Sid-GITR record, 0 to 6 hours, coracle at 22,000 feet, 248° T from surface zero, Shot Umbrella.

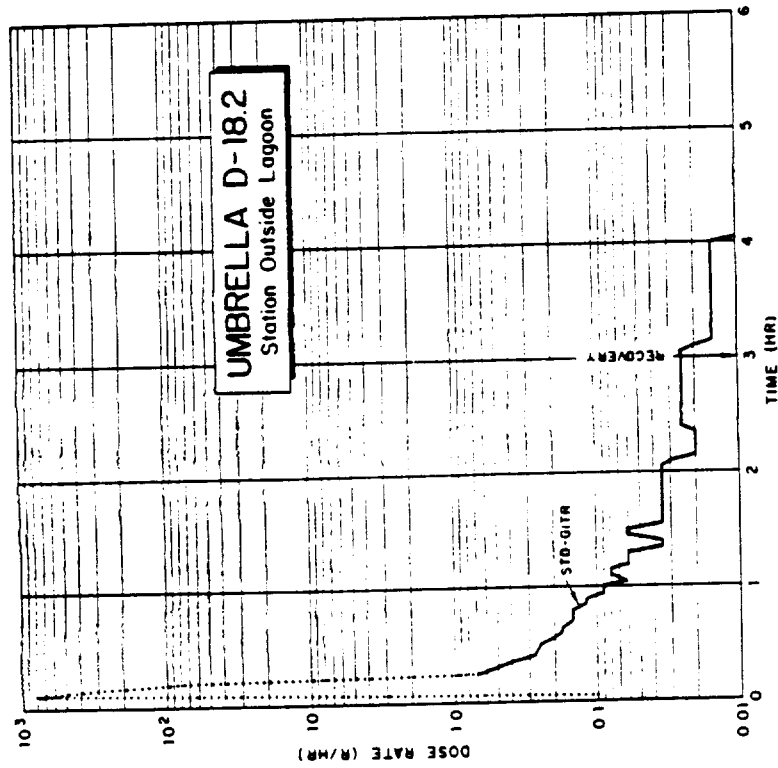


Figure 3.176 Sid-GITR record, 0 to 6 hours, coracle at 18,220 feet, 250.2° T from surface zero, Shot Umbrella.

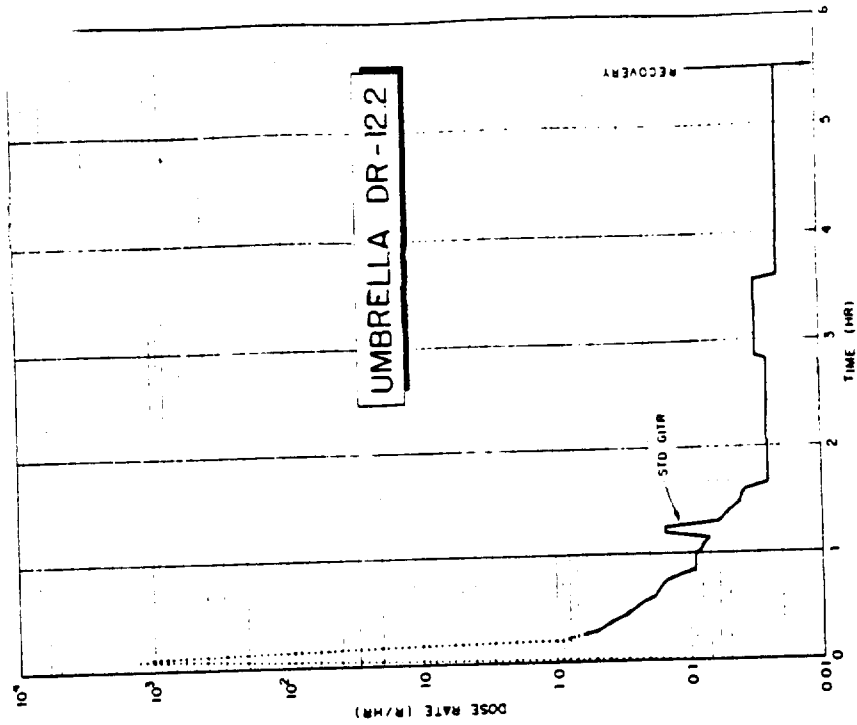


Figure 3.179 Sid-GITR record, 0 to 6 hours, coracle at 12,230 feet, 262.5° T from surface zero, Shot Umbrella.

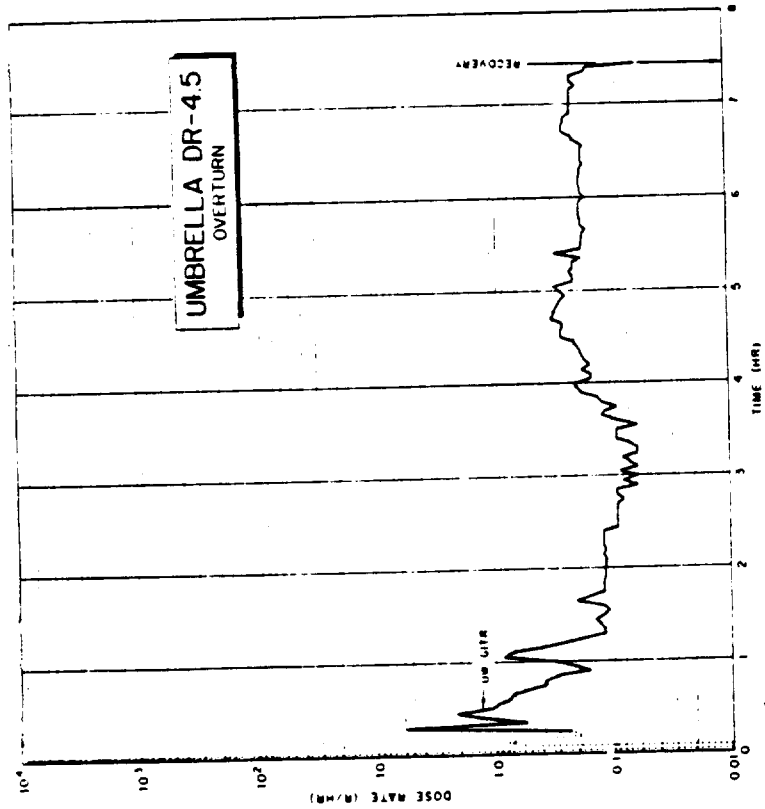


Figure 3.178 UW-GITR record, 0 to 6 hours, coracle at 4,530 feet, 263.5° T from surface zero, Shot Umbrella.

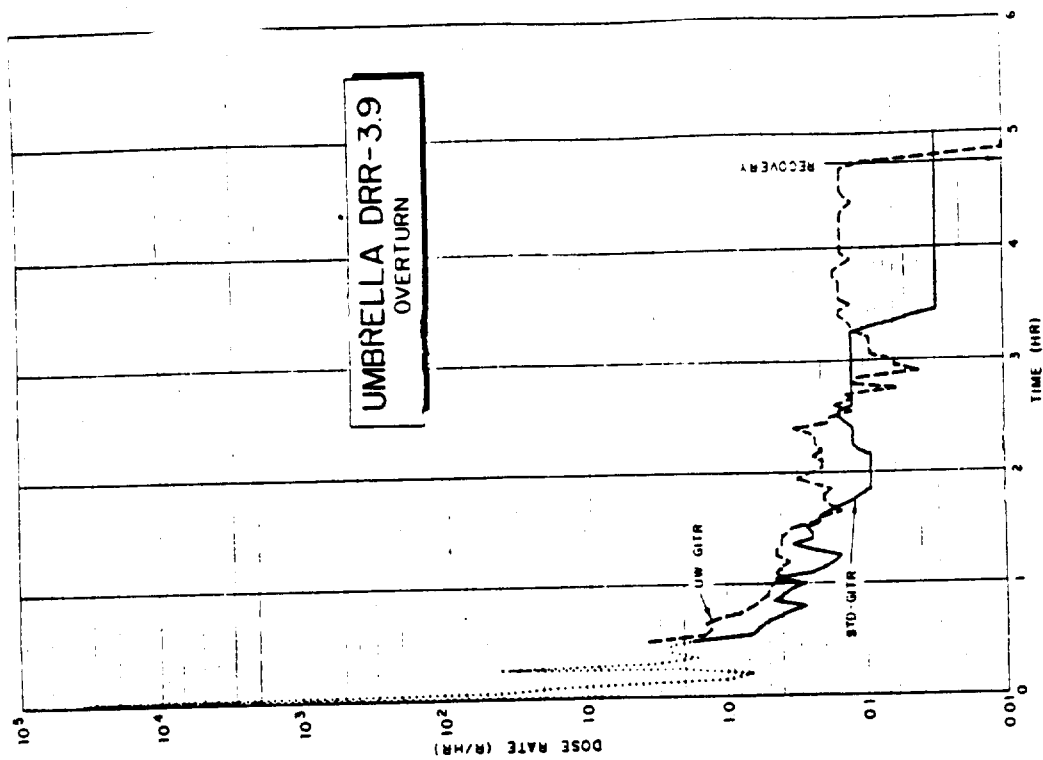


Figure 3.181 Std- and UW-GTR records, 0 to 6 hours; coracle at 3,940 feet, 279.1° T from surface zero, Shot Umbrella.

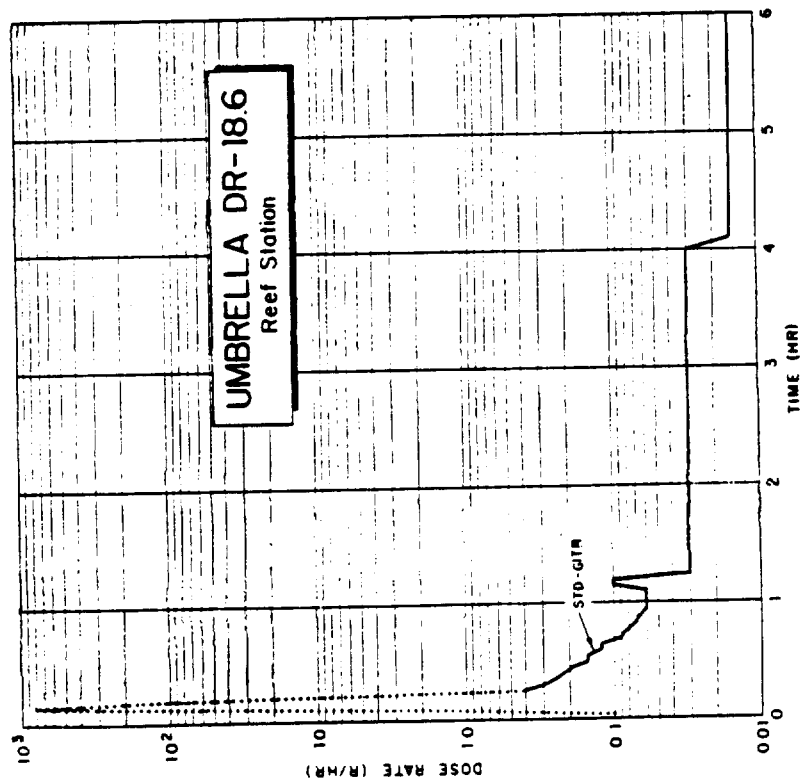
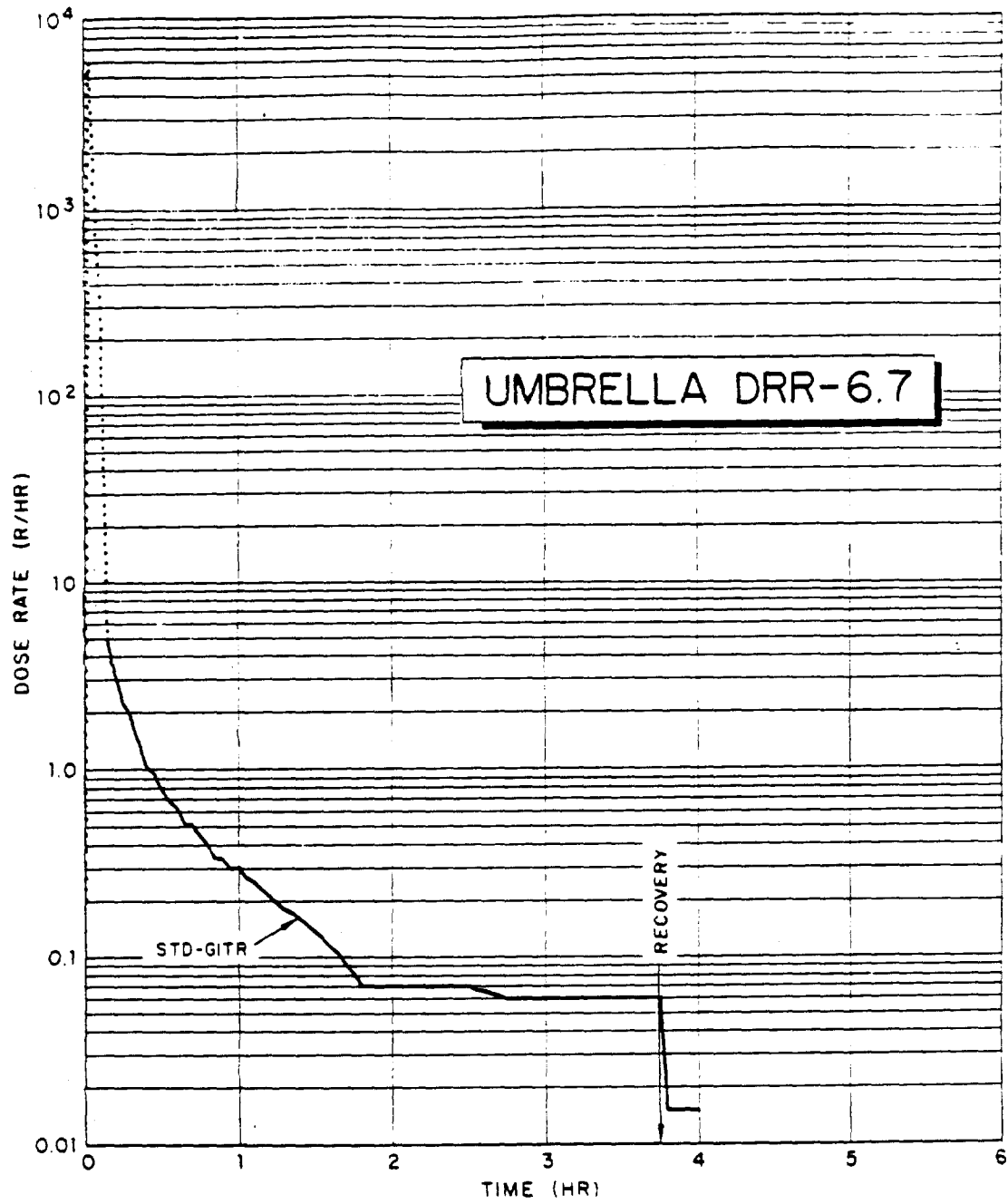


Figure 3.180 Std-GTR record, 0 to 6 hours, coracle at 18,600 feet, 261° T from surface zero, Shot Umbrella.



**Figure 3.182** Std-GITR record, 0 to 6 hours, coracle at 6,740 feet, 278.1° T from surface zero, Shot Umbrella.

mr. hr. This low reading could be explained by assuming that the coarser suspended material (probably in the form of  $\text{CaCO}_3$ ) sank, scavenging most of the radioactive debris as it did so.

### 3.4 GAMMA RADIATION FIELDS ABOARD TARGET SHIPS

Gamma fields aboard all target ships were measured by a std-GITR detector similar to that used on the coracles. Although tape readout in some cases was accomplished by a different method, limits of accuracy and restrictions similar to those already described for coracle records apply to shipboard gamma records (Sections 3.1.1 and 3.4.1). Most recorder transports used aboard the ships were the 60-hour type (Section 2.2.1) rather than the 12-hour type used in the coracles, and the detector was mounted in a different casing (Figure 2.3). Since deposited radioactive material may be neglected, the difference in response due to detector mounting should be minimal; however, the lower tape transport speed and the fact that the shipboard installations had no timing blank (Section 2.2.7) combined to reduce time resolution to about  $\pm 3$  seconds. The 60-hour tape transport was used aboard all target ships with the exception of the pilot house and centerline-forward stations on the EC-2 for Shot Umbrella. The slow transport speed was selected, despite the risk of saturation, so that in the event of large deposits of radioactive material, the decay rate would be recorded for a sufficient length of time to permit a complete radiological survey of the vessel before the GITR record terminated.

In addition to the GITR's, film packs were placed at approximately 20 locations aboard the target vessels (Section 1.3.3) to establish a relationship between GITR stations and other shipboard positions. The reported accuracy of these film packs is  $\pm 20$  percent (Section 2.2.5), but the correlation between film pack and solid angle plots versus frame number (Section 3.4.2) suggests higher accuracy. After each shot, a precise radiological survey of all topside decks was made with calibrated Cutie Pies (Model CP-3DM beta-gamma survey meter, Reference 103) in an attempt to extend GITR and film pack data to still other shipboard locations.

The final positions and attitudes of all target ships are tabulated in Table 3.26 (References 75 and 104); movement of the ships after each shot has been estimated from photographs and is also included in the table. This movement of the ships should be remembered when considering these shipboard records. After Wahoo, the EC-2, DD-474, and DD-592 all changed positions shortly after zero time (Figure 2.1). After Umbrella, the DD-474 broke her stern mooring and swung on her forward anchor. The final position of the DD-474 was about 500 feet upwind on the starboard quarter of the DD-592 with her bow into the wind (Figure 2.2). Ship movement probably took place during the first 20 minutes after zero time; however, the DD-474 GITR records for Umbrella suggest that the ship did not move very far from its original position during the first 5 minutes. All target ships were equipped with full washdown, which was started at the time of final evacuation (H-4 hours on Wahoo and H-2 hours on Umbrella) and was fueled to run 14 hours. The washdown systems operated as planned, with the single exception of the system on the DD-474 during Shot Wahoo. This ship did not appear to have washdown operating forward at shot time.

3.4.1 Gamma Dose Rate versus Time. Because of a mutual interest in the gamma radiation fields aboard the three destroyers, Projects 2.1 and 2.3 both used the records obtained by the weather deck GITR's at the bow, amidship-port, and amidship-starboard positions. Project 2.1 obtained dose rate information from these instruments, using the 704 computer on Parry Island rather than the GITOUT device used for the coracle records. Since the two methods of readout are entirely compatible, the information obtained by Project 2.1 has simply been recast by this project into a form identical to that used for the coracle records.

In brief, the 704 program, described in References 57 and 86, is identical to the time-between-pulse method described for the GITOUT device. Only the initial rise in dose rate on the low-range channel and the subsequent high-range channel record were read out, using the 704 computer. The timing channel on the shipboard tapes was first monitored to detect possi-

ble variations in the original recording speed, which, if found, were compensated by subprogramming the 704 computer. The high-range channel on the GITER tape was fed into the computer where the time between each radiation pulse was measured against a 1-Mc timing signal in the computer. Each radiation pulse interrupted the timing signal long enough to store the cumulated time during the previous interval in the computer memory bank. Since only 48 msec (a time much shorter than the duration of a radiation pulse from the GITER) were required by the 704 to store the cumulated time, the timing signal for the next interval could be started by the same radiation pulse; thus, complete time-between-pulse information was obtained. Usually all information on the high-range channel of a GITER could be stored in the 704 memory bank. The computer was then programmed to compute the average dose rate over each interval between radiation pulses, to compute the dose increments and to sum the time intervals. The GITOUT procedure is more accurate than the 704 procedure, since it uses the timing channel information on the tape; however, the difference in accuracy between the 704 and the GITOUT cannot be more than 1 percent.

GITER records from the EC-2 and the platform station aboard the DD-592 and all remaining low-range channel information from the destroyers were read out, using the GITOUT and the fixed-interval-counting method described in Section 3.1.1. All 60-hour tapes had to be electronically stretched, a process that is also described in Section 3.1.1. The records for 0 to 15 minutes and 0 to 6 hours are presented in this section (Figures 3.183 through 3.206); the records for 0 to 2.5 minutes are included in Section 3.2. Since no timing blank (Section 2.2.7) was included in the shipboard control system, zero time was established by measuring 5 minutes on the GITER timing channel starting from the minus-5-minute EG&G signal. Prior to evacuation of the ships for Umbrella, some GITER's were started manually. Zero time on these records was established by matching first dose rate peaks with GITER's that received the minus-5-minute signal, aboard the same vessel. Zero time on the EC-2 records for Umbrella was determined by calculating the time of the first peak on the basis of nearby coracle records.

Unmodified dose rates are presented, since any radioactive material deposited on the decks was probably removed either by the water accompanying the deposition or by the washdown system. The measurements represent gamma dose rates resulting from airborne radioactive material at specific positions aboard stationary ships under washdown. Unfortunately, nine of the GITER's saturated at peak dose rate for about 15 seconds during Umbrella; thus, exact cumulative doses cannot be computed. The peak dose rates for the destroyers have been reconstructed by Project 2.1, using the unsaturated records obtained from GITER's installed inside the ships. These reconstructed peaks are shown as a dashed line on the appropriate records. The total cumulative dose has been determined by numerical integration, using a straight line between the two dose rate points bounding the period of saturation. The difference between this integrated dose and the corrected film pack dose approximates the dose received during saturation. In all cases, more than half the total dose was received during the brief interval of saturation. These values together with the cumulative dose at various times after zero time for the non-saturated shipboard records are presented in Table 3.27. The total doses registered by film packs positioned within 3 feet of the GITER detector are also given for comparison.

For greater ease of comparison with the coracle data, the time and dose rate of the major peaks shown by the shipboard records are summarized in Table 3.28. The normalized doses have also been computed for various times after zero time as described in Section 3.3.2 and are presented in Table 3.29. Because corrections for waterborne radioactivity cannot be accurately made, the cumulative normalized dose is stopped as soon as the gamma record indicates completion of surge transit; therefore, comparison must be made with the observed dose cumulated over the same time interval. Although the cumulative normalized dose contains a number of inherent inaccuracies, it may be used to estimate the relative total amounts of radioactive base surge transiting a given ship.

During both Wahoo and Umbrella, the GITER record obtained at the bow station aboard the DD-593 is about double the other records obtained aboard that ship. The difference between the corrected film pack dose and the total cumulative dose computed from the GITER record is

also larger than normal. The possibility exists that this detector was double pulsing (a malfunction that would cause a dose rate about twice the actual dose rate); however, the instrument was checked after each shot and found to be operating perfectly. Furthermore, the record from this station agrees with those obtained from other GITR's aboard the same ship after passage of the base surge. The records are, therefore, considered reliable. Although no completely satisfactory explanation for the discrepancy has yet been advanced, the most likely possibility is that the bow records for the DD-593 are the result of an extreme case of ship retardation (Sections 3.3.2 and 3.4.3).

In many instances during Umbrella, the film pack dose is understandably higher than the cumulative GITR dose, since the GITR was saturated during peak dose rate (Table 3.27). This difference, however, occurs at the forward station aboard the EC-2 during Wahoo where there is no evidence of GITR saturation. The EC-2 was so oriented for Wahoo that the forward end was engulfed by the base surge slightly ahead of the rest of the ship. Although this difference might account for a higher total dose at the forward station, it does not account for the difference between the film pack dose and the total cumulative GITR dose. Superstructure shielding effects (Section 3.4.2), ship retardation (Sections 3.3.2 and 3.4.3), or variation in deposition at the two locations can be postulated but cannot be conclusively demonstrated.

Like those from the coracles, the shipboard records (Figures 3.183 through 3.194) may be divided into characteristic types (Table 3.11). The general discussion of all shipboard records has been incorporated with that of the coracle records (Section 3.3.2). The shipboard records are presented in this section, using the same format and key previously described for the coracles. The records are individually discussed here to indicate possible modifications due to the superstructure or ship movement. In general the shipboard and coracle records are so similar that the effects of the ship's superstructure on the free-field gamma radiation is not immediately apparent. An analysis of shipboard film pack doses, however, gives definite evidence of superstructure effects and may be used in conjunction with cumulative GITR doses to estimate the magnitude of such effects (Sections 3.4.2 and 3.4.3).

For Wahoo, the shipboard records from the DD-474 and DD-592 are limited to film pack and meter survey information, because a power failure aboard both ships prevented receipt of the radio signals that started the project instruments (Section 2.1.1). When this information is considered, the fact that both ships moved after the detonation should be borne in mind (Figure 2.1). At 20 minutes after Wahoo, the DD-474 had moved about 900 feet farther downwind, and the DD-592 had moved about 500 feet farther downwind.

During Wahoo, the EC-2 was anchored halfway between a crosswind and an upwind position at 2,300 feet from surface zero with the starboard side facing surface zero obliquely. At 20 minutes after Wahoo, the EC-2 had moved an additional 600 feet crosswind (Figure 2.1); however, the estimated maximum movement during base surge transit is 200 feet. The EC-2 was so oriented that the bow was first engulfed by the base surge as evidenced by the slight difference in time of peak between the forward and after stations. The abrupt decrease in dose rate (Figures 3.183 and 3.184) immediately after the first peak is probably due to the passage of the upwind surge beyond the ship. The gently sloping plateau from 2 to 4 minutes represents an inner edge transit of the upwind surge with some additional contributions from white water, which reached the ship at approximately 2 minutes. The gamma record persists about 4 minutes after the final transit of the primary surge photo-boundary  $P_0$  (Appendix F). Using the reported surface wind this delay in final transit could indicate a tail (Appendix F) of approximately 6,200 feet, but a more probable cause is the temporary retention of surge remnants in turbulent eddies associated with the superstructure (ship retardation). The fact that all shipboard detectors were installed in positions that are both distant and shielded from waterborne activity probably accounts for the absence of dose rate spikes caused by these sources.

The records for the DD-593 during Umbrella (Figures 3.185 and 3.186) represent a nearly central cross section of the base surge, clearly showing an intersurge decrement. The ship was positioned with the stern into the wind; thus, the starboard side faced the hot line (Appendix F). The records from the starboard and port GITR's do not, however, show any significant

differences. The special case of the bow GTR is discussed in Section 3.4.3. The prolonged sloping plateau extending from about 11 to 17 minutes is again most probably due to superstructure turbulence, although a long record due to a base surge tail is also possible (compare Station D 8.0). The earliest arrival of waterborne sources is about 12 minutes. If such sources did reach the ship, their arrival was masked by the last stages of base surge transit. Later records (Figures 3.197 and 3.198) show the arrival of white water at about 1 hour. The bow and the port GTR register similar peak dose rates, but there is considerable difference between these records and that of the starboard GTR. Such differences could be caused by a nonuniform distribution of radioactivity within the white water boundary.

During Umbrella, the EC-2 was positioned at 1,650 feet crosswind with the port side facing surface zero. No ship movement was observed after Umbrella. The records (Figures 3.187 and 3.188) represent a central transit, which is close to being an inner edge transit. The central decrement appears to have been recorded, but the high minimum dose rate in the first valley suggests contributions from a nearby inner base surge edge, although superstructure turbulence could also be a contributing factor. The prolonged record from 3 to 5 minutes is most probably due to ship retardation. At 3 minutes, the white water boundary is approximately 1,000 feet radially beyond the EC-2; however, the record shows little contribution from this source. As suggested previously, the shielded location of the shipboard detectors probably accounts for the reduced influence of waterborne sources.

The records for the DD-474 during Umbrella (Figures 3.189 and 3.190) represent a central cross section of the base surge, but possible effects due to the failure of the stern anchor swinging the ship must be considered. The DD-474 started with the stern toward surface zero and the port side facing the hot line; 20 minutes later it was 500 feet farther downwind with the bow toward surface zero and the starboard side facing the hot line. Very little change in the ship's position could have taken place during the transit of the downwind surge, but the lower dose rates recorded by the port GTR during upwind surge transit suggest partial superstructure shielding. The slightly higher dose rates recorded by the bow GTR are also the result of differences in shielding. The prolonged gamma record from about 4 to 8 minutes is probably due to temporary retention of the surge by superstructure turbulence. A central decrement is, nevertheless, clearly recorded. The longer significant record of the starboard GTR in comparison to the port GTR also supports the turbulent retention hypothesis, but this difference is not consistently borne out by records from the other ships. Arrival of radioactivity in foam would be masked by base surge transit; however, its final departure is calculated at 22 minutes. The rise in dose rate between 22 and 26 minutes may, however, be due to such sources. At approximately 0.9 and again at 3.9 hours (Figures 3.201 and 3.202), there are relatively sudden changes in the dose rate from waterborne sources suggesting rates of travel of 1 and 1.5 knots, respectively.

The records for the DD-592 during Umbrella (Figures 3.191 and 3.192) also represent a central transit, which should be similar, since the DD-474 and DD-592 are at nearly the same downwind distance 20 minutes after the shot. The DD-592 was oriented broadside with the starboard side facing surface zero. Because of the ship's greater distance from surface zero, the times and heights of peaks are later and lower. The bow and platform GTR records track each other closely as might be expected, since they both represent relatively exposed instrumentations. No large increase in dose rate with increasing detector height is shown, indicating that both the bow and the platform instruments must subtend about the same solid angle of the surge (Section 3.4.2). The port and starboard GTR records are lower than the bow and platform records because of their relatively shielded locations. Again, the upwind transit is longer than would be expected on the basis of cloud photography. The prolonged record is probably due to ship retardation although the ship's crosswind attitude should minimize such retardation effects. The DD-592 was in white water from very early time. Later records (Figures 3.203 and 3.204) indicate waterborne sources until 4.7 hours; thus, if the 6-minute upwind white water boundary is used, a speed of 0.2 knot again results.

The records for the DD-593 during Umbrella (Figures 3.193 and 3.194) also represent a central transit. The ship was anchored with the stern toward surface zero and the port side toward the hot line. No movement was observed after the shot. The records are comparable to those obtained on the other destroyers. The valley occurring around 4.2 minutes corresponds to the passage of the base surge center over the ship. The minimum dose rates for all shipboard records of the central decrement are discussed in Section 3.3.2. The higher minimum dose rate recorded by the starboard GTR is consistent with the ship's orientation, since this instrument would be more influenced by the inner edge of the base surge. The prolonged upwind surge transit is again probably due to superstructure turbulence effects. As during Wahoo, the bow GTR record during surge transit is abnormally high, a fact which is further discussed in Section 3.4.3. The later records (Figures 3.205 and 3.206) show increased dose rates due to waterborne sources from 60 to 84 minutes and again from 2.3 to 2.6 hours. The earlier peaks may be due to radioactive foam. The later peaks indicate a speed of 0.3 knot, which is similar to the previously calculated speeds for white water. The earlier peaks, however, indicate a speed nearly three times this value.

3.4.2 Variation of Shipboard Dose with Position. Two means of extending the measurement of gamma radiation exposure to additional weather deck positions were attempted. Approximately 20 NBS film packs (Section 2.2.5) were placed in specially designed holders aboard each of the target ships, as shown in Figures 1.12 through 1.14. The packs were placed exactly 3 feet above the deck and, in the case of film packs associated with GTR's, they were mounted on a pipe stand so that the film would be exposed to the same gamma environment as the GTR detector itself. These film pack stations represented the first attempt to extend GTR measurements to other locations. The second extension consisted of a pattern of marked meter survey points within 3 feet of every film pack, augmented by approximately 30 additional marked points distributed over all important weather decks (Figures 1.12 through 1.14).

As soon after the shot as radiological safety permitted, all marked points were surveyed with Cutie Pies (Model CP-3DM beta-gamma survey meter, Reference 103) calibrated on a Co<sup>60</sup> range within 6 days of the survey. At each point, four meter readings were taken exactly 3 feet above the deck with the meter probe pointed at 90° intervals relative to the bow.

These survey readings were averaged to compensate for possible variations caused by the ship's superstructure. The NBS film packs were also recovered at the time of this meter survey. Data obtained from all shipboard film packs together with the survey results are given in Tables 3.30 and 3.31.

A control group of similar NBS film packs were exposed on a Co<sup>60</sup> range at times sufficiently close to shot time so that no specific correction would be required for latent image fading (Reference 49). The film packs recovered from the target ships were then interpreted by means of these control films (Section C.4). Although film pack doses show the usual relationship to the GTR cumulative doses if the effects of superstructure shielding are taken in account, no relationship can be established between the survey readings and film pack doses. This lack of correspondence is probably due to the fact that the principal radiation exposure occurs during transit of the base surge while wind and washdown obscure any possible regularity in deposition.

A detailed analysis of the film pack doses indicates that the ship's superstructure has a detectable influence on the total gamma dose and thus probably on dose rate. Plots of the recorded film pack dose versus frame number give a characteristic curve shape for each ship regardless of ship's attitude or distance from surface zero (Figures 3.207 through 3.212). The regularity of these curve shapes is definite evidence of superstructure effect. If the free-field radiation is assumed to be uniform (this assumption can be valid only for relatively small masses of radiating cloud if all evidence is considered), the dose received by film packs would be influenced by the unobstructed solid angle subtended at the film.

Consequently, the approximate solid angle subtended by each major component of the ship's superstructure was calculated for each film pack location, using the DD-592 plans and photographs. This simplified treatment makes no allowance for variation in the shielding charac-

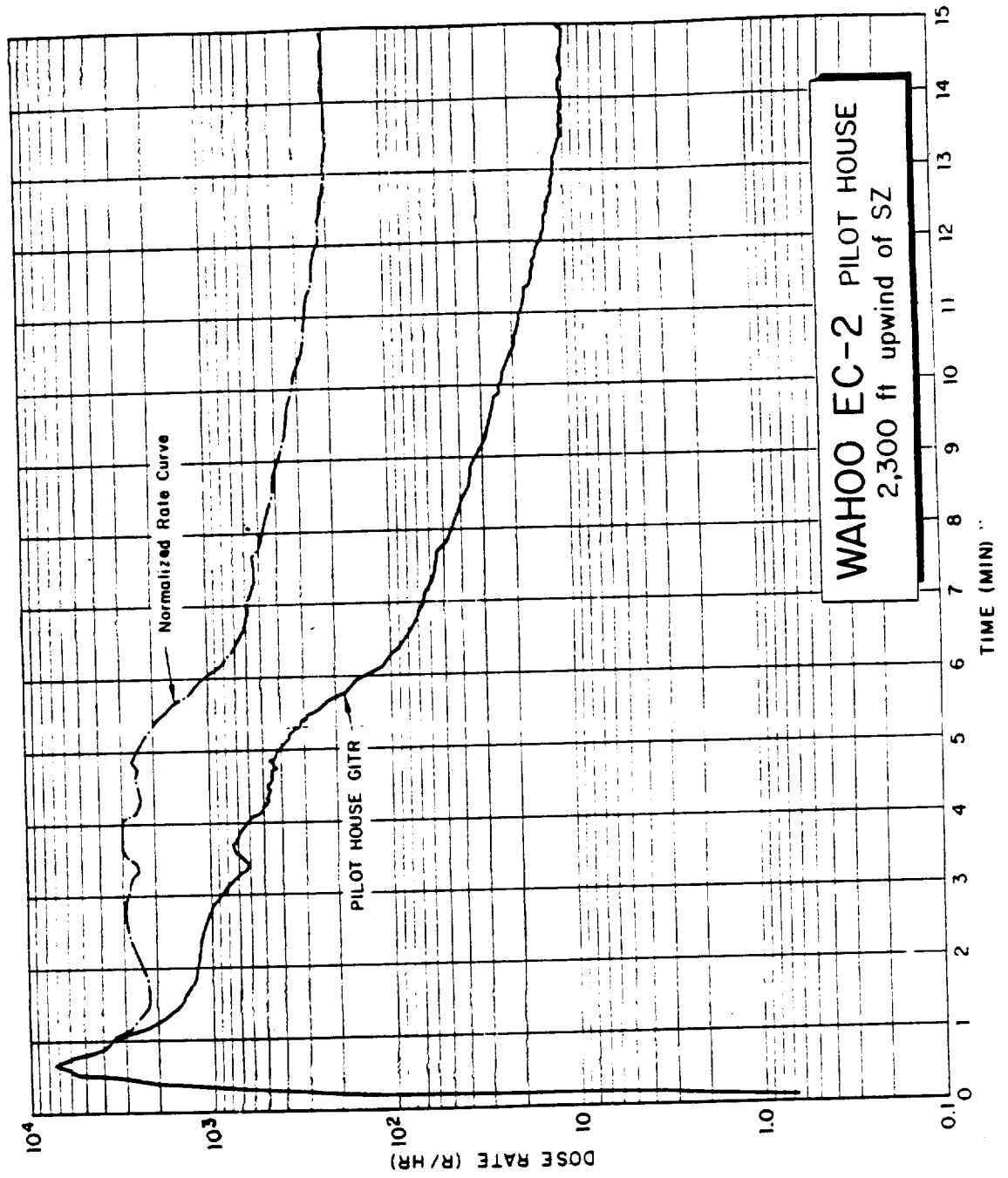


Figure 3.183 GITR record, 0 to 15 minutes, for EC-2 at 2,300 feet, 28.5° T from surface zero, Shot Wahoo. (GITR installed inside pilot house.)

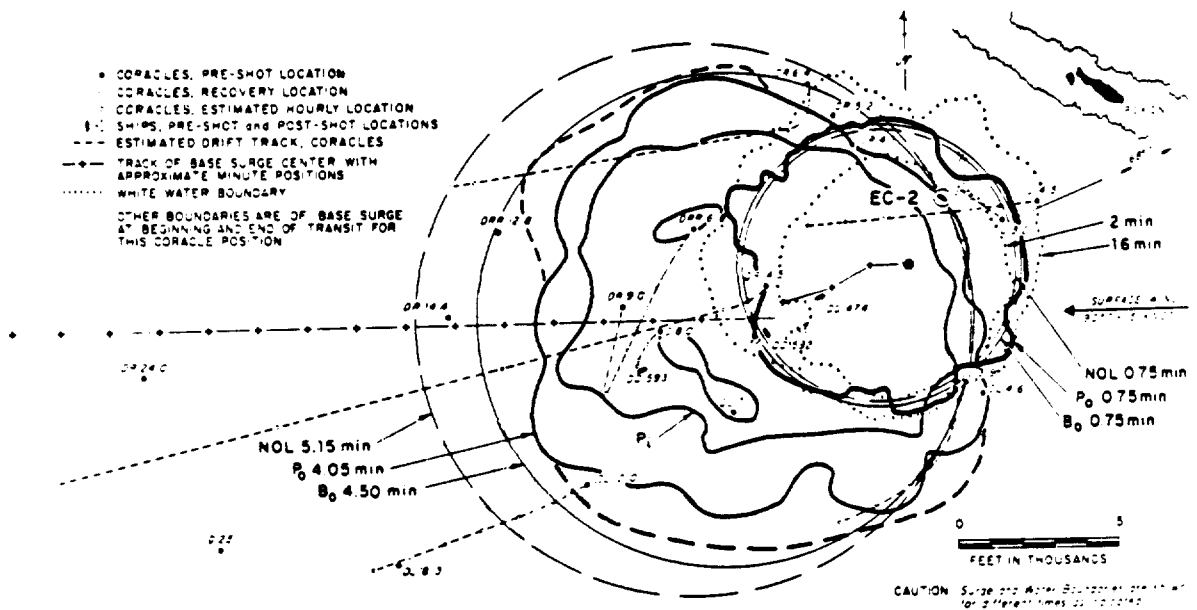
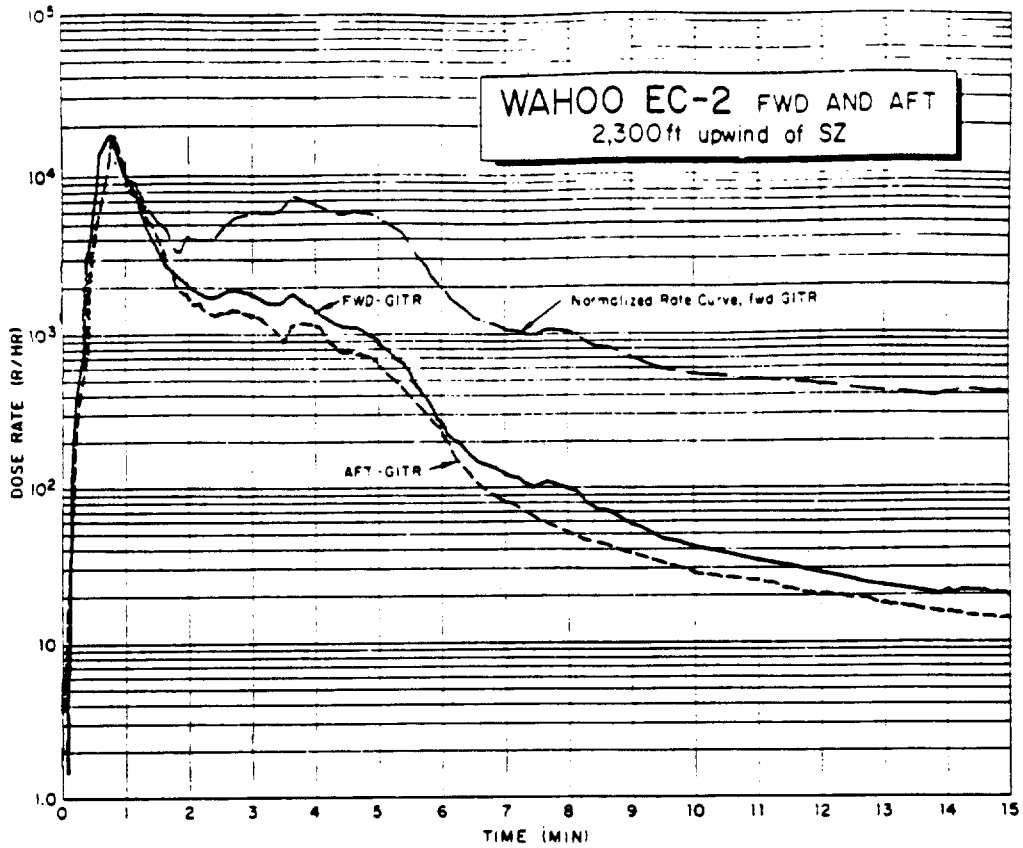


Figure 3.184 Transit dose rate record and data summary for EC-2, Shot Wahoo. (GITR's installed on centerline at Frame 48, forward, and Frame 137.5, aft, main deck.) See key preceding Table 3.11.

# WAHOO EC-2 fwd

Position: 2,500 feet,  
0.25 °T from Surface Zero

Complete Records (Unless Otherwise Indicated): Std-GITR, FF

Special Conditions: scrapped on 200 ft, post-shot position 2700 ft, possible self interference

## GENERAL INFORMATION

Type of Transit: Tower Edge, IE Type of Record: N<sub>1</sub> (EC-2, fwd)  
 Max. Dose Rate: 17.5 r/hr at 2.25 min. Total Dose: 3.2 r  
 Film Pack Dose: Tripod 335 r, Float — r. Total Surge: 650 (Transit from 0 to 10 min)

## SURGE BOUNDARIES

Photographic Boundary			Radiological Boundary		Source Center	Tail Length
TOA (min)	Center (ft)(min)	TOC (min)	TOA (min)	TOC (min)	relative to P <sub>0</sub> (ft)	(ft)
<u>0.60</u>	<u>2300/0</u>	<u>4.05</u>	<u>0.65</u>	<u>8.14</u>	<u>+760</u>	<u>6200</u>

## APPROACH VELOCITIES

Photographic (Vis.)					Radiological (r-of-r)			
minus 100 ft (k)	minus 200 ft (k)	minus 300 ft (k)	minus 500 ft (k)		1600 ft (k)	1200 ft (k)	400 ft (k)	
<u>P<sub>0</sub> 32</u>	<u>32</u>	<u>32</u>	<u>32</u>		90°	<u>43</u>	<u>39</u>	<u>34</u>
<u>B<sub>0</sub> 36</u>	<u>36</u>	<u>36</u>	<u>36</u>		60°	<u>47</u>	<u>41</u>	<u>32</u>

## WATER-BORNE SOURCES

(cf. Boundary Plot)

	Foam (min)	Water (min)
Obs. TOA	<u>ask</u>	<u>ask</u>
Obs. TOC	<u>ask</u>	<u>21.5</u>

## BOMB GENERATED WAVES

Wave No.	1st	TOA	min
	2nd	"	"
	3rd	"	"
	4th	"	"

## MISCELLANEOUS DATA

TOTAL SURGE DEPOSITION (IC)

c/min at 22 days: —  
 Approx. Fissions: —

ESTIMATED DEPOSIT DOSE RATE  
 (converted to Std-GITR response at 1min)

GITR Background: — r/hr  
 Survey Meter: — r/hr  
 IC Total: — r/hr

Initial Dose: 17.0 r  
 Shine Dose: 6.08 r  
 (for 38% of Peak)

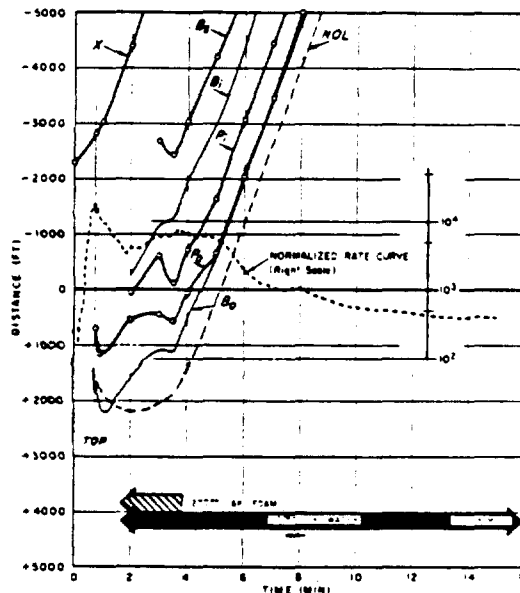


Figure 3.184 Continued.

155

**WAHOO DD-593** stbd      Position: 8,700 feet,  
250 °T from Surface Zero  
 Complete Records (Unless Otherwise Indicated): Std-GITR, EP  
 Special Conditions: possible self-interference

**GENERAL INFORMATION**  
 Type of Transit: Control, C      Type of Record: IC (DD-523, 761)  
 Max Dose Rate: 2256 r/hr at 2.73 min.      Total Dose: 221 r  
 Film Pack Dose: Tripod 265 r, Float — r. Total Surge: 2200 (Transit from 2 to 15 min)

**SURGE BOUNDARIES**

Photographic Boundary			Radiological Boundary		Source Center relative to P <sub>0</sub> (ft)	Tail Length (ft)
TOA (min)	Center (ft)(min)	TOC (min)	TOA (min)	TOC (min)		
<u>2.25</u>	<u>1500/6.2</u>	<u>11.15</u>	<u>2.61</u>	<u>16.53</u>	<u>+260</u>	<u>8300</u>

**APPROACH VELOCITIES**

	Photographic (Vis.)				Radiological (r-of-r)		
	minus 100 ft (k)	minus 200 ft (k)	minus 300 ft (k)	minus 500 ft (k)	1600 ft (k)	1200 ft (k)	400 ft (k)
P <sub>0</sub>	<u>17</u>	<u>17</u>	<u>17</u>	<u>17</u>	90° <u>28</u>	<u>26</u>	<u>22</u>
B <sub>0</sub>	<u>26</u>	<u>26</u>	<u>26</u>	<u>26</u>	60° <u>31</u>	<u>27</u>	<u>21</u>

**WATER-BORNE SOURCES**  
 (cf. Boundary Plot)

	Foam (min)	Water (min)
Obs. TOA	<u>11.30</u>	<u>4.5</u>
Obs. TOC	<u>12.50</u>	<u>12.0</u>

**BOMB GENERATED WAVES**

Wave No.	1st	TOA	2nd	3rd	4th
	—	—	—	—	—

**MISCELLANEOUS DATA**

TOTAL SURGE DEPOSITION (IC)  
 c/min at 22 days: —  
 Approx. Fissions: —

ESTIMATED DEPOSIT DOSE RATE  
 (converted to Std-GITR response at 1 min)

GITR Background: — r/hr  
 Survey Meter: — r/hr  
 IC Total: — r/hr

Initial Dose: — r  
 Shine Dose: — r  
 (for 38% of Peak)

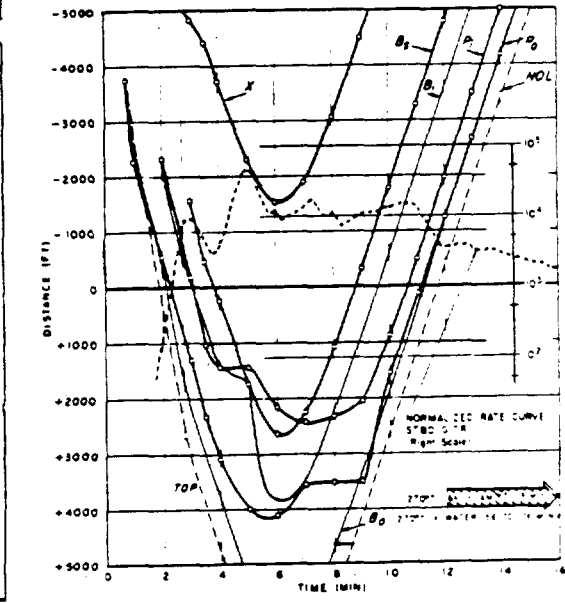


Figure 3.185 Continued.

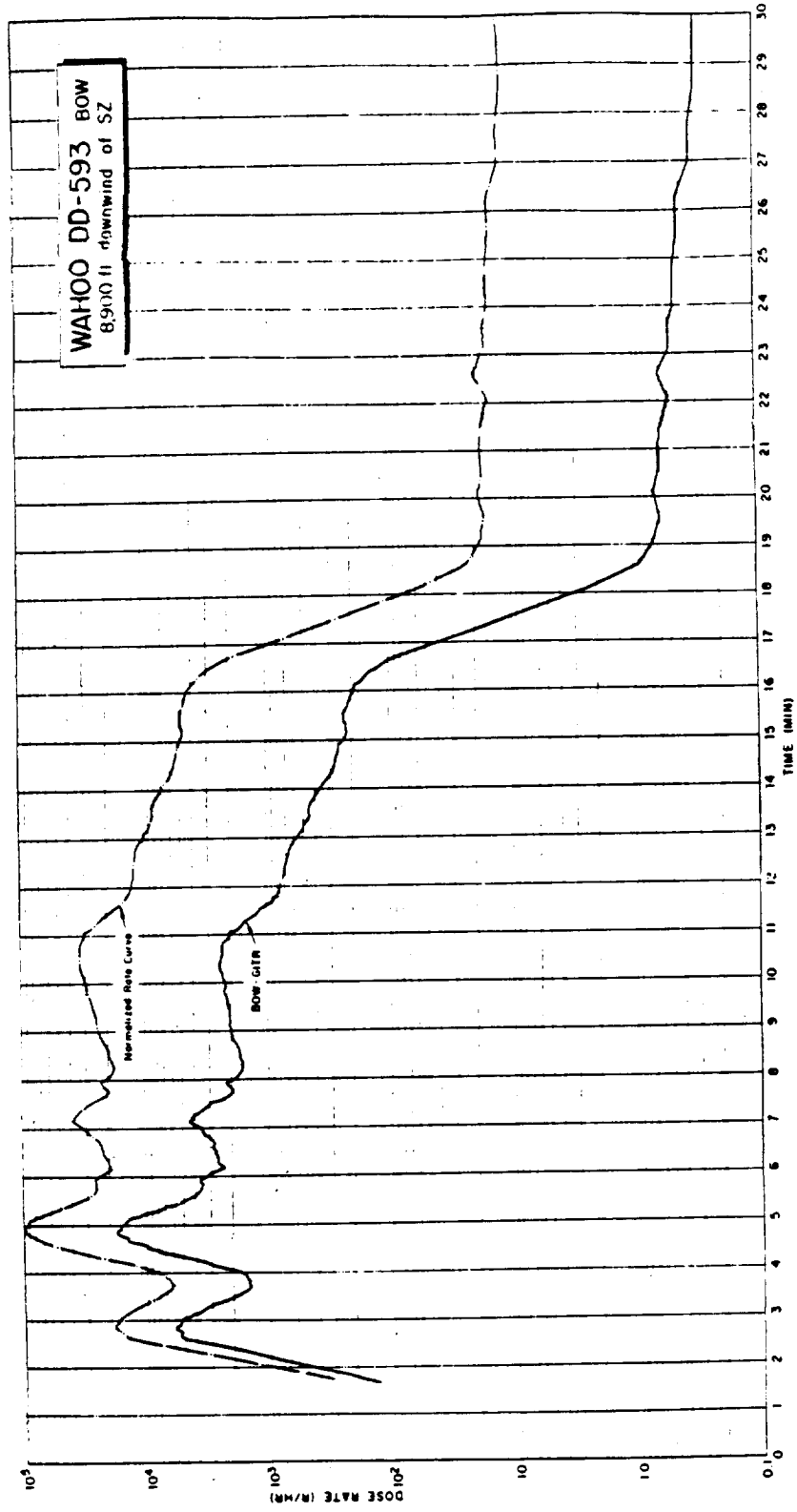


Figure 3.186 GTR record, 0 to 30 minutes, for DD-593 at 8,900 feet, 250° T from surface zero, Shot Wahoo. (GTR installed on centerline, Frame 21, bow, main deck.)

153

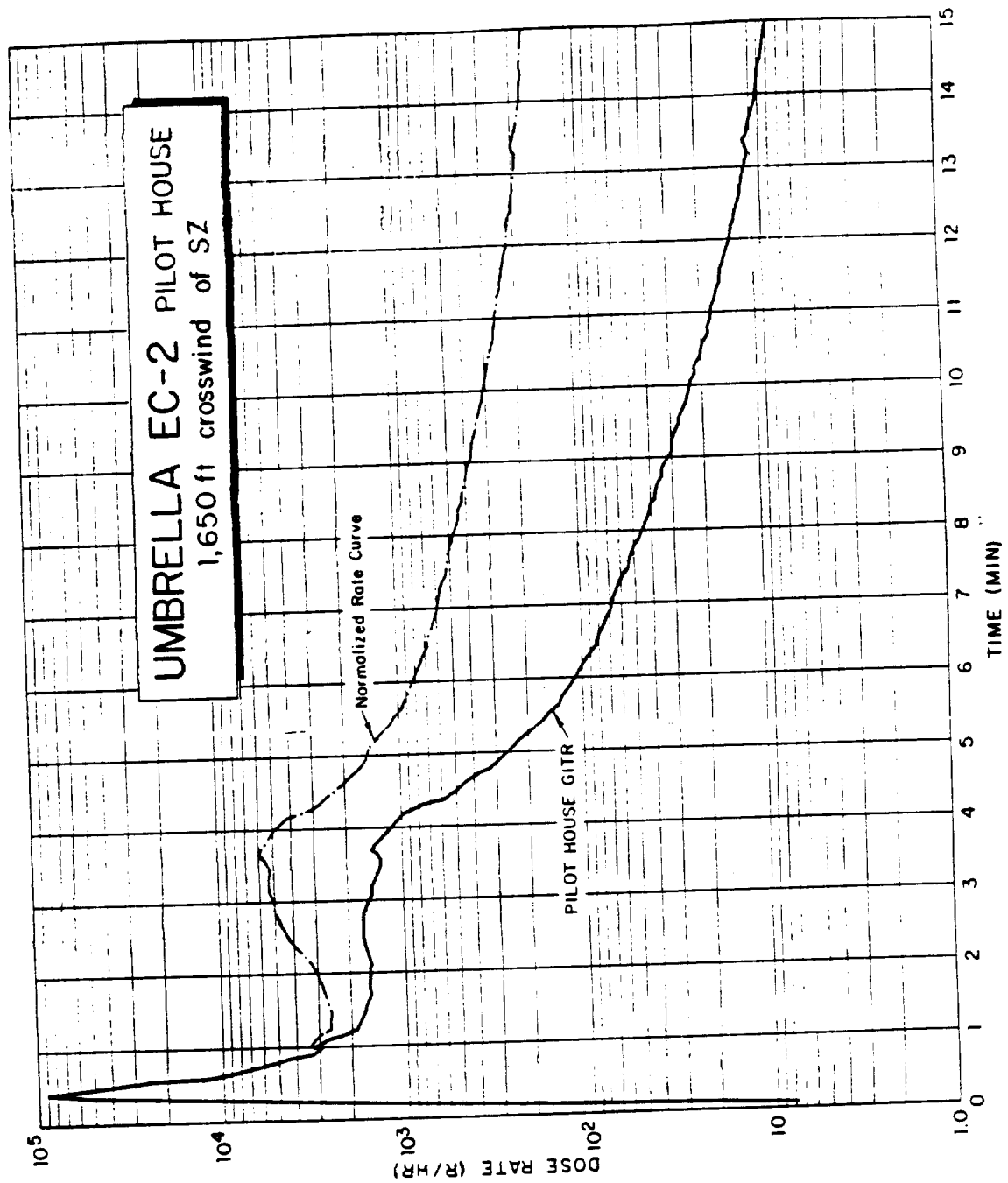


Figure 3.187 GTR record, 0 to 15 minutes, for EC-2 at 1,650 feet, 158° T from surface zero, Shot Umbrella. (GTR installed inside pilot house.)



# UMBRELLA EC-2 fwd

Position: 1.650 feet,  
152 °T from Surface Zero

Complete Records (Unless Otherwise Indicated): SPD-GITR

Special Conditions: saturated; possible self interference

## GENERAL INFORMATION

Type of Transit: Central C Type of Record: V<sub>2</sub> (EC-2 fwd)  
 Max. Dose Rate: 5.28 r/hr at --- min. Total Dose: 1432 r (converted FD)  
 Film Pack Dose: Tripod 1150 r, Float --- r. Total Surge: 1500 (Transit from 0 to 5 min)

## SURGE BOUNDARIES

Photographic Boundary			Radiological Boundary		Source Center relative to P <sub>0</sub>	Tail Length
TOA (min)	Center (ft)	TOC (min)	TOA (min)	TOC (min)	(ft)	(ft)
<u>&lt; 0.64</u>	<u>1650/0</u>	<u>3.12</u>	<u>SAT.</u>	<u>5.28</u>	<u>(-500)</u>	<u>440(0)</u>

## APPROACH VELOCITIES

Photographic (Vis.)				Radiological (r-of-r)		
minus 100 ft (k)	minus 200 ft (k)	minus 300 ft (k)	minus 500 ft (k)	1600 ft (k)	1200 ft (k)	400 ft (k)
<u>(40-60)</u>				90°	<u>---</u>	<u>---</u>
				60°	<u>---</u>	<u>---</u>

## WATER-BORNE SOURCES

(cf. Boundary Plot)

	Foam (min)	Water (min)
Obs. TOA	<u>rise</u>	<u>rise</u>
Obs. TOC	<u>rise</u>	<u>none</u>

## BOMB GENERATED WAVES

Wave No.	1st	TOA	min
2nd	"	"	"
3rd	"	"	"
4th	"	"	"

## MISCELLANEOUS DATA

### TOTAL SURGE DEPOSITION (IC)

c/min at 22 days: ---  
 Approx. Fissions: ---

### ESTIMATED DEPOSIT DOSE RATE (converted to Std-GITR response at 1min)

GITR Background: --- r/hr  
 Survey Meter: --- r/hr  
 IC Total: --- r/hr

Initial Dose: ? r  
 Shine Dose: ? r  
 (for 38% of Peak)

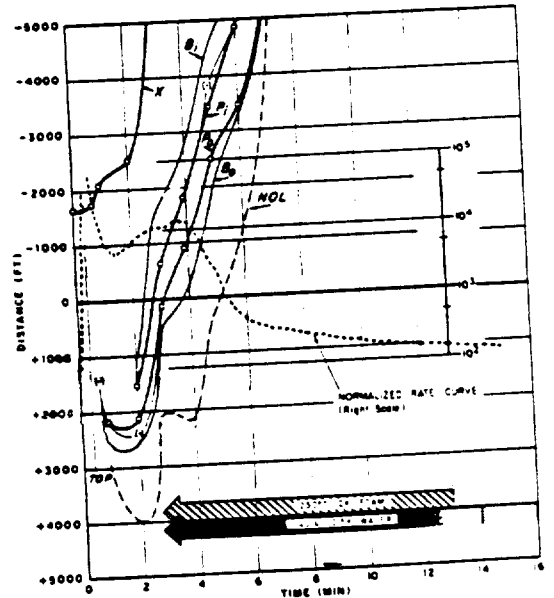


Figure 3.188 Continued.

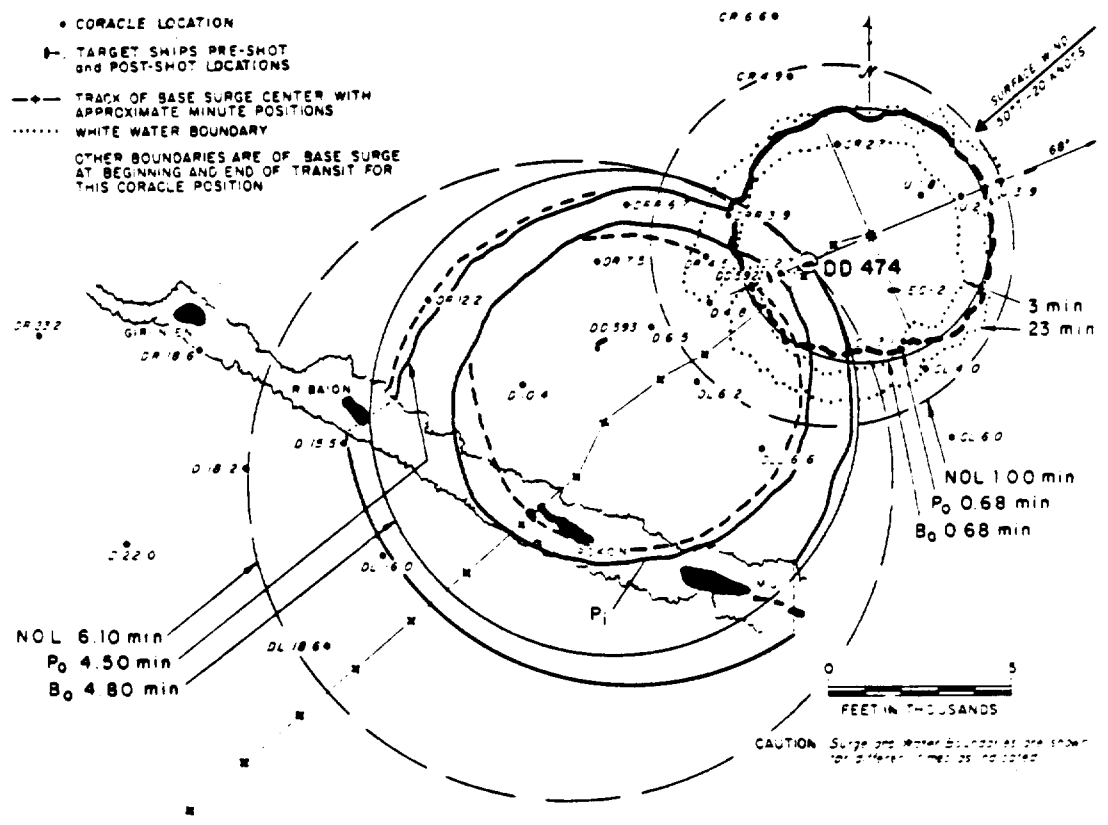
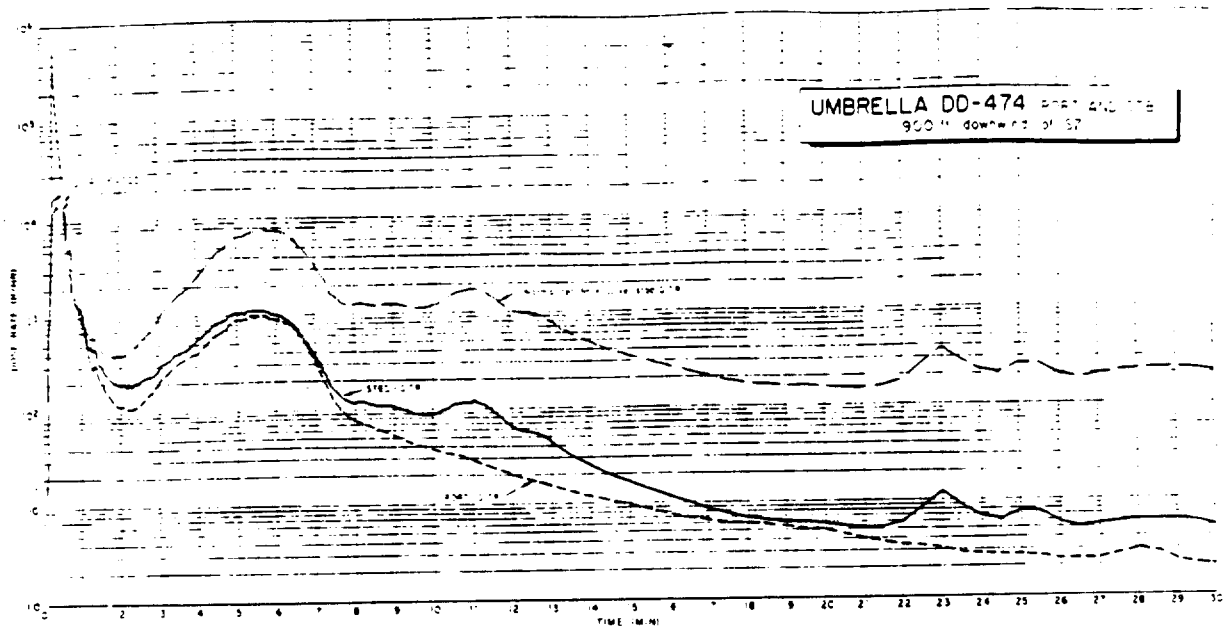


Figure 3.189 Transit dose rate record and data summary for DD-474, Shot Umbrella. (GITR installed on main deck, Frame 136, port, and Frame 136, starboard.) See key preceding Table 3.11.

1103

# UMBRELLA DD-474 stbd

Position: 330 feet,  
24.7 °T from Surface Zero

Complete Records (Unless Otherwise Indicated): Std-GITR, =P

Special Conditions: rotated, in swing & tilted 200 ft, possible self interference

## GENERAL INFORMATION

Type of Transit: Through the Center TIC Type of Record: U (Std-GITR 74-1)

Max. Dose Rate 5.25 r/hr at — min. Total Dose: 275 r (Converted ==)

Film Pack Dose: Tripod 125 r, Float — r. Total Surge: 125 (Transit from 0 to 10 min)

## SURGE BOUNDARIES

Photographic Boundary			Radiological Boundary		Source Center relative to P <sub>0</sub> (ft)	Tail Length (ft)
TOA (min)	Center (ft)(min)	TOC (min)	TOA (min)	TOC (min)		
<u>&lt; 500</u>	<u>320/18</u>	<u>4.50</u>	<u>sat</u>	<u>(210) w/w</u>	<u>—</u>	<u>210</u>

## APPROACH VELOCITIES

Photographic (Vis.)					Radiological (r-of-r)		
minus 100 ft (k)	minus 200 ft (k)	minus 300 ft (k)	minus 500 ft (k)	1600 ft (k)	1200 ft (k)	400 ft (k)	
<u>P<sub>0</sub></u>	<u>40-50</u>			<u>90°</u>	<u>—</u>	<u>—</u>	
<u>B<sub>0</sub></u>				<u>60°</u>	<u>—</u>	<u>—</u>	

## WATER-BORNE SOURCES

(cf. Boundary Plot)

	Foam (min)	Water (min)
Obs. TOA	<u>msk</u>	<u>msk</u>
Obs. TOC	<u>26</u>	<u>270</u>

## BOMB GENERATED WAVES

Wave No.	1st	2nd	3rd	4th	TOA	min
					<u>—</u>	<u>—</u>
					<u>—</u>	<u>—</u>
					<u>—</u>	<u>—</u>

## MISCELLANEOUS DATA

### TOTAL SURGE DEPOSITION (IC)

c/min at 22 days: —

Approx. Fissions: —

### ESTIMATED DEPOSIT DOSE RATE (converted to Std-GITR response at 1min)

GITR Background: — r/hr

Survey Meter: — r/hr

IC Total: — r/hr

Initial Dose: at 0.125 r

Shine Dose: at 80 r  
 (for 38% of Peak)

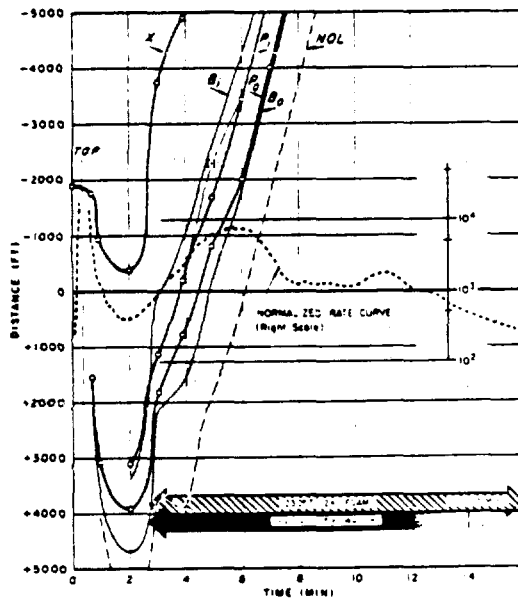


Figure 3.189 Continued.

150

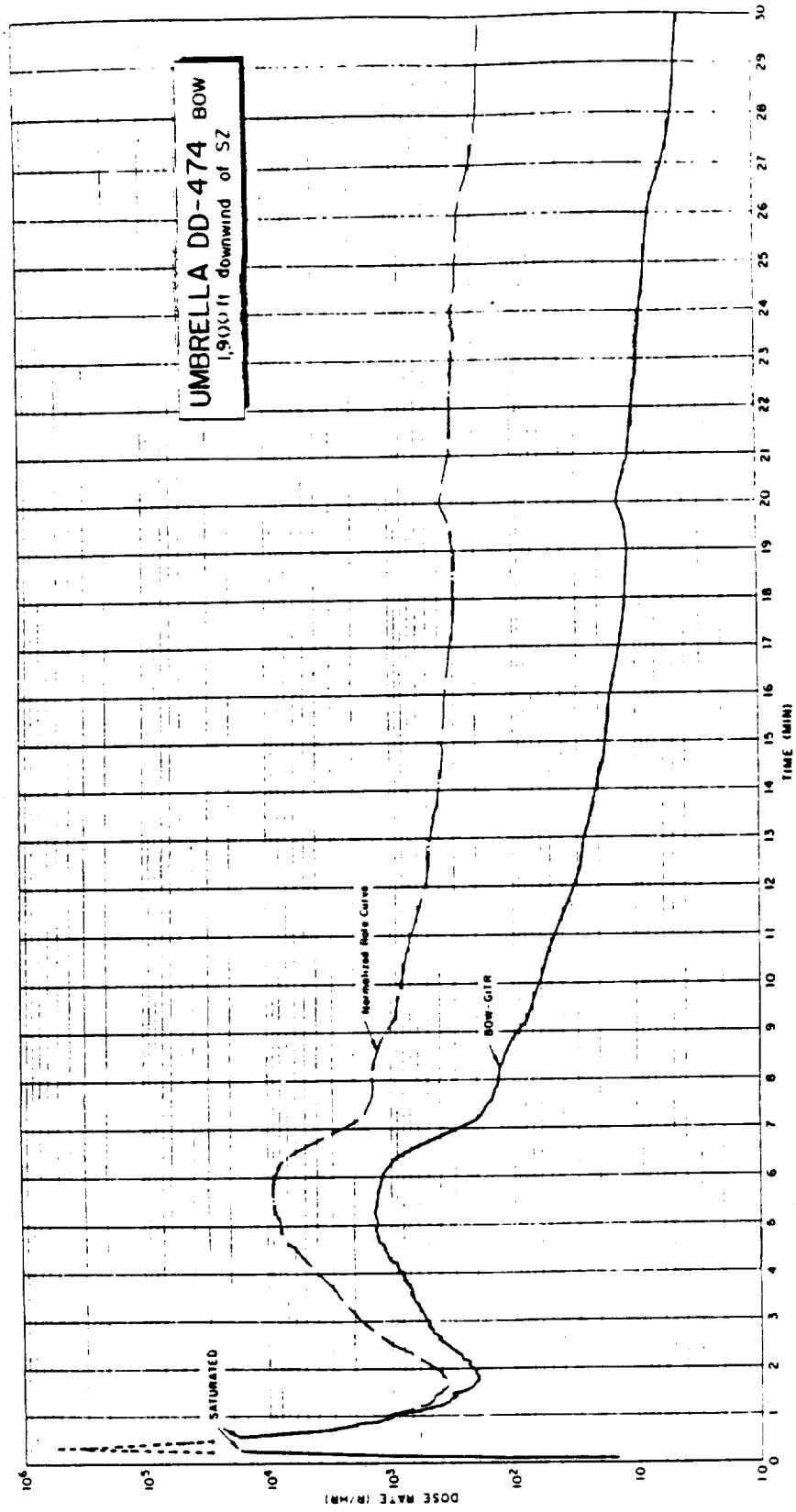


Figure 3.190 GATR record, 0 to 30 minutes, for DD-474 at 1,900 feet, 245.7° T from surface zero, Shot Umbrella. (GATR installed on centerline, Frame 21, bow, main deck.)

165

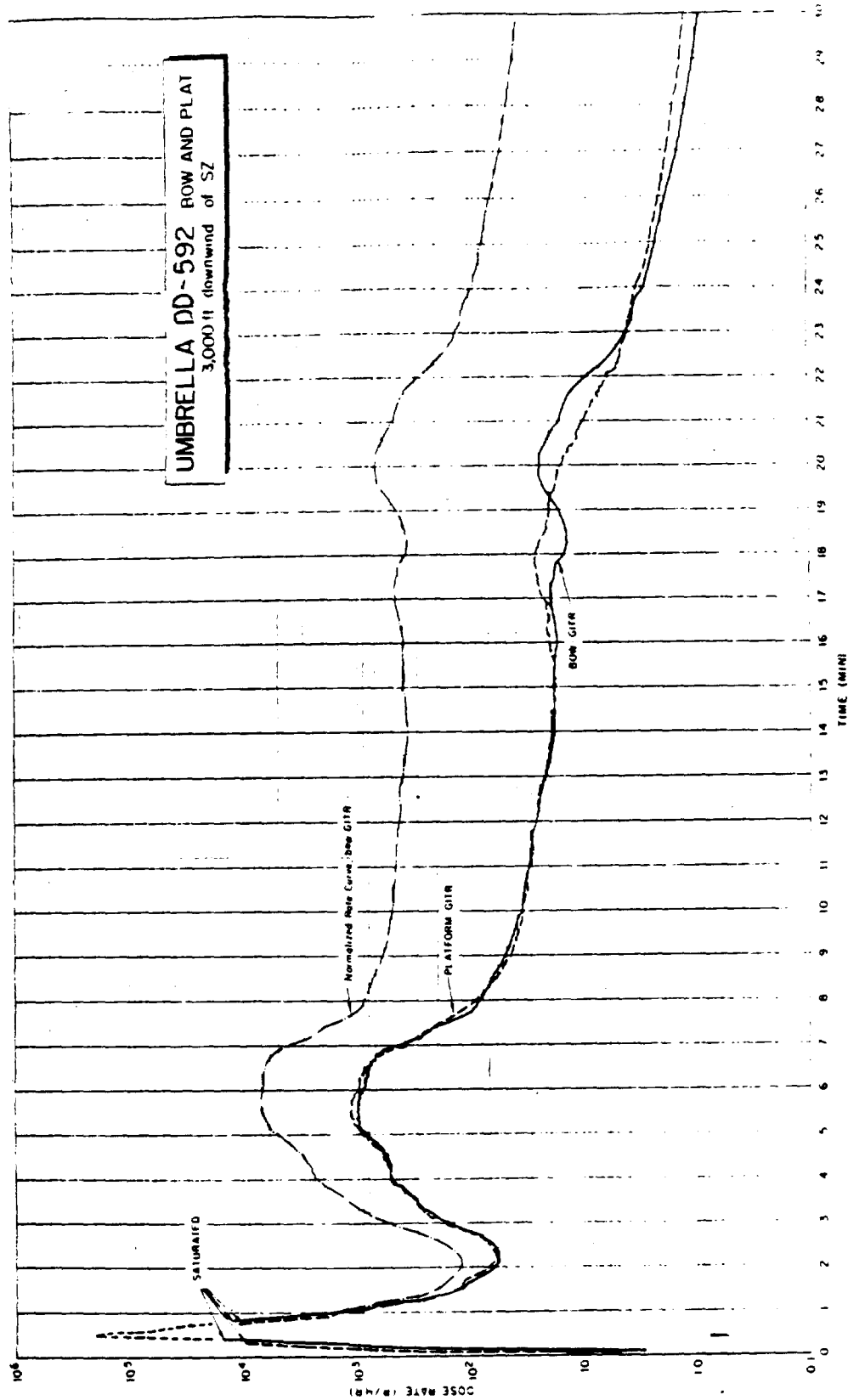


Figure 3.191 GTR record, 0 to 30 minutes, for DD-592 at 3,000 feet, 248.5° T from surface zero, Shot Umbrella. (GTR installed on centerline, Frame 21, bow, main deck, and top of 5-inch gun director, platform.)

166

**UMBRELLA DD-592 stbd**

Position: 3,000 feet,  
298.5°T from Surface Zero

Complete Records (Unless Otherwise Indicated): Std - GTR, FP

Special Conditions: saturated, possible self interference

**GENERAL INFORMATION**

Type of Transit: Through the Center, TIC Type of Record: U, (DD-592, stbd)  
 Max Dose Rate: saturated r/hr at      min. Total Dose: 688 r (Converted FP)  
 Film Pack Dose: Tripod 550 r, Float      r. Total Surge: 930 (Transit from 0 to 10 min)

**SURGE BOUNDARIES**

Photographic Boundary			Radiological Boundary		Source Center	Tail Length
TOA	Center	TOC	TOA	TOC	relative to P <sub>0</sub>	
(min)	(ft)/(min)	(min)	(min)	(min)	(ft)	(ft)
<u>&lt; 2.68</u>	<u>900/2.0</u>	<u>5.15</u>	<u>sat.</u>	<u>7.52</u>	<u>(-500)</u>	<u>4800</u>

**APPROACH VELOCITIES**

Photographic (Vis.)					Radiological (r-of-r)			
minus	minus	minus	minus		1600ft	1200ft	400ft	
100 ft	200 ft	300 ft	500 ft		(k)	(k)	(k)	
(k)	(k)	(k)	(k)					
				P <sub>0</sub>	90°	<u>    </u>	<u>    </u>	<u>    </u>
				B <sub>0</sub>	60°	<u>    </u>	<u>    </u>	<u>    </u>
	<u>(40-50)</u>							

**WATER-BORNE SOURCES**

(cf. Boundary Plot)

	Foam (min)	Water (min)
Obs. TOA	<u>msk</u>	<u>msk</u>
Obs. TOC	<u>2.6</u>	<u>2.80</u>

**BOMB GENERATED WAVES**

Wave No.	1st	TOA	min
2nd	"	<u>    </u>	"
3rd	"	<u>    </u>	"
4th	"	<u>    </u>	"

**MISCELLANEOUS DATA**

TOTAL SURGE DEPOSITION (IC)  
 c/min at 22 days:       
 Approx. Fissions:     

ESTIMATED DEPOSIT DOSE RATE  
 (converted to Std-GTR response at 1min)

GTR Background:      r/hr  
 Survey Meter:      r/hr  
 IC Total:      r/hr

Initial Dose: est. 0.030 r  
 Shine Dose: est 54 r  
 (for 38% of Peak)

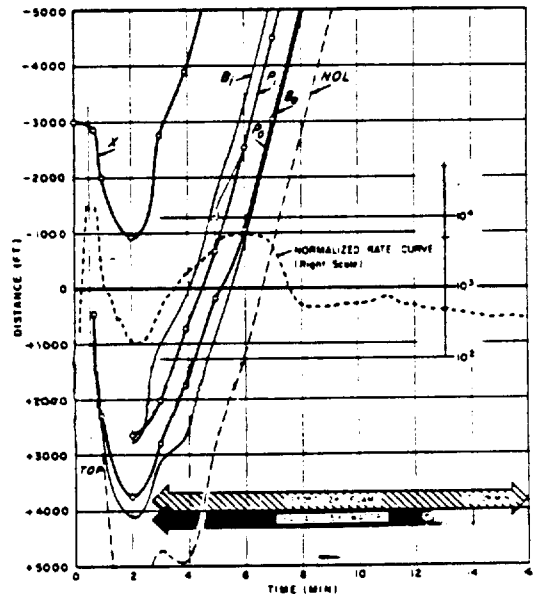


Figure 3.192 Continued.

164

# UMBRELLA DD-593 part

Position: 7,900 feet,  
242.2 °T from Surface Zero

Complete Records (Unless Otherwise Indicated): Std-GITR, FP

Special Conditions: possible self-interference

## GENERAL INFORMATION

Type of Transit: Central, C Type of Record: V, (DD-593, ...)  
 Max Dose Rate: 5500 r/hr at 1.72 min. Total Dose: 64.8 r  
 Film Pack Dose: Tnpod 54 r, Float — r. Total Surge: 290 (Transit from 1 to 10 min)

## SURGE BOUNDARIES

Photographic Boundary			Radiological Boundary		Source Center relative to P <sub>0</sub> (ft)	Tail Length (ft)
TOA (min)	Center (ft)(min)	TOC (min)	TOA (min)	TOC (min)		
<u>2.15</u>	<u>1940/4.3</u>	<u>7.90</u>	<u>1.58</u>	<u>9.36</u>	<u>-1290</u>	<u>3700</u>

## APPROACH VELOCITIES

	Photographic (Vis.)				Radiological (r-of-r)		
	minus 100 ft (k)	minus 200 ft (k)	minus 300 ft (k)	minus 500 ft (k)	1600 ft (k)	1200 ft (k)	400 ft (k)
P <sub>0</sub>	<u>12</u>	<u>10</u>	<u>9</u>	<u>9</u>	90° <u>35</u>	<u>32</u>	<u>27</u>
B <sub>0</sub>	<u>14</u>	<u>13</u>	<u>13</u>	<u>11</u>	60° <u>34</u>	<u>33</u>	<u>26</u>

## WATER-BORNE SOURCES

(cf. Boundary Plot)

	Foam (min)	Water (min)
Obs. TOA	<u>12.5</u>	<u>50</u>
Obs. TOC	<u>15</u>	<u>150</u>

## BOMB GENERATED WAVES

Wave No.	1st	TOA	min
2nd	"	"	"
3rd	"	"	"
4th	"	"	"

## MISCELLANEOUS DATA

TOTAL SURGE DEPOSITION (IC)  
 c/min at 22 days: —  
 Approx. Fissions: —

ESTIMATED DEPOSIT DOSE RATE  
 (converted to Std-GITR response at 1min)

GITR Background: — r/hr  
 Survey Meter: — r/hr  
 IC Total: — r/hr

Initial Dose: — r  
 Shine Dose: — r  
 (for 38% of Peak)

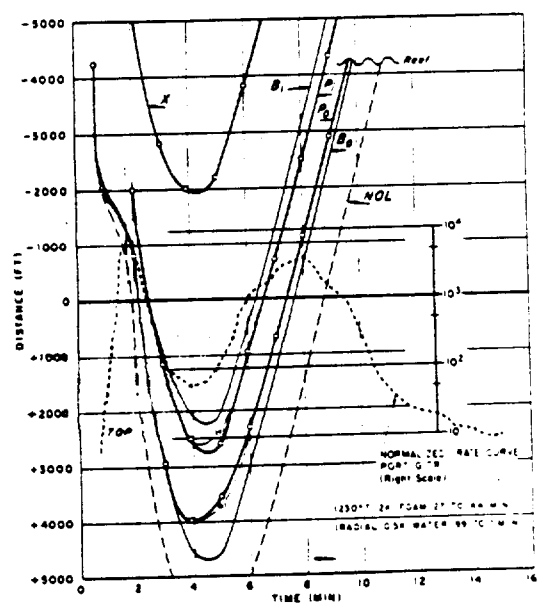


Figure 3.193 Continued.

168

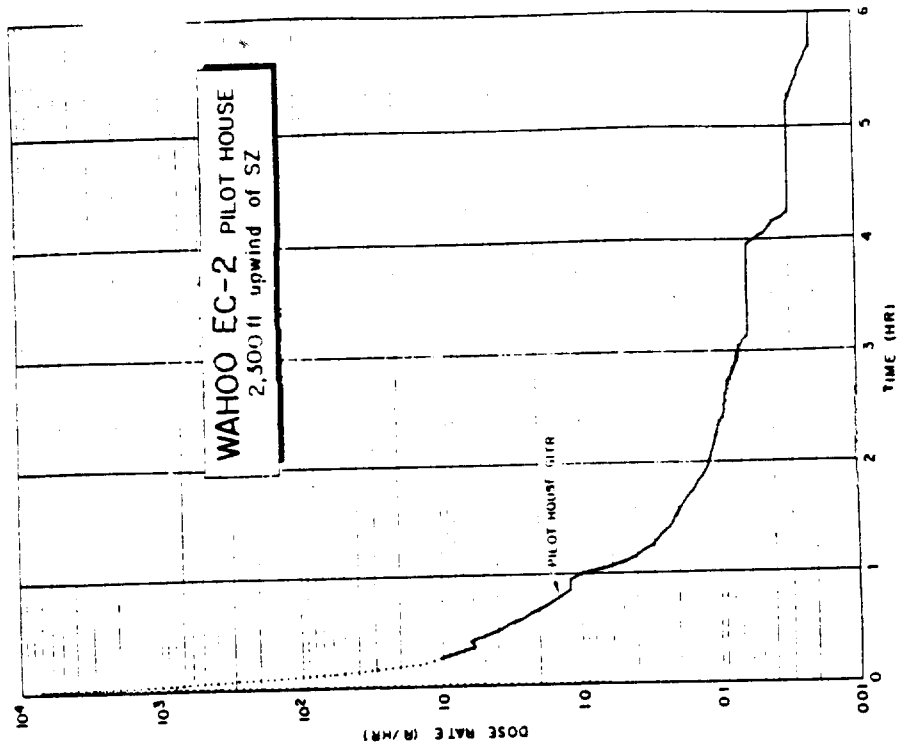


Figure 3.195 GTR record, 0 to 6 hours, for EC-2 at 2,300 feet, 28.5° T from surface zero, Shot Wahoo. (GTR installed inside pilot house.)

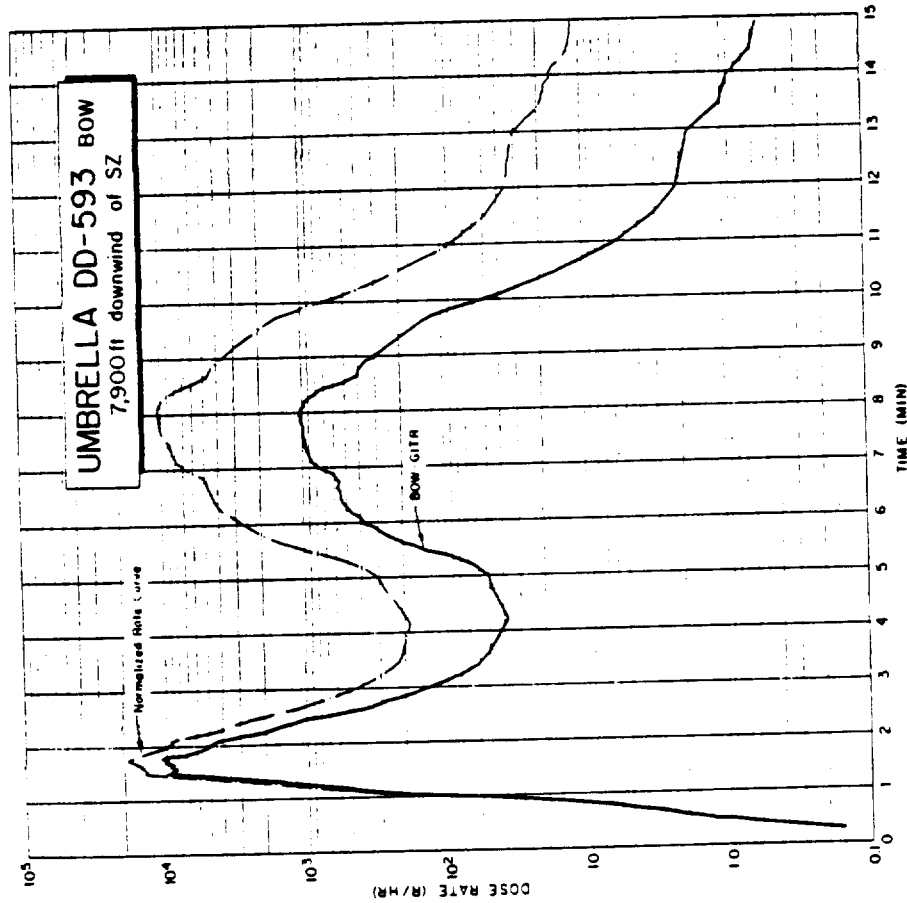


Figure 3.194 GTR record, 0 to 15 minutes, for DD-593 at 7,900 feet, 249.2° T from surface zero, Shot Umbrella. (GTR installed on centerline, Frame 21, bow, main deck.)

120

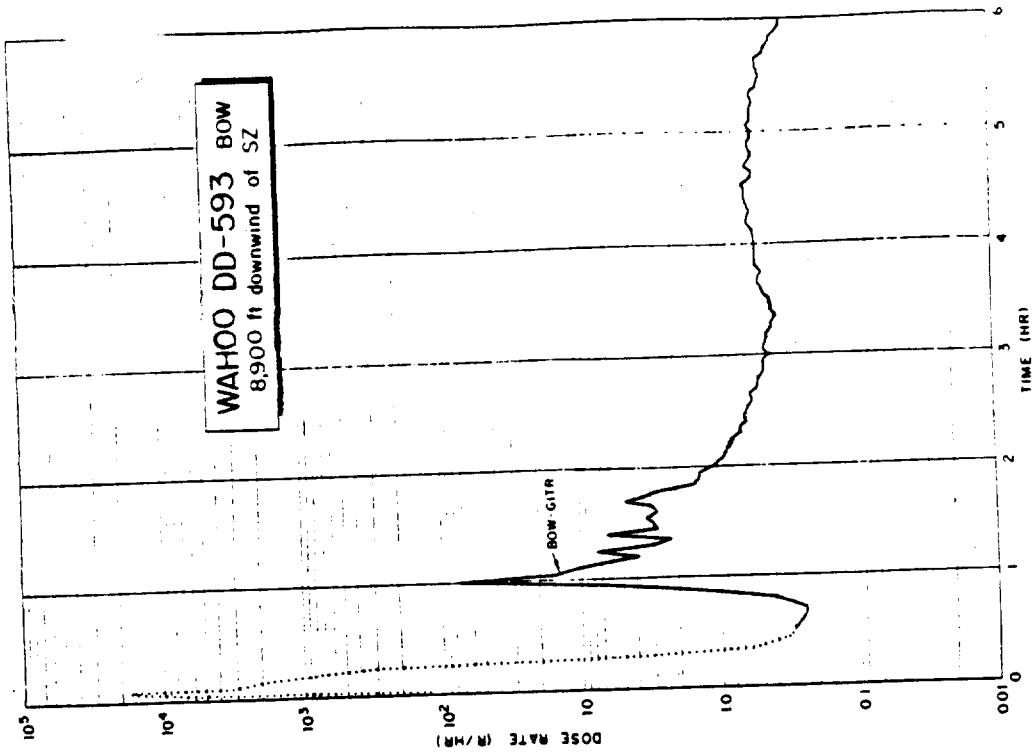


Figure 3.197 GTR record, 0 to 6 hours, for DD-593 at 8,900 feet, 250° T from surface zero, Shot Wahoo. (GTR installed on centerline, Frame 21, bow, main deck.)

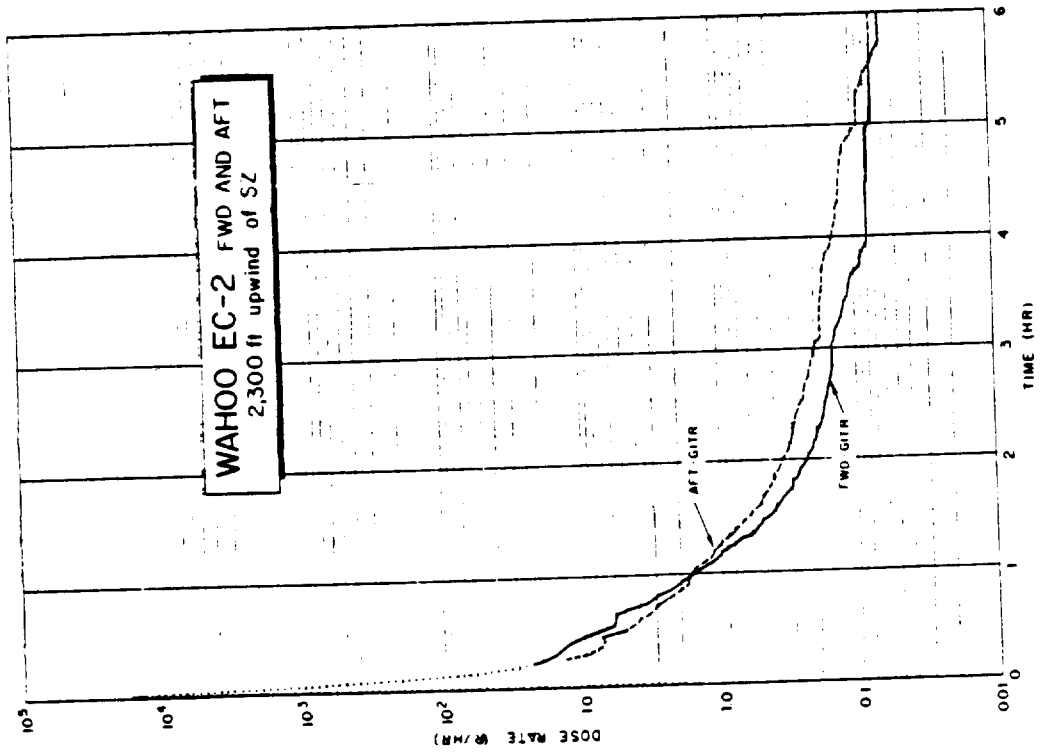


Figure 3.196 GTR record, 0 to 6 hours, for EC-2 at 2,300 feet, 28.5° T from surface zero, Shot Wahoo. (GTR installed on centerline, Frame 48, forward, and Frame 137.5, aft, main deck.)

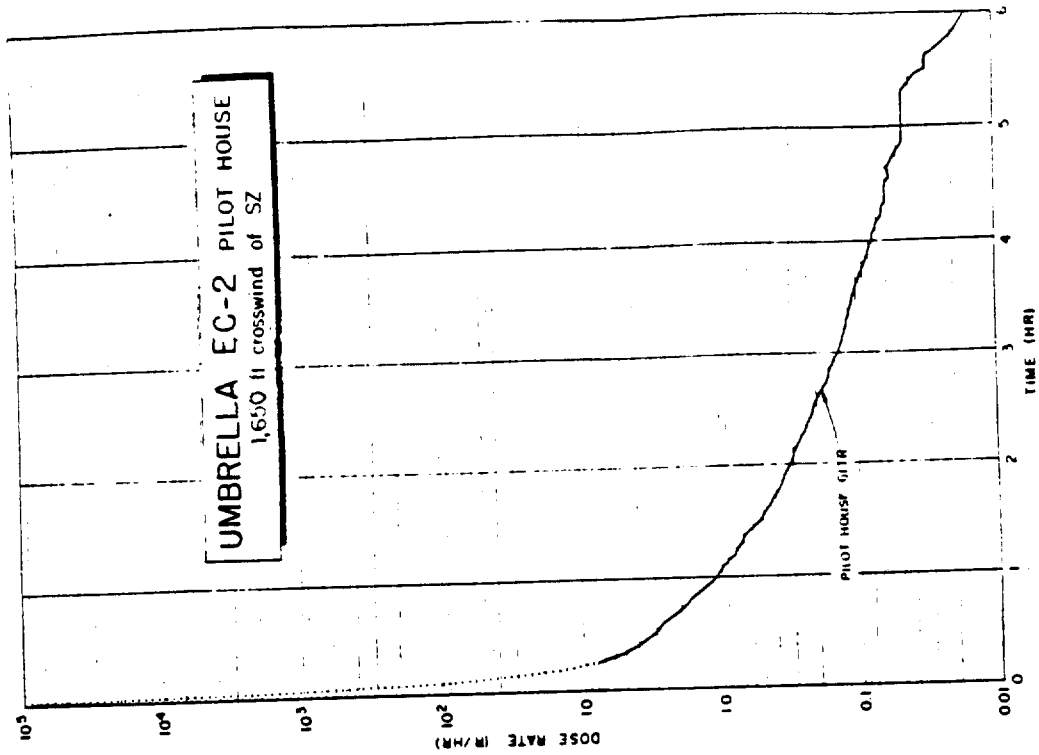


Figure 3.199 GTR record, 0 to 6 hours, for EC-2 at 1,650 feet, 158° T from surface zero, Shot Umbrella. (GTR installed inside pilot house.)

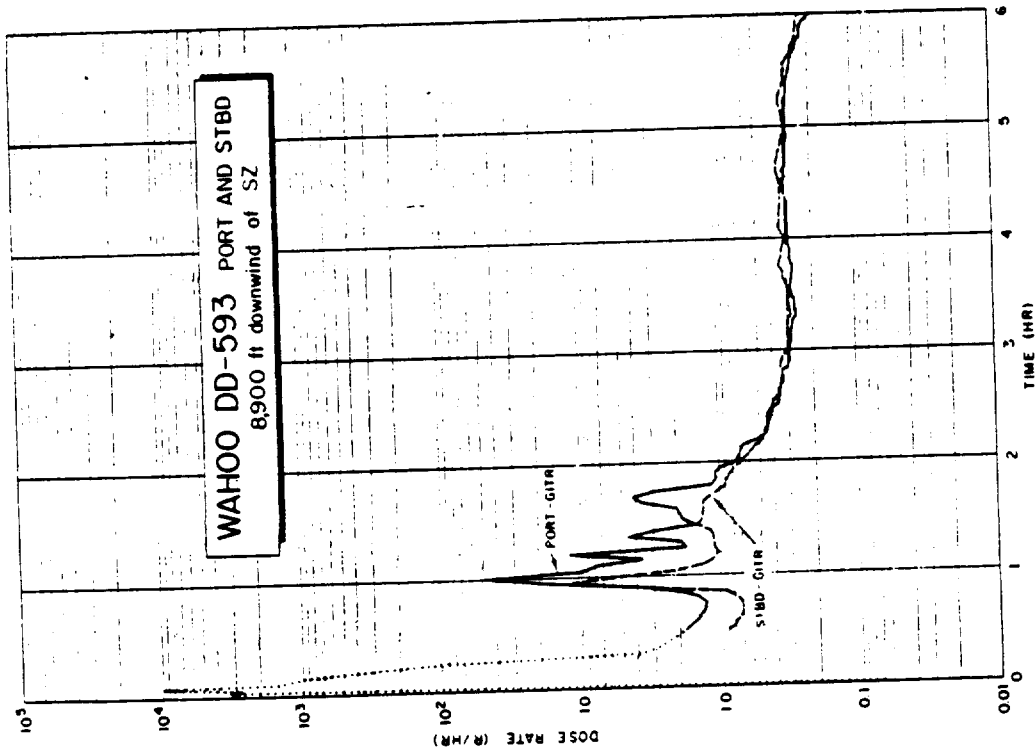


Figure 3.198 GTR record, 0 to 6 hours, for DD-593 at 8,900 feet, 250° T from surface zero, Shot Wahoo. (GTR installed on main deck, Frame 136, port, and Frame 136, starboard.)

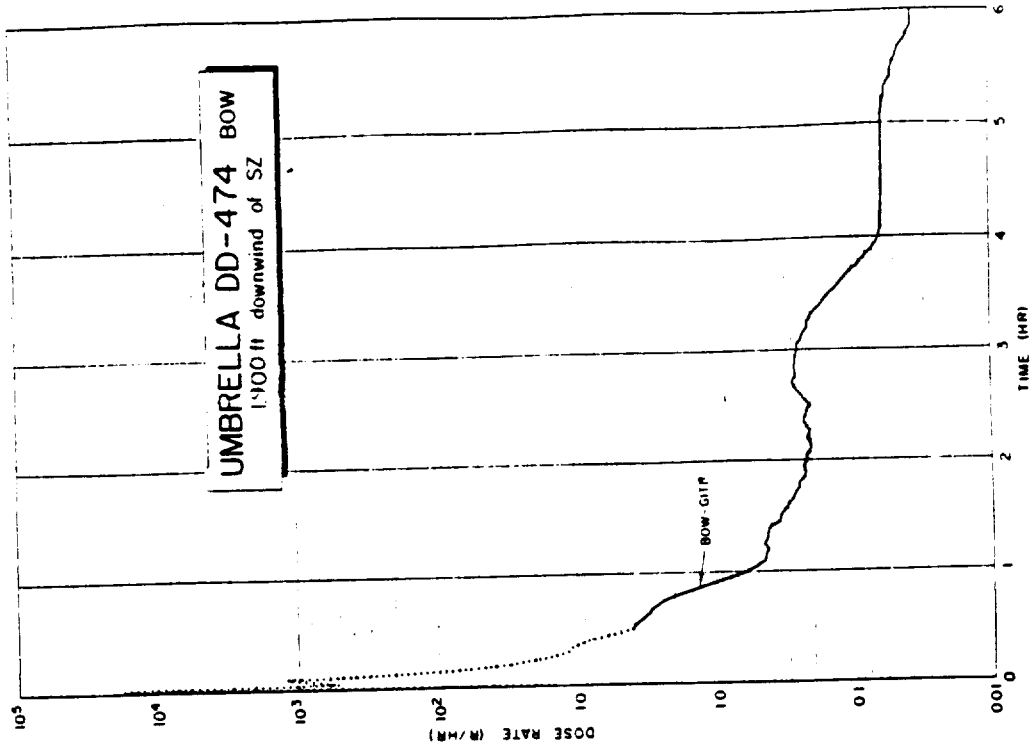


Figure 3.201 GTR record, 0 to 6 hours, for DD-474 at 1,900 feet, 245.7° T from surface zero, Shot Umbrella. (GTR installed on centerline, Frame 21, bow, main deck.)

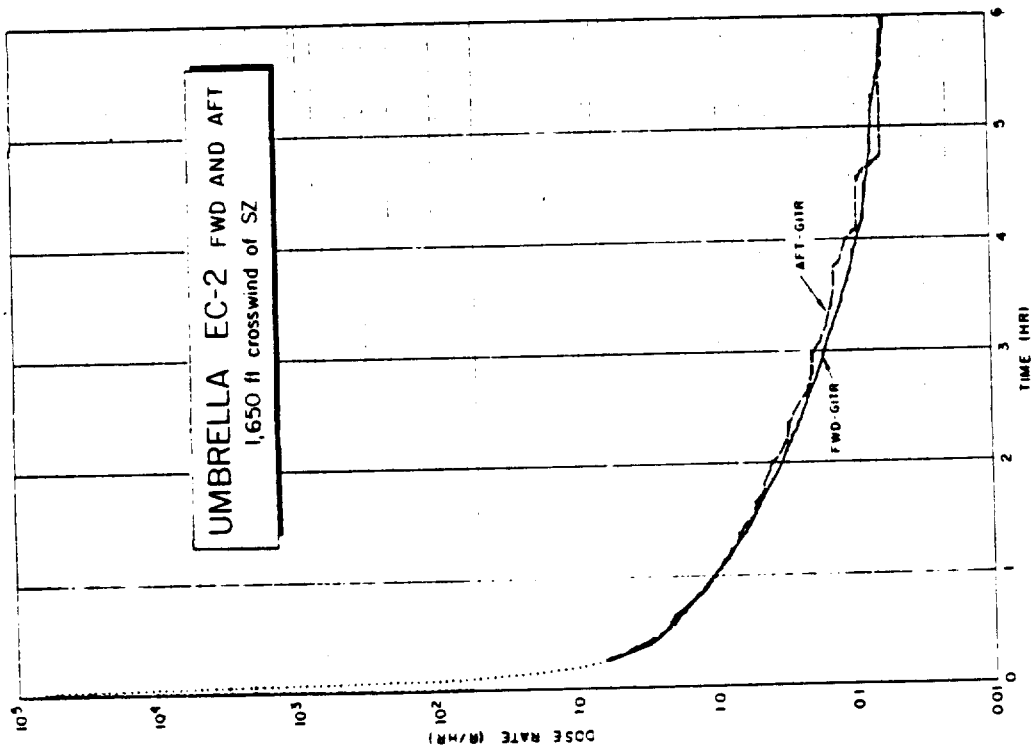


Figure 3.200 GTR record, 0 to 6 hours, for EC-2 at 1,650 feet, 158° T from surface zero, Shot Umbrella. (GTR installed on centerline, Frame 48, forward, and Frame 137.5, aft, main deck.)

100

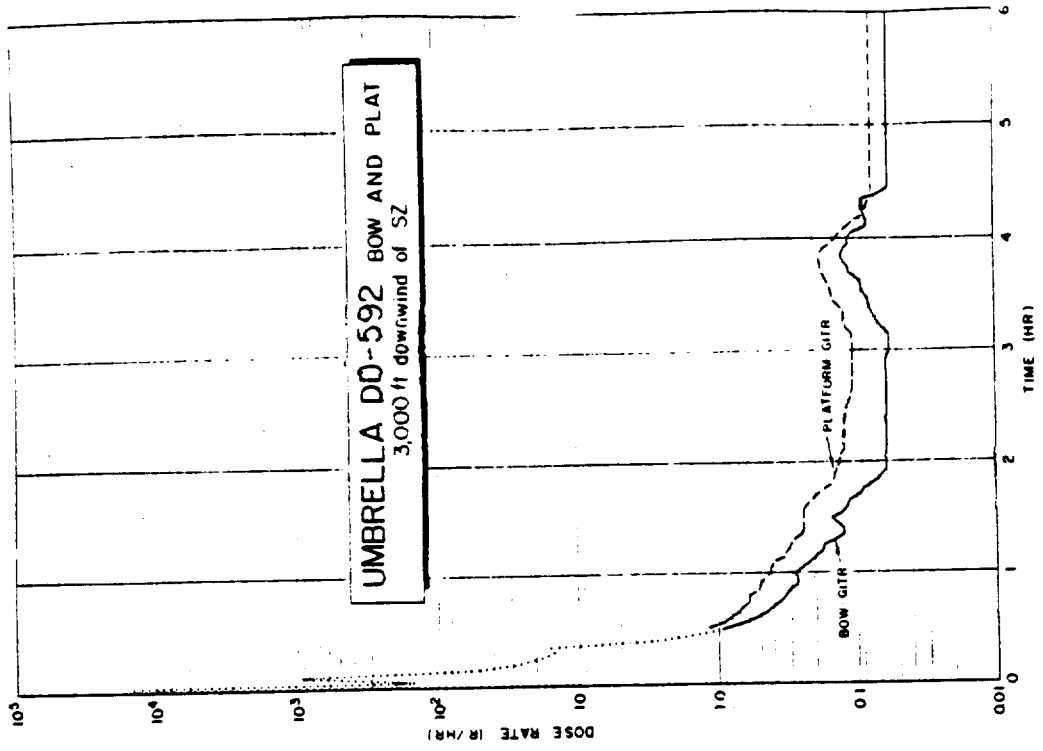


Figure 3.203 GTR record, 0 to 6 hours, for DD-592 at 3,000 feet, 248.5° T from surface zero, Shot Umbrella. (GTR installed on centerline, Frame 21, bow, main deck and top of 5-inch gun director, platform.)

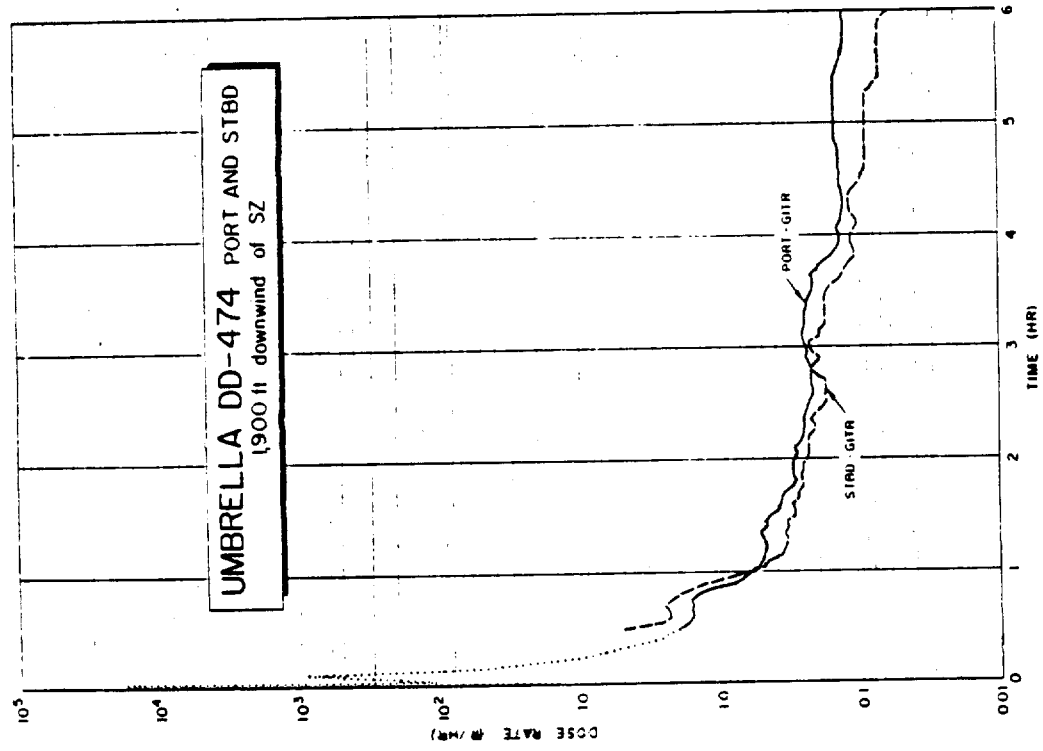


Figure 3.202 GTR record, 0 to 6 hours, for DD-474 at 1,900 feet, 245.7° T from surface zero, Shot Umbrella. (GTR installed on main deck, Frame 136, port, and Frame 136, starboard.)

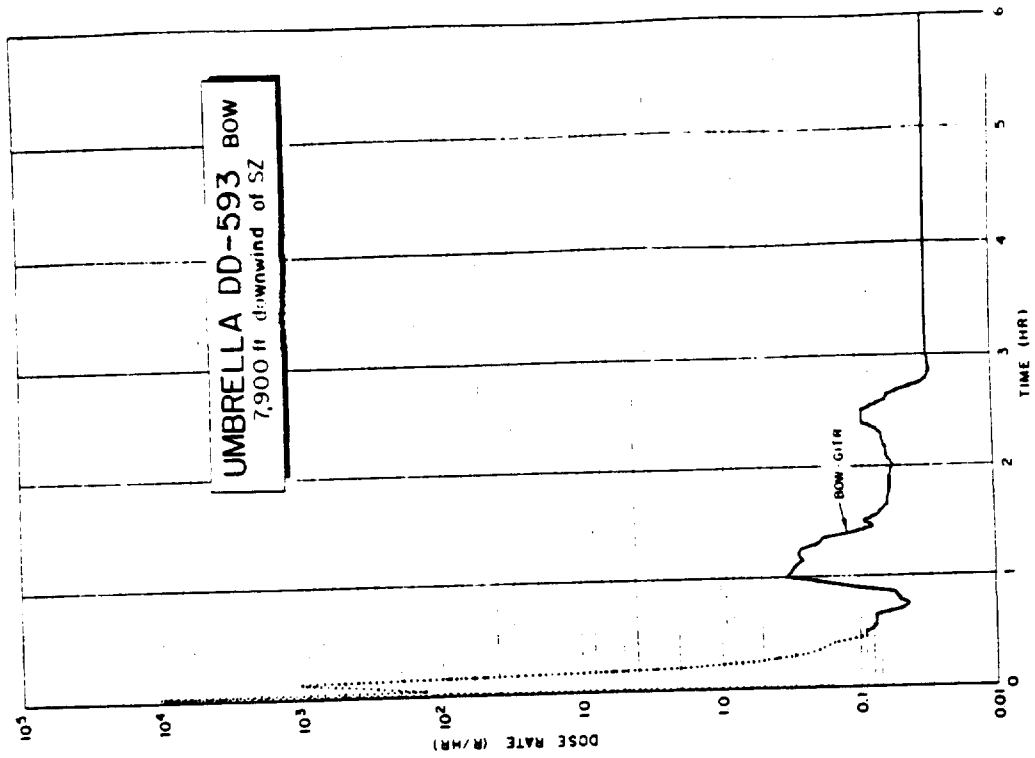


Figure 3.205 GTR record, 0 to 6 hours, for DD-593 at 7,900 feet, 249.2° T from surface zero, Shot Umbrella. (GTR installed on centerline, Frame 21, bow, main deck.)

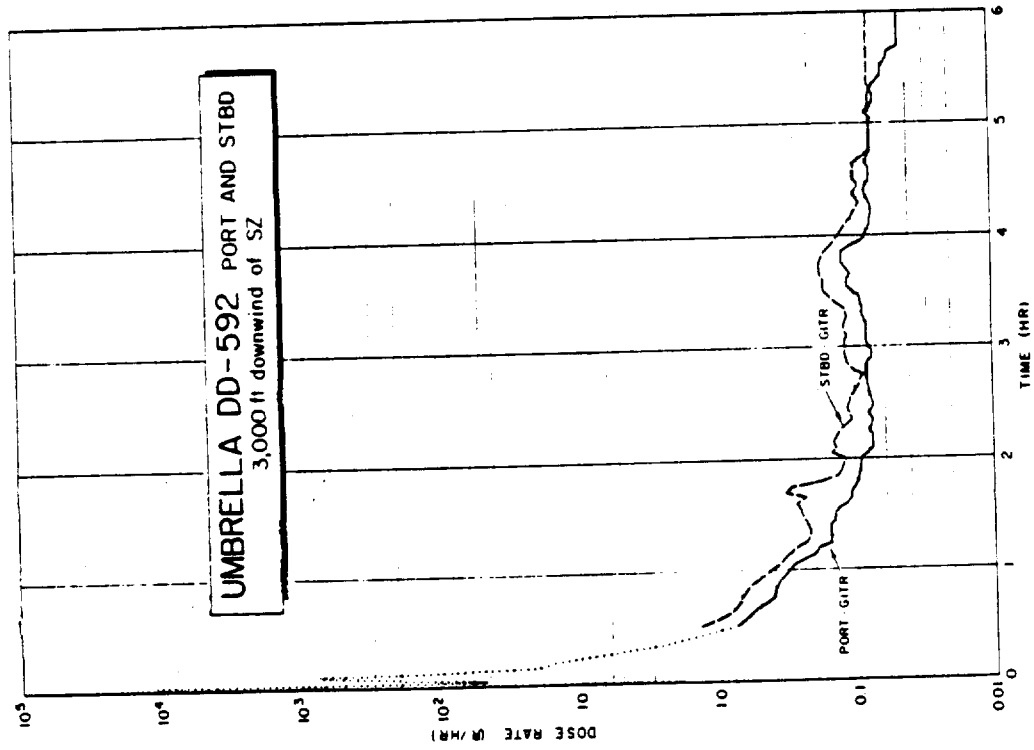


Figure 3.204 GTR record, 0 to 6 hours, for DD-592 at 3,000 feet, 248.5° T from surface zero, Shot Umbrella. (GTR installed on main deck, Frame 136, port, and Frame 136, starboard.)

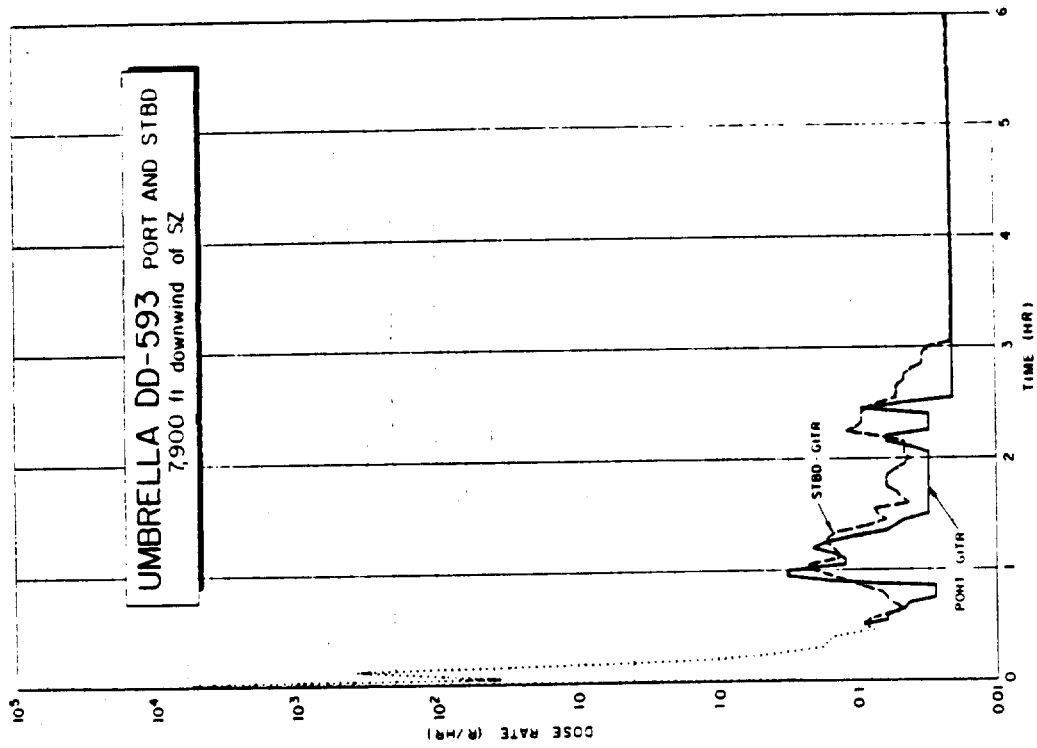


Figure 3.206 GTR record, 0 to 6 hours, for DD-593 at 7,900 feet, 249.2° T from surface zero, Shot Umbrella. (GTR installed on main deck, Frame 136, port, and Frame 136, starboard.)

TABLE 3.30 SNIPBOARD FILM PACK DOSES AND ASSOCIATED SURVEY READINGS

Film Pack Station Number	DD-474		DD-592		DD-593		Film Pack Station Number	EC-2	
	Survey*	Film	Survey*	Film	Survey*	Film		Survey*	Film
	mr/hr	r	mr/hr	r	mr/hr	r		mr/hr	r
<b>Wahoo:</b>									
3	30	1,020	47	605	26	235	1	20	30
6**	39	1,280	36	700	25	265	6	9	25
8	54	920	96	610	31	230	15	7	17
9	52	750	80	380	51	162	17**	7	24
11	42	850	60	505	33	198	24	18	15
12	22	910	25	510	20	205	29	5	31
17**	22	1,230	26	740	22	330	32	6	27
19	26	720	28	415	17	168	35	6	29
20	20	810	33	445	18	200	38	6	26
21	56	810	63	410	32	198	41	6	17
23	62	595	100	325	39	165	44	5	16
24	74	850	78	575	26	260	45	6	10
27**	32	1,150	39	615	24	280	47	8	18
30	22	1,000	80	555	24	225	49	10	18
37	26	610	34	395	26	168	55	7	23
40	29	1,500	42	445	18	325	56	7	16
42	47	800	34	800	36	195	63**	5	31
52 (54 on DD-592)	53	1,070	56	430	38	198	72	12	26
56	22	960	41	520	20	203	77	5	13
57	23	910	31	500	16	199	79	12	23
59	10	1,100	28	600	11	245	Pilot House**	6	9
Plat-Pt	16	1,320	15	760	9	368			
Plat-Stbd	16	1,700	15	850	9	335			
<b>Umbrella:</b>									
3	12	lost	21	430	6	51	1	23	58
6**	17	700	20	550	8	59	6	17	62
8	15	630	20	395	6	49	15	18	76
9	13	470	34	300	7	37	17**	19	96
11	20	520	22	355	7	39	24	30	71
12	14	590	16	340	4	45	29	29	60
17**	7	840	14	470	5	64	32	21	60
18	9	460	19	200	6	35	35	16	1,000
20	18	470	16	255	5	35	38	16	74
21	30	460	34	275	5	36	41	20	65
23	23	345	28	180	8	31	44	25	57
24	5	470	23	340	8	38	45	25	49
27**	22	660	22	490	7	54	47	34	63
30	14	530	19	330	7	43	49	22	58
37	16	350	17	215	6	36	55	14	55
40	20	910	18	340	6	65	56	17	52
42	27	lost	26	630	8	45	63*	16	1,150
52 (54 on DD-592)	22	480	26	290	8	43	72	16	71
56	16	610	20	320	6	46	77	17	35
57	17	520	18	280	4	37	79	18	40
59	9	680	16	395	2	52	Pilot House**	16	37
Plat-stbd	400	860	200	505	150	70			
Plat-port	400	lost	200	550	150	71			

\* Survey times for Wahoo were: 0840-1024M, 18 May for EC-2 (pilot house, 1015M, 21 May); 0949-1000 18 May for DD-474; 0826-0848M, 18 May for DD-592; and 0902-0928M, 18 May for DD-593.

Survey times for Umbrella were: 0943-1039M, 10 June for EC-2; 1053-1128M, 10 June for DD-474 (port and starboard platform, 1305M, 9 June); 1015-1047M, 10 June for DD-592 (port and starboard platform, 1300M, 9 June); and 0914-0954M, 10 June for DD-593 (port and starboard platform, 1300M, 9 June).

\*\* Aboard destroyers, GTR's were associated with film pack stations as follows: Bow-GTR = film pack station 17, Port GTR = film pack station 27, Starboard GTR = film pack station 6, Platform GTR = port and starboard platform film pack station on the DD-592 only.

Aboard the EC-2, GTR's were associated with film pack stations as follows: Pilot house GTR = pilot house film pack, Forward GTR = film pack station 63, Aft GTR = film pack station 17.

Film pack stations are presented graphically in Figures 1.12, 1.13 and 1.14.

TABLE 3.31 AVERAGE SHIPBOARD SURVEY READINGS NOT ASSOCIATED WITH FILM PACKS  
(Average of four directional readings at each station, see text)

Sta. No.	DD-474		DD-592		DD-593		Sta. No.	EC-2	
	Wahoe	Umbralla	Wahoe	Umbralla	Wahoe	Umbralla		Wahoe	Umbralla
	HT Date: 5/10/58 HT Time: 0740-1009	HT Date: 6/10/58 HT Time: 1053-1128	HT Date: 6/10/58 HT Time: 0800-0900	HT Date: 6/10/58 HT Time: 1015-1047	HT Date: 6/10/58 HT Time: 0900-0928	HT Date: 6/10/58 HT Time: 0914-0954		HT Date: 6/10/58 HT Time: 0740-1004	HT Date: 6/10/58 HT Time: 1003-1048
	HT	HT	HT	HT	HT	HT		HT	HT
1	26	11	26	28	23	6	2	7	19
2	26	11	26	28	26	6	3	10	18
3	30	16	33	26	22	6	4	13	16
4	36	15	33	26	23	6	5	15	19
5	37	16	40	20	25	6	6	16	20
10	30	16	70	30	26	6	8	17	17
13	22	17	42	14	18	4	9	5	16
14	30	10	35	20	24	4	10	5	15
15	22	10	22	20	24	4	11	5	15
16	20	8	21	13	21	4	12	5	16
19	17	12	23	14	15	5	13	6	17
22	51	26	100	30	27	6	14	7	17
25	35	22	32	22	21	7	16	6	17
26	40	20	36	22	29	8	18	8	17
28	31	24	50	22	29	8	19	9	17
29	23	12	43	23	24	8	20	9	18
31	26	10	41	26	52	7	21	8	18
32	22	8	52	22	21	8	22	8	19
33	26	10	37	20	23	8	23	9	20
34	37	15	21	18	24	8	25	6	20
35	16	16	20	17	18	4	26	5	20
36	17	16	20	18	16	4	27	5	20
38	30	23	36	20	20	4	28	5	30
39	31	22	43	18	18	5	30	7	31
41	31	23	28	24	21	5	31	10	40
43	20	16	40	28	17	6	33	8	25
44	25	20	39	24	20	4	34	5	16
45	25	18	30	14	18	6	36	6	18
46	21	14	24	10	19	6	37	6	18
47	22	19	35	24	23	4	39	0	15
48	20	21	31	26	16	4	40	7	22
49	23	12	30	29	20	6	42	8	28
50	26	15	34	28	23	6	43	5	24
51	29	18	33	25	20	6	46	8	43
52	-	-	40	28	-	-	42	11	25
53	29	20	36	26	16	6	50	8	18
54	33	20	-	-	18	5	51	8	20
55	33	25	53	23	25	6	52	7	16
58	37	26	50	20	22	6	53	7	16
							54	7	14
							57	8	18
							58	7	16
							59	6	15
							60	6	14
							61	4	14
							62	5	14
							64	10	16
							65	13	16
							66	9	16
							67	9	16
							68	9	15
							69	12	16
							70	13	18
							71	12	18
							73	8	19
							74	7	20
							75	8	23
							76	5	18
							78	6	16
							80	11	18

127

teristics of the various superstructure components; however, where a relatively thin section of the superstructure subtended more than 10 percent of the total unobstructed solid angle, an approximate shielding factor was estimated, using the ship's plans and a gamma energy of 1 Mev. Plots of the approximate effective solid angle subtended by the radiating cloud are presented in Figures 3.213 and 3.214. A comparison of these plots with similar film pack plots demonstrates the effect of the ship's superstructure conclusively. A more refined treatment of this problem would probably yield an even closer correspondence between film pack doses and the total solid angle subtended.

3.4.3 Conversion Factors. Although the effect of superstructure shielding has been demonstrated in the previous section, the calculation of conversion factors from isodose contours to shipboard exposures is subject to many errors. The variable nature of the radiological event at close ranges and the nonuniform distribution of radioactive material within the base surge are the principal sources of difficulty. These uncertainties can cause error even in the simple extension of a shipboard GTR measurement to another shipboard position where a film pack reading has been made. Because of these difficulties, the estimated conversion factors are restricted to total cumulative dose only. All factors should be used with caution.

With the exception of the EC-2 during Wahoo and the DD-592 during Umbrella, the average total GTR dose and the average of the film pack doses from the exposed deck positions agree with the total dose estimated from the isodose contours to within  $\pm 15$  percent (see Tables 3.27 and 3.30, and Figures 3.103 and 3.109 for basic data). The film pack inside the pilot house on the EC-2 is omitted from these averages for obvious reasons, and the cumulative dose from the bow GTR on the DD-593 is also omitted for reasons discussed later. The average GTR dose is less than or equal to the total dose estimated from the isodose contours for Wahoo, whereas for Umbrella the average GTR dose is greater than the total dose estimated from the isodose contours. If only exposed shipboard positions are considered, the film pack data also shows some fairly consistent differences for the two detonations (Table 3.32). In general, the shipboard doses for Wahoo are approximately 10 percent lower than what would be expected from the isodose contours, whereas for Umbrella they are 10 percent higher. The data is, however, insufficient to make any further generalizations about the differences between Wahoo and Umbrella. The variations shown by the EC-2 during Wahoo and the DD-592 during Umbrella are most probably due to errors in the isodose contours in the region of these ships, although another possible explanation is discussed later.

Conversion factors that compensate for superstructure shielding can also be computed for each ship. Because of the paucity of GTR data, these conversion factors have been calculated from film pack data only. The average of all film pack doses aboard a given ship is low because of shielding effects, whereas that for the platform film packs and perhaps even for exposed positions on the superstructure decks is high because of the increased solid angle subtended by elevated positions. The average of all exposed deck positions is, therefore, selected as most representative of the free-field dose for a given ship, and all other shipboard FP doses have been normalized to these averages, to obtain the desired conversion factors (Table 3.33).

The plots of film pack dose versus frame number (Figures 3.207 through 3.212) show a fairly consistent difference between film pack doses on the opposite sides of the closer ships. This difference is consistent with the attitude of the ship if allowance is made for movement after zero time (Figures 2.1 and 2.2). On the DD-593, the most distant ship, this difference is so small as to be somewhat arbitrary. On the closer destroyers for both shots and on the EC-2 for Wahoo, the starboard side was exposed either to surface zero or to the track of the base surge center (the hot line) and the starboard film packs; with the exception of a few exposed positions on the superstructure, the starboard film packs reflect this orientation by registering a significantly higher dose than the port film packs. For Umbrella, the port side of the EC-2 was facing surface zero; however, neither the port or starboard film packs show a consistent pattern, although the port film packs generally tend to be higher.

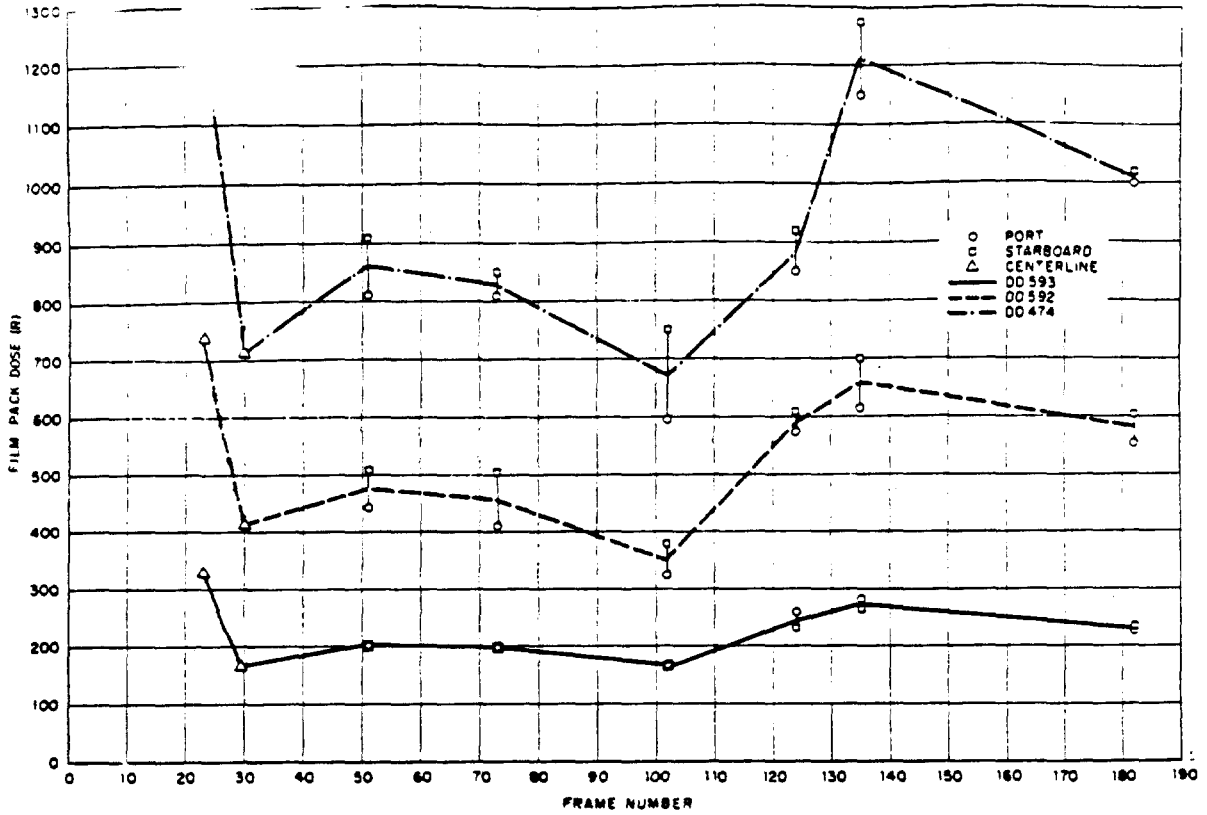


Figure 3.207 Plot of film pack dose readings on main deck of destroyers versus position along ship, Shot Wahoo. (Lowest frame numbers are forward; each frame number represents approximately 2 feet.)

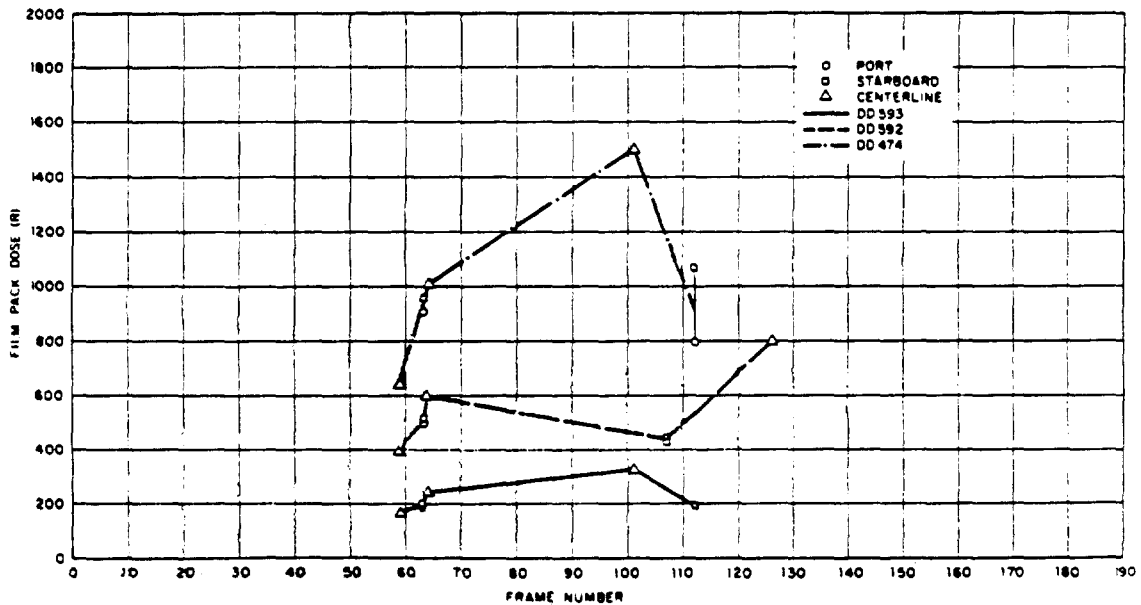


Figure 3.208 Plot of film pack dose readings on superstructures of destroyers versus position along ship, Shot Wahoo. (Lowest frame numbers are forward; each frame number represents approximately 2 feet.)

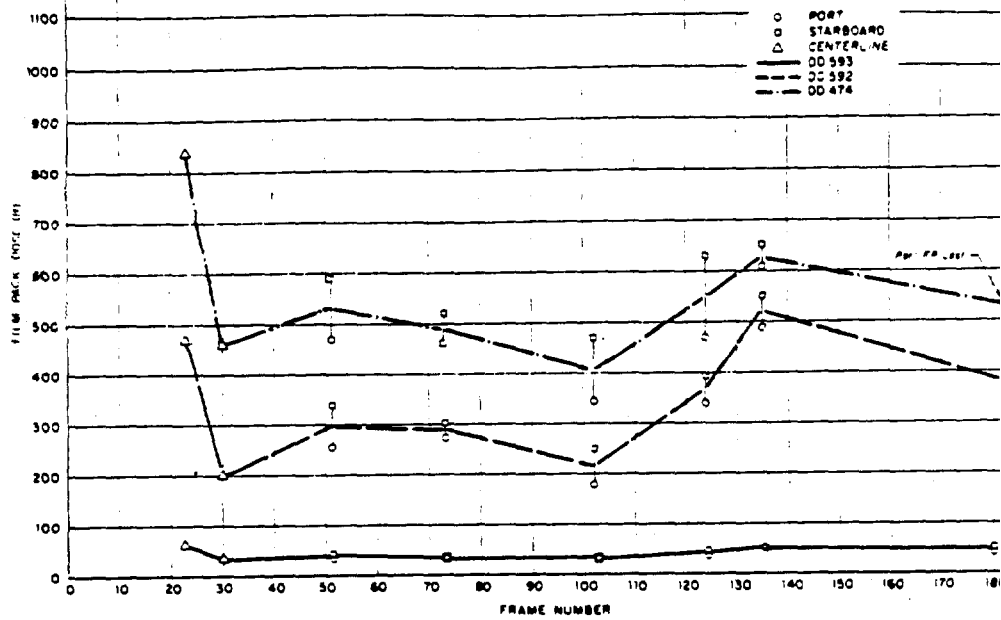


Figure 3.209 Plot of film pack dose readings on main deck of destroyers versus position along ship, Shot Umbrella. (Lowest frame numbers are forward; each frame number represents approximately 2 feet.)

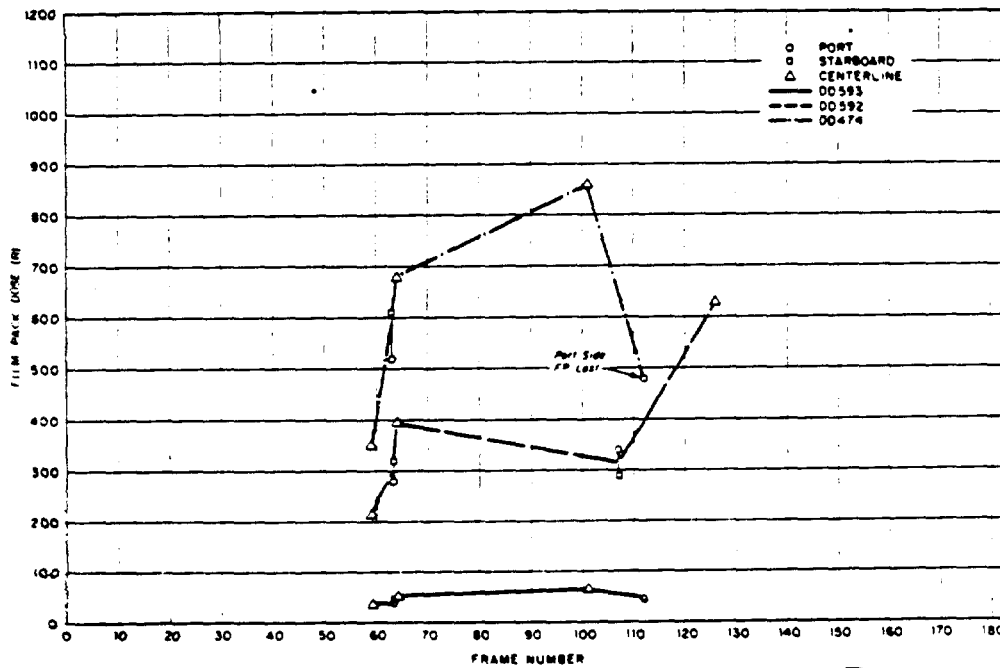


Figure 3.210 Plot of film pack dose readings on superstructure of destroyers versus position along ship, Shot Umbrella. (Lowest frame numbers are forward; each frame number represents approximately 2 feet.)

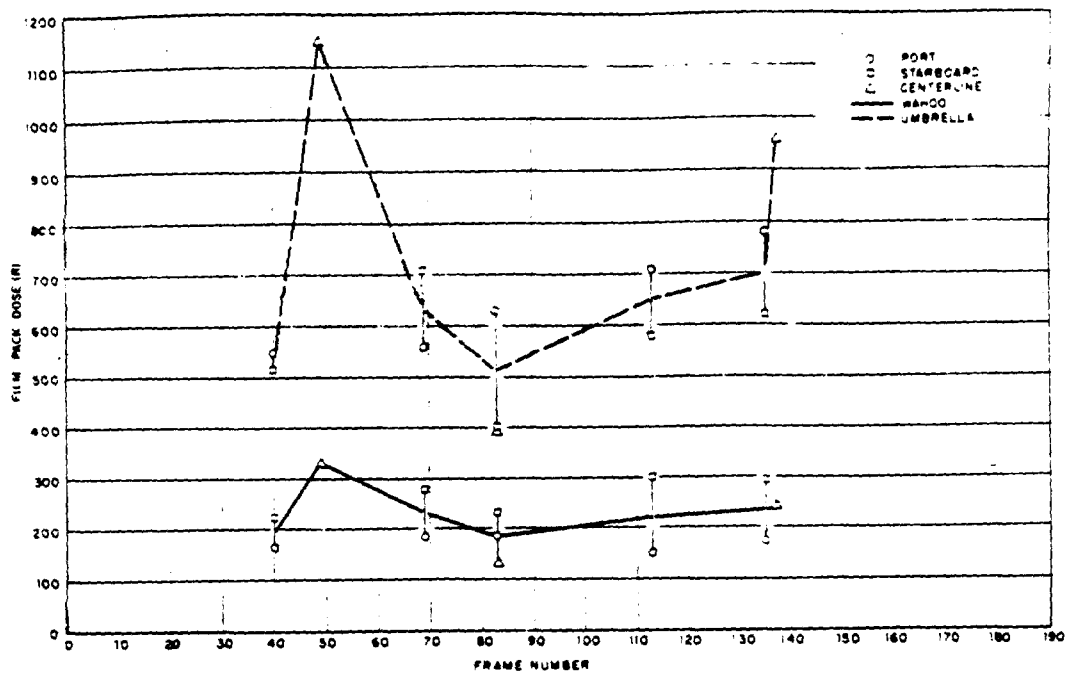


Figure 3.211 Plot of film pack dose readings on main deck of EC-2 versus position along ship, Shots Wahoo and Umbrella. (Lowest frame numbers are forward; each frame number represents approximately 2 feet.)

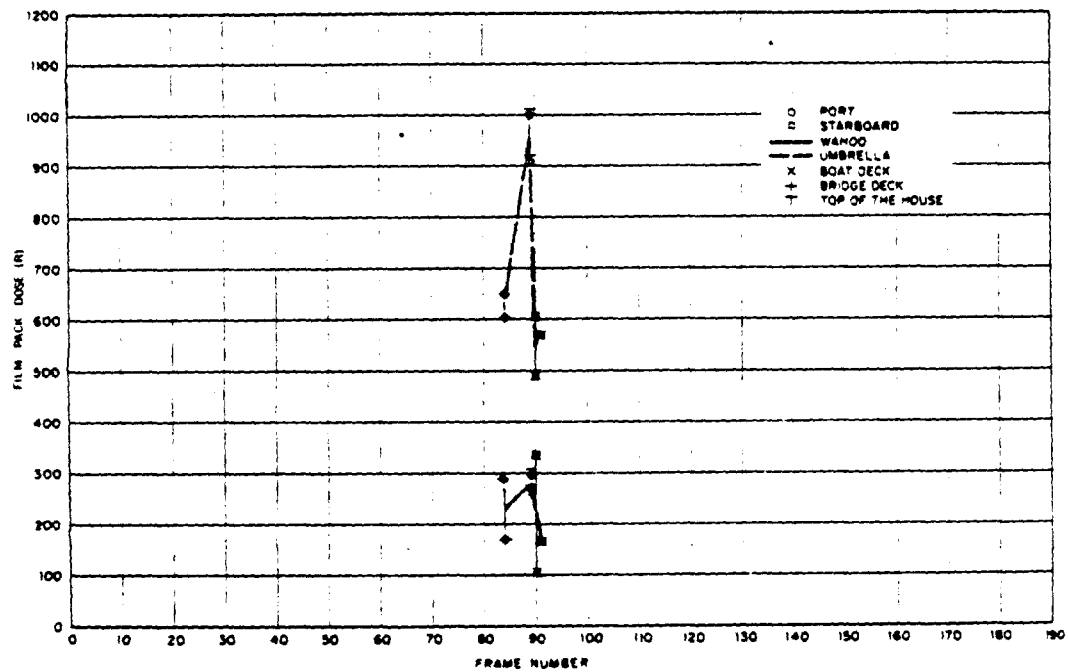


Figure 3.212 Plot of film pack dose readings on superstructure of EC-2 versus position along ship, Shots Wahoo and Umbrella. (Lowest frame numbers are forward; each frame number represents approximately 2 feet.)

181

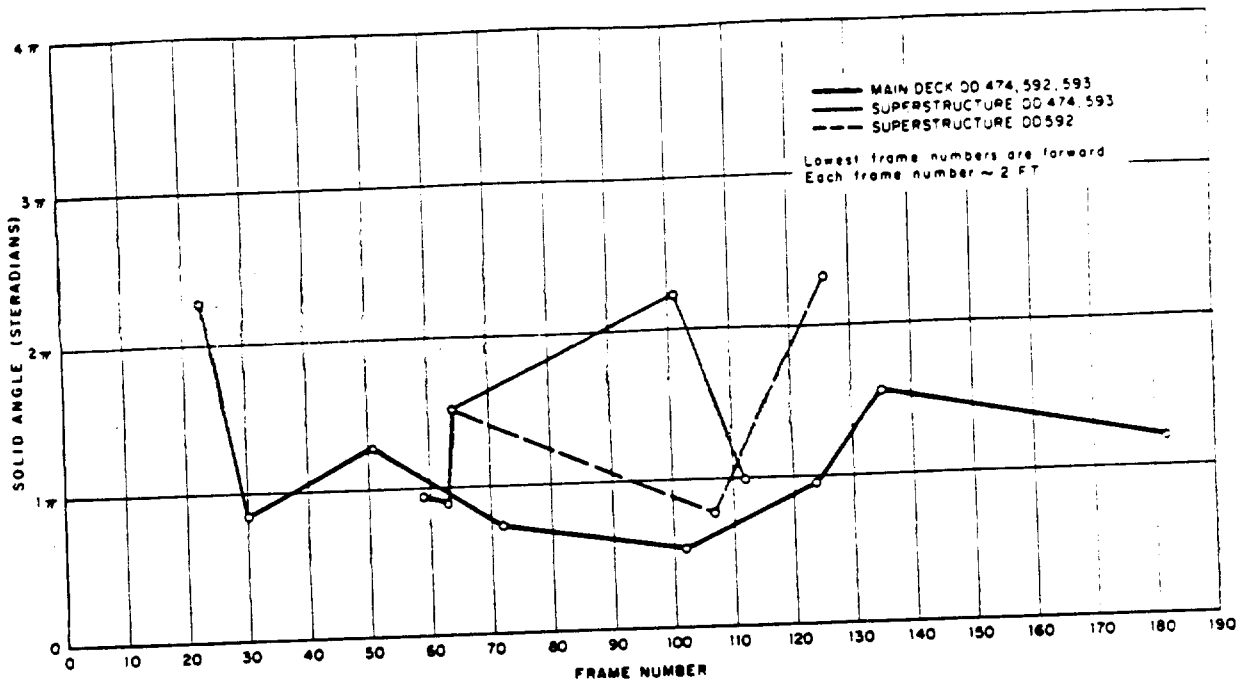


Figure 3.213 Estimated solid angle of cloud subtended by film packs plotted against frame number, destroyers. (Locations of film packs for all three DD's were identical for both shots.)

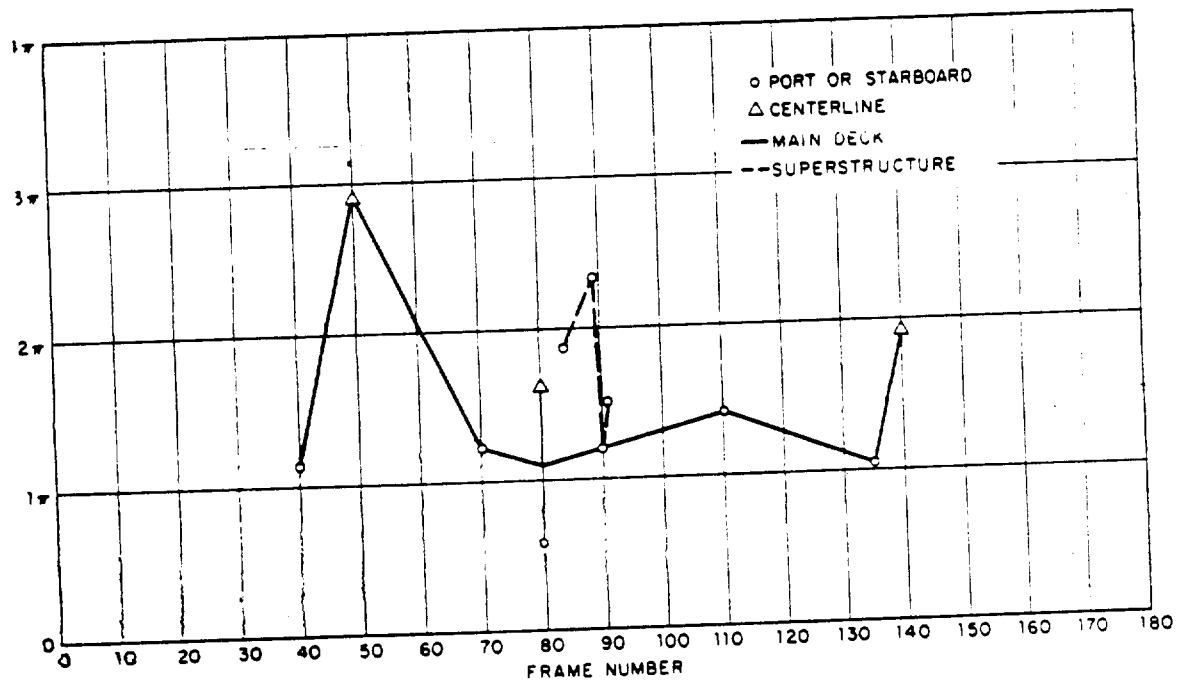


Figure 3.214 Estimated solid angle of cloud subtended by film packs plotted against frame number, EC-2. (Locations of film packs were identical for both shots.)

180

TABLE 3.12 AVERAGE SHIPBOARD DOSES AND DOSE RATIOS:

Ship	Est. From Isodose Contours	Ave GTR Dose*	Ratio: Ave GTR Isodose	Ave FP Dose*	Ratio: Ave FP Isodose	Ratio: Ave FP Ave Exp FP	Ave Exp FP Dose*	Ratio: Ave Exp FP Isodose	Ave Flat FP Dose	Ratio: Ave Flat FP Isodose	Ratio: Ave Flat FP Ave Exp FP
	F	F		F			F		F		
Maheo:											
DD-474	1,300	-	-	947	0.73	0.73	1,302	1.00	1,510	1.16	1.16
DD-592	800	-	-	528	0.66	0.74	714	0.89	805	1.00	1.13
DD-593	350	299	0.85	222	0.63	0.74	300	0.86	352	1.00	1.17
EC-2	900	276	0.31	238	0.26	0.02	289	0.32	-	-	-
Umbrella:											
DD-474	700	-	-	563	0.80	0.72	778	1.11	860	1.23	1.10
DD-592	380	-	-	351	0.92	0.66	535	1.41	528	1.39	0.99
DD-593	60	66	1.10	45	0.75	0.75	60	1.00	70	1.17	1.17
EC-2	900	-	-	656	0.73	0.62	1,055	1.17	-	-	-

\* Notes: Pilot house FP on EC-2 and platform FP's on DD's are omitted from average FP doses. Exposed FP's are 6, 17, 27, and 40 for DD 474 and DD 593, and 6, 17, 27 and 42 for DD 592. The cumulative dose from the GTR at bow station on DD 593 is omitted from GTR average.

TABLE 3.33 CONVERSION FACTORS FOR SUPERSTRUCTURE SHIELDING

Wahoo						Umbrella						Average conversion factor (both shots)		Variation of factor from shot mean	
Surge side* (stbd)		Center* Line		Other side* (port)		Surge side* (stbd)		Center* Line		Other side* (port)		(arg)*(ctr)	(other)	(arg)	(ctr)
Sta No.	Conv Factor	Sta No.	Conv Factor	Sta No.	Conv Factor	Sta No.	Conv Factor	Sta No.	Conv Factor	Sta No.	Conv Factor				
<u>DD-591</u>						<u>DD-591</u>						1.03		5	
		17	0.783			17	1.075					0.57		4	
		18	0.553			16	0.589			20	0.602	0.73		7.5	
12	0.693			25	0.459	12	0.755			21	0.589	0.66		1.5	
11	0.653			21	0.553	11	0.666			21	0.589	0.59		2	
9	0.576			23	0.457	9	0.602			21	0.422	0.75		6.5	
8	0.706			24	0.653	8	0.606			21	0.602	0.94		4	
6	0.923			27	0.883	6	0.896			27	0.345	0.78		2.5	
3	0.783			30	0.768	3	Lost			30	0.678	0.46		6	
		37	0.468			37	0.448					1.16		2	
		40	0.152			40	1.165					0.72		0	
52	0.922			42	0.164	52	0.614			42	Lost	0.76		2.5	
56	0.737			57	0.737	56	0.781			57	0.666	0.85		5	
		59	0.845			59	0.870					0.01		2	
												0.705		(ave var 4%)	
<u>DD-592</u>						<u>DD-592</u>						0.76		8	
		17	1.036			17	0.879					0.57		21	
		18	0.581			18	0.374			20	0.476	0.63		6	
12	0.714			20	0.623	12	0.636			21	0.514	0.69		3	
11	0.707			21	0.574	11	0.664			21	0.514	0.545		3	
9	0.572			23	0.455	9	0.561			23	0.336	0.90		7	
8	0.854			24	0.805	8	0.739			24	0.636	1.00		2.5	
6	0.980			27	0.861	6	1.022			27	0.316	0.82		16	
3	0.847			30	0.777	3	0.804			30	0.617	0.57		2.5	
		37	0.553			37	0.402					0.475		5.5	
54	0.602			40	0.623	54	0.542			40	0.636	1.15		2.5	
		42	1.120			42	1.175			42	1.175	0.67		6.3	
56	0.728			57	0.700	56	0.598			57	0.524	0.79		14	
		59	0.840			59	0.739					0.61		(ave var 8%)	
<u>DD-593</u>						<u>DD-593</u>						0.87		23	
		17	0.667			17	1.059					0.57		2	
		18	0.559			18	0.585			20	0.585	0.72		5	
12	0.683			20	0.666	12	0.751			21	0.601	0.66		1	
11	0.659			21	0.659	11	0.651			21	0.601	0.59		5	
9	0.556			23	0.549	9	0.619			23	0.512	0.80		3	
8	0.766			24	0.666	8	0.813			24	0.635	0.94		12	
6	0.882			27	0.932	6	0.985			27	0.902	0.82		5	
3	0.783			30	0.759	3	0.852			30	0.718	0.58		4	
		37	0.559			37	0.601					1.08		0	
		40	1.082			40	1.085					0.70		7	
52	0.659			42	0.649	52	0.718			42	0.752	0.72		7	
56	0.676			57	0.663	56	0.768			57	0.768	0.84		7	
		59	0.816			59	0.868					0.72		3	
												0.72		(ave var 5%)	
<u>DD-594</u>						<u>DD-594</u>						0.65		28	
		63	1.159			63	1.090			56	0.492	1.13		3.5	
		49	0.640			49	0.531			72	0.673	0.71		15	
72	0.969			47	0.640	72	0.597			79	0.384	0.42		12	
79	0.813			47	0.640	79	0.378					0.55		22	
1	1.038			24	0.360	1	0.673			1	0.549	0.88		16	
6	1.021			15	0.605	6	0.739			6	0.588	0.88		4	
		17	0.841			17	0.910					0.56		2.5	
		44	0.571			44	0.540					0.81		43	
29	1.199			45	0.360	29	0.464			29	0.574	0.81		23	
32	1.003			41	0.588	32	0.616			32	0.574	0.94		8.5	
35	0.863			38	0.917	35	0.863			35	0.948	0.93		(ave var 14%)	

\* Note: The side of the ships facing surface zero or the hot line is called the Surge side (arg); the opposite side is called the Other side (other). Positions on the center line are indicated by (ctr).

The conversion factors presented in Table 3.33 have, therefore, been calculated for the exposed and for the shielded side of a ship. A comparison of the destroyer conversion factors determined for the two shots indicates that, although they are fairly constant, there can be variations as large as 20 percent of the mean. The comparison is by no means as good for the EC-2. These discrepancies (and possibly the abnormally high record for the bow station aboard the DD-593) are probably due to local turbulence caused by the ship's superstructure (Section 3.3.2).

Since a high reading was obtained at the bow station on the DD-593 on both shots and since no fault can be found with the detector, the reading is considered valid. Furthermore, this GTR record agrees with the other weather deck records after passage of the base surge. As previously suggested, eddies caused by the superstructure may temporarily retain remnants of the base surge at specific locations. A plot of the difference between the bow station and the other two stations aboard the DD-593 versus time (Figure 3.215) yields a record resembling that characteristic of the particular shot. The integrated dose under these curves is 288 r for Wahoo and 93 r for Umbrella. Similar eddy effects are postulated aboard all target ships (Sections 3.3.2 and 3.4.1). The temporary retention of surge in turbulent eddies surrounding the ship's superstructure would have highly variable effects and cannot be conclusively demonstrated by the available data. A short retention at early time could result in a significant additional dose; however, the case of the bow station on the DD-593 appears extreme. Possibly, these effects may be more pronounced after the base surge has slowed down to surface wind velocities and at times when the surge transit dose is not masking. Although retardation and temporary retention of the surge by the ship's superstructure seems a reasonable explanation for the prolonged gamma records after upwind surge transit, the extension to the bow records for the DD-593 is at best difficult, and no completely satisfactory explanation has yet been advanced.

Although the eddy hypothesis cannot be conclusively demonstrated, it does indicate possible errors in the assumption that the cumulative dose received aboard a ship corresponds to that which would be predicted on the basis of the ship's position relative to the isodose contours and superstructure shielding factors. With these reservations, the dose determined from the isodose contours may be assumed to represent that received at an exposed position well away from the superstructure on a stationary ship under full washdown. This dose may then be converted to other less exposed positions on the weather decks, using the conversion factors listed in Table 3.33. This type of conversion may, of course, be extended to inner compartments using the film pack data obtained by Project 2.1. It is impossible to estimate the true accuracy of this procedure; therefore, these conversion factors must be used with caution. This statement is particularly true if this information is further extended to the case of moving ships.

### 3.5 CHARACTERISTICS OF AIRBORNE RADIOACTIVE MATERIAL

Since the chemical and physical parameters of base surge are indirectly associated with the principal objectives of this project, only a brief summary of the Hardtack results is given here. The two subjects covered in detail are (1) fractionation and (2) base surge collection aboard the DD-592. Fractionation of radionuclides deposited on coracle surfaces becomes important when determining the maximum possible contribution to the free-field dose from such sources. The special collections aboard the DD-592 give some indication of the amount of water accompanying deposition at distances of approximately 3,000 feet from surface zero. This region is beyond the maximum throwout radius for both shots and yet still appears to be within a zone of heavy water deposition (Section 3.3.1). This water probably contains significant amounts of either dissolved or entrained fission products, but, according to the GTR records at these locations, most of this radioactive material was rapidly washed from coracle and ship surfaces. Deposition from the base surge at greater distances is very light and does not appear to be accompanied by such large amounts of water.

More detailed reports of the results obtained from the Hardtack samples may be found in the following reports: radiochemical analysis and fractionation (References 105 and 106);

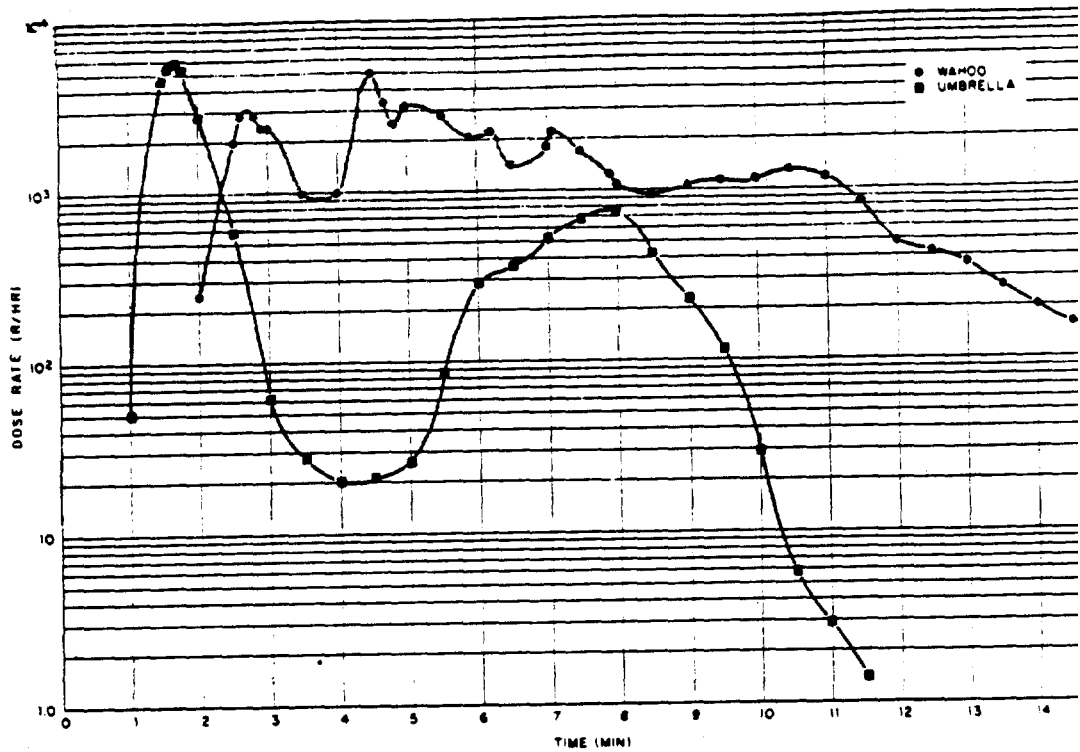


Figure 3.215 Dose rate difference shown by the bow GTR aboard the DD-593.

amounts of induced  $\text{Cl}^{38}$  (Reference 107); decontamination studies (Reference 108); and plume trajectories (Reference 109).

**3.5.1 Fractionation.** Fractionation is indicated by the pronounced differences in decay curves obtained from the various samples collected by the project. To establish the importance of the radiation due to deposited material relative to the free-field radiation during base surge transit, some systematic means of correcting for possible fractionation of the deposited material was required. Coracle recovery operations prevented the counting of IC collections at times earlier than about 11.5 hours on Wahoo and about 13.5 hours on Umbrella. Since decays could not be run on each IC tray, there did not appear to be any reliable means of correcting the observed counts back to the time of deposition. A detailed examination of the IC decays suggests, however, that the observed fractionation has some regular correlation with the history of the radioactive material immediately prior to collection. It should be emphasized that these analyses of decay characteristics are made upon limited observations. Nevertheless the apparent trends seem at least sufficient for the purposes of this project, especially since conclusions based upon this data are supported by information from other sources (Section 3.3.1).

IC trays that were continuously exposed or that are known to have been altered by coracle overturn have been eliminated from consideration; thus, only 21 decay curves for representative 1-minute IC collections (Table 3.34) are available for comparison. The 37- and 40-minute collections from Station CR 2.7 for Umbrella are also included in this group since, although the coracle is reported as overturned, the IC cannot have operated in an overturned position to expose these trays. Nevertheless, these collections are probably the result of an arming error and thus represent those of an overturned coracle, in which case they should most resemble the "water" decay described later. Each IC decay was plotted from 0.5 to 60 days on a separate sheet of transparent semilogarithmic paper, using identical scales; smooth curves were then drawn so that they passed through all plotted points. By comparison of these curve shapes on a light table, it was found that the curves could be grouped into two general classes whose characteristic shapes could not be superimposed. No real distinction between collections from the two shots could, however, be made.

These decay curves have been assembled into two families and normalized at 22 days (a time which produces the narrowest pencil of lines between 20 and 40 days) and are presented in Figures 3.216 and 3.217. The family of decay curves represented in Figure 3.216 is typical of collections that were probably deposited directly from transiting airborne material; whereas that in Figure 3.217 is typical of collections that could only have resulted from some secondary process, such as radioactive water splashed into the collector. These two characteristic types of decay were, therefore, called the "base surge" or "early" decay and the "water" or "late" decay, respectively. For ease of comparison, a best line has been faired through these two families of curves, and these two lines together with the standard decay curve and the gamma-intensity-decay unit (GIDU) decay curve obtained by Project 2.1 (Section B.2) are presented in Figure 3.218. Note that the early collections approximate the standard decay curve prior to 22 days, whereas the late collections approximate it from this time to 60 days. One Umbrella collection (DL 16.0 at 6 minutes) does not follow any of the decay curves over the entire 60-day interval. The collections from DL 16.0 and D 22.0 for this shot are both so close to background that their decay curves may have been influenced by changes in counter background. Other decay curves obtained from IC trays that jammed in an exposed position or from other collections that were continuous throughout the event are presented in Figure 3.219. These curves possess a variety of shapes, which vary between the early and late characteristics.

In addition to this possible division into two families, there also appears to be characteristic subvariations in the shape of the base surge decay family (Figure 3.216). A more detailed comparison of the curves for Wahoo and Umbrella samples indicates that a further subdivision may be possible (Figures 3.220 and 3.221). The collections corresponding to the plotted curves are given in Table 3.34. Although the correspondence is not perfect, there is a fairly consistent change in curve shape with time of deposition, particularly for collections widely separated in

TABLE 3.34 CHARACTERISTIC DECAY CURVES FOR IC COLLECTIONS

The IC collections are designated by the location of the collection followed by a time indicating the time at which the 1-minute collection ceased. For a more detailed description, see Section D.2. (Also see Figures 3.220 and 3.221.)

IC Collection	Decay Curve No.	Characteristic Family	IC Collection	Decay Curve No.	Characteristic Family
Wahoo:			Umbrella:		
CL 3.9, 2 min	3	Early	U 2.7, 2 min	2	Early
CL 3.9, 3 min	2a	Early	U 2.7, 3 min	3	Early
CL 4.6, 3 min	2a	Early	CL 4.0, 2 min	4	Early
CL 7.1, 4 min	3	Early	CL 4.0, 4 min	4	Early
DL 7.1, 9 min	1	Late	DL 6.2, 2 min	3a	Early
DR 4.5, 9 min	1	Late	DL 16.0, 6 min	4a	Neither
DR 24.0, 52 min	1	Late	D 18.2, 7 min	none	Early?
DRR 6.8, 2 min	2	Early	D 22.0, 9 min	none	Early?
DRR 6.8, 3 min	2	Early	DR 12.2, 5 min	4a	Early
DRR 12.8, 44 min	1	Late	CR 2.7, 37 min	1	Late (overturn)
CR 6.4, 2 min	3	Early	CR 2.7, 40 min	1	Late (overturn)
CR 6.4, 3 min	3	Early			

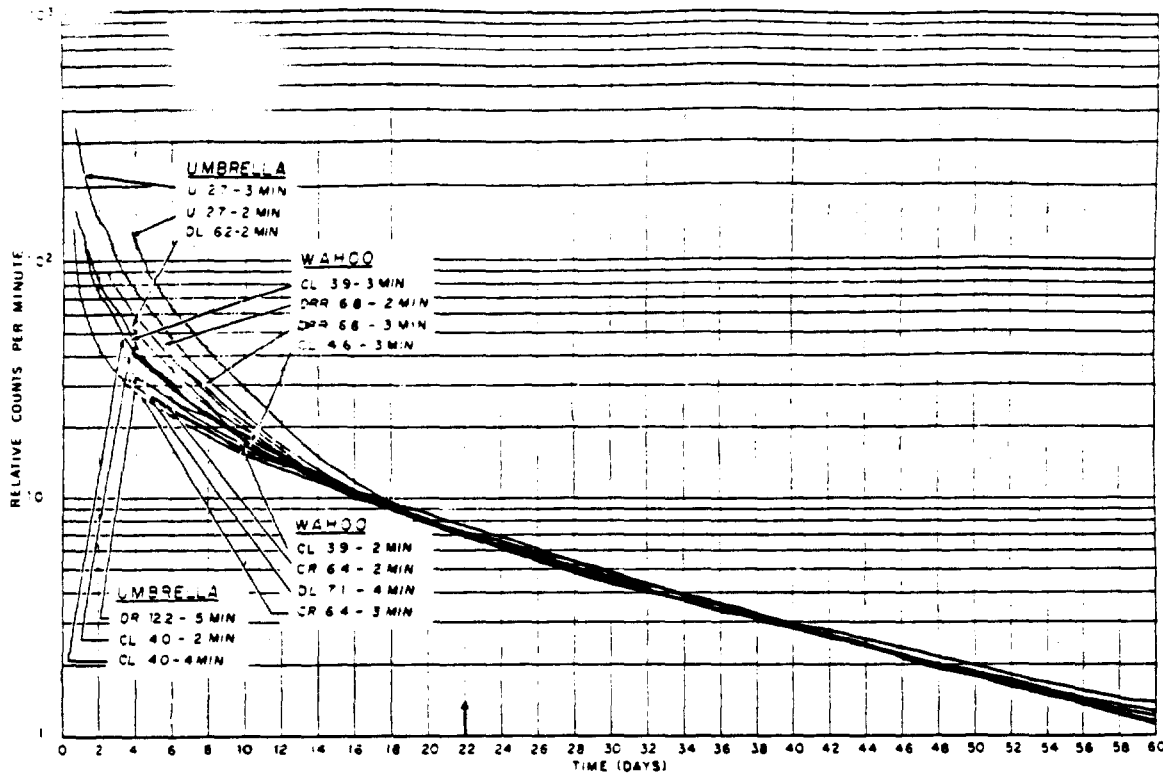


Figure 3.216 Family of decay curves for early IC collections.

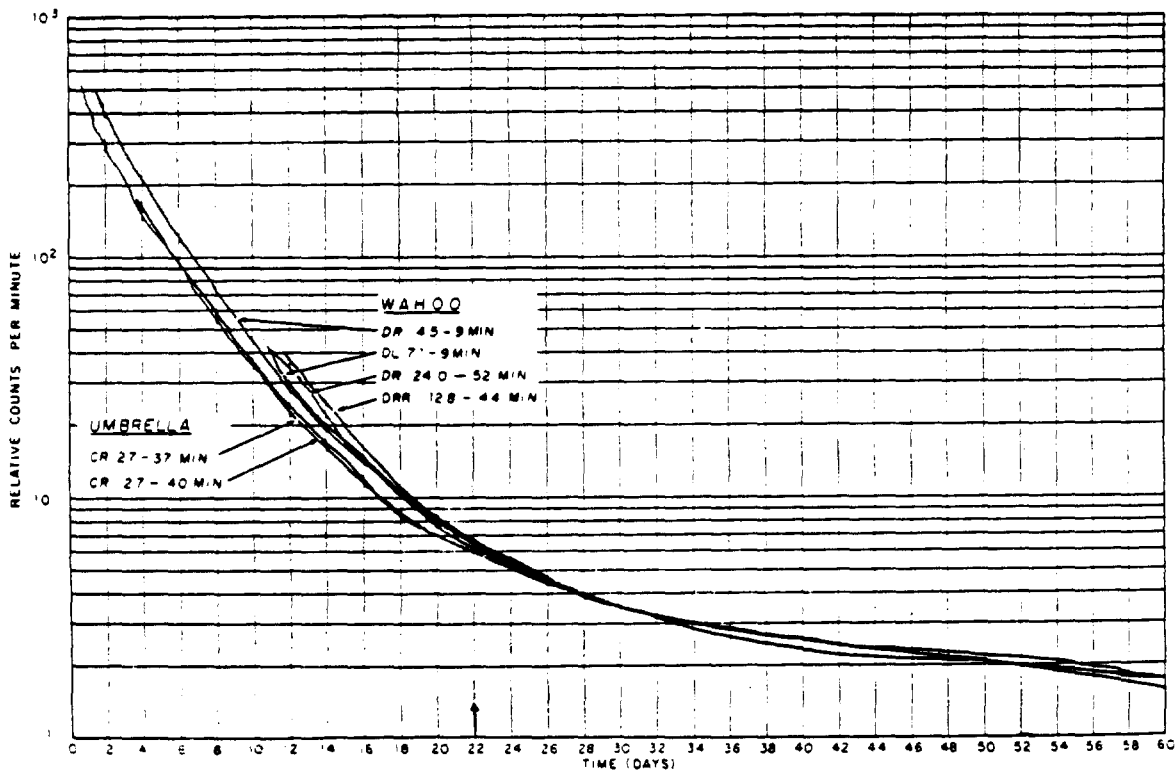


Figure 3.217 Family of decay curves for late IC collections.

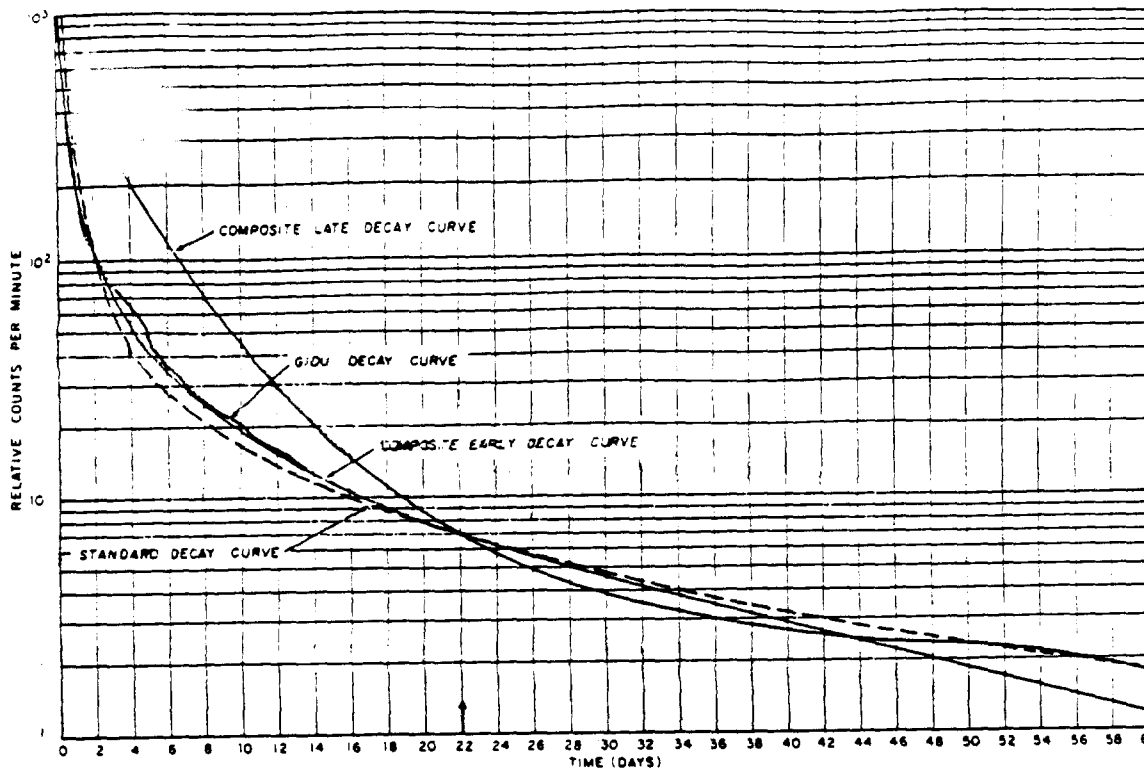


Figure 3.218 Comparison of characteristic decay curves with standard decay curve.

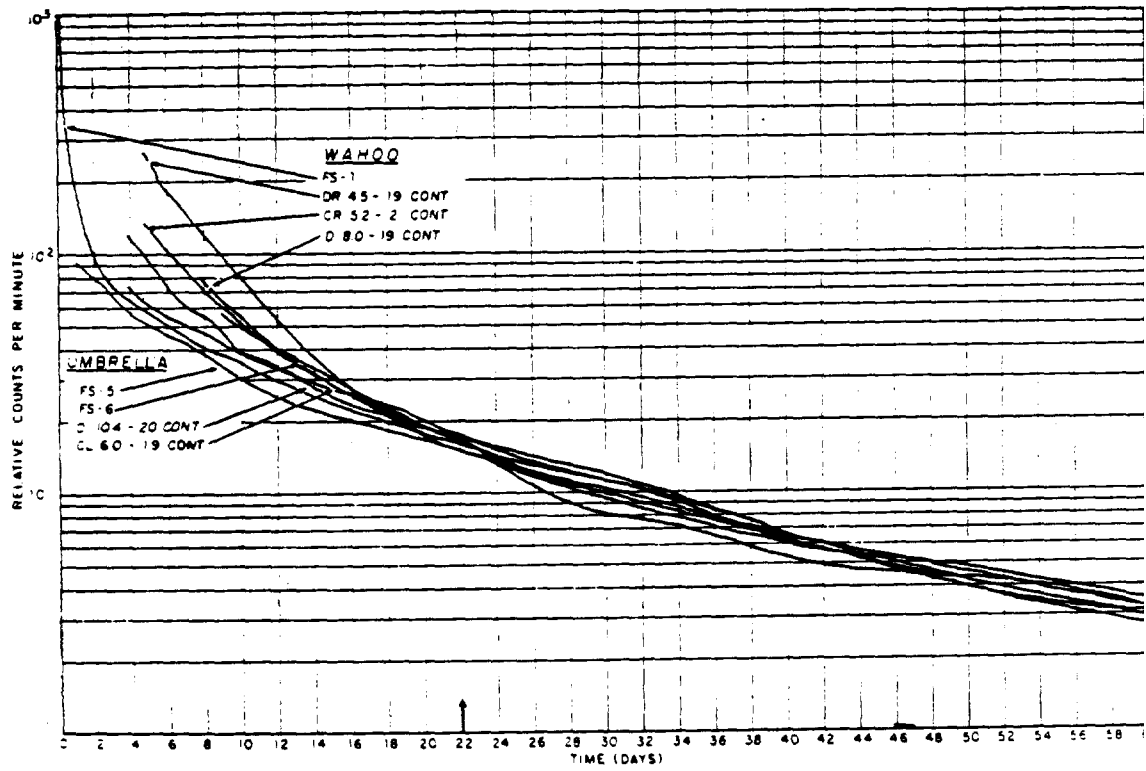


Figure 3.219 Family of decay curves for various continuous collections.

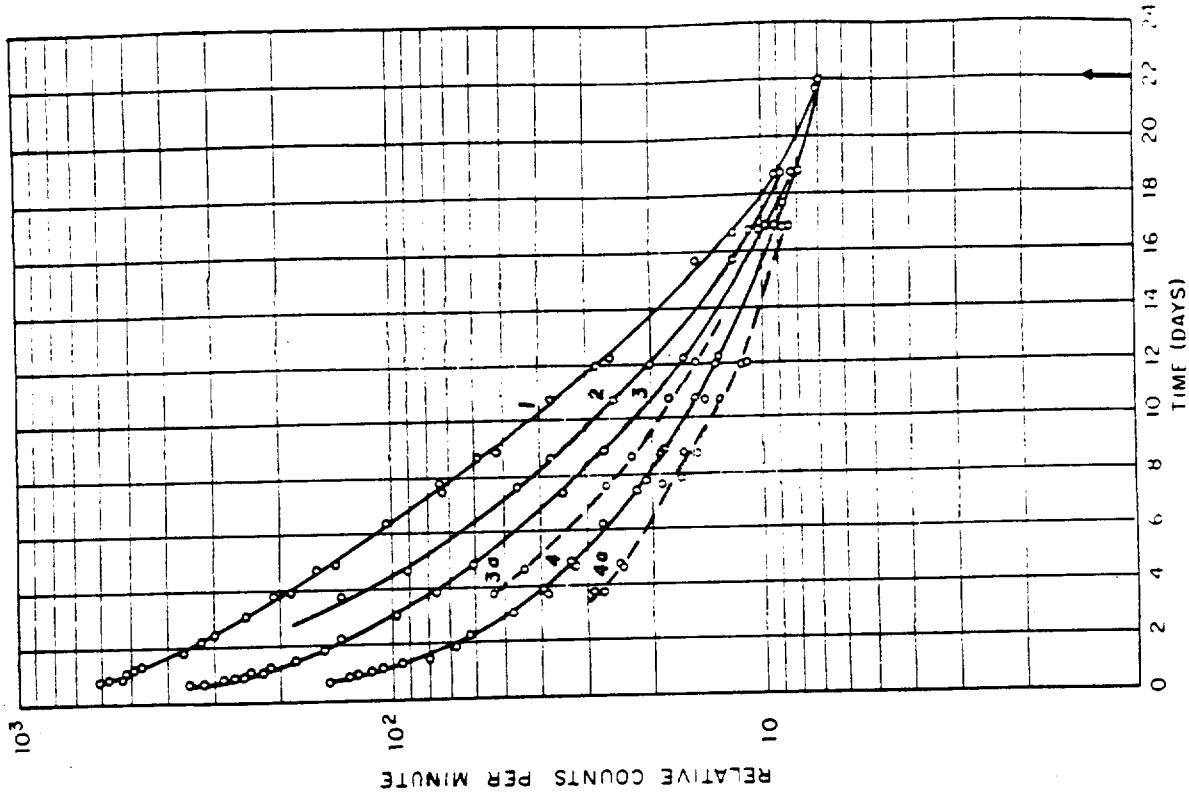


Figure 3.221 Possible subfamily of early decay curves, Shot Unabrella.

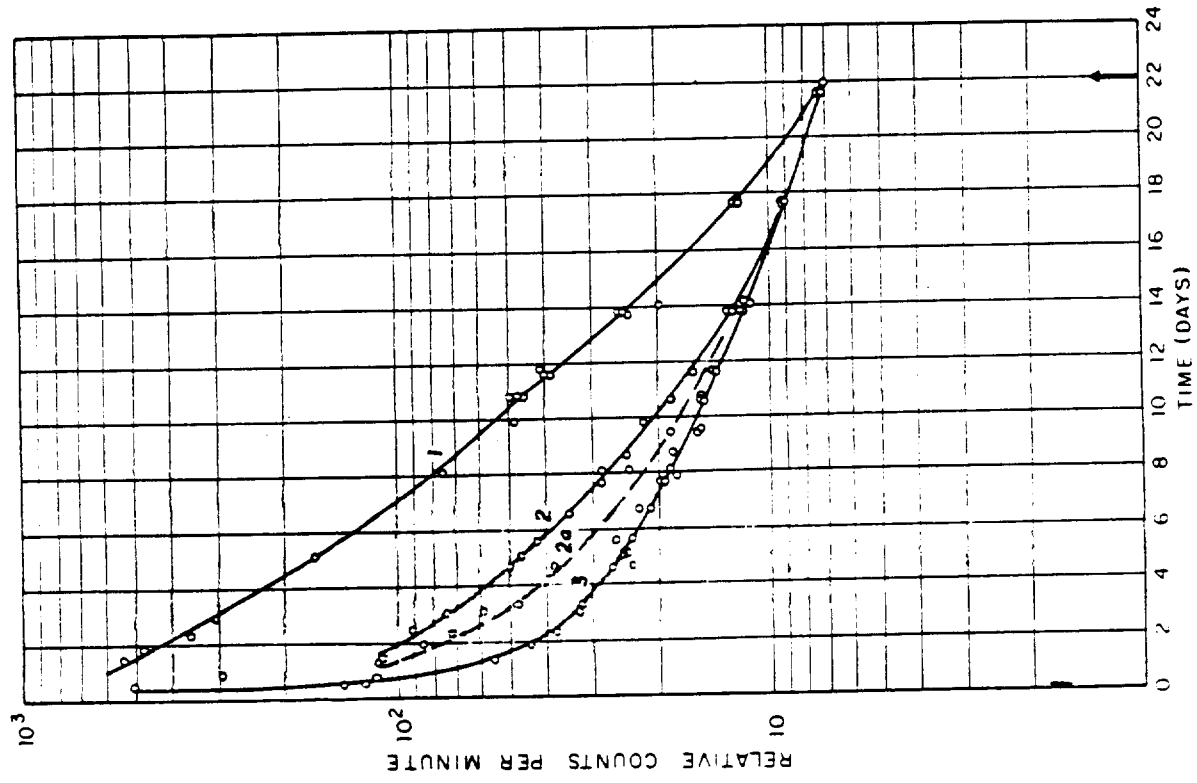


Figure 3.220 Possible subfamily of early decay curves, Shot Walton.

time. Since the exact time of collection cannot be established with an accuracy greater than  $\pm \frac{1}{2}$  minute, the characteristic decay curves for the two shots are combined for the correction of all IC collections (Figure 3.36). If these combined curves are accepted, the characteristic shape of decay curves for collections made in the first minute resembles that which would be expected from samples deficient in short-lived or enriched in long-lived fission products.

The decay shapes for samples collected during the next 4 or 5 minutes show an apparently continuous variation with time of collection, which could be duplicated by the addition of short-lived or depletion of long-lived fission products. After about 5 minutes, the base surge decays no longer exhibit any significant change with time of collection. In specific instances where a direct contribution from radioactive water is suspected (U 2.7 on Umbrella), the observed decay curve is intermediate between a base surge decay and a water decay. Contrarily, the water decay curves, while quite distinct from the base surge family, show little variation with either time or location of collection.

In general, the characteristic IC decays seem to depend primarily upon whether the deposition resulted from the base surge or from other sources with secondary modifications dependent upon the time of collection. Although the location of collection necessarily affects the time of deposition, this single factor in itself has apparently little significance. The data available is not sufficient to demonstrate the suggested time dependence conclusively; however, it is sufficient to suggest that a more rigorous investigation of this phenomenon on future underwater detonations might be rewarding.

Further evidence of the fractionation of Hardtack samples is found in the radiochemical analysis of a number of samples collected at various surface stations for both Wahoo and Umbrella and of a few cloud samples collected by LASL aircraft shortly after zero time (Reference 105). In summary, these analyses show evidence of extreme fractionation of certain radionuclides with respect to  $\text{Mo}^{99}$ . Zirconium, ruthenium, tellurium, and total rare earths showed little fractionation, but the nuclides with gaseous precursors exhibit considerable fluctuation. The base surge samples for Wahoo show  $\text{Sr}^{89}$  enrichments greater than 20, whereas the  $\text{Ba}^{140}$  enrichments of the samples are approximately a third of those observed for  $\text{Sr}^{89}$ . Conversely, base surge samples for Umbrella are enriched in  $\text{Sr}^{89}$  by factors ranging between 3 and 10, with  $\text{Ba}^{140}$  enrichments as great as twice those observed for  $\text{Sr}^{89}$ . Ocean water samples from both events were deficient in both  $\text{Sr}^{89}$  and  $\text{Ba}^{140}$  by factors as large as 2, whereas a crater sample from Umbrella was deficient in  $\text{Sr}^{89}$  by a factor of 10. Exact statement of all these results is given in Reference 105.

The change in relative  $\text{Sr}^{89}$  and  $\text{Ba}^{140}$  fractionation reported for Wahoo and Umbrella may represent an example of fractionation of gaseous fission products at venting. The suggestion that the IC decays demonstrate a consistent change dependent upon time of deposition during the first minutes after detonation invites some preliminary speculation on possible fractionation mechanisms that might be operative during the early stages of base surge generation. The gaseous precursors of such radionuclides as  $\text{Sr}^{89}$  and  $\text{Ba}^{140}$  may not be dissolved in the water droplets comprising the plumes and base surge, whereas most nonvolatile fission products could be effectively scavenged either in the ocean prior to venting or subsequently by these same liquid droplets. So long as these precursors remain gaseous, they can exist independently, going into solution in the liquid droplets at rates that are slow in comparison to the rate of surge development. Upon decay to a nonvolatile daughter, however, the radionuclide would be strongly attracted to any available surface. Since in the column and early base surge a very large area of liquid surface exists, the rapid incorporation of these nonvolatile radionuclides can be presumed.

Assuming that only a small percentage of the total fission products becomes airborne after an underwater detonation but that a large proportion of the volatile products escape when the explosion bubble reaches the water surface and become mixed with the column and base surge, it seems reasonable to suppose that base surge droplets would become increasingly enriched with the decay products of the gaseous radionuclides. Assuming that various small percentages of the total fission products escape at bubble surfacing time, the calculated enrichment with

respect to  $\text{Mo}^{99}$  for various radionuclides with volatile precursors indicates changes in nuclide composition with time, which are in rough agreement with the observed values for  $\text{Sr}^{89}$  and  $\text{Ba}^{140}$  on Wahoo and Umbrella. If this hypothesis is accepted, it would be reasonable to expect that, because of the later surfacing time on Wahoo, a larger proportion of  $\text{Ba}^{140}$ , which has shorter-lived gaseous precursors than  $\text{Sr}^{89}$ , would remain with the ocean water. The early surfacing of Umbrella would permit a larger proportion of the volatile precursors of  $\text{Ba}^{140}$  to escape. These would then be rapidly scavenged by airborne droplets. It would appear that both these effects have been observed (Reference 105). The speculations offered here cannot be considered conclusive; they do, however, appear to justify the limited observations made during Operation Hardtack and suggest that more precise investigation into such possible mechanisms might further elucidate the fractionation phenomenon.

Other miscellaneous samples collected by various simple means gave further evidence of fractionation. These samples included ocean-water samples, funnel samples, bottom samples, and cloud samples. The ocean-water samples were simply collected in polyethylene bottles. The funnel samplers (FS) described in Sections 1.33 and 2.2.6 were placed at a number of positions within the array in a special bracket that permitted helicopter recovery immediately after the shot; thus, decay information from H+4 hours was obtained for both Wahoo and Umbrella. Cloud samples were obtained for Project 2.3 by the LASL cloud-sampling aircraft. Cloud samples were collected on 2-inch-square filter paper patches placed upon the large filter paper normally used by LASL for aircraft sampling. A single bottom sample was obtained from the Umbrella crater on 13 June 1958 by means of an improvised bottom trawl. The locations and times of collection for all these miscellaneous samples are summarized in Table 3.35. The crystal decay curves obtained for some of these samples are presented in Figures 3.222 and 3.223. All these decays were counted on Shelf 1 of End-Window Gamma Counter 2 (described in Section 3.3.1). The distance from the support of Shelf 1 to the bottom of the crystal is 21 mm (conversion factor from Shelf 1 to Shelf 5 is 0.173). The cloud sample filter patches were digested by vigorous stirring in nitric acid, and the resulting suspension was filtered and made up to 50 ml. A 2-ml aliquot of this filtrate was distributed over the collecting surface of a blank IC tray, which was then counted.

All FS's were treated in a similar manner. These samples were made up to a known volume, and an aliquot of the resulting solution was distributed over an IC tray as summarized in Table 3.36. Similarly a 3-ml aliquot of the H+2 hour ocean-water sample for Umbrella was distributed over an IC tray and counted. The Umbrella crater sample was also counted by first dissolving 2.4 grams of the air-dried mud in nitric acid and then distributing the solution over an IC tray. The treatment of these miscellaneous samples permits comparison with decays determined for the IC collections if correction for shelf geometry is made. Funnel Sample 1 and Cloud Sample 1 for Wahoo were also counted in a 4 $\pi$  gamma ionization chamber (Reference 110). The relative ionization readings versus times are presented in Figure 3.224.

**3.5.2 Physical and Chemical Properties.** The majority of project instrumentation was specifically designed for the measurement of the gamma fields resulting from an underwater detonation. Only those instruments installed on the platforms aboard each target destroyer (Sections 1.3.3 and 2.2.6) were designed to provide samples from which physical and chemical properties could be determined. Thus, the conclusions presented in this report are obtained from a limited number of samples collected at no more than three downwind positions. During Wahoo, samples were obtained from the DD-593 only because of the power failure aboard the DD-474 and DD-592 prior to the shot. During Umbrella, nearly complete sets of samples were obtained from the DD-592 and DD-593, those aboard the DD-474 having been destroyed by what appeared to be the impact of the water-laden base surge moving at its initially high velocity.

The AFI installed on the platform aboard the DD-592 (Figures 1.13, 1.16, and 2.8) is fully described in Section 2.2.6. A series of samples are collected at a rate of 10 ft<sup>3</sup>/min on DMT filters, each backed by reservoirs that act as liquid traps. Thus, the sample is separated at the time of collection into liquid and solid fractions. A total collection by the AFI is composed

TABLE 3.35 MISCELLANEOUS SAMPLE DATA

Type of Sample	Location of Installation or Collecting Agency	Actual Position		Time of Collection	
		Bearing From Surface Zero	Distance From Surface Zero	EPG Date 1958	EPG Time
		deg (true)	ft		
Wahoo:					
Funnel Sample 1	YC-2	29	2,100	16 May	1530
Funnel Sample 2	YC-1	29	3,600	18 May	1030
Funnel Sample 3	YC-5	244.5	4,500	18 May	1130
Funnel Sample 4	YC-6	248	6,500	18 May	1130
Cloud Sample I	Aircraft	(altitude of 1,900 ft)		16 May	1356
Cloud Sample II	Aircraft	(altitude of 2,500 ft)		16 May	1408
Ocean Water I	Bolster	158	1,500	16 May	1509
Ocean Water II	Rehoboth	(11° 19.0' N lat. 162° 00.5' E long.)		17 May	1000
Umbrella:					
Funnel Sample 5	YFNB 12	068	2,350	9 June	1248
Funnel Sample 6	YC-7	96	3,150	9 June	1249
Funnel Sample 7	EC-2	158	1,650	10 June	0930
Funnel Sample 8	NOL-55	251.3	5,620	10 June	1245
Cloud Sample I	Aircraft	(altitude of 850 ft)		9 June	1126
Ocean Water I	Radsafe LCM	039	370	9 June	1232
Ocean Water II	Munsee	248	4,400	10 June	1200
Crater Sample	Project LCM	(Approximately SZ)		13 June	1445

TABLE 3.36 SUMMARY FOR FUNNEL SAMPLES

All measurements in milliliters.

Sample Number	Recovered Volume	Equivalent Sea Water *	Sample Made Up to Total Volume	Aliquot Placed on IC Tray
FS-1	5 to 10	15.0	50	0.50
FS-5	77	83.2	100	0.10
FS-6	336	363.7	500	0.50
FS-7	11	12.8	50	5.0
FS-8	45	65.9	100	5.0

\* Determined by chloride analysis.

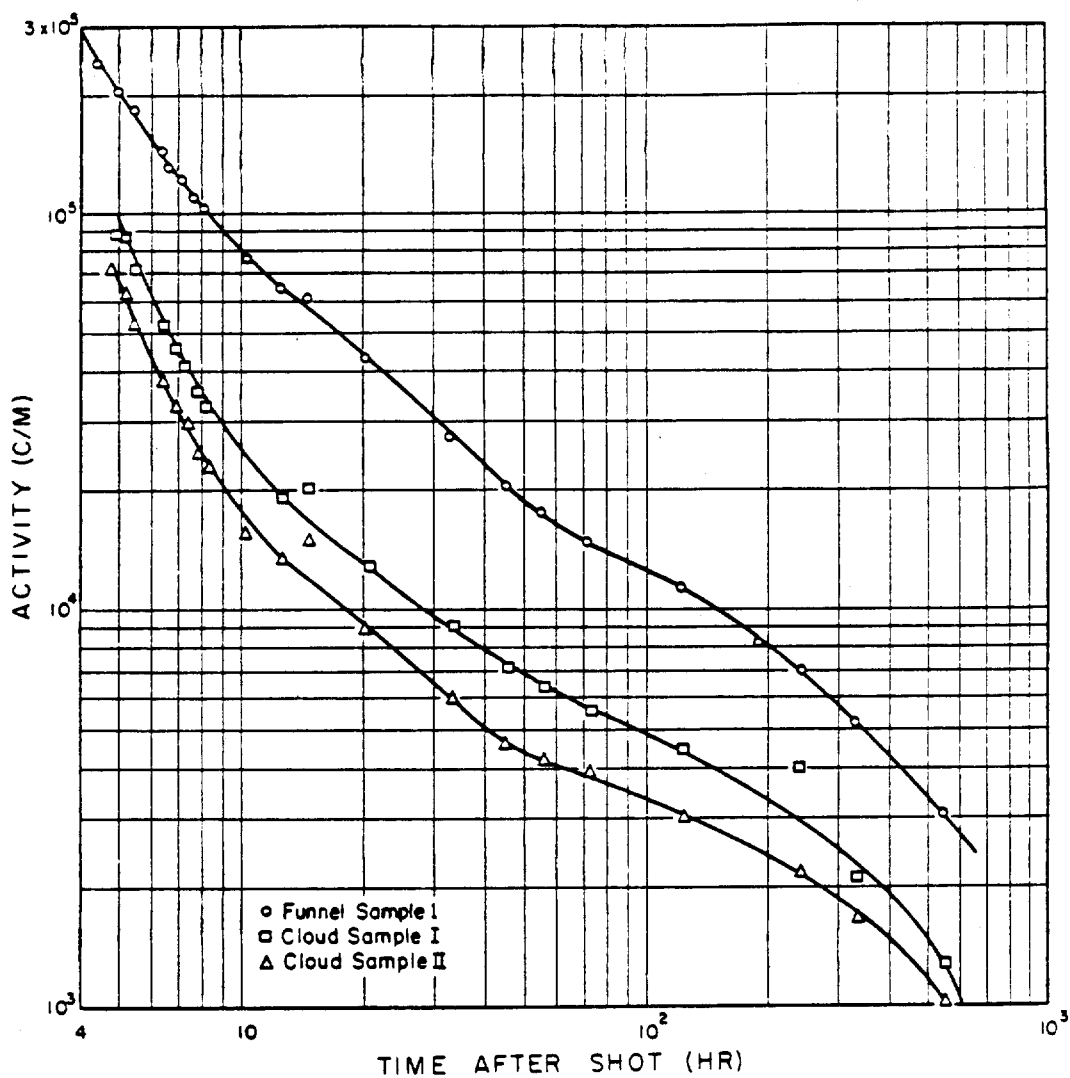


Figure 3.222 Decay of funnel and cloud samples determined by End-Window Gamma Counter 2, Shot Wahoo.

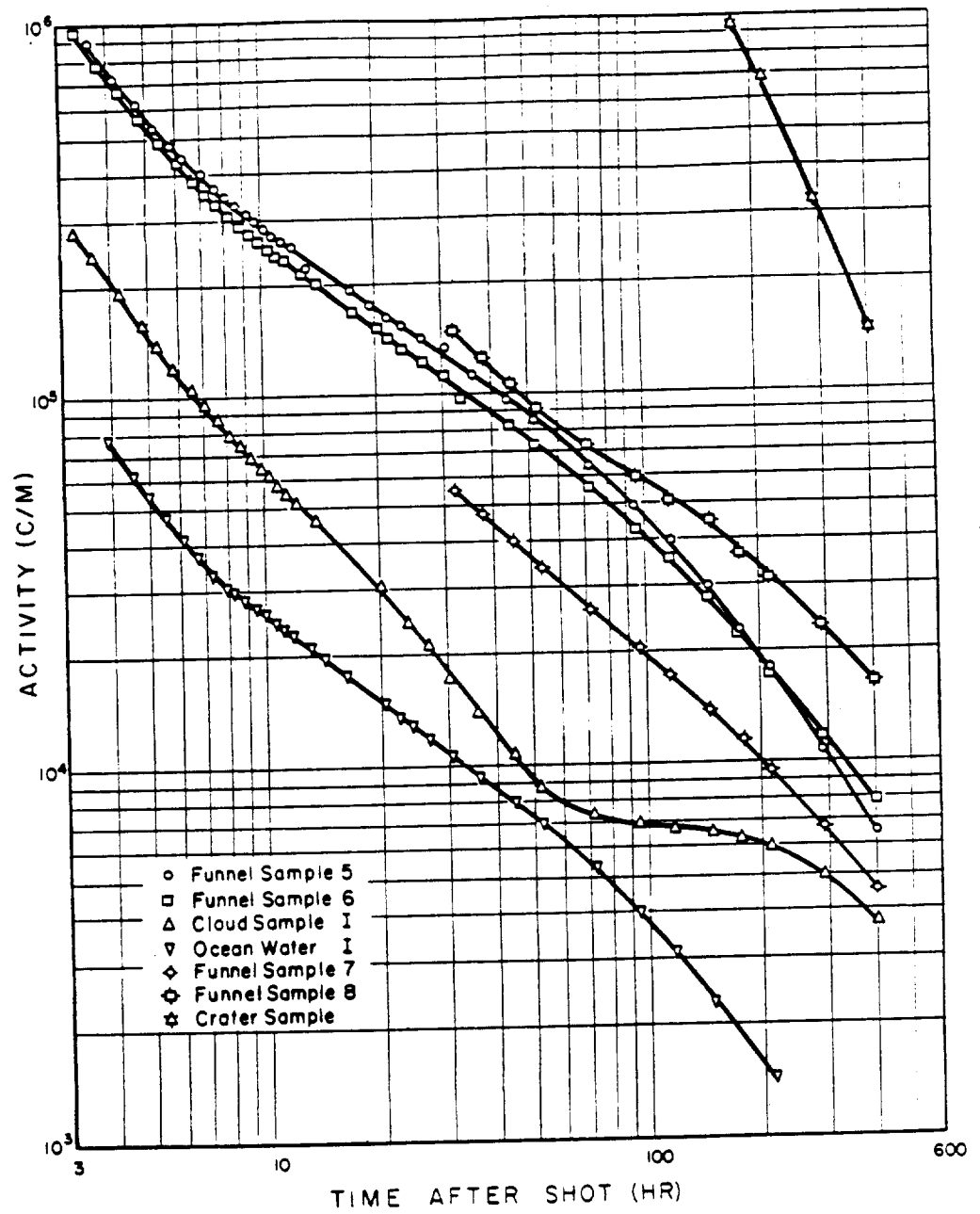


Figure 3.223 Decay of funnel, cloud, ocean-water, and crater samples determined by End-Window Gamma Counter 2, Shot Umbrella.

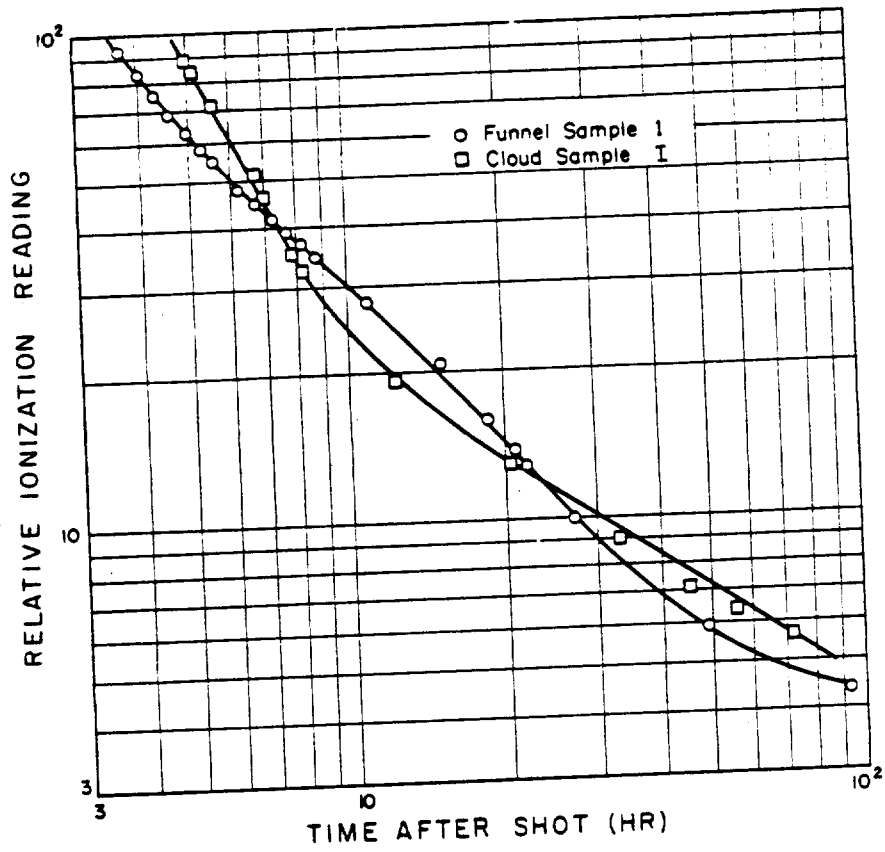


Figure 3.224 Decay of funnel and cloud samples determined by  $4\pi$  gamma ionization chamber, Shot Wahoo.

of 30 pairs of liquid and solid fractions, 20 of which are collected over a consecutive sequence of 2-minute intervals (designated 2-1, 2-2, etc., in Table 3.37) and 10 of which are collected over a simultaneous consecutive sequence of 10-minute intervals (designated 10-1, 10-2, etc., in Table 3.37). For Umbrella, both sampling sequences were started by a radiation trigger at zero time; however, only a partial collection was obtained. Because of misalignment of the indexing switches by shock, the last two sampling heads in the 10-minute sequence did not open and the last 10 collections of the 2-minute sequence were probably obtained without any vacuum being applied to the sampling head. Thus, although the analytical results for all collections are tabulated, only Samples 10-1 through 10-8 and 2-1 through 2-10 are considered truly representative. All AFI samples were sealed upon recovery and returned to NRD L for analysis. When recovered in the field, the first samples in both the 2-minute and the 10-minute series were heavily loaded with visible residue, which upon cursory inspection resembled pulverized coral.

Upon arrival at NRD L, each sampling head containing its water reservoir (Figure 2.9) was first counted on the bottom shelf of a doghouse counter—a 1-inch-diameter, 1-inch-thick, thallium activated NaI crystal canned in spun aluminum and installed inside a large lead shield into which samples as large as 18 by 22 inches can be placed (Reference 33). The shelf-to-crystal distance is 3 feet. The water reservoirs were then removed and the volume of the contents measured. If the reservoirs were dry, 25 ml of distilled water was added. A 4-ml aliquot of the liquid phase was then counted in a well counter—a 1 $\frac{3}{4}$ -inch-diameter, 2-inch-thick, thallium activated NaI crystal containing a central well  $\frac{3}{4}$  inch in diameter and 1 $\frac{1}{2}$  inches deep sealed in a  $\frac{1}{32}$ -inch spun aluminum can (Reference 110). About 150 ml of chloroform was used to dissolve the DMT filters and to rinse out the sampling head. The solution and rinse were then filtered through an HA Millipore filter (a cellulose nitrate membrane having a controlled pore size of 0.45 micron). The residue was distributed as uniformly as possible over a circle 34 mm in diameter and was washed with additional chloroform to assure complete removal of DMT. The residue was dried overnight in a desiccator, weighed, then mounted on a plastic cap and counted on Shelf 5 of End-Window Gamma Counter 3 (an instrument similar to that used in the EPG). After removal of the DMT filter, the empty sampling head was again counted in the doghouse counter. Large amounts of residual activity appeared to be adsorbed on the bottom screen and aluminum walls and was extremely difficult to remove. Counts of the discarded chloroform filtrates containing the dissolved DMT filters indicated that less than 1 percent of the activity was lost in the transfer to HA Millipore filters.

A summary of AFI results is presented in Table 3.37. All counts have been reduced to a fifth-shelf end-window gamma counter response at 6 days after zero time. Conversion factors were obtained by comparing the doghouse counts of two AOC samples obtained aboard the DD-592 during Umbrella with the well counts and end-window counts of aliquots from the same AOC samples. The factor converting a doghouse count to a fifth-shelf end-window count is approximately 100 (the exact value varies between 99 and 103 for the period of 5 to 45 days). A similar factor converting the well counts at 6 days to end-window counts at 6 days is 0.27. Since the time of count can cause a significant variation in this factor, all other measurements have been brought to the time of this measurement using the observed decay curves. The decays for both the solid and liquid fractions of Samples 10-3, 10-8, and 2-11 are presented in Figures 3.225 through 3.227.

The liquid fractions of the AFI samples obtained during Umbrella are first considered. Samples 10-1 and 2-1 have about equivalent amounts of water associated with them; since Samples 2-2 through 2-5 are dry, all this liquid must have been deposited in the first 2 minutes after zero time. The inside diameter of the AFI sampling heads is 3.55 inches; therefore, if uniform deposition is assumed, the collection corresponds to a rainfall of about 7 in/hr. Photographic evidence from Wahoo gives a maximum crosswind throwout radius of about 1,800 feet (Section 3.3.1); trajectories for downwind positions for both Wahoo and Umbrella are not expected to be much greater. Thus, massive deposition of water from such sources seems unlikely. All evidence indicates that base surge was in the neighborhood of the DD-592 at about 1 minute; however, the ship's washdown must also be considered as another possible source of the liquid

TABLE 3.37 ACTIVITY OF AIR FILTRATION INSTRUMENT (AFI) SAMPLES  
 (All counts converted to end-window gamma counter at 6 days after detonation)\*\*

Sample	Collection Interval (min after zero time)	Total Sample Count	Total Solid Count	Total Liquid Count	Total Counts Remaining on Sampling Head Walls	Sum of Solid, Liquid and Remainder Counts
		(10 <sup>5</sup> c/min)	(c/min)	(c/min)	(10 <sup>5</sup> c/min)	(10 <sup>5</sup> c/min)
10-1	0-10	62.0	114,818	81,000	8.59	1.05
10-2	10-20	3.09	614	dry	2.44	2.44
10-3	20-30	3.13	952	dry	2.66	2.66
10-4	30-40	3.15	902	dry	2.74	2.75
10-5	40-50	3.09	192	dry	2.29	2.29
10-6	50-60	6.21	3,076	49,200	2.26	2.78
10-7	60-70	3.39	2,210	dry	2.37	2.39
10-8	70-80	13.9	15,412	19,287	3.15	3.49
10-9*	(80-90)†	11.1	10,148	3,330	4.72	4.86
10-10*	(90-100)†	228.0	101,202	410,145	23.9	29.0
2-1	0-2	39.3	43,672	74,167	4.17	5.35
2-2	2-4	3.03	2,936	dry	1.63	1.66
2-3	4-6	4.66	10,984	dry	3.11	3.22
2-4	6-8	5.01	13,068	dry	2.76	2.89
2-5	8-10	2.70	776	dry	1.58	1.53
2-6	10-12	2.24	726	dry	1.74	1.74
2-7	12-14	1.89	636	dry	1.60	1.60
2-8	14-16	4.79	570	dry	2.98	2.99
2-9	16-18	3.23	2,018	dry	2.75	2.76
2-10	18-20	6.93	9,804	dry	2.54	2.64
2-11*	(22-22) ?	9.07	38,472	dry	4.43	4.51
2-12*	(22-24)†	4.11	8,504	dry	2.61	2.69
2-13*	(24-26)†	4.30	7,864	dry	3.18	3.26
2-14*	(26-28)†	5.38	4,428	dry	6.16	6.20
2-15*	(28-30)†	2.75	2,890	dry	2.21	2.23
2-16*	(30-32)†	3.04	4,058	dry	2.19	2.22
2-17*	(32-34)†	6.22	16,694	dry	4.32	4.51
2-18*	(34-36)†	3.25	3,226	dry	2.33	2.36
2-19*	(36-38)†	2.90	1,384	dry	2.69	2.71
2-20*	(38-40)†	2.80	1,276	dry	2.67	2.68

\* Note: Questionable samples. For full description, see text.

\*\* Note: Total sample counted on U+5 days in doghouse counter.

Solid samples counted on U+12 days in end-window gamma counter.

Liquid samples counted on U+6 days in well counter.

Remainder on sampling head walls counted from U+9 to U+12 days in doghouse counter.

Description of conversion factors applied is given in text.

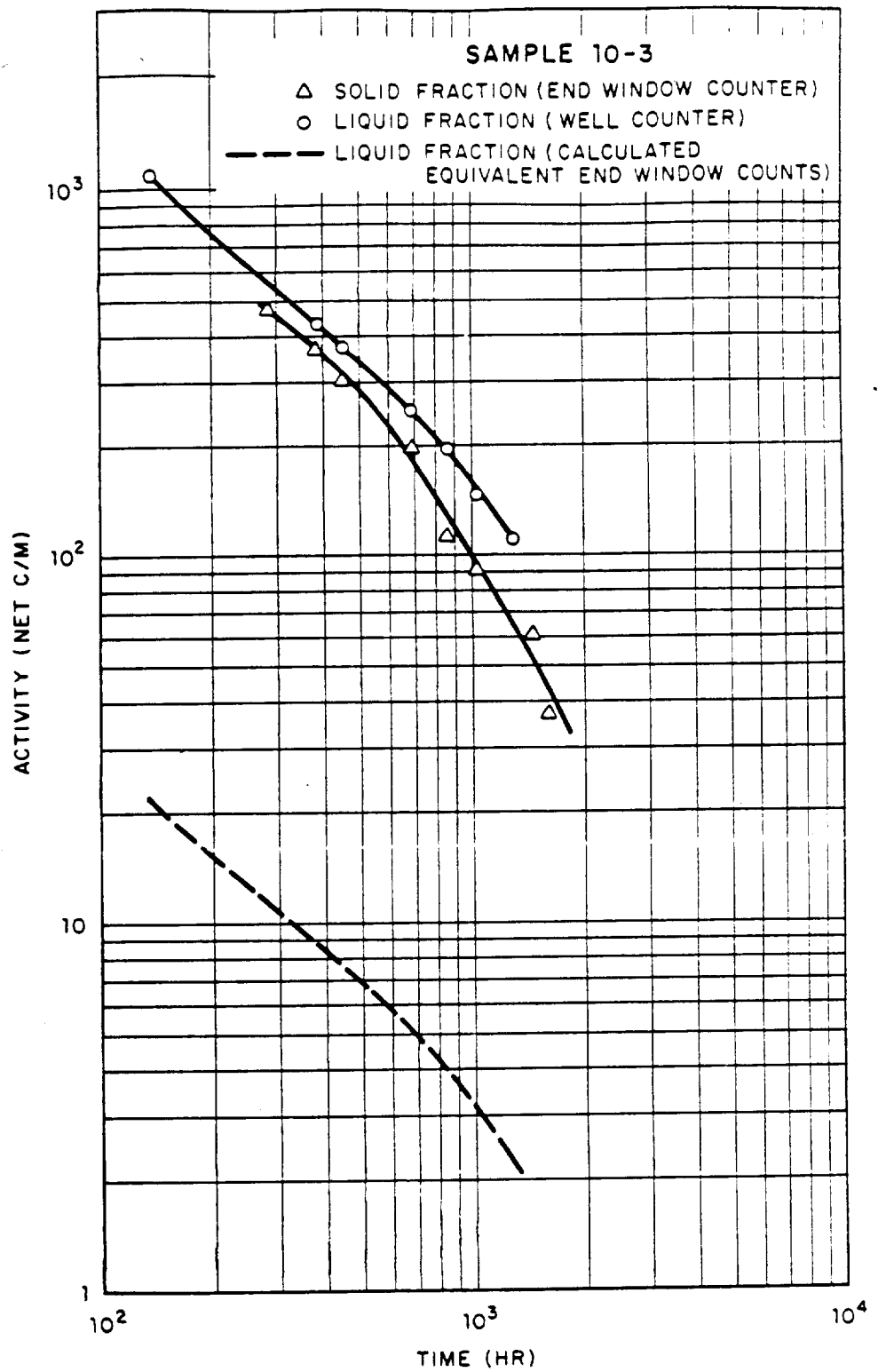


Figure 3.225 Decay of liquid and solid fractions of AFI Sample 10-3, Shot Umbrella.

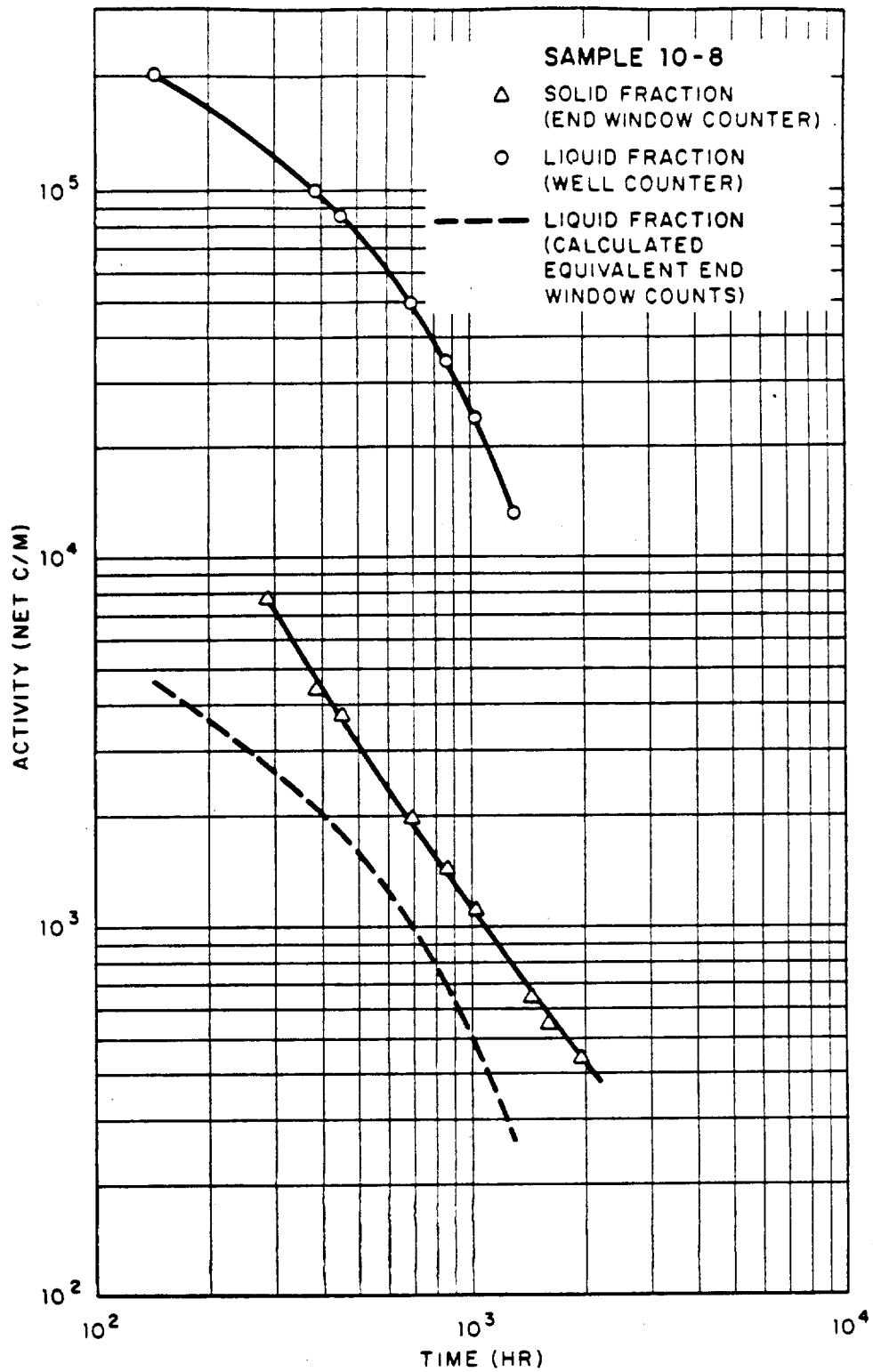


Figure 3.226 Decay of liquid and solid fractions of AFI Sample 10-8, Shot Umbrella.

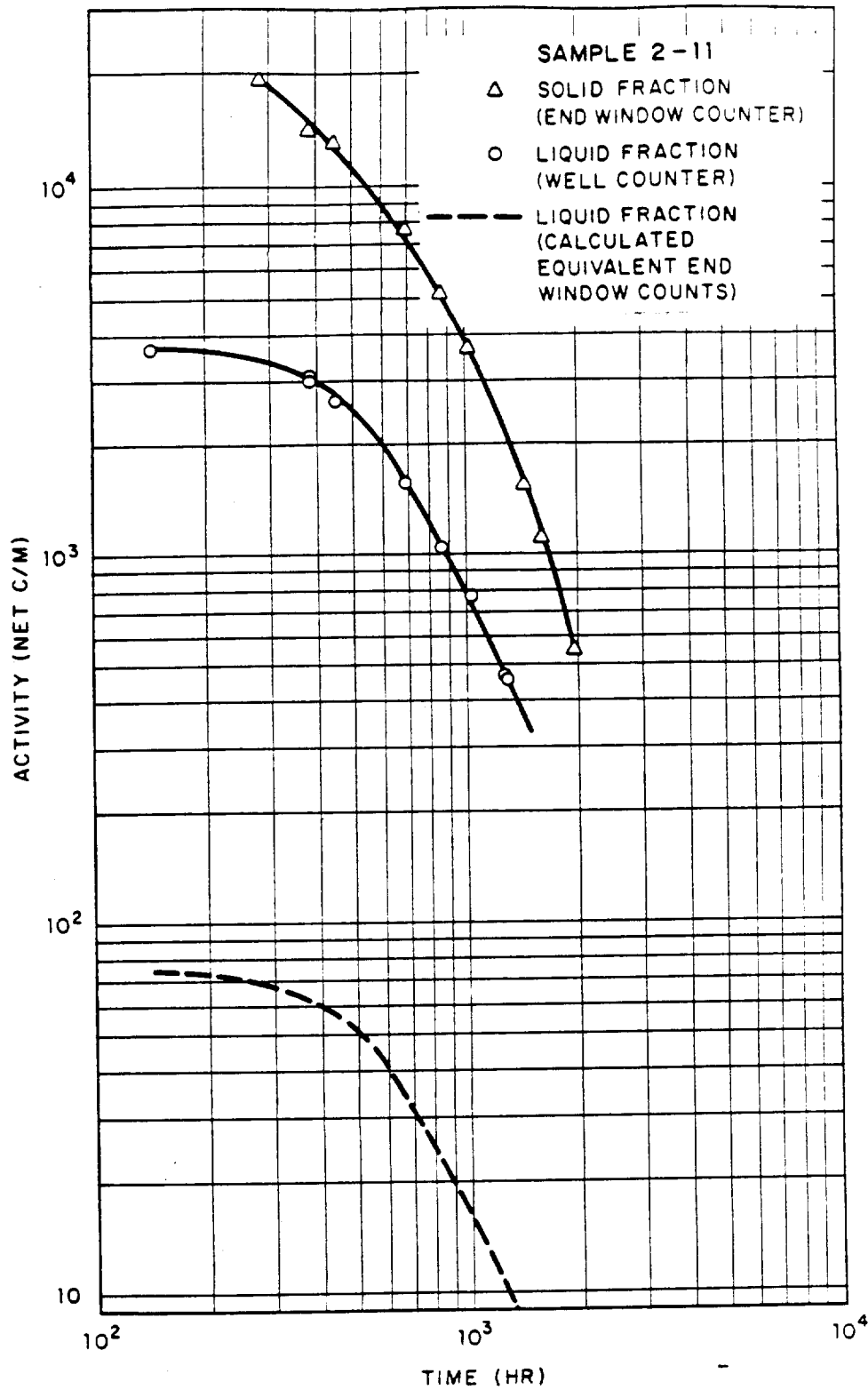


Figure 3.227 Decay of liquid and solid fractions of AFI Sample 2-11, Shot Umbrella.

0502

collected by the AFI. Washdown at first appears to be the only possible source for the liquid fractions collected later than a few minutes after zero time. The data does not, however, support this supposition. Because of the position of the washdown spray nozzles relative to the platform, only a light spray could have reached the AFI—a supposition that is supported by motion-picture photography of the ships under washdown. If washdown were the source, then it should also account for the heavy deposition of radioactive material in the later AFI collections. To obtain active deposits of this magnitude, the water pumped through the washdown system would have to be about 700 times more radioactive than that actually observed in the vicinity of the DD-592 by the early recovery team, which boarded the vessel at about H + 2 hours. Although small areas of such highly radioactive water might exist, any contaminating event of this magnitude caused by washdown at these later times would certainly have registered as a pronounced rise in the GTR dose rate; no such large increase in dose rate was recorded.

Although washdown may have made minor intermittent contributions, a more reasonable explanation of both the liquid and the solid fractions of Samples 10-6, 10-8, 10-9, and 10-10 is that the deposition occurred during the first minute after zero time when Samples 10-1 and 2-1 were collected. Base surge arriving at the DD-592 was traveling at a velocity between 40 and 50 knots (Section 3.3.4) and AFI Samples 10-10, 2-10, and 2-20 were close to the starboard edge of the platform, the side which faced surface zero. The impact of the base surge tore all the Project 2.2 animal cages along the starboard edge out of their mounting brackets and thus could easily have been sufficient to force considerable liquid into closed AFI sampling heads. Both rows of 2-minute sampling heads were shielded from the direct impact of the base surge by the starboard IC collector; however, the 10-minute sampling heads near the starboard edge must have received the full force of the impact. Thus, these later AFI collections are interpreted as additional evidence for a heavy liquid deposition associated with radioactive material occurring during the first few minutes.

The specific activity of the liquid fraction is almost exactly the same for Samples 10-1 and 2-1 and is about the same order of magnitude for all liquid fractions except Sample 10-6 (Table 3.38). Not all AFI samples, however, show a consistent relationship between the total chloride content and the total activity of the liquid and solid fraction. A limited number of chloride analyses (Volhard) were run on selected IC trays, and these show a similar lack of correspondence. Thus, although the individual radioactive droplets are undoubtedly comprised of sea water, large amounts of nonactive sea-water droplets appear to mask any possible relationship between total activity and chloride content.

The specific activity of the solid material recovered from the DMT filter shows wide fluctuation, which may be attributed to the variable inclusion of nonradioactive solids and to the large amounts of activity lost to the walls of the sampling head. The specific activities are not, therefore, considered truly representative and have not been included in Table 3.39. Furthermore, when this solid material is leached with warm water, a considerable proportion of the total weight is found to be soluble. This soluble material, when crystallized, was petrographically identified as salt. Consequently, the approximate concentrations of sodium and chloride ions in the filtrate were determined by flame photometry and Volhard analysis respectively and are summarized in Table 3.39.

The relative activity of the remaining solids and the filtrate could not be determined, since the separation was made too long after the time of detonation. The amount of solid material remaining after leaching could not be determined directly, because the preparation of the sample for particle size work did not permit accurate second weighings. This amount has, however, been estimated as a percentage of the original weight recovered from the filter by assuming that the sum of the sodium and chloride determinations approximate the total weight of material in solution. Since other ions known to be in sea water have not been taken into account, the percentages presented in Table 3.39 are probably high.

Interpretation of the AFI data is made difficult both by apparent sample bias due to the turbulence over the platform and by the high loss of activity to the walls of the sampling head. The material balance for an individual sampling head is good when wall losses are included; however,

TABLE 3.36 SUMMARY OF LIQUID FRACTION MEASUREMENTS

Sample	Collection Interval (min after zero time)	Original Liquid Volume	Final Volume	Well Counter Count for 4 ml Aliquot (22300 14 June)	Calculated Total End-Window Count at 6 Days After Detonation	Specific Activity (end-window at 6 days)	Chloride Analysis of 5 ml Aliquot
		ml	ml	c/ml	c/min	c, ml, ml	m.eq.
10-1	0-10	39	39	417,104	81,000	2,077	2.90
10-2	10-20	dry	25	1,368	-		
10-3	20-30	dry	25	1,080	-		
10-4	30-40	dry	25	1,272	-		
10-5	40-50	dry	25	2,388	-		
10-6	50-60	58 (leaked)	58	16,960	49,200	843	2.90
10-7	60-70	dry	25	1,024	-		
10-8	70-80	19	19	203,024	19,287	1,015	2.92
10-9*	(80-90)?	3	25	26,640	3,330	1,110	3.99
10-10*	(90-100)?	235	235	349,068	410,145	1,745	2.85
2-1	0-2	36	36	412,036	74,167	2,060	
2-2	2-4	dry	25	1,064	-		
2-3	4-6	dry	25	1,176	-		
2-4	6-8	dry	25	1,376	-		
2-5	8-10	dry	25	2,396	-		
2-6	10-12	dry	25	1,012	-		
2-7	12-14	dry	25	1,396	-		
2-8	14-16	dry	25	1,240	-		
2-9	16-18	dry	25	1,284	-		
2-10	18-20	dry	25	872	-		
2-11*	(22-22)?	dry	25	3,716	-		
2-12*	(22-24)?	dry	25	2,090	-		
2-13*	(24-26)?	dry	25	1,634	-		
2-14*	(26-28)?	dry	25	1,040	-		
2-15*	(28-30)?	dry	25	1,060	-		
2-16*	(30-32)?	dry	25	988	-		
2-17*	(32-34)?	dry	25	2,376	-		
2-18*	(34-36)?	dry	25	1,360	-		
2-19*	(36-38)?	dry	25	1,152	-		
2-20*	(38-40)?	dry	25	1,080	-		

\*Note: questionable samples. For full description see text.

TABLE 3-5) SUMMARY OF SOLID FRACTION MEASUREMENTS

Sample	Collection Interval (min after zero time)	Weight of Solids Remaining on DMT Filter	Analysis After Leaching Remaining Solids With 150 ml of Chloroform		Percent Solids Remaining After Leaching (based on NaCl)	Total End-Window Count (1930Z 20 June)	Calculated Total End-window Count at 6 Days After Detonation
			Milliequiv of Na <sup>+</sup> in Filtrate (Flame photometry) (Volhard)	Milliequiv of Cl <sup>-</sup> in Filtrate			
		gms	m.eq.	m.eq.	%	c/min	c/min
10-1	0-10	0.2093	1.8	2.4	39	57,409	114,818
10-2	10-20	0.0086	0.011	0.017	90	307	614
10-3	20-30	0.0241	-	-	-	476	932
10-4	30-40	0.0127	0.10	0.13	46	451	902
10-5	40-50	0.0062	0.033	0.045	62	96	192
10-6	50-60	0.1736	1.7	2.1	35	1,538	3,076
10-7	60-70	0.1561	1.5	1.9	34	1,105	2,210
10-8	70-80	0.1784	-	-	-	7,706	15,412
10-9*	(80-90)?	0.0260	-	-	-	5,074	10,148
10-10*	(90-100)?	1.0261	3.8	5.3	73	50,601	101,202
2-1	0-2	0.6907	2.8	3.5	72	21,836	43,672
2-2	2-4	0.0403	0.35	0.45	40	1,468	2,936
2-3	4-6	0.0328	0.30	0.38	38	5,492	10,984
2-4	6-8	0.0107	0.075	0.097	52	6,534	13,068
2-5	8-10	0.0055	0.010	0.017	85	383	766
2-6	10-12	0.0040	0.017	0.026	67	363	726
2-7	12-14	0.0049	0.017	0.023	75	318	636
2-8	14-16	0.0439	0.26	0.40	54	285	570
2-9	16-18	0.0152	0.11	0.15	49	1,009	2,018
2-10	18-20	0.0125	0.079	0.10	57	4,902	9,804
2-11*	(22-22)?	0.0135	-	-	-	19,236	38,472
2-12*	(22-24)?	0.0199	0.13	0.17	55	4,252	8,504
2-13*	(24-26)?	0.0137	0.10	0.14	46	3,932	7,864
2-14*	(26-28)?	0.0172	0.12	0.16	51	2,214	4,428
2-15*	(28-30)?	0.0073	0.036	0.044	67	1,445	2,890
2-16*	(30-32)?	0.0305	0.24	0.33	44	2,029	4,058
2-17*	(32-34)?	0.0436	-	-	-	9,347	18,694
2-18*	(34-36)?	0.0406	0.34	0.44	33	1,613	3,226
2-19*	(36-38)?	0.0068	0.030	0.041	38	692	1,384
2-20*	(38-40)?	0.0078	0.025	0.041	48	638	1,276

\* Note: Questionable samples. For full description, see text.

53 67

a comparison of the 2-minute and 10-minute series is poor, being particularly so at later times. The AFI data does indicate that large amounts of water were associated with the activity in the base surge during the first minute, after which time the base surge appears to be composed principally of small droplets or nearly dry aggregates of salt slurry. This later stage is suggested by laboratory tests of the DMT filter, which indicate that the filter retains less than 1 percent of the salt contained in clean sea water or in a suspension of Umbrella crater material in sea water. The possibility that the activity in the later AFI samples is simply a general background due to very fine droplets accompanying the initial base surge exists, but it is considered remote.

Microscopic examination of the solid residue from the AFI samples indicated that the size distribution determination originally intended would be largely useless. The material ranged between 10 and 80 microns in diameter and appeared under the petrographic microscope to be largely  $\text{CaCO}_3$  and crystalline salt with a few opaque particles of iron oxide and some siliceous material probably not of device origin. Only one classical iron sphere (Reference 18) was observed; this single sphere was not, however, radioautographed. Spectrochemical analysis of this material confirmed the petrographic findings and also indicated the presence of other elements usually reported in fallout material (see Table 3.40).

As demonstrated by the theoretical considerations in Reference 90, the size distribution of the liquid drops comprising the base surge is undergoing large and rapid changes. The duration of the surge is so short that it is unlikely that equilibrium conditions are attained before deposition. Furthermore, the ambient conditions within the base surge are not precisely known; therefore, their effect on the ultimate particle size distribution cannot be precisely determined. Only instruments that could give some indication of droplet size distribution were the two differential flow collectors installed aboard the DD-592, which were loaded with trays containing special reagent films and a few vertical panels containing similar reagent films (Reference 111). Unfortunately, the amounts of water accompanying the base surge were so large as to render the reagent films unreadable.

Limited size information was obtained from a number of the vertically mounted cellulose acetate sheets installed aboard the DD-593 only. These samples were recovered and returned to NRDL for analysis. Size data was obtained from these sheets using the isopiestic technique described in Reference 112. This procedure is based on the fact that hygroscopic sea-salt clusters will absorb water, if the relative humidity exceeds 75 percent, until the resulting solution reaches a dilution at which the vapor pressure of the drops and the humid atmosphere are equal. Thus, the acetate sheets were placed in an atmosphere maintained at approximately 80-percent relative humidity until the impinged salt particles had absorbed sufficient water to form little hemispheres of solution in equilibrium with ambient conditions. By measuring the volume of these equilibrium hemispheres, the weight of salt deposited on the sheet and hence the equivalent sea-water droplet diameter could be determined. The results of this analysis showed a few large droplets of about 0.5-mm diameter with the preponderance of the droplet diameters being 20 to 40 microns. According to the mathematical analysis in Reference 112, this type of collection would be very inefficient for the collection of droplets less than 10 microns in diameter; therefore, the actual median size for the droplet population may have been considerably less than 20 microns in diameter.

A radioautograph of these sheets showed most droplets to be weakly radioactive. X-ray diffraction of the solids included in these droplets revealed the presence of  $\text{CaCO}_3$  as both calcite and aragonite for Wahoo but only as aragonite for Umbrella. Diffraction also showed evidence of quartz and calcium silicates on both shots. A few water-insoluble crystals (between 10 and 20 microns) that appeared more active than the rest of the material were also found on both shots. No radioactive iron spheres were observed in these samples. The apparent absence of the iron spheres typically associated with tower or megaton-range barge shots should be noted. A few large coral grains were included in the Umbrella droplets, and a number of weakly radioactive filamentous structures were observed on both shots. These fibers were generally insoluble in dilute nitric-hydrochloric acid mixtures but readily soluble in hot nitric-perchloric acid.

TABLE 3.40 SPECTROCHEMICAL ANALYSIS OF SELECTED SAMPLES

Element	Air Filtration Instrument Samples				Coral Soil	Lagoon Bottom (Umbrella crater)
	10-1	10-6	10-10	2-1		
Ag	T	T	T	T	O	T
Al	S	M	S	VS	T	S
B	T	T	T	T	T	T
Ba	W	T	T	T	T	W
Ca	VS	M	S	S	VS	VS
Cr	T	T	T	T	O	W
Cu	W	W	W	W	T	W
Fe	S	S	S	S	T	M
Mg	VS	S	VS	VS	VS	VS
Mn	W	W	W	W	T	W
Mo	W	O	W	T	O	
Na	VS	M	S	S	M	S
Ni	T	O	T	T	O	
P						T
Pb	W	W	W	W	O	
Si	M	W	M	M	W	M
Sn	W	T	W	W	O	W
Sr	M	T	W	W	M	M
Ti	T	T	T	T	O	
V	O	O	T	T	O	
Zn	T	T	T	T	O	

Key: Trace, 0.001 to 0.01 percent; Weak, 0.01 to 0.1 percent; Moderate, 0.1 to 1.0 percent; Strong, 1.0 percent; Very Strong, 10 percent; and O, not detected.

Upon strong ignition, the fibers would char but retain most of their form, turning slowly to a white salt, which was then easily soluble in dilute HCl. The fibers, therefore, appear to be an organic material.

Emission spectra of these droplet residues revealed the presence of macroscopic amounts of aluminum and iron presumably from the device casing. Macroscopic amounts of calcium and magnesium were also observed; these elements are probably due to the inclusion of coralline material and thermally altered sea salts.

In addition to the radiochemical determinations of samples from the destroyers, IC samples from coracles were subjected to the standard analysis for molybdenum (Reference 114). The total fissions determined from  $\text{Mo}^{99}$  analysis are presented in Table 3.41 together with the net activity of the analyzed tray on Shelf 5 of End-Window Gamma Counter 3 (a counter system similar to that described in Section 3.3.1). The data may be used in conjunction with the IC decay data to obtain additional information on the gross fractionation of the fission product mixture, by plotting the change in fission product ratios with time, as described in Reference 115. No consistent variation with time of collection or with distance from surface zero could be established for the total fissions determined from  $\text{Mo}^{99}$  analysis of the IC trays. The lack of a consistent variation with distance is probably due to the fact that the selected IC trays do not represent a total sample. Additional  $\text{Mo}^{99}$  analyses of total samples from Wigwam and Umbrella are given in Reference 105.

Special rapid recovery techniques were also employed to permit early chemical analysis of gross fallout collections for induced  $\text{Cl}^{38}$ . The rapid analytical techniques and a full account of

A theoretical capture-to-fission ratio of 0.0028 has been calculated in Reference 116. The difference between the calculated and observed ratios is believed to be caused by the marked fractionation of the different nuclides used for the fission determinations.

## Chapter 4

### CONCLUSIONS AND RECOMMENDATIONS

Drawing conclusions in a Weapon Test (WT) Report is always a difficult and somewhat hazardous undertaking. Since the primary objective of a WT report is the promulgation of data obtained on a given test series as rapidly as possible, little opportunity exists for critical analysis, yet the drawing of conclusions definitely implies such critical analysis. Furthermore, certain important pieces of information such as a detailed analysis of technical photography are not available at present writing. Despite the lack of time and information, a number of tentative and somewhat general conclusions are possible. Although the temptation constantly exists, both the writer and the reader must be exceptionally careful not to project the partially analyzed data beyond the region of established fact without taking note of the departure. It is emphasized, finally, that all data contained in this report is properly applied only to stationary ships exposed to the specific radiological environments encountered. Any extension of this data to moving ships or to other types of nuclear devices should be recognized as an extension and performed with special care.

#### 4.1 CONCLUSIONS

The gamma records resulting from the passage of airborne radioactive material are sufficiently characteristic so that records from Shots Wahoo and Umbrella can usually be distinguished by inspection, this statement being especially true for downwind locations. The records for Shot Wahoo are unexpectedly complex, showing in one instance at least nine significant peaks in dose rate (Station D 8.0, Figure 3.70). Because of this complexity, the exact time history of dose rate for a given point near surface zero can probably never be predicted for an underwater shot of this nature. The gamma-time-intensity records for Shot Umbrella are relatively simple by comparison. In most instances, the Umbrella records contain a single high peak in dose rate followed at a later time by a prolonged and relatively low increase in dose rate.

The highest recorded dose rate for Wahoo is 42,500 r/hr at 1.63 minutes and at a distance of 4,500 feet downwind of surface zero; that for Umbrella is 200,000 r/hr at 0.32 minute and at 1,760 feet upwind of surface zero, although a maximum dose rate has been estimated by Project 2.1 (Reference 86). In spite of generally higher peak dose rates during Umbrella, the cumulative dose for the entire event is usually larger for a given Wahoo station than for a similar Umbrella station. This difference is probably due to the prolonged nature of the total Wahoo event.

The cloud of airborne radioactive debris contributing the significant fraction of the total radiation is apparently rather low, since an analysis of the gamma records at a number of fixed locations indicates that the surface winds are the principal mechanism of transport at distances greater than  $7,500 \pm 1,500$  feet downwind of surface zero. High-altitude winds and hodographic plotting are, therefore, not required for the prediction of radiological fields resulting from this type of underwater shot. At distances closer than about 7,000 feet, the radioactive material appears to move outward with velocities on the order of 100 ft/sec.—These rates of expansion do not compare well with published fluid-model studies of base surge.

An inspection of the isodose contours for the two underwater shots indicates that gamma doses in excess of 100 r occur within the first 15 minutes at downwind distances less than 16,000 feet from Wahoo surface zero and 14,000 feet from Umbrella surface zero. Since the airborne radioactive material is greatly influenced by the surface wind, the direction of closest approach is from upwind; however, because of the rapid and energetic transport mechanisms that appear to be operative and the possible existence of radioactive remnants trailing behind the receding surge, close approaches should be made with extreme caution. According to the isodose contours, an upwind approach as close as 4,000 feet is possible on either Wahoo or Umbrella without exceeding a 100-r dose. To assure a total free-field dose of less than 25 r, minimum downwind and upwind distances of 30,000 and 5,000 feet for Wahoo and 24,000 and 4,500 feet for Umbrella would have to be maintained. Because of the existence of pronounced lobes, particularly on the Umbrella isodose contours, it may be possible to approach to much closer downwind distances; however, since the exact location of the areas between such lobes of higher dosage cannot be predicted, the larger distances have been quoted.

#### 4.2 RECOMMENDATIONS

Although considerable information concerning the radiological environment associated with underwater nuclear detonations has been obtained, a large number of questions remain unanswered. If any nuclear devices are fired underwater in the future, another attempt to document the radiation fields should be made with instruments specifically designed to obtain more information on the mechanism of base surge formation and its relationship to the observed radiation fields. The differences between Wahoo and Umbrella indicate that depth of burst has a pronounced influence on the radiation fields produced. The similarity between Wigwam and Wahoo suggests that, however, the most extensive changes occur as the depth of burst approaches zero, probably because of differences in bubble stage upon breaking the water surface. Therefore, a series of underwater detonations commencing at the surface and gradually increasing in depth should be fully documented. Such a series could probably consist of fractional-kiloton devices. On all future tests, the density of stations documenting the radiological event should be two to three times that employed by this project. There should be much greater use of film packs, both fixed and floating.

The feasibility of radar spotting of film packs and large elements has been demonstrated and should be used more extensively. Lack of accurate position information was one of the project's greatest difficulties. A second great difficulty is lack of micrometeorological information over the entire area traversed by the base surge. The use of surface wind information provided by a station some 6 miles from surface zero is probably not justified. The problem of complete

micrometeorological documentation is difficult but one which must be solved if any precise analysis of transport mechanism is to be made. Perhaps, radar tracking of a number of reflectors dropped by parachute just prior to zero time could be used to define the microstructure of surface wind currents.

Certain early collections of radioactive material deposited from the base surge suggest that fractionation of fission products is a time-dependent process. On any future underwater detonations, this hypothesis should be carefully investigated. By obtaining a series of discrete samples of base surge during the first 5 or 10 minutes after zero time and by measuring their decay immediately after collection, considerable insight into the problem of fractionation might be obtained. With this information, questions concerning amount and rate of deposition from the base surge could be more accurately answered. These same samples could also be employed to obtain more information on the size of the individual base surge droplet and its variation with time. This information also has a direct bearing on the amount and rate of deposition from the base surge.

More information on the precise mechanism of radial expansion for white water is needed to analyze both the relative importance of this source of radiation and the true magnitude of forces that can be exerted by such an expansion. Photographic evidence suggests that the expansion of white water is due to the rapid overlaying of surface waters by aerated water upwelling around surface zero rather than a more massive toroidal circulation.

Finally, the project recommends that a complete operational analysis for moving ships be made on the basis of the data contained in this report and the final reduced photographic information on surge movement. The procedures for the delivery of nuclear antisubmarine weapons (Reference 3) can then be modified on the basis of this operational analysis.

## Appendix A

### THEORY AND PREDICTION

This appendix contains additional material used primarily for theoretical analysis and prediction of the radiation fields expected from the two underwater detonations. Since this same material is also helpful in the interpretation of some of the results presented in this report, it has been summarized briefly in the following sections.

#### A.1 FACTORS FOR THEORETICAL CALCULATIONS

All factors used in the calculation of the relative contributions to the total gamma field have been tabulated in as compact a form as possible. A more detailed discussion of these factors may be found in the literature cited.

#### A.2 THEORETICAL DEPOSITION FROM A RADIOACTIVE CLOUD

Calculated values of the free-field dose expressed as a percentage of the gross gamma field are presented in Table A.8 for a number of cloud slopes (Section 1.3.1). The values for cloud slopes of 0.17 and 0.05 are also plotted in Figures 1.5 and 1.6.

#### A.3 MODEL FOR AN INCLINED WALL OF APPROACHING BASE SURGE

To analyze the gamma radiation fields due to the base surge, it is useful to deduce the radiation intensity at a stationary detector as it is approached by a radiating cloud of finite thickness whose leading and trailing edges are sloped away from the detector position at a specified angle. The theoretical considerations in Reference 46 and the base surge photography establish this angle at  $60^\circ$ . The direct solution of this problem leads to an intractable analytical expression; therefore, the following geometrical approximations are employed to obtain the desired solution.

An inclined cloud of infinite height and breadth but of finite thickness approaching along the ocean's surface is assumed to continue to infinity beneath the ocean surface (Figure A.3). The radiation intensity from both the real cloud and its imaginary extension below the ocean's surface is exactly that which would be observed at a point a distance  $\sqrt{3}/2 h$  above a slab of homogeneously distributed radioactivity whose thickness is  $\sqrt{3}/2 s$ , where  $h$  is the distance along the ocean's surface to the leading edge of the real cloud. The analytical expression for such a slab is integrable (Reference 39), and the resultant radiation intensity may be computed. If now an imaginary ocean surface is drawn below the true surface so that the surface is a mirror image of the true surface, it is obvious that the radiation intensity due to the real cloud is exactly half that due to the slab of homogeneous activity less the radiation due to the infinitely long trapezoidal strip bounded by the true ocean surface and its mirror image. The radiation resulting from such a strip has been calculated in Reference 119, on the attenuation of gamma radiation by iron plates, if the special case of an iron plate of zero thickness is considered. Thus, by first calculating the radiation intensity from a slab of homogeneously distributed radioactivity then subtracting the intensity due to a trapezoidal strip whose width is  $h$  on the surface toward the detector, and finally dividing the difference by two, the radiation fields due to base surge approaching at an angle of  $60^\circ$  were computed for a number of distances from the leading edge to the detector. The results of these calculations are presented in Section 1.3.2.

The model used is not exact, since in most cases the base surge approaches a given detector as a curved surface; thus, the intensity at a distance  $h$  from the closest point on this curved surface would be less than that from the straight leading edge assumed in the model. The radius of curvature of the base surge front encountered under actual conditions is so large, however, that the difference between these two situations is negligible, particularly when the calculated intensities are used only to compute velocity of approach from the rate of rise of the gamma dose rate record.

#### A.4 WIND CORRECTION FACTORS

The velocity components of the wind along each of the station radii are tabulated for a number of reported surface winds. A plus sign indicates that the velocity component should be added, to compensate for wind effects; a minus sign indicates the reverse procedure. The official surface winds are 15 knots from 090° T for Wahoo and 20 knots from 050° T for Umbrella. The range of surface winds appearing in the following table was selected after inspecting continuous records of the surface wind made at the Eniwetok Weather Station.

During Wahoo, the record fluctuates between 080° and 100° T with speeds between 10 and 15 knots, whereas during Umbrella the variation is between 040° and 070° T with speeds between 10 and 20 knots. A few additional surface wind records have been included from the USS Rehoboth (AGS-50) for Wahoo and the USS Boxer (LPH-4) for Umbrella. The wind speeds reported by the Rehoboth were consistently lower than those reported by the Eniwetok weather station and probably should not be used.

#### A.5 PREDICTED RADIATION CONTOURS

Prior to Shots Wahoo and Umbrella, the radiation contours resulting both from radioactive debris raining out of the cloud and from upwelling contaminated water were predicted. The contours were calculated from data available prior to Operation Hardtack (References 8, 14, 22, 24, 39, and 40) for helicopter operations over radex areas and are presented in Figures A.4 and A.5. The values were determined by calculating the radiation intensity due to deposited material 3 feet above an infinite plane (Reference 22) and then converting this intensity to that which would be expected at 10 feet over a body of water, assuming that all activity is retained in a surface layer 2 meters thick. The 5-r/hr boundary obtained from these calculations was then moved in hourly increments on the basis of available current information for the area (Reference 53). Throughout the calculations, all required estimations were purposely chosen so that fields finally obtained could not reasonably be higher than predicted. The predicted data presented must not be mistaken for actual radiation fields observed after either shot.

TABLE A.3 PERTINENT ATTENUATION COEFFICIENTS

Time After Fission	Average Photon Energy*, E	Total Absorption Coefficients							
		Air		Salt Water		Aluminum + Fiberglass		Styrofoam	
		Mass** Attenuation	Linear Attenuation	Mass** Attenuation	Linear Attenuation	Mass Attenuation	Linear Attenuation	Mass Attenuation	Linear Attenuation
min.	Mev/photon	cm <sup>2</sup> /g	cm <sup>-1</sup>	cm <sup>2</sup> /g	cm <sup>-1</sup>	cm <sup>2</sup> /g	cm <sup>-1</sup>	cm <sup>2</sup> /g	cm <sup>-1</sup>
1	1.212	0.058	6.7 x 10 <sup>-5</sup>	0.063	0.064	0.054	0.14	0.058	1.6 x 10 <sup>-2</sup>
5	1.146	0.059	6.8 x 10 <sup>-5</sup>	0.065	0.066	0.055	0.15	0.059	1.6 x 10 <sup>-2</sup>
10	1.029	0.061	7.1 x 10 <sup>-5</sup>	0.069	0.070	0.060	0.16	0.061	1.7 x 10 <sup>-2</sup>
15	0.974	0.063	7.3 x 10 <sup>-5</sup>	0.071	0.073	0.062	0.16	0.063	1.8 x 10 <sup>-2</sup>
20	0.946	0.065	7.5 x 10 <sup>-5</sup>	0.072	0.074	0.063	0.17	0.065	1.8 x 10 <sup>-2</sup>
25	0.924	0.066	7.6 x 10 <sup>-5</sup>	0.073	0.075	0.064	0.17	0.066	1.9 x 10 <sup>-2</sup>
30	0.914	0.067	7.7 x 10 <sup>-5</sup>	0.074	0.076	0.065	0.17	0.067	1.9 x 10 <sup>-2</sup>
Average	1.02		7.2 x 10 <sup>-5</sup>		0.071		0.16		1.7 x 10 <sup>-2</sup>

\* Values interpolated from data in Table A.1.  
 \*\* Reference 35.

TABLE A.4 GEOMETRIC PARAMETERS OF CORACLE

See Figure A.1.

- a. Radius of dome = 3.5 inches.
- b. Height of dome = 18.0 inches.
- c. Height of center of sensitive volume above deck = 14.7 inches.
- d. Height of center of sensitive volume above water line = 4.06 feet.
- e. Height of center of sensitive volume above keel = 5.29 feet.
- f. Radius of flat coracle deck = 3.66 feet.
- g. Radius of coracle (maximum) = 4.5 feet.
- h. Intersection with water surface of tangent to point of coracle rolloff = 12 feet. Average thickness of absorbing material along stated tangent = 1 inch of fiberglass. Approximate linear attenuation factor = 0.67.
- i. Intersection with water surface of tangent to edge of aluminum case = 8.3 feet. Average thickness of absorbing materials along stated tangent = 46 inches of aluminum plus 0.5 inch of fiberglass. Approximate linear attenuation factor = 0.68.
- j. Intersection with water surface of tangent to edge of Styrofoam = 6.6 feet. Average thickness of absorbing materials along stated tangent = 0.28 inch of aluminum plus 0.5 inch of fiberglass plus 12 inches of Styrofoam. Approximate linear attenuation factor = 0.69.
- k. Radius at water line = 3.8 feet.
- l. Draft (fully instrumented) = 14 inches.

TABLE A.5 BUILDUP FACTORS FOR WATER

From Reference 37.

Number of Mean Free Paths	e <sup>-μx</sup>	Buildup Factor*				
		0.25 Mev	0.5 Mev	1.0 Mev	2.0 Mev	3.0 Mev
μx						
1	0.37	3.3	2.6	2.2	1.9	1.7
2	0.14	7.0	5.0	3.7	2.8	2.4
3	0.05	14.0	9.5	5.5	3.8	3.2
4	0.02	21.0	14.0	7.9	4.9	4.0
5	0.01	34.0	20.0	10.0	6.0	4.7

\* Approximate expressions for buildup factor B with estimation of the validity:

Average Photon Energy:	Expression	Validity:
0.25 Mev	B = (1 + 4.2μx)	Poor
0.5 Mev	B = (1 + 2.6μx)	Poor
1.0 Mev	B = (1 + 1.5μx)	Fair
2.0 Mev	B = (1 + 0.9μx)	Good
3.0 Mev	B = (1 + 0.72μx)	Good

TABLE A.6 GAMMA INTENSITIES OF FINITE CLOUDS EXPRESSED AS A PERCENTAGE OF AN INFINITE CLOUD, 1-Mev GAMMA ENERGY

See Figure A.2.

Number of Mean Free Paths $\mu_A R$	Radius of Finite Cloud		Q*	Percentage of Flux From Infinite Cloud
	m	ft		pct
1	140	459	1.02	41
2	280	918	1.73	69
3	420	1,380	2.15	86
4	560	1,840	2.33	93
5	700	2,300	2.43	97
$\infty$	$\infty$	$\infty$	2.50	100

$$* Q = K \left[ 1 - e^{-\mu_A R} (\mu_A R + 1) \right] - e^{-\mu_A R} + 1$$

TABLE A.7 DIRECTIONAL RESPONSE OF LOW-RANGE STD-GITR DETECTOR

Measuring Solid Angle From Top As 0°				
Increment of Solid Angle From To		Solid Angle Subtended	Average Response Over Increment	Average Response Normalized to Total Response of 1.00
0	20	0.054	1.00	
20	45	0.226	1.02	1.02
45	110	1.061	1.02	
		$\Sigma = 1.341$		
110	135	0.365	0.996	
135	140	0.059	0.970	
140	145	0.053	0.950	
145	150	0.047	0.930	0.97
150	155	0.040	0.905	
155	160	0.034	0.872	
		$\Sigma = 0.598$		
160	165	0.026	0.838	
165	170	0.019	0.805	
170	175	0.011	0.775	0.81
175	180	0.004	0.750	
		$\Sigma = 0.060$		

TABLE A.6 VALUE OF  $I_A$  EXPRESSED AS A PERCENTAGE OF  $I_D$

$I_A$  = free-field gamma intensity.  
 $I_D$  = gross or total radiation intensity.

$$I_D = I_A = 1.54t^{-1.2} \int_{t_0}^t n_A(t) dt \text{ for } V_p = 0.3 \text{ cm/sec}$$

time of arrival =  $t_0$

a*	$(t_0 a)^{-1.2}$	$I_A$	$I_D = I_A$	$I_A/I_D$ (percent)		
				$V_p = 0.30$	$V_p = 3.0$	$V_p = 30$
$t_0 = 1 \text{ minute; cloud slope} = 0.3$						
1.0	1.000	0	0	100	100	100
1.5	0.615	2770	1.067	99.9	99.6	99.3
2.0	0.435	3920	3.01	99.9	99.2	98.9
2.4	0.350	4410	4.75	99.9	99.0	98.3
2.6	0.318	4580	5.64	99.9	98.8	97.9
2.8	0.291	4710	6.52	99.9	98.6	97.2
3.0	0.268	4820	7.43	99.8	98.5	96.6
3.2	0.248	4900	8.23	99.8	98.1	95.9
3.4	0.230	4950	8.87	99.8	97.7	95.3
3.6	0.215	4980	9.34	99.7	97.3	94.4
4.0	0.190	4730	10.0	99.6	96.5	93.2
5.0	0.145	4570	10.4	99.3	93.8	89.6
6.0	0.117	840	10.0	98.8	89.3	85.6
7.0	0.0970	349	9.15	97.4	79.2	27.6
8.0	0.0826	0	8.00	0	0	0
$t_0 = 2 \text{ minutes; cloud slope} = 0.25$						
1.0	0.435	0	0	100	100	100
1.5	0.268	1210	0.921	99.9	99.2	98.9
2.0	0.190	1710	2.63	99.8	98.4	96.6
2.4	0.152	1920	4.12	99.7	97.8	95.3
2.6	0.138	1990	4.90	99.7	97.5	94.1
2.8	0.127	2050	5.70	99.7	97.2	92.8
3.0	0.117	2100	6.50	99.6	97.0	91.4
3.2	0.108	1870	7.14	99.6	96.3	90.2
3.4	0.100	1670	7.70	99.5	95.6	88.5
3.6	0.0934	1480	8.21	99.3	94.7	86.3
4.0	0.0826	1190	8.67	99.2	93.1	82.7
5.0	0.0630	682	9.08	98.6	88.2	82.8
6.0	0.0509	369	8.71	97.7	82.4	29.4
7.0	0.0425	152	8.00	94.9	65.3	15.8
8.0	0.0360	0	6.99	0	0	0
$t_0 = 3 \text{ minutes; cloud slope} = 0.17$						
1.0	0.268	0	0	100	100	100
1.5	0.162	742	0.837	99.8	98.8	98.8
2.0	0.117	1030	2.43	99.7	97.7	97.2
2.4	0.0934	1130	3.80	99.6	97.4	95.6
2.6	0.0850	1220	4.53	99.6	96.4	94.9
2.8	0.0778	1260	5.21	99.5	96.0	94.6
3.0	0.0719	1290	5.98	99.5	95.5	94.3
3.2	0.0664	1150	6.60	99.4	94.5	93.1
3.4	0.0615	1020	7.10	99.3	93.6	91.4
3.6	0.0573	910	7.54	99.1	92.3	89.4
4.0	0.0508	730	8.00	98.9	90.0	87.6
5.0	0.0389	420	8.40	98.0	83.3	28.7
6.0	0.0312	225	8.01	96.5	73.6	21.8
7.0	0.0260	93.6	7.34	92.7	56.0	11.2
8.0	0.0221	0	6.43	0	0	0
$t_0 = 5 \text{ minutes; cloud slope} = 0.10$						
1.0	0.145	0	0	100	100	100
1.5	0.0893	402	0.774	99.8	98.1	95.0
2.0	0.0630	569	2.18	99.6	96.3	92.3
2.4	0.0508	639	3.44	99.4	94.7	89.9
2.6	0.0462	664	4.09	99.3	94.1	88.8
2.8	0.0425	685	4.75	99.3	93.4	87.9
3.0	0.0389	700	5.39	99.2	92.8	86.4
3.2	0.0360	683	5.96	99.0	91.2	84.9
3.4	0.0335	556	6.43	98.8	89.6	83.4
3.6	0.0312	493	6.79	98.6	87.9	81.2
4.0	0.0278	398	7.30	98.1	84.3	77.9
5.0	0.0210	227	7.56	96.7	78.9	73.0
6.0	0.0169	122	7.26	94.3	56.4	14.3
7.0	0.0141	50.8	6.44	89.2	43.3	7.1
8.0	0.0120	0	5.81	0	0	0
$t_0 = 10 \text{ minutes; cloud slope} = 0.05$						
1.0	0.0630	0	0	100	100	100
1.5	0.0389	175	0.674	99.6	96.2	92.1
2.0	0.0278	246	1.90	99.2	92.8	86.2
2.4	0.0221	279	3.00	98.9	90.2	81.1
2.6	0.0200	288	3.55	98.7	89.1	80.7
2.8	0.0195	314	4.38	98.6	87.7	81.7
3.0	0.0189	304	4.69	98.4	86.6	79.3
3.2	0.0185	270	5.14	98.1	83.9	74.3
3.4	0.0183	242	5.59	97.8	81.3	70.3
3.6	0.0182	215	5.87	97.3	78.6	66.9
4.0	0.0180	173	6.30	96.4	73.2	21.4
5.0	0.00915	98.6	6.99	93.7	59.9	13.0
6.0	0.00735	52.9	6.30	89.3	45.5	7.0
7.0	0.00610	20.0	5.75	77.6	25.8	3.0
8.0	0.00520	0	5.05	0	0	0

207

TABLE 1. WIND CORRECTIONS

Nominal Direction	Bearing From SZ	Distance From SZ	Correction Factors* (in knots)						
			Emmett Surface Winds				USS Beizer Wind		
			080°T		090°T		100°T		060°T
15k	10k	15k	10k	15k	10k	7k			
		True	Fc						
<b>Waboo:</b>									
U 3.2	066	3,250	+14.6	+9.70	+13.7	+9.14	+12.4	+ 8.29	+6.79
U 4.0	059	3,100	+14.0	+9.34	+12.8	+8.57	+11.3	+ 7.55	+6.54
U 4.5	066	4,500	+14.6	+9.70	+13.7	+9.14	+12.4	+ 8.29	+6.79
CL 3.9	159	3,900	+ 2.86	+1.91	+ 5.37	+3.58	+ 7.72	+ 5.15	+1.34
CL 4.6	151-1/2	4,600	+ 4.76	+3.17	+ 7.16	+4.77	+ 9.33	+ 6.22	+2.22
DL 7.1	231-1/2	7,100	-13.2	-8.79	-11.7	-7.83	- 9.94	- 6.63	-6.15
DL 12.0	237	12,000	-13.8	-9.20	-12.6	-8.39	-11.0	- 7.31	-6.44
DL 18.3	241	18,000	-14.2	-9.46	-13.1	-8.75	-11.6	- 7.77	-6.62
D 8.0	256-1/2	8,000	-15.0	-9.98	-14.6	-9.72	-13.8	- 9.17	-6.99
D 14.4	247-1/2	14,400	-14.6	-9.76	-13.9	-9.24	-12.6	- 8.43	-6.83
D 24.0	249	23,100	-14.7	-9.82	-14.0	-9.34	-12.8	- 8.57	-6.87
IR 4.8	261	4,500	-15.0	-9.99	-14.9	-9.92	-14.3	- 9.56	-6.99
IR 8.0	263	8,950	-15.0	-9.99	-14.9	-9.92	-14.3	- 9.56	-6.99
IR 14.4	265	14,400	-14.9	-9.96	-14.9	-9.96	-14.5	- 9.66	-6.97
IR 23.1	263	24,000	-15.0	-9.99	-14.9	-9.92	-14.3	- 9.56	-6.99
IRR 6.8	281	6,800	-14.0	-9.34	-14.7	-9.82	-15.0	-10.0	-6.54
IRR 12.8	276	12,800	-14.4	-9.61	-14.9	-9.94	-15.0	- 9.98	-6.73
CR 4.1	336	4,100	- 3.63	-2.42	- 6.10	-4.07	- 8.38	- 5.59	-1.69
CR 5.2	334-1/2	5,200	- 4.00	-2.67	- 6.45	-4.30	- 8.72	- 5.81	-1.87
CR 6.4	332	6,400	- 4.64	-3.09	- 7.04	-4.69	- 9.24	- 6.16	-2.16
<b>Ships</b>									
EC-2	028-1/2	2,300	+ 9.33	+6.22	+ 7.16	+4.77	+ 4.76	+ 3.17	
DD-474	251	2,900	-14.8	-9.88	-14.2	-9.46	-13.1	- 8.75	
DD-592	245-1/2	4,900	-14.5	-9.68	-13.8	-9.10	-12.4	- 8.24	
DD-593	250	8,900	-14.8	-9.85	-14.1	-9.40	-13.0	- 8.66	

Correction Factors* (in knots)							
Emmett Surface Winds				USS Beizer Wind			
040°T		050°T		060°T		070°T	
20k	15k	20k	15k	20k	15k	20k	15k
045°T							
18k							

<b>Umbrella:</b>											
U 1.8	051.8	1,760	+19.6	+14.7	+20.0	+15.0	+19.8	+14.8	+19.0	+14.2	+17.95
U 2.7	067	2,700	+17.8	+13.4	+19.1	+14.3	+19.8	+14.9	+20.0	+15.0	+16.70
U 3.9	068	3,990	+17.7	+13.2	+19.0	+14.3	+19.8	+14.8	+20.0	+15.0	+16.56
CL 3.1	163.7	3,060	-11.1	- 8.32	- 8.04	- 6.03	- 4.74	- 3.56	- 1.29	- 0.960	- 8.64
CL 4.0	158.5	3,990	- 9.54	- 7.16	- 6.34	- 4.76	- 2.96	- 2.22	+ 0.524	+ 0.393	- 7.17
CL 6.0	158.9	6,010	- 9.66	- 7.24	- 6.48	- 4.86	- 3.10	- 2.32	+ 0.664	+ 0.498	- 7.29
DL 6.6	207.5	6,580	-19.5	-14.6	-18.4	-13.8	-16.8	-12.6	-14.6	-11.0	-17.55
DL 6.2	230.4	6,220	-19.7	-14.9	-20.0	-15.0	-19.7	-14.8	-18.8	-14.1	-17.9
DL 16.0	237.1	15,980	-19.1	-14.3	-19.8	-14.9	-20.0	-15.0	-19.5	-14.6	-17.6
DL 18.6	233.5	18,650	-19.4	-14.6	-20.0	-15.0	-19.9	-14.9	-19.2	-14.4	-17.79
D 2.7	248	2,670	-18.6	-14.0	-19.6	-14.7	-20.0	-15.0	-19.8	-14.8	-17.29
D 4.8	247.9	4,770	-17.7	-13.2	-19.0	-14.3	-19.8	-14.8	-20.0	-15.0	-16.60
D 6.5	248	6,500	-17.7	-13.2	-19.0	-14.3	-19.8	-14.8	-20.0	-15.0	-16.55
D 10.4	247.5	10,380	-17.7	-13.3	-19.1	-14.3	-19.8	-14.9	-20.0	-15.0	-16.61
D 15.5	249.1	15,470	-17.5	-13.1	-18.9	-14.2	-19.7	-14.8	-20.0	-15.0	-16.41
D 18.2	250.2	18,220	-17.3	-13.0	-18.8	-14.1	-19.8	-14.8	-20.0	-15.0	-16.30
D 22.0	248	22,000	-17.7	-13.2	-19.0	-14.3	-19.8	-14.8	-20.0	-15.0	-16.55
IR 4.5	263.5	4,530	-14.5	-10.9	-16.7	-12.5	-16.3	-13.8	-19.4	-14.6	-14.05
IR 7.5	265.5	7,530	-15.2	-11.4	-17.2	-12.9	-18.7	-14.0	-19.7	-14.7	-13.68
IR 12.2	266.5	12,230	-14.5	-10.9	-16.9	-12.6	-18.5	-13.9	-19.5	-14.6	-14.29
IR 18.6	261	18,600	-15.1	-11.3	-17.1	-12.8	-18.7	-14.0	-19.6	-14.7	-14.58
IR 23.2	264.5	23,240	-14.3	-10.7	-16.5	-12.4	-18.2	-13.6	-19.4	-14.5	-13.84
IRR 3.9	279.1	3,940	-10.3	- 7.70	-13.1	- 9.82	-15.5	-11.6	-17.5	-13.1	-10.57
IRR 6.7	278.1	6,740	-10.6	- 7.92	-13.4	-10.0	-15.7	-11.8	-17.6	-13.2	-10.80
CR 2.7	340.9	2,670	+10.0	+ 7.53	+ 6.88	+ 5.16	+ 3.50	+ 2.62	+ 0.035	+ 0.026	+ 9.00
CR 4.9	334	4,930	+ 8.14	+ 6.10	+ 4.84	+ 3.63	+ 1.40	+ 1.05	- 2.08	- 1.56	+ 5.86
CR 6.6	337.3	6,610	+ 9.28	+ 6.88	+ 5.94	+ 4.46	+ 2.54	+ 1.90	- 0.942	- 0.706	+ 6.83
<b>Ships</b>											
EC-2	158	1,650	- 6.84	- 5.13	- 3.48	- 2.61	0	0	+ 3.48	+ 2.61	- 4.65
DD-474	245.7	1,900	-17.9	-13.4	-19.2	-14.4	-19.9	-14.9	-19.9	-15.0	-16.76
DD-592	248.5	3,000	-17.8	-13.4	-19.1	-14.3	-19.9	-14.9	-15.0	-15.0	-16.71
DD-593	249.2	7,900	-17.7	-13.3	-19.1	-14.3	-19.8	-14.9	-20.0	-15.0	-16.64

\* Use signs as given to obtain wind corrected velocities.

278

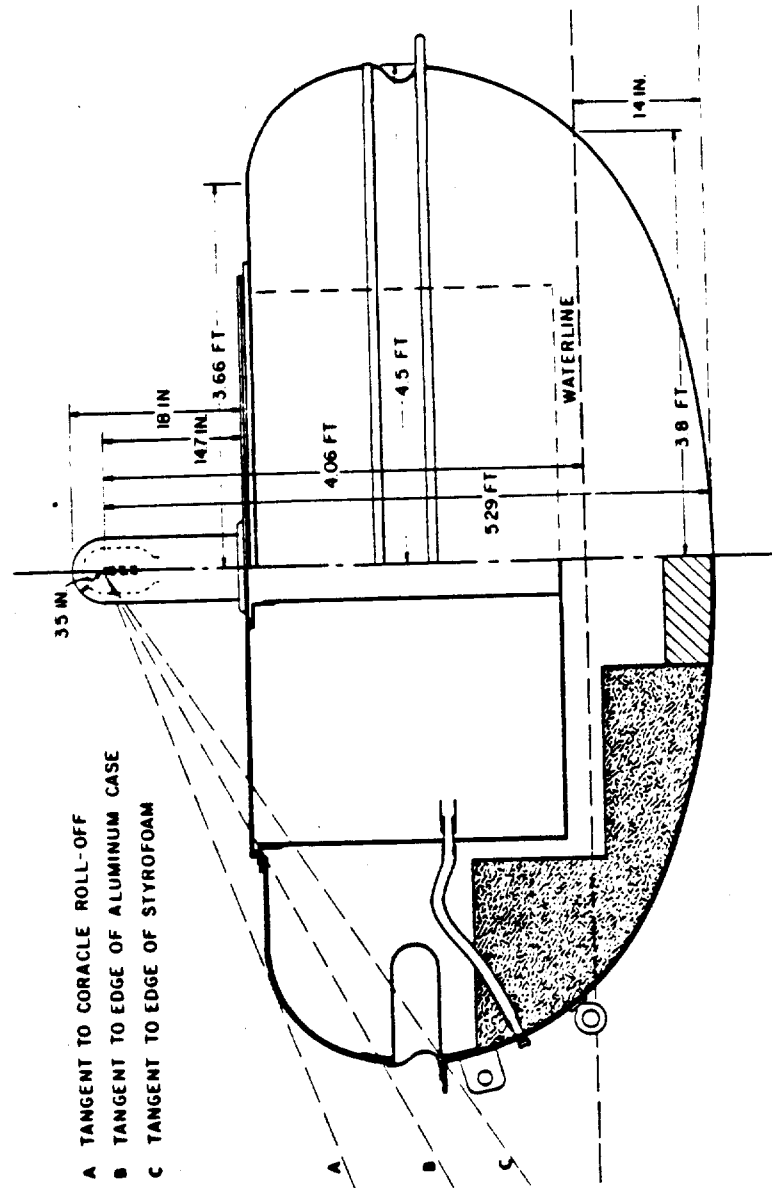


Figure A.1 Coracle dimensions.

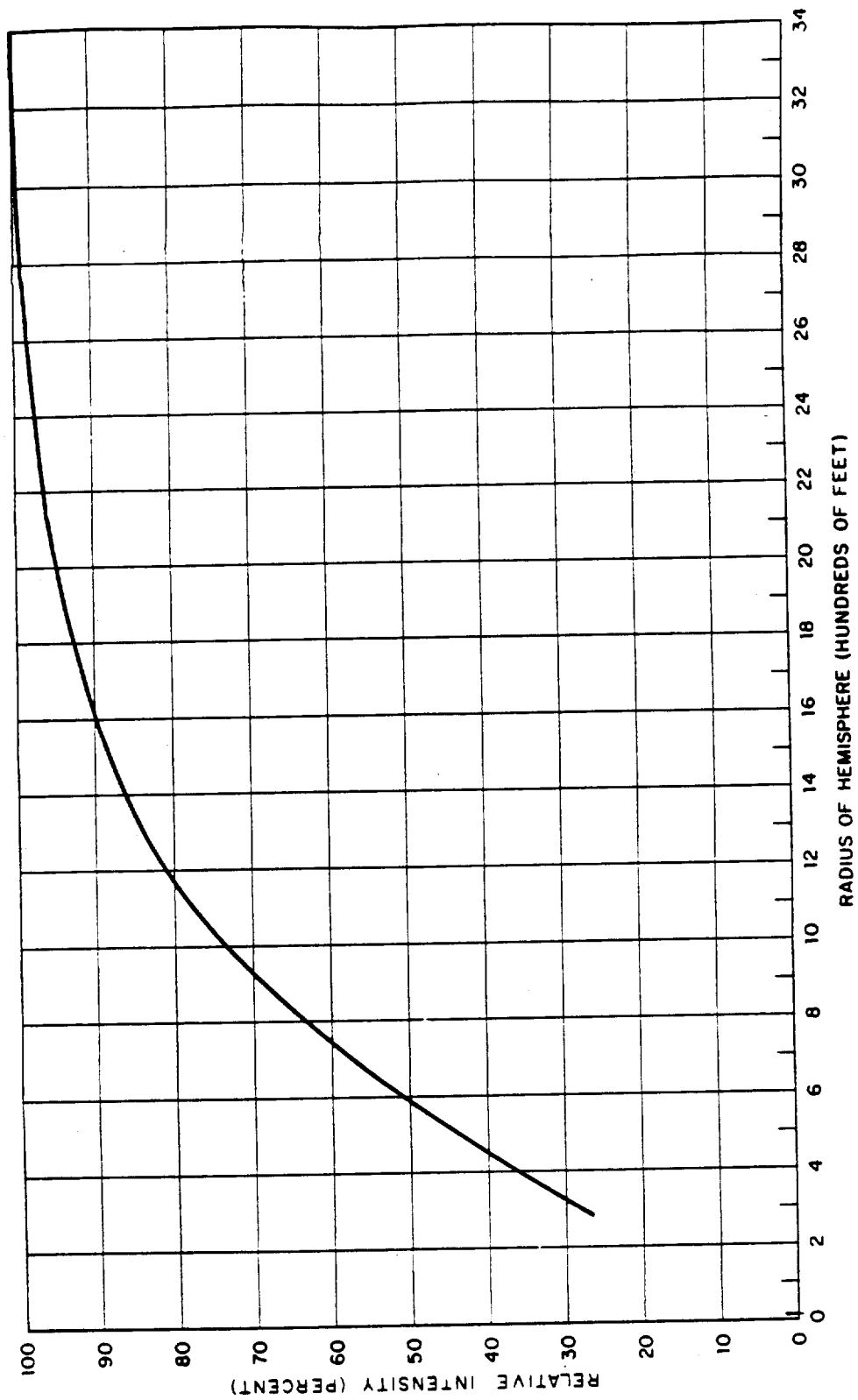


Figure A.2 Relative gamma intensity for finite hemispheres of uniformly distributed activity (1 Mev gamma energy).

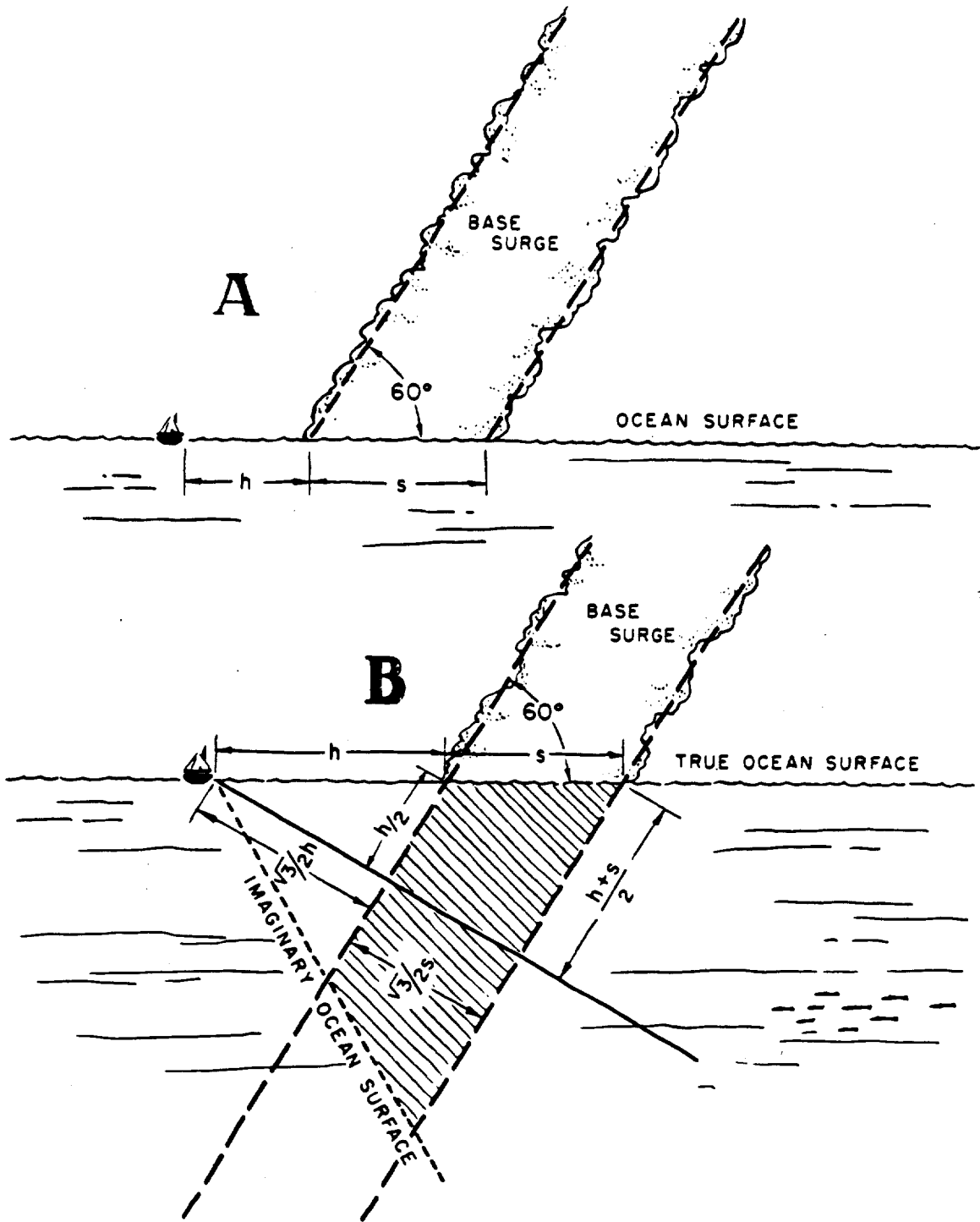


Figure A.3 Diagram of 60° cloud model.

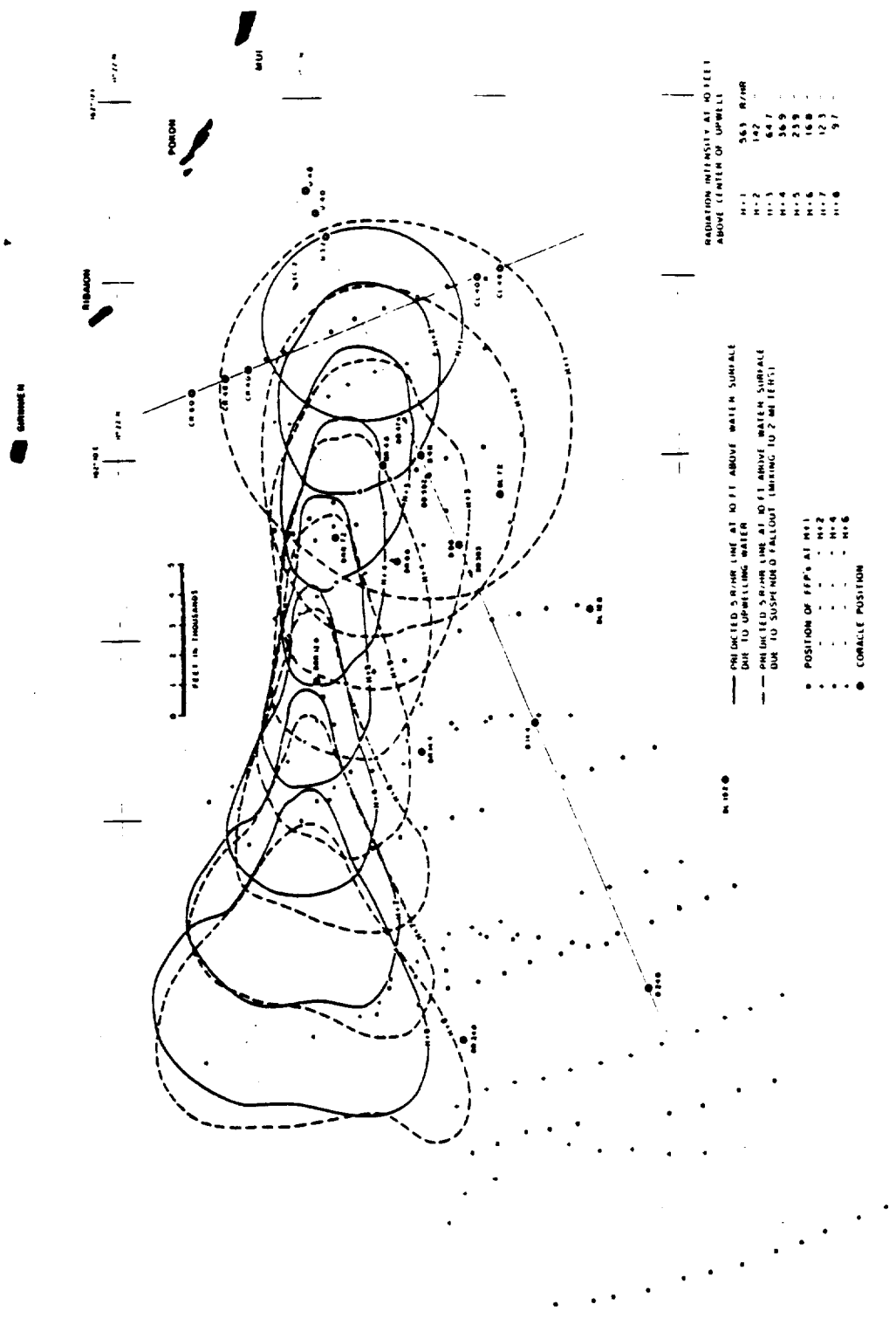


Figure A.4 Proposed array including FFP positions and predicted radiation fields, Shot Wahoo.

236



## Appendix B

### INSTRUMENTS AND DECAY

This appendix contains a detailed description of the detecting instruments of primary importance to the project, together with certain early-time decay curves used throughout the body of this report. This information is not currently available in the literature.

#### B.1 INSTRUMENTS

Since the GTR 103 is basic to the project, it is described in greater detail. This instrument is a dose-increment recorder consisting of: (1) two concentric ionization chambers with recycling electrometers, (2) a magnetic-tape recorder, (3) a mechanical timer, and (4) a control circuit and a battery power supply (Figures 1.4 and B.1). The externally mounted detector unit is connected to the main instrument assembly within the case itself.

The detector consists of a low-range ionization chamber constructed around a high-range ionization chamber, with each chamber connected to a recycling electrometer. These electrometer circuits use a CK 5886 tube connected as a cathode-coupled blocking oscillator with the interelectrode capacity of the first grid below the predetermined triggering level of the positive voltage shift on the first grid (Figure B.2). When a predetermined voltage level is reached, the circuit is triggered and generates a pulse of fixed amplitude at the cathode. The pulse causes the first grid to conduct and to transfer a constant, predetermined charge to the chamber. Simultaneously, the pulse is recorded on magnetic tape. The pulse terminates at the cathode in approximately 500  $\mu$ sec, and the tube is left nonconducting with a negative voltage on the first grid, thus completing the cycle.

The gamma dose increment required to discharge the ionization chamber is directly proportional to the amount of charge transferred to the chamber (Figures B.3 and B.4). The charge transferred during each cycle is constant but dependent upon the triggering level of the electrometer, which is controlled by the adjustable bias voltage of the second grid. Calibration of detectors is achieved by adjustment of the bias voltage until a predetermined dose increment causes the electrometer to cycle (Section C.1). The calibration control for each chamber is located on the moistureproof electrometer housing attached to the base of the chamber assembly.

The ionization chambers are constructed of thin-walled spun-aluminum shells mounted concentrically. Cylindrical and hemispherical surfaces are used wherever possible to establish optimum voltage gradients for efficient charge collection. The chambers are filled with pure argon at 7.5 psi and sealed by softsoldering over nickel-plated surfaces. The volumes of the two chambers are 1.475 and 14.0  $\text{cm}^3$  for the low-range and high-range chambers, respectively. The sensitivity ratio of 1,000 between the two ranges is achieved by the design value of the input capacity of the electrometer circuits. A lead-tin filter over the entire outer surface of the detector provides uniform energy response from about 100 kev to 2 Mev (Figure C.1).

The record is made on 900-foot lengths of instrumentation-quality magnetic tape spooled on standard 5-inch reels. The tape is 0.25 inch wide and has a polyester backing 0.001 inch thick. A Brush Electronic Company BK 1303-1 three-channel recording head, driven to tape saturation, records unidirectional pulses on the tape. The maximum usable pulse packing is 400 pulses per inch of tape. Recording intervals of 12 hours and 60 hours are used with tape transport speeds of 0.25 in/sec and 0.05 in/sec, respectively. These speeds are accurate to  $\pm 2$  percent for the entire recording interval. Both recorders are of identical construction with the exception of the drive motors. A single 6.7-volt mercury-battery stack having a

capacity of 14,000 ma-hr powers each recorder. The 12-hour recorder is driven by a 2-watt motor operating at a speed of 6,000 rpm and regulated by a centrifugal governor. A 0.75-watt, chronometrically governed motor rotating at 900 rpm operates the 60-hour recorder. Both recorders utilize gear reduction and worm-gear drive. The tape is guided in the conventional manner. Metal friction plates on the feed spindle establish an average tape tension of about 4 ounces. Contacts on the recorder turn off the instrument when a conductive section of tape at the end of the reel passes over them causing a circuit closure. Both recorders were developed at NRDL in conjunction with the Precision Instruments Company, San Carlos, California.

The dose increments chosen for the low- and the high-range ionization chambers are 0.243 mr and 0.243 r, respectively. As radiation data is recorded on the two channels of the three-channel tape, pulses are recorded on the third channel at 3.75-second intervals to establish a time reference for data reduction. The time pulses are generated by a cam-operated switch driven by a low-power, 6-volt chronometrically governed motor. The accuracy of these pulses is  $\pm 0.5$  percent. The timer is manufactured by the Haydon Company and is used because of its known accuracy and high reliability.

The function of the control circuit is to start and stop the instrument. Power to all the motors and to the filaments is controlled by means of a latching relay. This relay can be activated locally by a switch on the instrument or remotely by a contact closure through a cable into the instrument. The instrument can be turned off by deactivation of the relay with the switch on the instrument or by the tape-actuated turnoff switch on the recorder.

Mercury batteries are used to power the motors and the filaments, to take advantage of the high current capacity and flat-discharge characteristics these batteries offer. In addition, a mercury battery with very low current drain is used in the electrometer-calibration circuit to restrict calibration shift to less than  $\pm 1$  percent during the expected life of the battery. Chamber bias and transistor bias are supplied by carbon batteries. With the exception of the motor battery, the minimum battery life is in excess of 250 hours. However, the 12-hour recorder can be operated in excess of 26 hours and the 60-hour recorder in excess of 80 hours without a battery change.

All components are designed to operate under the following maximum conditions: (1) a shock of 15 g for 11 msec in all planes, (2) vibrations of 12 g at frequencies up to 45 cps in all planes, (3) temperature within the detector of 120° F, (4) temperature within the main instrument assembly of 155° F, (5) ambient relative humidity of 100 percent, and (6) a static overpressure of 5 psi. During the operation, satisfactory performance beyond these limits was frequently observed.

## B.2 DECAY CURVES

Throughout this report, the ionization chamber decay curve in Reference 89, extrapolated to early time by means of data in Reference 36, has been used repeatedly and has been referred to as the standard decay curve. Since this entire curve is not available in a single reference, it is reproduced here (Figure B.5). In addition to the standard decay curve, the crystal decay curve of Reference 120, the gamma intensity decay unit (GIDU) decay curve (Figure B.6), and the IC decay curve S-IV (Section 3.3.1) have also been reproduced in Figure B.5. The GIDU was installed aboard the DD-592 where it collected a total sample of deposited material for the first 4 minutes after zero time. This total sample was then conducted into a shielded chamber where a GTR immediately started recording decay. The design and operation of this unit is more fully described in Reference 86; however, the Umbrella decay from 6 minutes is included in this report for comparison with other decay curves (Figure B.6). For very early times, the decay curve of Reference 87 is used and is also reproduced here for greater convenience (Figure B.7).

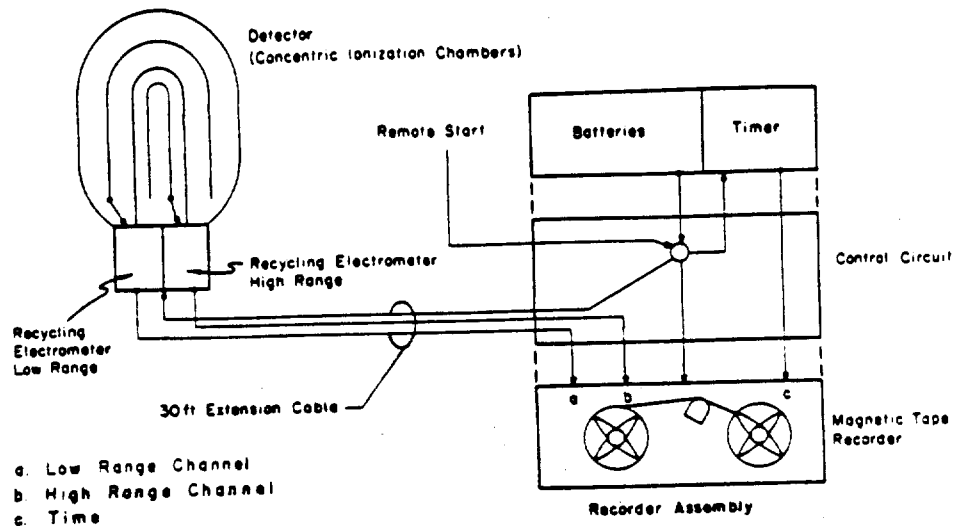


Figure B.1 Block diagram of GTR 103 with remote detector.

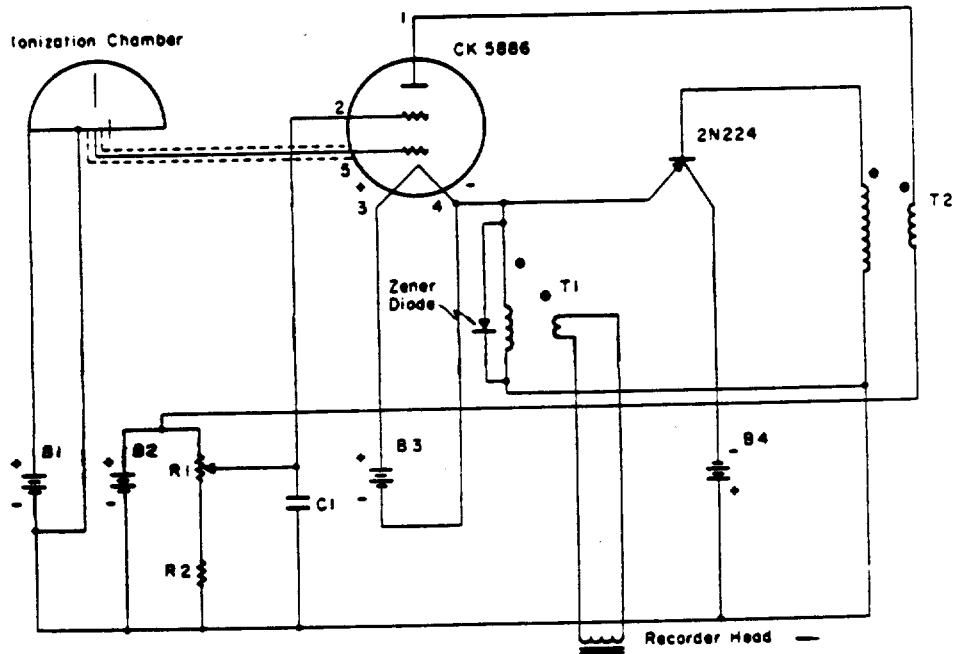


Figure B.2 Simplified schematic diagram of GTR 103 recycling electrometer.

336

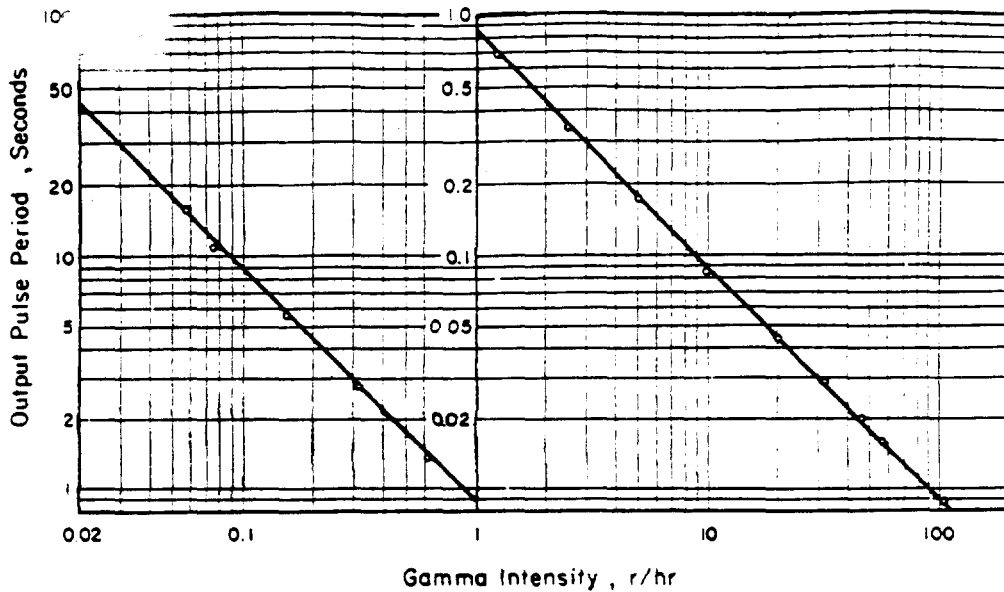


Figure B.3 GITR 103 low-range detector output pulse period as a function of gamma intensity for  $\text{Co}^{60}$  and  $\text{Cs}^{137}$ . The longitudinal axis of the detector and the beam are parallel, and the electronics housing is directed away from the source.

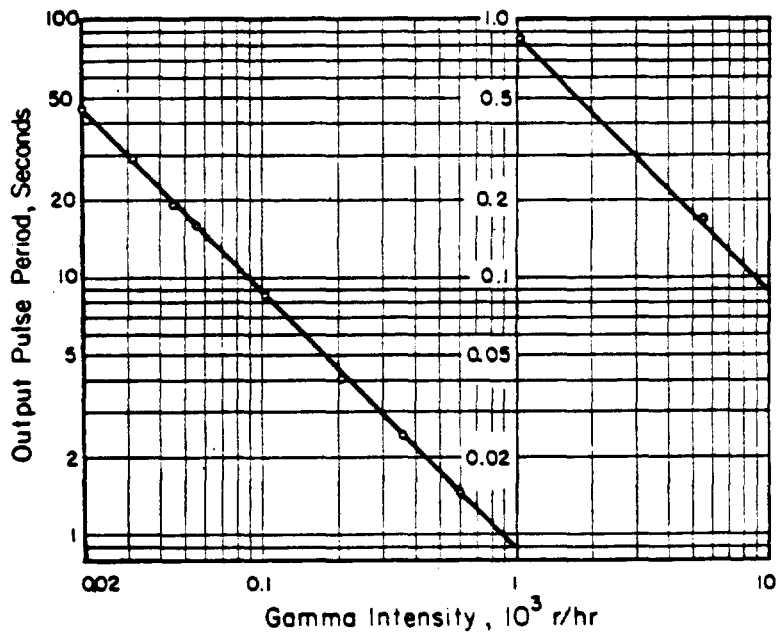
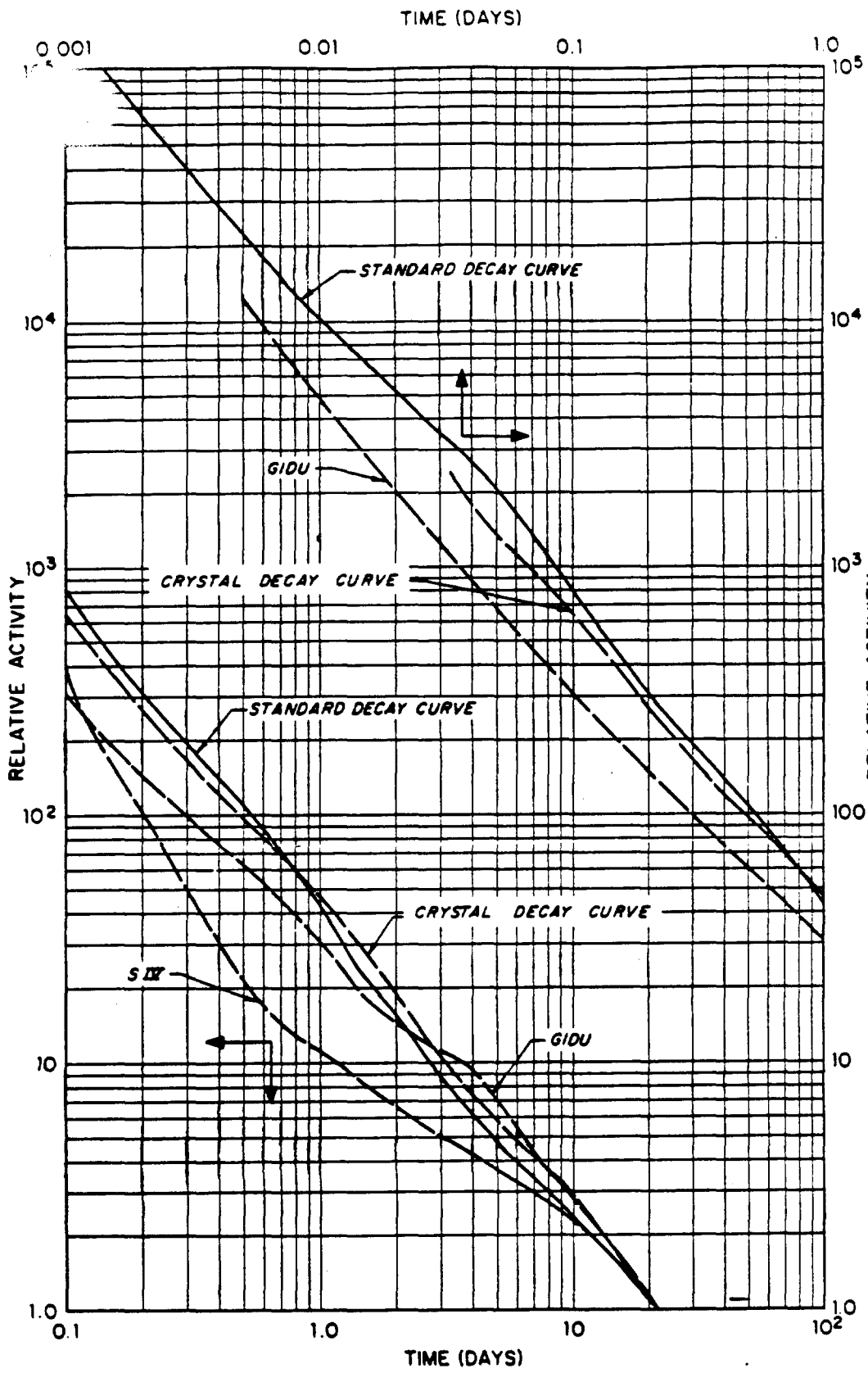


Figure B.4 GITR 103 high-range detector output pulse period as a function of gamma intensity for  $\text{Co}^{60}$  and  $\text{Cs}^{137}$ . The longitudinal axis of the detector and the beam are parallel, and the electronics housing is directed away from the source.

227



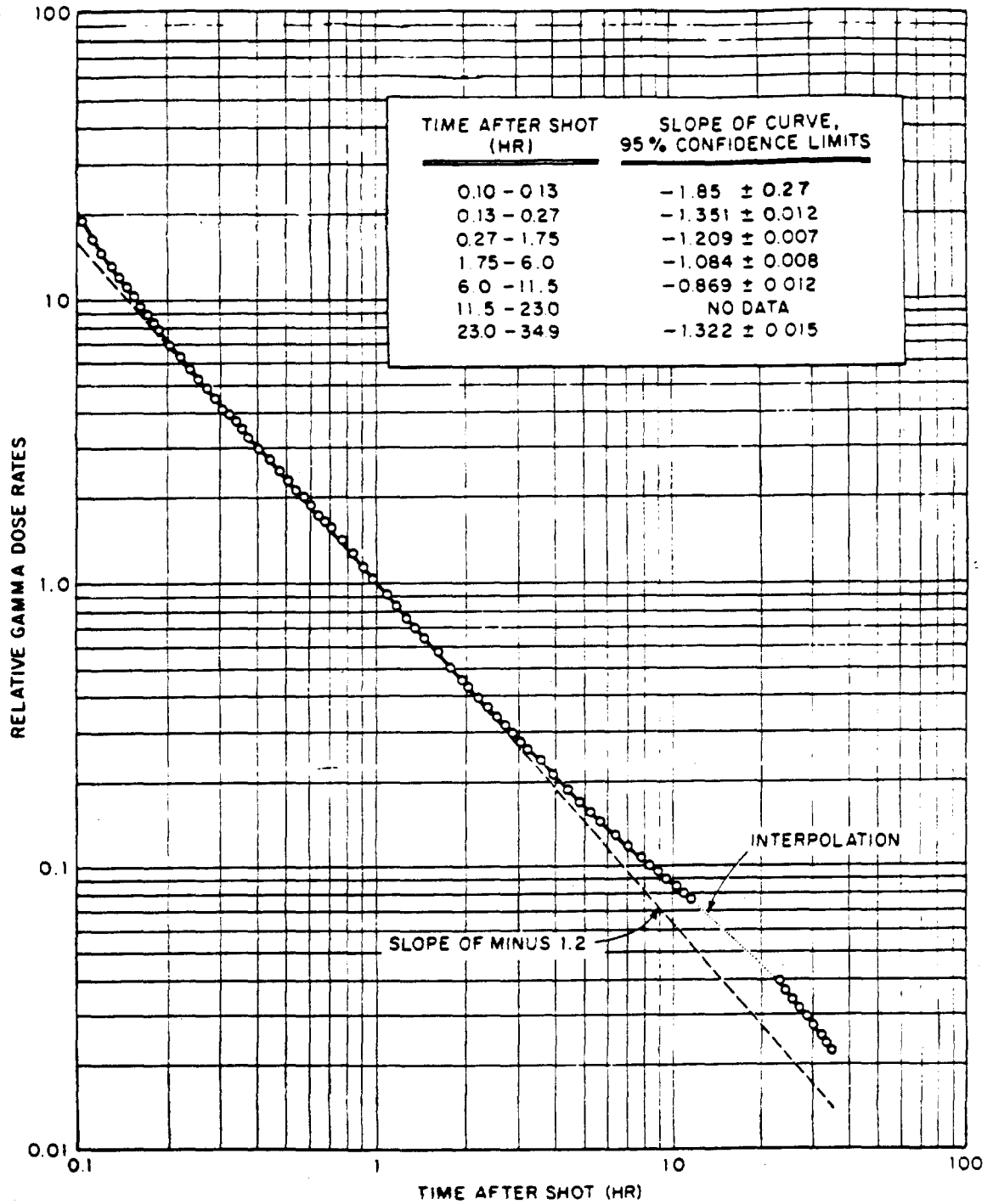


Figure B.6 Early decay determined by GIDU aboard DD-592.

207

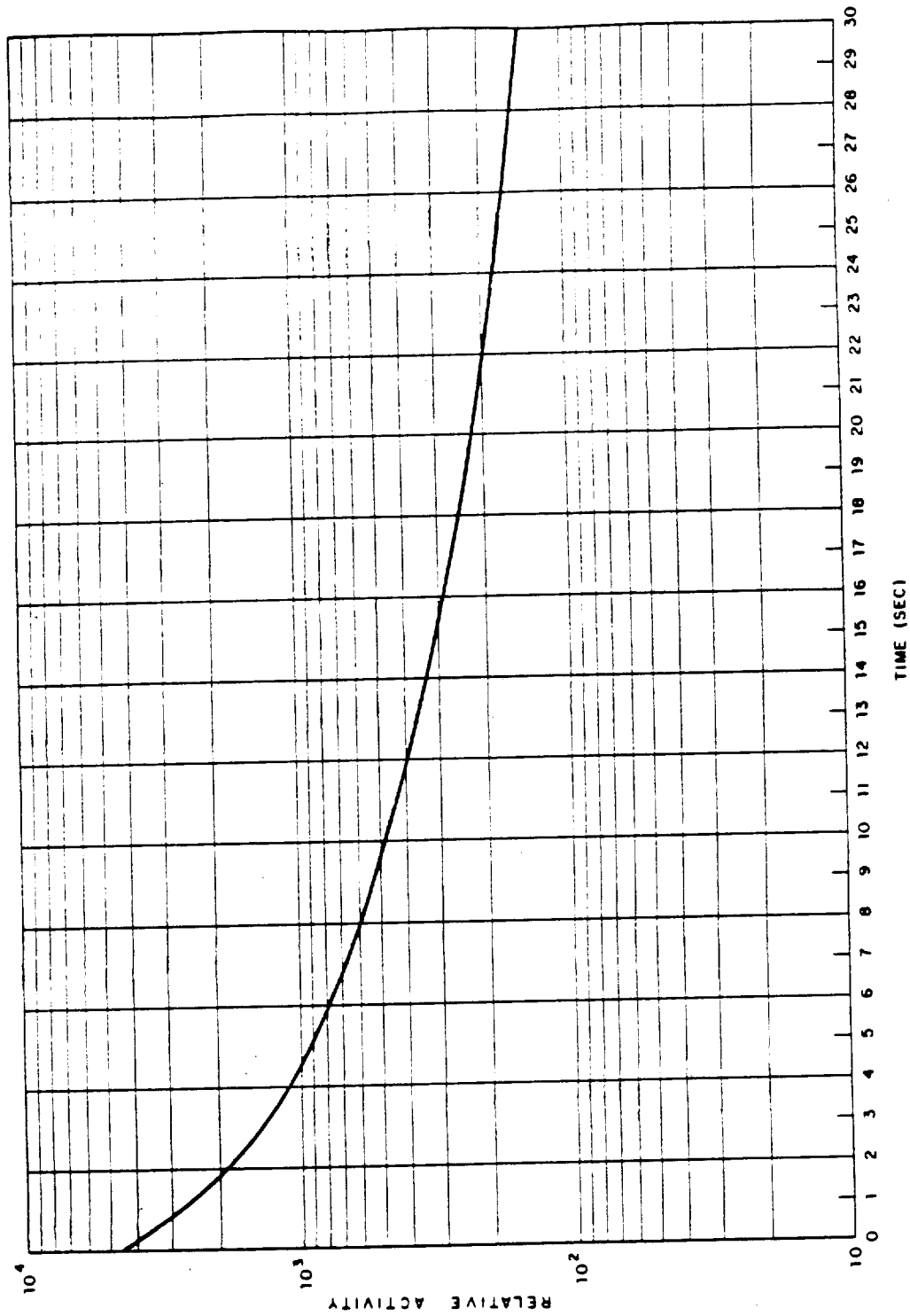


Figure B.7 Scintillation counter decay of fission products following thermal neutron fission of  $U^{235}$  (abstracted from Reference 87).

## Appendix C

### CALIBRATION AND RESPONSE

This appendix contains a more detailed description of all calibration procedures and response factors used by the project. Some of this material appears in separate reports but has been gathered together here for greater convenience.

#### C.1 STANDARD GITR CALIBRATION AND RESPONSE

All GITR detectors were calibrated at NRDL with  $\text{Co}^{60}$  sources standardized to within 3 percent. Calibration was performed with the detector in a standard orientation, the longitudinal axis of the detector and the beam parallel with the electrometer housing facing away from the source (source at  $0^\circ$ ).

The energy response of the detectors was determined at NRDL, using  $\text{Co}^{60}$  and  $\text{Cs}^{137}$  sources and broad-beam X-rays with effective energies of 180, 120, 70, and 35 keV. The response is uniform within 10 percent from approximately 100 keV to 2 MeV when the detector is surrounded by 0.13 inch of aluminum (Figure C.1). The directional response of the detectors was also determined by using these sources. Typical directional responses for the std-GITR and the UW-GITR are reproduced in Figures C.2 and C.3 for rotation about an axis orthogonal to the longitudinal axis of detector. Rotation about the longitudinal axis produces a completely uniform response.

Optimum reliability and accuracy was assured by recalibrating each detector before and after each shot with a 120-curie  $\text{Cs}^{137}$  source installed in a trailer specially designed for the purpose. This source was standardized to the  $\text{Co}^{60}$  sources by means of a Victoreen 70-A R-meter and various calibrated chambers. Maximum reproducibility was assured by using a jig that exactly positioned each detector in the calibration beam in a radiation field of 57.0 r/hr. The calibration radiation pulse output of the detector was then adjusted to a period of 0.016 and 15.5 seconds for the low-range and the high-range channels, respectively. The low-range period of 0.016 second (instead of 0.0155 second) compensated for the 0.5-msec recycling time of the detector electrometer circuit. The calibration field was too low to permit a similar compensation for the high-range chamber. All calibrations are estimated to be accurate within 5 percent for the period of use between preshot and postshot calibration.

#### C.2 ASEL-GITR CALIBRATION AND RESPONSE

The directional response of the ASEL detectors was determined at NRDL, using an X-ray beam that peaks at 120 keV. The corrected output of the X-ray was 2,100 r/hr, and the precise energy of the 120-keV beam is given in Figure C.1. Typical directional responses for rotation about and orthogonal to the longitudinal axis of the high- and low-range ASEL detectors are presented in Figures C.4 through C.7.

The basic calibration and energy response of each detector was determined at ASEL. A typical energy response for the ASEL detector is given in Figure C.8. The dose rate response from 40 r/hr to  $10^7$  r/hr was determined for all detectors, using X-ray and Van de-Graaf sources. At EPG, the lower range of these dose rate responses was rechecked for all detectors on 2 May and again on 22 May, using a 200-curie  $\text{Co}^{60}$  source with a  $15^\circ$  beam. This source produced a maximum field sufficiently uniform for calibration to 8,000 r/hr. A typical dose rate calibration curve for a high-range detector is reproduced in Figure C.9. The radiation pulse data

for detector was converted to dose rate, using such a curve specifically determined for each detector.

### C.3 END-WINDOW GAMMA COUNTER RESPONSE

The relative response for a point gamma source on the fifth shelf of End-Window Gamma Counter 2 is given in Table C.1 and plotted in Figure C.10. Without a detailed knowledge of the energy spectra of the samples counted and without a complete analysis of distributed source effects, the energy response presented cannot be applied to the measurements obtained for the IC trays with an accuracy greater than  $\pm 30$  percent. Assuming an average energy of 0.7 Mev at the time of counting, the efficiency of the End-Window Gamma Counter 2 was probably between 0.25 and 0.45 percent.

### C.4 FILM CALIBRATION

All films used in the NBS film holders were recalibrated at EPG, using a 200-curie  $\text{Co}^{60}$  source. Control films were exposed over a period extending from H+1 to H+31 for Wahoo and from H-22 to H+8 hours for Umbrella, and the development of all film was delayed until at least H+144, to reduce possible errors due to latent image fading. The calibration curves used to interpret Wahoo and Umbrella film densities are given in Figures C.11 through C.14.

All film densities were determined with an Eberline FD-2 film densitometer; however, the conversion from density to gamma dose was done manually, using the curves given. The energy response of these films in the NBS holders has been determined in Reference 121, and a summary of the results is presented in Figures C.15 and C.16. The directional response was consistent with data given in Reference 63.

### C.5 EMPIRICAL CORRELATION BETWEEN STD-GITR AND IC

In the event of heavy deposition from the base surge, the free-field dose rate might have to be estimated from the gross gamma dose rate; the relative contribution from material deposited on coracle and detector surfaces being known. Therefore, an empirical relationship was established between a known distribution of radioactive material per unit area on the coracle surfaces, as indicated by the IC, and the resultant total field measured by the std-GITR. This conversion factor was determined by some preliminary experiments prior to departure for EPG; but, since the relative contribution from deposited material appears to be small, no detailed evaluation of the conversion factor has been attempted.

Deposition from base surge was simulated by spraying a  $\text{La}^{140}$  slurry over the upper section of a coracle. The technique of spraying relatively uniform deposits of radioactive material over various surfaces has been previously developed by NRDL (References 122 and 123). The project made use of the facility established at Camp Stoneman, California. The upper section of a coracle, including the instrument well and all instruments, was mounted on roller tracks so that the sensitive volume of the std-GITR detector was exactly 4.06 feet above the concrete floor (the expected distance for the detector above the ocean surface). The scattering and albedo data for concrete (References 124 and 125) indicated that the backscatter from the ocean surface for 1-Mev gammas was closely approximated by the concrete floor at this distance. The coracle with its assemblage of instruments in operation was then drawn through the spray system, which deposited a known amount of  $\text{La}^{140}$  slurry over all coracle surfaces. The coracle was then removed from the spray area, and the resultant gamma field was measured first with the GITR in the normal coracle position and then at various distances above the coracle deck. The IC trays that collected the  $\text{La}^{140}$  slurry were recovered immediately and counted on Shelf 5 End-Window Gamma Counter 2, the same counter used for all subsequent IC tray counts in EPG (Section 3.3.1). The IC tray counts, corrected for coincidence loss and decay, were used to determine the ratio between the IC counts and the GITR record (Figure C.17). This relationship was determined to be:

$$I_{\text{GITR}} = \beta C_{\text{IC}}$$

where  $I_{\text{GITR}}$  is the radiation intensity (r/hr) due to deposited activity,  $C_{\text{IC}}$  is the gamma activity (C/min) of the IC tray determined on Shelf 5 of End-Window Gamma Counter 2 and corrected to time of deposition, and  $\beta$  is a constant empirically determined to be  $0.71 \times 10^{-7}$ .

If this data had been required for an interpretation of the Hardtack data, energy corrections would have been required and it would have been necessary to repeat the preliminary experiment with greater precision. It is used in this report to convert IC tray counts at 22 days to a std-GITR response for the sole purpose of establishing the approximate magnitude of the maximum dose rate due to deposited radioactivity. Since an analysis of the material deposited from the base surge after either shot (Reference 105) showed considerable enrichment in  $\text{Ba}^{140}$ - $\text{La}^{140}$  and since the relative importance of these radionuclides is greatest at about 22 days (Reference 126), the energy spectrum of the deposited material at this time most closely approximates that of the  $\text{La}^{140}$  slurry used to determine the conversion factor.

A comparison of the experimental with the theoretical decrease in relative intensity with height above the coracle deck is given in Figure C.18. The empirical curve agrees with the theoretical curve within the limits of experimental error; the differences in shape are probably due to differences in energy. These curves were useful in converting survey meter dose rates into maximum probable std-GITR dose rates.

#### C.6 UNDERWATER RESPONSE OF STD-GITR

The std-GITR detector in an underwater casing (Section 2.2.2) was immersed into a 6-foot diameter tank containing known concentrations of  $\text{Cs}^{137}$ ,  $\text{La}^{140}$ , and  $\text{Co}^{60}$  in sea water. The recorded GITR dose rate above 20 mr/hr is directly proportional to concentrations in the sea water. The empirically determined conversion factor from the UW-GITR dose rate in r/hr to concentration in photons/sec per liter is  $3.5 \times 10^7$ . Assuming no fractionation and neglecting induced activity, concentrations so expressed may be converted to fissions/ml with an estimated accuracy of  $\pm 20$  percent, using the average photon energies summarized in Section A.1.

The GITR detector in its underwater casing is calculated to have a total response of approximately  $3\pi$  steradians; this response agrees with the experimentally determined underwater response to within 10 percent. Since the source is distributed entirely around the detector, the underwater response is considered to be the most accurate determination of total response. A complete description of these underwater measurements may be found in Reference 127.

TABLE C.1 RELATIVE ENERGY RESPONSE FOR END-WINDOW GAMMA COUNTER 2 FOR A POINT SOURCE ON SHELF 5

Energy	Relative Response	Energy	Relative Response
Mev	pct	Mev	pct
0.025	0.0528	0.40	0.487
0.03	0.2896	0.50	0.416
0.04	0.680	0.60	0.376
0.05	0.926	0.8	0.327
0.06	1.0425	1.0	0.296
0.08	1.1175	1.5	0.249
0.10	1.1542	2.0	0.226
0.15	1.055	3.0	0.207
0.20	0.886	4.0	0.200
0.30	0.612		

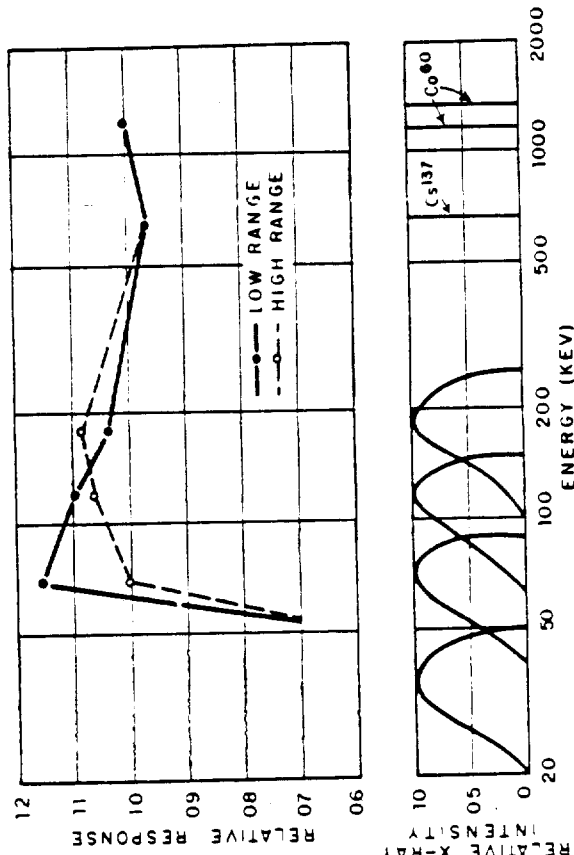


Figure C.1 Energy response characteristics of the GTR 103 detector for parallel beam radiations. The longitudinal axis of the detector and the beam were perpendicular. Response is normalized to 1.0 for  $Co^{60}$ . Values for 0.13-inch aluminum shield.

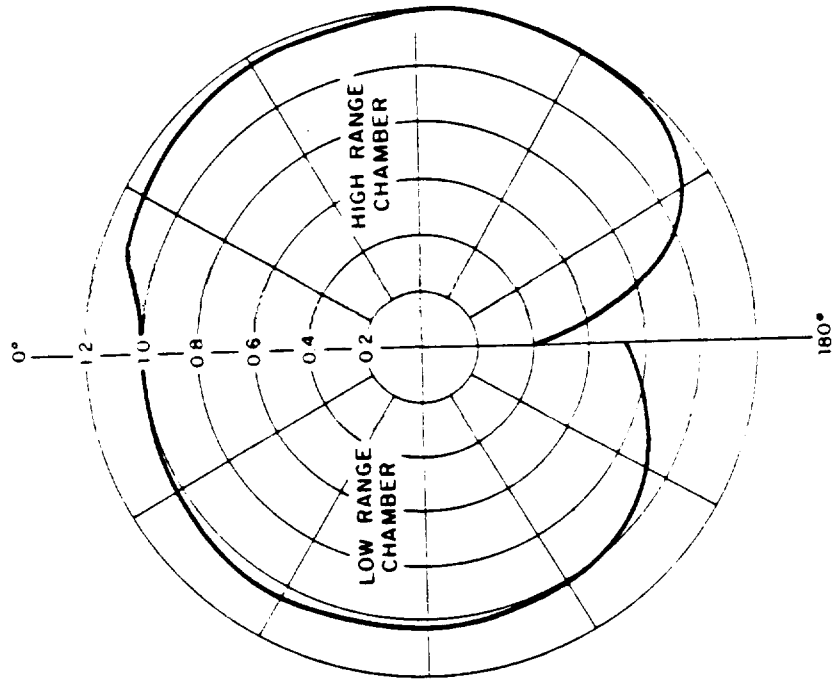


Figure C.2 Directional response characteristics of the std-GTR detector for parallel beam radiation ( $Co^{60}$ ). Response is symmetrical about the longitudinal axis of the detector for both ranges.

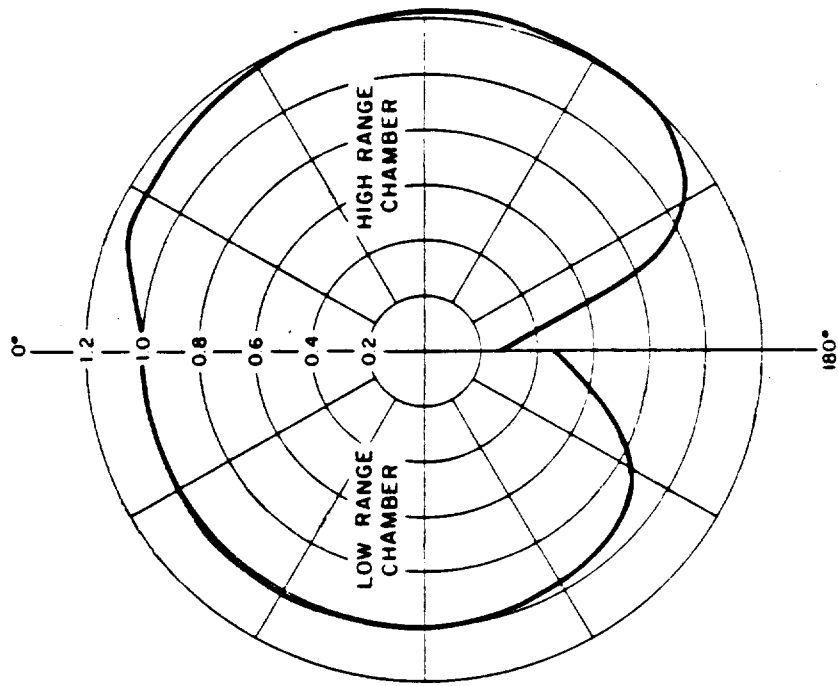


Figure C.3 Directional response characteristics of UW-GITR detector for parallel beam radiation ( $Co^{60}$ ). Response is symmetrical about the longitudinal axis of the detector for both ranges.

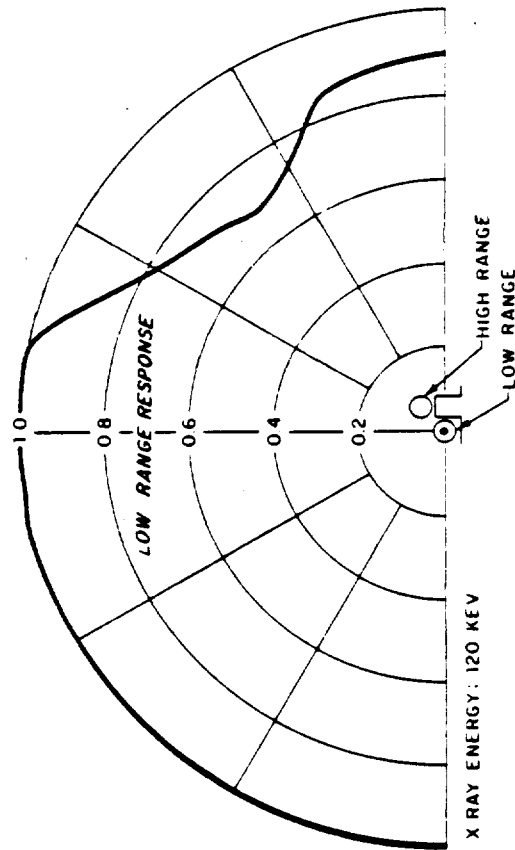


Figure C.4 Directional response of ASEIL-GITR low-range detector in a plane perpendicular to the detector axis. The diagram in the center of the plot shows the arrangement of the two detectors used in the field and the approximate center of the sensitive volume (high-range detector was included to obtain typical shielding).

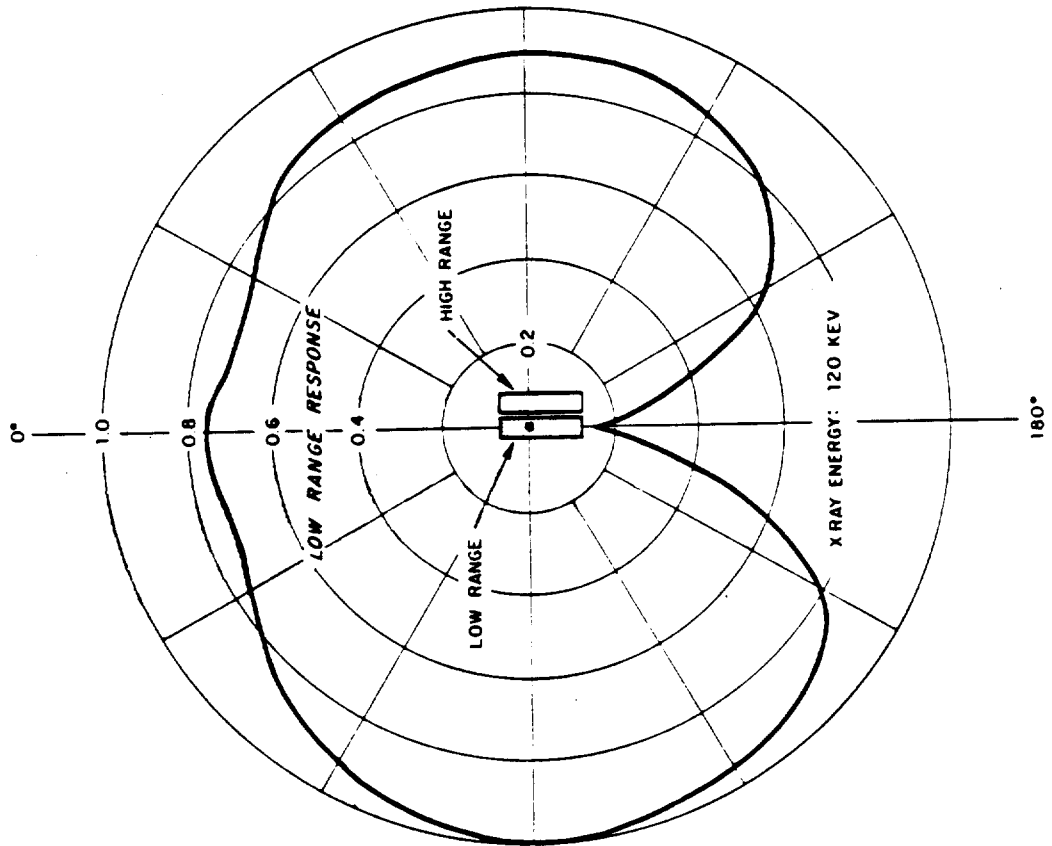


Figure C.5 Directional response of ASE-L-GITR low-range detector in the plane of the detector axis. The diagram in the center of the plot shows the arrangement of the two detectors used in the field and the approximate center of the sensitive volume (high-range detector was included to obtain typical shielding).

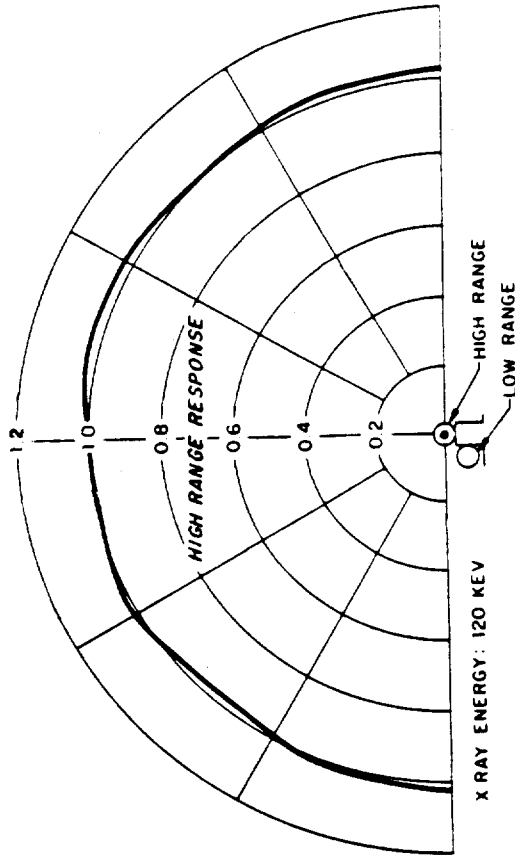


Figure C.6 Directional response of ASE-L-GITR high-range detector in a plane perpendicular to the detector axis. The diagram in the center of the plot shows the arrangement of the two detectors used in the field and the approximate center of the sensitive volume (low-range detector was included to obtain typical shielding).

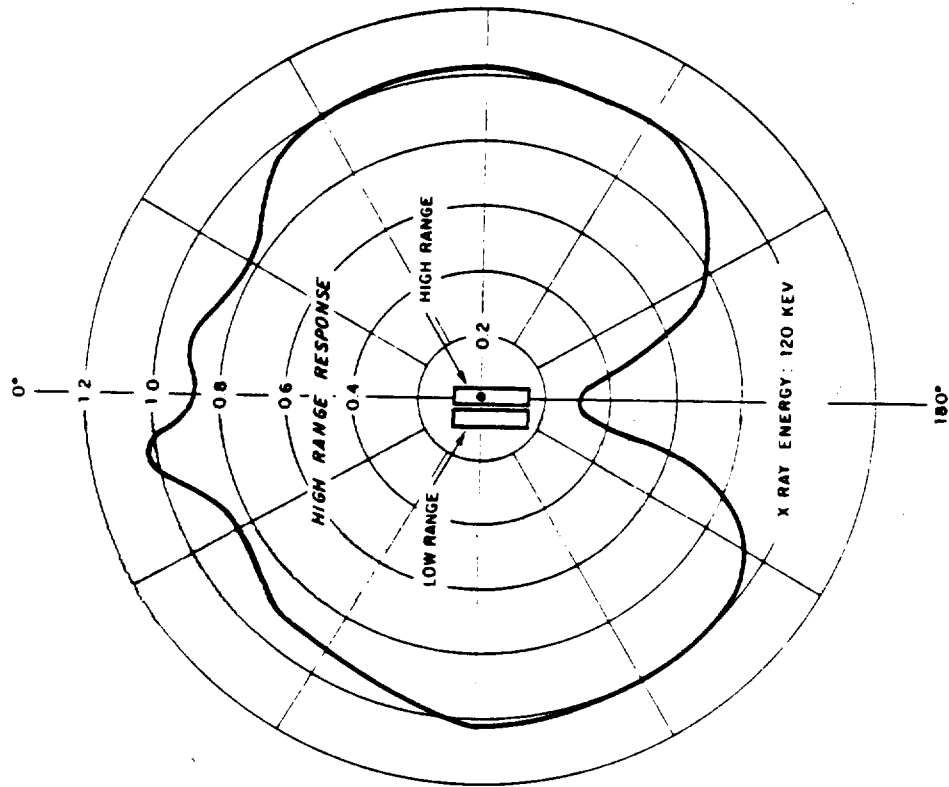


Figure C.7 Directional response of ASEL-GITR high-range detector in the plane of the detector axis. The diagram in the center of the plot shows the arrangement of the two detectors used in the field and the approximate center of the sensitive volume (low-range detector was included to obtain typical shielding).

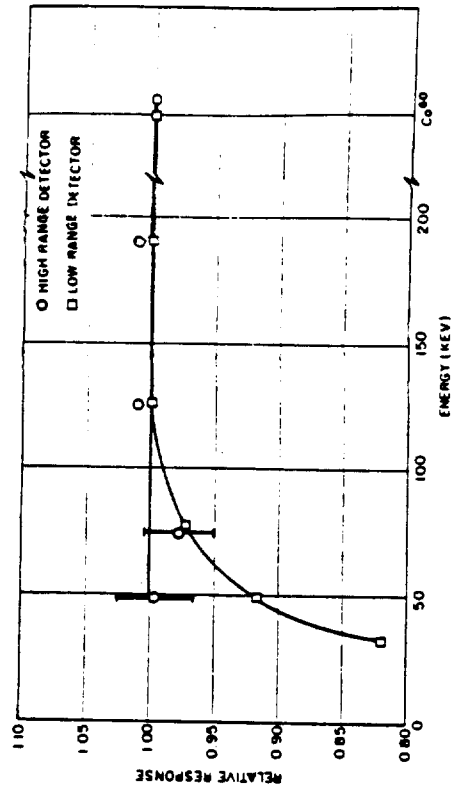


Figure C.8 Energy response characteristics of the ASEL-GITR for parallel beam radiations.

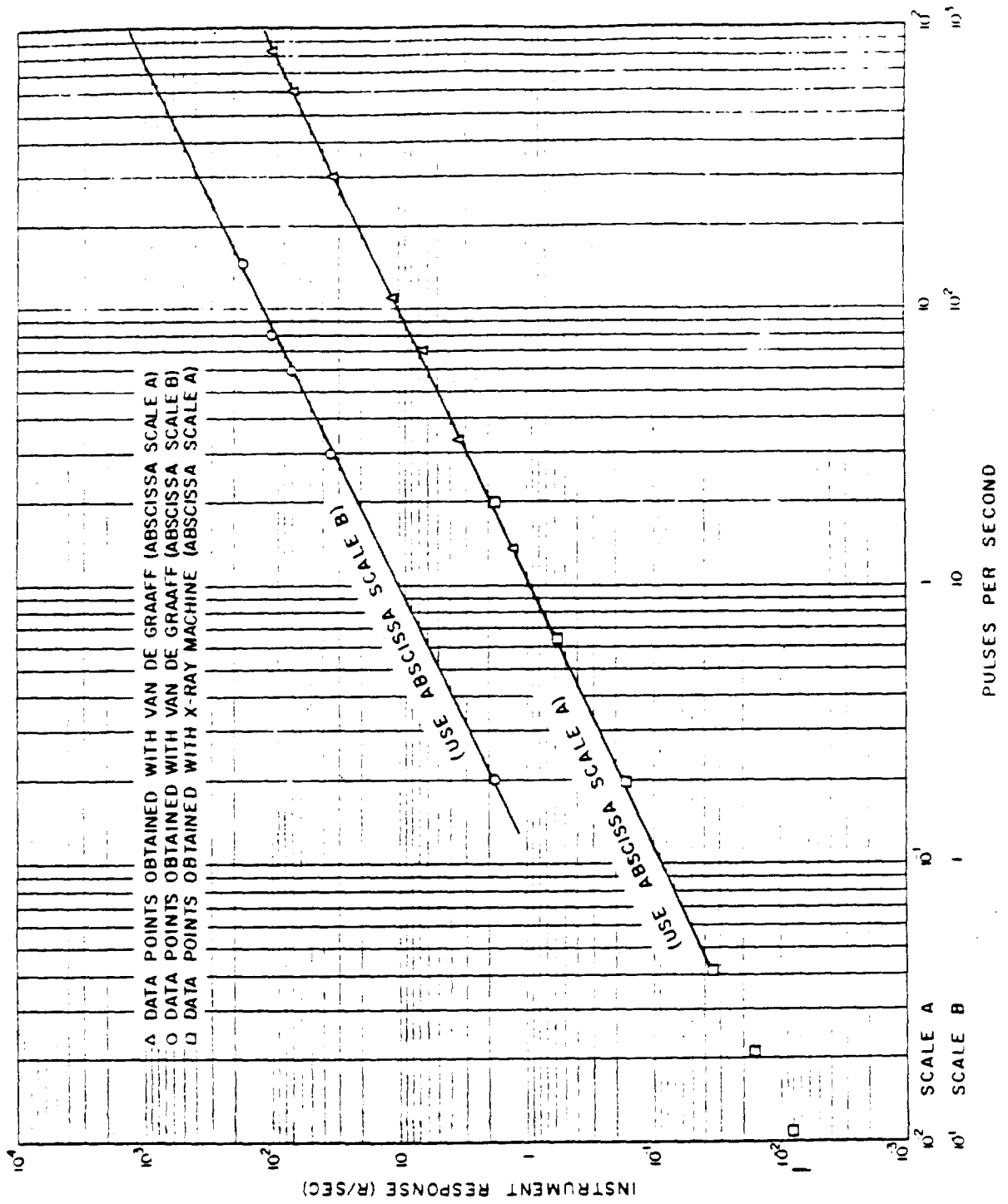


Figure C.9 Typical calibration curve for ASEL-GITR high-range detector.

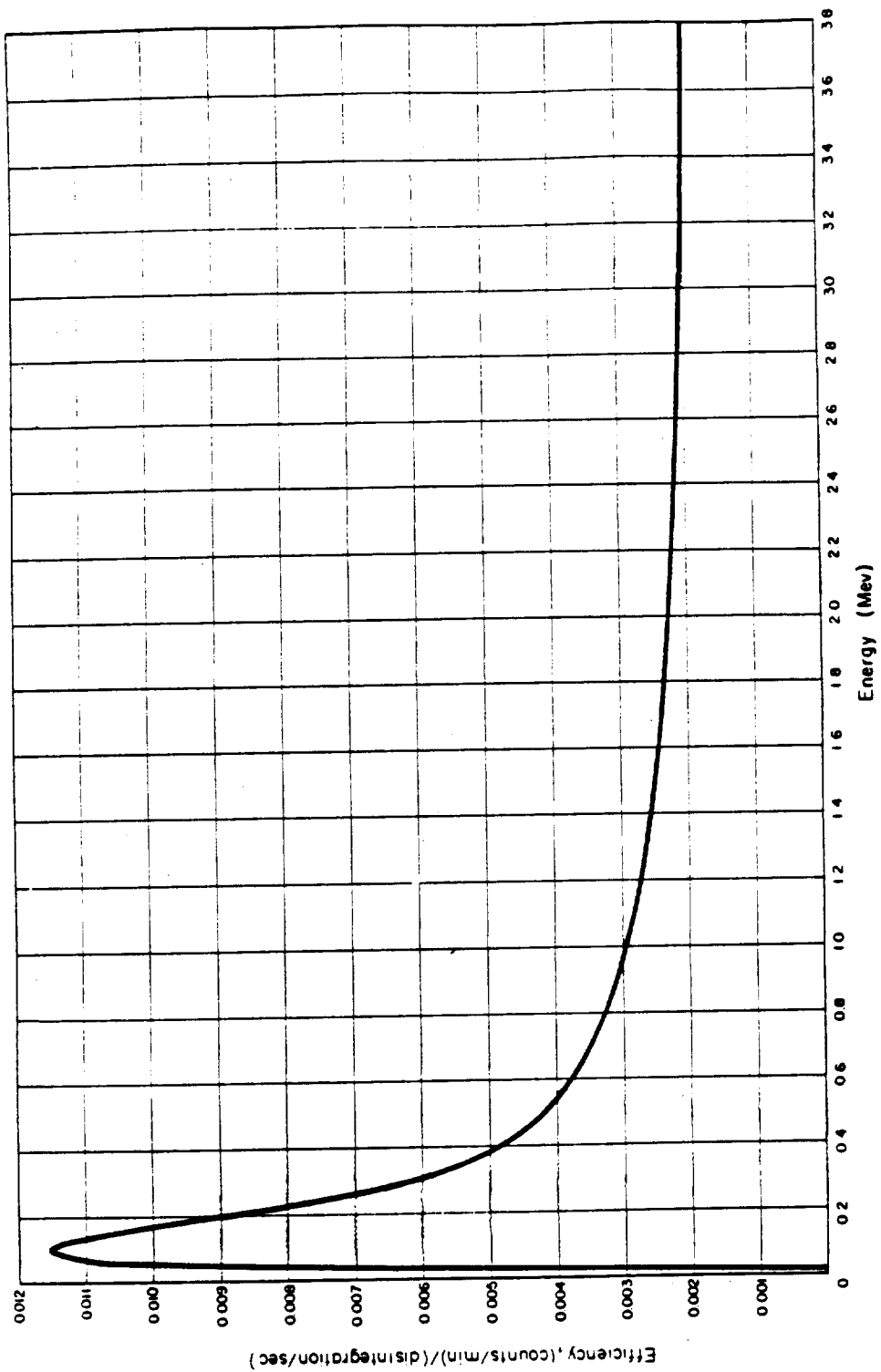


Figure C.10 Relative energy response for End-Window Gamma Counter 2 (for a point source on Shelf 5).

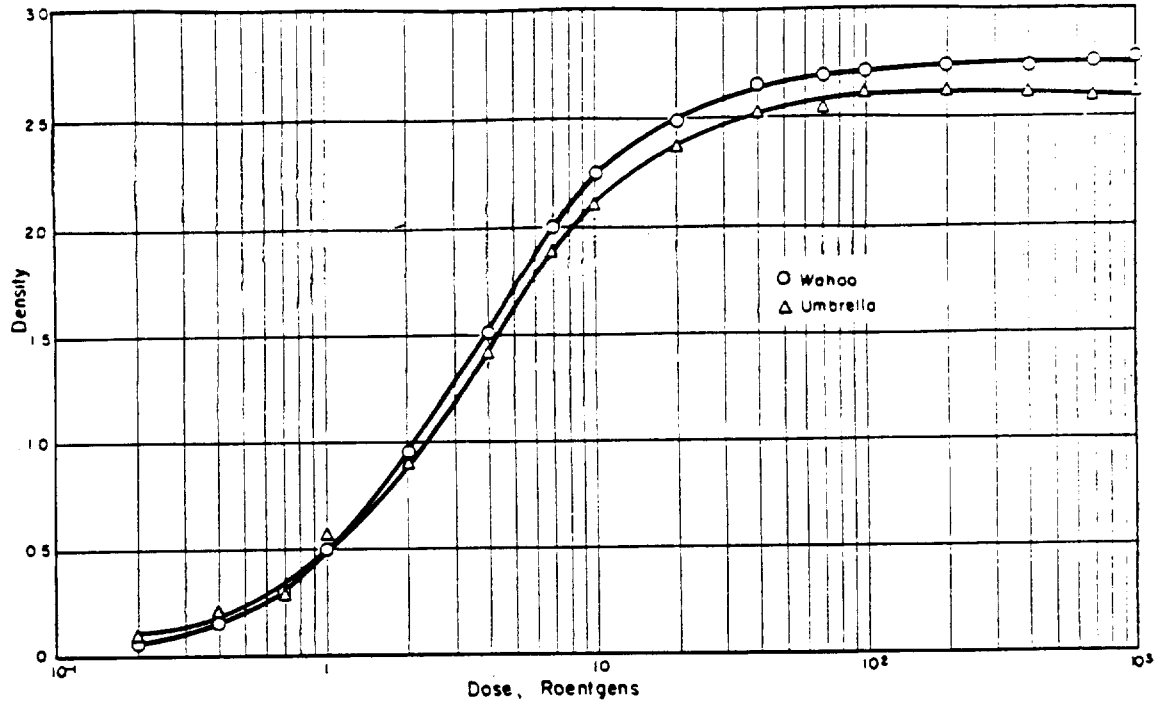


Figure C.11  $Co^{60}$  calibration curves for 502 emulsion.

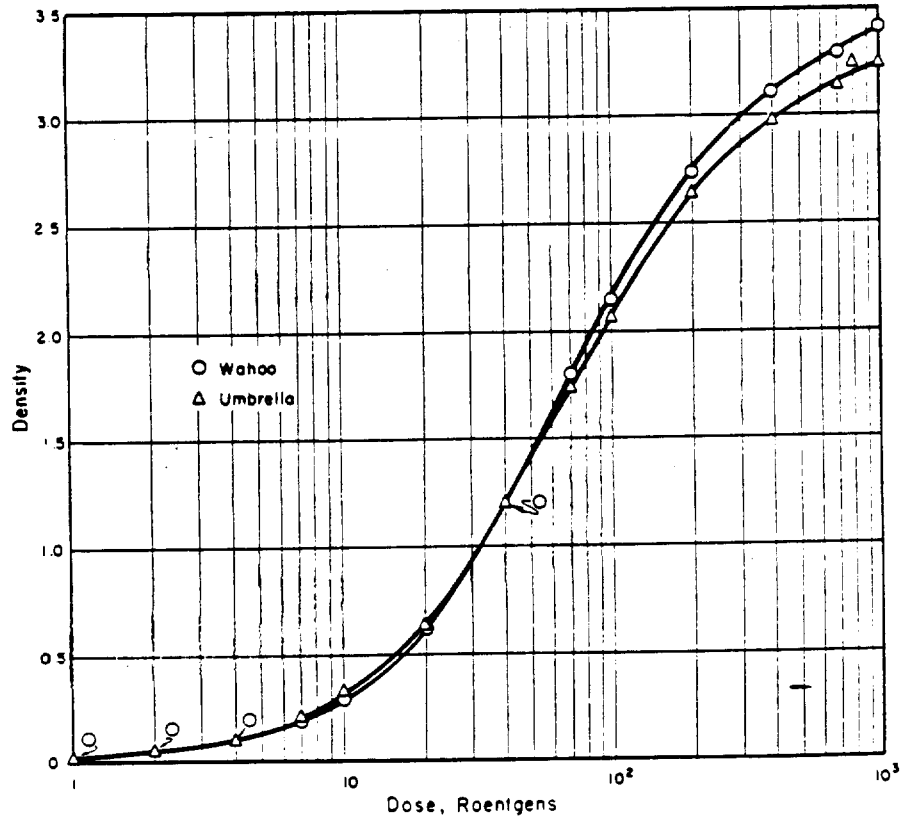


Figure C.12  $Co^{60}$  calibration curves for 834 emulsion.

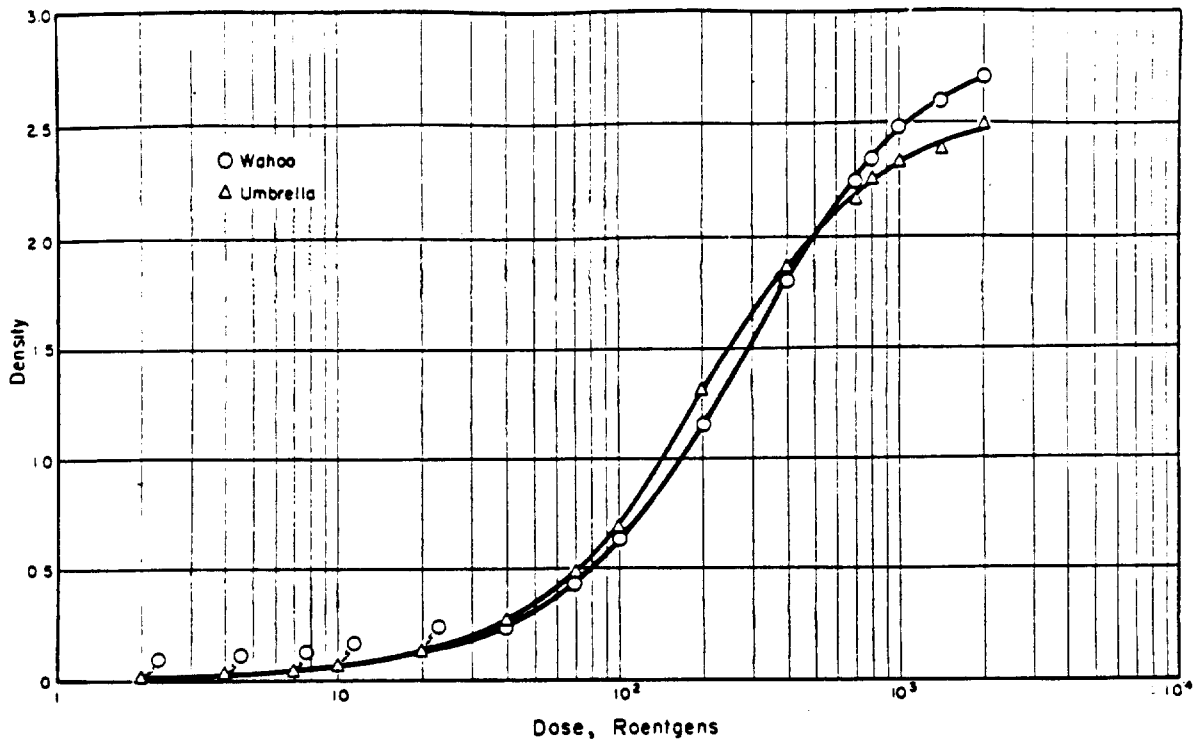


Figure C.13  $\text{Co}^{60}$  calibration curves for 1290 emulsion.

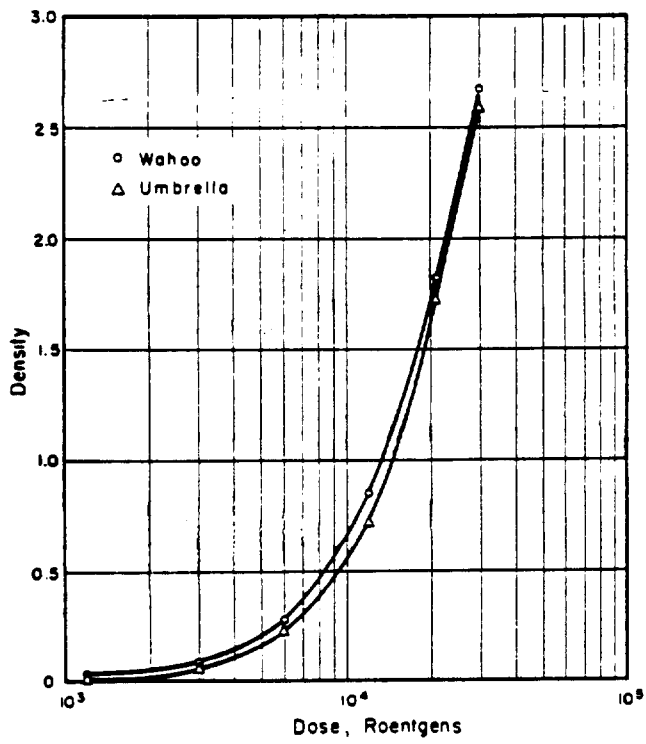


Figure C.14  $\text{Co}^{60}$  calibration curves for 548-0 emulsion.

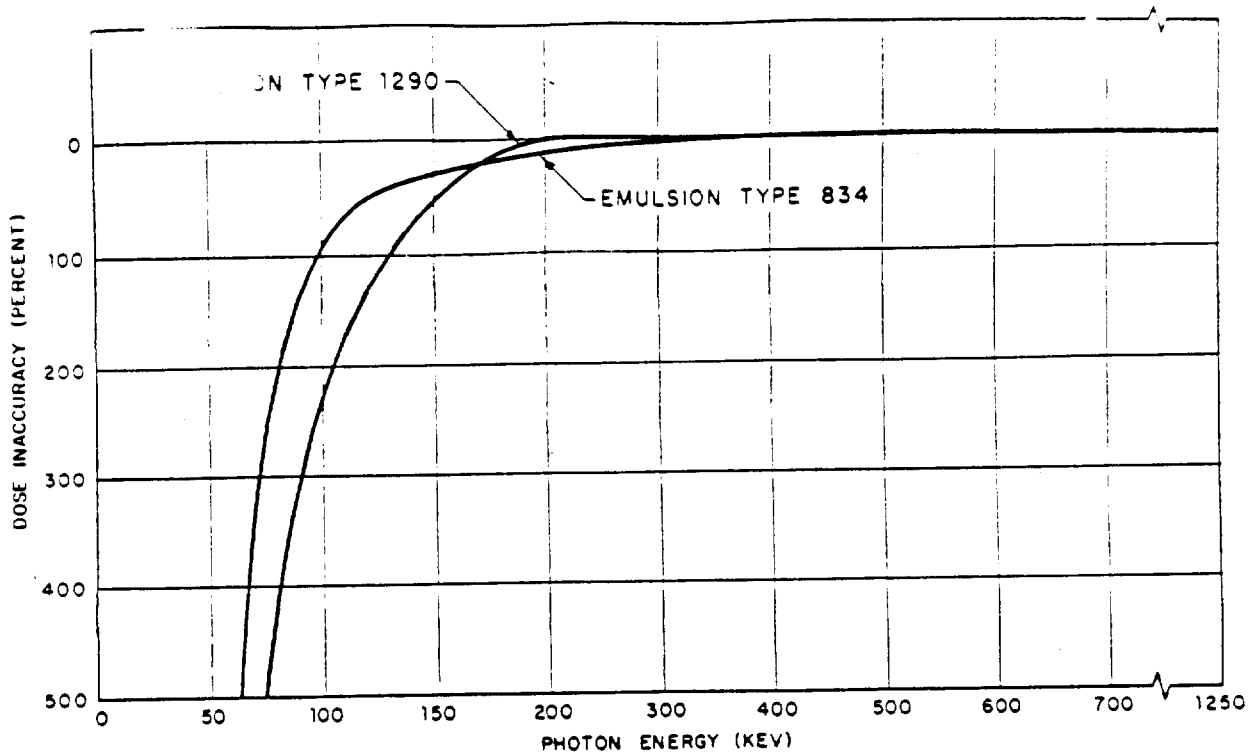


Figure C.15 Energy response for emulsions used in film packs (dose inaccuracy).

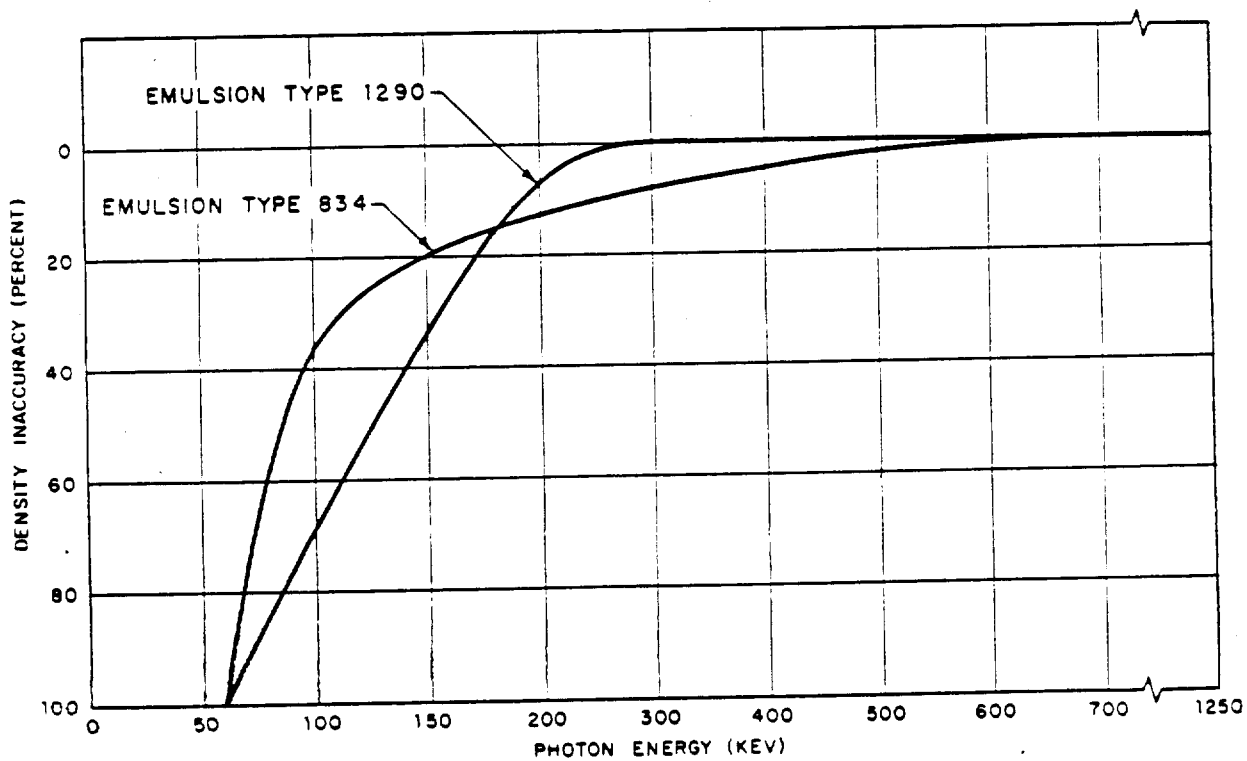


Figure C.16 Energy response for emulsions used in film packs (density inaccuracy).

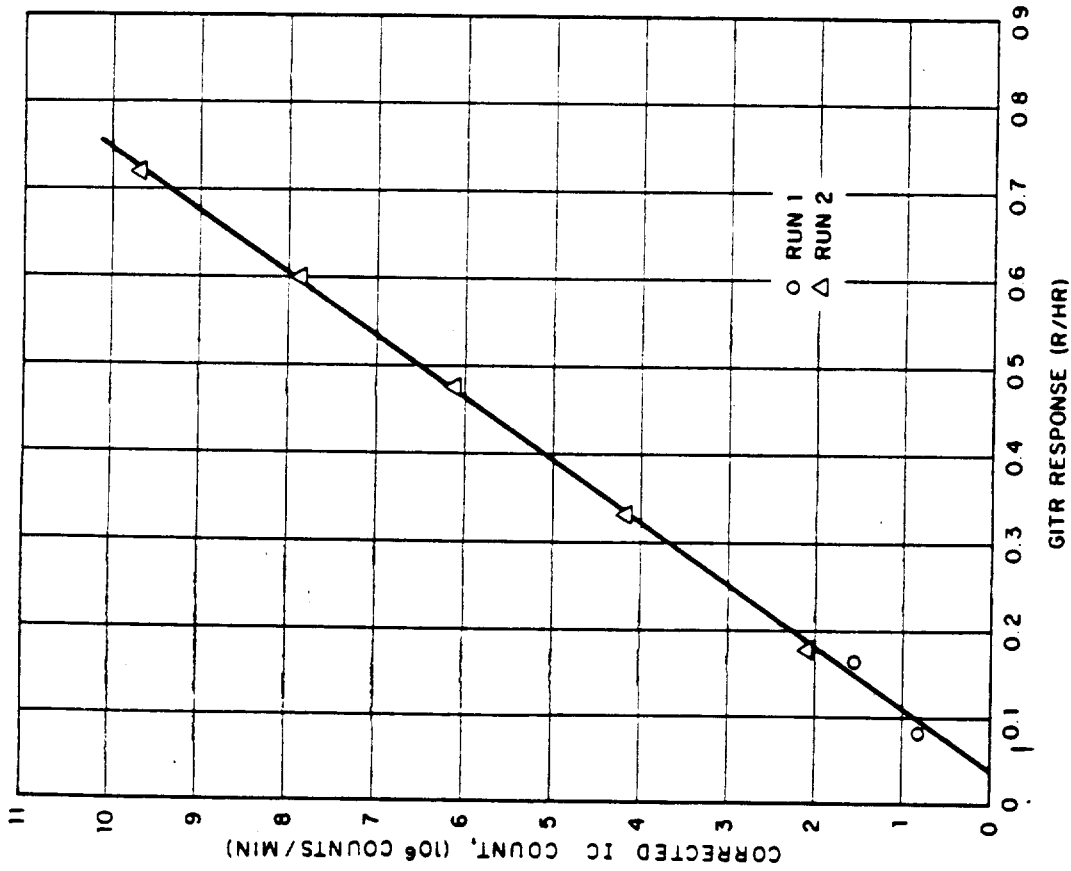
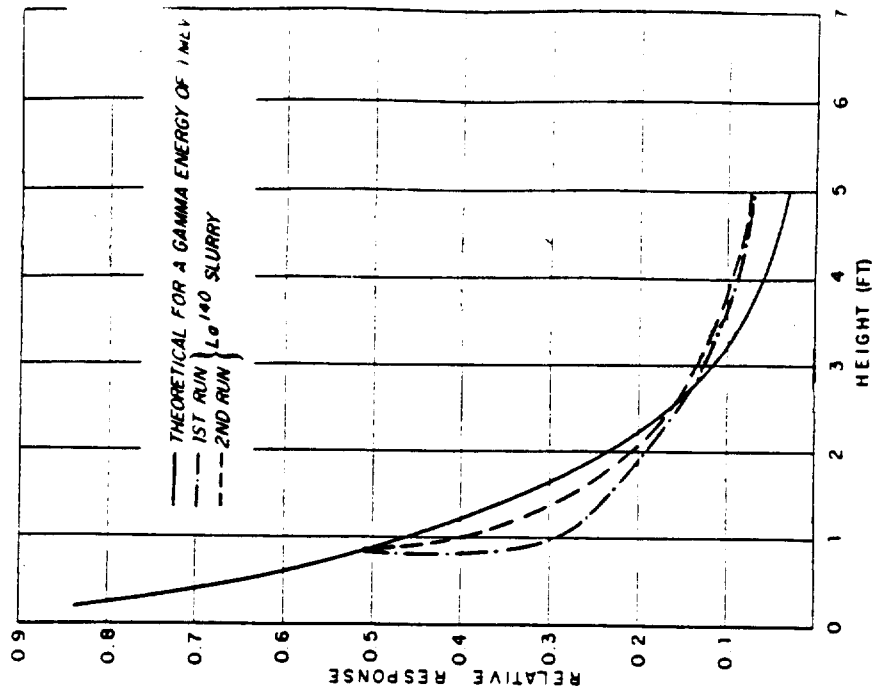


Figure C.17 Relationship between std-GITR response and deposited activity determined by IC. (IC tray counts on Shelf 5 of End-W Window Gamma Counter 2.)



C.18 Variation of GITR reading as a function of height above a contaminated coracle deck.

243

## Appendix D

### ORIGINAL DATA

This appendix contains all the original counting data used in the body of this report, since this information in unmodified form may be useful for studies not attempted by the project. For greater convenience, a limited amount of descriptive and analytical material has been included.

#### D.1 LINEAR FREE-FIELD AND SHIPBOARD RECORDS

A linear presentation of the gamma records was used in the Interim Test Report (ITR-1621). These records are preliminary uncorrected results plotted automatically by the GITOUT. Since ITR's are destroyed after the final reports are issued, these original linear presentations are reproduced here. They may be helpful in indicating the relative importance of specific features of the total gamma record for quick tactical considerations. No particular attempt has been made to correct these records; therefore, they must be regarded as approximate. Not all records contained in the ITR are reproduced. The discussions in Section 3.3.2 and 3.4.1 are equally applicable to those records that do appear here.

#### D.2 METER SURVEY DATA FOR CORACLES

The coracles were surveyed with a Cutie-Pie (CP-3DM beta-gamma survey meter, Reference 103) shortly after recovery. For Wahoo, the meter probe was held 3 feet above the IC port roughly in the center of the coracle. Since the coracle background was so low after Umbrella, the meter probe was held 3 inches above the IC port. The survey meter data may be converted to approximate std-GITR response by the factors 2.3 and 0.36 for Wahoo and Umbrella, respectively. The original and converted data is presented in Table D.1. A plot of this data versus distance from surface zero (Figure D.34) indicates that the general background for Wahoo was about a factor of 10 higher than that for Umbrella.

#### D.3 IC COUNTING DATA

All IC trays were counted on Shelf 5 in one of two end-window gamma counters described in Section 3.3.1. Counter 2 was used at the EPG, and Counter 1 was used at NRDL. The two counters were nearly identical, no conversion factor from one to the other being necessary. Upon recovery of the coracles in the field, all IC trays were immediately removed to a laboratory at the site where they were given a preliminary count with a MX-5 survey meter with its probe positioned exactly  $\frac{1}{8}$  inch above the center of each IC tray. This reading was used to distinguish trays having significant radioactive deposits, so that maximum counting time could be assigned to trays having usable data and so that decay counts on the most active samples could be started immediately. After this initial count at EPG, all IC trays were returned to NRDL where a second count of all collections was made. Trays were shipped in individual plastic bags, which precluded cross-contamination during shipment.

The tray counts for a complete set of IC trays (both exposed and unexposed trays in the case of IC collectors which jammed) were plotted, and a background for the entire set of trays was determined. These backgrounds for the tray set are reported as "collection bkgd (measured)" at the beginning of each table of original counts; backgrounds determined from the counts for a complete IC tray set and backgrounds calculated for other times using the standard decay curve

are indicated; these are reported as "collection bkgd (calculated)." A plot of collection background versus distance from surface zero (Figure D.35) is similar to that for the survey meter data (Figure D.34). Again the general background for Wahoo appears to be about a factor of 10 higher than Umbrella. These collection backgrounds were subtracted from all IC data used in the body of this report. It should be reiterated that the IC was designed to assess deposited material under conditions of heavy deposition originally expected from these underwater detonations. Under the conditions of light deposition, occasionally coupled with high transport velocities, the IC data suffers both from an appreciable collection bias and from statistical variation between samples.

Unmodified Wahoo tray counts are presented in Tables D.2 through D.12 and unmodified Umbrella tray counts in Tables D.13 through D.27. Complete data for the first 15 minutes of collection is presented; after this time, only collections significantly above collection background are reported. The IC collections are designated by the location of the collection followed by a time indicating the time at which the 1-minute collection ceased. The abbreviation "cont" following the time designator indicates that the IC stuck at the tray in question; therefore, the tray was exposed continuously from 1 minute prior to the indicated time until the coracle was recovered. When the time designator is included in parenthesis, the tray was never actually exposed but was intended to be exposed at that time. Since the top tray was exposed from 1 minute prior to the shot to approximately zero time, it is frequently omitted from plots of IC collections; counting data for omitted trays is, however, included. Omitted trays are designated by an X or, if more than one, by a series of X's.

#### D.4 IC DECAY DATA

The counting procedure and method of designating IC collections are described in Section D.2. In most cases, the most radioactive tray was returned to NRDL for a decay count, while the second most radioactive tray was retained at the EPG for a decay count. In a few instances, a decay started at the EPG was continued at NRDL, thus affording two points on a decay curve. Decay data for Wahoo is presented in Tables D.28 through D.44 and those for Umbrella in Tables D.45 through D.60. Slopes determined on the basis of two points are presented in Table D.61 for trays not decayed but counted once at the EPG and once at NRDL.

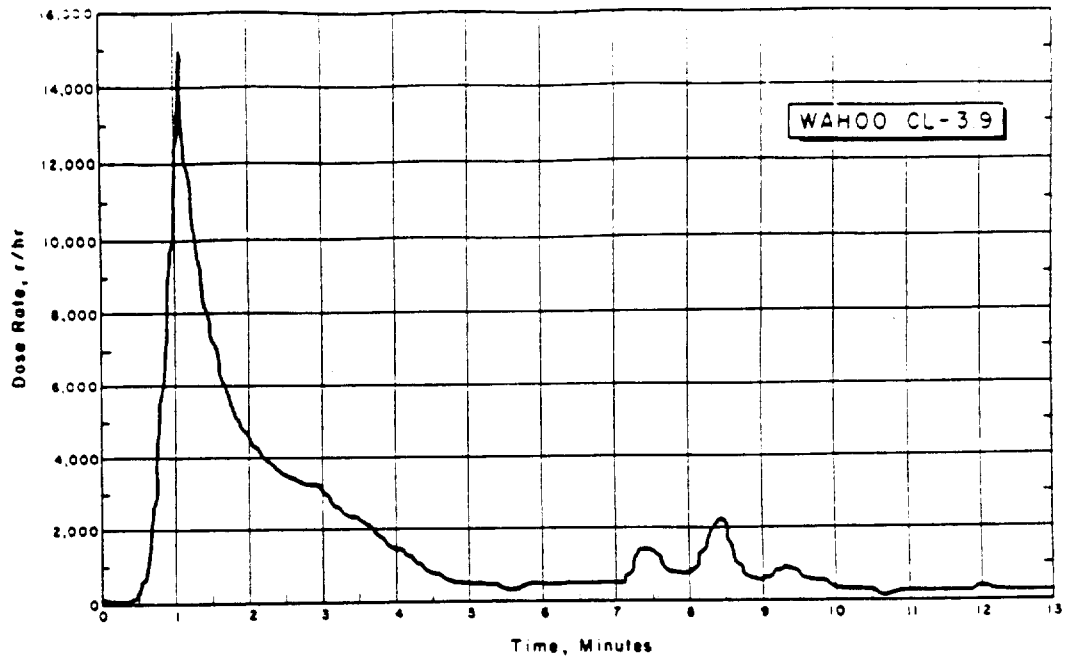


Figure D.1 Approximate linear gamma dose rate record for coracle at 3,900 feet, 159° T from surface zero, Shot Wahoo. Warning: Increase values read from this gamma record by 10 percent.

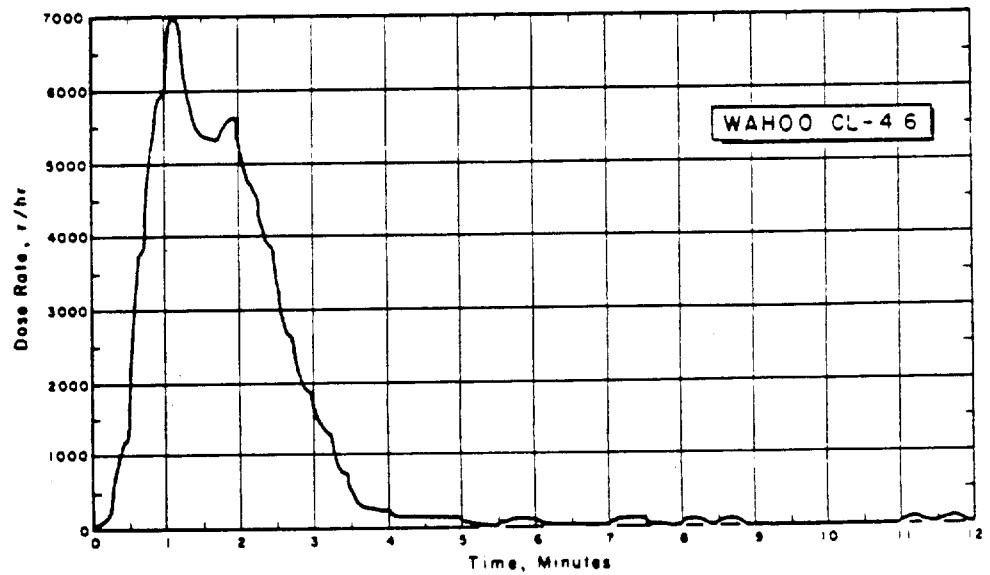


Figure D.2 Approximate linear gamma dose rate record for coracle at 4,600 feet, 151.5° T from surface zero, Shot Wahoo.

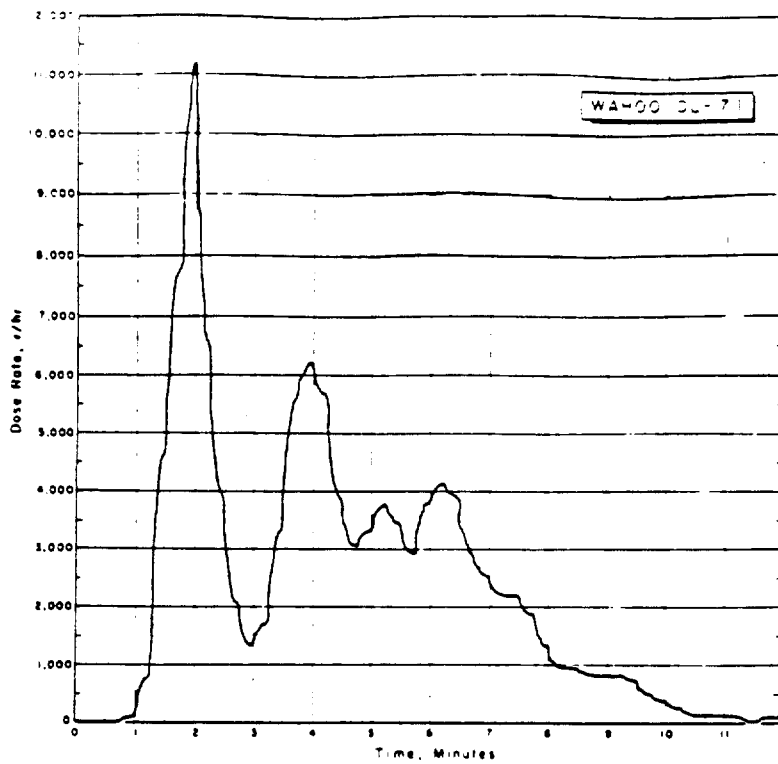


Figure D.3 Approximate linear gamma dose rate record for coracle at 7,100 feet, 231.5° T from surface zero, Shot Wahoo.

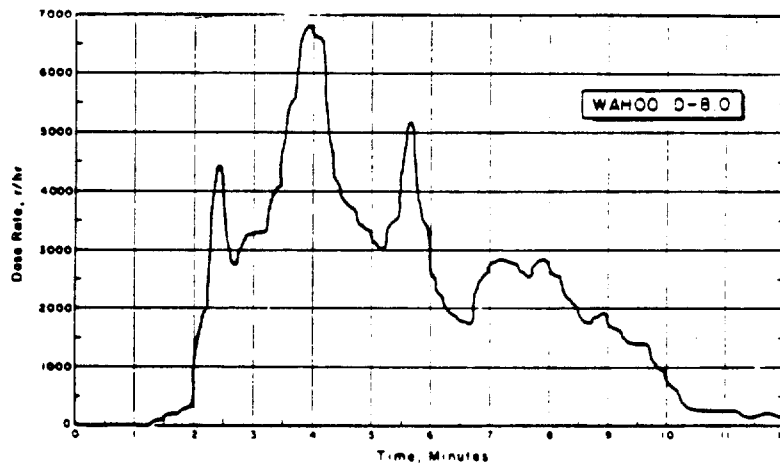


Figure D.4 Approximate linear gamma dose rate record for coracle at 8,000 feet, 256.5° T from surface zero, Shot Wahoo. Warning: Increase values read from this gamma record by 10 percent.

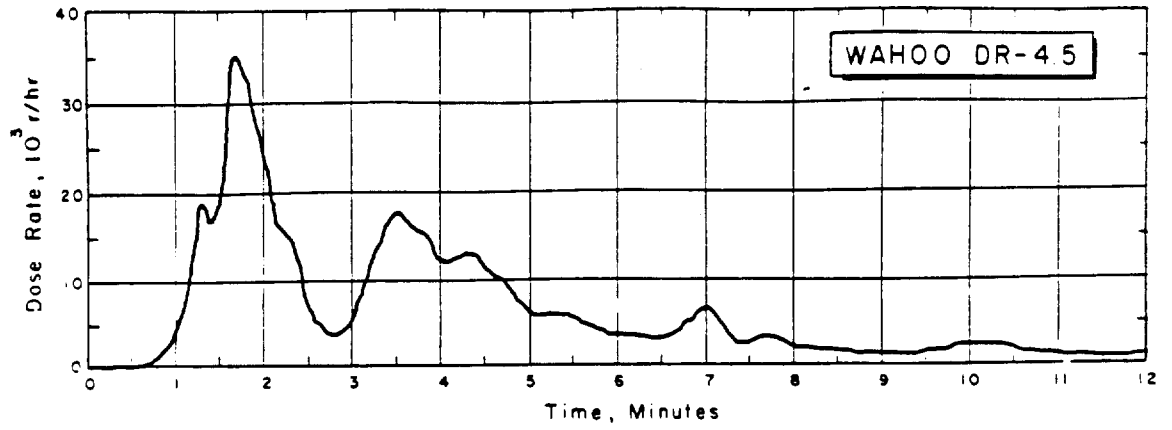


Figure D.5 Approximate linear gamma dose rate record for coracle at 4,500 feet, 263° T from surface zero, Shot Wahoo. Warning: Increase values read from this gamma record by 10 percent.

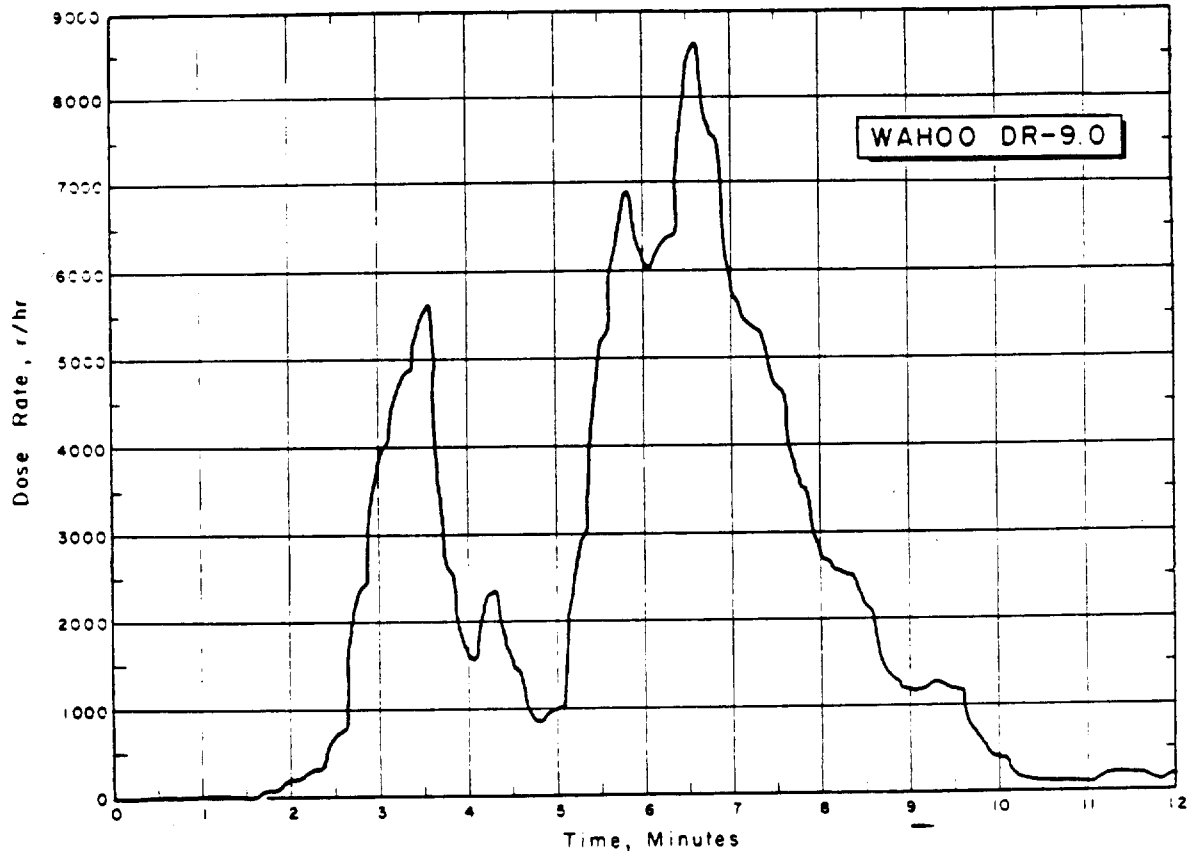


Figure D.6 Approximate linear gamma dose rate record for coracle at 8,950 feet, 263° T from surface zero, Shot Wahoo.

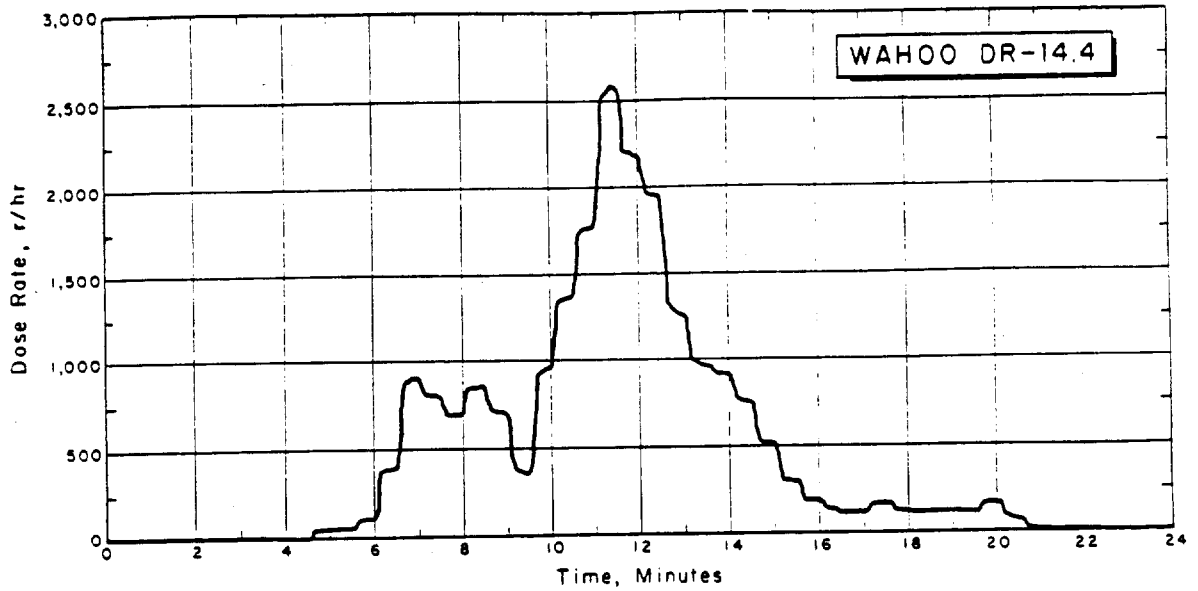


Figure D.7 Approximate linear gamma dose rate record for coracle at 14,400 feet, 265° T from surface zero, Shot Wahoo. Warning: Increase values read from this gamma record by 10 percent.

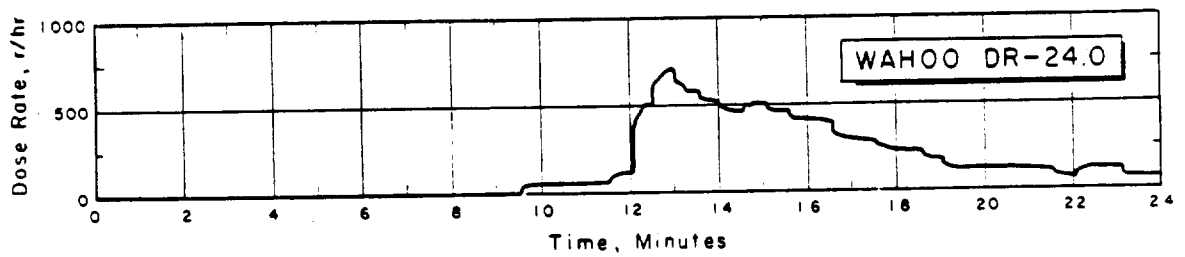


Figure D.8 Approximate linear gamma dose rate record for coracle at 24,000 feet, 263° T from surface zero, Shot Wahoo.

227

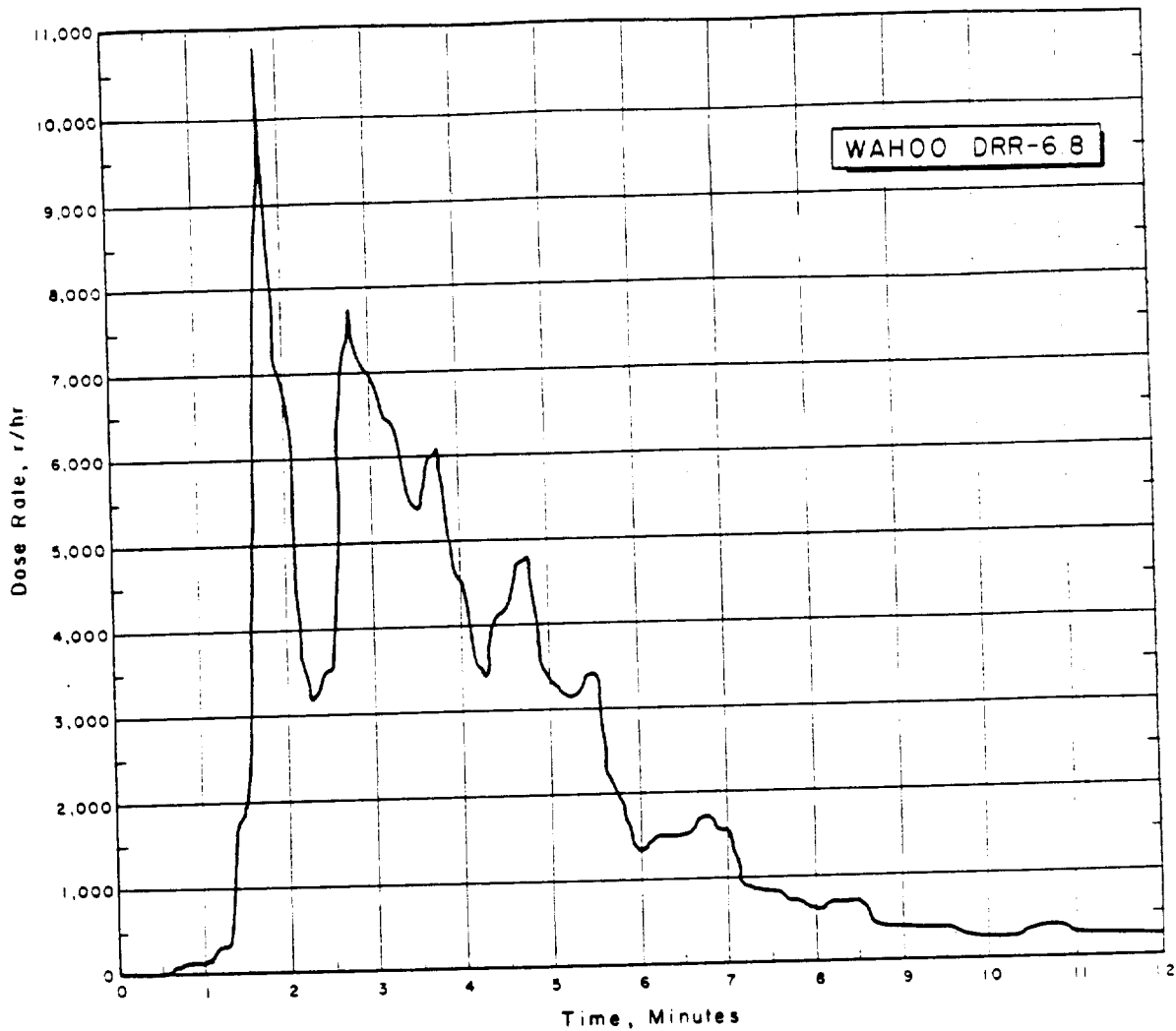


Figure D.9 Approximate linear gamma dose rate record for coracle at 6,800 feet, 281° T from surface zero. Shot Wahoo. Warning: Increase values read from this gamma record by 10 percent.

25

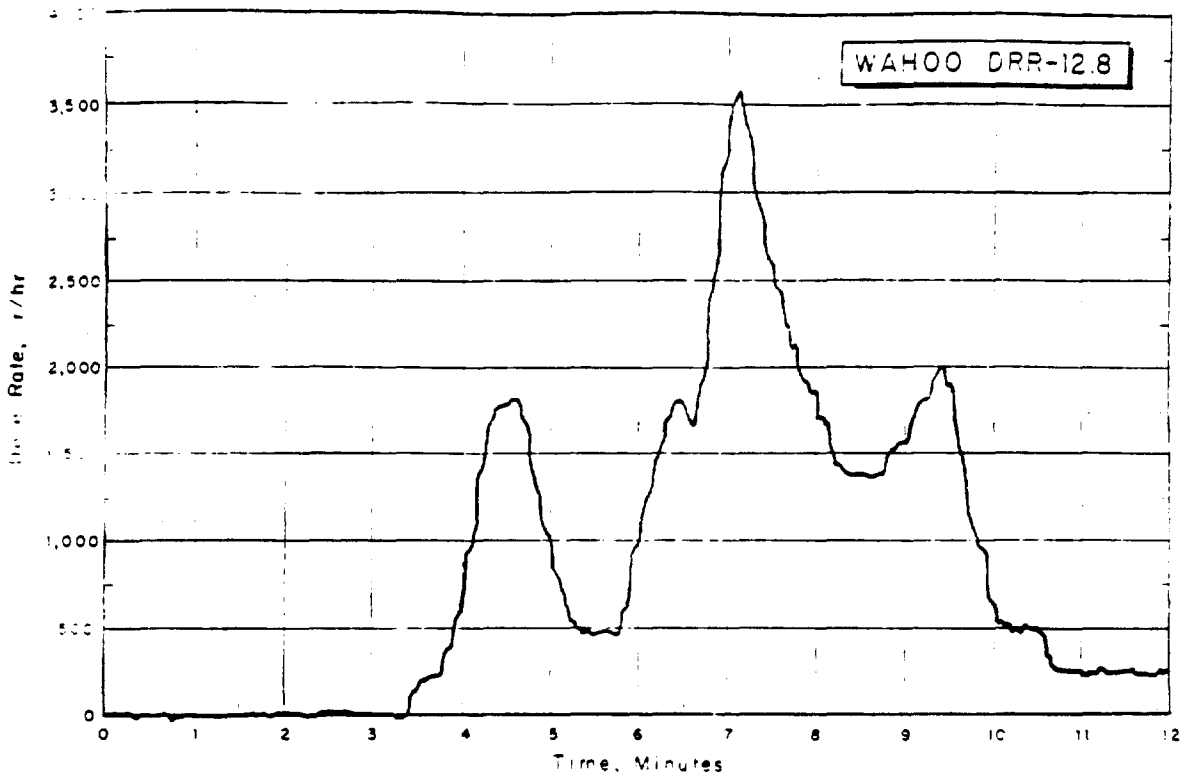


Figure D.10 Approximate linear gamma dose rate record for coracle at 12,800 feet, 276° T from surface zero, Shot Wahoo.

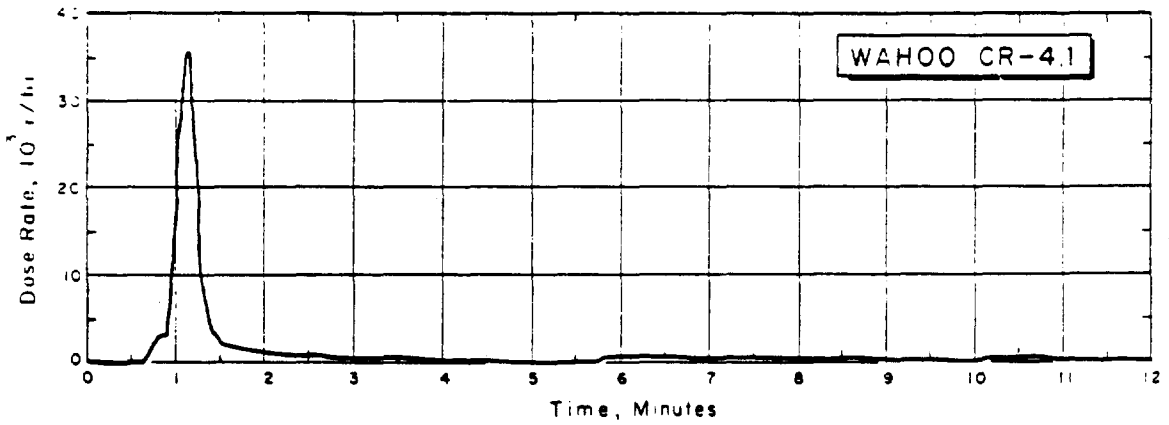


Figure D.11 Approximate linear gamma dose rate record for coracle at 4,100 feet, 336° T from surface zero, Shot Wahoo. Warning: Increase values read from this gamma record by 10 percent.

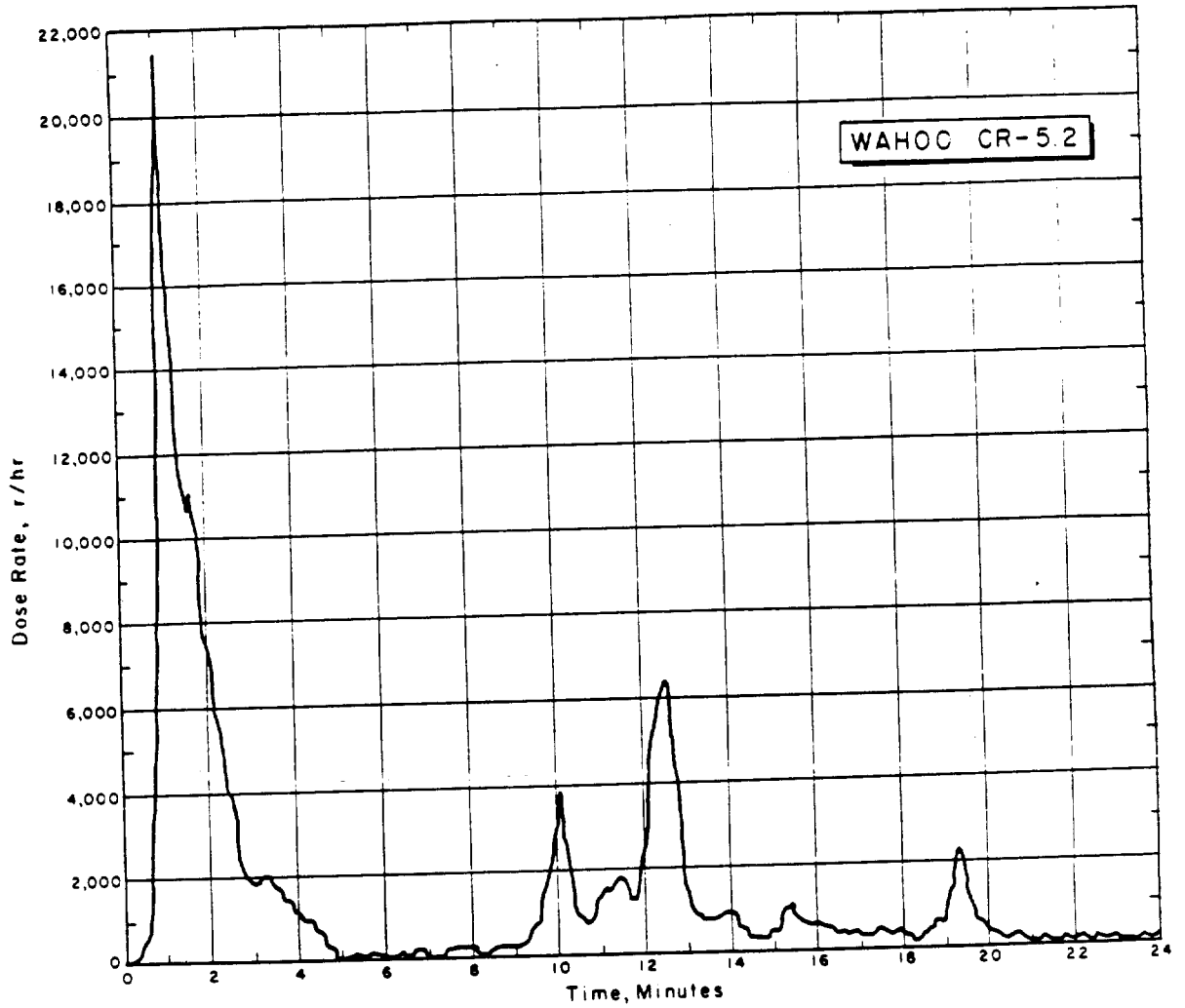


Figure D.12 Approximate linear gamma dose rate record for coracle at 5,200 feet, 334.5° T from surface zero, Shot Wahoo. Warning: Increase values read from this gamma record by 10 percent.

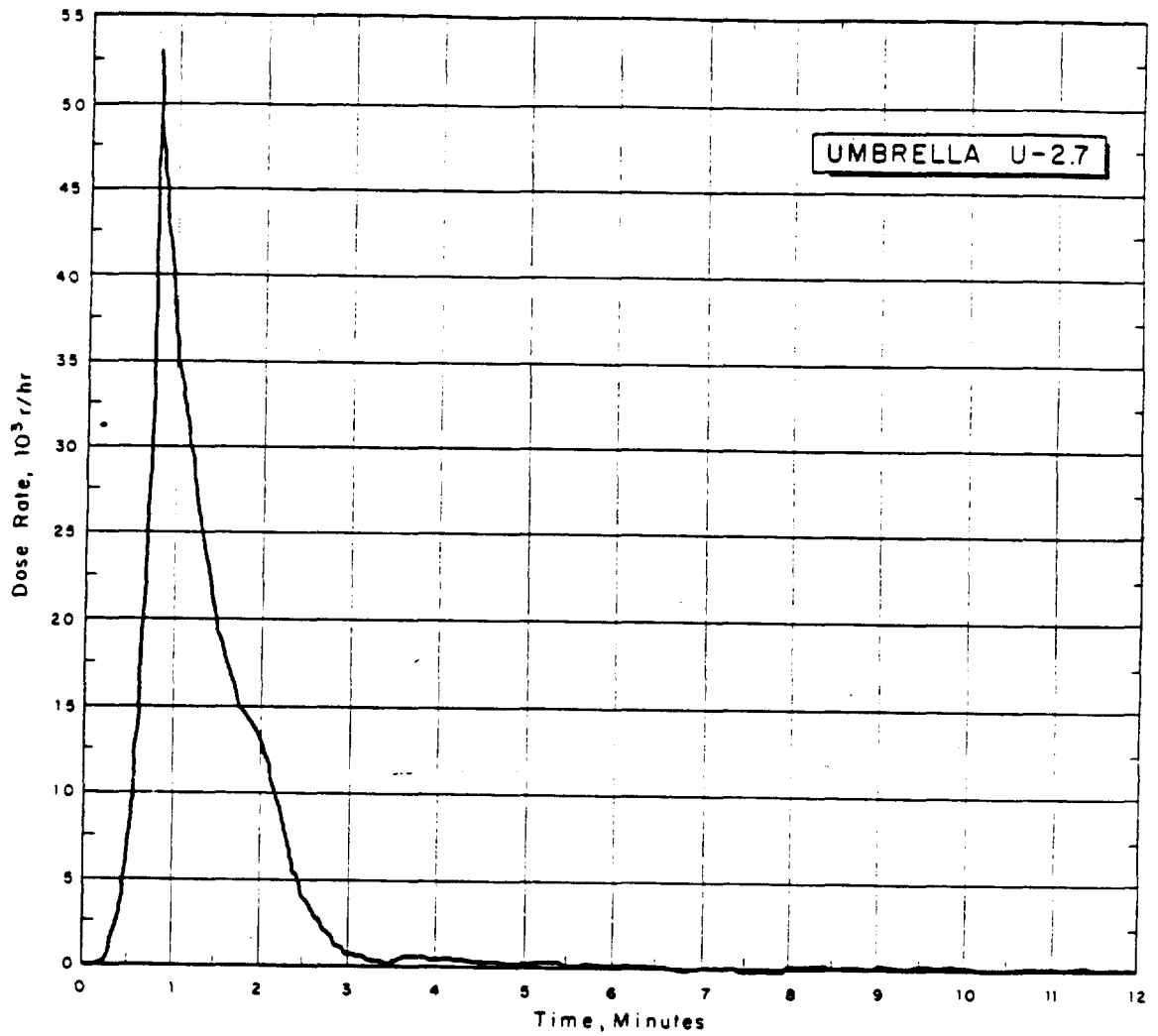


Figure D.13 Approximate linear gamma dose rate record for coracle at 2,700 feet, 67° T from surface zero, Shot Umbrella.

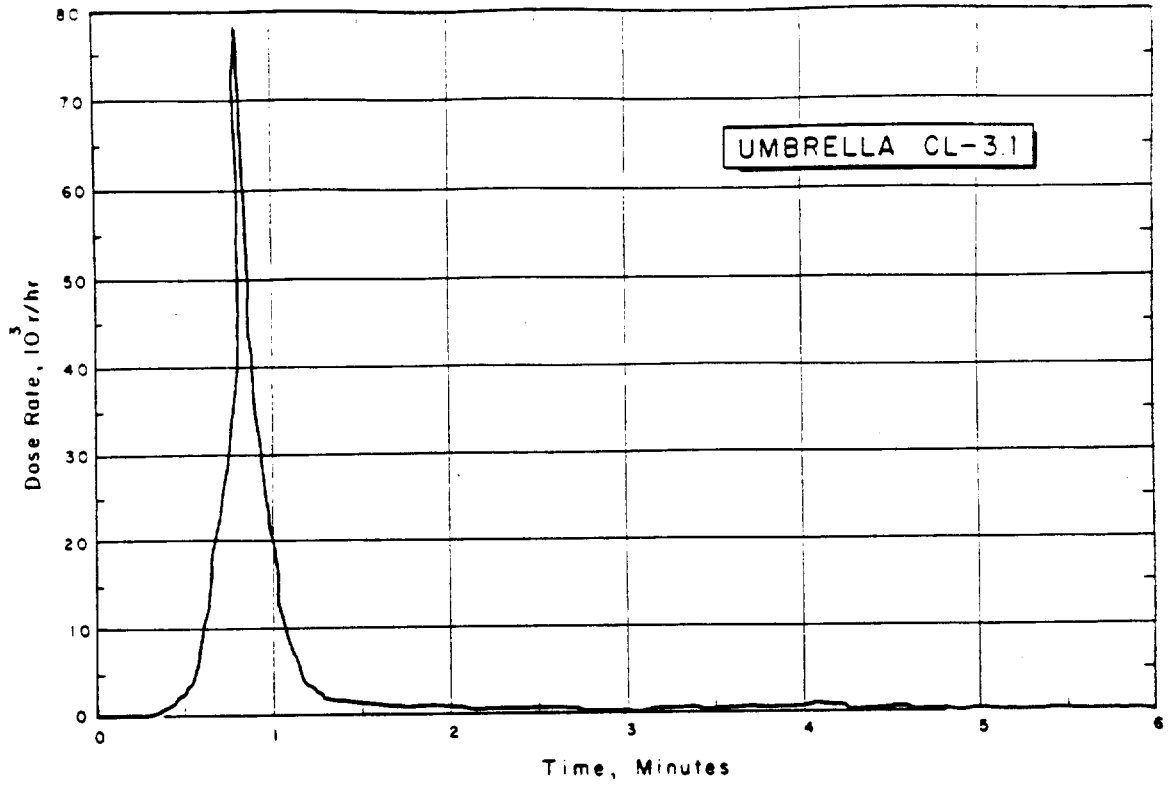


Figure D.14 Approximate linear gamma dose rate record for coracle at 3,060 feet, 163.7° T from surface zero, Shot Umbrella.

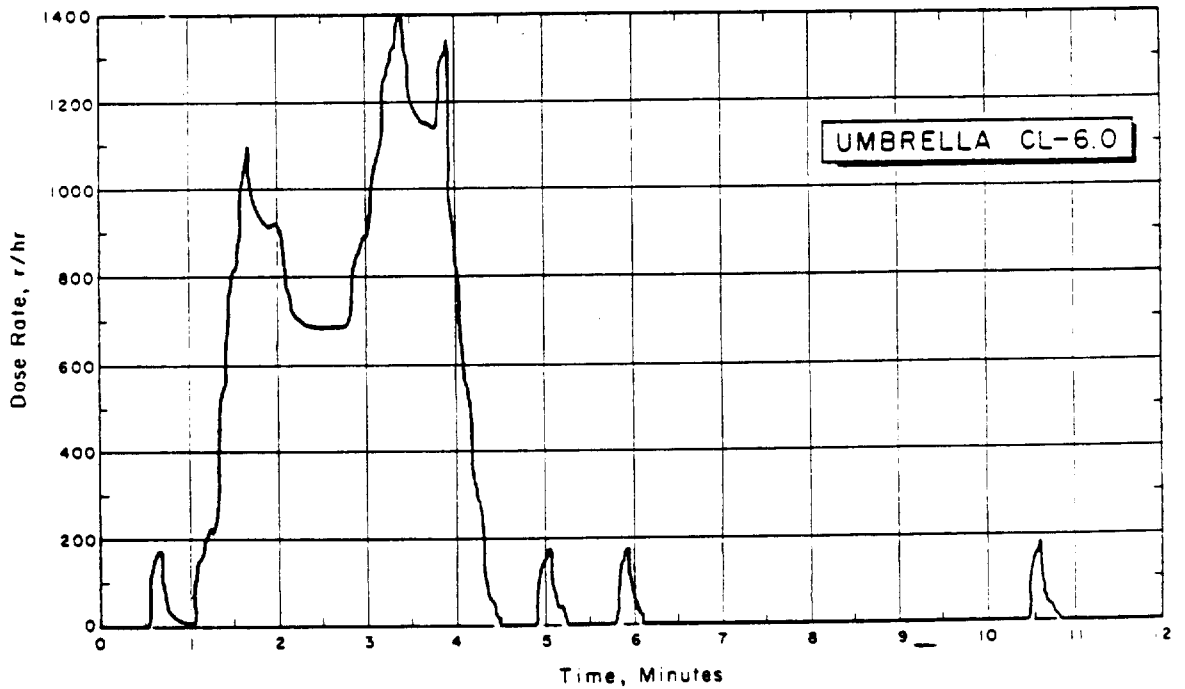


Figure D.15 Approximate linear gamma dose rate record for coracle at 6,010 feet, 158.9° T from surface zero, Shot Umbrella. Warning: Increase values read from this gamma record by 10 percent.

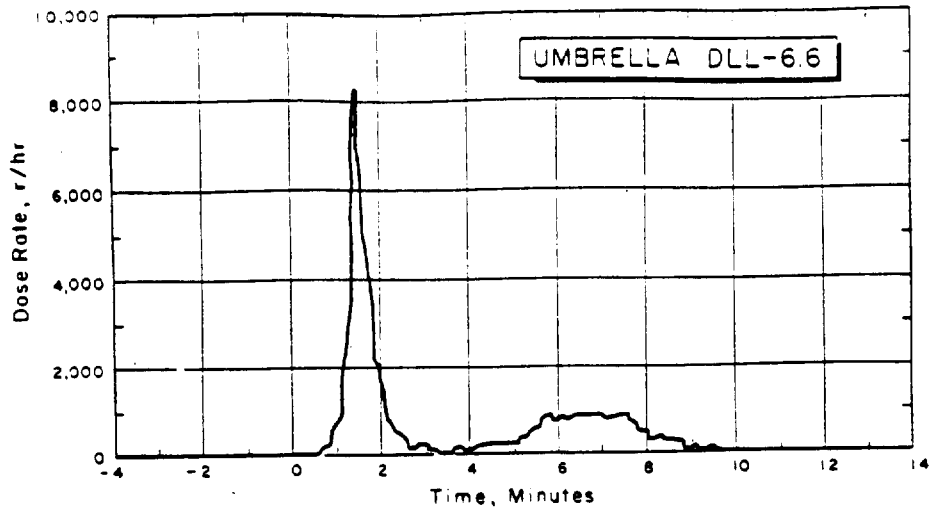


Figure D.16 Approximate linear gamma dose rate record for coracle at 6,580 feet, 207.5° T from surface zero, Shot Umbrella.

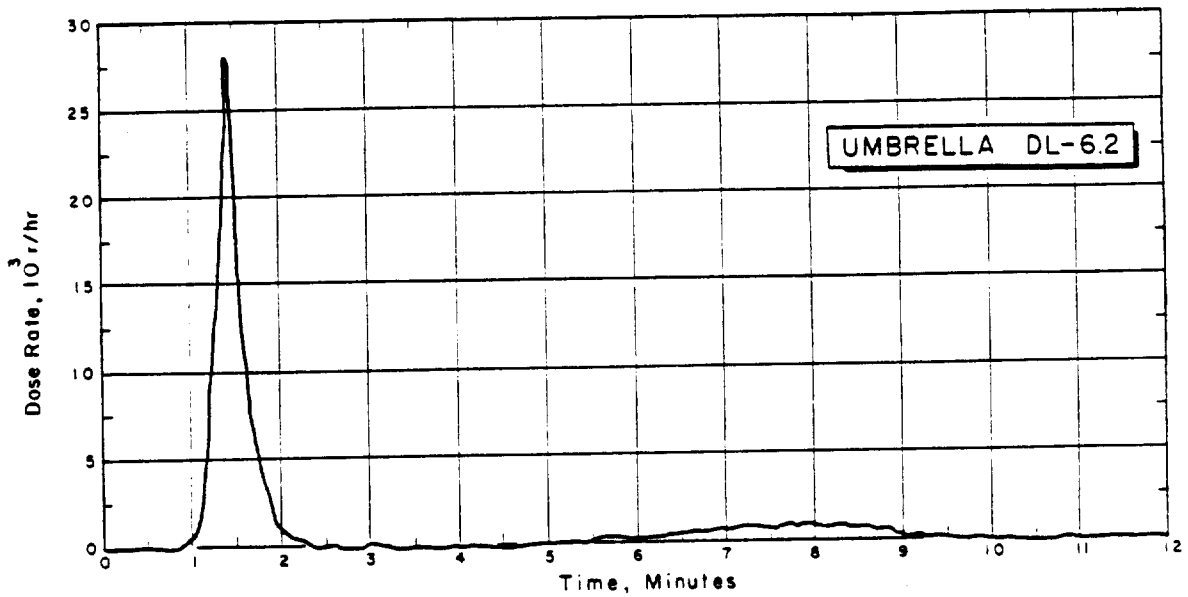


Figure D.17 Approximate linear gamma dose rate record for coracle at 6,220 feet, 230.4° T from surface zero, Shot Umbrella.

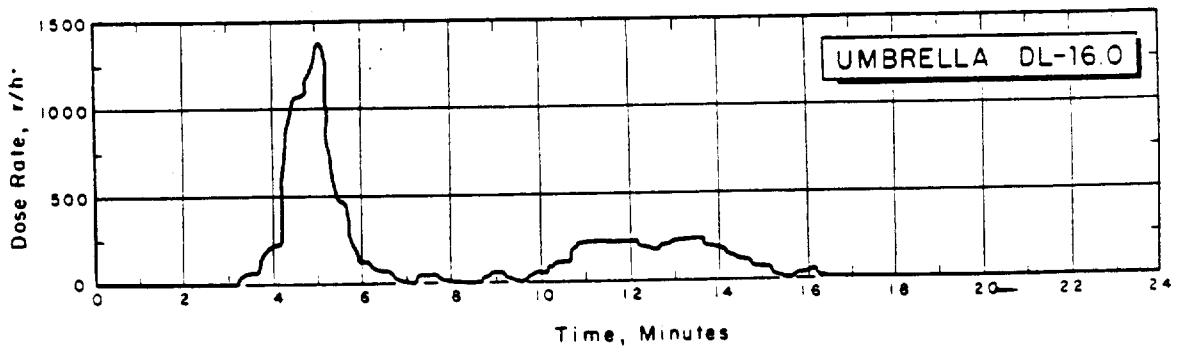


Figure D.18 Approximate linear gamma dose rate record for coracle at 15,980 feet, 237.1° T from surface zero, Shot Umbrella.

250

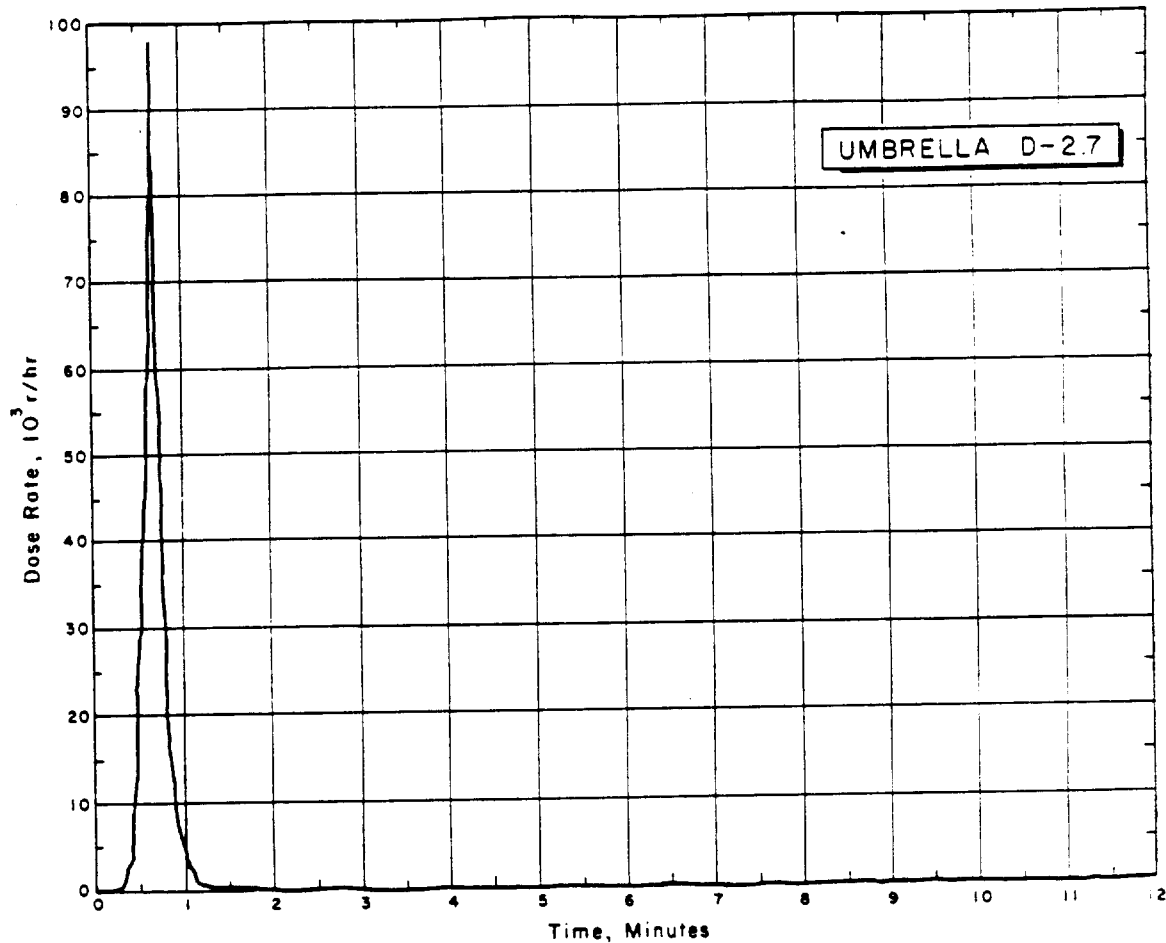


Figure D.19 Approximate linear gamma dose rate record for coracle at 2,670 feet, 248° T from surface zero, Shot Umbrella.

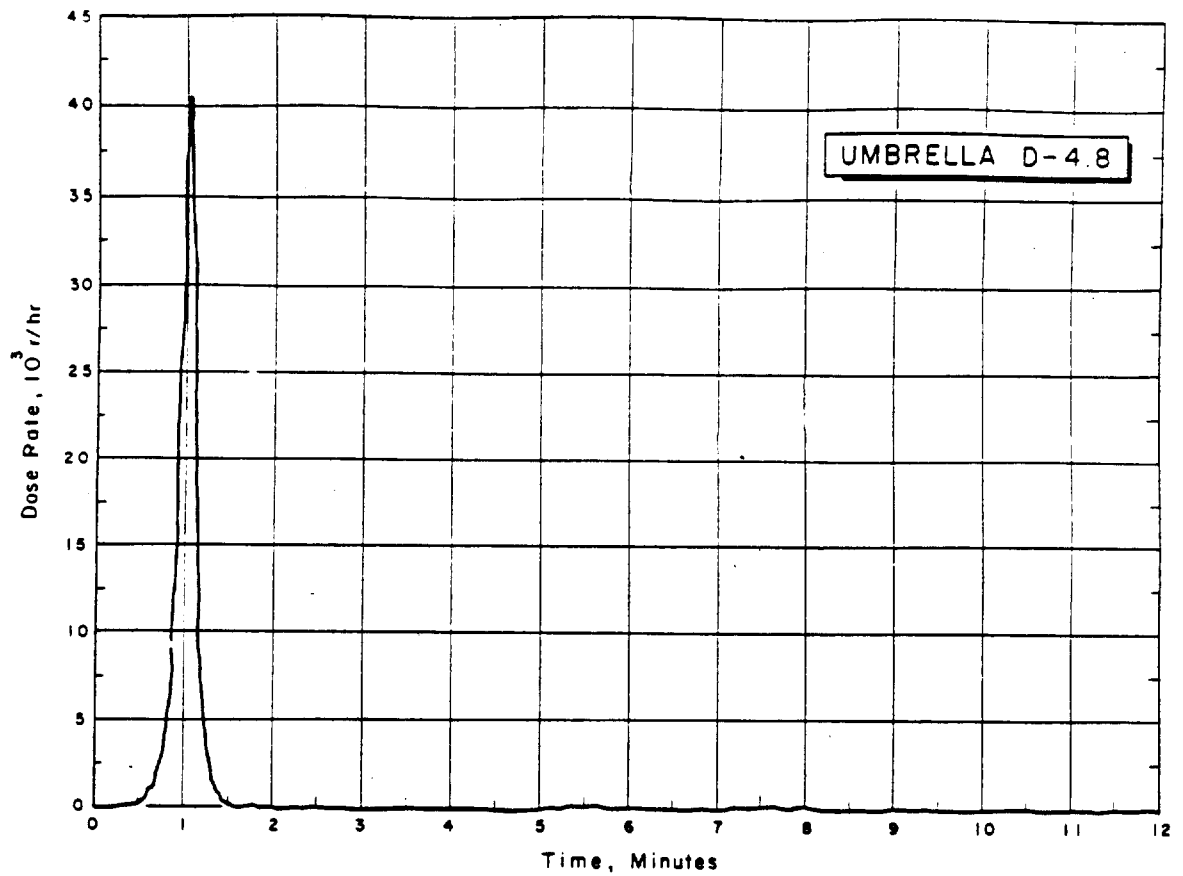


Figure D.20 Approximate linear gamma dose rate record for coracle at 4,770 feet, 247.9° T from surface zero, Shot Umbrella.

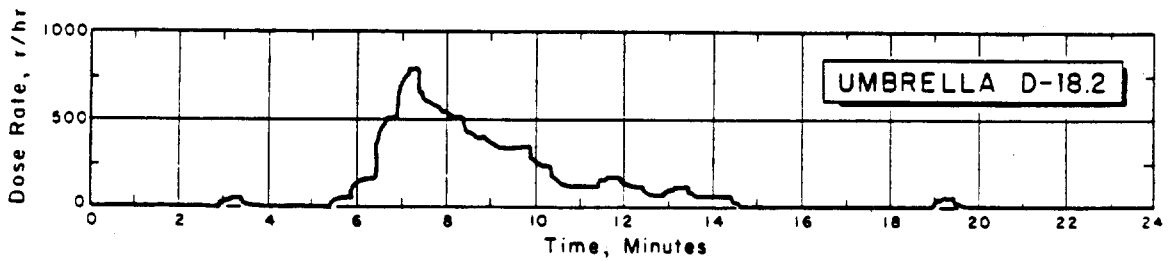


Figure D.21 Approximate linear gamma dose rate record for coracle at 18,220 feet, 250.2° T from surface zero, Shot Umbrella.

257

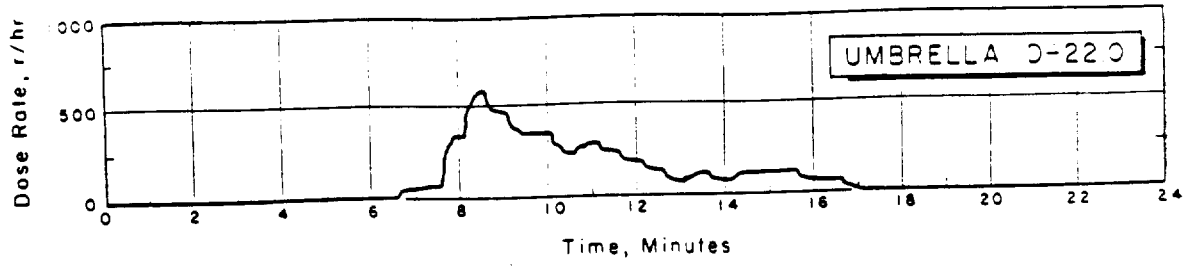


Figure D.22 Approximate linear gamma dose rate record for coracle at 22,000 feet, 248° T from surface zero, Shot Umbrella.

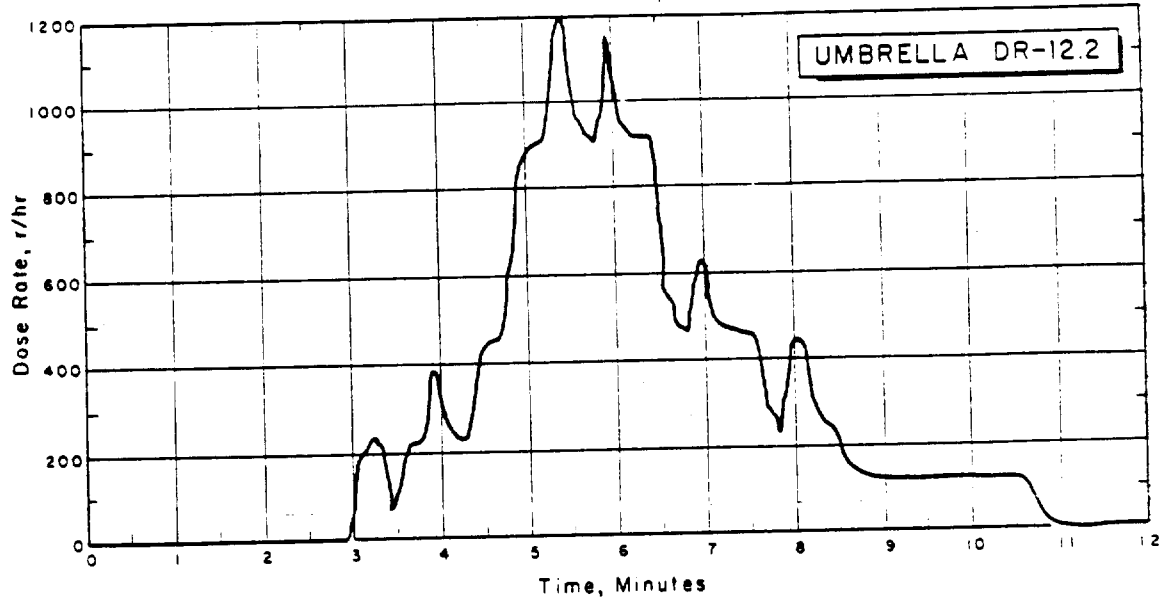


Figure D.23 Approximate linear gamma dose rate record for coracle at 12,230 feet, 262.5° T from surface zero, Shot Umbrella. Warning: Increase values read from this gamma record by 10 percent.

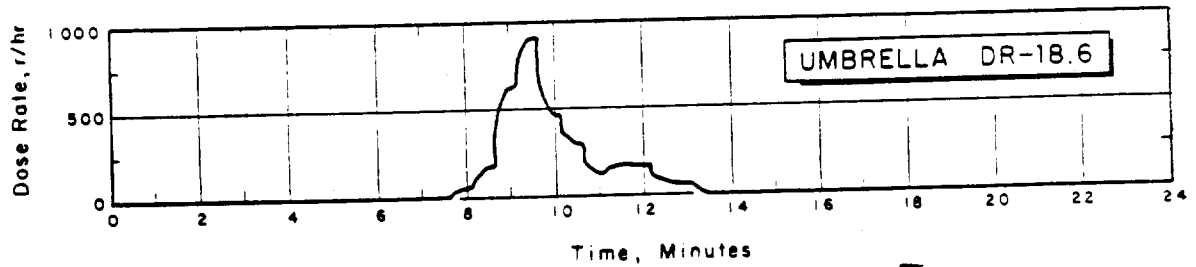


Figure D.24 Approximate linear gamma dose rate record for coracle at 18,600 feet, 261° T from surface zero, Shot Umbrella.

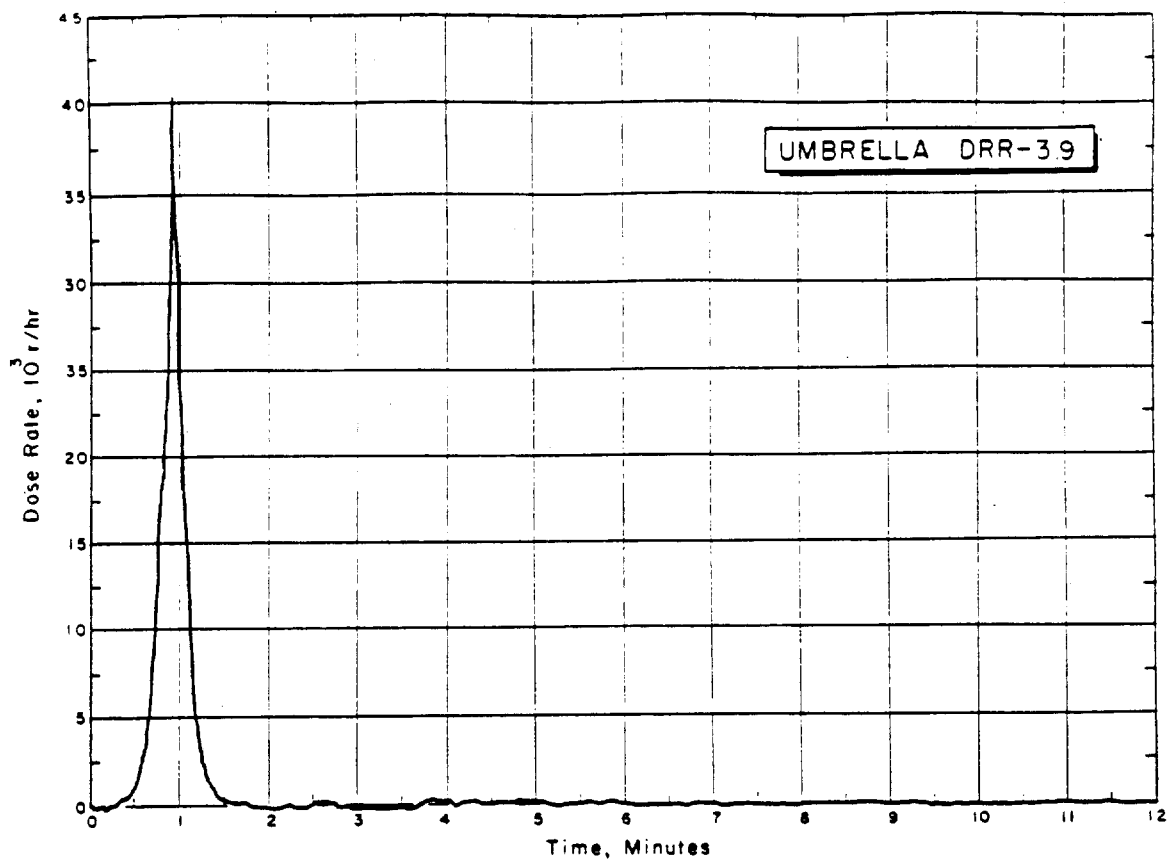


Figure D.25 Approximate linear gamma dose rate record for coracle at 3,940 feet, 279.1° T from surface zero, Shot Umbrella.

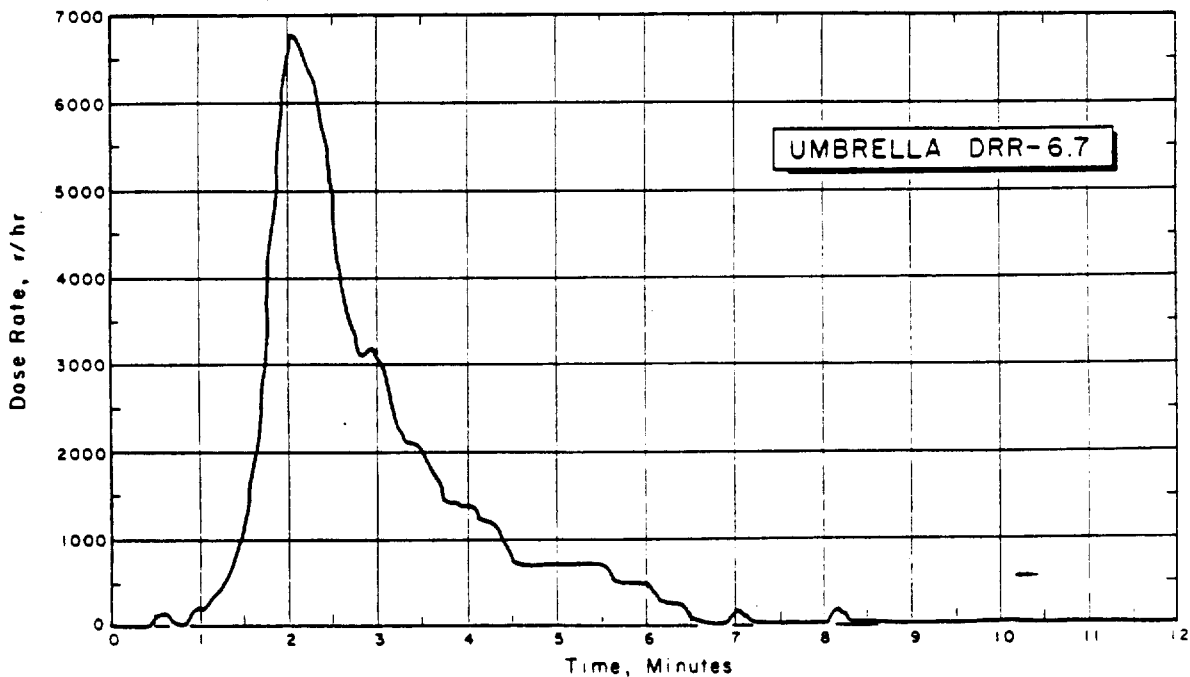


Figure D.26 Approximate linear gamma dose rate record for coracle at 6,740 feet, 278.1° T from surface zero, Shot Umbrella.

2-7

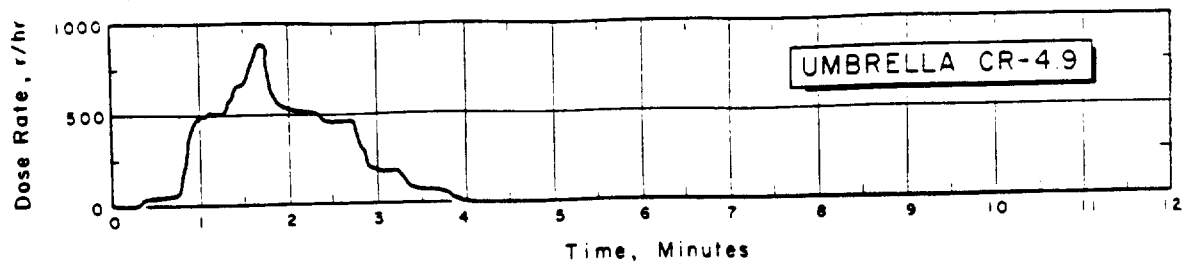


Figure D.27 Approximate linear gamma dose rate record for coracle at 4,910 feet, 334° T from surface zero. Shot Umbrella. Warning: Increase values read from this gamma record by 10 percent.

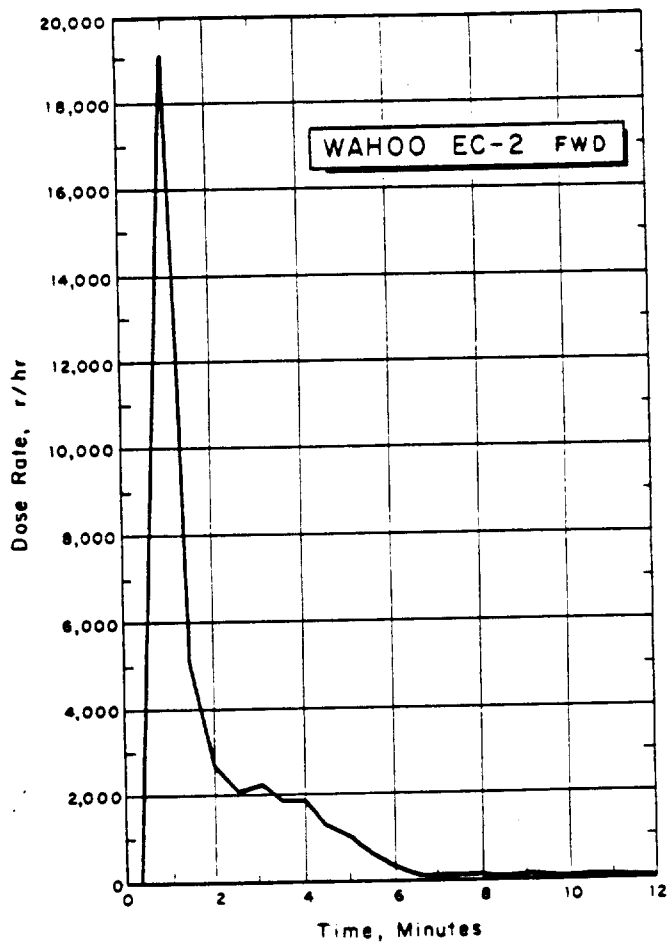


Figure D.28 Approximate linear gamma dose rate record for ship at 2,300 feet, 28.5° T from surface zero. Shot Wahoo. Warning: Increase values read from this gamma record by 10 percent.

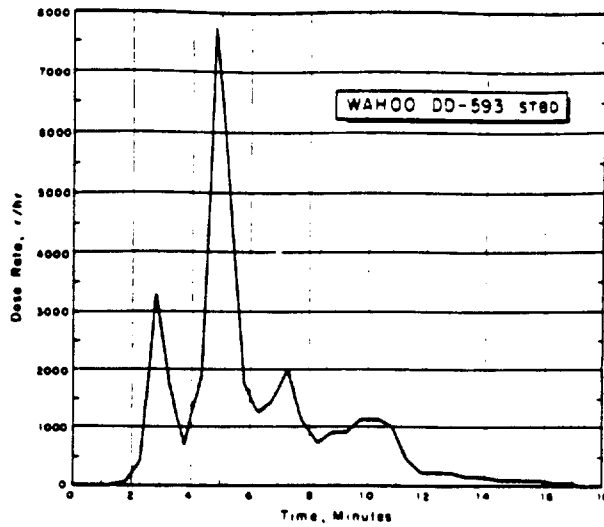


Figure D.29 Approximate linear gamma dose rate record for ship at 8,900 feet, 250° T from surface zero, Shot Wahoo. Warning: Increase values read from this gamma record by 10 percent.

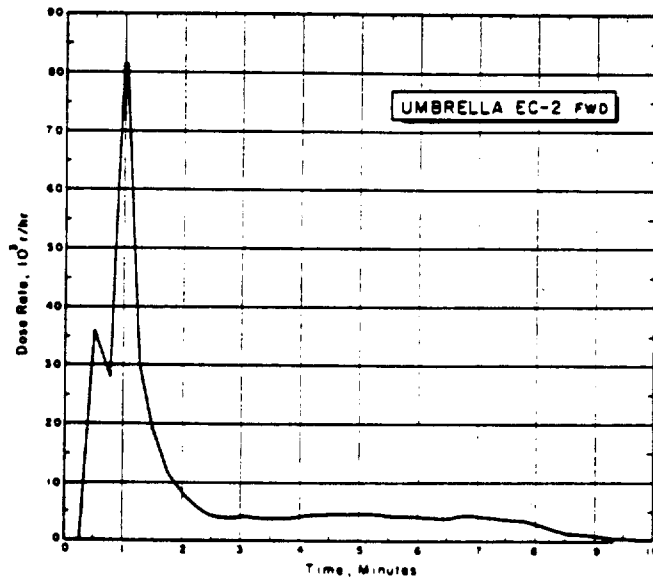


Figure D.30 Approximate linear gamma dose rate record for ship at 1,650 feet, 158° T from surface zero, Shot Umbrella.

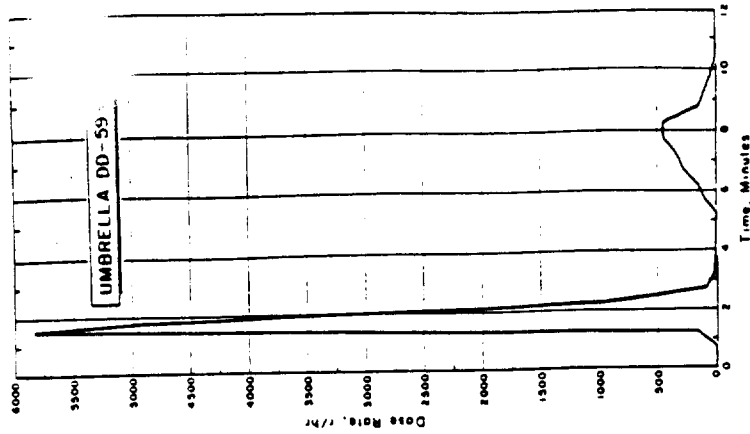


Figure D.31 Approximate linear gamma dose rate record for ship at 1,900 feet, 245.7° T from sur-face zero, Shot Umbrella.

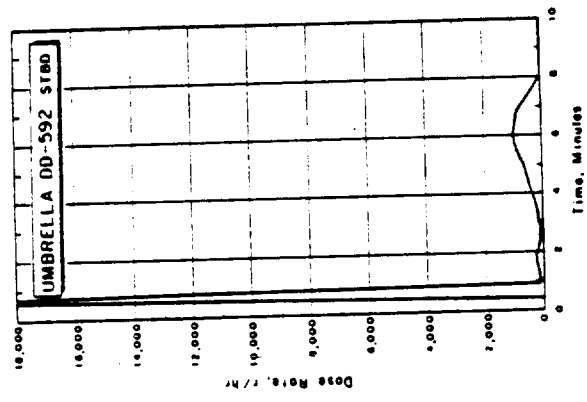


Figure D.32 Approximate linear gamma dose rate record for ship at 3,000 feet, 248.5° T from sur-face zero, Shot Umbrella.

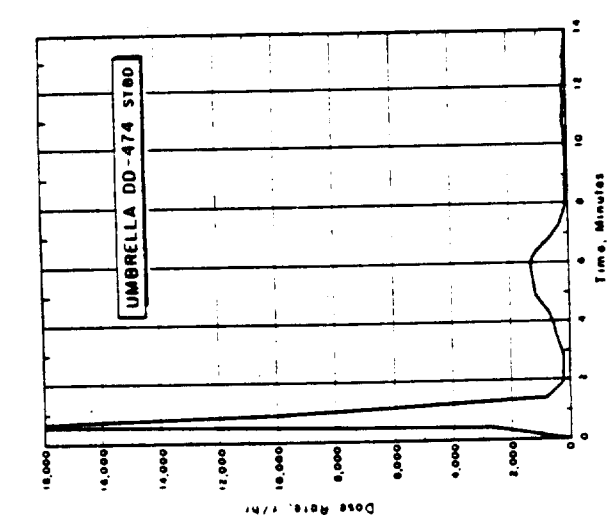


Figure D.33 Approximate linear gamma dose rate record for ship at 7,900 feet, 249.2° T from sur-face zero, Shot Umbrella.

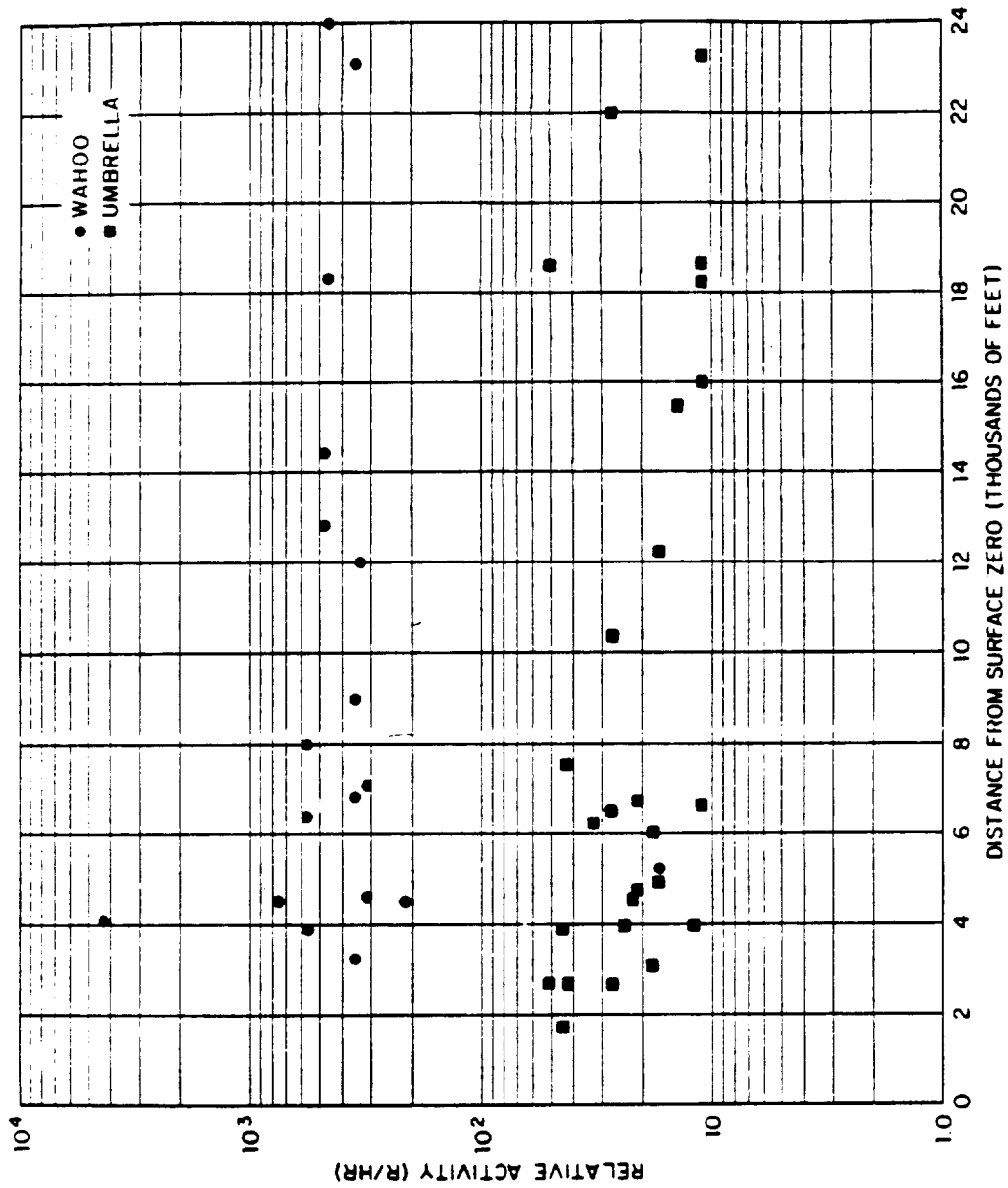


Figure D.34 Variation of meter survey of coracles with distance (converted to std-GTR response at 1 minute).

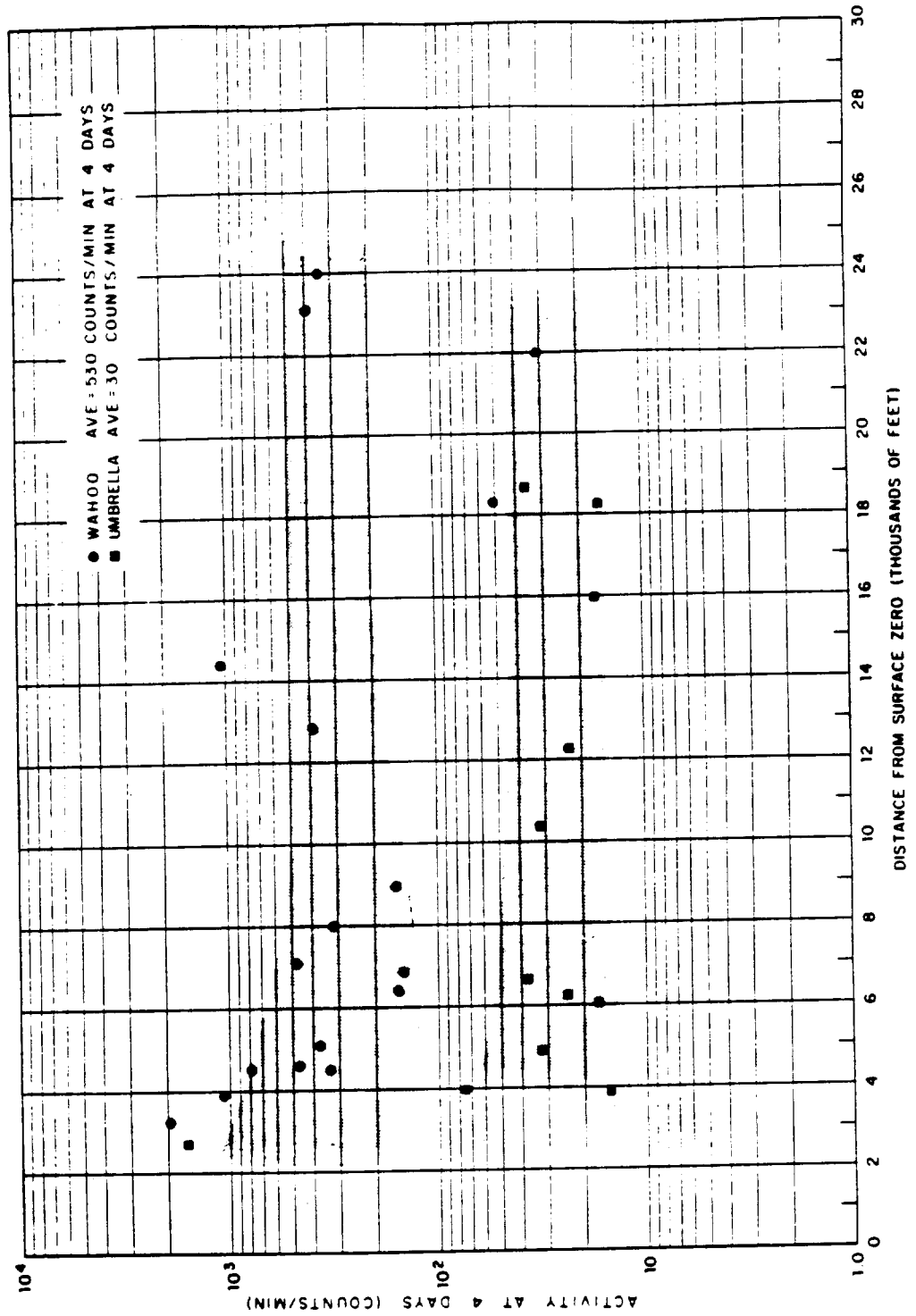


Figure D.35 Tray set background for IC collections.

26+

## Appendix E

### SUMMARY OF OTHER UNDERWATER DETONATIONS

A brief summary of pertinent shot and weather data for Shots Baker and Wigwam is presented in Tables E.1 through E.3. This material has been abstracted from References 8, 9, 14, 24, 35, 54, 99, 101, and 128 through 131.

#### E.1 GENERAL CONDITIONS

The general conditions are listed in Table E.1.

#### E.2 SHOT BAKER

The surface waters were illuminated by the fireball for a few milliseconds, this luminosity disappearing as the bubble reached the surface. Following the appearance of the slick, a conical spray dome began to form at about 4 msec after zero time; its initial rate of rise was approximately 2,500 ft/sec. A few milliseconds later, plumes began to form. These plumes rapidly overtook the spray dome and formed a hollow column approximately 8,000 feet high and 2,000 feet in diameter (estimated thickness of the column walls is 300 feet). The fireball was briefly visible near the top of this column but was quickly obscured by the development of a large cumuliform cloud capping the column. Massive bodies of water fell from the periphery of this cumuliform cloud, reaching the surface at approximately 10 seconds. Also at 10 seconds, a base surge generated by the collapsing column expanded outward rapidly and reached a height of 500 feet at 12 seconds. The cumuliform cloud persisted during the base surge formation, and a heavy rain was observed to fall from it from approximately 1 to 2.5 minutes; the annular ring of maximum rainfall had approximate inner and outer diameters of 4,000 and 6,000 feet, respectively. After about 5 minutes, the base surge lifted from the water surface and rose to form a part of the lower cloud deck. A moderate to heavy rain lasting for nearly an hour fell from this lower cloud deck.

An initial dose rate greater than 10,000 r/hr was reported aboard the LCT-874 at 7,260 feet and 48° T of surface zero. Peak dose rates of 4,000 r/hr at 2 minutes, 180 r/hr at 5 minutes, 220 r/hr at 6 minutes, and 900 r/hr at 7 minutes were recorded aboard the LCT-874 (7,260 feet, 48° T from surface zero), USS Crittenden (APA-77) (5,025 feet, 276° T from surface zero), USS Carterett (APA-70) (9,720 feet, 256° T from surface zero), and LCI-332 (5,610 feet, 88° T from surface zero), respectively.

#### E.3 SHOT WIGWAM

The first evidence of detonation was an expanding disk on the water surface indicating the arrival of the shock wave. The expanding disk appeared as a white area with a dark fringe and reached a radius of 7,000 feet.

The spray dome appeared at 386 msec after the appearance of the first surface effects (called surface zero time or SZT) reaching a maximum radius of 7,000 feet at 1 second and a maximum height of 160 feet at 2.5 seconds after its initial appearance. Also at 2.5 seconds, a second dome of extremely spiky appearance rose above the first spray dome. The tallest spikes reached a height of 900 feet at approximately 8 seconds.

About 2.85 seconds after the first visible effects on the surface, a condensation cloud appeared directly above the burst as a result of the passage of the air shock wave. A second, less clearly defined condensation cloud appeared about 8.5 seconds after SZT.

The spray domes were broken up by large irregular plumes at approximately 10 seconds after SZT. The first plumes were predominantly vertical and denser than the spray in the domes. These plumes reached a maximum height of 1,450 feet and an aggregate diameter of 2,000 feet at 19 seconds. A second group of plumes, appearing at lower levels, developed at approximately 16 seconds. The entire plume formation fell back to the surface covering an area 3,100 feet in diameter at 25 seconds. A third plume formation became visible at 35 seconds, reaching a height of about 770 feet.

The plumes broke up into a fine spray, spreading out radially to form a base surge that was first evident at 13 seconds. The development of the base surge from both the primary and secondary plumes was continuous. The base surge was clearly identifiable at approximately 26 seconds, attaining a maximum height of 1,900 feet at 4 minutes. The base surge moved downwind as a low-lying cloud and remained visible for about 23 minutes.

A white circular patch of foam was observed about surface zero after the base surge had thinned sufficiently to make it visible. At 1.5 minutes, the patch's diameter was 6,300 feet; it continued to expand to a diameter of 10,400 feet at 13 minutes, at which time it became difficult to distinguish.

The YAG-39, which was steaming at approximately 10 knots, encountered a radioactive cloud about 13 minutes after zero time at approximately 28,000 feet downwind (bearing 200° T from surface zero). Gamma intensity measurements of greater than 400 r/hr were recorded during the period from 16 to 19 minutes. By 22 minutes, the radiation field had dropped off to a level of 1 r/hr. Assuming that the observed decay exponent (-1.5) is valid for early times, the radiation intensity was estimated to be about 10,000 r/hr at 2 minutes after SZT. The overall dose accumulated topside on the YAG-39 with the washdown system in operation was about 30 r. Phosphate glass dosimeters placed in the vicinity of YC-473 (shot barge) recorded total gamma doses of approximately 3,600 r.

TABLE E.1 SHOT DATA AND SURFACE WEATHER AT SHOT TIME,  
SHOTS BAKER AND WIGWAM

	Baker	Wigwam
Yield, kt		
Weapon depth, feet		
Water depth, feet		
Zero time		
Zero coordinates		
Surface wind direction, °T		
Surface wind speed, knots		
Sea level pressure, mos		
Free-air surface temperature, °F		
Relative humidity, pct		
Tide		
Sea state		

\* Wave heights given here are the average of the  $\frac{1}{3}$  highest waves.

TABLE E.2 COLUMN AND BASE SURGE DATA, SHOT BAKER

Column height	4,100 feet at 10 seconds		
	7,600 feet at 60 seconds		
Column diameter (at throat)	1,950 feet		
Time of first appearance of base surge	10 seconds		
	Radial Velocity (knots)	Height (ft)	Radius (ft)
Base surge at 30 sec	42	620	3,000
40 sec	36	690	3,600
50 sec	32	850	4,200
60 sec	28	980	4,800
90 sec	20	1,350	6,000
2 min	15	1,580	6,900
3 min	10	1,800	8,100

TABLE E.3 SPRAY DOME AND BASE SURGE DATA,  
SHOT WIGWAM

Maximum height of spray dome	900 feet	
Maximum diameter of spray dome	14,000 feet	
Time of first appearance of base surge	13 seconds	
	Radial Velocity (knots)	Height (ft)
Base surge at 30 sec	67	500
40 sec	44	600
50 sec	31	700
60 sec	23	800
90 sec	14	1,200
2 min	12	1,400
3 min	11	1,700

## Appendix F

### GLOSSARY

A large number of alphabetic abbreviations are frequently used in the text of this report because of the rather unwieldy descriptive names applied to specialized project equipment. Furthermore, certain common words are used in a specialized or restrictive sense when discussing the phenomena connected with the underwater events. For greater convenience, these terms are assembled and briefly defined here. When additional discussion of the word or abbreviation appears in the text, a section reference is given parenthetically following the definition. The glossary is preceded by the key used in the summary presentation of the gamma records in Sections 3.3.2 and 3.4.1.

#### KEY FOR MASTER TABLE (TABLE 3.11) AND FOR INDIVIDUAL STATION DATA (Figures 3.66 through 3.96)

1. Gamma dose rate record: gamma dose rate versus time corrected for instrument response; type of detector indicated. Normalized rate curve for instrument shown from 1 minute until end of record.
2. Transit plot: plan view of various surge boundaries at beginning and end of transit. Boundaries shown for times indicated. Letter designators for boundaries same as those given in tabulated section of this key.
3. Tabular data: same key applicable also for master table (Table 3.11).

General: letter designators and other general symbols used in the table:

- = no data available      ( ) = value is estimated      [ ] = see notes for boundary plot

CA = point of closest surge approach

calc = calculated data

CR = point where  $B_0$  recedes

DD = drifting

ED = inner edge influences

EX = expanded surge boundary

OL = station outside lagoon

OV = coracle overturned

obs = observed data

poss = possibly

msg = observation expected but not observed

msk = observation masked by a concurrent event

n.a. = not applicable, occurrence is unlikely

NC = not central decrement

neg = negative value

RF = reef station

sat = instrument saturated

WW = interference due to white water

XTP = extrapolated data

Records: records given are complete unless parenthetically indicated or modified as stated.

Modifying conditions: basis of estimated time of overturn given in parenthesis: (no 2nd rise) = the instrument failed to record the passage of the upwind surge accurately; (sec-GITR track) = the secondary GITR tracked the std-GITR until the time of the estimate; GITR OK = std-GITR was not damaged by overturn; GITR damaged = std-GITR damaged by overturn.

Types of transit are illustrated in Figure 3.63; the letter designators used are:

C = central transit

D = distant transit

SN = skirting transit, an upwind event

TN = total envelopment, an upwind event

5.8

E = edge transit  
IE = inner edge transit  
OE = outer edge transit  
PN = partial transit, an upwind event

TTC = transit through the center, center passes at 1,000 feet or less

Types of records: more fully described in Section 3.3.2; the letter designators used are:

M = record typical for station almost missed by surge  
N<sub>1</sub> & N<sub>2</sub> = records typical for stations experiencing an edge transit

W<sub>1</sub> & W<sub>2</sub> = characteristic Wahoo records  
U<sub>1</sub> & U<sub>2</sub> = characteristic Umbrella records

Surge boundaries: These and other surge parameters are illustrated in Figure 3.63; the letter designators used are:

B<sub>i</sub> = inner primary smooth boundary  
B<sub>o</sub> = outer primary smooth boundary  
B<sub>s</sub> = outer secondary smooth boundary  
H = hypothetical surge center

NOL = NOL smooth boundary  
P<sub>1</sub> = inner photo-boundary of primary surge  
P<sub>o</sub> = outer photo-boundary of primary surge  
S<sub>o</sub> = outer photo-boundary of secondary surge  
X = photographic surge center

Total surge: normalized dose cumulated over time indicated.

Surge boundaries: photo-TOA and photo-TOC given for outer primary photo-boundary only; distance and time of closest approach of X given if <5,000 feet; rad-TOA = average of 38 and 100 percent of TOP; rad-TOC = time normalized rate curve drops below 10<sup>3</sup> r/hr; source center = distance of P<sub>o</sub> at TOP; length of tail calculated using official surface wind speed.

Approach velocities: Photo-velocities calculated for boundary indicated at specified distances greater than that at TOP. Rad-velocities calculated for rise from 5 to 100 percent of peak for models indicated, (see also Section A.3).

Waterborne sources: Calculated water and foam movements for drifts and sets or radial expansions indicated.

Bomb-generated waves: Calculated as described in Section 2.3.2.

4. Boundary plot: distance of various surge boundaries shown as a function of time; normalized rate curve with logarithmic scale superimposed; calculated water and foam movements shown at bottom; values in brackets are read from dashed boundaries, which compensate for surge disappearance (see text).

AFI: Air filtration instrument, a device which collects a sequence of aerosol samples on a chemical filter (see Section 2.2.6).  
A-frame: A simple pipe frame used to support lightweight hoisting equipment, usually mounted on the front of a vehicle.  
AOC: Always-open collector, a large tray for collection of fallout (see Section 2.2.6).  
ASEL: Army Signal Engineering Laboratory, Ft. Monmouth, New Jersey.  
ASEL-GITR: Army Signal Engineering Laboratory gamma-intensity-time recorder, an instrument developed at ASEL to measure high gamma dose rates; also called the Gustave I (see Section 2.2.3).  
ASW: Antisubmarine warfare, used in this report with the connotation that the weapons used are nuclear.  
AVR: A high-speed launch used for aviation rescue work.  
background: Normal radiation intensities of instrument readings due to natural causes or from uncontrolled sources not under study.  
ball crusher: A device used for detecting the bottom when placing deep anchors.  
base surge: The apparently fine liquid aerosol that moves outward rapidly from the subsiding column of water after detonation of an underwater nuclear device. The base

surge is probably radioactive or carries radioactive material with it. For detailed discussion of gamma records, base surge may be subdivided into primary and secondary base surge (see Figure 3.63). Primary base surge is the surge generated by collapse of the first column formed and is outermost. Secondary base surge (whose existence is postulated on the basis of photographic records of secondary plumes and other corroborative evidence) advances radially behind the primary base surge.

- base surge decay curve: Same as early decay curve.
- boundary plot: A plot of various photographically determined base surge boundaries versus time, used for correlating specific features of the gamma dose rate records with these photographic boundaries.
- BWA: Beach work area, an area on Parry Island specially equipped for the staging and instrumenting of coracles.
- CIC: Combat information center, a highly centralized information and control center aboard combatant ships.
- CL: Crosswind left, an abbreviation used to designate an approximate radial line 90° to the left when looking down the downwind leg of the target array (~158° T).
- cloud: An aerosol or body of airborne liquid droplets, usually used with the connotation that the droplets are radioactive or are associated with airborne radioactive material. The meaning of cloud is sometimes extended to include the entire aerial environment, such as material that is in the process of falling to the surface.
- cloud slope: A term used in discussion of stationary cloud models in order to avoid expressions implying movement, such as time of arrival. Cloud slope is the rate at which the concentration of radioactive material in a hypothetical model increases with time (see Section 1.3.1).
- column: The mass of solid water, liquid aerosol, and gaseous material that is blown into the air by an underwater nuclear detonation. The energy of this mass falling back to the surface generates the base surge.
- coracle: A circular floating platform specially designed to mount project instruments (see Section 1.3).
- CR: Crosswind right, an abbreviation used to designate an approximate radial line 90° to the right when looking down the downwind leg of the target array (~338° T).
- cross-contaminate: An uncontrolled interchange of material between two individual samples occurring at time of collection or during subsequent handling.
- D: Downwind, an abbreviation used to designate the approximate radial line extending down the downwind leg of the target array (~248° T).
- decrement: A presumed decrease in the concentration of airborne radioactive material within the visible base surge, resulting in a decrease in the observed dose rate. Such a decrease may be located centrally (central decrement) or between the primary and secondary base surges (intersurge decrement). (See Figure 3.63.)
- deposit dose or dose rate: The gamma dose or dose rate resulting from radioactive material deposited on surfaces.
- DL: Downwind left, an abbreviation used to designate the approximate radial line 15° to the left when looking down the downwind leg of the target array (~233° T).
- DLL: Downwind left left, an abbreviation used to designate the approximate radial line 30° to the left when looking down the downwind leg of the target array (~218° T).
- DMT: dimethylterephthalate, a crystalline material used to form the chemical filter in air filtration instrument (see AFI).
- DR: Downwind right, an abbreviation used to designate the approximate radial line 15° to the right when looking down the downwind leg of the target array (~263° T).
- DRR: Downwind right right, an abbreviation used to designate the approximate radial line 30° to the right when looking down the downwind leg of the target array (~278° T).

**DUKW:** A small amphibious surface craft capable of being used either in the water or on land.

**early decay curve:** Any of a family of decay curves presumed to be characteristic of radioactive material deposited from the base surge during the first 5 minutes of its existence.

**early gamma dose:** An expression arbitrarily defined in this report as the gamma radiation dose received within the first minute after zero time. (See initial dose.)

**EC-2:** A Liberty ship used on this operation as a floating platform for instruments.

**EG&G:** Edgerton, Germeshausen, and Grier, Inc., a contractor providing timing and firing service to the Task Force.

**EMBL:** Eniwetok Marine Biology Laboratory, a laboratory on Parry Island.

**envelopment:** A term used in a special sense to describe movement of the complex base surge over a position upwind of surface zero. Envelopment may be skirting, partial, or total as illustrated in Figure 3.63.

**EPG:** Eniwetok Proving Ground, the area surrounding Eniwetok and Bikini atolls in the Marshall Islands.

**fallout:** Particulate material raining down from or falling out of clouds or other aerosols produced by atomic devices, usually used with the connotation that the material is radioactive or carries with it radioactive debris from the device.

**FFP:** Floating film pack, any of several types of simple floats designed to support film packs at the water surface; the term includes both float and film pack (see below).

**film pack:** An assemblage of special photographic films so packaged as to give a reliable measurement of total gamma dose (see Section 2.2.5).

**float:** Any surface buoy; however, the term is frequently used to designate a small circular float which contains a film pack (see Section 2.2.5).

**Flowrator:** A commercially produced instrument that measures the rate of fluid flow through a closed system.

**flyaway:** Any of several specially scheduled flights usually direct to the continental U. S. for the principal purpose of returning short-lived radioactive samples to home laboratories for analysis. The various flyaways are usually designated by their departure time relative to a specific shot, e. g., Wahoo plus 10-hour flyaway or 10-hour flyaway.

**FP:** An abbreviation for film pack.

**fractionation:** Alteration of the normal spectrum of fission products resulting from a nuclear detonation by mechanical or chemical separation. Fractionation is usually expressed in terms of R-values. (See R-value.)

**free-field:** An arbitrary term defined to mean the radiation field near the water surface resulting from a cloud of airborne radioactive material unmodified by any projections above the water surface (see Section 1.1).

**FS:** Funnel sample, a fallout sample collected by means of a funnel and bottle (see Section 3.5.1).

**Getok Hill:** A spiritual sanctuary for harassed members of the project.

**GIDU:** Gamma-intensity-decay unit, an instrument that flushed radioactive fallout collected until H + 4 minutes into a lead shield where a continuous decay record was started immediately.

**GITOUT:** An electronic device that automatically reads out the gamma-intensity-time recorder tapes and plots the data (see Section 2.2.8).

**GITR:** Gamma-intensity-time recorder, an instrument that measures gamma intensity as a function of time and records this information on magnetic tape (see Section 2.2.1).

**gross gamma field:** Arbitrarily defined as the total, uncorrected gamma field exactly as measured by a detecting instrument.

**Gustave I:** An ASEL-GITR.

**H and N:** Holmes and Narver Inc., the site contractor providing construction and housing services.

hot line: The line along which the greatest deposition of radioactive material is expected for atomic clouds whose maximum height does not exceed 2,000 feet, this line nearly coincident with the track of the center of the radioactive cloud.

hypocentral surge center, H: the presumed location of the base surge center at a specific time determined simply by moving surface zero downwind in accordance with the official Task Force surface winds.

IC: Incremental collector, an instrument that makes a sequence of passive fallout collections on small trays (see Section 2.2.4).

ICB: Instrument control box, a switching and timing device that controls coracle instruments (see Section 2.2.7).

identifier: A larger float used to aid in spotting and identifying floating film packs from the air; also an alphabetic or numerical symbol designating instrument position at given station (see Section 2.2.5).

initial dose or dose rate: Dose or dose rate from radiation occurring shortly after zero time during the venting of the radioactive products.

intensity: A term used for both source intensity and dose rate.

isodose contour: a boundary drawn for a specified time after a nuclear detonation, along which the cumulative radiation dose to that time is presumed to be the same.

ITR: Interim Test Report.

LASL: Los Alamos Scientific Laboratory, Los Alamos, New Mexico.

late decay curve: A decay curve presumed to be characteristic of radioactive material deposited later than 5 minutes, possibly from such sources as white water.

LCM: A small amphibious attack craft capable of carrying vehicles and making landings directly on beaches.

LCU: A large amphibious attack craft capable of carrying several vehicles and a small crane, and capable of making landings directly on beaches.

LD<sub>50</sub>: Lethal dose 50 percent. For a stated type of radiation, the dose which results in 50-percent fatalities in a population of exposed organisms within a stated period of time after irradiation, usually 30 days.

M: The alphabetic time zone designator for the EPG indicating the time zone 12 hours later than Greenwich Mean Time (GMT).

M-boat: An LCM.

NBS: National Bureau of Standards, Washington, D. C.

NOL: Naval Ordnance Laboratory, Silver Spring, Maryland.

NRDL: U. S. Naval Radiological Defense Laboratory, San Francisco, California.

OCC: Open-close collector; a large tray that is opened to collect fallout and later closed (see Section 2.2.6).

PDST: Pacific Daylight Saving Time. Seven hours earlier than Greenwich Mean Time (GMT).

photo-: a prefix used to indicate that the parameter in question is photographically determined as distinguished from one that is determined on the basis of the dose rate records.

photo-boundary: any of several base surge boundaries determined from aerial photographs.

photographic surge center, X: the presumed location of the base surge center at a specific time defined as the center of the circle that best fits the outer photo-boundary of the primary surge at the time in question. This center is presumed to move in accordance with this photo-boundary up to the time of the last reliable boundary (3.5 minutes for Wahoo and 6 minutes for Umbrella) after which it moves in accordance with the official Task Force surface winds.

plume: One of the several large masses of water thrown upward and outward radially by an underwater water explosion.

R-value: The ratio of the observed amount of a given radionuclide to the amount expected from thermal neutron fission of U<sup>235</sup>, calculated on the basis of some reference radionuclide whose amount is also determined. When the reference radionuclide is not specified, Mo<sup>99</sup> is usually implied through common usage.

rad-: prefix used to indicate that the parameter in question is determined on the basis of the dose rate records as distinguished from one determined photographically.

radex area: radiological exclusion area. An area to which access is limited or prohibited due to the presence of generally distributed radioactive material constituting a personnel contamination hazard.

radiation pulse: A square wave pulse recorded on magnetic tape by the recycling of a GITR ionization chamber. For the high-range channel of the std-GITR, each radiation pulse represents a dose increment of 0.243 r. A low-range radiation pulse is one-thousandth of the high range.

residual dose rate: The radiation field due to deposited radioactive material, which remains after passage of the radiating cloud.

sec-GITR: Secondary gamma-intensity-time recorder, a term used to designate an underwater GITR that failed to drop. Records produced by the underwater GITR under these circumstances were similar to those produced by the standard GITR.

shadow bias: alteration of fallout collections caused by particle trajectories in the neighborhood of surfaces vertical to the prevailing wind.

shine: A term used in this report to distinguish radiation emanating beyond the visible boundaries of a diffuse body of radioactive aerosol from the field within said diffuse body.

SIO: Scripps Institution of Oceanography, La Jolla, California.

smooth boundary: An imaginary base surge boundary defined by the circle best approximating any of the several photo-boundaries. (See photo-boundary.)

source center: A point within a diffuse body of radioactive aerosol at which the dose rate reaches peak intensity probably as a result of optimum geometry.

source intensity: The energy emitted at a radioactive source, used here as the number of Mev emitted per unit time per unit volume or area.

spike: A sharp rise and fall in gamma dose rate as seen on a plot of gamma intensity versus time, with the connotation that the peak dose rate is very much higher than the dose rate either before or after the peak.

SRC: Sample recovery center, an area specially arranged to maintain records and contamination control during sample recovery operations.

standard decay curve: A decay curve for mixed fission products at early times selected from the latest literature available at the time of writing (References 36 and 89) and used consistently throughout this report (see Section B.2).

standoff distance: The distance a ship delivering a weapon must maintain in order to avoid tactical damage, usually used in the report with the connotation that the weapon is nuclear.

std-GITR: Standard gamma-intensity-time recorder, a GITR with a 12-hour tape transport mounted in the center of a coracle deck (see Section 2.2.1).

subsurface buoy: A 3-foot diameter buoy placed at a depth of 150 feet below the surface when establishing a deep anchor (see Section 2.3.1).

surface zero: The point at the water surface directly over the point of detonation of an underwater shot.

surge: An abbreviation for base surge in general or a specific segment of the base surge. When modified by the adjectives upwind or downwind, the term is used in the more restrictive sense of the upwind or downwind portions of a torus assumed to represent a generalized base surge (Figure 3.63).

survey point: A mark painted in a known location on a ship's deck indicating that a survey meter reading is to be taken at that point (see Section 3.4.2).

SZ: Surface zero.

tail: A remnant of radioactive aerosol trailing behind the base surge proper. The meaning is extended to include radioactive aerosol temporarily detained in turbulent eddies associated with ship superstructures and streaming downwind from the ship after passage of the base surge (see Section 3.3.2).

**T-boat:** An LCU. (See LCU.)

**throwout:** Massive ejections from a detonation, which follow a ballistic trajectory. These ejections from an underwater detonation are principally water and, thus, follow the usual modified ballistic trajectory.

**time of arrival:** Arbitrarily defined as the lapse in time from detonation to some specified point on the increasing slope of the first major dose rate peak at a specific location; abbreviated TOA. Other definitions are also possible (see Section 3.3.4).

**time of cessation:** Arbitrarily defined as the lapse in time from detonation to the point at which the dose rate curve of the major event drops to background or nearly so; abbreviated TOC. TOC is determined in this report by inspection of the normalized rate curve (see Section 3.3.4).

**time of peak:** The lapse in time from detonation to the first major dose rate peak; abbreviated TOP.

**TOA:** Time of arrival.

**TOC:** Time of cessation.

**TOP:** Time of peak.

**transit:** A term used in a special sense to describe passage of the complex base surge over a fixed position. Transit may be through the center, central, inner edge, edge, outer edge, or distance as illustrated in Figure 3.63.

**transit plot:** A plan view of the probable photo-boundaries and smooth boundaries at the times of their individual initial and final transits at a given station. These plots are useful for intercomparison of the dose rate records from several stations.

**tripod:** A three-legged mast installed on coracles to aid in handling at sea (Figure 1.2).

**U:** Upwind, an abbreviation used to designate the approximate radial line extending along the upwind leg of the target array ( $\sim 68^\circ$  T).

**upwelling water:** Subsurface water moving upward to the surface as a result of bomb energy, usually with the connotation that this water is radioactive.

**UW-GITR:** Underwater gamma-intensity-time recorder, a detector modified to detect gamma fields underwater.

**valley:** A marked decrease in dose rate occurring between two dose rate peaks.

**visual approach velocity:** Any of several approach velocities for the photographically determined base surge boundaries.

**water decay curve:** Same as late decay curve.

**water dose rate:** Gamma radiation due to fallout remaining suspended in the surface water layer.

**white water:** Water containing visible amounts of bottom material pulverized and suspended by the detonation, with the usual connotation that this water is very radioactive.

**WT:** Weapons Test Report, of which this report is an example.

**Z:** The alphabetic time zone designator for Greenwich Mean Time (GMT).